SOURCE TERM SAFETY ASSESSMENT OF RADIONUCLIDE RELEASES UNDER SEVERE ACCIDENT CONDITIONS AT INDIAN POINT 3 NUCLEAR POWER PLANT

Prepared for:
New York Power Authority

by

RISK MANAGEMENT ASSOCIATES
2903 Dietz Farm Road NW
Albuquerque, New Mexico 87107

and

NEW YORK POWER AUTHORITY
123 Main Street
White Plains, New York 10601

July 10, 1984

Table of Contents

List of Tables

List of Figures

Acknowledgements

The authors of this report wish to thank the many individuals and organizations which contributed their time, expertise, and, in some cases, their work. Firstly, to Dr. William Stratton, Dr. Walton Rodger, Messrs. James Davis and Herschel Specter for their constant help and advice throughout the project and their valuable assistance in reviewing this report. Special thanks go to Ms. Ellen Lepper of Potomac Communications Group for her valuable help in communicating our ideas. The efforts of various national laboratories for initially developing the computer code sets utilized in this work merit special mention. They are the Battelle Columbus Laboratory, Sandia National Laboratory, and Oak Ridge National Laboratory. The assistance of several individuals who made valuable contributions should also be noted. They are: Dana Powers of Sandia for core-concrete aerosol generation rates and insight of radioisotope chemistry, and Dr. Richard A. Martin of Los Alamos National Laboratory for the fission product resuspension model.

1.0 EXECUTIVE SUMMARY AND INTRODUCTION

In November 1983, the New York Power Authority (NYPA) undertook a detailed analysis of the radionuclide releases under postulated severe accident conditions. The objective was to examine the physical and chemical behavior of four fission product species under the most severe accident conditions to more precisely determine the fraction of reactor core releases that would remain in the primary system of the reactor, the fraction that would end up in the containment, and the fraction that could ultimately reach the environment, assuming that the containment eventually overpressurized and failed. The analyses were based on accident scenarios taken from the Indian Point Probabilistic Safety Study and focused on those that were risk dominant.

1.1 Background

This assessment of radionuclide releases is an extension of two plant-specific studies. The first was a safety study using probabilistic techniques (the Indian Point Probabilistic Safety Study, or IPPSS) in which the accident sequences most likely to result in substantial public risk were identified and their potential public health consequences were calculated. The second was a sensitivity study by NYPA and another utility to determine the relationship between the quantity and type of radioactive releases or "source term" and public health consequences.

The NRC's landmark reactor safety study, WASH-1400, published in 1975, used source term values which, reviews of actual nuclear accidents and more recent research efforts have suggested, are unrealistically high and that magnify the consequences, especially early fatalities. The scientific investigation that was stepped up after the Three-Mile Island accident in 1979 shows that the use of more realistic source terms reduces the magnitude of the public health consequences significantly. NYPA sensitivity study, for example, indicated that a ten-fold reduction of the WASH-1400-type source term could result in a four hundred-fold reduction in the maximum number of early fatalities--where the peak value for

fatalities decreased from 8,000 to 20, assuming evacuation--and that a 45-fold reduction eliminates all early fatalities, even without evacuation.

Given the enormity of these reduction factors and their potential significance, NYPA began determining the extent to which earlier studies and generic analyses may have overstated the accident consequences for specific accident scenarios. The work described below reflects the computation state-of-the-art and the expert opinions of scientific specialists as to the technical correctness of the analytical approach taken.

1.2 Source Term and Public Risk

Protection of the health and safety of the public has been a "first principle" of nuclear power plant technology since its commercialization more than 30 years ago. The scientific and technical community has amassed a considerable body of knowledge about nuclear plant operations, the potential for accidents occurring, and the attendant risks to the public. Active research programs and refinements in the analytical tools continue, particularly since the accident at the Three-Mile Island Nuclear Plant in 1979.

Estimates of public risk are grounded in three interrelated factors:

- the frequency of specific events occurring that could lead to an accident involving a radiation release;
- the quantity, type and timing of the release of radioactive material that would escape the reactor containment building if it is overpressurized and failed or bypassed; and
- the effects of emergency planning actions to mitigate the consequences of the accident to the public.

The second factor is known as the "accident source term." If reactor core fission products are released from the fuel under severe accident

conditions, a number of physical and chemical factors, as well as the plant configuration which establishes a pathway to the environment, determine the amount of fission products released.

From a public health standpoint, the degree of risk represented by a particular radioactive material under accidental release conditions is influenced by the decay rate of the fission product, its chemical form, the type of radiation it gives off, and its interaction with individual biological systems. If the source term for a postulated severe accident is overestimated, then the predicted health and economic consequences of the accident will be overestimated as well. Hence, the growing interest in more accurate source terms.

Although many researchers agree that the source-term values presently used by the Nuclear Regulatory Commission are unrealistically large, there has been much uncertainty over the extent of their overestimation. A diverse but complementary array of research programs is being carried out in the United States and other countries by government and industry to add to the technical understanding and thereby arrive at a new consensus for establishing more accurate source term estimates. NYPA is actively involved in source term research, and is working closely with regulatory agencies and other research institutions to help resolve technical differences and to integrate the results of its work into the accumulated body of knowledge that will lead to improved understanding of the potential consequences of reactor accidents.

1.3 Evolution of Source Term Analysis

Brookhaven National Laboratory published the first analysis of the potential consequences of a severe nuclear power plant accident in 1957 for the Atomic Energy Commission, the predecessor agency to the U.S. Nuclear Regulatory Commission (NRC). The most serious postulated accident considered in the WASH-740 study assumed a source term that consisted of the instantaneous release of 50% of the noble gases (xenon and krypton), 50% of the halogens (mainly iodine), and 50% of the solid fission products from the reactor core. Little scientific information was available at the time, particularly about the transport of fission products from the reactor core to the containment, and then to the outside atmosphere. The

assumed release values were deliberately high to compensate for the limited state of knowledge that existed at this time.

In the early 1960s the concept of "maximum credible accident" was adopted by the nuclear regulatory agency as a means for establishing an upper bound for the consideration of potentially severe but very low probability accidents. This maximum credible case resulted in releases of fission products from the reactor core to the containment and then to the environment. A technical document, TID-14844, was used to estimate the source term for this hypothetical accident. The TID source term, as it was called, assumed that 100% of the inventory of noble gases, 25% of the iodine, and 1% of the fission products would escape the core region and reach the environment outside the plant. Again in this instance, the accident scenarios were not plant-specific, and the chemical and physical processes involved in fission product release were not analyzed.

The next milestone development in reactor safety analysis came in 1975 with the publication of the NRC's Reactor Safety Study (WASH-1400). WASH-400 was the first comprehensive attempt to use probabilistic techniques to estimate the likelihood and potential consequences of reactor accidents. Unlike its forerunners, WASH-1400 analyzed specific accident scenarios and modeled some of the physical processes involved in radiation release. However, where gaps existed in the data, large fission product releases were purposely assumed. Most affected by this approach were the source-term assumptions for the risk-dominant accident scenarios about which little was known. For those scenarios, the source-term values were essentially the same as those calculated 10 years earlier in the TID-14844 report. To that extent, source-term values have remained essentially unchanged and unexamined for nearly 20 years; they still contain the high values deliberately, but arbitrarily chosen as conservatisms to account for uncertainties in experimental data and computational methodology.

The extent to which source-term values may be overstated received little attention until recently because safety studies showed that the risk of severe reactor accidents was exceedingly small compared with other industrial accident risks, even when predicated on "conservative" source

terms. However, post-accident measurements inside the reactor containment building at Three-Mile Island revealed such a wide disparity between the predicted and actual effects of that accident that major R&D efforts were started.

The hypothesis underlying current source-term research is that earlier studies had ignored or underestimated certain natural processes--gravity, aerosol physics, chemical solubility and reactivity, physical plate-out and sorption--that would keep releases relatively low even if the reactor containment building failed. These factors, say researchers, are certain to come into play in varying degrees for all situations.

Current source-term research programs are designed to obtain a detailed understanding of specific fission product species that are released when reactor fuel is overheated or melted. Briefly, they include laboratory-scale tests of the effects of melting and other variables on fission product formation and the reaction of fission products with other substances, such as metal or water. They also include large-scale experiments to study the behavior of fission products as they are transported through a reactor's internal systems under accident conditions. Data from these experiments are then used to validate the predictive analytic methods used. The data and validated methodology help improve the models of the physical and chemical processes that, in turn, are used to estimate more realistic source terms.

The NYPA study of source terms takes advantage of the current state-of-the-art in the input values and analytic models selected for its investigation. The study findings represent a tangible step forward in determining the more realistic risks from potential reactor accidents and enchanced safety of nuclear power plant operation.

1.4 Accident Data

Past reactor accidents provide some insight and corroborating evidence that fission product releases are overestimated using current source-term analyses. The accident record, though limited, shows that the presence of water and steam in an accident environment play a key role in limiting the

release of fission products--especially iodine, the dominant contributor to the early fatality risk. In all LWR accidents and destructive tests to-date, no more than 0.5% of the available iodine has ever been released to the environment and only limited quantities of other fission products, e.g. cesium and tellurium, have been detected when water was present.

One such accident occurred in 1961 at the SL-1 reactor, a 3-megawatt prototype at the Idaho National Reactor Testing Station. The sudden removal of a control rod during a maintenance procedure led to a power excursion which resulted in substantial core melting and release of fission products from the fuel. Despite the fact that this prototype military reactor was housed in a vented sheet metal building, not a containment, less than 0.5% of the iodine in the core reached the outside of the building. And while 5-10% of the total fission product inventory escaped the reactor vessel, all but about 0.1% remained within the building.

More recently, and perhaps more representative of potential releases in commercial nuclear power plants today, was the TMI-2 accident in 1979 in Pennsylvania. The TMI accident was not the most severe type of accident postulated in reactor safety analyses; however it was one in which significant radioactive releases could be expected under current source-term analyses. In that partially mitigated loss-of-coolant accident involving substantial core damage, the actual release of radioiodine to the environment was only about 18 curies out of the 64 million curies of iodine that were released from the fuel. This was less than 1/100,000th of the amount that was predicted by the theoretical models and the conservative assumptions used at the time. The evidence also suggests that the water present absorbed the fission product compounds that posed the highest potential public health risks.

1.5 NYPA Study Scope

The accident sequences which form the basis of this investigation were identified as the risk-dominant scenarios in the detailed Probabilistic Safety Study (IPPSS) conducted on Indian Point 2 and 3 in 1982. The IPPSS study found that two slow containment overpressurization sequences, one

involving a pump seal LOCA and the other involving a transient event with failure of the off-site and on-site electric power and loss of the auxiliary feedwater system (TMBL) represented the most serious risks, as did an interfacing systems LOCA or "V" sequence. The "V" sequence was not investigated as part of this analytical source-term effort because technical assessment revealed that the sequence can be eliminated through plant modifications. Both overpressurization sequences were studied.

1.6 Selection of Analytical Software and Analytical Approach.
The computer code set for the source term study of both accident sequences consisted of MARCH 2.0, MERGE, CORSOR, TRAP-MELT, and MATADOR II, followed by the use of the CRAC-2 code to calculate accident consequences in terms of potential health effects.

The MARCH 2.0 code was used to perform the thermal-hydraulic calculations for each accident sequence, yielding core exit gas flow rates and temperatures, as well as core node temperatures.

MERGE, CORSOR, and TRAP-MELT were combined into a single computer code (the M-C-T code) to compute the primary system temperatures along the gas flow path, using the core exit gas flow rates and temperatures, until the first radionuclides were released. Then the M-C-T code used the core node temperatures calculated previously to determine the release rates for four fission product species: cesium iodide, cesium hydroxide, tellurium, and aerosol. These release rates were used next to calculate primary system retention from the time of first fission product releases through melt-through of the lower reactor head system and depressurization of the primary system.

After the release rates were determined, the M-C-T code calculated the amount of fission products retained in the primary system and the inventory released to the containment. At the same time, temperatures were calculated for each primary system structure based on the energy transfer from both the gas flow and fission product deposition, until lower reactor head melt-through.

The MATADOR II code used at that juncture simulated sudden depressurization of the primary system, whereby any undeposited fission products (whether in vapor form or condensed on particles) are transferred instantaneously to the containment. Fission product behavior in the containment is then analyzed for a 24-hour period, beginning with the lower reactor head melt-through, after which the containment is assumed to fail and release its airborne contents to the environment in a "puff".

Finally, the newly calculated source terms were used as the input to the CRAC-2 code to calculate consequences.

A number of analytical improvements were incorporated in the study design. The combination of MERGE, CORSOR, and TRAP-MELT into a single computer code, whereby MERGE and CORSOR became subroutines of TRAP-MELT enabled the investigators to simulate the dynamics of the accident sequences in greater detail. The M-C-T code improvements include modeling of fission product heating and energy depositions, energy losses for different types of insulation, and fission product resuspension. Fission product removal in the containment was modeled with a "bin" representation of the particle size distribution rather than a log-normal distribution. The physical phenomena were represented on a more time-consistent basis by structuring all codes to run on the same time scale. And finally, by modeling discrete core nodes and their behavior over time, a more accurate understanding of core temperature flux, gas flow and fission product release was possible.

Other key assumptions and input variables are presented in the full technical study.

1.7 Summary Discussion of Results

Table 1 shows the effect of various modeling additions and changes to the computer code on the final environmental release source term. Table 2 shows the distribution of the fission products in terms of the fraction of core inventory contained in the primary system, retained in the containment (both in the melt and as vapor), and released to the environment.

In the two accident sequences studied, the volatile fission products--cesium iodide, cesium hydroxide, and tellurium--are completely released during the meltdown process; their fraction remaining in the melt is zero. The tellurium fraction remaining in the primary system is very close to 1.0 for both accident sequences; this is a result of its high deposition velocity for chemisorpiton onto steel surfaces of the primary system.

The retention of the cesium iodide and cesium hydroxide by the primary system is quite different for the two accident sequences analyzed. In the pump seal LOCA sequence, with its higher gas flow rates between volumes, the vapor forms of the volatiles are carried from the hotter volumes of the system to cooler volumes where they condense onto either structures or aerosol particles, and subsequently settle. Accordingly, for this sequence the primary system retains a larger fraction of both cesium iodide and cesium hydroxide than it does in the TMLB sequence. In the TMLB sequence, gas flows between volumes at a lower rate, which causes revolatization of the condensed volatiles from structures heated by the fission products. The revolatized fission product species enter the gas stream but they remain in the hotter volumes for a longer period of time because of the lower gas flow rate. Less of the cesium iodide and cesium hydroxide are thereby retained in the primary system at the time that the lower reactor head is assumed to fail.

In both sequences, more cesium hydroxide is retained than cesium iodide. The cesium hydroxide has a higher deposition velocity for chemisorption onto stainless steel surfaces in the primary system than cesium iodide, so much so that the deposition velocity for cesium iodide chemisorption was assumed to be zero.

The containment retains a significant amount of the fission product species, between the time of their release from the primary system and the time of their assumed "puff" release from the containment. The volatile species, when released from the primary system as vapors, condense quickly onto the aerosol particles suspended in the containment atmosphere. In that form, they settle out of the containment atmosphere during the interval between failure of the primary system and containment failure.

Analyses show that virtually all of this settling out of fission products occurs during the first six-to-eight hours after the accident begins. Thereafter, the settling out process reaches an essentially asymptotic value which prevails until the time of containment failure.

Figures 1 through 4 show selected plots of the behavior of the fission products in the primary system and in containment for the TMLB and Pump Seal LOCA, respectively.

In this analysis of thermal response, it is important to note that the primary system for both accident sequences achieves an elevated pressure at the same time that the hot leg and/or surge line reach temperatures that threaten the integrity of the primary system. These temperature levels occur considerably sooner than failure of the lower reactor vessel-head. It is, therefore, highly likely that the primary system would fail in a manner different from what has been predicted to date by analyses which contain no treatment of fission product heating of structural materials. When fission product heating of structural materials is incorporated in the analysis, the primary system fails before the lower reactor vessel-head fails.

The effect of fission product heating and revolitization is shown in the second plot on Figures 1 and 3, according to the fission product heat deposited in the different volumes of the primary system. The effect is more noticeable in the Pump Seal LOCA sequence (Figure 3) where the gas flow rates between volumes is considerably higher, but it is nevertheless discernible in the TMLB sequence (Figure 1) with its lower flow rates. In both cases, the fission product heat in the upper plenum reaches a peak, then decreases. The peaking effect is caused by the revolitization of the volatile species and their transfer into the downstream volumes. This downstream movement is indicated by the sudden increase in fission product heat in those downstream volumes at the same time the upper plenum experiences a decrease in heat.

Fission product revolitization is also illustrated in the plots of retention factors in the different primary system volumes whereby the peaking and subsequent rapid decreases in retention factors mark the

revolitization process. For the specie tellurium, revolitization is considerably less significant than the chemisorption process. Tellurium's high deposition velocity for chemisorption onto stainless steel surfaces binds the tellurium on primary system surfaces even in the presence of the elevated temperatures calculated.

Figures 2 and 4 present the composite behavior of fission products in the containment. They show that the containment system removes the suspended fission products rapidly, within six to eight hours after accident initiation. Only a small fraction of the cesium and iodine species remain suspended in the atmosphere.

This results, combined with the non-dispersive melt-through of the lower reactor head--the primary system has already been depressurized by the hot-leg or the surge line failure--tends to remove some of the emphasis placed today on specifying the mode of a late containment failure. In other words, containment failure six to eight hours after the accident begins leads to similar consequences, all of which are small.

Table 3 shows that the fission product inventory calculated and available for release under these conditions is a factor of about 1000 lower than WASH-1400 source terms. The consequence analysis performed using the revised source terms shows that there are no early fatalities by virtue of the low amount of fission products released to the environment at containment failure and that latent fatalities are a factor of 1,000 smaller than those calculated with WASH-1400 source terms. Table 4 provides additional details.

1.8 Study Conclusions

1. The calculated source terms for two risk dominant accident scenarios at Indian Point 3 are a small fraction of the source terms calculated in two previous studies: the Indian Point Probabilistic Safety Study (IPPSS) and the WASH-1400 study.

2. Because the fission products suspended in the containment atmosphere are removed by natural processes within a period of

approximately six to eight hours from the beginning of the accident, the mode of late containment failure is not judged to be critical.

3. The analytical ability to estimate the time of containment failure within a margin of at least two to three hours raises questions about the need for further research into primary system retention of fission products. This is true for the Indian Point 3 nuclear power plant and most likely for all dry containment PWRs.

4. The fission products released from the primary system, and those aerosols released from the core-concrete interaction, are readily removed by natural processes occurring in the containment. Most important of these is particle agglomeration and gravitational settling. In addition, condensation of volatile species onto aerosol particle surfaces is a dominant means of volatile fission product removal from the containment atmosphere.

5. Iodine and cesium are the major contributors to the early and latent fatality risks, respectively. It was found that after six to eight hours their environmental release fractions are insensitive to the modeling of fission product heating, the type of insulation on the primary system, and whether or not log-normal or bin models were used to depict particle agglomeration. These modeling differences are of interest in calculating the location of fission product species early in the accident sequences. However, after a few hours, and long before the containment overpressurizes, low concentrations of iodine and cesium are found in the containment atmosphere for all models.

6. Fission product heating of structure surfaces in the primary system plays an important role in the primary system retention of fission products.

7. Fission product heating of structural surfaces in the primary system, especially in the hot-leg and surge line for the TMLB sequence, is the most probable cause of primary system failure and depressurization prior to lower reactor head failure.

TABLE 1

EFFECTS OF VARIOUS PHENOMENA ON
IODINE AND CESIUM RELEASE FRACTIONS (AT 24 HOURS)

PHENOMENON	IODINE RELEASE FRACTION	CESIUM RELEASE FRACTION
1) *With/Without Primary System Insulation	$2.0 \times 10^{-5}/2.04 \times 10^{-5}$	$1.6 \times 10^{-5}/1.73 \times 10^{-5}$
2)**With/Without Fission Product Heating	$4.5 \times 10^{-6}/4.9 \times 10^{-6}$	$3.1 \times 10^{-6}/3.4 \times 10^{-6}$
3)**Log-normal vs. "bin" particle modeling	$3.03 \times 10^{-5}/4.5 \times 10^{-6}$	$1.15 \times 10^{-5}/3.4 \times 10^{-6}$
4) *With/Without Core Concrete aerosol	$2.0 \times 10^{-5}/2.3 \times 10^{-5}$	$1.6 \times 10^{-5}/1.84 \times 10^{-5}$

* For TMLB case only

** For Pump Seal LOCA case only

TABLE 2

DISTRIBUTION OF FISSION PRODUCTS, FRACTION OF CORE INVENTORY

TMLB

	CsI	CsOH	Te	Ba	Ru	La
Primary System	.22	.32	.9999	.18	4.3×10^{-2}	3.4×10^{-5}
Containment (failure 24/hrs-puff release)	.78	.68	1.0×10^{-4}	.13	1.8×10^{-3}	1.6×10^{-3}
Remaining in Melt	0	0	0	.69	.9549	.9984
Released to Environment	1.9×10^{-5}	1.7×10^{-5}	6.5×10^{-9}	3.1×10^{-6}	1.5×10^{-6}	5.4×10^{-6}

Pump Seal LOCA

	CsI	CsOH	Te	Ba	Ru	La
Primary System	.67	.80	.998	.26	6.3×10^{-2}	5.1×10^{-5}
Containment (failure 24/hrs-puff release	.33	.20	2.0×10^{-4}	.16	9.9×10^{-3}	1.6×10^{-3}
Remaining in Melt	0	0	0	.58	.9266	.9984
Released to Environment	4.2×10^{-6}	2.7×10^{-6}	3.3×10^{-9}	2.4×10^{-9}	7.7×10^{-7}	2.5×10^{-6}

TABLE 3

FRACTION OF CORE INVENTORY AVAILABLE FOR RELEASE

F.P. SPECIES	FRACTION OF INVENTORY		WASH-1400*
	TMLB EVENT	PUMP SEAL LOCA	SOURCE TERMS
Iodine	2.0×10^{-5}	4.5×10^{-6}	0.7
Cesium	1.6×10^{-5}	3.1×10^{-6}	0.5
Tellurium	6.5×10^{-9}	3.3×10^{-9}	0.3
Barium/Strontium	3.1×10^{-6}	2.4×10^{-6}	0.06
Ruthenium	1.5×10^{-6}	7.7×10^{-7}	2.0×10^{-2}
Lanthanum	5.4×10^{-6}	2.5×10^{-6}	4.0×10^{-3}
Noble Gases	0.90	0.90	0.90

* Source terms for Pump Seal Loca were not explicitly developed in WASH-1400.

TABLE 4

CRAC-2 Results with NYPA Source Terms*

and WASH-1400 Source Terms**

	Conditional Probability NYPA Source Terms		Conditional Probability WASH-1400 Source Terms	
No. of People Affected	Early Fatalities	Latent Fatalities	Early Fatalities	Latent Fatalities
1	0	0.991	.998	1.0
2	0	0.763	.995	.999
5	0	0.339	.994	.999
10	0	1.6×10^{-1}	.986	.999
20	0	6.4×10^{-2}	.979	.996
50	0	9.6×10^{-3}	.958	.982
100	0	0	.929	.976
200	0	0	.784	.957

*TMLB Accident Sequence
**PWR - 2 Release Category

2.0 SELECTION OF ANALYTICAL SOFTWARE*

The selection of analytical software for evaluating a matter as complex and dynamic as accident source terms is an extremely important task in that the validity of the results is highly dependent on the acceptability of the computer codes employed. Perhaps the most critical factor in the code selection process is validation of the codes with respect to experimental evidence. Furthermore, in order to validly interpret the results from these analyses, it is important to determine the sensitivity of these results to the input parameters.

With these considerations in mind, the TRAP-MELT computer code, developed under the auspices of the U.S. Nuclear Regulatory Commission (USNRC) was selected for this study. TRAP-MELT and its companion codes, MERGE and CORSOR, are presently being used in conjunction with the BMI-2104 work-in-progress, under USNRC auspices. The development of these codes spans a period of several years during which time there have been numerous iterations between experiemental data and analytical models.

The codes are essentially a combination of empirical formulations and mechanistic representation of physical phenomena involved in fission product behavior. Wherever experimental data is insufficient to perperly define a phenomenon, bounding assumptions have been made. Thus the shortcomings of the codes described in subsequent sections, tend to yield conservative resutlts. In some instances, due to developmental resource contraints, analytical simplifications of behavioral models in the codes were used. These simplifications, however, were judged to have no significant impact on the conclusion of this study.

Another important reason for the selection of the TRAP-MELT, MERGE and CORSOR codes was the extensive effort presently underway to validate these codes. From reviews of the literature on the subject, it is evident that

---

* The majority of the information contained in this section is extracted from material presented during the peer review process for BMI-2104 and contained in ORNL/TM-8842, Draft.

these validation efforts will help refine the models in order to better represent the phenomena and thereby reduce the conservatism implicit in the current versions. It is not believed likely that discovery of new phenomena or major errors in modeling of known phenomena will result from these efforts.

Significant efforts are being expended at Oak Ridge National Laboratory to document all code validation efforts. In addition, Sandia National Laboratories has performed a detailed study of sensitivities and uncertainties inherent in the suite of codes selected for this analysis. The work described in subsequent sections of this report takes full advantage of these efforts, as well as other code validation experiements planned in the near future.

The TRAP-MELT, MERGE and CORSOR codes were written in a manner that made their combinatin into a single code possible. This removed a major shortcoming found in separate use of the codes, namely that they did not represent the effect of fission product heating on the primary system retention. By combining the codes, the fission product removal mechanisms and accompanying thermal-hydraulic processes could be properly coupled.

The remainder of this section describes the status of various code validation efforts. Essentially, these efforts fall into three categories. The first deals with the release rates of the fission products and inert aerosols from the core region during the core melting. The second deals with further definition of the chemistry of fission product behavior in the primary system, while the third category deals with the behavior of aerosols in both the primary system and the containment.

2.1 MERGE Validation

Los Alamos National Laboratory is studying the upper plenum flow behavior using a multi-dimensional computer code. The Los Alamos work is intended to validate MERGE results analytically. Overall, MERGE is accepted widely as the state-of-the-art for heat transfer calculations. No further efforts are currently planned for its validation.

2.2 CORSOR Validation

CORSOR is based on the fission product and structural material release model used in the technical basis report, NUREG-0772 [1] and in the emergency planning analysis report, ORNL/TM-8275 [2]. CORSOR was selected for this study for its ease of application and apparently successful use in three similar accident analyses which employed the code and its basic release models.

2.2.1 Comparison of CORSOR with Other Core Source Term Models

For most severe accidents the core source term can be defined as the amount of material carried past the top of the fuel rod plenums. All materials, radioactive and nonradioactive, should be accounted for, and the physical and chemical forms of the transported materials should be specified. For purposes of this discussion, the process can be divided into three steps: (1) initial transport of material into the flowing steam-hydrogen atmosphere, (2) proportionation into vapor and solid aerosol particles, and (3) deposition of vapor and solid particles in the cooler upper regions of the core. A comparison of the characteristics of the CORSOR code with other core source term models using either fractional release rate or vapor saturation is given in Table 2.1.

SASCHA. [4-7] The SASCHA code uses fundamentally the same fission product/fuel/structural material release model as CORSOR. Most of the CORSOR release rate coefficients are strongly influenced by SASCHA results. Accident analyses performed by KfK do not reflect any adjustment of experimental release rates for scale-up or geometry changes as the core melts, wherein the presumed melting temperature for the fuel and structural material (corium) combination is 2400° C.

CORE MELT. [8-9] The core melt experimental apparatus at ORNL is similar to SASCHA in that simulants are used in miniature unirradiated fuel rods to determine fission product behavior. The cluster of rods is heated inductively in steam, and the effects of stainless steel and control rod alloys are explored. The mass of material in a test is 4 to 5 times that of SASCHA. Full-scale core releases are calculated by using the same

total fraction of a species released in the core melt tests. The chemical atmosphere toward the center of the cluster is reducing as evidenced by low Te and Ru releases and high Ba and Sr releases.

FISREL [10] This British model also uses fractional release rates as the basis for fission product release. Details of selection of the release rate coefficients are presented in ND-R-610(S) [11]. However, the release of structural materials is treated as a vaporization process and not as fractional release. In the Cambridge paper [10], the vapor pressures of the major components of Inconel (grid spaces) were calculated using Raoult's law and then four different mass transfer models were used to calculate the vaporization and deposition behavior in the upper cooler portions of the core. Calculated releases were much lower for these materials than found in Appendix B of NUREG-0772 [1]. FISREL uses MARCH for all time-temperature behavior.

IDCOR. An IDCOR-sponsored accident analysis [12] uses the Steam Oxidation Model [12] for calculating fission product release from the fuel matrix. Time, temperature, gas composition and flow rate are determined by the PWR Heat-up Code. [13] The Steam Oxidation Model for fission product release is based on grain growth observations (grain boundary sweeping as the grains grow) for UO_2 sintered in steam. The fractional fission product release rates initially are higher than CORSOR rates but decrease with time at fixed temperatures as a result of decreasing grain growth. For example, at 2 min and 1800°C, the Steam Oxidation release rate for volatile fission products is 5 times that in NUREG-0772.

For fission products such as Ba, Sr, and Ru, it is assumed that there is sufficient transport to the fuel surface that gas flowing by the fuel is saturated with vapor according to pressures calculated with the SOLGASMIX-PV [14] program. The SOLGASMIX-PV computer code calculates the species and partial pressures of all the released fission products. The potential for condensation in the cooler upper core regions is accounted for, but the extent of formation of aerosol particulates, the deposition of particles, and the condensation of vapors were not included in the Cambridge paper. [12]

As in FISREL, structural materials are released according to their calculated vapor pressures and gas flow rates. More than one chemical species of an element is included if present in significant quantity. Saturation is assumed to occur in the hottest core nodes.

FASTGRASS. FASTGRASS [15] is a mechanistic code that includes all of the important release mechanisms working simultaneously. Derived primarily for fission gas release, it has been expanded to include iodine and cesium releases.

ANL-VFP [16] The ANL volatile fission produce release model calculates release behavior according to the chemistry of the fission products in the UO_2 matrix. Iodine, cesium, and molybdenum releases have been calculated. Their relative release rates are compared with the fission gases. Absolute release rates are obtained by assuming that the fission gases escape as in NUREG-0772 [1].

ANS-5.4 [17] This empirical model uses Booth-Rymer-Beck equations for diffusional releases from equivalent spheres. This is the only model that calculates separately the releases of radioactive isotopes with short half-lives. The data base for this code was derived from fission gas release, but the diffusion coefficients were modified to include iodine, cesium, and tellurium releases.

The fractional release rate model is used by CORSOR, NUREG-0772, and SASCHA for calculating the release of all core materials. A danger of applying the fractional release rate model to structural materials is that with low gas flow rates, for example, saturation of the gas might be exceeded. Similarly, with high gas flow rates evaporation might be under-estimated. In FISREL the vapor saturation model was used for structural materials transport, but mass transfer coefficients were used both for evaporation and later condensation in the cooler upper positions of the core. FISREL found much less material leaving the core, compared with the same scenario calculated with NUREG-0772 fractional release rates.

The vapor saturation model was used to calculate structural material release in the Browns Ferry SASA study [18] of a station blackout

accident. Excluding fission products, the model predicted the vaporization of only 13.3 kg of the components of stainless steel, Zircaloy-2, and UO_2. It is quite likely, however, that the release of highly volatile components, especially if present in small quantities, can be handled better with the fractional release rate model. Examples are Mn, Sn (cladding) and Cd, although for a molten source this should not be true.

Very little experimental data are available to compare the two models, fractional release rate or vapor saturation. SASCHA data were reviewed as part of the Browns Ferry SASA study [18, 20]. It was found that the flowing gas did not saturate with any of the melt species, probably as a result of poor contact between gas flowing above the crucible and the melt species. The data support the concept of a natural convection region existing between the melt and the flowing gas, with saturation occurring only in the boundary layer above the melt. Structural materials have not yet been added to the HI fission product release tests at ORNL [21-24].

2.2.2 Comparison of CORSOR and Recent Experimental Fractional Release Rate Coefficients

A series of figures follows in which the current CORSOR release rate coefficients are compared with pertinent experiment results. Most of the test results shown are from SASCHA simulant fuel tests or the HI series of tests in which high burnup commercial fuel was used. Note that much of the NUREG-0772 data base is not used, either because it applied to non-accident environments (inert atmospheres), or because it used very small fuel samples with only trace irradiation.

Several release rate coefficients were usually extracted from each SASCHA test since total element release was available as a function of both time and temperature. For the HI series tests, the release rate coefficient was calculated using total element release, including amounts released during heatup and cooldown, but the time period used in the calculation excluded the time involved in heatup and cooldown.

Tables 2.2A and 2.2B summarize the different operating conditions for the various ORNL tests. One of the problems encountered with any fission

product release correlation is the restriction provided by the cladding. CORSOR (and NUREG-0772) release rates are releases from fuel and cladding. At temperatures below 1400°C, before oxidation results in cladding fragmentation, the fuel rod can be expected to have only one opening. Differences in the initial gap inventory of tests HBU-11 and BWR-3 [25, 26] account for the deviations from the CORSOR correlation line. It appears that the data from short duration tests produce high release rates as calculated by the fractional release rate method.

All of the figures include a dashed line representing a recommended change for CORSOR which have not yet been adopted. Points marked "relative volatility study" [18, 20] are the average of many different types of fission product release tests but are most heavily influenced by the older SASCHA tests performed in both steam and air.

Xenon and Krypton release. Fission gas releases at high temperatures have been observed to be similar to those of cesium and iodine [18, 20, 25]. It is therefore recommended that the same release rate coefficients be used for Xe, Kr, Cs, and I. An important difference is that the fission gases accumulate in the plenum and open void spaces of a fuel rod during normal operation of the reactor and are released from the rod at the time of rupture. This burst release is included in CORSOR.

Cesium and iodine release. The release rates for cesium and iodine calculated from fission product release tests performed at ORNL [21-27] are shown in Figure 2.1. With each pair of release rates, the number of minutes of test duration is also indicated.

Cesium and iodine release rates for SASCHA tests performed in steam are shown in Figure 2.2 [3 - 7]. The simulant pellets containing iodine and cesium prepared for SASCHA contain the simulants in relatively open voids of the pressed but unsintered UO_2 pellets. It is reasonable to expect rapid release compared with real fission products formed within the pellet grains.

Results from the PBF severe core damage scoping test differ from those from the results of the ORNL HI series tests. Data from PBF steam grab

samples indicate that the cesium and iodine fractional release rates were approximately a factor of 100 lower than CORSOR rates in the 1730-2080°C range [28]. Cesium and iodine that had plated out on surfaces between the fuel assembly and sample collection point would not have been measured by the steam samples.

A very large release or flush-out of cesium and iodine occurred during quenching and reflooding of the PBF test core. A model for this phenomenon should be included for any accident in which it is important; however, in all but exceptional cases, cesium and iodine dissolved in the reflood water are likely to remain there and not escape into the containment atmosphere or escape outside of containment. Accident analysts certainly need to be aware of this important release mechanism, but inclusion of it is not expected to affect release from the containment building. Accordingly, CORSOR does not include a reflood model.

Tellurium release. The release of tellurium in steam tests is shown in Figure 2.3. CORSOR now uses the two-stage tellurium model presented at the Cambridge meeting [29]. The model assumes retention of most of the tellurium by the Zircaloy cladding until the cladding becomes nearly completely oxidized. Then the tellurium release rate increases to the same rates used for Xe, Kr, I, and Cs.

Release of fission product and control rod silver. SASCHA release rates for silver are shown in Figure 2.4. The releases for both types of simulant silver are similar. The release rate of control rod silver decreases with time, possibly due to of gradual dilution by or alloying with other materials in the core mockup.

Antimony release. The release of fission product antimony is shown in Figure 2.5. The agreement of SASCHA test data with CORSOR is good. Results of the HI series tests (ORNL) suggest lower releases, but the ^{125}Sb activity used to monitor antimony release is too low in these tests to assure complete analyses [21 - 24]. Data for SASCHA tests performed in air, as shown in Figure 2.6, indicate somewhat lower release rates for antimony.

Barium release. SASCHA release rates for barium are shown in Figure 2.7. Release rates are much higher in the presence of a reducing atmosphere than in a steam atmosphere. Therefore, a significant release rate change for Ba is recommended for CORSOR, although it has not yet been incorporated in the code.

Molybdenum release. Molybdenum volatility is also strongly affected by the oxidation potential of the gas flowing over the SASCHA melt. A significant reduction in the CORSOR release rate is recommended, as shown in Figure 2.8.

Ruthenium, zirconium, and UO_2 release. From the relatively little information about ruthenium and zirconium, and UO_2 release tests, as shown in Figure 2.9, reduction in the CORSOR release rates is recommended. No significant change in fission product zirconium is suggested. UO_2 release should be treated as a vaporization process allowing for reductions of the exposed surface area before gross failure of the cladding occurs.

Release of structural materials. SASCHA release rates for various structural and control rod materials are shown in Figure 2.10. These materials should also be treated by the vapor pressure method; however fractional release rates can be used in the interim until the mechanics of vaporization are worked into the CORSOR model.

2.2.3 CORSOR Validation Needs

Fission Product Release Data Needs

The release rates for fission gas, cesium, and iodine are more accurate than for other fission products since more data are available. Their high release rates usually result in 90% release from the core during meltdown type accidents. Refinement would probably not change the total release significantly.

Release data for fission products Te, Sb, Ba, Sr, Mo, and Ru are especially needed. All of these exhibit sensitivity to the oxygen

potential of the environment or to the oxidation of the Zircaloy cladding. These effects need to be considered in planning and conducting the tests.

Structural Material Release Data Needs

More structural material, fuel rod, and control rod release data are needed. At present SASCHA is the only data source available. PBF [28] and HI series tests [21 - 24] have yet to include either structure or control rod materials. Data are also unavailable for B_4C in a complete accident environment.

Fission Product Release Model Improvements

The fractional rate release model could be improved by decreasing the release rate with time at a given temperature. This would not affect those accidents in which the temperature changes continuously.

Inclusion of a liquefaction release expression should also be considered. The ORNL HI tests with high burnup fuel do not show enhanced release when clad melting occurs. The PBF severe damage scoping test with low burnup fuel did show an increased release at the time of clad melting [28, 29]. More information would be helpful.

A quench release model is needed for those accidents in which rapid cooling occurs. Both the PBF severe damage scoping test and the TMI-2 accident indicated a large quenching release when cold water came in contact the hot fuel.

A leach release model should be included for those accidents in which water eventually circulates through the overheated core. TMI-2 should provide much information about this mechanism.

Structural Release Model Improvements

Experimental verification of the vaporization model is lacking. The vaporization release model applies only to accidents with positive upward flow of steam and hydrogen. Some variation must be developed for those accidents in which steam flow is very low or in which core leakage occurs

at the bottom (the Brown Ferry scram discharge volume leak accident, for example) [30, 31].

Further study of species partial pressures, mass transfer efficiency, vapor-to-solids partitioning, and the effect of melting and other geometry changes is needed.

2.2.4 Experiments Underway or Planned

HI-series tests at ORNL continue in the temperature range 1700-2000°C with plans to reach 2400°C. Discussions are in progress to alter the original work plan to permit earlier testing with stainless steel clad silver alloy and other structure-type materials. None have been included in tests to-date. Increasing effort is being made to obtain more complete information regarding Te, Sb, Ba, Sr, Mo, Ru, UO_2, and PuO_2 releases. SASCHA simulant pellets will be used in some future tests.

Core-melt tests continue at ORNL. Additional analyses are required before the release data can be converted to temperature dependent release rates.

The PBF severe fuel damage tests are in progress. They are much larger scale tests than any other and are very realistic regarding inclusion of core materials such as grid spacers and control rods.

The KfK SASCHA tests are now devoted to the effect of corium-concrete reactions on fission product release. No further corium-only tests are planned.

2.2.5 CORSOR Validation Discussion Summary

1. The fractional rate release model used in CORSOR appears satisfactory for the calculation of fission product release from fuel and cladding.
2. Significant reductions in release rates for fission products Ba, Sr, Mo, and Ru are recommended. Minor changes are suggested for other fission products in order to achieve a uniform mathematical format.
3. Partition of the released fission products into 60% aerosol solids and 40% vapor, plus simple provisions for particle deposition and vapor condensation in the cool portions of the core, have been adopted for the NYPA study.

4. A vaporization model for structural materials (stainless steel and Inconel), fuel rod cladding and UO_2, and control rod silver alloy is proposed. A method of accounting for the effects of exposed surface area, degree of saturation, phase changes, partitioning between aerosol particles and vapor fractions, deposition of particles and condensation of vapor in the cool upper portions of the core is suggested. Fraction release rates of these materials are recommended for use until the vaporization model can be implemented.
5. Review of the state-of-the-art indicates that additional data are needed for the release of fission products, Te, Sb, Ba, Sr, Mo, and Ru. The release rates for these species are sensitive to the composition of the atmosphere and/or to oxidation of the Zircaloy cladding.
6. The vaporization release of structural material components is not verifiable until these materials are included in more realistic experiments in the future.

2.3 TRAP-MELT Validation Discussion Summary

In the NYPA study, the most important processes in determining the vapor and aerosol retention in the RCS for various accident sequences include:

- vapor condensation/evaporation onto aerosols and wall surfaces
- vapor sorption onto aerosols and wall surfaces
- aerosol agglomeration
- aerosol deposition by settling
- aerosol deposition by thermophoresis
- turbulent deposition of aerosols (in V Sequence)

The TRAP-MELT code models the transport, deposition, and interactions of vapors and aerosols as they flow through the RCS for various accident sequences relevant to PWRs and BWRs.

The known validation experiments for TRAP-MELT are less comprehensive than that entire set of phenomena at scales and conditions utilized in the NYPA study. There have been experiments in which a number of the aerosol processes -- agglomeration, gravitational settling, thermophoresis, and diffusive plateout -- have occurred simultaneously. However, even these

do not reflect the high aerosol concentrations or the directed flow patterns projected for this study.

2.3.1 TRAP-MELT Validation Needs

The additional validation needs for TRAP-MELT are judged to be as follows:

1. Integral experiments with characteristic sources -- species, mixtures, and quantities (high aerosol number densities).
2. Large-scale experiments to evaluate aerosol and vapor transport under conditions where 3-D effects in the upper plenum are present.
3. Small-scale experiments to provide additional information on fission product species interactions with surfaces -- involving deposition velocity and chemical transformation measurements -- over a broad range of temperatures.
4. Small-scale experiments under upper plenum conditions to evaluate:
   - aerosol plateout/settling in a flowing system
   - conditions needed for aerosol resuspension
   - potential for fission product vapor sorption on aerosols (adsorption isotherms and kinetics).

2.3.2 TRAP-MELT Experiments

Major experiments are underway or planned to help validate TRAP-MELT. Only those programs that are either partially funded or are under consideration by the NRC are discussed here.

Power Burst Facility (PBF) Severe Fuel Damage (SFD)

The PBF SFD Phase-2 experiments are contemplated as an international cooperative effort, sponsored by the NRC, at the Idaho National Engineering Laboratory (INEL). The objectives of the Phase-2 experiments include:

1. Performing realistic integral tests to define the chemical compositions and amounts of materials that evolve from fuel under postulated LWR core-melt accident conditions;
2. Performing experiments related to vapor and aerosol transport through the upper plenum in LWR core-melt accidents, and to obtain sufficient transport, deposition, and thermal-hydraulic data from these tests that the test results can be compared with predictions from TRAP-MELT calculations.

Assuming that the experiments are performed as planned, in-pile and under conditions directly simulating those expected for key LWR accident sequences, they could have the following value:

1. Because the tests would be done with real fuel in the appropriate thermo-physical environment, the release rates of fission products and structural/control rod materials from the fuel bundle should be similar to real accident behavior.
2. Since the release of vapors and aerosols from the fuel bundle would closely approximate the reactor environment and the timing of the accident, the chemical and physical interactions occurring between materials as they move through the upper plenum and deposit onto surfaces would more closely resemble those that would occur in core-melt accidents. Determination of the amounts and chemical forms of materials deposited onto surfaces and transported through the upper plenum would provide direct data for comparison with TRAP-MELT code predictions.

Although alternatives to the PBF proposal are being considered, the test train proposed by INEL would be inserted into a pressure housing so that the high pressures needed for some experiments -- up to 2500 psia -- can be produced. The fuel assembly for the tests would consist of 28 fuel rods and four control rods mounted in a 6 x 6 array (12.6 mm pitch) without the corner rods included. The proposed fuel rods are roughly one meter long and would be pre-irradiated to a burnup of about 35,000 MWd/t, typical of PWR power levels. Short-time preconditioning at power in the PBF would allow the inventory of short-lived isotopes to be re-built. The control rod material proposed to be used for PWR-type tests would be an Ag-In-Cd mixture. The fuel would be contained in a zircaloy-lined thoria crucible.

The somewhat simplified upper plenum section for the proposed PBF SFD Phase-2 tests would simulate as much as possible the surface-to-volume (S/V) ratio of the structure components above the reactor core in a PWR plenum. A fairly good simulation of the S/V ratios of the reactor plenum end box, grid, and flange can be made, but the S/V ratio for the proposed simulated upper plenum region is higher than the S/V ratio expected in the upper plenum in a real PWR.

The following measurement equipment are proposed to be located in the plenum region of the experiment:

1. A video probe to measure the surface temperature of the fuel bundle as a function of time;
2. A continuous vapor/aerosol sampler to collect samples of materials released from the fuel bundle and rapidly transport those samples to a collection media located outside of the test rain housing. This sampler would determine the quantities and chemical forms of materials released from the bundle as a function of time, and measure the size distribution of the aerosols produced;
3. An upper-plenum deposition system consisting of discrete and integrated deposition samples. These samples would be removed after the test and analyzed for the amounts and chemical forms of materials deposited in the upper plenum region of the test train.

The proposed Phase-2 measurement system for sampling inside the test train complements the measurement system for sampling the materials that are transported out of the test train used in Phase-1 experiments.

The proposed test matrix for the PBF SFD Phase-2 tests consists of two experiments involving PWR simulations of the expected TMLB and V sequence accident conditions. If funding is available, two additional tests would simulate the PWR S_2D sequence and a BWR sequence -- either a TC or a TW sequence. The first experiment is currently scheduled to be performed in April 1985, the second experiment in October 1985, and any additional tests in 1986.

Marviken Aerosol Transport Tests

The Marviken Aerosol Transport Test (ATT) Project is an internationally-funded effort supported by the NRC, EPRI, Sweden, and a number of other foreign countries. The primary objective of the project is (16) "to create a data base on overheated core materials within typical LWR primary systems for risk-dominant scenarios." A secondary objective is "to provide a large scale demonstration of the behavior of aerosols in primary systems."

The important characteristics of the proposed experiments, relative to TRAP-MELT validation, are:

1. They are essentially full-scale experiments. At this scale, it should be possible to produce the expected interactions between forced flow and natural convection flow.
2. The complex geometries of the PWR and BWR upper plenums will be simulated.
3. The tests will be performed at high aerosol concentrations with aerosols that simulate those expected to be released from the core. Interactions between structural aerosols and fission product vapors that might absorb or condense onto them should occur.

The experiments will be performed at the Marviken test facility in Sweden. The basic arrangement of the components of the ATT test facility include a reactor vessel tank, a vapor/aerosol generator, a pressurizer, a relief tank, and associated piping. The reactor vessel is a tank of 164 m^3 internal volume. Internals to the reactor vessel will be interchangeable to simulate the upper plenum structures of both PWRs and BWRs. A full-scale pressurizer and relief tank are the other two large tanks in the system. Vapor and aerosol characteristics and transport behavior in each of the three volumes will be measured in the tests.

Materials will be vaporized using either a group of small plasma arc heaters or one large plasma arc heater; total power input required for these devices will likely range from 3-5 MW. The materials to be vaporized are grouped into so-called "fissium" and "corium" mixtures. The fissium mixture will consist of simulants for volatile fission products primarily the iodine, cesium, and tellurium groups; present plants call for vaporizing up to 100 kg of this mixture. The corium mixture consists of structural and control rod type materials -- including things like Fe, Cr, Ag, and Cd metals; present plans call for vaporizing up to 455 kg of this mixture.

The proposed test matrix consists of one shakedown test for flow calibration, followed by six experiments on a range of transients possible in PWR and BWR severe accidents. The first three tests will be fissium-only tests; the first two by direct injection of fissium into the pressurizer, and the third by vaporizing fissium, then injecting it into

the reactor vessel. Tests 4 through 6 will simultaneously vaporize both fissium and corium mixtures in the reactor vessel. In terms of accident sequences, tests 3 and 5 will simulate both V and AD sequences; test 4 will simulate the TMLB sequence; and test 6 will simulate a BWR intermediate LOCA sequence. These six planned experiments were to be completed in October 1984.

Sandia High Temperature Fission Product Chemistry and Transport Experiments

This NRC-funded program at Sandia's Fission Product Reaction Facility has the following overall objectives:

1. To define the theromadynamic data and chemical reaction characteristics of the fission products of interest;
2. To examine the chemistry and transport of fission products in typical steam and hydrogen environments; and
3. To compare the observed behavior of the fission products with predictions made by purely thermodynamic calculations.

These experiments are important to TRAP-MELT validation for two reasons. First, the values of fission product vapor deposition velocities used in TRAP-MELT are obtained from the results of these experiments. Second, results from these tests will provide data on the relative importance of the various chemical reactions that could occur within the RCS; this data will determine the important reactions and reaction products that should be modeled within TRAP-MELT.

Three different types of experiments are performed in the Sandia test program. The first series studies the chemistry resulting from the reaction of single and multiple fission product species with structural materials in a steam/hydrogen environment at temperatures up to 1100°C. (The Sandia facility provides reaction residence times from seconds to as long as several hours to allow chemical and physical reactions to occur among the materials.) A second set of experiments utilizes a microbalance set-up; these tests are done largely to study the kinetics of vapor-wall reactions. A third type of experiment uses a transpiration apparatus; these experiments are performed to study vapor-vapor reactions (although some vapor-wall reactions have also been studied.)

Some of the material reactions studied in the Sandia tests performed to date include:

1. TELLURIUM with: 304 Stainless Steel; Oxidized 304 Stainless Steel; Inconel 600; Oxidized Inconel 600; Silver; Zircaloy; and Tin.
2. CESIUM HYDROXIDE, CESIUM IODIDE with: 304 Stainless Steel; Inconel; Silver; and Boron Carbide.
3. BORON CARBIDE with: Steam/Hydrogen; CsOH/Steam/Hydrogen; and CsI/Steam/Hydrogen.
4. MISCELLANEOUS REACTIONS: CsOH with HI or I; and CsI with O_2.

The experiments of most immediate application to TRAP-MELT validation are those where estimates of deposition velocities are made for Te and CsOH.

ORNL TRAP-MELT Validation Tests

The ORNL TRAP-MELT Validation Test Program, which is funded by the NRC, was initiated in April 1982. The overall objective of this project is to perform small-scale experiments related to deposition and transport of aerosols and fission products in the reactor primary vessel under simulated LWR core-melt accident conditions. The test results will provide part of the data base for validation of the models in TRAP-MELT. Because they are small-scale, simple geometry tests, results from the tests should be somewhat easier to interpret than those from experiments performed in more complex geometries or performed in-pile. Comparisons of measured results should be quite instructive, especially in understanding the results from the more complex PBF and Marviken experiments.

The experiments to be performed in this program are all related to aerosol deposition and transport in the LWR primary vessel. They include three different types of tests:

1. Aerosol Transport

These tests are to investigate aerosol deposition and transport under upper plenum conditions for a range of possible core-melt accident conditions. Test results will largely be used to validate the models for aerosol agglomeration, thermophoretic deposition, and settling for upper plenum flow conditions. In the experiments, aerosols will be

generated in a 10-inch diameter, 9-feet long vertical pipe using a plasma torch aerosol generator. Measurements will be made of pipe wall thermal gradients, aerosol plateout and settling in the pipe, aerosol leakage out of the pipe, and the aerosol mass concentration in the pipe. Ten aerosol transport tests are planned; test parameters include aerosol residence times in the pipe (10 to 100 s), aerosol material (zinc or iron oxide), pipe wall temperatures (varying the wall thermal gradients), and gas type flowing through the pipe (argon or argon plus superheated steam). Later tests may add internal surface area for settling and impaction.

2. Aerosol Resuspension Tests

These tests are to investigate aerosol resuspension phenomena that might occur in the reactor pressure vessel under core-melt accident conditions. These experimental results will be used as a basis for developing a resuspension correlation missing at the present time in TRAP-MELT. In the experiments, aerosols will be generated with a plasma torch and deposited onto collection foils; the mass of aerosols resuspended from the collection foils, as a function of flow conditions (Reynold's numbers) past the foil surface, will be measured. Under test condition, air flows of up to 200 SCFM through a 3-inch diameter pipe can be attained; this is equivalent to maximum plug flow velocities of 21 m/s, or maximum Reynold's numbers of 60,000, through the pipe. Eight aerosol resuspension experiments are planned. Parameters varied in the experiments include deposited aerosol material (zinc or iron oxide), amount of aerosol deposited onto collection foils (calculations indicate that these loadings could be in the range of 0.01 to 0.1 g/cm^2 for accident conditions), and flow gas (argon or argon plus steam).

3. Fission Product Transport Tests

These tests are to investigate the reactor vessel transport of fission product species liberated under a range of core-melt accident conditions. They differ from the aerosol transport tests in that a mixture of materials will be liberated from a simulated fuel bundle. The core-melt aerosols and fission-product species will be generated using a core-melt induction furnace heating technique developed in the NRC Aerosol Release and Transport Program (17). Using the furnace, 1-kg of simulated fuel

bundles will be heated to temperatures in the range of 2400° C, and the aerosols and vapors produced will move through and deposit in a small-scale upper-plenum simulator located above the bundle. Measurements of the amounts and types of materials deposited in the simulator and transported out will be made. Six fission product transport tests are planned. Parameters to be varied include the fuel bundle composition (PWR or BWR material mixes), initial upper plenum structure temperatures, and flow residence times.

The present project schedule calls for all 24 experiments to be completed by May 1985.

Fission Product Interaction with Aerosols Tests ORNL

The ORNL Fission Product Interaction With Aerosols Program, funded by the NRC in April 1983, is "to provide experimental data on the rates of adsorption (combustion/evaporation) onto aerosol/wall surfaces for key fission products." A secondary objective is to provide sorption capacity with respect to the competition between structural surfaces and aerosol surfaces for the sorption of fission product vapors. They are the first experiments to use the key aerosol and fission product vapor materials that could be released from the core in core-melt accidents. The exit sample will be analyzed to determine the quantity of aerosol, the quantity of vapor associated with the aerosol, and the free vapor concentration. In addition, the flow tube can be surveyed at the end of the experiment to determine the amount of aerosol and vapor deposited in it. Test results, then, will provide data on the quantity of vapor sorped on a suspended aerosol for a specified time of mixing plus the relative sorption on the tube wall.

The aerosol generator will be based on a commercial plasma spray system. Selection of aerosol materials, temperatures, times of mixing, and concentrations will depend on the results from the static tests. Each aerosol will be first tested with CsOH and CsI vapors; the system will then be modified for tests with Te vapor.

The present schedule calls for the static tests to end in August 1985, and for the dynamic tests to end in November 1985.

2.3.3 TRAP-MELT Validation Discussion Summary

1. The purely aerosol models used in TRAP-MELT have a good level of validation based on single-component aerosol tests performed under well-mixed aerosol conditions. These models have not yet been compared with experiments performed under conditions where mixtures of aerosols are generated at high concentrations, and under the thermal-hydraulic conditions associated with the reactor vessel upper-plenum. Experiments of this type are planned.
2. The values for "deposition velocities" used in TRAP-MELT to calculate vapor sorption onto surfaces need a more complete data base (tests done over a range of temperatures) for CsI, CsOH, and Te. Experiments are planned and being performed to produce this data base.
3. The major shortcomings in the application of TRAP-MELT to this study lie in the essentially one-dimensional nature of the control volume code formalism, and in the non-unified treatment of thermal-hydraulics and aerosol/fission product transport within the primary reactor vessel. At issue is the applicability under the recirculatory flow/geometry conditions existing in the primary reactor vessel and upper plenum region.
4. There are processes not now treated in TRAP-MELT that could make a significant difference in the calculated results. These processes are: surface chemical reactions that might lead to more volatile species or retain condensed species, aerosol deposition by impaction, and aerosol resuspension.
5. Further assessments are needed, i.e., TRAP-MELT uses internal thermal hydraulic/mass transfer correlations that are for turbulent, well-developed steady-flow conditions. In addition, the internal model used to assess the strength of natural convection (and to calculate an effective Reynold's number) appears to be inappropriate for the confined geometry in the reactor vessel. Also, the values used for the mixed aerosol effective density, shape factors, and gas-to-particle effective density are speculative. Furthermore, the use of a net velocity (Stokes-convective) is not appropriate for gravitational settling. Finally, the properties for the carrier fluid are for steam only.

2.4. REFERENCES

1. Technical Bases for Estimating Fission Product Behavior During LWR Accidents, NUREG-0772 (June 1981).
2. S. J. Niemczyk and L. M. McDowell-Boyer, Technical Considerations Related to Source Term Assumptions for Emergency Planning and Equipment Qualifications, ORNL/TM-8275 (September 1982).
3. H. Albrecht, V. Matschoss, and H. Wild, "Experimental Investigation of Fission and Activation Product Release from LWR Fuel Rods at Temperatures Ranging from 1500-2800°C," in Proceedings of the Specialists' Meeting on the Behavior of Defected Zirconium Alloy Ceramic Fuel in Water Cooled Reactors, CONF-790935-3 (September 1979).
4. H. Albrecht and H. Wild, "Investigation of Fission Product Release by Annealing and Melting of LWR Fuel Pins in Air and Steam," in Proceedings of the Topical Meeting on Reactor Safety Aspects of Fuel Behavior, Sun Valley, ID (August 2-6, 1981).
5. H. Albrecht, "Fission Product Release Program at the SASCHA Facility," BMFT/USNRC Core Melt Information Exchange Meeting (October 27-28, 1982).
6. H. Albrecht, "Out-of-Pile Release Tests Under Core Melting Conditions," OECD-NEA-CSNI/IAEA Specialists' Meeting on Water Reactor Fuel Safety and Fission Product Release in Off-Normal and Accident Conditions, RISO National Laboratory (May 16-20, 1983).
7. H. Albrecht and H. Wild, "Behavior of I, Cs, Te, Ba, Ag, In, and Cd During Release from Overheated PWR Cores," in Proceedings of the International Meeting on Light Water Reactor Severe Accident Evaluation, Cambridge, MA, (August 28 - September 1, 1983).
8. G. W. Parker, G. E. Creek, and A. L. Sutton, Jr., "Influence of Variable Physical Process Assumptions on Core-Melt Aerosol Release," in Proceedings of the International Meeting on Thermal Nuclear Reactor Safety, NUREG/CR-0027, Vol. 2, pp. 1078-89 (February 1983).
9. G. W. Parker, A. L. Sutton, Jr., and G. E. Creek, "Core-Melt Aerosol Release and Transport," in Aerosol Release and Transport Program Quarterly Report for October-December 1982, NUREG/CR-2809, Vol. 4 (ORNL/TM-8397/V4) (May 1983).
10. P. N. Clough, H. C. Starkie, and A. R. Taig, "Modelling of Whole-Core Release of Fission Products in PWR Core Melt Accidents," in Proceedings of the International Meeting on Light Water Reactor Severe Accident Evaluation, Cambridge, MA, (August 28 - September 1, 1983).

11. J. H. Gittus, PWR Degraded Core Analysis, ND-R-610(S) (April 1982).
12. B. R. Sehgal and D. Cubicciotti, "Fission Product Core Material Sources in Degraded Accidents," in Proceedings of the International Meeting on Light Water Reactor Severe Accident Evaluation, Cambridge, MA, (August 28 - September 1, 1983).
13. T. Y. Han, P. I. Nakayama, and R. G. Stuart, "User's Manual and Modeling for the PWR Heatup Code," Vol. II, Draft Final Report for the IDCOR Subtask 15.1 (January 1983).
14. G. Eriksson, Chem. Scripta 8, 100 (1975). Modified in T. M. Besmann, SOLGASMIX-PV, A Computer Program to Calculate Equilibrium Relationships in Complex Chemical Systems, ORNL/TM-5775 (1977).
15. J. Rest, "A Generalized Model for Predicting Radionuclide Source Terms for LWR Degraded Core Accidents," in Proceedings of the International Meeting on Thermal Nuclear Reactor Safety, NUREG/CP-0027, Vol 1, pp. 111-21 (February 1983).
16. S. W. Tam, P. E. Blackburn, and C. E. Johnson, "Effect of Core Chemistry on Fission Product Release,"in Proceedings of the International Meeting on Thermal Nuclear Reactor Safety, NUREG/CP-0027, Vol. 1, pp. 101-10 (February 1983).
17. S. E. Turner et al., Background and Derivation of ANS-5.4 Standard Fission Product Release Model, NUREG/CR-2507 (January 1982).
18. R. P. Wichner et al., Station Blackout at Browns Ferry Unit One -- Iodine and Noble Gas Distribution and Release, NUREG/CR-2181, Vol. 2 (ORNL/NUREG/TM-455/V2) (August 1982).
19. R. M. Elrick and R. A. Sallach, "Fission Product Chemistry in the Primary System" in Proceedings of the International Meeting on Light Water Reactor Severe Accident Evaluation, Cambridge, MA, (August 28 - September 1, 1983).
20. R. A. Lorenz, "The Vaporization of Structural Materials in Severe Accidents," in Proceedings of the International Meeting on Thermal Nuclear Reactor Safety, NUREG/CP-0027, Vol. 2, pp. 1090-99 (February 1983).
21. M. F. Osborne, R. A. Lorenz, J. R. Travis, and C. S. Webster, Data Summary Report for Fission Product Release Test HI-1, NUREG/CR-2928 (ORNL/TM-8500) (December 1982).
22. M. F. Osborne, R. A. Lorenz, J. R. Travis, C. S. Webster, and K. S. Norwood, Data Summary Report for Fission Product Release Test HI-2, NUREG/CR-3171 (ORNL/TM-8667) (in publication).

23. M. F. Osborne, R. A. Lorenz, K. S. Norwood, J. R. Travis, and C. S. Webster, Data Summary Report for Fission Product Release Test HI-3, NUREG/CR-3335 (ORNL/TM-8793) (in preparation).
24. M. F. Osborne, R. A. Lorenz, K. S. Norwood, and R. P. Wichner, "Fission Product Release Under LWR Accident Conditions," in Proceedings of the International Meeting on Light-Water Reactor Severe Accident Evaluation, Cambridge, MA, (August 28 - September 1, 1983).
25. R. A. Lorwenz, J. L. Collins, M. F. Osborne, R. L. Towns, and A. P. Malinauskas, Fission Product Release from BWR Fuel Under LOCA Conditions, NUREL/CR-1772 (ORNL/NUREG/TM-388) (July 1981).
26. R. A. Lorenz, J. L. Collins, A. P. Malinauskas, O. L. Kirkland, and R. L. Towns, Fission Product Release from Highly Irradiated LWR Fuel, NUREG/CR-0722 (ORNL/NUREG/TM-287/R2) (February 1980).
27. R. A. Lorenz, J. L. Collins, A. P. Malinauskas, M. F. Osborne, and R. L. Towns, Fission Product Release from Highly Irradiated LWR Fuel Heated to 1300-1600°C in Steam, NUREG/CR-1386 (ORNL/NUREG/TM-346) (November 1980).
28. D. J. Osetek, K. Vinjamuri, D. E. Kudera, and R. R. Hobbins, "Iodine and Cesium Behavior During the First PBF Severe Fuel Damage Test,"in Proceedings of the International Meeting on Light Water Reactor Severe Accident Evaluation, Cambridge, MA, (August 28 - September 1, 1983).
29. R. A. Lorenz, E. C. Beahm, and R. P. Wichner, "Review of Tellurium Release Rates from LWR Fuel Elements Under Accident Conditions,"in Proceedings of the International Meeting on Light Water Reactor Severe Accident Evaluation, Cambridge, MA, (August 28 - September 1, 1983).
30. S. A. Hodge et al., SBLOCA Outside Containment at Browns Ferry Unit One - Accident Sequence Analysis, NUREG/CR-2672, Vol. 1 (ORNL/TM-8119/V1) (November 1982).
31. R. P. Wichner et al., Analysis of a Small-Break LOCA Outside Containment at Browns Ferry Unit One -- Iodine, Cesium, and Noble Gas Distribution and Release, NUREG/CR-2672, Vol. 2 (ORNL/TM-8119/V2) (in technical review.)

Table 2.1 CHARACTERISTICS OF VARIOUS RELEASE MODELS

Code name	Time, temperature, gas flow source	Fission product release		UO2	Control rods		Stainless steel and inconel
		Xe, Kr, I, Cs, Te Sr, Ba, Ru, Mo, Zr			Cladding	Ag-In-Cd or B_4C	
CORSOR	MARCH	Frac/min	Frac/min	Frac/min	Frac/min	None	Frac/min
NUREG-0772	MARCH	Frac/min	Frac/min	Frac/min	Frac/min	None	Frac/min
SASCHA	MELSIM	Frac/min	Frac/min	Frac/min	Frac/min	Frac/min	Frac/min
Browns Ferry SASA	MARCH	Frac/min	Frac/min	Vapor	Vapor	None	Vapor
FISREL	MARCH	Frac/min	Frac/min	Frac/min	Vapor	None	Vapor
EPRI/IDCOR	PWR heatup	Steam oxidation	Vapor	Vapor	Vapor	Vapor, 1400°C max	Vapor
FASTGRASS		Mechanistic					
ANL-VFP		RCB[a]	RCB				
ANSI-5.4		ESD[b]					

[a] Relative chemical behavior
[b] Equivalent sphere diffusion, or Booth/Rymer/Beck Model.

Table 2.2A OPERATING CONDITIONS FOR ORNL FISSION PRODUCT RELEASE TESTS

Test no.	Temperature (°C)	Heatup rate (°C/s)	Cooldown rate (°C/s)	Time at temperature (min)	Heatup/ cooldown allowance (min)	Steam flow (°C/min STP) (min)	Inert gas flow (L/min STP)
HBU-11	1200	0.16	0.30	10	13	1.32	0.34 (He)
BWR-3	1200	0.11	0.31	10	17	1.00	0.30 (He)
HT-1	1325	9.9	12.2	10	0.25	0.72	0.87 (He)
HT-2	1445	11.1	11.1	7	0.25	0.94	0.87 (He)
HT-3	1610	6.7	17.0	3	0.38	1.02	0.87 (He)
HT-4	1400	18.5	11.0	0.33	0.20	0.93	0.79 (He)
HI-1	1400	0.97	0.60	30	3.8	1.00	0.50 (Ar)
HI-2	1700	1.04	1.17	20	2.5	0.99	0.33 (Ar)
HI-3	2000	2.78	1.67	20	1.3	0.30	0.30 (He)
HI-4	1875	1.93	1.58	20	1.6		

TABLE 2.2B. RELEASE OF KR, CS, AND IN IN ORNL FISSION PRODUCT RELEASE TESTS

Test No.	Temp. (°C)	Fuel Source	% Gap Inventory	Adjusted test duration (min)	Release of fission products				
					85Kr	Cs		I	
					(%)	(%)	(frac/min)	(%)	(Frac/min)
HBU-11	1200	H. B. Robinson	0.3	23	0.47	3.11×10^{-2}	1.35×10^{-5}	4.80×10^{-2}	2.09×10^{-2}
BWR-3	1200	Peach Bottom-2	14	27	1.08	1.846	6.90×10^{-4}	2.986	1.12×10^{-3}
HT-1	1325	H. B. Robinson	0.3	10.25	1.07	0.112 x 2	2.18×10^{-4}	0.165 x 2	3.22×10^{-4}
HT-2	1445	H. B. Robinson	0.3	7.25	5.0	4.82 x 2	1.40×10^{-2}	2.35 x 2	6.64×10^{-3}
HT-3	1610	H. B. Robinson	0.3	0.53	2.8	3.054 x 2	1.19×10^{-1}	1.75 x 2	6.72×10^{-2}
HI-1	1400	H. B. Robinson	0.3	33.8	2.83	2.04	6.10×10^{-4}	1.75	5.22×10^{-4}
HI-2	1700	H. B. Robinson	0.3	22.5	51.5	50.5	3.13×10^{-2}	53.0	3.36×10^{-2}
HI-3	2000	H. B. Robinson	0.3	21.3	59.0	57.7	4.04×10^{-2}	35.4	2.05×10^{-2}
HI-4	1875	Peach Bottom-2	10.0	21.6		31.9	1.78×10^{-2}	24.65	1.31×10^{-2}

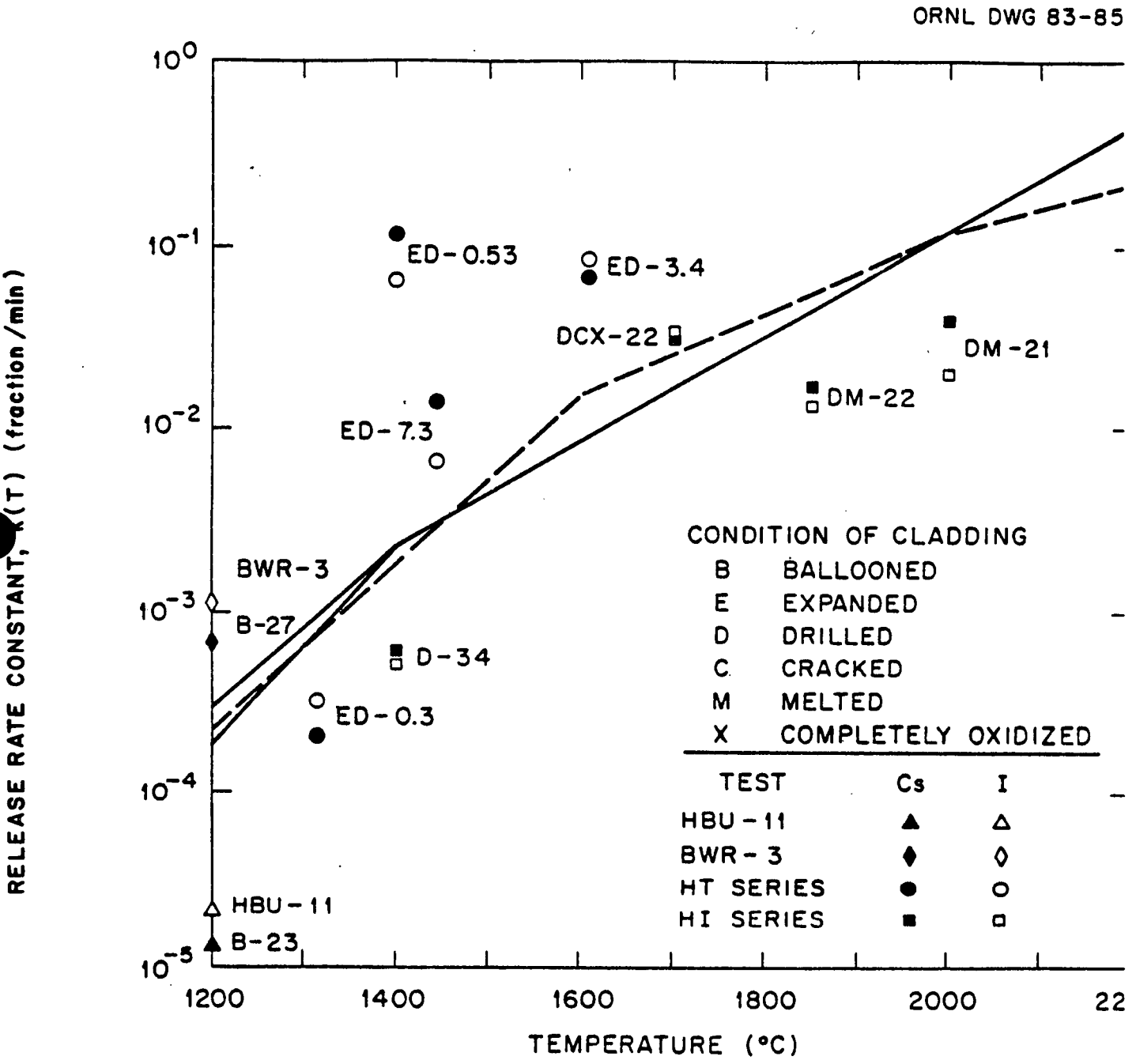

RELEASE OF CESIUM AND IODINE IN ORNL STEAM TESTS

FIGURE 2.1

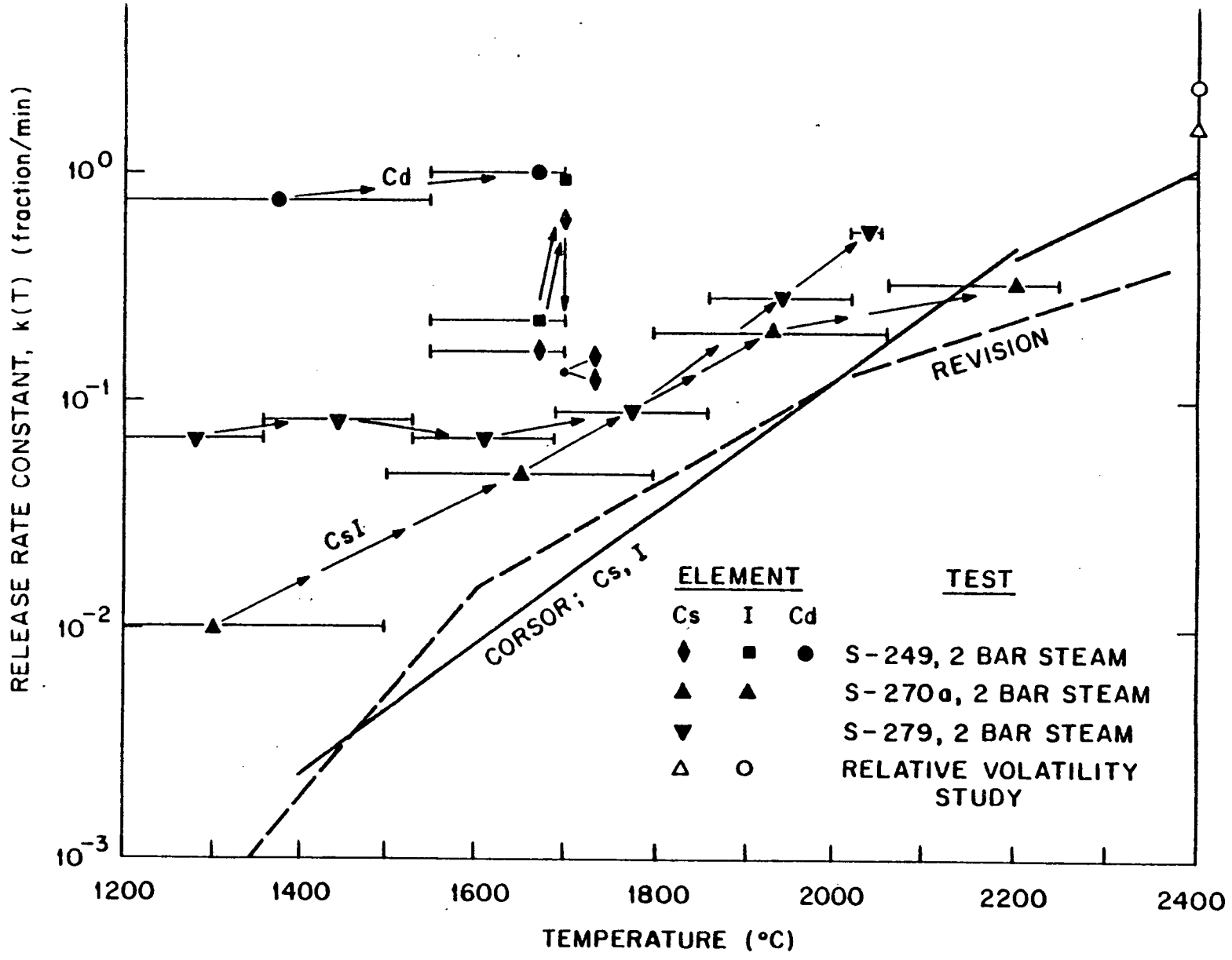

RELEASE OF CESIUM, IODINE, AND CADMIUM IN SASCHA STEAM TESTS

FIGURE 2.2

ORNL-DWG 83-653

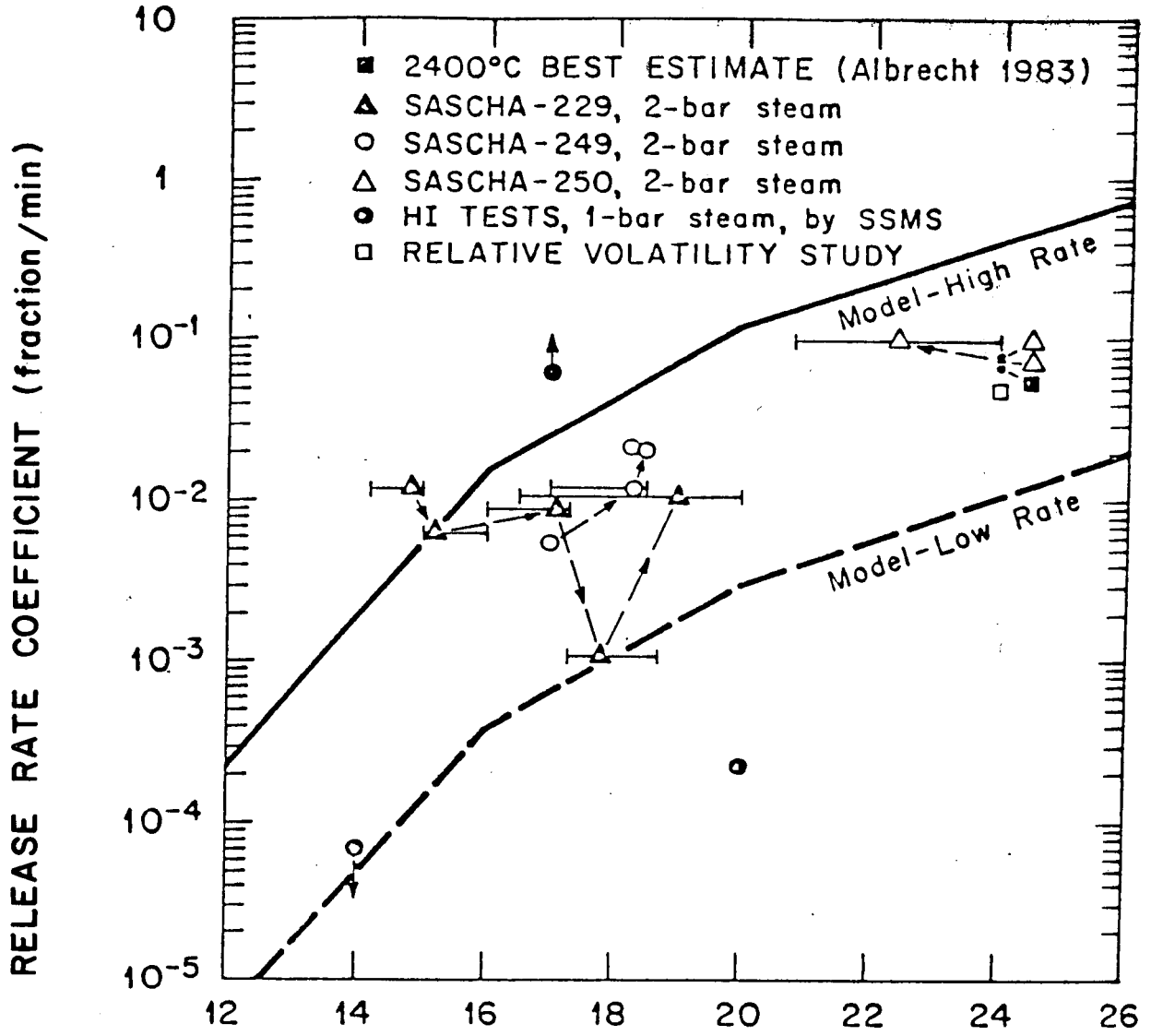

TELLURIUM RELEASE RATES

FIGURE 2.3

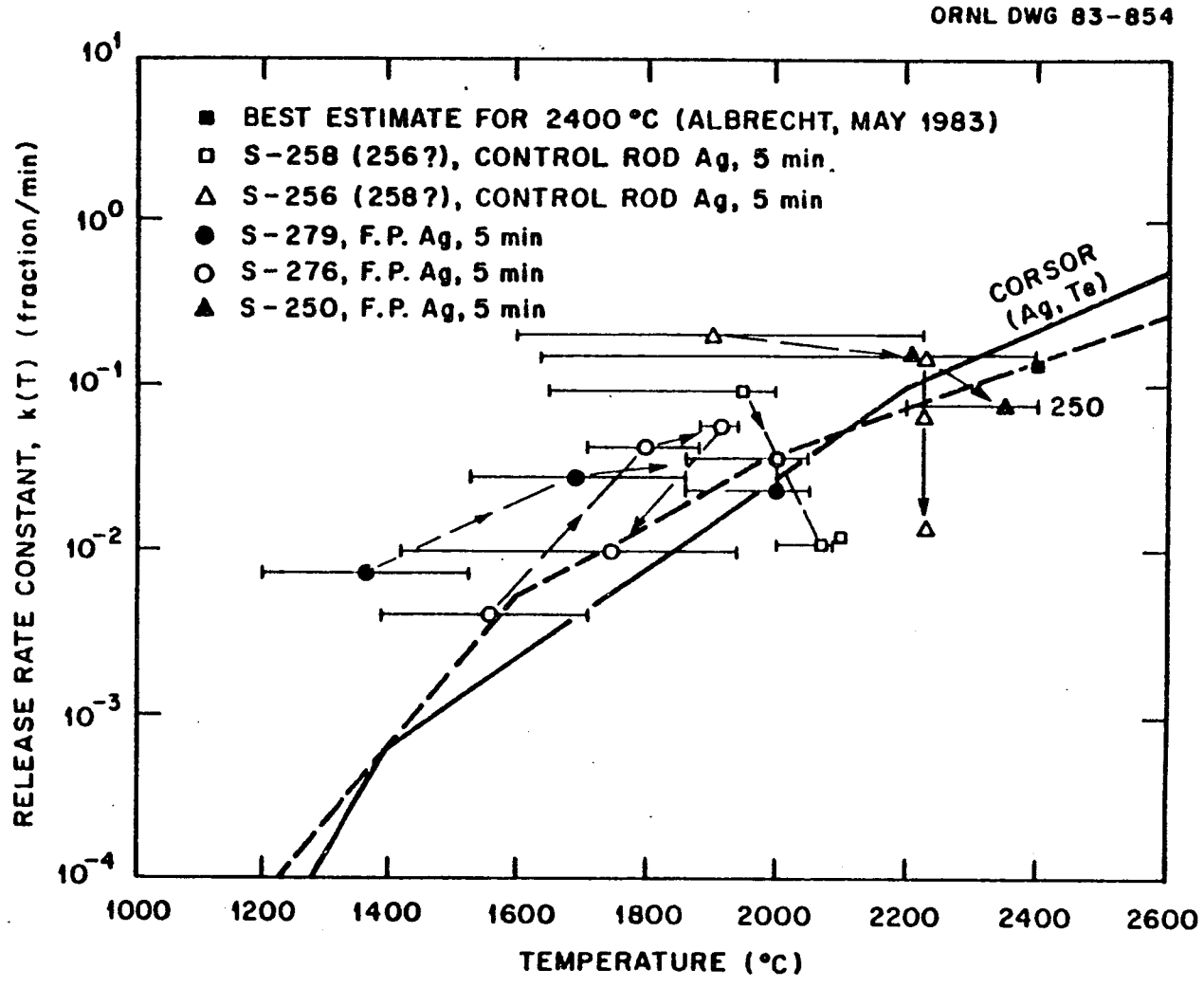

SILVER RELEASE RATES IN SASCHA TESTS WITH 2 BAR STEAM

FIGURE 2.4

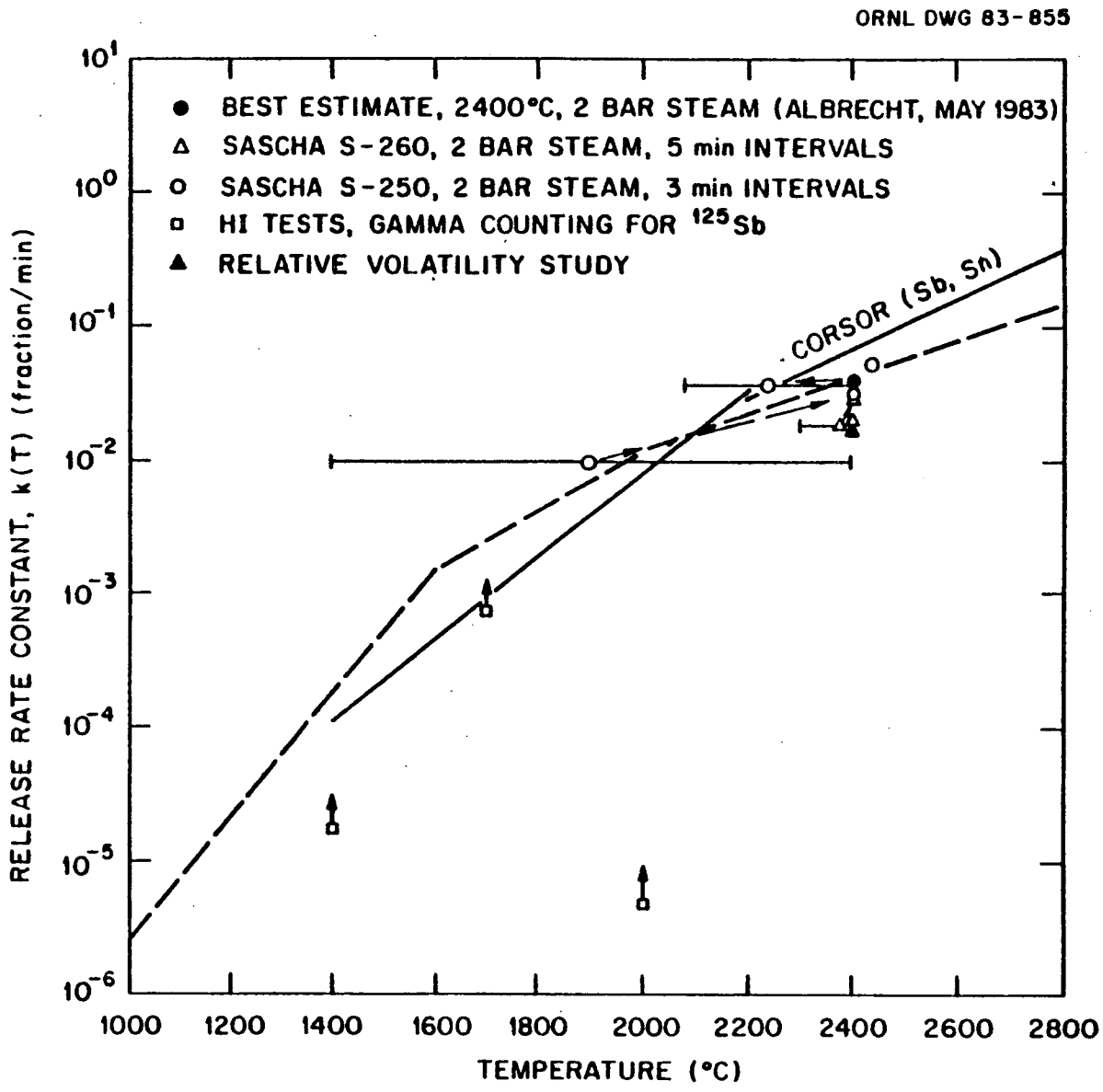

ANTIMONY RELEASE RATES IN STEAM

FIGURE 2.5

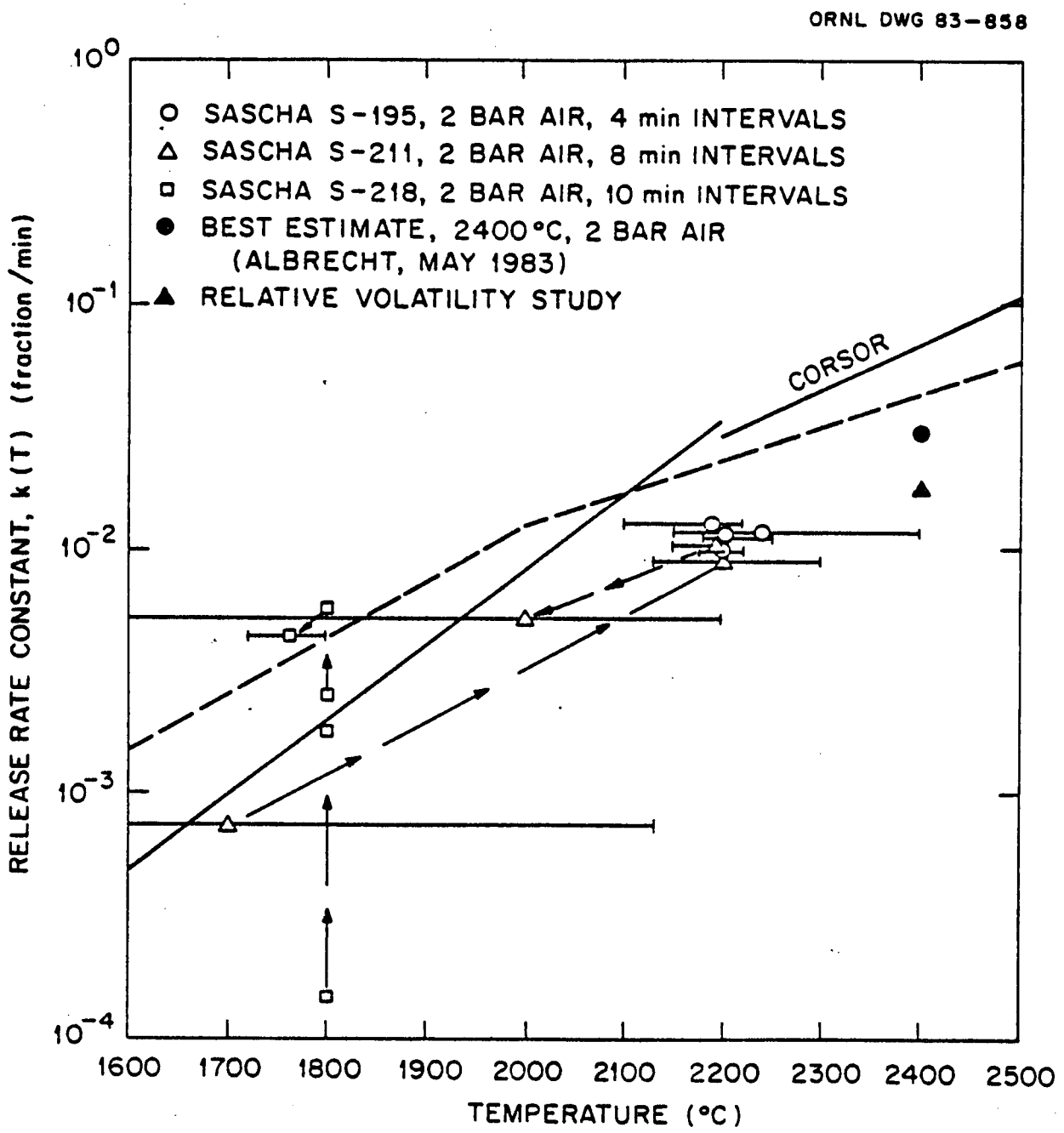

RELEASE RATES FOR ANTIMONY IN AIR

FIGURE 2.6

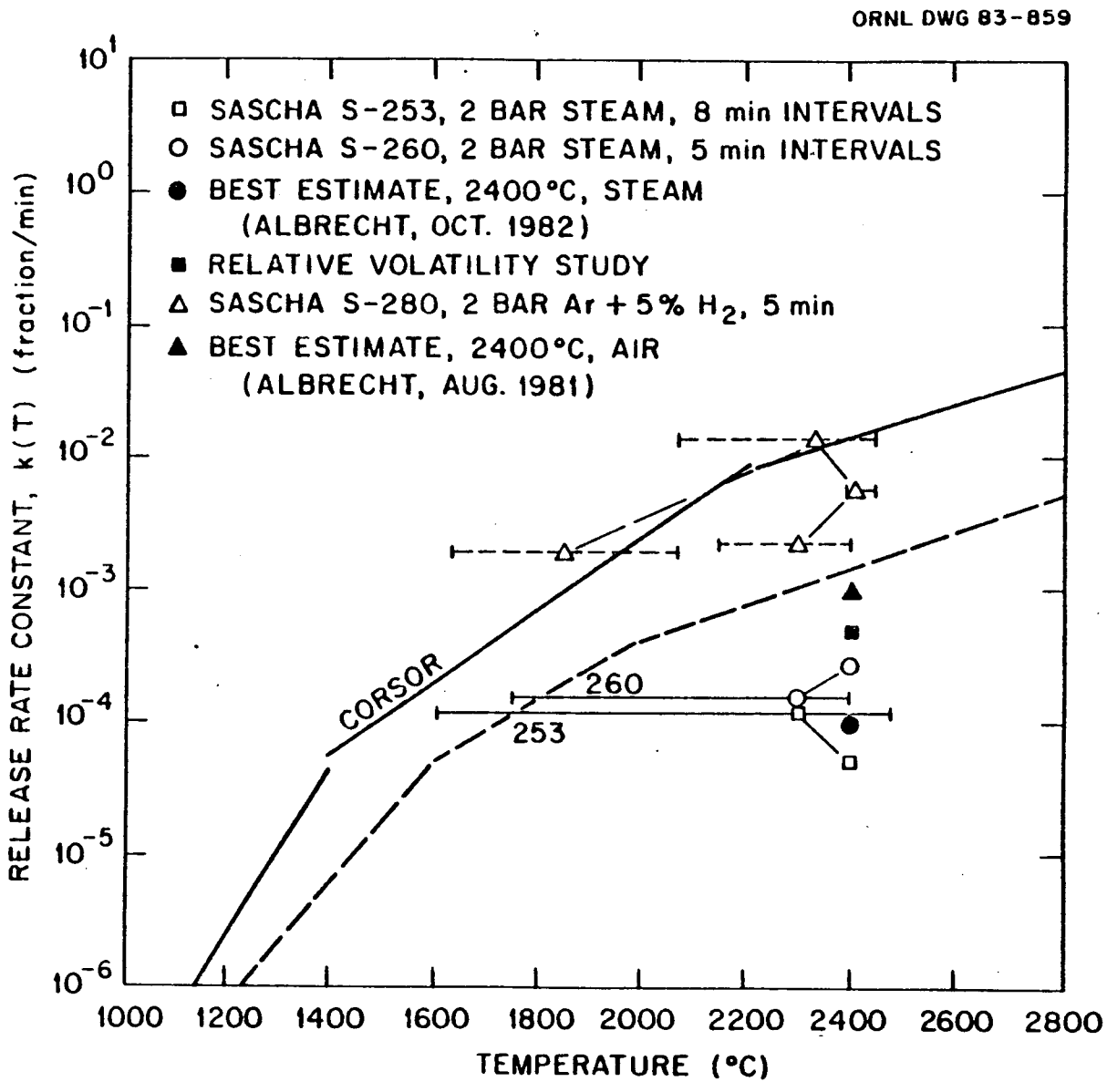

BARIUM RELEASE RATES

FIGURE 2.7

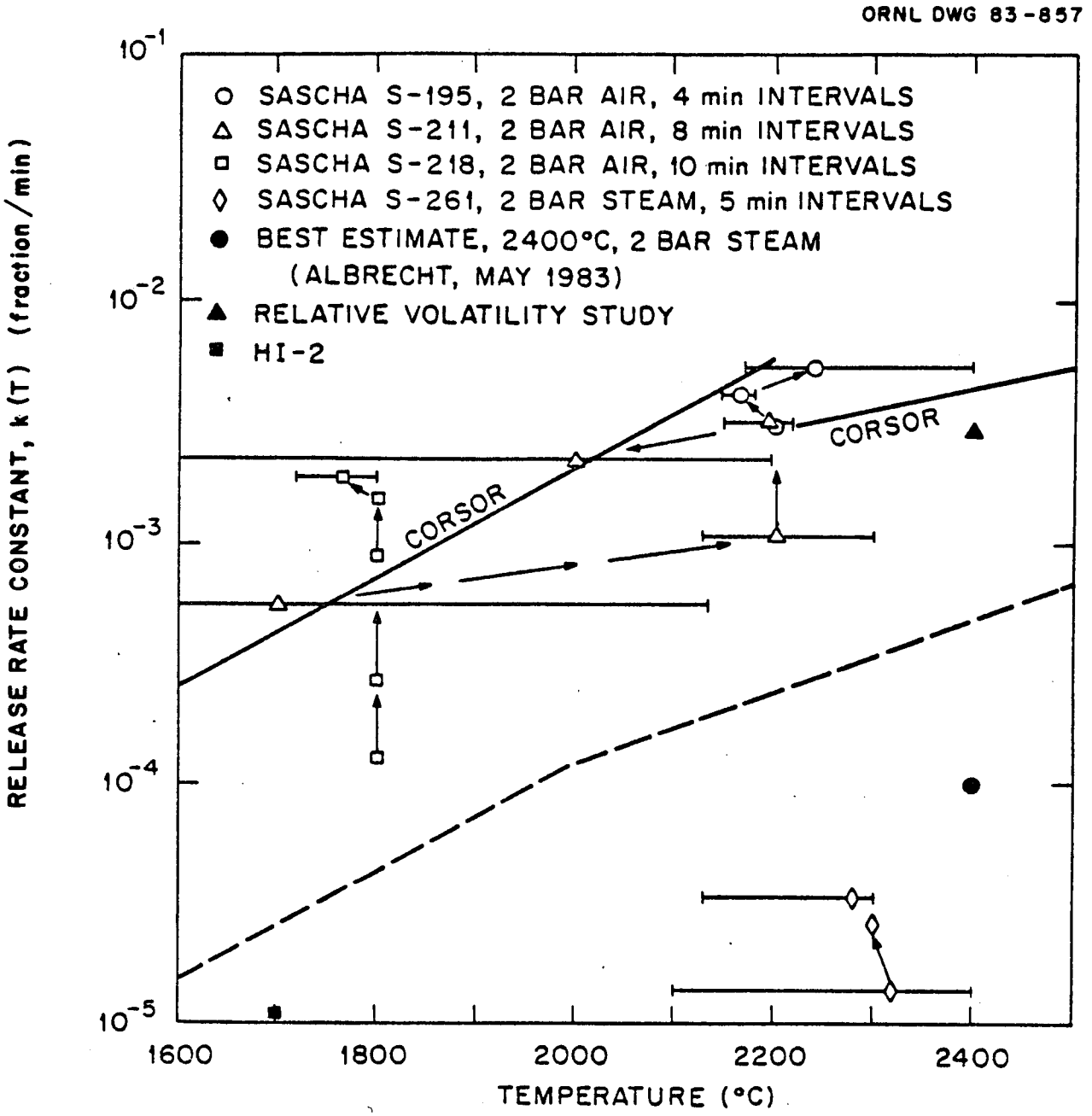

RELEASE RATES FOR MOLYBDENUM IN STEAM AND AIR

FIGURE 2.8

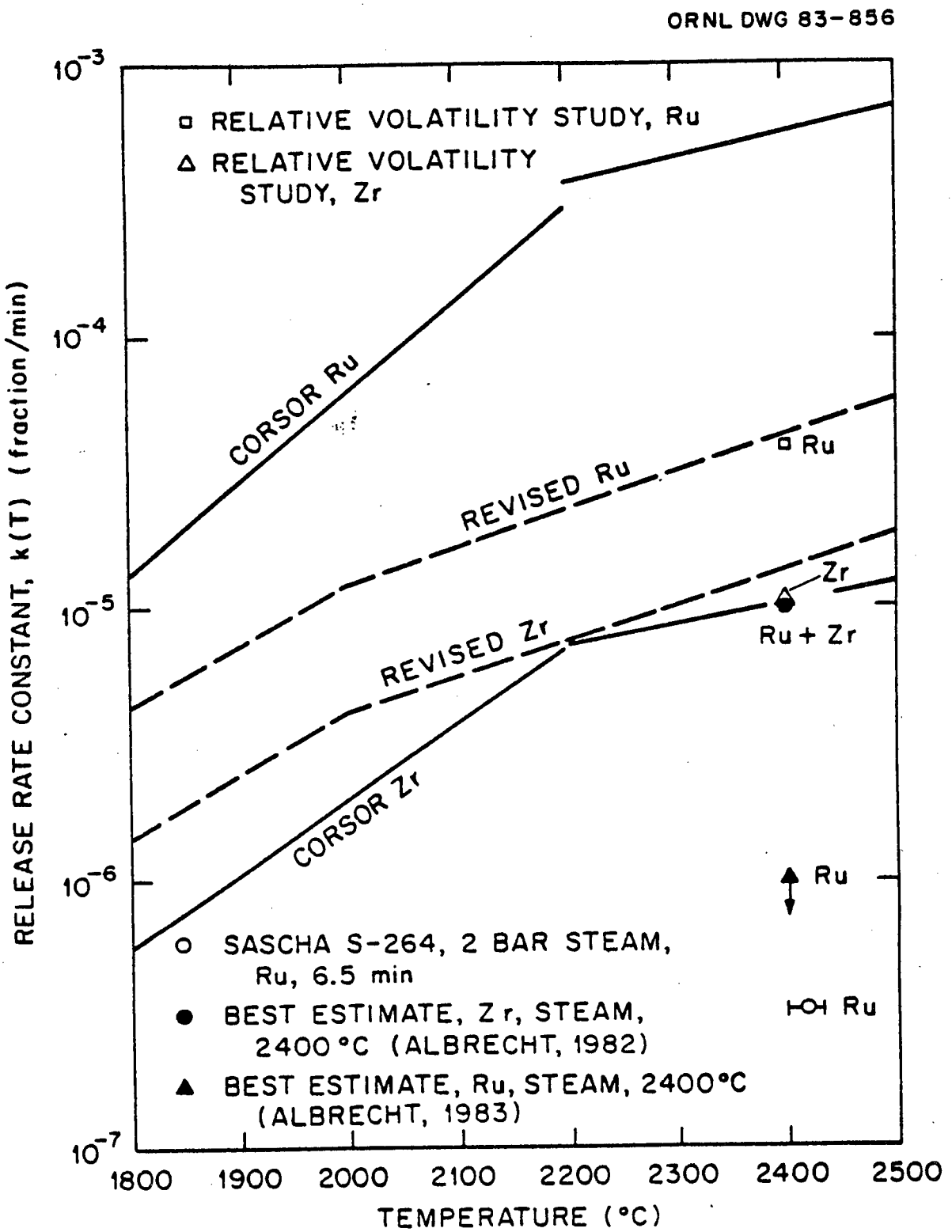

RELEASE RATES FOR RUTHENIUM AND ZIRCONIUM

FIGURE 2.9

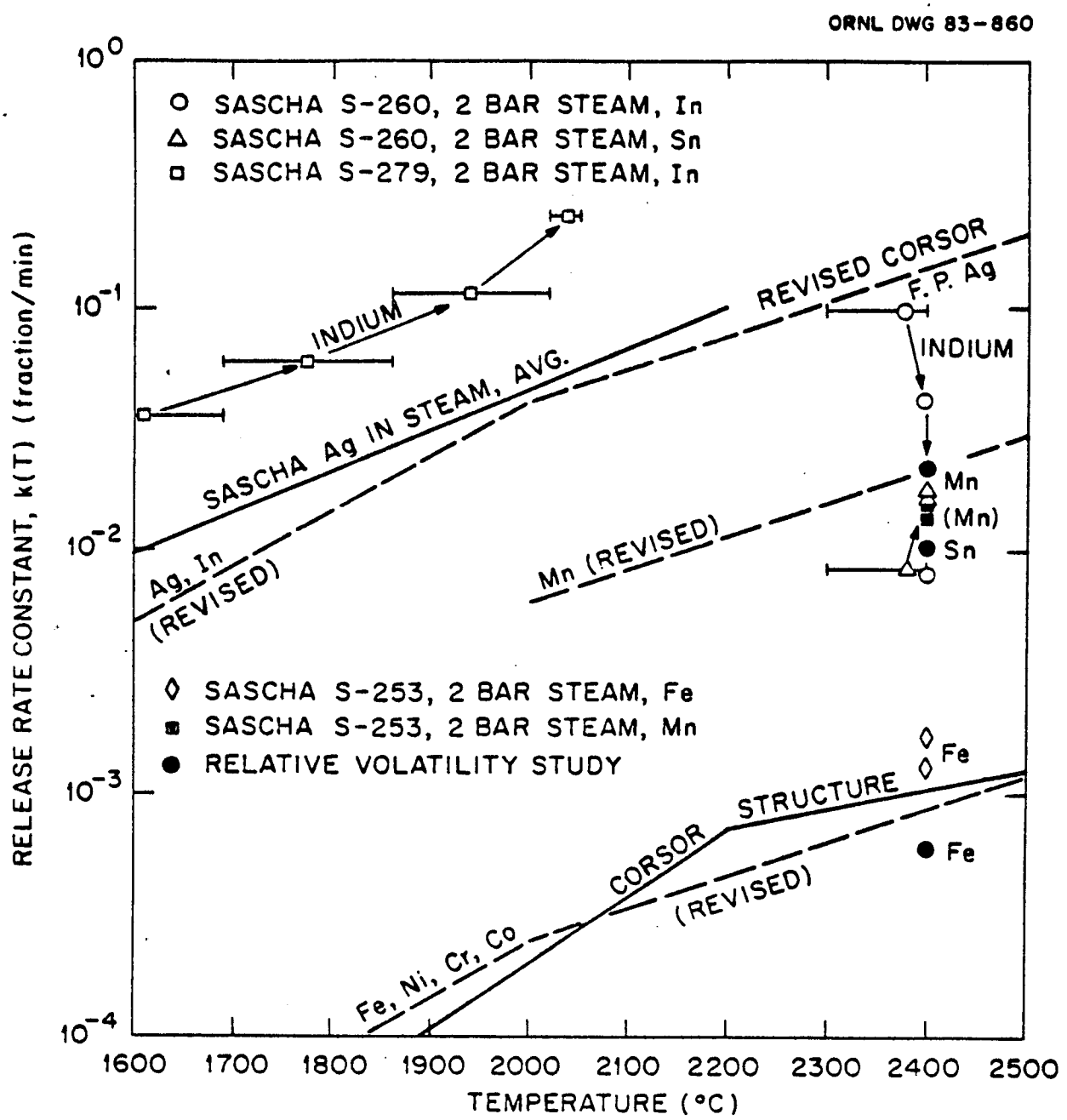

RELEASE RATES FOR VARIOUS MATERIALS IN STEAM

FIGURE 2.10

3.0 APPROACH TO ANALYSIS

The scope of this this study is to develop more precise set of source terms for the radiological releases associated with the most consequence-significant accident scenarios hypothesized for IP-3. These source terms have been developed using the latest mechanistic representations of radionuclide behavior contained in the MARCH 2.0, M-C-T and MATADOR computer codes. The M-C-T and MATADOR II computer codes are fully described and discussed in Appendices B and C, respectively.

The basis for selecting the accident sequences studied and the overall analytical approach depicted in Figure 3.1 are briefly discussed here.

3.1 Accident Sequences

The basis for the selection of accident sequences for source term evaluation is their relative contribution to plant risk. NYPA and its contractors have performed an extensive probabilistic risk study for IP-3, the 1982 Indian Point Probabilistic Safety Study or IPPSS. The most risk significant accident sequences identified in the IPPSS analysis are the rapid developing interfacing systems LOCA ("V"-sequence), and the slow overpressurization accident. The overpressurization accident sequences assume the loss of all off-site and on-site power followed by degradation of main coolant pump seals, leading to a small-LOCA (Loss of Coolant Accident). In a variation of this type of accident, a TMLB sequence assumes no pump seal leakage. The remainder of the IPPSS accident sequences have negligible risk significance and therefore will not be analyzed in this report. Each analyzed sequence is discussed in detail below.

3.1.1 V-Sequence

The classical V-sequence for IP-3 is not a physically realizable scenario. Various plant specific design characteristics impact the V-sequence to such an extent; its likelihood is extremely low for this plant. It is therefore not included in the source term analysis. An in-depth analysis justifying the above statement is appended (see Appendix A) to this report for completeness.

3.1.2 TMLB Sequence

A TMLB Sequence at IP-3 is postulated as a result of a transient initiated by a complete loss of on-site and off-site power followed by the complete loss of all core and containment cooling. Intermediate steps include loss of feedwater and auxilliary feedwater to the steam generators, thereby drying out the steam generators. This in turn increases pressure in the primary system up to the PORV (Pressure Operated Relief Valve) setpoint at which time blowdown of the primary system occurs. The path taken by the radioactive materials during the core melt is shown in Figure 3.2.

3.1.3 Pump Seal LOCA Sequence

The pump seal LOCA sequence begins in essentially the same manner as the TMLB sequence. However, at approximately 30 minutes into the sequence, the reactor cooland pump seals begin to leak as a result of the thermal degradation caused by loss of all cooling to the seals. The assumed leak rate is approximately 1200 gpm. Following the pump seal degradation, the accident appears to behave like a small break LOCA. The path for core melt releases associated with this sequence is shown in Figure 3.3. Note that in the later stages of this sequence, the flow through the PORV ceases as the primary system pressure decreases.

The analytical models for the TMLB and pump seal LOCA sequences are shown in Figures 3.4, 3.5, and 3.6.

3.2 Analytical Tools

Essentially three computer codes, MARCH 2.0, M-C-T, and MATADOR II were used. Limited input from a fourth computer code, VANESA, supplied the aerosol source rates from core-concrete interactions for MATADOR II. Figure 3.1 depicts the overall analytical flow employed in this study. Appendices B and C contain a detailed discussion of M-C-T and MATADOR II respectively.

3.2.1. MARCH 2.0

The MARCH 2.0 code analyzes the thermal-hydraulic response of the reactor core, the primary coolant system, and the containment system in Light Water Reactor systems for accidents involving some level of engineered safety feature inoperability. While MARCH 2.0 primarily addresses

accidents leading to complete core meltdown, it can also be used to treat events involving only partial core degradation and to assess the minimum levels of engineered safety feature operability required to cope with various accident events. MARCH 2.0 analyses provide the essential thermal-hydraulic input conditions required by the fission product transport codes such as TRAP-MELT, CORRAL-II, and MATADOR II.

MARCH 2.0 simulates the entire accident sequence, from the initiating accident event through the attack of the containment basemat, for a variety of accident initiators and reactor system designs. More specifically, depending on the reactor design and accident sequence, the code can evaluate:

1. Heatup of the primary and secondary coolant inventories, pressure rise to the relief/safety valve settings and subsequent boiloff.

2. Initial blowdown of the primary coolant for small and intermediate breaks in the primary system.

3. Generation and transport of heat within the core and associated coolant, if any, including boiloff of water from the reactor vessel.

4. Heatup of the fuel following core uncovery, including the effects of Zircaloy-water reactions.

5. Melting and slumping of the fuel onto the lower core support structures and into the lower head of the reactor vessel.

6. Interaction of the core debris with residual water in the reactor vessel.

7. Interaction of the core debris with the reactor vessel lower head and the subsequent melt-through or pressure-driven failure of the reactor vessel lower head.

8. Interaction of the core debris with the water in the reactor cavity, including chemical reactions and their effects.

9. Attack of the concrete basement by the core and structural debris.

10. The relocation of the decay heat source, as fission products are released from the fuel and transported to the containment.

11. Mass and energy additions to the containment associated with all the foregoing phenomena, containment temperature and pressure response, including the effects of passive and active containment safety features.

12. Effects on the containment pressure and temperature response resulting from the burning of hydrogen and other combustibles.

13. Failure of the containment and leakage to the environment.

The assumptions and approximations inherent in the code treat these phenomena in a consistent manner. A number of designated user options are offered to modify certain accident sequences or to explore the effects of various modeling assumptions. The results of the MARCH 2.0 calculations are sensitive to the user options selected.

3.2.2 M-C-T

M-C-T simulates the release and subsequent behavior of fission products inside the primary system during a severe accident. The computer code consists of three modules, M, C, and T. The first module, M, processes the MARCH 2.0 output and calculates the surface temperatures in the primary system. The second module, C, calculates the release rates of the fission product species, based on the temperature-time histories of the fuel nodes, as calculated by MARCH 2.0. The third module, T, evaluates the retention of fission products in the primary system and calculates the release rates of the fission products from the primary system.

The M-C-T program flow is shown in Figure 3.7. The analysis commences with the execution of the M module in its first mode (run 1) in order to process the MARCH 2.0 input data. This initial run develops the input information needed for the execution of the M module in its second mode (run 2). Run 2 generates the primary system surface temperatures needed

execute the T module. Module M runs until core uncovery is reached at which time modules M and T are executed to simulate fission product heating.

The C module calculates the release rates of the fission product species from the fuel during the progression of the accident. Its input consists of the temperature-time histories of the fuel nodes, as defined by MARCH 2.0. Output from the C module consists of time histories for the release rates of fission product species, and other core structural materials.

The T module, run concurrently with the M module, analyzes the retention capability of the primary system based on the temperatures supplied by run 2 of the M module and the volatile and aerosol release rates supplied by the C module. Moreover, the T module calculates the release rate-history of the primary system volatile and aerosol inventory.

3.2.3 MATADOR II

MATADOR II analyzes the behavior of radionuclides in the presence of vapors and aerosols in Light Water Reactor containments under severely degraded core conditions. In MATADOR II, radionuclides can exist in five states; as vapor, condensed on suspended particles, condensed on structural walls, deposited by particle settling and chemisorbed. Radionuclides in the aerosol state exist in up to twenty discrete particle sizes or "bins" calculated internally by MATADOR II. The radionuclides can also be picked up by spray water droplets and and be located in bulk water in the sump or on the containment floor. Radionuclides can be collected by other engineered safety systems besides sprays such as filters, ice condensers, pressure supression pools, etc. The transfer and removal of radionuclides by these systems (called DF transfers) are achieved by the use of decontamination factors and do not enter into the rate equations discussed in Appendix C.

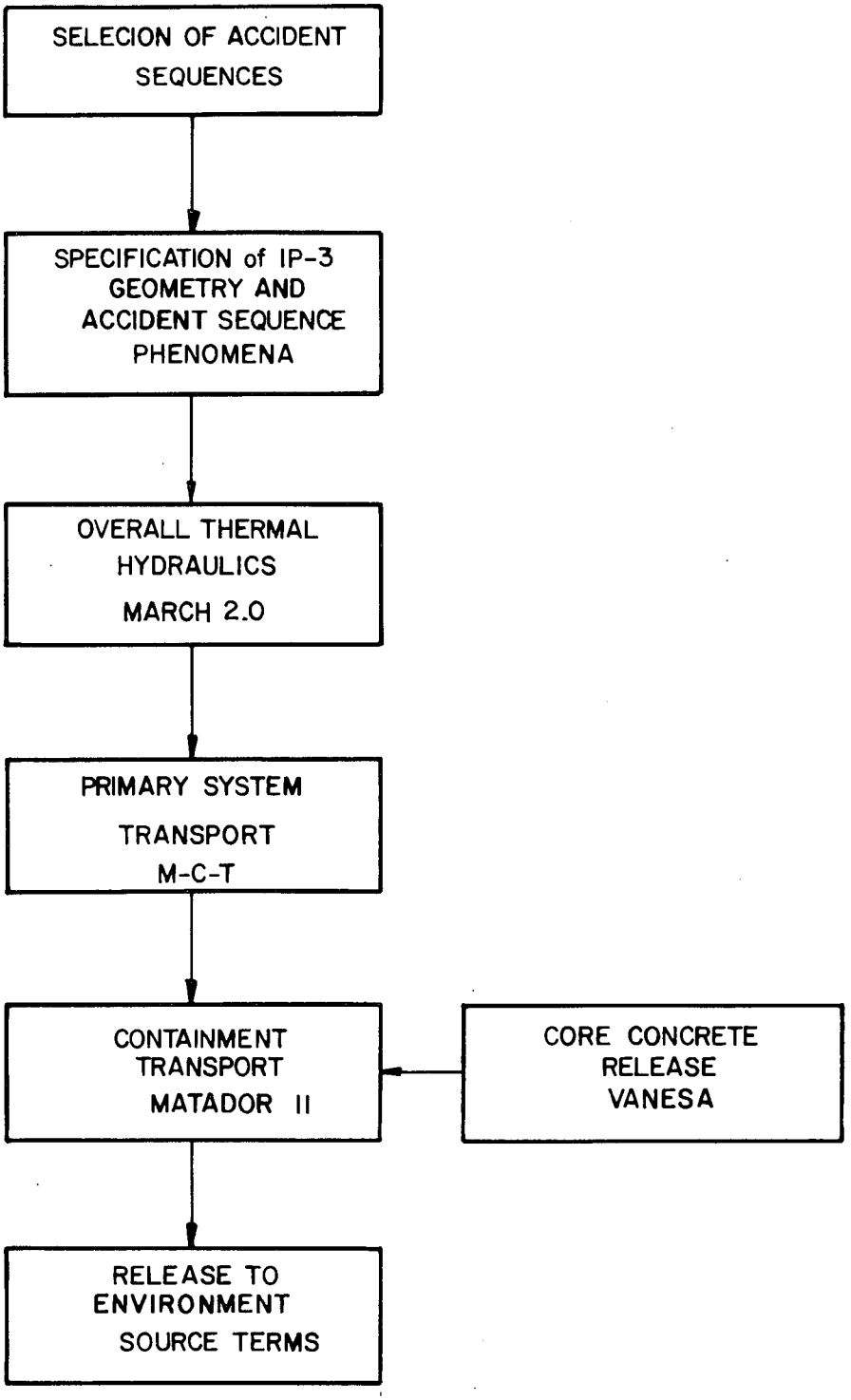

FIGURE 3.1 IP-3 SOURCE TERM ANALYSIS APPROACH

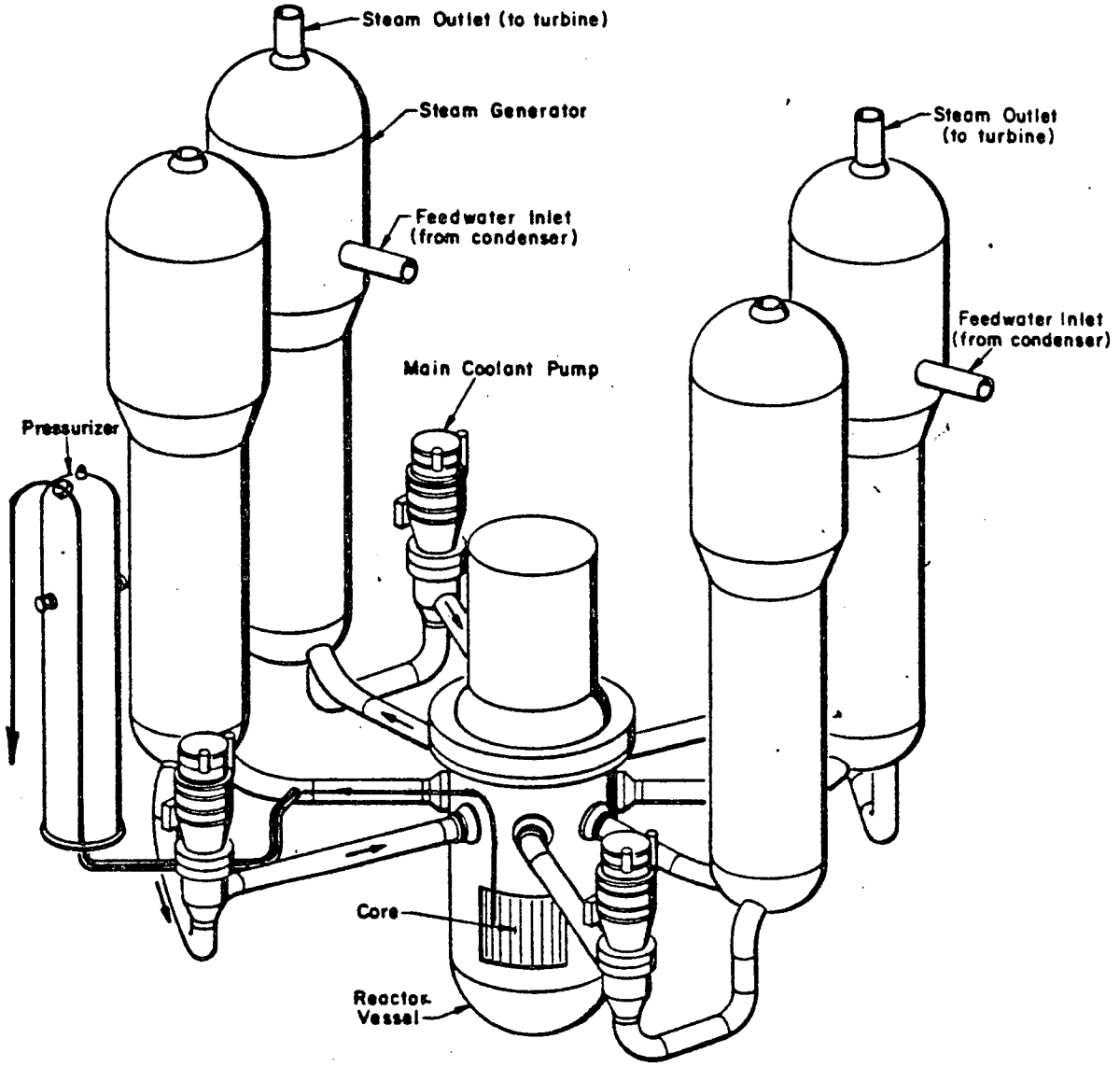

FIGURE 3.2 Fission Product Release Path for a TMLB Sequence

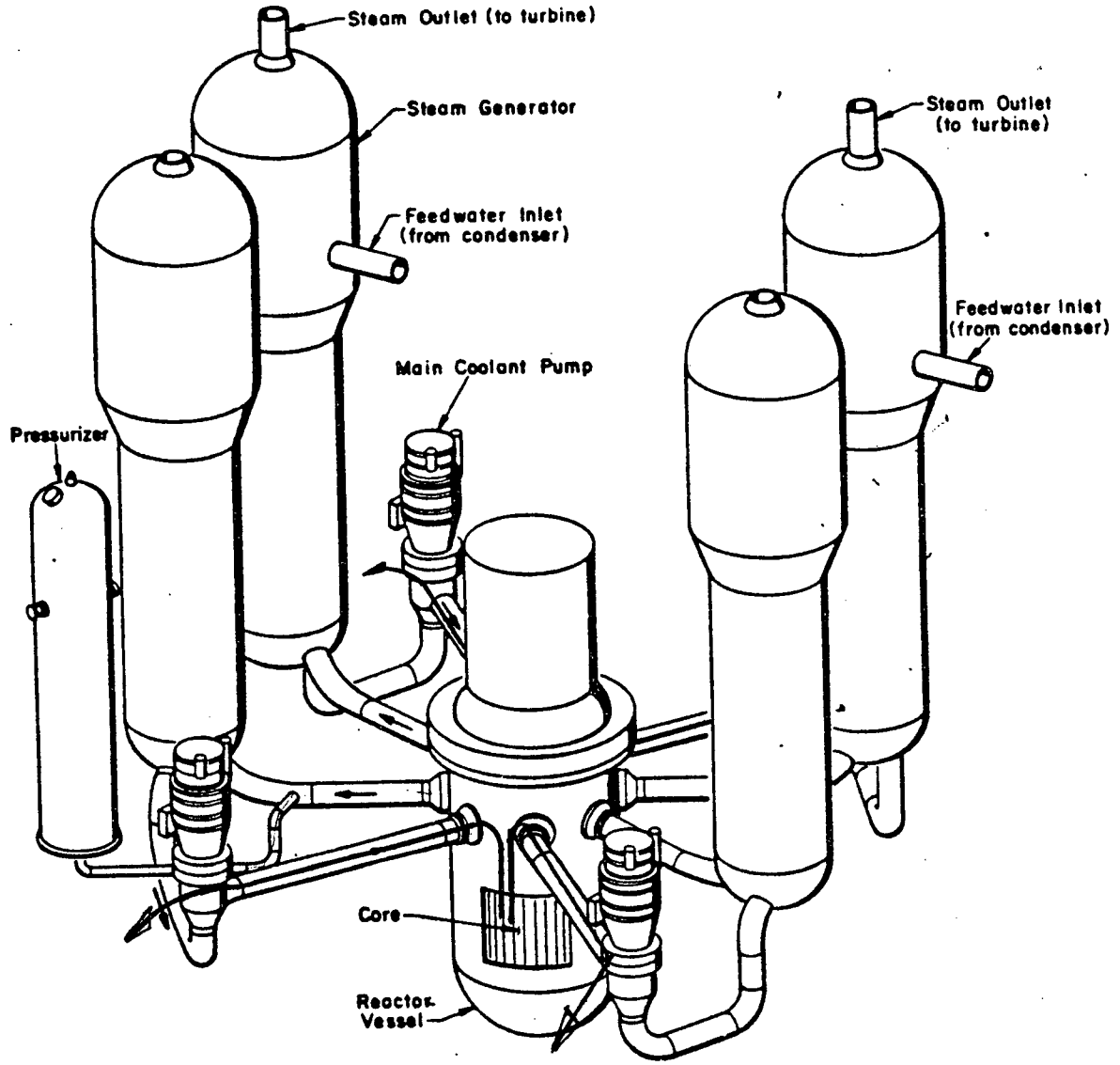

FIGURE 3.3 Fission Product Release Path for a Pump Seal LOCA

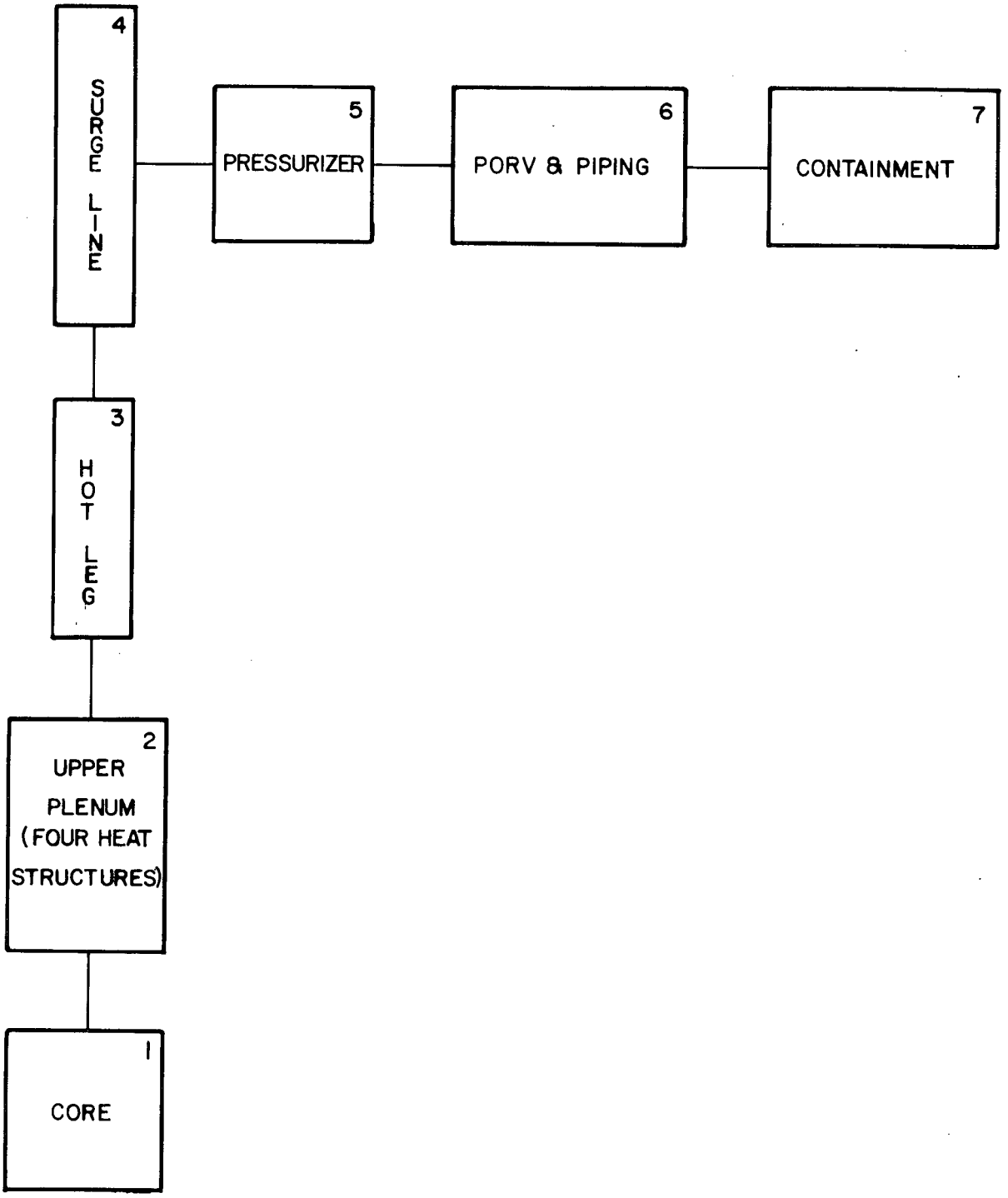

FIGURE 3.4

M Module/T Module Model

for TMLB Sequence

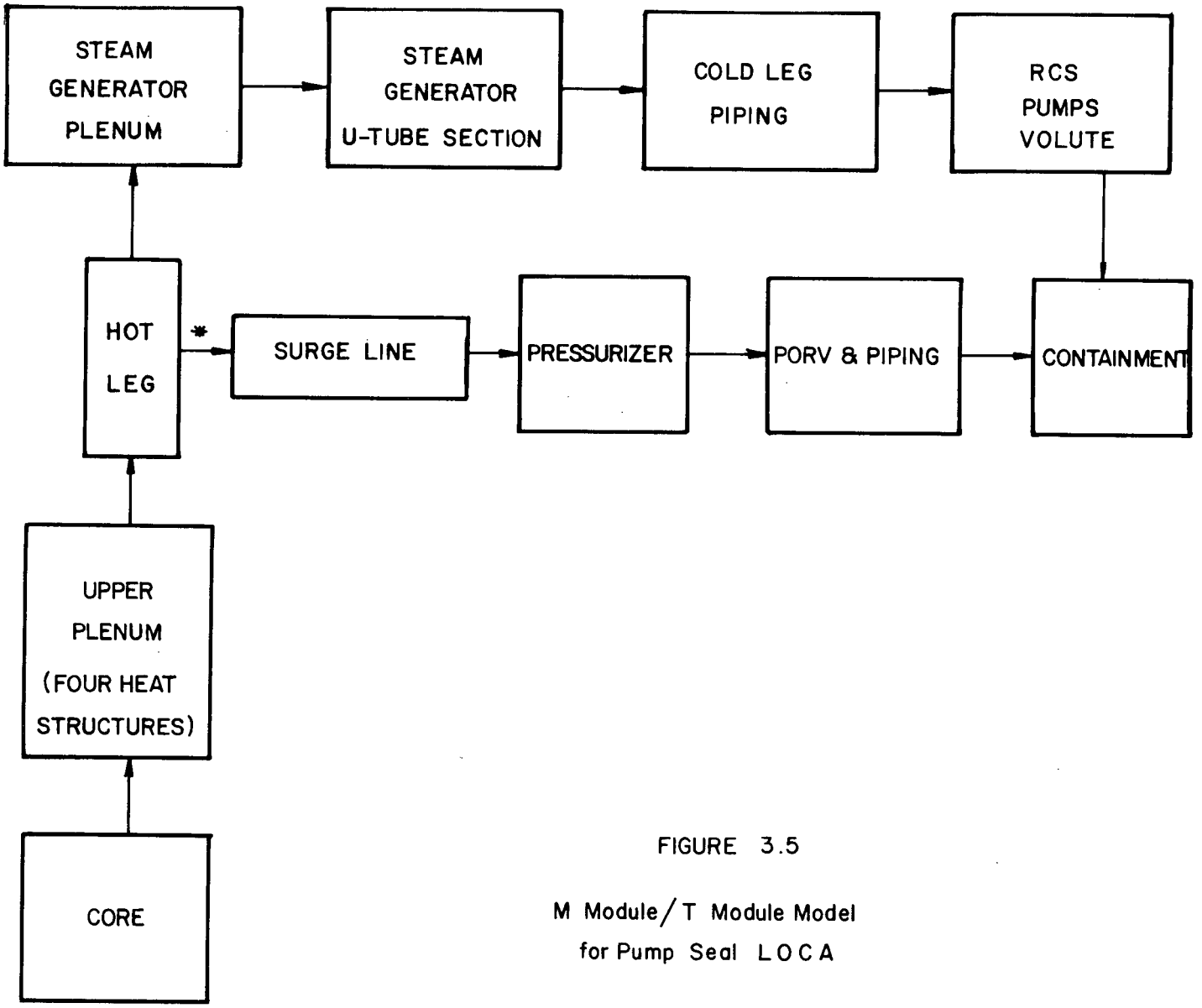

FIGURE 3.5

M Module/T Module Model
for Pump Seal LOCA

* Flow path exists only during first 30 minutes of accident.

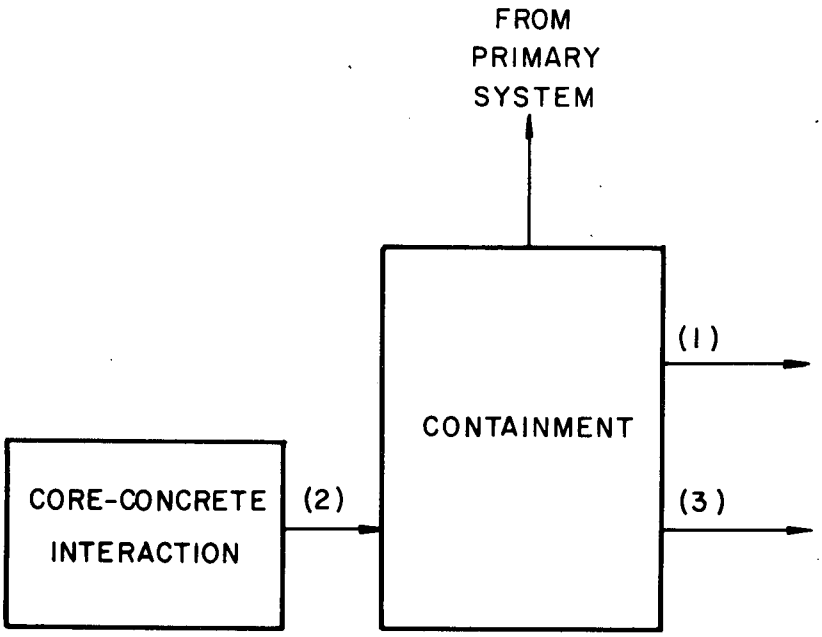

(1) CONTAINMENT LEAKAGE AT DESIGN LEAK RATE

(2) STARTS WHEN REACTOR VESSEL FAILS

(3) RELEASES COMMENCES WHEN CONTAINMENT FAILS

FIGURE 3.6

MATADOR MODEL FOR

TMLB AND PUMP SEAL LOCA

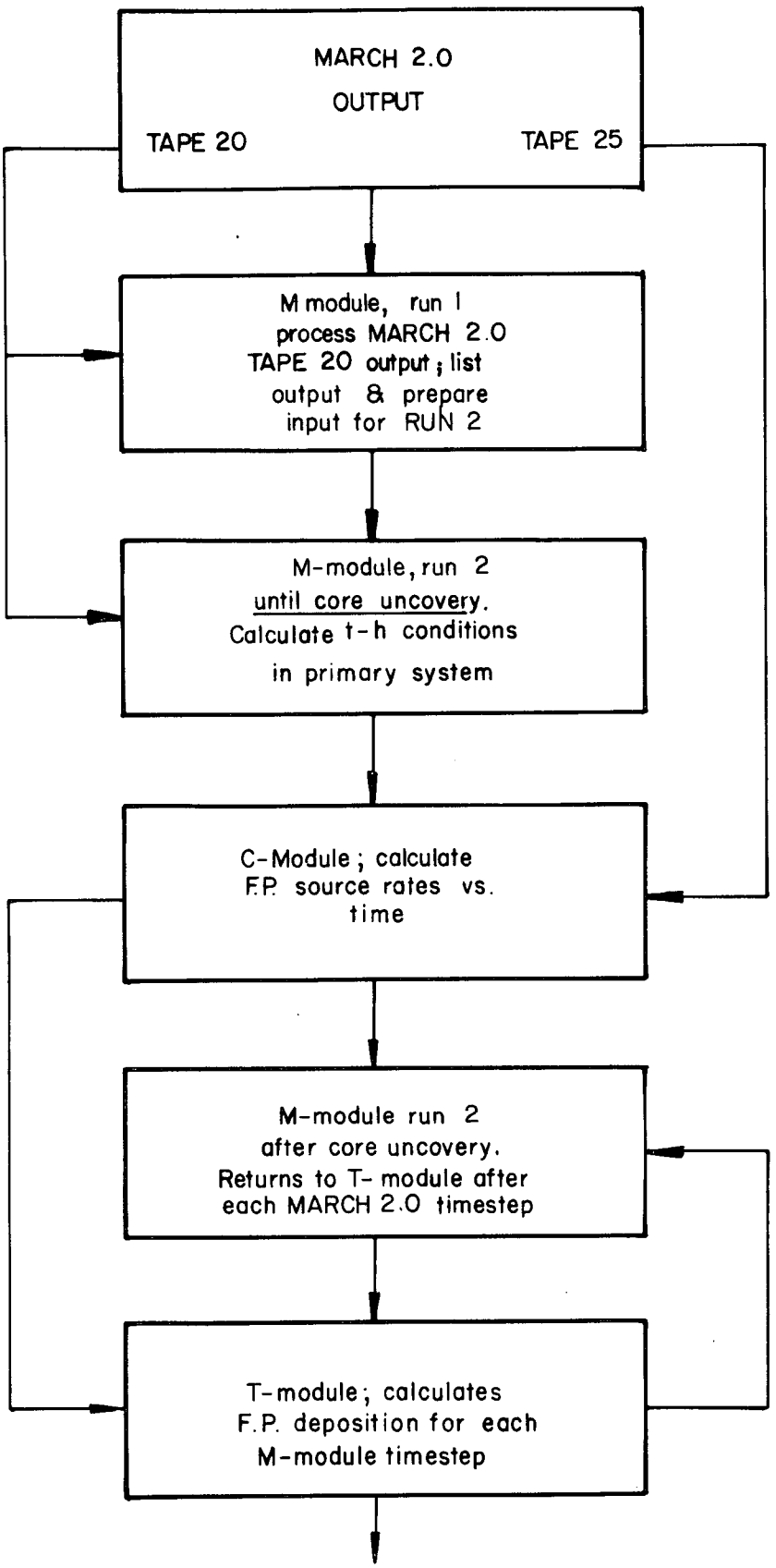

Figure 3.7 M-C-T Program flow

4.0 ASSUMPTIONS AND INPUTS FOR THE ANALYSES OF IP-3 ACCIDENT SEQUENCES

This section describes the assumptions and code inputs employed in the performance of the source terms analyses. The information is presented in a manner consistent with the flow of the analyses. Thus, the input parameters for the MARCH 2.0 are presented and discussed first, followed by the input discussion to the M, C, and the T module of the M-C-T code. Lastly, the input description for the MATADOR analysis is presented and discussed.

4.1 MARCH 2.0 Input

The MARCH 2.0 code performs a deterministic analysis of the behavior of a severe accident sequence. The code user specifies the boundary conditions for the accident, such as: the size and location of a primary system break, the control parameters and level of operability of safety systems, the conditions leading to containment failure, and the size of the leak in the failed containment. Since some of the phenomena modeled by the code are not well-understood, options are available in the code that allow variations in modeling the phenomena, requiring considerable judgment on the part of the analyst.

Table 4.1 shows the general parameters selected for each major system or component used in MARCH 2.0. Table 4.2 shows the specific input data for the TMLB accident sequence and Table 4.3 show the input parameters for the Pump Seal LOCA.

The most results-sensitive MARCH 2.0 input parameters are identified below, along with some rationale for the values chosen in each case. The parameters of interest are: FCOL, FDROP, IBEDC, IBEDS, ICON, IHR, IMWA, MELMOD, MWORNL, IAXC, ICONV, IRAD.

FCOL, FDROP - consistent with other analyses, a value of .75 was chosen for the fractions of core melted prior to core slumping and collapse into the lower plenum, respectively.

IBEDC, IBEDS - consistent with other analyses, the Lipinski debris bed model was chosen to model core quenching before and after core collapse into bottom head.

ICON - credit was taken for steam condensation in the cooler steam generator and subsequent return of the condensate to the reactor vessel.
IHR - radiation heat tranfer from the rods to the steam was included in the calculations.
IMWA - metal-water reaction was not stopped by node (fuel pin) melting as long as there was a supply of steam available. Even though there could be blockage which would interrupt steam flow axially to nodes above the lowest melted node, it was assumed that steam could flow radially to these nodes where oxidation would continue. Sensitivities of the results to this assumption show small effects on the total oxidation of zirconium whether metal-water reaction was stopped above the lowest melted node IMWA=2 or in each melted node, IMWA=1.
MELMOD - consistent with numerous other analyses, meltdown model A was used.
MWORNL - the Zr-steam oxidation rate was calculated using the following model features: (1) oxygen deprivation due to hydrogen blanketing and/or lack of steam, (2) automatic time step reduction and interactive solution for solid-state oxidation rate, (3) more representative geometric model for gaseous diffusion oxidation rate, (4) laminar/turbulent flow condition, (5) improved physical model (Urbanic - Heindrick) for solid state oxidation rate.
IAXC - axial heat conduction in fuel rods is included.
ICONV -complete Dittus-Boelter and forced laminar convection model with calculated gas properties was used.
IRAD - radiation heat transfer, including core-to-water, core-to-upper gridplate and pin-to-pin radiation interchanges were included. The inclusion of pin-to-pin radiation heat transfer produces a smoothing of the core temperature distribution, more rapid heating of the cooler nodes, extension of core meltdown by a few minutes and an increase in the metal water reaction.

4.2 M-C-T Input

The M-C-T code consists of three distinct modules, each performing a separate analytical function. Thus, the M-Module calculates the gas flows, gas temperatures and structures temperatures for the primary system; the C-module calculates the source rates of the different

radionuclide species; and the T-module calculates the deposition rates of the different radionuclide species on the primary system surfaces, and communicates this information to the M-module to account for the heating of structures by the deposited material. Therefore, the input to M-C-T is organized into three parts as shown in Tables 4.4 and 4.5. There, the input for the TMLB, and the Pump Seal LOCA are listed and the breakpoints in inputs for the different modules are clearly shown.

The primary system was modeled by dividing it into specific control volumes. These volumes were chosen to represent the physical distinctions which actually exist. Thus the hot leg was modeled as Volume 3, and the surge line, being separate from the hot leg, as Volume 4, while the pressurizer was modeled as Volume 5. The control volumes for the TMLB Sequence and the Pump Seal LOCA are shown on Figures 4.1 and 4.2 respectively.

The complexity of the upper plenum with respect to heat transfer and temperature response has been modeled by dividing it into four distinct heat structures, according to such geometric parameters as openings in the guide tubes, part length vs. full length performation, and material thicknesses. The upper core plate, upper support structure, upper core barrel and support comprise heat structure 1. The support columns comprise heat structure 2 and guide tubes comprise the remainder of the heat structures. Since flow rates are not a factor in the portion of the upper plenum between the upper support structure and the reactor head, that section of the upper plenum was not modeled.

As Figures 4.1 and 4.2 indicate, the control volumes are connected serially, meaning that the models assume no parallel flows. Under actual TMLB conditions, however, some minimal flow into the steam generators would be expected, especially during the periods of low gas flows out of the PORV. This flow is expected to have little or no effect on fission product deposition. For the other accident sequence, Pump Seal LOCA, this limitation does not apply.

In the case of the Pump Seal LOCA, blowdown through all four loops was modeled by analyzing the system behavior in one loop, and extrapolating that behavior to the overall system.

4.3 MATADOR II Input

The input into the MATADOR II code consists of control parameters, containment thermal - hydraulic data, containment geometric parameters, and fission product inventories and source rates. The analytical model employed for the IP-3 analysis is depicted in Figure 4.3.

The IP-3 containment is modeled as a single volume which obtains fission product sources from the primary system and core-concrete interaction. At containment failure, the containment contents were assumed to be released as a "puff." Tables 4.6 and 4.7 list the MATADOR II input for the TMLB and Pump Seal LOCA, respectively. In both cases, containment failure at 24 hours was assumed, even though containment failure was calculated to occur long after the assumed 24 hours.

Table 4.1 - IP-3 Plant-Data Input to MARCH 2.0

SYSTEM OR COMPONENT	PARAMETERS INCLUDED
General containment data	Total volume; number of compartments; volume and dimensions of compartments; initial pressure, temperature, and humidity.
Heat sink	Number and compartment location of heat-sink slabs; materials in slab, including density, heat capacity, and thermal conductivity; heat-transfer area, thickness, and heat-transfer coefficient for the liner-concrete interface.
Ice condenser (not applicable)	Mass of ice; temperature of ice; temperatures of water drained from ice bed; temperature of gas leaving ice bed.
Suppression pool (not applicable)	Mass of water; temperature of water; water volume; air volume.
Containment floor (for core-concrete interactions)	Thickness density, thermal conductivity, temperature, and composition of concrete containment floor.
ECC tanks	Pressure, temperature, and water mass of accumulators and/or upper head injection tanks.
ECC pumps	Start time, nominal flow rate, nominal and shut-off pressure of all pumps, including high-pressure injection, safety injection, low-head pumps, and any additional pumps; minimum sump inventory and temperature to avoid pump cavitation.
ECC heat exchangers	Heat-exchanger capacity; primary and secondary flow rates and temperatures for ECC and containment-spray heat exchangers.
Containment coolers	Number and location of coolers; air-flow rate and inlet temperature; secondary flow rate and inlet temperature.

Table 4.1 (Continued)

SYSTEM OR COMPONENT	PARAMETERS INCLUDED
Containment sprays	Flow rate and spray-drop diameter of containment-spray system.
Auxiliary feedwater	Flow, temperature, and start time of auxiliary feedwater pumps.
Water-supply	Mass of water in condensate-storage tank; mass of water in the refueling-water storage tank (RWST); fractional value of RWST to start recirculation of ECC and containment sprays; minimum sump mass to avoid cavitation.
Core	Initial thermal power; total number of fuel rods in core; active fuel height; liquid level; mass of UO_2, Zircaloy, and miscellaneous metal; fuel-rod diameter; fuel-pellet diameter; hydraulic diameter; cladding thickness; density, conductivity; and heat capacity of core material; peaking factors.
Vessel	Core diameter; flow area; cross-sectional area; mass, heat capacity, temperature, and heat-transfer area of internal structures; mass, diameter, and thickness of bottom head; location and size of leaks.
Reactor-coolant system	Volume; initial primary steam volume; pressure; safety-relief-valve pressure setpoint and rated capacity.
Steam generator	Initial mass of water in steam generator; volume of steam generator; setpoint of secondary steam-generator relief valve.

TABLE 4.2 MARCH 2.0 INPUT FOR THE IP-3 TMLB SEQUENCE

```
100=   51768001TMLBP001IP-3 TMLBP DELAYED CONTAINMENT FAILURE
110= &CHANGE
120= ACBRK=-1.0,CPSTP=500.,FDRP=-1.,HIMX=-1.,HIOX=-1.,ID=51768001,
130= IFISH=-1,
140= IFPM=10,IFPV=10,IGASX=10,IHOTX=10,IPLOT=0,IS=10,JS=0,LST7=1,
150= MEL=10,
160= NCRST=1,
170= NCT7=1,PFAIL=-1.,PRST=149.,TFX=-1.,TMX= -1.,TRST=1440.,WALLX=-1.,
180= NCT20=1,NCT12=1,NCT25=1,NCT30=1,
190= &END
200= TMLBP PUMP SEAL INTACT - IP 3
210= &NLMAR
220= CMDN=0.15,CMHI=.167,CMHZ=.138,CMLO=.0003,CMON=.148,CMUP=.125,
230= CMXX=.148,
240= DTINIT=.02,HIG=.55,HIOXY=.05,H2DIST(1)=140.,H2DN=.09,H2HI=.10,
250= H2HZ=.06,
260= H2LO=.0001,H2ON=.08,H2UP=.041,H2VO=352.8,H2VX=11650.,H2XX=.08,
270= IBLDF=0,IBLDI=1,IBLDP=50,IBRK=0,IBURN=-1,IBURNJ=1,IBURNL=1,
280= IBURNM=1,
290= ICBRK=1,ICE=0,ICKV=0,IECC=0,IFPSM=2,IFPSV=2,IPDEF=0,IPDTL=7,
300= IPLOT=3,
310= ISPRA=0,
320= ITRAN=1,IU=-0,IXPL=0,NINTER=60,NPAIR=0,TAP=2.6E6,TIME=0.,
330= VOLC=2.61E6,
340= IGNITE(1)=10*0,
350= &END
360= &NLINTL
370= &END
380= IRON    CONCRETE
390= DOME    CYLINDERMISC. FECONCRETEWET WALLS
400=
410= &NLSLAB
420= DEN(1)=487.,157.,DTDX(1)=2*0.,HC=.133,.238,HIF(1)=2*100.,
430= IVL(1)=4*1,
440= IVR(1)=4*1,
450= IVL(5)=1,IVR(5)=1,MAT1(1)=4*1,MAT2(1)=4*2,MAT1(4)=2,MAT2(3)=1,
460= MAT1(5)=1,
470= MAT2(5)=1,NMAT=2,NNO1(1)=2*3,NNO2(1)=2*9,NNO1(3)=3,8,NNO2(3)=2*0
480= NNO1(5)=3,
490= NNO2(5)=0,NOD(1)=1,4,5,12,NSLAB=5,SAREA(1)=30138.,64423.,34000.,
500= 61000.,36904.,
510= TC(1)=25.,.8,TEMP(1)=38*110.,IPRINT=0,
520= X(1)=0.,.015,.03,.04,.06,.1,.18,.34,.66,1.3,2.58,3.5,
530= X(13)=0.,.015,.03,.04,.06,.1,.18,.34,.66,1.3,2.58,4.5,
540= X(25)=.0,.02,.04166,
550= X(28)=.0,.01,.03,.07,.15,.31,.63,1.,
560= X(36)=0.,.041,.083,
570= &END
580= &NLECC
590= ACMO=173000.,CSPRC=.023,DTSUB=-100.,ECCRC=.023,NP=0,P(1)=0.,
600= PACMO=662.,PHH=0.,
```

TABLE 4.2 (CONTINUED)

```
 610= PHLO=0.,PLH=0.,PLO(1)=0.,PLLO=0.,PSIS=1463.,PSLO=0.,PUHIO=662.,
 620= RWSTM=2.89E6,
 630= STP(1)=1.0E6,STPHH=1.0E6,STPLH=1.0E6,STPSIS=1.0E6,TACM=125.,
 640= TM(1)=0.,
 650= TMHH=0.,
 660= TMLH=0.,TMSIS=0.,TRWST=120.,TUHI=580.,UHIO=0.,WEC(1)=0.,
 670= WHH1=0.,WLH1=0.,
 680= WSIS1=-650.,WTCAV=0.,
 690= &END
 700= &NLECX
 710= &END
 720= &NLCSX
 730= &END
 740= &NLCOOL
 750= &END
 760= &NLMACE
 770= AREA(1)=23580.,AVBRK=7.07,CVBRK=.583,
 780= C1(1)=10000.,
 790= C2(1)=.583,
 800= C3(1)=.785,C4(1)=0.,DCF=1.,DCFICE=1.,DTO=.05,DTPNT=30.,DTS=1440.,
 810= FALL=1.,FSPRA=0.,
 820= HMAX=280.,HUM(1)=.5,IBETA=0,ICECUB=0,IDRY=1,IVENT= 0 ,
 830= IWET=2,JRPV1=1,JRPV2=1,
 840= JRPV3=1,N=1,NC(1)=1,NCAV=-1,NCUB=1,NRPV1=1,
 850= NRPV2=1,NS(1)=2,
 860= NSMP=1,NSMP2=1,NT(1)=7,PO=15.0,STPECC=1.E6,
 870= STPSPR=1.E6,
 880= TEMPO(1)=120.,TSTM=105.,TVNT1=10000.,TVNT2=10000.,
 890= TWTR=190.,TWTR2=130.,
 900= VC(1)=2.61E6,VCAV=9857.,VDRY=0.,VFLR=6441.,VTORUS=0.,
 910= WPOOL=0.,
 920= TPOOL=100.,WVMAKS=0.,WVMAX=0.,WICE=0.,TICE=0.,PVNT=0.,
 930= &END
 940= &NLBOIL
 950= AB(1)=16*0.,ABR(1)=-1,ABRK=0.,ACOR=54.39,AH(1)=100.,188.,
 960= 158000.,150.,150.,340.,
 970= ANSK=0.,ASR(1)=-1.,ASRV=0.,AR(1)=50.,.78,36.,0.,-2.,-4.,
 980= ATOT=105.5,CM(1)=1200.,
 990= 912.,427235.,4000.,7886.0,7262.,CLAD=.001815,CONB=5.,
1000= CSRV=5966.67,
1010= D=.03517,
1020= DC=10.,DD(1)=.3,1.,.065,.1,.5,.443,DF=.03049,DH=.05069,
1030= DHEAT(1)=200*0.,
1040= DPART=.0164,DTK=1000.,DTPN=-15.,DTPNTB= 15.,DUO2=.03049,
1050= F(1)=.47,.49,.53,.64,.77,.95,1.12,1.27,1.35,1.44,1.47,1.5,1.5,
1060= 1.47,1.44,1.35,1.27,1.12,.95,.77,.64,.53,.49,.47,
1070= FDCR=.5,FCOL=.75,FDROP=.75,FLD=0.,FM=0.,FPV(1)=2*.05,.9,FR=0.,
1080= FULSG=307235.,FZMCR=1.,FZOCR=1.,FZOS1=0.,F12=.445,H=12.,
1090= HO=115.67,HW=300.,
1100= IBEDC=3,IBEDS=3,ICON=1,IDECAY=0,IFP=2,IHC=0,IHR=1,IMWA=3,
1110= IMZ=100,
1120= ISAT=0,ISG=3,
1130= ISTM=0,ISTR=3,KRPS=0,MELMOD=1,MWORNL=1,NDTM=100000,NDZ=24,
1140= NDZDRP=2,NNT=43425,
```

TABLE 4.2 (CONTINUED)

```
1150= NR=39351,PF(1)=1.09,1.11,1.1,1.1,1.12,1.11,1.09,1.1,1.01,.75,
1160= PORB=.4,
1170= PSET=2350.,
1180= PSG=1100.,PSR(1)=16*-1.,PVSL=2265.,QPUMP1=1.E-10,QPUMP2=1.E-10,
1190= Q235U=200.,
1200= QZERO=10.32E9,
1210= RHOCU=54.1,R1=1,R2=10,R239U=0.8,TAFW=100.,TALF1=1.0E10,
1220= TALF2=1.0E10,
1230= TB(1)=16*1.E6,TCAV=1251,TDK=0.,TFAIL=1832.,TFEOO=600.0,
1240= TFUS=5320.,
1250= TGOO=572.0,
1260= TMAFW=1.E6,TMB=1.,TMELT=4130.,TMLEG(1)=3*1.E6,TMSG1=1.E6,
1270= TMSG2=1.E6,
1280= TMUP1=1.E6,
1290= TMUP2=1.E6,TMYBK=1.E6,TPM=1.,TPN=200.,TPUMP1=1.E6,TPUMP2=1.E6,
1300= TRPS=0.,
1310= TSB(1)=.25,TSCT(1)=0.,TT(1)=6*542.6,TT(3)=511.6,
1320= TSB(2)=.05,TSCT(2)=80.,TSB(3)=.50,TSCT(3)=100.,
1330= VF(1)=.047,.062,.083,.062,.062,.062,.083,.124,.166,.249,
1340= VOLP=12224.,
1350= VOLS=720.,WAFW=6.673E3,WATBH=48000.,WDED=30489.,WFE2=8000.,
1360= WMUP1=0.,
1370= WMUP2=0.,
1380= WTRSG=307235.,XOO=3.28E-6,YB=0.,YBR(1)=16*-1.,YBRK=0.000,
1390= YBRK2=1000.,
1390= YBRK2=1000.,
1400= YLEG=20.,
1410= YLEG2=1000.,YSR(1)=16*-1.,YSRV=37.65,YT=0.,IGRID1=1,IGRID2=0,
1420= IHEAD=-1,
1430= ISRV=1,
1440= WCST=5.E6,TFAIL2=1832.,IPRIMP=0,NZPLT(1)=7*0,NRPLT(1)=7*0,
1450= &END
1460= &NLRAD
1470= IAXC=1,ICONV=1,IRAD=2,ECROS=.7,ELONG=.214,ESTRU=.6,EWAT=.95,
1480= PITCH=.04692,
1490= TFAILB=1832.,VIEW=2.0,WBAR=4770.,
1500= &END
1510= &NBWRIN
1520= &END
1530= &NLHEAD
1540= COND=5.,DBH=14.72,E1=.8,E2=.5,FOPEN=0.,THICK=.443,THKF=10.,
1550= TMLT=4130.,TVSL=500.,FHEAD=1.,SIGF=50000.,
1560= WFEC=9800.,WGRID=73706.,WHEAD=67865.,WUO2=220300.,WZRC=47400.,
1570= &END
1580= &NLHOT
1590= ACAV=254.0,CON=5.,DP=.12,FLRMC=0.,IDBED=0,IHOT=101,MWR=1,
1600= NSTOP=1000,
1610= PORO=.4,
1620= TCORM=3275.,TMS=2600.,TPOOLH=254.93,TQNCH=0.,WTR=0.,
1630= &END
1640= &NLINTR
1650= CAYC=.015,CPC=1.45,DENSC=2.4,DPRIN=3600.,DT=.5,
1660= EPSI(1)=.5,.5,8*0.,
1670= FC1=.0,FC2=.04,
```

TABLE 4.2 (CONTINUED)

```
1680= FC3=.61,FC4=.024,FIOPEN=.5,FRCW=1.,HIM=.01,HIO=.01,IGAS=0,
1690= IWRC=0,
1700= NEPS=2,R=6000.,
1710= RBR=.135,RO=312.6,TAUL=.5,TAUS=5.,TDC=1375.,
1720= TEPS(1)=0.,3.6E7,8*0.,
1730= TIC=293.0,
1740= TF=259200.,TPRIN=0.,WALL=300.,ZF=1000.,
1750= &END
```

TABLE 4.3 MARCH 2.0 INPUT FOR THE IP-3 PUMP SEAL LOCA SEQUENCE

```
100=  51768001SEALOCA1IP-3 SEALS DELAYED CONTAINMENT FAILURE
110= &CHANGE
120= ACBRK=-1.0,CPSTP=300.,FDRP=-1.,HIMX=-1.,HIOX=-1.,ID=51768002,
130= IFISH=-1,
140= IFPM=10,IFPV=10,IGASX=10,IHOTX=10,IPLOT=0,IS=10,JS=0,LST7=1,
150= MEL=10,
160= NCRST=1,
170= NCT7=1,PFAIL=-1.,PRST=149.,TFX=-1.,TMX= -1.,TRST=1440.,WALLX=-1.,
180= NCT20=1,NCT12=1,NCT25=1,NCT30=1,
190= &END
200= TMLBP PUMP SEAL LOCA
210= &NLMAR
220= CMDN=0.15,CMHI=.167,CMHZ=.138,CMLO=.0003,CMON=.148,CMUP=.125,
230= CMXX=.148,
240= DTINIT=.02,HIG=.55,HIOXY=.05,H2DIST(1)=140.,H2DN=.09,H2HI=.10,
250= H2HZ=.06,
260= H2LO=.0001,H2ON=.08,H2UP=.041,H2VO=352.8,H2VX=11650.,H2XX=.08,
270= IBLDF=0,IBLDI=1,IBLDP=50,IBRK=0,IBURN=-1,IBURNJ=1,IBURNL=1,
280= IBURNM=1,
290= ICBRK=1,ICE=0,ICKV=-1,IECC=0,IFPSM=2,IFPSV=2,IPDEF=0,IPDTL=7,
300= IPLOT=3,
310= ISPRA=0,
320= ITRAN=1,IU=-0,IXPL=0,NINTER=60,NPAIR=0,TAP=2.6E6,TIME=0.,
330= VOLC=2.61E6,
340= IGNITE(1)=10*0,
350= &END
360= &NLINTL
370= &END
380= IRON    CONCRETE
390= DOME    CYLINDERMISC. FECONCRETEWET WALLS
400=
410= &NLSLAB
420= DEN(1)=487.,157.,DTDX(1)=2*0.,HC=.133,.238,HIF(1)=2*100.,
430= IVL(1)=4*1,
440= IVR(1)=4*1,
450= IVL(5)=1,IVR(5)=1,MAT1(1)=4*1,MAT2(1)=4*2,MAT1(4)=2,MAT2(3)=1,
460= MAT1(5)=1,
470= MAT2(5)=1,NMAT=2,NNO1(1)=2*3,NNO2(1)=2*9,NNO1(3)=3,8,NNO2(3)0,
480= NNO1(5)=3,
490= NNO2(5)=0,NOD(1)=1,4,5,12,NSLAB=5,SAREA(1)=30138.,64423.,34000.,
500= 61000.,36904.,
510= TC(1)=25.,.8,TEMP(1)=38*110.,IPRINT=0,
520= X(1)=0.,.015,.03,.04,.06,.1,.18,.34,.66,1.3,2.58,3.5,
530= X(13)=0.,.015,.03,.04,.06,.1,.18,.34,.66,1.3,2.58,4.5,
540= X(25)=.0,.02,.04166,
550= X(28)=.0,.01,.03,.07,.15,.31,.63,1.,
560= X(36)=0.,.041,.083,
570= &END
580= &NLECC
590= ACMO=173000.,CSPRC=.023,DTSUB=-100.,ECCRC=.023,NP=0,P(1)=0.,
600= PACMO=662.,PHH=0.,
```

TABLE 4.3 (CONTINUED)

```
 610= PHLO=0.,PLH=0.,PLO(1)=0.,PLLO=0.,PSIS=1463.,PSLO=0.,PUHIO=662.,
 620= RWSTM=2.89E6,
 630= STP(1)=1.0E6,STPHH=1.0E6,STPLH=1.0E6,STPSIS=1.0E6,TACM=125.,
 640= TM(1)=0.,
 650= TMHH=0.,
 660= TMLH=0.,TMSIS=0.,TRWST=120.,TUHI=580.,UHIO=0.,WEC(1)=0.,
 670= WHH1=0.,WLH1=0.,
 680= WSIS1=-650.,WTCAV=0.,
 690= &END
 700= &NLECX
 710= &END
 720= &NLCSX
 730= &END
 740= &NLCOOL
 750= &END
 760= &NLMACE
 770= AREA(1)=23580.,AVBRK=7.07,CVBRK=.583,
 780= C1(1)=10000.,
 790= C2(1)=.583,
 800= C3(1)=.785,C4(1)=0.,DCF=1.,DCFICE=1.,DTO=.05,DTPNT=30.,DTS=4320.,
 810= FALL=1.,FSPRA=0.,
 820= HMAX=280.,HUM(1)=.5,IBETA=0,ICECUB=0,IDRY=1,IVENT= 0 ,
 830= IWET=2,JRPV1=1,JRPV2=1,
 840= JRPV3=1,N=1,NC(1)=1,NCAV=-1,NCUB=1,NRPV1=1,
 850= NRPV2=1,NS(1)=2,
 860= NSMP=-1,NSMP2=1,NT(1)=7,PO=15.0,STPECC=1.E6,
 870= STPSPR=1.E6,
 880= TEMPO(1)=120.,TSTM=105.,TVNT1=10000.,TVNT2=10000.,
 890= TWTR=190.,TWTR2=130.,
 900= VC(1)=2.61E6,VCAV=9857.,VDRY=0.,VFLR=6441.,VTORUS=0.,
 910= WPOOL=0.,
 920= TPOOL=100.,WVMAKS=0.,WVMAX=0.,WICE=0.,TICE=0.,PVNT=0.,
 930= &END
 940= &NLBOIL
 950= AB(1)=16*0.,ABR(1)=.0135,ABRK=0.0,ACOR=54.39,AH(1)=100.,188.,
 960= 158000.,150.,150.,340.,
 970= ANSK=0.,ASR(1)=.0,ASRV=0.,AR(1)=50.,.78,36.,0.,-2.,-4.,
 980= ATOT=105.5,CM(1)=1200.,
 990= 912.,427235.,4000.,7886.0,7262.,CLAD=.001815,CONB=5.,
1000= CSRV=5966.67,
1010= D=.03517,
1020= DC=10.,DD(1)=.3,1.,.065,.1,.5,.443,DF=.03049,DH=.05069,
1030= DHEAT(1)=200*0.,
1040= DPART=.0164,DTK=1000.,DTPN=-5.,DTPNTB= 5.,DUO2=.03049,
1050= F(1)=.47,.49,.53,.64,.77,.95,1.12,1.27,1.35,1.44,1.47,1.5,1.5,
1060= 1.47,1.44,1.35,1.27,1.12,.95,.77,.64,.53,.49,.47,
1070= FDCR=.5,FCOL=.75,FDROP=.75,FLD=0.,FM=0.,FPV(1)=2*.05,.9,FR=0.,
1080= FULSG=307235.,FZMCR=1.,FZOCR=1.,FZOS1=0.,F12=.445,H=12.,
1090= HO=115.67,HW=300.,
1100= IBEDC=3,IBEDS=3,ICON=1,IDECAY=0,IFP=2,IHC=0,IHR=1,IMWA=3,
1110= IMZ=100,
1120= ISAT=0,ISG=3,
1130= ISTM=0,ISTR=3,KRPS=0,MELMOD=1,MWORNL=1,NDTM=100000,NDZ=24,
1140= NDZDRP=2,NNT=43425,
```

TABLE 4.3 (CONTINUED)

```
1680= IWRC=0,
1690= NEPS=2,R=6000.,
1700= RBR=.135,R0=312.6,TAUL=.5,TAUS=5.,TDC=1375.,
1710= TEPS(1)=0.,3.6E7,8*0.,
1720= TIC=293.0,
1730= TF=259200.,TPRIN=0.,WALL=300.,ZF=1000.,
1740= &END
```

TABLE 4.3 (CONTINUED)

```
1150= NR=39351,FF(1)=1.09,1.11,1.1,1.1,1.12,1.11,1.09,1.1,1.01,.75,
1160= PORB=.4,
1170= PSET=2350.,
1180= PSG=1100.,PSR(1)=25000.,PVSL=2265.,QPUMP1=1.E-10,QPUMP2=1.E-10,
1190= Q235U=200.,
1200= QZERO=10.32E9,
1210= RHOCU=54.1,R1=1,R2=10,R239U=0.8,TAFW=100.,TALF1=1.0E10,
1220= TALF2=1.0E10,
1230= TB(1)=30.,TCAV=1251,TDK=0.,TFAIL=1832.,TFEOO=600.0,
1240= TFUS=5320.,
1250= TGOO=572.0,
1260= TMAFW1.E6,TMB=3.,TMELT=4130.,TMLEG(1)=3*1.E6,TMSG1=1.E6,
1270= TMSG2=1.E6,
1280= TMUP1=1.E6,
1290= TMUP2=1.E6,TMYBK=1.E6,TPM=1.,TPN=200.,TPUMP1=1.E6,TPUMP2=1.E6,
1300= TRPS=0.,
1310= TSB(1)=.25,TSCT(1)=0.,TT(1)=6*542.6,TT(3)=511.6,
1320= VF(1)=.047,.062,.083,.062,.062,.062,.083,.124,.166,.249,
1330= VOLP=12224.,
1340= VOLS=720.,WAFW=6.673E3,WATBH=48000.,WDED=30489.,WFE2=8000.,
1350= WMUP1=0.,
1360= WMUP2=0.,
1370= WTRSG=307235.,XOO=3.28E-6,YB=0.,YBR(1)=16.0,YBRK=0.0,
1380= YBRK2=1000.,
1390= YLEG=20.,
1400= YLEG2=1000.,YSR(1)=16*-1.,YSRV=37.65,YT=0.,IG
1400= YLEG2=1000.,YSR(1)=16*-1.,YSRV=37.65,YT=0.,IGRID1=1,IGRID2=0,
1410= IHEAD=-1,
1420= ISRV=1,
1430= WCST=5.E6,TFAIL2=1832.,IPRIMP=0,NZPLT(1)=7*0,NRPLT(1)=7*0,
1440= &END
1450= &NLRAD
1460= IAXC=1,ICONV=1,IRAD=2,ECROS=.7,ELONG=.214,ESTRU=.6,EWAT=.95,
1470= PITCH=.04692,
1480= TFAILB=1832.,VIEW=2.0,WBAR=4770.,
1490= &END
1500= &NBWRIN
1510= &END
1520= &NLHEAD
1530= COND=5.,DBH=14.72,E1=.8,E2=.5,FOPEN=0.,THICK=.443,THKF=10.,
1540= TMLT=4130.,TVSL=500.,FHEAD=1.,SIGF=50000.,
1550= WFEC=9800.,WGRID=73706.,WHEAD=67865.,WUO2=220300.,WZRC=47400.,
1560= &END
1570= &NLHOT
1580= ACAV=254.0,CON=5.,DP=.12,FLRMC=0.,IDBED=0,IHOT=101,MWR=1,
1590= NSTOP=1000,
1600= PORO=.4,
1610= TCORM=3275.,TMS=2600.,TPOOLH=254.93,TQNCH=0.,WTR=0.,
1620= &END
1630= &NLINTR
1640= CAYC=.015,CPC=1.45,DENSC=2.4,DPRIN=3600.,DT=.5,
1650= EPSI(1)=.5,.5,8*0.,
1660= FC1=.0,FC2=.04,
1670= FC3=.61,FC4=.024,FIOPEN=.5,FRCW=1.,HIM=.01,HIO=.01,IGAS=0,
```

TABLE 4.4 M-C-T INPUT FOR THE IP-3 TMLB SEQUENCE

M-MODULE INPUT

```
100= -1
110= 0
120= 1
130= 1.
140= 0
150= 1
160= 744
170= 779
180= 0
190= 0
200= 10000
210= 0
220= 6
230= 0
240= 1
250= 572. 665.93 1241. 12.08 12.08 4 8069.8 .19 690.8 1.693 99.64
260= 572. 665.93 86.68 16.33 16.33 1 1415.15 .208 124. 2.42 4.59
270= 572. 665.93 51.85 71.7 71.7 1 1250.13 .104 215.9 .96 .723
280= 572. 665.93 1808. 50.14 50.14 1 22054.0 .36 1111.4 6.51 38.13
290= 350. 665.93 60.22 77.5 77.5 1 449.17 .0338 242. .995 .777
300= 120. 665.93 1. 1. 1. 1 1. 1. 1. 1. 1.
310= 250.
320= 0 4.5
330= 1 4.5
340= 1 4.5
350= 0 4.5
360= 0 4.5
370= 0 4.5
380= 572. 8069.8 690.8 1.693 99.64 12.08 .19
390= 572. 2916.0 826.13 .266 3.694 12.1 .0417
400= 572. 587.5 107.55 .412 1.575 12.1 .125
410= 572. 2900.4 1528.7 .1241 14.55 12.1 .0417
420= 0. 0. 0.
430= 0. 0. 0.
440= 0. 0. 0.
450= 0. 0. 0.
460= 0. 0. 0.
470= 0. 0. 0.
480= 2388.
490= 0 1 0 0 0 0 0
500= 0 0 1 0 0 0 0
510= 0 0 0 1 0 0 0
520= 0 0 0 0 1 0 0
530= 0 0 0 0 0 1 0
540= 0 0 0 0 0 0 1
550= 1. 1. 1. 1. 1. 1.
560= 0 0 0 0 0 0
570= 18
580= 744 753 762 771 780 739 798 807 816 825 834 843 852 861 870 875
590= 879 882 885
600= 0
610= 0. 10.32E9 7.88E5
```

TABLE 4.4 (CONTINUED)

```
 620= 3
 630= 5
 640= 100. 10000. 1000000.
 650= .093 .099 .099 .675 .061
 660= .16 .033 .033 .722 .029
 670= .043 .057 .057 .875 .0093
 680= 0. 0. 0. 0. 0. 0. 0.
                              C-MODULE INPUT
 690= 129. 182.001 129.
 700= 10
 710= 24
 720= 10
 730= 1.09 1.11 1.1 1.1 1.12 1.11 1.09 1.1 1.01 .75
 740= .47 .49 .53 .64 .77 .95 1.12 1.27 1.35 1.44 1.47 1.5 1.5 1.47
 750= 1.44 1.35 1.27 1.12 .95 .77 .64 .53 .49 .47
 760= .047 .062 .083 .062 .062 .062 .083 .124 .166 .249
 770= 167.32 13.83 298.95 15.42 28.77 0. 1. 70.44 324.2 247. 101009.5
 780= 21500. 205.60 64215. 178.41 55.21 2232. 419. 140.
                              T-MODULE INPUT
 790= TMLBP-PUMP SEALS INTACT
 800= 10000.
 810= 13.2
 820= 0
 830= 0
 840= 0.0 3180. 2.0
 850= .0001 .1 .1
 860= 5 6 5 2
 870= I2       CSI      CSOH     AEROSOL TE
 880= 0 0 0 0 0 0
 890= 1 0 0 0 0 0
 900= 0 1 0 0 0 0
 910= 0 0 1 0 0 0
 920= 0 0 0 1 0 0
 930= 0 0 0 0 1 0
 940= 3
 950= 1 1 0
 960= 1 1 1
 970= 1 1 1
 980= 1 1 0
 990= 1 1 0
1000= 0 0 0
1010= 1
1020= 1
1030= 1
1040= 1
1050= 1
1060= 1
1070= 0
1080= 1 1 1 1 1 0
1090= 1.
1100= 1.
1110= 1.
1120= 1.
1130= 1.
1140= 1.
1150= 1.
1160= 1
```

TABLE 4.4 (CONTINUED)

```
1170= 12.08 1.693 99.644 99.644 12.08
1180= 16.33 2.42 4.59 62. 16.33
1190= 71.7 .96 .723 107.95 71.7
1200= 50.14 6.51 38.13 38.13 50.14
1210= 77.5 .995 .777 121. 77.5
1220= 1.E4 1.0 1.E4 1.E4 1.E4
1230= 0 0 0 0 0
1240= 1 0 0 0 0 0
1250= 1 0 0 0 0
1260= 1 0 0 0 0 0
1270= 1 0 0 0 0
1280= 1 0 0 0 0 0
1290= 1 0 0 0 0
1300= 1 0 0 0 0 0
1310= 0 1 0 0 0
1320= 1 0 0 0 0 0
1330= 1 0 0 0 0
1340= 1 0 0 0 0 0
1350= 1
1360= 0.
1370= 1.7
1380= 1
1390= 0.
1400= .05
1410= 3. 3. 3. 3. 3. 3.
```

TABLE 4.5 M-C-T INPUT FOR THE IP-3 PUMP SEAL LOCA SEQUENCE

M-MODULE INPUT

```
100= -1
110= 0
120= 1
130= 0.25
140= 0
150= 1
160= 418
170= 488
180= 0
190= 0
200= 10000
210= 0
220= 7
230= 0
240= 1
250= 572. 656.27 1241. 12.08 12.08 4 8069.8 .19 690.8 1.693 99.64
260= 572. 656.27 86.68 16.33 16.33 1 1415.15 .208 124. 2.42 4.59
270= 572. 656.27 246.42 3.77 3.77 1 1835.150 .217 109.1 4.52 37.60
280= 556. 656.27 700.86 59.53 59.53 1 20382.82 .00417 39500. .096 10.674
290= 542. 656.27 136.02 24.26 24.26 1 2227.24 .198 196.6 2.58 5.24
300= 542. 656.27 192. 6.48 6.48 1 4895. .5 160.2 4.79 19.4
310= 120. 572. 1. 1. 1. 1 1. 1. 1. 1. 1.
320= 250.
330= 0 1.
340= 1 4.5
350= 1 4.5
360= 0 1.
370= 1 4.5
380= 1 4.5
390= 0 1.
400= 572. 8069.8 690.8 1.693 99.64 12.08 .19
410= 572. 2916.0 826.13 .266 3.694 12.1 .0417
420= 572. 587.5 107.55 .412 1.575 12.1 .125
430= 572. 2900.4 1528.7 .1241 14.55 12.1 .0417
440= 0. 0. 0.
450= 0. 0. 0.
460= 0. 0. 0.
470= 0. 0. 0.
480= 0. 0. 0.
490= 0. 0. 0.
500= 0. 0. 0.
510= 2242.
520= 0 1 0 0 0 0 0 0
530= 0 0 1 0 0 0 0 0
540= 0 0 0 1 0 0 0 0
550= 0 0 0 0 1 0 0 0
560= 0 0 0 0 0 1 0 0
570= 0 0 0 0 0 0 1 0
580= 0 0 0 0 0 0 0 1
590= 1. .25 1. 1. 1. 1. 1.
600= 0 0 0 0 0 0 0
```

TABLE 4.5 (CONTINUED)

```
 610= 18
 620= 417 453 489 507 525 543 561 579 597 615 633 651 669 687 702 720
 630= 738 756 770
 640= 0
 650= 0. 10.32E9 7.88E5
 660= 3
 670= 5
 680= 100. 10000. 1000000.
 690= .093 .099 .099 .675 .061
 700= .16 .033 .033 .722 .029
 710= .043 .057 .057 .875 .0093
 720= 0. 0. 0. 0. 0. 0. 0. 0.
                          C-MODULE INPUT
 730= 98.0 166.92 98.0
 740= 10
 750= 24
 760= 10
 770= 1.09 1.11 1.1 1.1 1.12 1.11 1.09 1.1 1.01 .75
 780= .47 .49 .53 .64 .77 .95 1.12 1.27 1.35 1.44 1.47 1.5 1.5 1.47 1.44
 790= 1.35 1.27 1.12 .95 .77 .64 .53 .49 .47
 800= .047 .062 .083 .062 .062 .062 .083 .124 .166 .249
 810= 167.32 13.83 298.95 15.42 28.77 0. 1. 70.44 324.17 247.0 101009.5
 820= 21500. 205.60 64215. 178.41 55.21 2232. 419. 140.
                          T-MODULE INPUT
 830= TMLBP-PUMP SEALS FAIL AT 30 MINUTES INTO ACCIDENT
 840= 30000.
 850= 17.21
 860= 0
 870= 0
 880= 0. 4129.5 2.0
 890= .0001 .1 .1
 900= 5 7 5 2
 910= I2       CSI      CSOH     AEROSOL TE
 920= 0 0 0 0 0 0 0
 930= 1 0 0 0 0 0 0
 940= 0 1 0 0 0 0 0
 950= 0 0 1 0 0 0 0
 960= 0 0 0 1 0 0 0
 970= 0 0 0 0 1 0 0
 980= 0 0 0 0 0 1 0
 990= 3
1000= 1 1 0
1010= 1 1 1
1020= 1 1 0
1030= 1 0 0
1040= 1 1 1
1050= 1 1 1
1060= 0 0 0
1070= 1
1080= 1 1 1 1 1 1 0
1090= 1 1 1 1 1 1 0
1100= 1. 4. 1. 1. 1. 1. 1.
1110= 1
1120= 12.08 1.693 99.644 99.644 12.08
1130= 65.32 9.68 18.36 248. 65.32
```

TABLE 4.5 (CONTINUED)

```
1140= 15.08 18.08 150.4 436. 15.08
1150= 238.12 .2572 42.696 42.696 238.12
1160= 97.04 10.32 20.96 393.2 97.04
1170= 25.92 19.16 77.6 320.4 25.92
1180= 1.E4 1.0 1.E4 1.E4 1.E4
1190= 0 0 0 0 0
1200= 1 0 0 0 0 0 0
1210= 1 0 0 0 0
1220= 1 0 0 0 0 0 0
1230= 1 0 0 0 0
1240= 1 0 0 0 0 0 0
1250= 1 0 0 0 0
1260= 1 0 0 0 0 0 0
1270= 0 1 0 0 0
1280= 1 0 0 0 0 0 0
1290= 1 0 0 0 0
1300= 1 0 0 0 0 0 0
1310= 1
1320= 0.
1330= 1.7
1340= 1
1350= 0.
1360= .05
1370= 3. 3. 3. 3. 3. 3. 3.
```

TABLE 4.6 MATADOR II INPUT FOR THE IP-3 TMLB SEQUENCE

```
100= 0
110= 1
120= 0.01
130= 10
131= 0. 0. 599.9 0. 600. 2.6389E-5 6.E4 2.6389E-5 9.E4 1.2121E-5 1.2E5 1.4167E-
132= 1.8E5 8.9744E-6 2.4E5 5.6945E-6 3.3E5 3.7037E-6 4.2E5 3.E-6
133= 5000. .125
140= TRAPMELT SIMULATION OF CONTAINMENT FP REMOVAL - TMLB CASE
150= 10000.
160= 83.88
170= 0
180= 0
190= 10910. 86400. 2.5
200= .0001 0.1 0.1
210= 8 2 5 2
220= I2      CSI       CSOH     AEROSOL TE       BA       RU       LA
230= 0 0
240= 1 0
250= 3
260= 1 1 1
270= 0 0 0
280= 1
290= 1 0
300= 1 0
310= 1. 1. 1. 1. 1. 1. 1.
320= 1
330= 182. 135. 1.43E4 23580. 182.
340= 1.E4 1. 1.E4 1.E4 1.E4
350= 2
360= 10910. 86410.
370= 0.0019 0.0019
380=  13
390= 10910. 10932. 11304. 13614. 17364. 25470. 38484. 49086. 57534.
400= 63000. 66900. 83520. 86880.
410= 55.93 90.38 80.26 70.94 65.76 67.13 64.84 64.54 64.87 65.19
420= 69.36 75.28 77.01
430= 13
440= 10910. 10932. 11304. 13614. 17364. 25470. 38484. 49086. 57534.
450= 63000. 66900. 83520. 86880.
460= 262.5 302.8 292.6 282.1 275.5 276.1 273.1 272.7 273.1 273.6
470= 324. 349. 355.4
480= 13
490= 10910. 10932. 11304. 13614. 17364. 25470. 38484. 49086. 57534.
500= 63000. 66900. 83520. 86880.
510= 238.4 251.55 283.5 280.5 274.5 275.3 272.5 272.2 272.6 273. 319.
520= 343.3 349.4
530= 2
540= 10910. 86410.
550= 14.7 14.7
560= 2
570= 10910. 86410.
580= 120. 120.
590= 2
600= 10910. 86410.
610= 120. 120.
```

TABLE 4.6 (CONTINUED)

```
 620= 1
 630= 10. 0. 0. 0. 0.
 640= 0. 0. 0. 0. 0.
 650= 1
 660= 2.23E4 1.138E3 0. 0. 0.
 670= 0. 0. 0. 0. 0.
 680= 1
 690= 1.214E5 3.37E3 0. 0. 0.
 700= 0. 0. 0. 0. 0.
 710= 1
 720= 0. 6.15E4 0. 0. 0.
 730= 0. 0. 0. 0. 0.
 740= 1
 750= 3.034 1.933E-7 0. 0. 0.
 760= 0. 0. 0. 0. 0.
 770= 1
 780= 0. 8.36E2 0. 0. 0.
 790= 0. 0. 0. 0. 0.
 800= 1
 810= 0. 6.94E2 0. 0. 0.
 820= 0. 0. 0. 0. 0.
 830= 1
 840= 0. 1.66 0. 0. 0.
 850= 0. 0. 0. 0. 0.
 860= 0 0
 870= 0 0 0 0 0
 880= 0 0
 890= 0 0 0 0 0
 900= 0 0
 910= 0 0 0 0 0
 920= 1 0
 930= 0 1 0 0 0
 940= 20
 950= .109E5 .197E5 .209E5 .221E5 .233E5 .245E5 .257E5 .269E5 .281E5 .305E5
 960= .329E5 .365E5 .377E5 .389E5 .401E5 .413E5 .425E5 .461E5 .485E5 .865E5
 970= 0. 1.638 17.15 37.87 51.52 112.7 130.2 28.21 22.4 28.98
 980= 35.21 43.19 48.3 49.63 56.98 27.79 13.58 5.6 5.53 0.
 990= 0 0
1000= 0 0 0 0 0
1010= 1 0
1020= 0 1 0 0 0
1030= 10
1040= .109E5 .197E5 .209E5 .221E5 .233E5 .245E5 .257E5 .269E5 .281E5 .865E5
1050= 0. 4.333E-2 9.59E-1 2.541 4.109 2.590 2.177 9.59E-3 0. 0.
1060= 1 0
1070= 0 1 0 0 0
1080= 8
1090= .109E5 .197E5 .209E5 .257E5 .329E5 .401E5 .485E5 .865E5
1100= 0. 0. 5.852E-8 9.03E-7 2.821E-3 3.43E-3 3.29E-4 0.
1110= 1 0
1120= 0 1 0 0 0
1130= 14
```

TABLE 4.6 (CONTINUED)

```
1140= .109E5 .197E5 .209E5 .221E5 .233E5 .245E5 .257E5 .269E5 .305E5 .365E5
1150= .401E5 .413E5 .485E5 .865E5
1160= 0. 3.565E-4 4.27E-2 3.087E-1 3.367E-1 6.202E-1 1.729E-1 1.162E-2 5.803E-3
1170= 8.68E-3 1.148E-2 1.393E-2 3.85E-3 0.
1180= 1 0
1190= 1
1200= 0.
1210= 2.4
1220= 1
1230= 0.
1240= .40
1250= 3. 3.
```

TABLE 4.7 MATADOR II INPUT FOR THE IP-3 PUMP SEAL LOCA SEQUENCE

```
100= 0
110= 1
120= 0.01
130= 10
131= 0. 0. 599.9 0. 600. 2.6389E-5 6.E4 2.6389E-5 9.E4 1.2121E-5 1.2E5 1.4167E-6
132= 1.8E5 8.9744E-6 2.4E5 5.6945E-6 3.3E5 3.7037E-6 4.2E5 3.E-6
133= 5000. .125
140= TRAPMELT SIMULATION OF CONTAINMENT FP REMOVAL - SEAL LOCA CASE
150= 10000.
160= 84.88
170= 0
180= 0
190= 10010. 86400. 2.5
200= .0001 0.1 0.1
210= 8 2 5 2
220= I2      CSI       CSOH     AEROSOL TE       BA       RU       LA
230= 0 0
240= 1 0
250= 3
260= 1 1 1
270= 0 0 0
280= 1
290= 1 0
300= 1 0
310= 1. 1. 1. 1. 1. 1. 1.
320= 1
330= 182. 135. 1.43E4 23580. 182.
340= 1.E4 1. 1.E4 1.E4 1.E4
350= 2
360= 10010. 86410.
370= 0.0019 0.0019
380=  13
390= 10010. 10026. 16302. 38160. 55290. 56676. 57996. 62040. 63960.
400= 64620. 69960. 77160. 86940.
410= 70.51 84.23 64.58 61.66 62.56 64.61 65.52 63.91 63.25 64.19 68.9 68.11
420= 69.45
430= 13
440= 10010. 10026. 16302. 38160. 55290. 56676. 57996. 62040. 63960. 64620.
450= 69960. 77160. 86940.
460= 281.4 296.6 273.8 269.2 272.7 297.6 308.4 285. 275.3 286.7 342.2 327.4
470= 337.7
480= 13
490= 10010. 10026. 16302. 38160. 55290. 56676. 57996. 62040. 63960.
500= 64620. 69960. 77160. 86940.
510= 244.33 254.56 272.78 268.61 272.22 287.23 272.1 275.94 273.92 275.12
520= 273.4 283.77 288.81
530= 2
540= 10010. 86410.
550= 14.7 14.7
560= 2
570= 10010. 86410.
```

TABLE 4.7 (CONTINUED)

```
 580= 120. 120.
 590= 2
 600= 10010. 86410.
 610= 120. 120.
 620= 1
 630= 10. 0. 0. 0. 0.
 640= 0. 0. 0. 0. 0.
 650= 1
 660= 1.313E3 8.444E3 0. 0. 0.
 670= 0. 0. 0. 0. 0.
 680= 1
 690= 3.434E3 3.406E4 0. 0. 0.
 700= 0. 0. 0. 0. 0.
 710= 1
 720= 0. 3.63E5 0. 0. 0.
 730= 0. 0. 0. 0. 0.
 740= 1
 750= 6.949 2.726E-11 0. 0. 0.
 760= 0. 0. 0. 0. 0.
 770= 1
 780= 0. 5.10E3 0. 0. 0.
 790= 0. 0. 0. 0. 0.
 800= 1
 810= 0. 4.17E3 0. 0. 0.
 820= 0. 0. 0. 0. 0.
 830= 1
 840= 0. 1.02E1 0. 0. 0.
 850= 0. 0. 0. 0. 0.
 860= 0 0
 870= 0 0 0 0 0
 880= 0 0
 890= 0 0 0 0 0
 900= 0 0
 910= 0 0 0 0 0
 920= 1 0
 930= 0 1 0 0 0
 940= 20
 950= .100E5 .197E5 .209E5 .221E5 .233E5 .245E5 .257E5 .269E5 .281E5 .305E5
 960= .329E5 .365E5 .377E5 .389E5 .401E5 .413E5 .425E5 .461E5 .485E5 .865E5
 970= 0. 1.638 17.15 37.87 51.52 112.7 130.2 28.21 22.4 28.98
 980= 35.21 43.19 48.3 49.63 56.98 27.79 13.58 5.6 5.53 0.
 990= 0 0
1000= 0 0 0 0 0
1010= 1 0
1020= 0 1 0 0 0
1030= 10
1040= .100E5 .197E5 .209E5 .221E5 .233E5 .245E5 .257E5 .269E5 .281E5 .865E5
1050= 0. 4.333E-2 9.59E-1 2.541 4.109 2.590 2.177 9.59E-3 0. 0.
1060= 1 0
1070= 0 1 0 0 0
1080= 8
1090= .100E5 .197E5 .209E5 .257E5 .329E5 .401E5 .485E5 .865E5
```

TABLE 4.7 (CONTINUED)

```
1100= 0. 0. 5.852E-8 9.03E-7 2.821E-3 3.43E-3 3.29E-4 0.
1110= 1 0
1120= 0 1 0 0 0
1130= 14
1140= .100E5 .197E5 .209E5 .221E5 .233E5 .245E5 .257E5 .269E5 .305E5 .365E5
1150= .401E5 .413E5 .485E5 .865E5
1160= 0. 3.565E-4 4.27E-2 3.087E-1 3.367E-1 6.202E-1 1.729E-1 1.162E-2 5.803E-3
1170= 8.68E-3 1.148E-2 1.393E-2 3.85E-3 0.
1180= 1 0
1190= 1
1200= 0.
1210= 2.4
1220= 1
1230= 0.
1240= .40
1250= 3. 3.
```

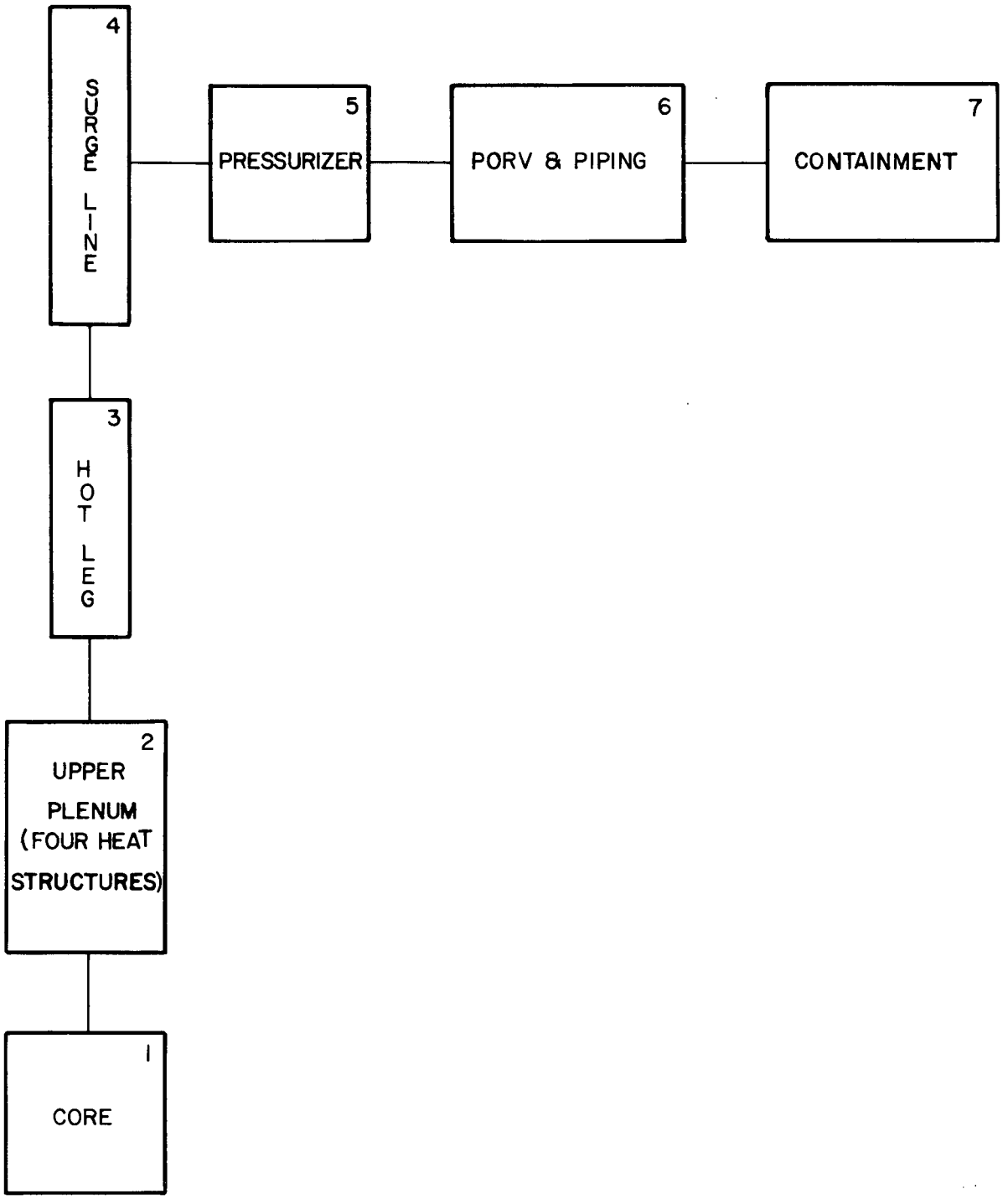

FIGURE 4.1

Control Volumes for

TMLB Sequence

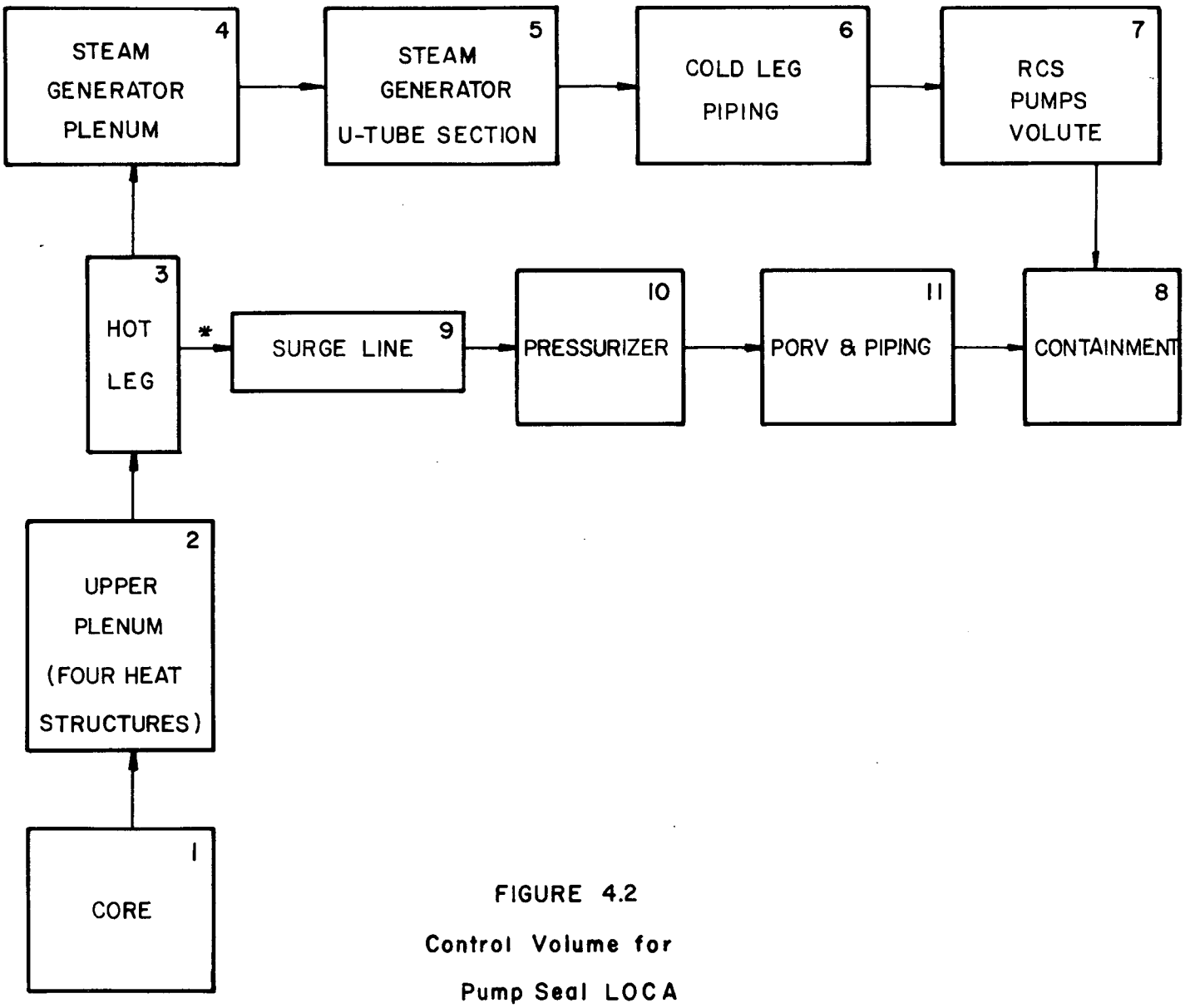

FIGURE 4.2

Control Volume for

Pump Seal LOCA

* Flow path exists only during first 30 minutes of accident

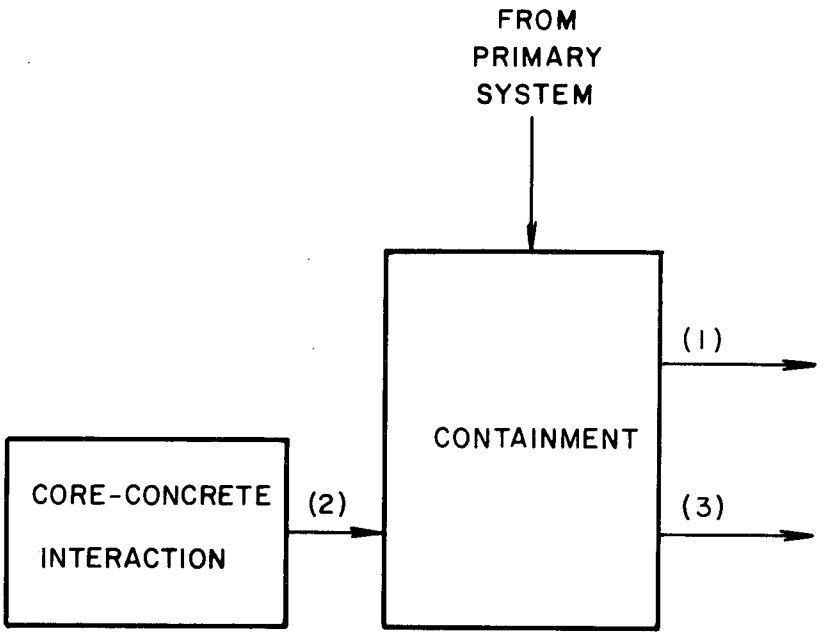

(1) CONTAINMENT LEAKAGE AT DESIGN LEAK RATE

(2) STARTS WHEN REACTOR VESSEL FAILS

(3) RELEASE COMMENCES WHEN CONTAINMENT FAILS

FIGURE 4.3

MATADOR MODEL FOR

TMLB AND PUMP SEAL LOCA SEQUENCE

During the depressurization stage, the steam generator secondary side water inventory is drastically reduced by blowdown of the steam safety valve. After blowdown, the secondary side feedwater inventory continues to be reduced at a slower rate. The slowdown is due to reduced heat transfer between the primary and secondary side, caused by the low feedwater levels on the secondary side.

Figures 5.3 and 5.4 show the water mass in the primary system and in the steam generator secondary side respectively. From Figure 5.1, when the steam generator heat transfer decreases at around 45 minutes, the primary system pressure increases to 2400 psia, causing the PORV to lift and deplete the primary system water inventory. Figure 5.3 shows a gradual decrease in water mass on the primary side until about 80 minutes into the accident, at which time the rate of water loss from the primary system accelerates.

Figure 5.2 shows the water-steam mixture level in the primary system. During the first 80 minutes of the accident, the water level remains essentially constant with a small increase at the 45 minute mark when the rate of heat exchange with the secondary side decreases. After about 80 minutes into the accident the water-steam mixture level drops rather rapidly. This rapid decrease in mixture level tracks the changeover from a liquid blowdown through the PORV to a mixture of water and steam, and finally to steam alone. The oscillations in primary system pressure in Figure 5.1 indicate the limitations of MARCH 2.0 in properly handling the two phase flow through the PORV. Consequently, the primary system pressure between approximately 80 minutes and 115 minutes are artificially high.

The oscillation and artificial increase in the primary system pressure speeds up the depletion of water in the primary system until the beginning of core uncovery, which is calculated to occur at 111 minutes. As the fuel is gradually uncovered, the rate of primary system water loss begins to decrease, slowly at first and more rapidly as core uncovery progresses. The tapering off of the curves in Figures 5.2 and 5.3 at approximately 120 minutes mark the decrease in steam production that accompanies complete uncovery of the core.

Figures 5.5 through 5.8 show the relationship between the fraction of the core which has melted, the fraction of the clad reacted through zirconium-steam reaction, the associated hydrogen mass in the primary system, and the total mass of hydrogen produced, respectively.

Note that the fraction of clad reacted increases at a fairly constant rate up to approximately 160 minutes, at which time the reaction rate increases before leveling off at around 50%. Comparing this curve against the fraction of core melted in Figure 5.5, the constant rate of clad reaction attained soon after 120 minutes is not tied to the fraction of core melted. In other words, the constant rate of clad reaction establishes itself prior to any core melting. The increase in the fraction of clad reacted, as well as the fraction of core melted after approximately 160 minutes, can be attributed to the increase in the overall core temperature after the bottom-most nodes in the core reach their melting temperature. This can be seen by examining Figures 5.9 through 5.12, which show the temperature responses of the core in terms of a maximum and average temperature, and temperature responses of selected core nodes, respectively.

5.1.2 MARCH 2.0 Results -- Containment

Figures 5.13 through 5.18 show the containment responses for the TMLB sequence. Figures 5.13 and 5.14 show the containment pressure and temperature. Figure 5.15 shows the mass of steam in containment vs. time, while Figures 5.16 through 5.18 deal with the hydrogen content and concentration in the containment during the course of the accident. All containment calculations have been carried out for 72 hours, and it should be noted that the containment pressure remains below the 141 psia containment failure pressure during the entire time.

Examining Figure 5.13, the containment pressure rises initially to about 42 psia from the blowdown of the primary system through the PORV into the containment. The decrease in pressure, at approximately 120 minutes, marks complete core uncovery, the corresponding decrease in steam production, and the decrease in the PORV flow rate. The containment pressure drops to a low of about 37 psia at approximately 181 minutes,

then increases very rapidly with lower reactor head failure and subsequent quenching of the debris in the reactor cavity water. The pressure spike from the two phenomena is approximately 90 psia, is followed by a decrease in containment pressure to approximately 65 psia as steam condenses on the containment structures. The containment pressure remains fairly steady at approximately 65 psia until approximately 1100 seconds into the accident, until condensation on containment structures and other heat sinks stops. Finally, containment pressure and temperature are observed to increase fairly quickly, and then at a steady rate for the remainder of the accident. The pressure and temperature response of the containment at that point is tied to the generation of non-condensibles from the core-concrete interaction and to deposition of the energy from that reaction into the containment atmosphere.

Figures 5.16 through 5.18 show the hydrogen parameters relative to the containment during the course of the accident. Note that at no time during the accident is a flammable mixture reached.

5.1.3 M-C-T Results* -- Fission Product Source Rates

Figures 5.19 through 5.22 show the mass release rates of the different chemical species of interest as well as the aerosols. The mass release rates in grams per second are considered in the analysis as the species source rates into the first volume of interest, the upper plenum. The computer code, CORSOR, has been modified to account for the possibility that not all particulates comprising the aerosol emitted from the fuel would be in solid form. This is particularly true of the silver component of the aerosol which would be emitted in liquified rather than solid form. Thus, it was assumed in all of the CORSOR calculations that 60% of the emitted aerosol would eventually find its way into the upper plenum as solids, whereas 40% would be retained in the core-region.

In the case of the silver component, however, it was assumed that all of the silver would be retained in the core-region, thereby eliminating the control rod silver from participation in the aerosol.

---

*Individual plots of the multiple plot figures discussed below may be found in Appendix D.

The mass release rates shown in Figures 5.19 through 5.22 depend entirely on the temperature histories of the core nodes discussed earlier. However, the release rate of tellurium depends directly on the zirconium oxidation rate. Figures 5.23 through 5.26, show the integrated releases of the chemical species of interest. All of these chemical species, including tellurium, are assumed to be released during the core-melt phase of the accident.

5.1.4. M-C-T Results -- Primary System Heatup

Figure 5.27 shows the response of the primary system to the gas flows carrying fission products coming out of the core. Figures 5.28 through 5.30 show the thermal response of the primary system structures to the energy transferred from the gas flow and from the fission products entrained in the gas stream as well as deposited on structural surfaces.

Figure 5.27 shows the gas flow out of the core in pounds per second over time. Initially, the gas flow rate is quite high as a function of the core-uncovery process. Once the core is uncovered at around 8000 seconds into the accident, the gas flow out of the core is composed mainly of the hydrogen which results from the metal water reaction. Steam from water evaporation is essentially consumed by the zirconium-water reaction and is not part of the gas flow out of the core.

At about 9800 seconds, the core begins to collapse into the lower plenum. The debris which falls into the lower head water generates moderate amounts of steam. This phenomena can be seen in Figure 5.27 by the moderate increase in the gas flow rate out of the core after 10,000 seconds into the accident, peaking at approximately 10,500 seconds. As the fallen debris is quenched, the steam rate decreasees.

Figure 5.28 shows the core-exit gas temperature over time. The temperature of the exit gas remains quite cool until approximately 6800 seconds into the accident and core-uncovery. At that time, the core-exit gas temperature increases rather rapidly from the heating of the steam hydrogen mixture by the uncovered nodes and from the metal water reaction. The core-exit gas temperature rises to about 3700 degrees F,

followed by a sharp increase to about 4100 degrees F, and then a rapid temperature decrease which corresponds to a decrease in the core-wide zirconium-water reaction.

Finally, as the debris slumps into the lower plenum, the gas temperature drops to approximately saturation temperature of the lower plenum water. As the debris heats the water to a full boil, the gas exiting from the boil-off increases correspondingly. Figures 5.29 and 5.30 show the thermal response of the primary system to the gas entering the upper plenum.

Figure 5.31 shows the fission product energy deposited on the primary system structures in the path of the gas. Figure 5.30 shows the thermal response of the upper plenum structures, as well as the downstream structures, to the entering gas. Initially, the upper plenum structures heat-up slowly at a nearly constant rate. At about 8000 seconds, the heat-up rate increases as the fission products are deposited in the upper plenum. Figure 5.31 shows the energy deposition from the fission products on the four heat structures in the upper plenum. The fission product energy begins to be deposited at about 7800 seconds, which coincides with an increase in the heat structure temperature. Figure 5.29 shows the upper plenum gas outlet temperature. The effects of the fission product energy can be seen at approximately 8000 seconds when the gas outlet temperature begins to accelerate.

At approximately 9600 seconds, an increase in the gas temperature is observed that can be attributed to the rapid increase in the gas inlet temperature shown in Figure 5.28. However, according to Figure 5.30, that gas exit temperature peak has very little effect on heat structure temperature. In fact, at that stage of the accident, the heat-up of the structures in the gas path is completely dominated by the energy transferred from the fission products to the structure, rather than from the gas to the structure.

Given the pressure conditions in the primary system during the accident, it is interesting to examine the heat-up of the hot leg and the surge line. The gas temperature in the hot leg is, in effect, the gas

temperature entering the surge line; the gas temperature in the surge line indicates the temperature history of the gas entering the pressurizer, and so on. The temperature responses of the hot leg and the surge line are shown in Figure 5.30.

The temperature response of the hot leg is primarily due to the energy transferred from the gas stream. At approximately 8000 seconds, fission products begin to deposit in the hot leg and heat its surface. The gas entering the hot leg is hot because its energy has not been removed by the structures in the upper plenum already heated by deposited fission products. The heat up rate of the hot leg is highly influenced by both the temperature of the gas flowing through the hot leg and the energy from the fission products deposited there.

Fission products initially deposited in the upper plenum later begin to re-volatilize and are carried in the vapor stream from the upper plenum to the hot leg. This re-volatilization can be observed in Figure 5.31 by the turn-around in the curve observed at approximately 10,500 seconds, and a corresponding increase in the fission product heat observed in the downstream volumes.

The heat-up rate of the surge line as shown in Figure 5.30 is initially influenced by the temperature of the gas entering the surge line, because the fission product energy from deposited material is initially fairly low as shown by Figure 5.31. At about 9600 seconds, the energy from deposited fission products increases slowly at first, then quite rapidly after about 10,300 seconds with the re-volatilization of the fission products deposited in the upper plenum and in the hot leg. This increase in fission product heat causes the increase in the rate of temperature rise in the surge line, observed at around 9600 seconds into the accident.

Given the pressure conditions of the primary system during the accident, both the hot leg and the surge line reach temperatures at which failure would more than likely occur. This defines another mode of primary system failure, one which could occur earlier than the calculated failure by melt through of the lower head by core debris.

This result has a dramatic effect on the subsequent course of events during the accident. For example, upon lower head melt-through, the core debris would no longer be dispersed by the flow surge up the cavity onto the containment floor; rather the core debris would drop by gravity onto the reactor cavity floor. Thus, the pressure spike in the containment as debris quenches the water collected on the containment floor would no longer be experienced. The effect of this finding on subsequent retention of the deposited fission products will be discussed later.

Since the heat up of the hot leg precedes the heat up of the surge line by several minutes, the rupture in the primary system would likely occur in the hot leg, at approximately 10,500 seconds, just about the time that the core collapses into the lower plenum.

Figure 5.29 shows the gas temperature exiting the pressurizer, while Figure 5.30 shows the temperature response of the pressurizer to the gas temperature exiting the surge line. The fission product energy deposited in the pressurizer is shown in Figure 5.31. Note that very little fission product energy is deposited in the pressurizer, until fission product re-volatilization begins to take place at about 9600 seconds. Thus, Figure 5.29 shows a fairly steady temperature increase in the pressurizer from about 570 degrees F to approximately 630 degrees F at around 9600 seconds. As fission products re-vaporize and are transported in the gas stream from one volume to another, an increase in the pressurizer temperature is noticed. This is caused by the increase in energy transferred from the fission products entrained in the gas to the pressurizer structure. Because of the very large mass of steel in the pressurizer structure, the temperature response of the pressurizer is quite slow, and remains well below 1000 degrees F at the time that the reactor vessel lower head is calculated to melt, at which point the calculations are stopped.

All of the calculations discussed to this point take into account the thermal properties of primary system insulation. Above approximately 1500 degrees F, the bonding agent present in the insulation of the primary system degrades, and breakdown of the insulation properties occurs.

Above that temperature, increased heat losses were calculated. With the increased heat losses, unacceptable stressing of the piping due to the local temperature gradients through the pipe wall occur. Consequently, pipe cracking would be expected. This temperature regime ranges from 1700 to 1900 degrees F, during which hot leg failure is assumed.

5.1.5 M-C-T Results -- Primary System Fission Product Retention

Figures 5.32 through 5.43 show the retention of the fission product species in the primary system as well as the release history of the species to the containment.

Figure 5.32 shows the retention of cesium iodide in the primary system. The retention factor, as applied here, is defined as the grams of cesium iodide retained in the entire primary system, divided by the grams of cesium iodide available in the reactor core. Thus, in the early stages of the accident, for example at 8000 seconds, the retention factor for cesium iodide is below 10%; however, that is because only a very small portion of the cesium iodide has been released and not because little cesium iodide has been trapped or retained in the primary system.

The overall retention factor of cesium iodide, top curve, increases at a fairly steady rate until it levels off at approximately 9200 seconds. This leveling off can be attributed to two factors. The first is that the release rate of the cesium iodide begins to decrease at that point in time; the second factor is the heatup of the primary system surfaces by the cesium iodide in each volume. The overall retention factor peaks out at about 90% at approximately 9800 seconds, and then drops to a low of about 20% at approximately 10,600 seconds into the accident. This drop is entirely due to re-vaporization of the cesium iodide and entrainment of the vapor in the gas flow stream. At approximately 10,600 seconds, the cesium iodide retention in the primary system increases slightly from the arrival and condensation of the cesium iodide vapors in the cooler portions of the primary system.

Figure 5.34 shows the masses of cesium iodide retained on the surfaces of the primary system through condensation and on the surfaces of the

deposited aerosol particles. During the initial stages of the accident, i.e., between 8000 seconds and approximately 9600 seconds, the primary means of cesium iodide removal is through condensation onto aerosol particles and subsequent deposition, rather than direct condensation on the structure surfaces. This is because the area-to-volume ratio of the aerosol particles is much greater than the area-to-volume ratio offered by the structure surfaces. At approximately 9200 seconds, the mass retained on the aerosol particles begins to level off as the temperature of the particles increases. At the same time, the mass retained on the walls due to condensation begins to become more important. Subsequently, the mass retained on the particles begins to drop whereas the mass retained on the structure surfaces begins to increase. This phenomenon can be explained by observing the temperatures in the volumes downstream of the hot leg. In other words, the surge line, the pressurizer, the PORV and the downstream piping begin to receive the cesium iodide in vapor form, as a result of the re-evaporation going on in the first two volumes, i.e., the upper plenum and the hot leg.

Bcause the surfaces of the downstream volumes are considerably cooler, especially the pressurizer and the PORV and its associated piping, the vapors which entered these volumes in the gas stream condense readily. Since the number of aerosol particles existing in those volumes is fairly small upon prior removal of aerosols in the upper plenum and hot leg, the area to volume ratio for cesium iodide vapor condensation onto the aerosol particles is no longer totally dominant. Therefore, simultaneous removal by condensation on walls and on the surfaces of particles takes place. This can be observed by the increase in the mass retained on particles at approximately 10,600 seconds into the accident, as well as the continued increase in the cesium iodide mass retained on walls at the same time.

Figure 5.32 shows the mass of cesium iodide in vapor and condensed forms released to the containment during the course of the accident. Note that essentially no cesium iodide is released to the containment until the primary system depressurizes. The release of cesium iodide proceeds at a very slow rate, with a gradual increase occurring at approximately 10,400 seconds into the accident, until the time of primary system

depressurization. Then all of the suspended aerosols plus any vapors are released to the containment through the opening in the lower reactor vessel head. This release is shown as the two spikes in Figure 5.33 at approximately 10,900 seconds.

The cesium iodide retention factor in each primary system volume is shown on Figures 5.32. The upper plenum retention increases to approximately 80%, and rapidly decreases to 0% when the cesium iodide is re-volatized.

In the case of the hot leg volume, the retention factor increases to about 10% at around 10,900 seconds. No sudden decrease in retention is experienced for two reasons. First, the vapor pressure of the cesium iodide is fairly high so no significant re-volatilization occurs at hot leg temperatures. Second, the hot leg temperature is high enough to prevent condensation of the cesium iodide re-volatilized in the upper plenum. Therefore, the retention factor in the hot leg remains fairly steady.

The surge line initially plays a small role in cesium iodide retention until approximately 9600 seconds, at which time the retention factor increases slowly and then more rapidly at approximately 10,400 seconds. This increase in the retention factor is due to the deposition in the surge line of the re-vaporized material from the upper plenum moved along by the gas flow. The cesium iodide retention factor in the surge line reaches approximately 12% and then levels off as the temperature in the surge line increases.

The retention factor in the pressurizer only begins to increase at approximately 10,400 seconds, and thereafter until depressurization of the primary system. No leveling off, as in the surge line, is observed because pressurizer temperatures never reach a high enough level to affect cesium iodide condensation.

Figure 5.32 demonstrates that at the time of the primary system depressurization, all of the retained cesium iodide is located in the hot leg surge line and the pressurizer. The remainder, or approximately 80% of the cesium iodide core inventory, is either in vapor form as part of the gas stream, or condensed on aerosol particles which have not yet deposited. The PORV and its downstream piping play an insignificant role in cesium iodide retention. Figure 5.33 shows that the cesium iodide,

which is released upon primary system failure, consists of approximately 92% vapor and 8% particulate form. This is consistent with the earlier observation that a very small aerosol content is present in the volumes upstream of the upper plenum and the hot leg volumes.

The plots showing the cesium iodide retention factor in each volume, Figure 5.32, can be easily used in conjunction with the known mass of cesium iodide core inventory to obtain the mass of cesium iodide retained in each volume over time. It should be noted that the retention factor is defined as the ratio of the total mass retained within a given volume to the total mass of the fission product species contained in the core at the beginning of the accident. The above observation is equally applicable to all the fission product species.

Figures 5.35 through 5.37 show the primary system retention of cesium hydroxide as well as its release history to the containment. Upon close examination, cesium hydroxide behaves similarly to cesium iodide, except that cesium hydroxide is readily removed by chemisorption onto structure surfaces, and by condensation onto structure surfaces and aerosol particles, as shown in Figure 5.37. The rapid increase in the cesium hydroxide mass retained by sorption at approximately 10,600 seconds, which was noticeable but to a much lesser extent, for the cesium iodide mass retained on walls, is attributed to the increase in gas flow rate from debris quenching upon core collapse into the lower plenum.

The retention factor for cesium hydroxide in the upper plenum does not drop to 0 as it did for cesium iodide, due to chemisorption. In fact, chemisorption of cesium hydroxide accounts for approximately 60% of the entire retention, and it takes place primarily in the upper plenum where temperatures are high enough to negate other means of removal. This phenomenom was not observed in the case of cesium iodide with its very low deposition velocity.

Figures 5.38 through 5.40 show the behavior and release of aerosols. The shape of the overall retention factor curve is derived from the nature of the release mechanisms of the aerosol from the core region. This can be

confirmed by examining the shape of the curve showing the cumulative release of aersol over time, Figure 5.25.

Figure 5.39 shows the aerosol mass released to the containment over time. Very little aerosol is released to containment until the primary system is depressurized when the lower reactor head fails. By comparing Figure 5.39 with Figure 5.38, it is seen that very little aerosol is suspended in the gas stream at the time of the primary system depressurization.

Figure 5.38 also shows the aerosol retention factors in the individual volumes. Because of low gas stream flow rates, a greater portion of the aerosol is deposited in the upper plenum; only a small percentage is carried into the downstream volumes.

Figures 5.41 through 5.43 show the behavior of tellurium in the primary system as well as its release to the containment. From Figure 5.41, it could be inferred that tellurium is readily retained in the primary system and is unaffected by the high structural and gas temperatures present. However, the latter comment is not totally true. Figure 5.43 shows the mass of tellurium retained as a result of condensing tellurium vapors on structural walls. The mass of tellurium retained increases until approximately 8800 seconds, at which time it is re-vaporized into the gas stream. The same is true for the tellurium condensed onto the suspended aerosol particles and subsequently deposited whereby the condensed tellurium is re-vaporized into the gas stream and the tellurium mass retained is turned around.

In order to understand why the overall tellurium retention in the primary system is unaffected by the tellurium re-vaporization, Figure 5.43, which also shows the tellurium mass retained by chemical sorption, should be carefully examined. Chemical sorption is a dominant removal process throughout the accident. The masses of tellurium which have been removed by condensing on structural walls and on aerosol particles are small compared with the mass of tellurium removed by chemical sorption. The dominance of the chemical sorption of tellurium over the other removal mechanisms is due to the high deposition velocity of tellurium onto

stainless steel surfaces. Therefore, when the tellurium vapors which have been condensed onto walls and aerosol particles are re-released into the vapor stream, they are very quickly removed by chemical sorption; hence the overall removal of tellurium in the primary system is unaffected by the re-vaporization of the condensed tellurium.

Figure 5.42 shows the tellurium mass released to the containment in vapor form as well as in particulate form. In both cases, it is evident that negligible amounts of tellurium are released from the primary system. Figure 5.41 shows the removal factors of tellurium in the individual volumes of the primary system. It is apparent that by far the most dominant retention takes place in the upper plenum, with the downstream volumes playing only a minor role in the retention of the tellurium specie.

5.1.6 MATADOR II Results

Figures 5.44 through 5.58 show the behavior of the fission product species in the containment following their release from the primary system. Figures 5.44 through 5.46 present the specific behavior of cesium iodide in the containment. Examination of these three figures reveals that approximately 30,000 seconds after the beginning of the accident essentially all of the cesium iodide initially present in the containment has settled out by natural processes, such as gravitational settling. Figure 5.45 shows that the cesium iodide mass retained in the containment reaches an asymptotic value by approximately 30,000 seconds into the accident. Figure 5.46 shows that the cesium iodide release to the environment also reaches an asymptotic value at approximately the same time. These results indicate that approximately 6 hours after cesium iodide is released from the primary system into the containment, natural processes remove essentially all of the suspended cesium iodide. Longer retention in the containment would only result in minimal additional removal of the fission product specie.

Figures 5.47 through 5.49 show the behavior of cesium hydroxide in the containment. Since cesium hydroxide exhibits behavior almost identical to that of cesium iodide, the observations and conclusions reached with

respect to the cesium iodide specie are applied equally to the cesium hydroxide specie.

Figures 5.50 through 5.52 present the behavior of inert aerosols in the containment. Figure 5.50 shows the mass of inert aerosol in the containment atmosphere over time. The initial suspended mass of approximately 50,000 grams is comprised of the inert aerosols released from the primary system upon its failure. This aerosol mass decreases until approximately 20,000 seconds, at which time the core concrete interaction begins to generate large amounts of aerosols. The subsequent shape of this plot shows the competition between the generation rate of the inert aerosols from this core-concrete interaction and the natural removal processes taking place in the containment. Thus, the decrease in the aerosol mass at approximately 28,000 seconds marks a decreased generation rate of aerosol combined with rapid settling out of the particles. The increase at approximately 32,000 seconds marks a sudden increase in the aerosol generation rate, followed by a gradual decrease in the generation rates until the assumed containment failure time at 24 hours.

Figure 5.51 shows initially that the aerosol mass retained by natural settling is fairly small, and that it increases at a slow rate. This is because the geometric mean radius of the aerosols released from the primary system on its failure is considerably smaller than the geometric mean radius of the aerosol particles generated by the core-concrete interaction. Therefore, as core-concrete interaction increases in importance, an increased rate of mass settling is observed until approximately 48,000 seconds, at which time the rate of settling decreases considerably. This decrease is brought about by a reduced aerosol source rate and by the fact that a majority of the larger particles suspended in the containment atmosphere have settled out and are no longer replenished by an active core-concrete interaction. The slow increase in particle settling observed after approximately 48,000 seconds indicates that a steady state condition is being reached between the source rate of particles and the agglomeration and settling out of the suspended particles.

The rate of removal continues to decrease with time because the agglomeration of particles takes place in a particle population of ever decreasing geometric mean radius. Since the particle population is composed of ever smaller particles, the removal rate for those particles continues to decrease. Figure 5.53 shows the particle mass median diameter in the containment over time. The effects of particle agglomeration and settling out are particularly obvious in the early stages (i.e., between the time of primary system release and the beginning of core-concrete interaction) and in the latter stages (from approximately 40,000 seconds until the end of the accident sequence).

Figures 5.54 through 5.58 show the behavior of tellurium, barium, ruthenium, and lanthanum in the containment during the 24 hours prior to containment failure. Tellurium exhibits a behavior quite similar to cesium iodide and cesium hydroxide. The three species are released primarily in a vapor form from the primary system. Upon release, the volatiles are very quickly condensed onto the inert aerosol particle surfaces and undergo removal by particle settling. Moreover, since all of the cesium iodide, cesium hydroxide and tellurium inventory present in the core at the beginning of the accident was released during the core melting, they are not present during the core-concrete interaction.

This is not true of the less volatile species: barium, ruthenium, and lanthanum. Figure 5.56 shows that barium is initially released from the primary system whereupon the initial inventory decreases as particles undergo agglomeration and settling. The sudden increase in the mass in containment atmosphere occurs when the barium is released from the core-concrete interaction. The rate of barium release from core-concrete interaction is rather large, resulting in an overall increase in the mass of barium contained in the containment atmosphere. The turnaround in the barium mass contained in the containment atmosphere marks a decrease in the source rate of barium from core-concrete interaction, at which time the removal processes through agglomeration and settling become dominant.

Figure 5.57 shows the behavior of ruthenium in the containment to be similar to that exhibited by the volatile species because the source rate

from core-concrete interaction for ruthenium is very small. Ruthenium has an initial mass of approximately 550 grams released from the primary system. Subsequently, ruthenium is removed through natural processes in the containment until the total mass of ruthenium in the containment atmosphere is small enough that the source rate of ruthenium for core-concrete interaction just balances out the removal rate of ruthenium. This happens at approximately 30,000 seconds and is shown as a fairly constant mass of ruthenium in the containment. At approximately 45,000 seconds, the mass of ruthenium in the containment begins to decrease very slowly. This is due to the decreasing source rate of ruthenium from core-concrete interaction and the increased dominance of the removal mechanisms.

Figure 5.58 shows the behavior and removal of lanthenum. Lanthanum exhibits a behavior very similar to that of barium and, therefore, the discussions associated with the behavior of barium apply equally to lanthanum.

In all cases, the containment plays a very important role in the removal of fission products released from the primary system. Of great importance is the rate at which the fission product species are removed from the containment atmosphere. As observed from the plots discussed above, only a tiny portion of the fission products initially released from the primary system remain suspended in the containment atmosphere after approximately 6 hours following their release. In addition, comparing Figures 5.44 and 5.47 to Figure 5.50, it is important to note that the removal rate of cesium iodide and cesium hydroxide from the containment atmosphere is not heavily influenced by the core-concrete generated inert aerosol. This result indicates that the inert aerosols released in conjunction with the primary system failure are sufficient to aid in the settling and agglomeration processes which control the removal of cesium iodide and cesium hydroxide. Thus, the inert aerosols released from core-concrete interaction do not play a major role in source term reduction.

5.2 Pump Seal LOCA Results

The pump seal LOCA is a variation of the TMLB accident sequence. Both begin in the same manner; however, after 30 minutes into a pump seal LOCA accident, the loss of cooling to the pump seals resulting from the loss of electric power causes the failure of the reactor coolant pump seals, and finally loss of reactor coolant inventory out of the seals. The pump seal LOCA in effect becomes a small LOCA with blowdown occurring in all four cold legs. The blowdown rate was assumed to be 300 gallons per minute per pump seal. The subsequent discussion deals with the results of the analysis performed to examine the behavior and fission product retention capability of the primary system under these conditions.

5.2.1 MARCH 2.0 Results -- Primary System and Containment

Figures 5.59 through 5.70 show the thermal-hydraulic behavior of the primary system following the occurrence of the TMLB-initiated pump seal LOCA. Figures 5.71 through 5.76 show the response of the containment to the blowdown from the four failed pump seals.

Figure 5.59 shows the primary system pressure response to the accident. For the first 30 minutes, the pressure response of the system matches that of the TMLB. Only after the first 30 minutes does the accident becomes a pump seal LOCA. At 30 minutes, a sudden drop in primary system pressure is observed as the pump seals fail, causing primary system depressurization and inventory loss. Figures 5.60 and 5.61 show the loss of primary system inventory. Throughout the accident, the primary system pressure does not reach the setpoint pressure of the PORV valve on the pressurizer; therefore, all of the primary system inventory loss is through the failed pump seals.

Shortly after the onset of the depressurization, the primary system pressure reaches the secondary side pressure, and steadies out until the water inventory in the steam generator is depleted by heat transfer from the primary side to the secondary side. The mass of water in the steam generator secondary side is shown in Figure 5.62. The depletion rate of the secondary side water from the steam generator is essentially identical

to the rate observed earlier during the TMLB accident. The sudden opening of a "hole" in the primary side caused by failure of the pump seals does not appear to have any appreciable effect on the rate of loss of feedwater from the steam generator. Observe that the total flow through the pump seals is not enough to remove the decay heat energy from the primary side. Therefore, the decay heat energy continues to be transferred from the primary side to the secondary side in the steam generator, thereby depleting the mass of water in the steam generator secondary side.

The primary system pressure stabilizes at approximately 1200 psi for about 20 minutes until the secondary side water inventory is depleted to the point where negligible heat transfer in the steam generators takes place from the primary to the secondary side. Then approximately 50 minutes into the accident, the primary system pressure begins to increase because the decay heat energy is now being stored in the primary system water with the subsequent pressurization of the primary system.

The total break flow through the failed pump seals is by itself insufficient to remove the decay heat generated from the primary system. Until the pressure build-up in the primary system is such that the break flow increases, only then can the break flow remove the decay heat energy from the primary system. Figure 5.60 reveals that at exactly that time, the water-steam mixture level has dropped to the elevation of the break, and blowdown effluent now changes from liquid to steam with a consequent rapid energy removal from the primary system.

This rapid energy removal results in a depressurization of the primary system as shown in Figure 5.59, starting at approximately 30 minutes. As a result of the change from a liquid blowdown to a steam blowdown, the rate of loss of inventory from the primary system decreases. The rate of energy removal from the primary system increases, mainly because of the higher energy content per pound of steam.

The core begins to uncover at approximately 81 minutes and is completely uncovered at approximately 100 minutes. Figures 5.63 and 5.64 show the fraction of core melted and fraction of clad reacted, respectively. The

cladding begins to oxidize at approximately 95 minutes and continues oxidizing at a rapid rate until approximately 115 minutes, at which time the rate decreases. Total oxidation continues at an ever decreasing rate until the core collapses into the lower plenum at approximately 155 minutes.

The rapid oxidization until about 115 minutes is caused by the large portion of the core that participates in the oxidation process. The radiation heat transfer from the hotter regions of the core to the cooler regions tends to reduce the heatup rate of the central portions, while increasing the heatup rate of peripheral portions. The net effect is that a large portion of the core heats up at approximately the same rate, and participates in the oxidation process at approximately the same rate. Thus, about 50% of the core melts rather quickly, with a noticeable slowing down in the melting rate thereafter. The slower rate of oxidation is due to the fact that the outermost radial regions of the core heat up at a considerably slower rate initially, and begin to heat up more rapidly only after the central portions of the core heat to temperatures where radiation heat transfer to the cooler portions begins to be appreciable.

Figures 5.65 and 5.66 show the instantaneous mass of hydrogen in the primary system and cumulative mass of hydrogen produced, respectively. Because the primary system is open to the containment throughout the entire accident, the instantaneous mass of hydrogen in the primary system reaches a peak. After the production rate of hydrogen begins to decrease, the instantaneous mass of hydrogen in the primary system decreases as the hydrogen is carried with the steam flow into the containment.

Figures 5.67 through 5.70 show the core maximum and core average temperatures, as well as temperature responses of selected core nodes. Note that the outer regions lag in temperature response behind the central regions. Moreover, it can be seen that central region 1 and middle region 5, have very similar temperature responses throughout most of the accident.

Figures 5.71 through 5.76 show the behavior of the containment during the accident. For the most part, the containment behavior is quite similar to

that described for the TMLB accident sequence, with only a few differences early in the accident. One of these differences is the lack of an appreciable pressure increase in the containment due to the failure of the lower reactor head. In the case of the pump seal LOCA, pressure in the primary system is quite low (approximately 200 psia) when the lower reactor head failure occurs; in the case of the TMLB accident sequence, the pressure was approximately 2400 psia when the lower head failure occurs. Therefore, when the lower head failure does occur, only a small pressure spike is observed on Figure 5.71. The later pressure spike observed on Figure 5.71, which stands between approximately 45 psia and 85 psia, is due to the quenching of the debris in the lower reactor cavity water. Thereafter, the subsequent behavior of the containment is similar to that described in the discussion of containment behavior for the TMLB sequence. Furthermore, at no time during the accident is the hydrogen concentration fraction in excess of flammability conditions.

5.2.2 M-C-T Results* -- Fission Product Source Rates

Figures 5.77 through 5.84 show the release rate and cumulative releases of the fission products and inert aerosols from the core following the initiation of the pump seal LOCA. As in the case of the TMLB accident sequence, the release rates for cesium iodide and cesium hydroxide are directly related to the temperature history of the fuel. Figures 5.77 and 5.78 should be studied in conjunction with the figures showing, not only the temperature response of the core as a whole, but also the temperature response of individual nodes as shown in Figures 5.67 through 5.70.

The release of the fission product tellurium is quite similar to the release of that specie in the TMLB sequence through the extensive oxidation of the zirconium during both of these accident sequences. From Figures 5.81 through 5.84, it is evident that the entire inventory of CsI, CsOH and tellurium is released from the core into the primary system gas stream prior to primary system failure. In the case of the pump seal LOCA, there was a substantially greater amount of aerosol generated as a

---

* Individual plots of the multiple plot figures discussed are provided in Appendix D.

result of the core meltdown process than in the case of the TMLB accident sequence. This is due to the somewhat hotter core temperatures lasting for a somewhat longer period of time in the pump seal LOCA sequence. From an overall standpoint, however, the release rates and the amounts of material released for the two accident sequences, the TMLB and the pump seal LOCA, do not differ from each other in any significant way.

5.2.3 M-C-T Results -- Primary System Heatup

The removal of fission products from the flowing gas stream is strongly dependent on the flow rate of the fission-product-bearing gas. The higher the flow rate of gas, the less deposition would be expected. This is due to the fact that the higher gas flow rates through a given volume would result in higher velocities and hence lower residence time.

Figure 5.85 shows the gas flow out of the core into the upper plenum for the pump seal LOCA. Initially, the gas flow rate out of the core into the upper plenum is quite high, then it decreases as the core uncovers. The gas flow rate decrease is due to the lower rate of steam production as the core uncovers and to steam consumption by the increasing metal-water reaction. The continuous depressurization of the primary system from the ruptured pump seals insures continued steaming due to flashing, even after the core is completely uncovered, as small amounts of energy are transferred to the water surface below the melting core. This is evident by a fairly steady gas flow rate out of the core after approximately 660 seconds into the accident as shown in Figure 5.85.

Figure 5.86 shows the core exit gas temperature over time. The exit gas temperature rises rapidly to approximately 4300 degrees F due to the rapid zirconium-steam oxidation. The temperature remains almost stable for about 800 seconds, and then begins to decrease. This leveling off and subsequent decrease reflects the decreasing rate of zirconium-steam reaction as limitations in steam supply or hydrogen blanketing begin to take effect. The noticeable jumps in the gas temperature on the downslope of the curve are due to the heat-up and oxidation of the cooler nodes located in the outer regions of the core. This rapid oxidation burst creates a momentary increase in the gas temperature. Core-wide, however,

the zirconium oxidation rate continues decreasing, thereby decreasing the gas temperature exiting the core region. The sudden drop in the gas exit temperature observed at approximately 9300 seconds signals the core slump and collapse into the lower plenum.

Before discussing the thermal response of the individual volumes in the gas flow path, note that the accident consists of a blowdown and subsequent gas flow through all four loops, as opposed to one loop in the TMLB case. Consequently, the gas flow out of the core shown on Figure 5.85 splits into four individual paths, each path carrying with it one-quarter of the fission product material airborne in the upper plenum. This flow-splitting has been accounted for in the analysis. The results of the thermal response analysis are presented as applied to the response of a single loop; however, the results of the fission product retention analysis apply to the entire reactor system, i.e., all four loops.

Figures 5.87 through 5.89 show the thermal response of the primary system to the gas flow entering the upper plenum. The gas flow rate out of the core into the upper plenum and its temperature history is shown on Figure 5.86. The effect of fission product deposition on the gas temperatures in each volume and on the heat structures, discussed in Section 5.1, is directly applicable and incorporated by reference here.

Figures 5.87 and 5.88 show that the initial gas temperature rise in the upper plenum, and the associated heat structure temperature rise, are due to the heat transferred from the gas flow stream to the structure and not to any energy transferred from the fission products. Figure 5.89 shows that energy transferred to the heat structures from fission products in the upper plenum does not become significant until approximately 6200 seconds into the accident. This clearly coincides with the initial rise in the gas temperature in the upper plenum, and the rise in the structure temperature in the same volume.

Figure 5.89 shows that the energy transferred to the heat structures in the upper plenum increases rapidly after about 6200 seconds and peaks out at approximately 7700 seconds. This peaking is from re-volatilization of

the volatile species that have been condensed on the structural surfaces, the entrainment of the vapors by the gas stream, and subsequent transport of these volatiles into other volumes downstream. Although the decrease in the energy transfer from the deposited fission products to the structures in the upper plenum is significant, the corresponding decrease in the heatup rate of the structure in the upper plenum is not as noticeable. This is because the core exit gas temperature reaches its peak at approximately the same time and remains at an elevated temperature for a significant period. By comparison, the overall heat transfer to the upper plenum structures is affected less by the evaporation of the fission products. At approximately 7800 seconds, the amounts of re-vaporized and entrained fission products being swept out of the upper plenum become smaller than the amounts of the fission products coming into the upper plenum from the core region. At that time, the fission product energy deposited in the upper plenum begins to increase until it decreases once again at approximately 9000 seconds. The gradual increase in the heat transfer to the upper plenum structures after about 7800 seconds is not due to an increase in the deposition rate of the volatile fission products. Rather, the flow rate out of the upper plenum into the hot legs is low enough that the amount of fission products coming into the upper plenum result in an overall increase in the vapor inventories of the different fission product species in the upper plenum.

It is informative to compare the overall heat structure temperature response in the upper plenum in this accident sequence to that of the TMLB sequence discussed in Section 5.1. Figure 5.30 for the TMLB case shows that the upper plenum structures heated up fairly slowly at first, but then the heat rate accelerated for the remainder of the accident sequence. Figure 5.88 for the pump seal LOCA sequence shows that the heat structures initially heat up fairly slowly, then more rapidly with fission product deposition, finally leveling off with the re-volatilization of the fission products and a decrease in the core exit gas temperature.

The flow rate out of the upper plenum into the hot legs is not sufficient to carry fission products away and thereby decrease the energy transfer to the upper plenum structures. However, the flows during the pump seal LOCA

sequence are high enough to produce considerably lower partial pressure of the volatiles in the upper plenum and re-volatilize the condensed volatiles at a lower temperature. Yet in the case of the TMLB sequence, the volatiles partial pressure was higher, requiring a higher temperature of the structures in order to achieve re-volatilization. Combined with the very low flow out of the upper plenum, the slower re-volatilization rate resulted in a higher energy transfer to the upper plenum structures and continued heatup. Because of the higher flows in the pump seal LOCA case, the energy transfer rate to the upper plenum structures is lower and causes the energy transfer from the gas to the structures to play a more significant role.

Figure 5.86 shows that the core exit gas temperature begins to drop rapidly, starting at approximately 7700 seconds. In combination with the decreased energy transfer rate from the fission products in the upper plenum, the overall heat structure temperature of that volume begins to level off and eventually decrease at approximately 9600 seconds.

Figures 5.87 and 5.88 also show the gas temperatures exiting the hot leg and the hot leg structure temperature. Figure 5.89 shows the corresponding energy transfer rate from the fission products in that volume to the hot leg structures. The effect of the fission product energy transfer to the structure is noticeable at approximately 6500 seconds when the temperature of the hot leg begins to increase at a steady rate. At approximately 8400 seconds, the temperature begins to level off. This leveling-off is due to the re-volatilization of the deposited volatiles and their entrainment in the gas stream, which then carries the volatiles into downstream volumes.

The temperature response of the hot leg in the case of the pump seal LOCA is somewhat different than for the TMLB because of its higher gas stream flow rates from the upper plenum to the downstream volumes. More fission products will find their way to the downstream volumes than in the TMLB case. Because more fission products are being contained within that volume, the hot leg heats up at a faster rate than in the case of the TMLB sequence. And because of the higher flow rates, the partial pressure of

the volatiles in vapor form is lower throughout the system. Therefore, re-volatilization of the condensed volatiles takes place at lower structure temperatures than in the TMLB case. Figure 5.89 shows that the fission product energy transfer rate through the hot leg structure peaks out at approximately 7800 seconds which corresponds to a structural temperature of approximately 2000 F.

At 7800 seconds the pressure in the system is only about 700 psia, making rupture of the hot leg piping doubtful. However, the hot leg temperature continues to increase, reaching nearly 2200 degrees F at approximately 9000 seconds. Combined with the pressure in the primary system at that point, the 2200 F temperature could indeed result in piping rupture.

Figure 5.88 shows the thermal conditions in the plenum of the steam generator. The structure does not begin to heat up significantly until after a rapid increase in the fission product energy transfer rate to the structure at approximately 7800 seconds, as shown in Figure 5.89. This coincides with the significant re-volatilization and consequent entrainment of the volatile vapors from the hot leg volume. It also coincides with rapid heat up in the steam generator plenum structure, as shown in Figure 5.88; at approximately 8500 seconds, re-volatilization of the deposited volatiles takes place. Figure 5.89 shows the energy transfer rates through the steam generator plenum.

Figures 5.88 also shows the thermal response and conditions in the U-tube of the steam generator. While a complete discussion will be presented later, note that there are essentially no horizontal surfaces for gravitational deposition in this particular volume. Only vapor condensation could act as the removal mechanism for fission products within the U-tube section of the steam generators.

Figure 5.89 shows the energy deposition rate due to the fission products in the U-tube section of steam generator. Significant energy deposition starts at approximately 7800 seconds, in parallel with upper plenum and hot leg re-volatilization of the fission products. This increase in the energy transfer rate result in the temperature behavior shown in

Figure 5.88, where the temperature of the structure initially increases very slowly as a function of the heat transfer from the gas stream to the structures. A gradual temperature rise follows because of the presence of the fission products in the U-tube section of the steam generator.

Figure 5.88 shows the thermal response of the two volumes downstream of the steam generator, i.e., the cold leg and the pump volute. Figure 5.89 shows the corresponding energy deposition rates from the fission products present in the two volumes.

The energy deposition rate in the cold leg increases steadily after 7800 seconds. This is due to the transport of the condensed volatiles on particles through the steam generator tubes to the cold leg. Further discussion of this behavior will follow.

Note that the amount of energy transferred from fission products to the pump volume is very small when compared to other upstream volumes. Both of these volumes remain quite cool throughout the duration of the accident. The bathtub shape of gas temperature exiting the pump volute during early stages of the accident is due to the fact that the pump volute is initially at the cold leg temperature. A large difference exists between the structure temperature and the gas entering the temperature of the volume. This large temperature difference manifests itself in a rapid increase in the structure temperature over time. An initial rapid drop in the gas exit temperature, followed by its asymptotic approach to the structure temperature, gives rise to the peculiar shape of the curve.

5.2.4. M-C-T Results -- Primary System Fission Product Retention

Figures 5.90 through 5.101 show the behavior of the fission products in the primary system, as well as the total releases of the different fission product species to the containment.

Figure 5.90 shows the retention factor of CsI in the primary system. The overall retention of CsI, top curve, peaks out at approximately 75%. Re-volatilization of the condensed CsI begins, and the retention factor decreases until approximately 8300 seconds. At that time, it increases

again upon the arrival of entrained vapors in the cooler downstream volumes, where the vapors begin to condense. The rise in the retention factor turns around again when the downstream volumes heat up to the re-volatilization temperature and the condensed CsI begins to re-volatilize again. The specifics of this transport will be discussed later.

Figure 5.92 shows the CsI mass retained on structural walls and deposited on aerosol particles. The initial retention of CsI by condensation on structural walls is small compared to the retention by deposition on aerosol particles. A peak occurs at approximately 7500 seconds due to the re-volatilization of the condensed CsI. This peak in retention through condensation on structural walls coincides with a peak in retention of CsI through deposition on aerosol particles. At approximately 8300 seconds, a turnaround in the CsI retained on walls and deposited particles takes place when the re-volatilized species arrive in the cooler volumes and condense on both structural walls and suspended aerosol particles.

Figure 5.90 shows that the CsI retention factor in the upper plenum and the hot leg reach a maximum at approximately 7300 seconds and 7500 seconds, respectively, followed by a rapid decrease. This is caused by re-volatilization of the condensed species after structural heat-up.

The shape of the CsI retention curve in the steam generator plenums, shown in Figure 5.90, shows similar behavior. At approximately 7000 seconds, the retention factor begins to increase, which is consistent with the leveling-off then rapid decrease in the retention factor of the upper plenum and the hot leg. The rapid decrease in the retention factor of the upper plenum and the hot leg accounts for the decrease in the overall retention factor at about 7500 seconds. The increase in the overall CsI retention factor at approximately 8300 seconds is governed by CsI retention in the steam generator plenums. At approximately 9500 seconds, this increase in the overall retention factor turns around and begins to decrease again as the condensed CsI re-volatizes in the steam generator plenums and the entrained vapors are carried into downstream volumes.

The steam generators were modeled as two separate volumes: the steam generator plenum as one volume, and the U-tube section of the steam generators downstream of the plenum as another volume. The CsI retention factor for these two volumes is shown in Figure 5.90. Because there are no horizontal surfaces for gravitational settling in the steam generator tubes, this mechanism for removal of suspensed aerosols was assumed to be non-existent in that volume. The entrained vapors from re-volatilization in the steam generator plenum, and to a lesser extent, the upper plenum and the hot leg entering the steam generator U-tube section, preferentially condense on the surfaces of the suspended particles because of area-to-volume ratio considerations, and are carried in that manner into the cold leg volume.

A considerable mass of CsI already condensed on particle surfaces quickly deposits gravitationally on the cold leg volume surfaces. This explains the small amount of CsI retained on the structural walls by condensation in the later stages of the accident, i.e., approximately 9700 seconds onwards.

It is important to reiterate that the steam generator tube section does not play a major role in the removal of volatile fission products. Because the volatiles arrive in the U-tube section "riding" on aerosol particle surfaces, and the steam generators are ineffective in removing these aerosols, the volatiles subsequently enter the cold leg. Figure 5.90 shows that the CsI retention factor in the cold leg increases significantly in the latter stages of the sequence due to that phenomenon. In fact, the majority of all the retained CsI eventually resides in the cold leg. This is further confirmed by Figure 5.91, which shows the CsI mass released to containment, either in vapor form or condensed on particle surfaces which exit the primary system through the break into containment. The amounts of CsI released to containment are essentially negligible until the primary system fails. At that time, CsI vapors entrained in the gas stream and not yet condensed, as well as CsI condensed on aerosol particles but not yet deposited, are assumed to be released to the containment atmosphere.

Figures 5.93 through 5.95 show the behavior of CsOH in the primary system and its release to the containment. The overall behavior of CsOH is quite similar to the behavior exhibited by CsI; the main difference is that CsOH has a non-zero deposition velocity for chemical sorption onto surfaces. Therefore, removal of CsOH by sorption onto steel surfaces is a significant removal mechanism. The mass of CsOH removed by this mechanism is shown in Figure 5.95. The amount of CsOH removed by sorption increases as the wall condensation removal mechanisms decrease. Specifically, as CsOH re-volatilizes, chemical sorption on surfaces becomes more competitive. The chemical sorption mechanism is evident when examining Figure 5.93. Following the initial rise in the retention factor of CsOH in the upper plenum and the hot leg, the retention factor decreases and steadies out at a small value which corresponds to the retention due to chemical sorption on the wall surfaces in these volumes.

Figures 5.96 through 5.98 show the behavior of aerosols and the release of aerosol particles into the containment. Figure 5.96 shows that about 90% of the aerosols released from the core into the gas stream are retained in the primary system. Because of the gas stream flow rate associated with the pump seal LOCA, the aerosol retention is distributed mostly among the upper plenum, the hot leg, the steam generator plenum and the cold leg. The hot leg accumulates the majority of the deposited aerosol. The aerosol retention factor in each volume is shown in Figures 5.96.

Figures 5.97 through 5.101 show the behavior of tellurium. Tellurium behaves much as it did in the TMLB sequence with chemisorption being the dominant removal mechanism in retaining almost the entire tellurium inventory in the primary system.

5.2.5 MATADOR II Results

Figures 5.102 through 5.116 present the results of the analyses of fission product behavior in containment, following release from the primary system which has undergone a pump seal LOCA. Comparison of these figures to the corresponding figures in section 5.1 for the TMLB sequence reveals that the behavior of the fission products in the containment associated with the pump seal LOCA is nearly identical to that exhibited by the fission

products in the containment following the TMLB accident sequence. Therefore, the discussion of results presented in Section 5.1.6 is directly applicable to the results presented in Figures 5.102 through 5.116.

5.3 Summary of Results and Conclusion

5.3.1 Summary of Results

The analytical results are summarized on Tables 5.1, 5.2 and 5.3. Table 5.1 shows a comparison of the calculated source terms by this analysis compared to the WASH-1400 source terms. Clearly, the calculated realistic source terms are several orders of magnitudes smaller than those of WASH-1400. Table 5.2 shows the effect of various modeling additions and changes to the computer code phenomenology on the final environmental release source term. Table 5.3 shows the distribution of the fission products in terms of the fraction of core inventory retained in the primary system, the fraction retained in the containment (both in the melt and as vapor), and the fraction released to the environment.

In the two cases analyzed, the volatiles (i.e., cesium iodide, cesium hydroxide, and tellurium) are completely released during the melt-down process; therefore, their fraction remaining in the melt is zero. Furthermore,the tellurium fraction remaining in the primary system is very close to "1" for both accident sequences. This is due to the high deposition velocity of tellurium for chemisorption onto steel surfaces of the primary system. However, the retention of cesium iodide and cesium hydroxide by the primary system for the two accident sequences is quite different. In the case of the pump seal LOCA, the primary system retains a larger fraction of both cesium iodide and cesium hydroxide, than in the TMLB case. The reason for this is the higher gas flow rates between volumes present during the pump seal LOCA accident sequence which carry the vapor form of the volatiles from hotter volumes to cooler volumes where the volatiles condense onto either structural surfaces or

aerosol particles, which subsequently settle out. In the case of the TMLB sequence, the retention of cesium iodide and cesium hydroxide in the primary system is low due to low gas flow rates between volumes and the re-volatilization of the condensed volatiles as a consequence of structural heating by fission products. The re-volatilized fission product species enter the gas stream; however, since the gas stream flows at a slow rate it is not readily moved into cooler volumes, causing the volatile species to remain in vapor form in the hotter volumes for a longer period of time. This results in lower overall retention by the primary system upon lower reactor head failure.

The somewhat larger retention of cesium hydroxide than cesium iodide for both accident sequences is because cesium hydroxide has a higher deposition velocity for chemisorption onto stainless steel surfaces in the primary system than cesium iodide. In fact, for these analyses the deposition velocity for cesium iodide chemisorption was assumed as zero.

The containment retention of the fission product species, between the time of release from the primary system and the time of release from the containment, is very high. This is due to the fact that the volatile species, when released from the primary system as vapors, quickly condense onto the aerosol particles suspended in the contained atmosphere and settle during the long time interval between the primary system failure and containment failure. Analyses show that this settling out of fission products occurs during the first six to eight hours after release from the primary system. After that duration, the settling out of the particles from containment atmosphere reaches an essentially asymptotic rate which continues until containment failure.

5.3.2 Conclusions

1. The calculated source terms for two accident sequence scenarios at Indian Point 3 are a small fraction of the source term calculated in the two previous relevant studies, the Indian Point Probabilistic Safety Study and the WASH-1400 study.

2. Because the fission products suspended in the containment atmosphere are removed by natural processes within a period of approximately six to eight hours after accident initiation, the mode of late containment failure is not critical.

3. The analytical ability to estimate the time of containment failure within a margin of at least two to three hours raises questions about the need for further research into primary system retention of fission products. This is true for the Indian Point 3 station, and most likely for all dry containment PWRs.

4. The fission products released from the primary system, and those released from the core-concrete interaction, are readily removed by natural processes occurring in the containment. Most important of these is particle agglomeration and gravitational settling. In addition, condensation of volatile species onto aerosol particle surfaces is a dominant means of volatile fission product removal from the containment atmosphere.

5. Iodine and cesium are the major contributors to the early and latent fatality risks, respectively. It was found that their environmental release fractions ar rather insensitive to the modeling of fission product heating, the type of insulation on the primary system, and whether or not log-normal or "bin" models were used to depict particle agglomeration. These modeling differences are of interest in calculating the location of fission product species early in the accident sequences. However, after a few hours, and long before the containment overpressurizes, low concentrations of iodine and cesium are found in the containment atmosphere for all models.

6. Fission product heating of structural surfaces in the primary system plays an important role in the primary system retention of fission products.

7. Fission product heating of structural surfaces in the primary system, especially the hot leg and the surge line for the TMLB sequence, is the most probable cause of primary system failure and subsequent depressurization prior to lower reactor head failure.

TABLE 5.1

FRACTION OF CORE INVENTORY AVAILABLE FOR RELEASE

F.P. SPECIES	FRACTION OF INVENTORY		WASH-1400*
	TMLB EVENT	PUMP SEAL LOCA	SOURCE TERMS
Iodine	2.0×10^{-5}	4.5×10^{-6}	0.7
Cesium	1.6×10^{-5}	3.1×10^{-6}	0.5
Tellurium	6.5×10^{-9}	3.3×10^{-9}	0.3
Barium/Strontium	3.1×10^{-6}	2.4×10^{-6}	0.06
Ruthenium	1.5×10^{-6}	7.7×10^{-7}	2.0×10^{-2}
Lanthanum	5.4×10^{-6}	2.5×10^{-6}	4.0×10^{-3}
Noble Gases	0.90	0.90	0.90

* Source terms for Pump Seal Loca were not explicitly developed in WASH-1400.

TABLE 5.2

EFFECTS OF VARIOUS PHENOMENA ON
IODINE AND CESIUM RELEASE FRACTIONS (AT 24 HOURS)

PHENOMENON	IODINE RELEASE FRACTION	CESIUM RELEASE FRACTION
1) *With/Without Primary System Insulation	$2.0 \times 10^{-5}/2.04 \times 10^{-5}$	$1.6 \times 10^{-5}/1.73 \times 10^{-5}$
2)**With/Without Fission Product Heating	$4.5 \times 10^{-6}/4.9 \times 10^{-6}$	$3.1 \times 10^{-6}/3.4 \times 10^{-6}$
3)**Log-normal vs. "bin" particle modeling	$3.03 \times 10^{-5}/4.5 \times 10^{-6}$	$1.15 \times 10^{-5}/3.4 \times 10^{-6}$
4) *With/Without Core Concrete aerosol	$2.0 \times 10^{-5}/2.3 \times 10^{-5}$	$1.6 \times 10^{-5}/1.84 \times 10^{-5}$

* For TMLB case only

** For Pump Seal LOCA case only

TABLE 5.3

DISTRIBUTION OF FISSION PRODUCTS, FRACTION OF CORE INVENTORY

TMLB

	CsI	CsOH	Te	Ba	Ru	La
Primary System	.22	.32	.9999	.18	4.3×10^{-2}	3.4×10^{-5}
Containment (failure 24/hrs-puff release)	.78	.68	1.0×10^{-4}	.13	1.8×10^{-3}	1.6×10^{-3}
Remaining in Melt	0	0	0	.69	.9549	.9984
Released to Environment	1.9×10^{-5}	1.7×10^{-5}	6.5×10^{-9}	3.1×10^{-6}	1.5×10^{-6}	5.4×10^{-6}

Pump Seal LOCA

	CsI	CsOH	Te	Ba	Ru	La
Primary System	.67	.80	.998	.26	6.3×10^{-2}	5.1×10^{-5}
Containment (failure 24/hrs-puff release	.33	.20	2.0×10^{-4}	.16	9.9×10^{-3}	1.6×10^{-3}
Remaining in Melt	0	0	0	.58	.9266	.9984
Released to Environment	4.2×10^{-6}	2.7×10^{-6}	3.3×10^{-9}	2.4×10^{-9}	7.7×10^{-7}	2.5×10^{-6}

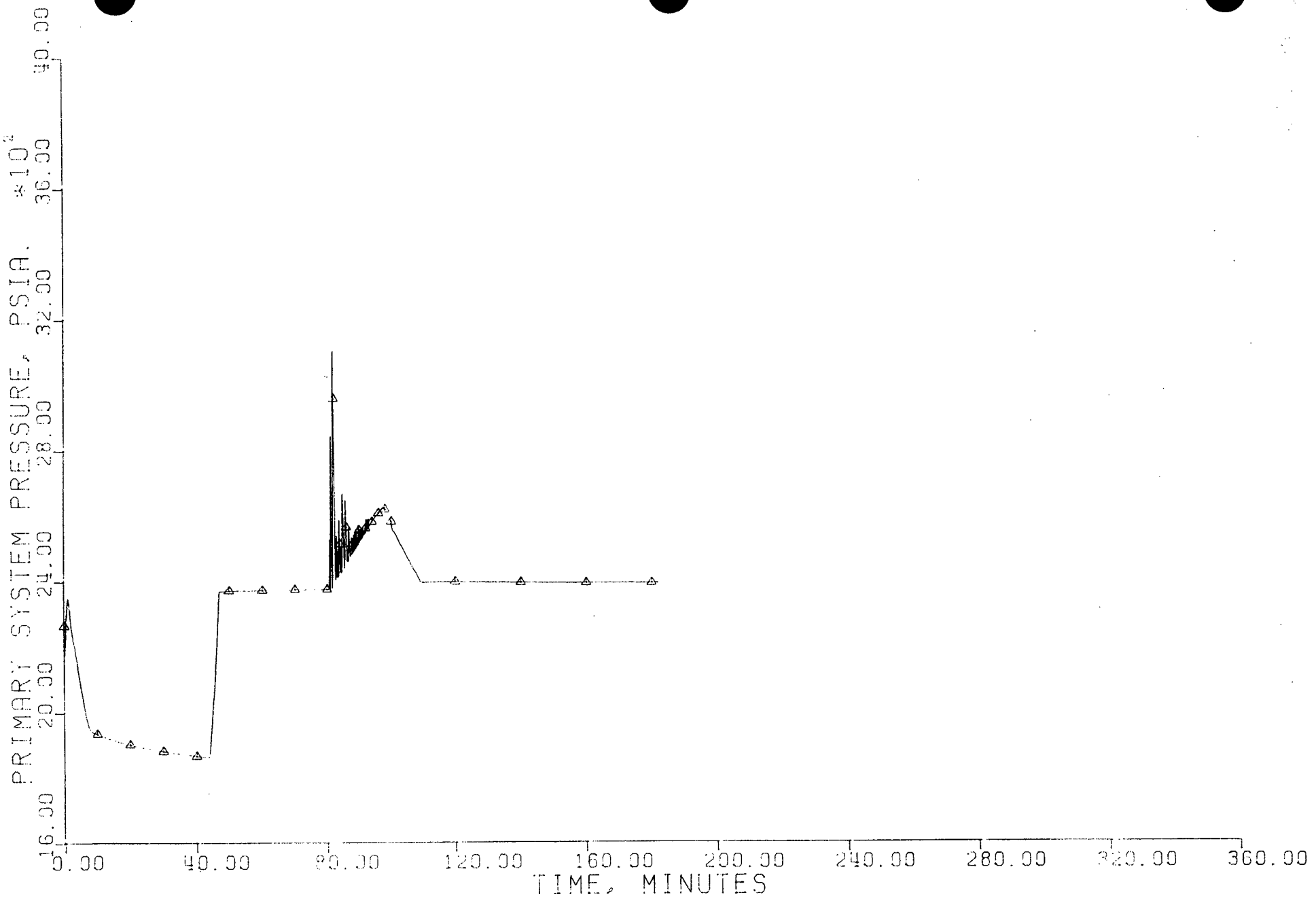
PRIMARY SYSTEM PRESSURE, PSIA. *10²
40.00
36.00
32.00
28.00
24.00
20.00
16.00
0.00
40.00
80.00
120.00
160.00
200.00
240.00
280.00
320.00
360.00
TIME, MINUTES

FIGURE 5.1

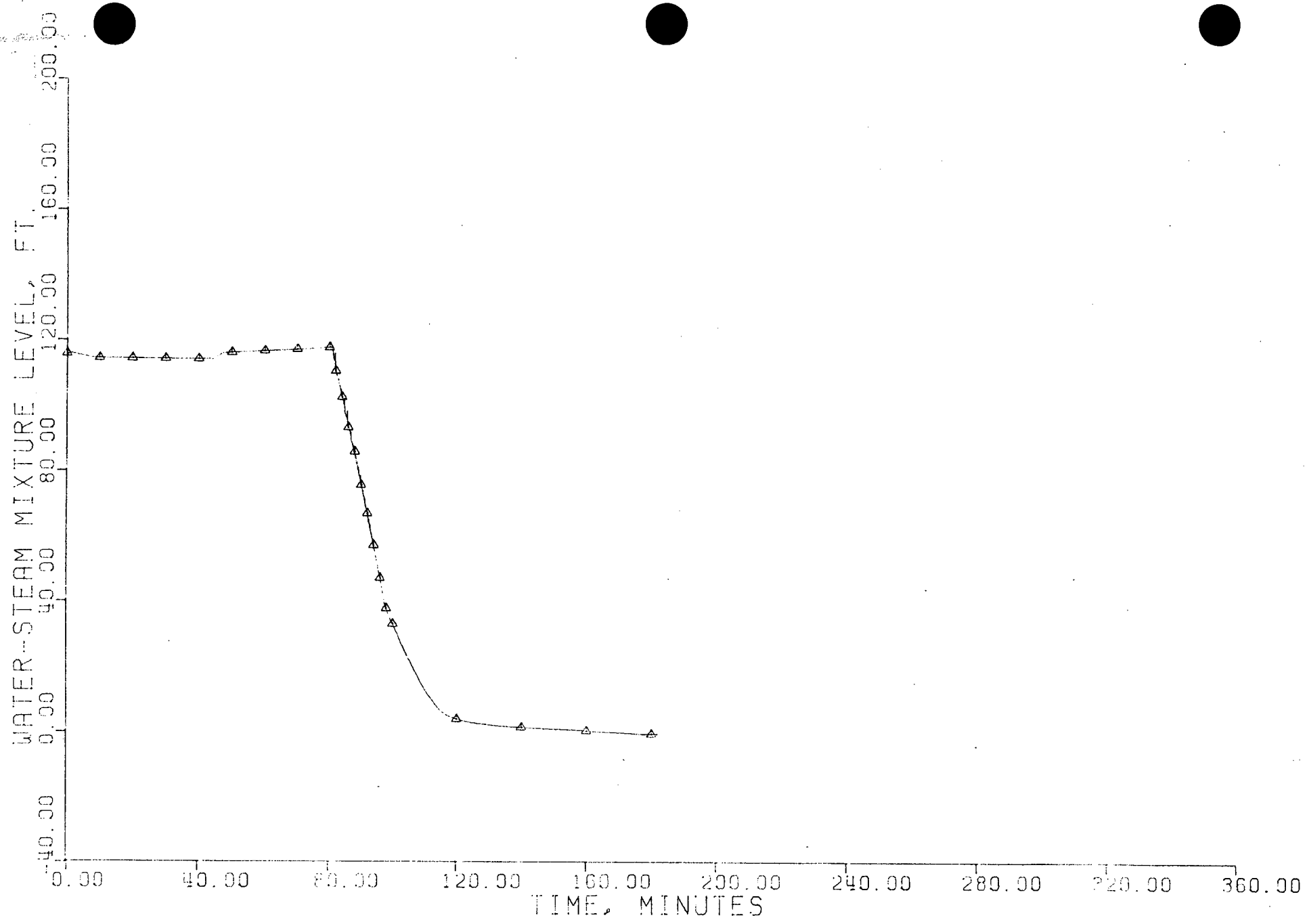
WATER-STEAM MIXTURE LEVEL, FT.
200.00
160.00
120.00
80.00
40.00
0.00
-40.00
0.00
40.00
80.00
120.00
160.00
200.00
240.00
280.00
320.00
360.00
TIME, MINUTES

FIGURE 5.2

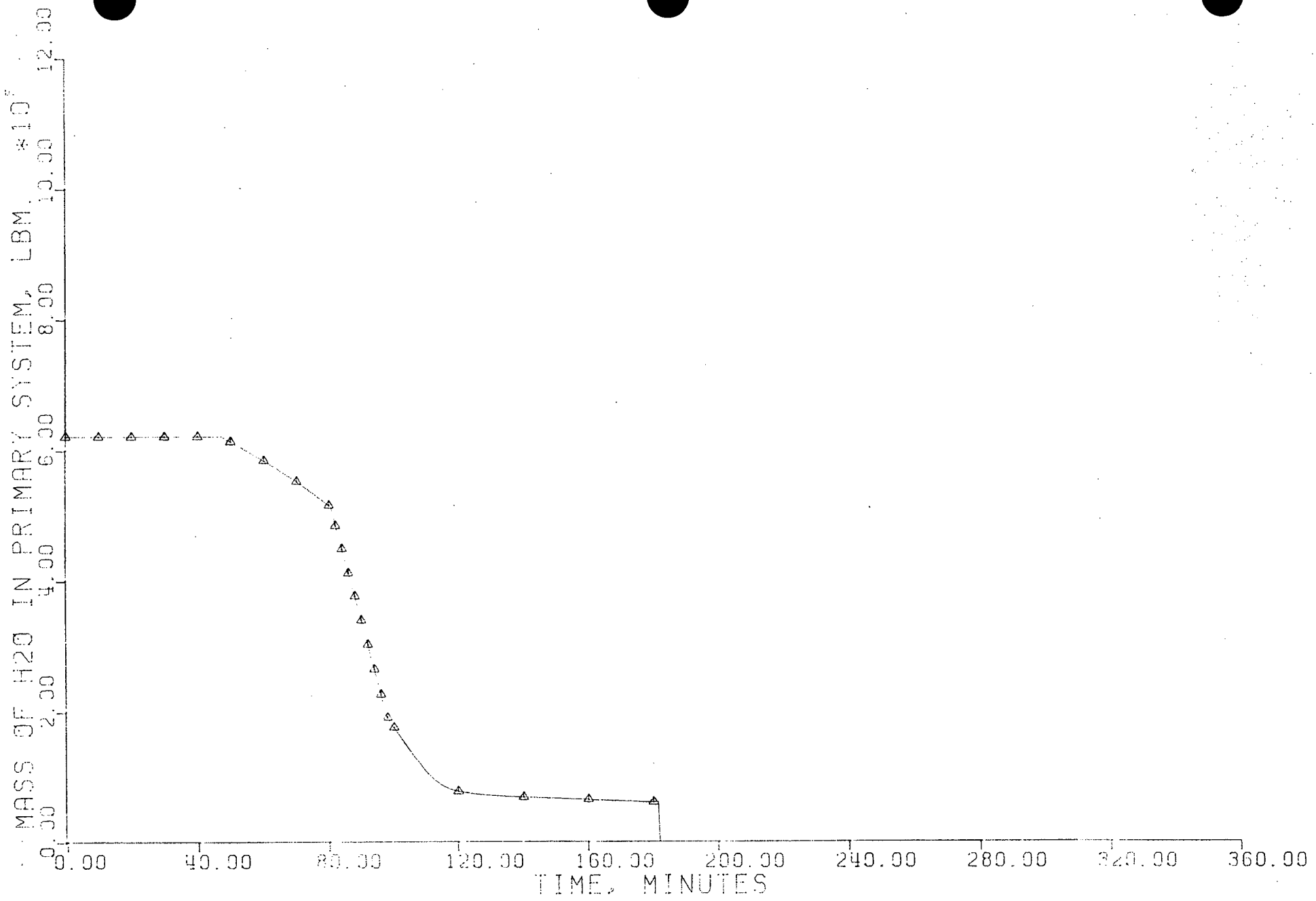
MASS OF H20 IN PRIMARY SYSTEM, LBM. *10
0.00
2.00
4.00
6.00
8.00
10.00
12.00
0.00
40.00
80.00
120.00
160.00
200.00
240.00
280.00
320.00
360.00
TIME, MINUTES

FIGURE 5.3

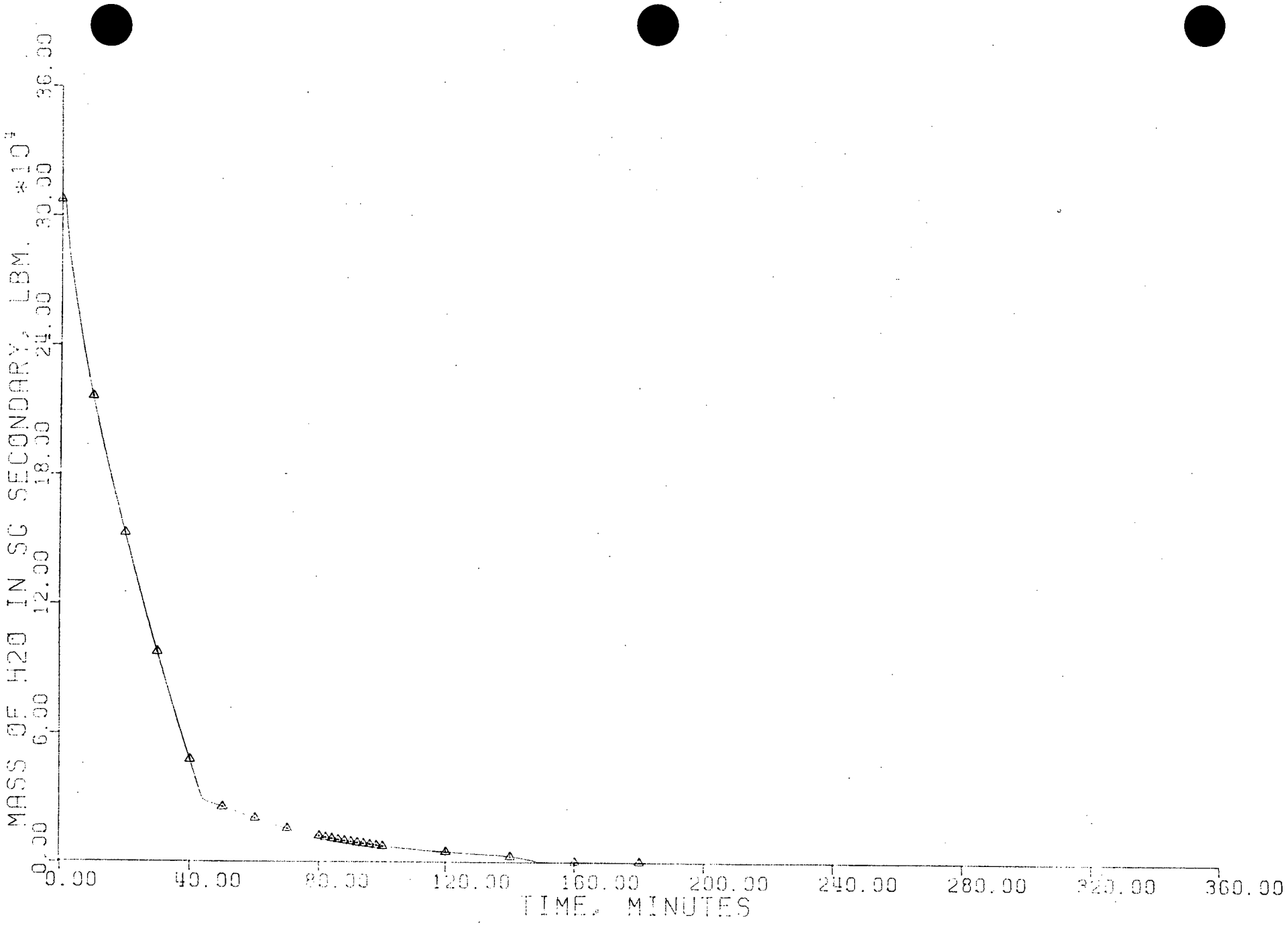
MASS OF H20 IN SC SECONDARY, LBM. *10**3
0.00
6.00
12.00
18.00
24.00
30.00
36.00
0.00
40.00
80.00
120.00
160.00
200.00
240.00
280.00
320.00
360.00
TIME, MINUTES

FIGURE 5.4

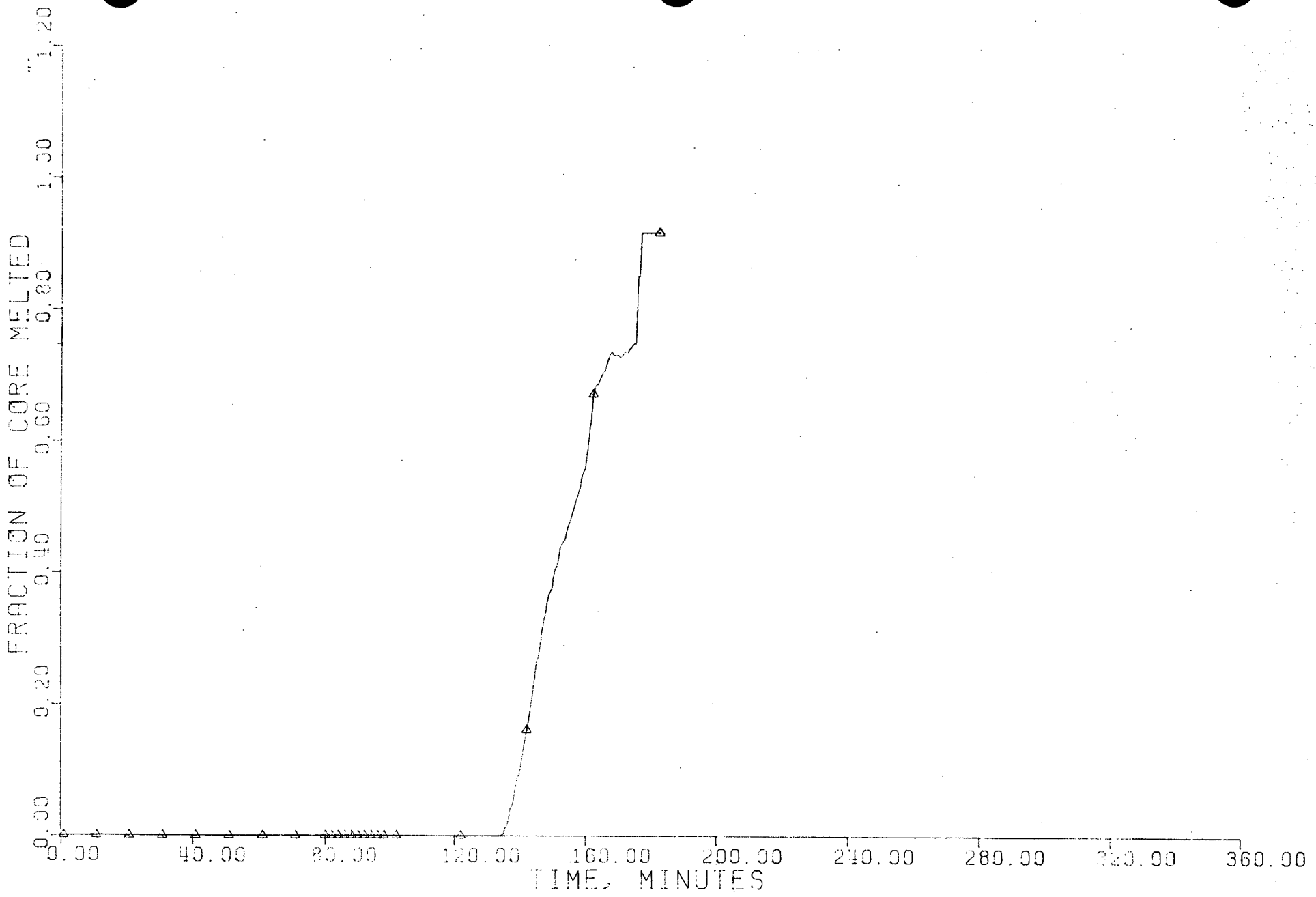
FRACTION OF CORE MELTED
0.00
0.20
0.40
0.60
0.80
1.00
1.20
0.00
40.00
80.00
120.00
160.00
200.00
240.00
280.00
320.00
360.00
TIME, MINUTES

FIGURE 5.5

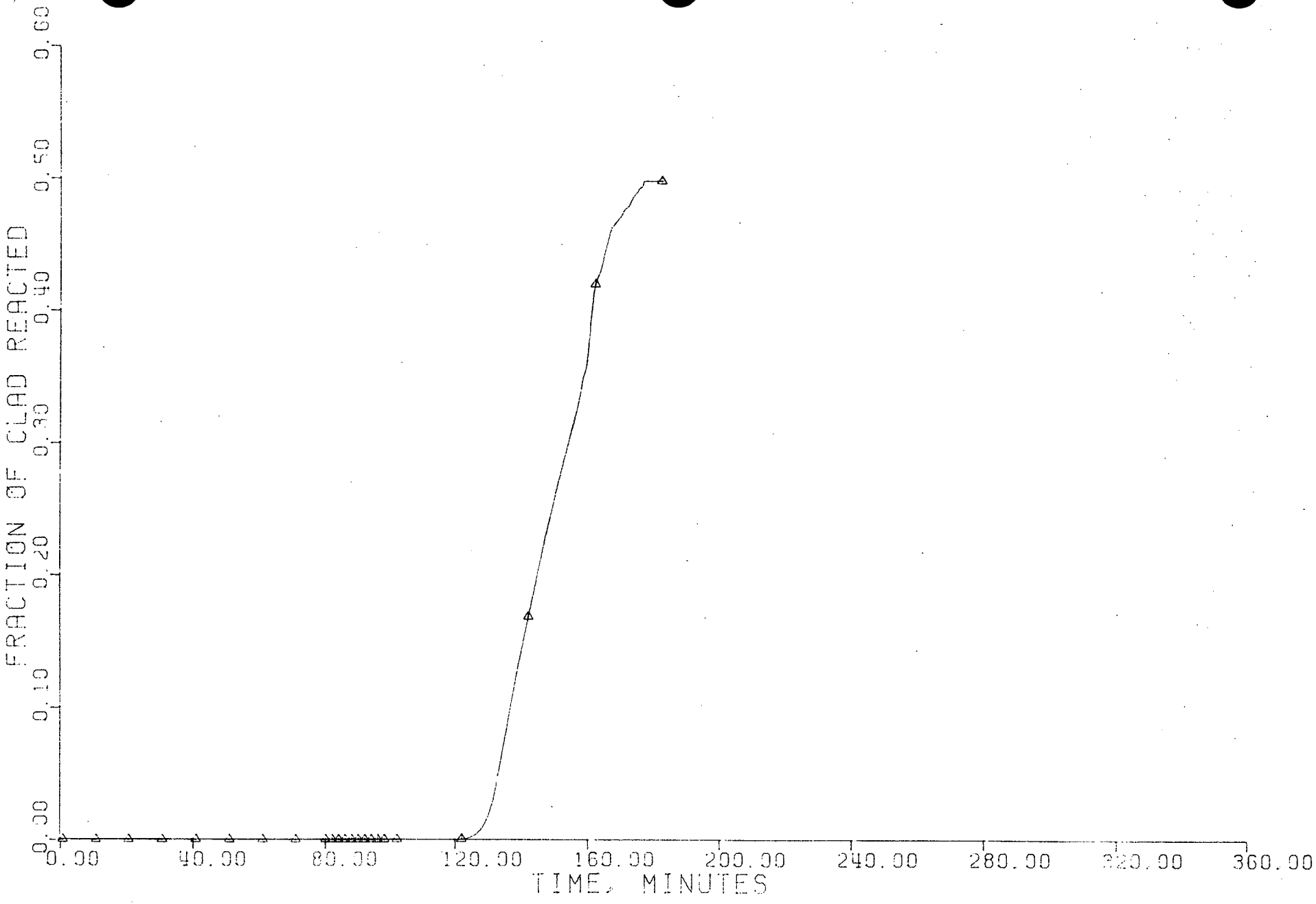
FRACTION OF CLAD REACTED
0.00
0.10
0.20
0.30
0.40
0.50
0.60
0.00
40.00
80.00
120.00
160.00
200.00
240.00
280.00
320.00
360.00
TIME, MINUTES

FIGURE 5.6

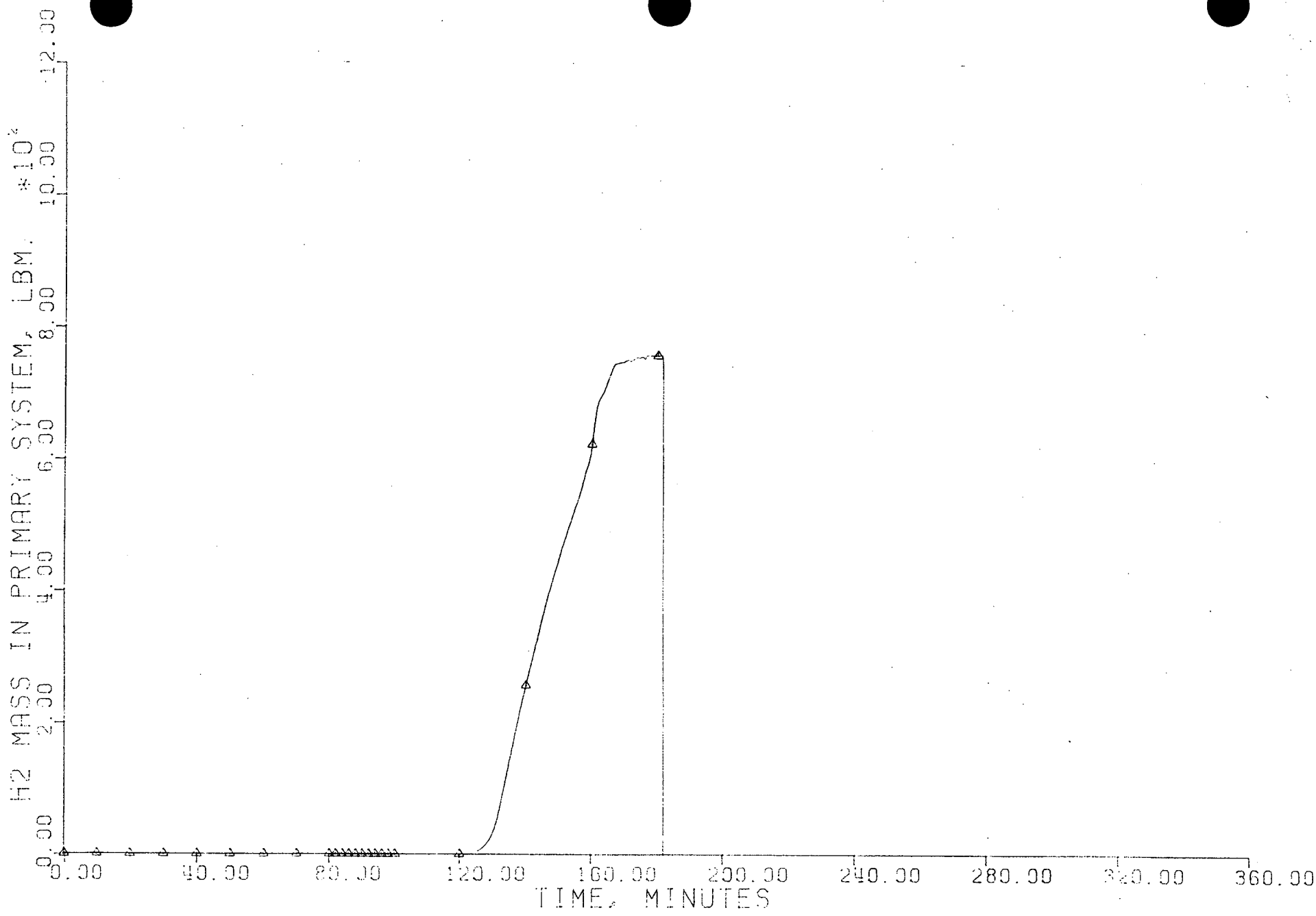
H2 MASS IN PRIMARY SYSTEM, LBM. *10²
0.00
2.00
4.00
6.00
8.00
10.00
12.00
0.00
40.00
80.00
120.00
160.00
200.00
240.00
280.00
320.00
360.00
TIME, MINUTES

FIGURE 5.7

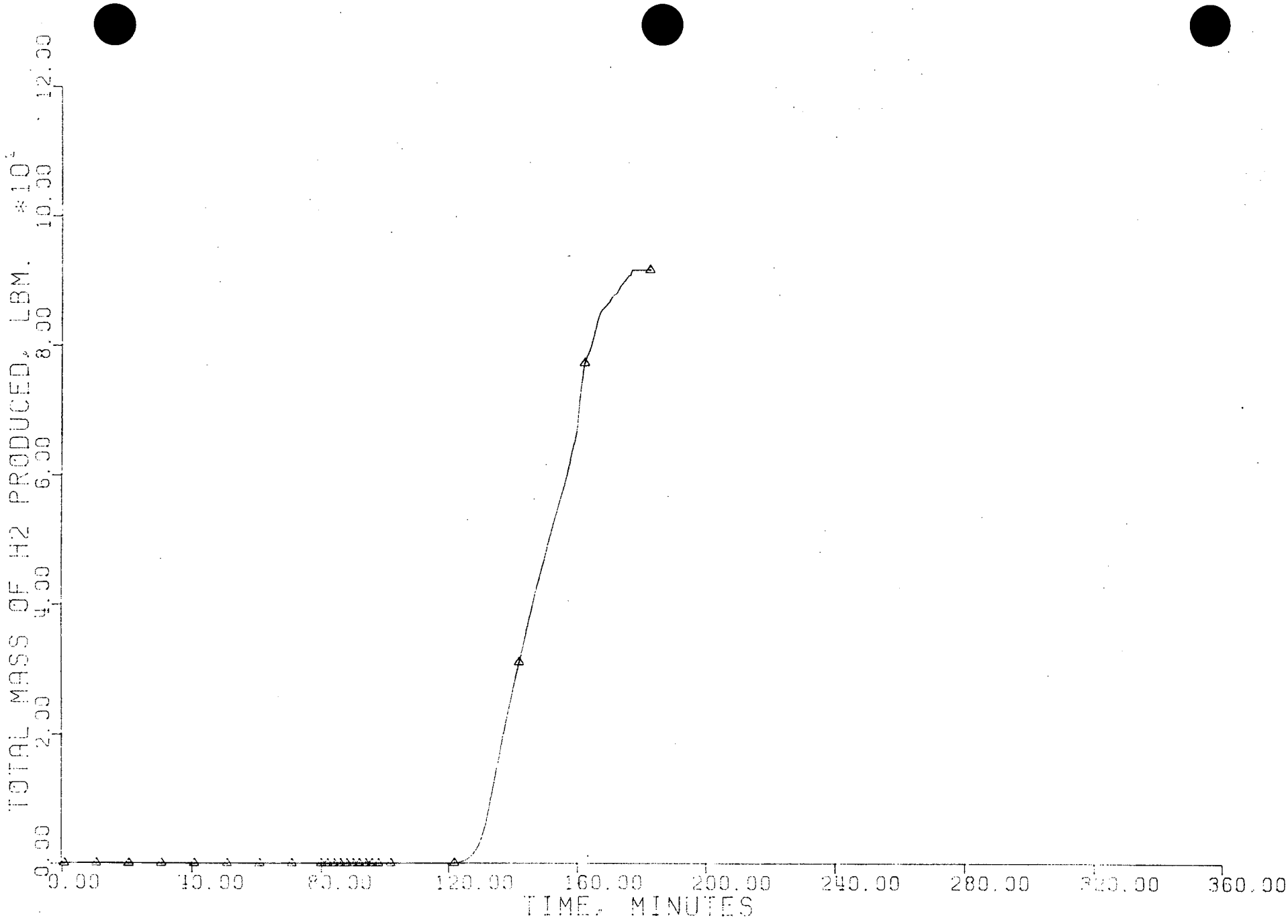
TOTAL MASS OF H2 PRODUCED, LBM. *10⁴
0.00
2.00
4.00
6.00
8.00
10.00
12.00
0.00
40.00
80.00
120.00
160.00
200.00
240.00
280.00
320.00
360.00
TIME, MINUTES

FIGURE 5.8

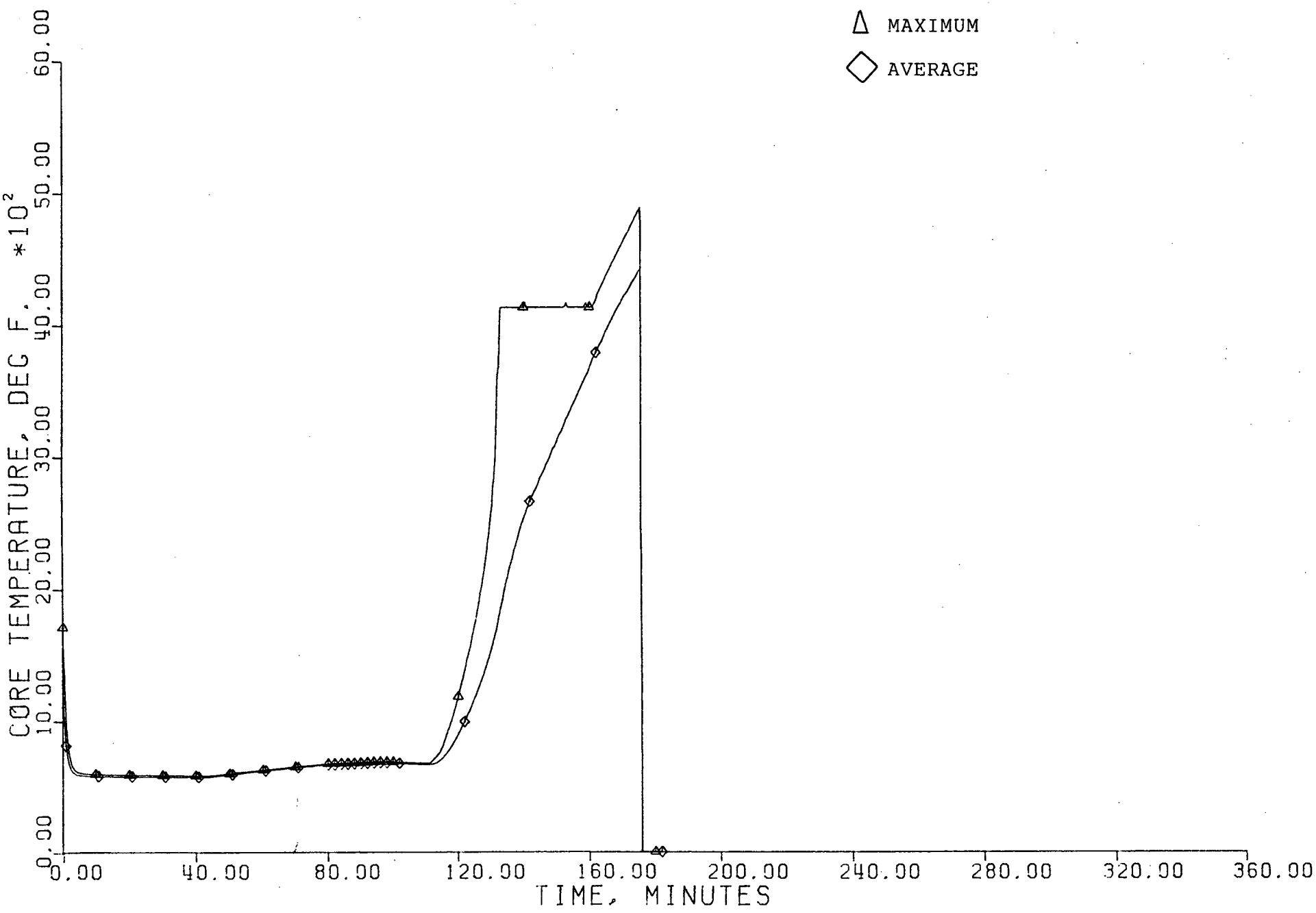
MAXIMUM
AVERAGE
CORE TEMPERATURE, DEG F. *10²
0.00
10.00
20.00
30.00
40.00
50.00
60.00
0.00
40.00
80.00
120.00
160.00
200.00
240.00
280.00
320.00
360.00
TIME, MINUTES

FIGURE 5.9

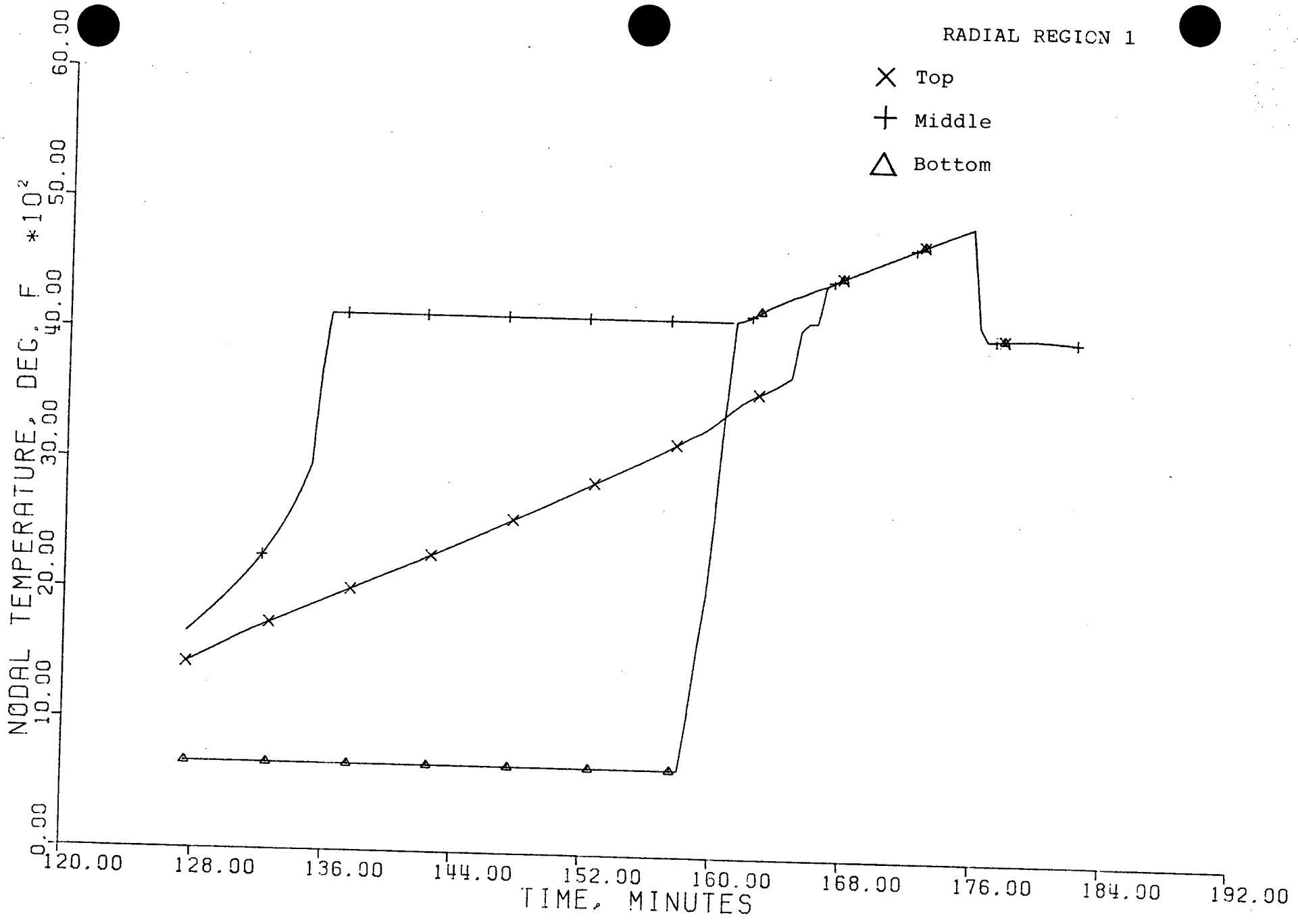
RADIAL REGION 1
Top
Middle
Bottom
NODAL TEMPERATURE, DEG. F *10²
60.00
50.00
40.00
30.00
20.00
10.00
0.00
120.00
128.00
136.00
144.00
152.00
160.00
168.00
176.00
184.00
192.00
TIME, MINUTES

FIGURE 5.10

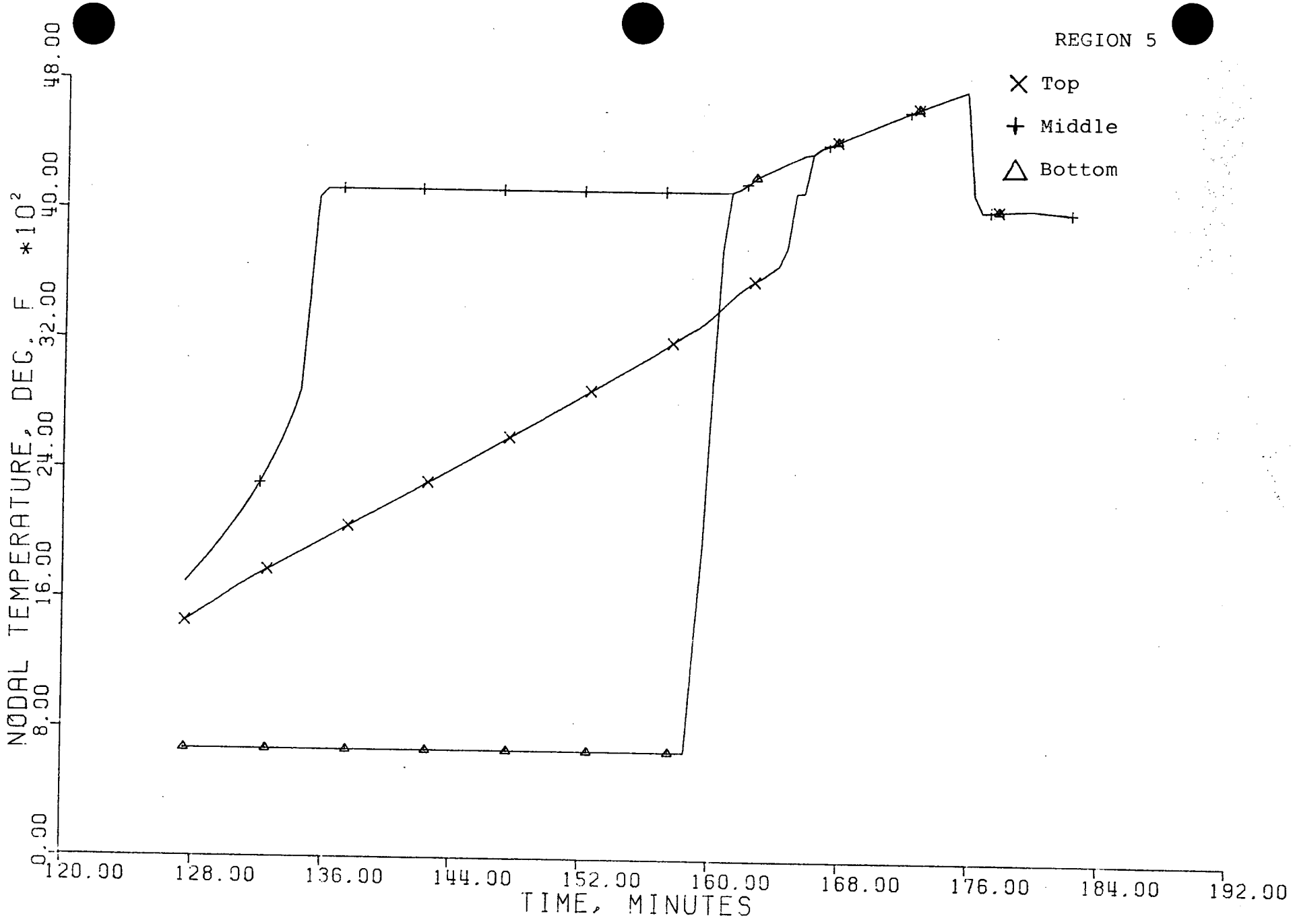
REGION 5
X Top
+ Middle
△ Bottom
NODAL TEMPERATURE, DEG. F *10²
0.00
8.00
16.00
24.00
32.00
40.00
48.00
120.00
128.00
136.00
144.00
152.00
160.00
168.00
176.00
184.00
192.00
TIME, MINUTES

FIGURE 5.11

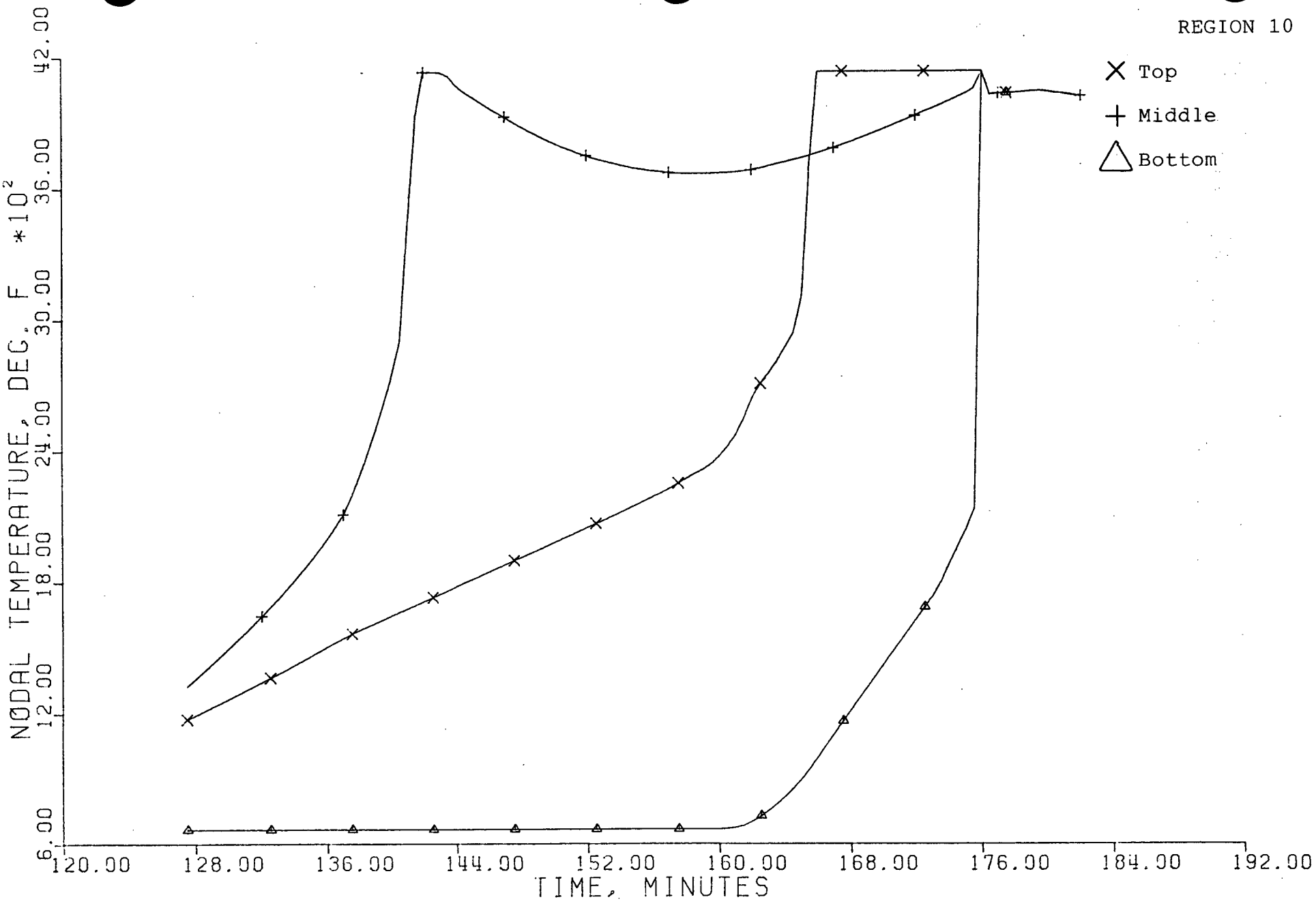
REGION 10
Top
Middle
Bottom
NODAL TEMPERATURE, DEG. F *10²
6.00
12.00
18.00
24.00
30.00
36.00
42.00
120.00
128.00
136.00
144.00
152.00
160.00
168.00
176.00
184.00
192.00
TIME, MINUTES

FIGURE 5.12

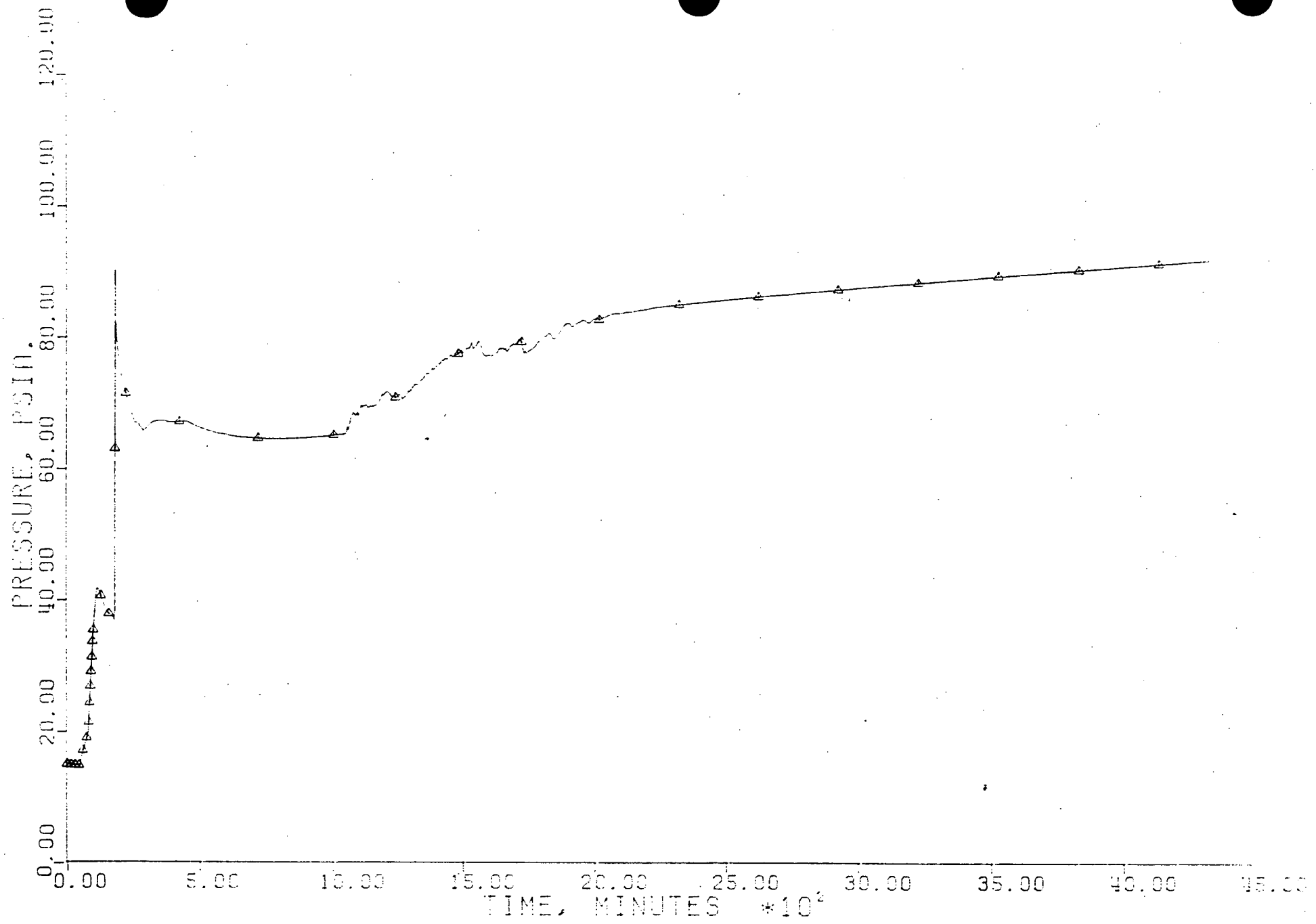
PRESSURE, PSIA.
0.00
20.00
40.00
60.00
80.00
100.00
120.00
0.00
5.00
10.00
15.00
20.00
25.00
30.00
35.00
40.00
TIME, MINUTES *10²

FIGURE 5.13

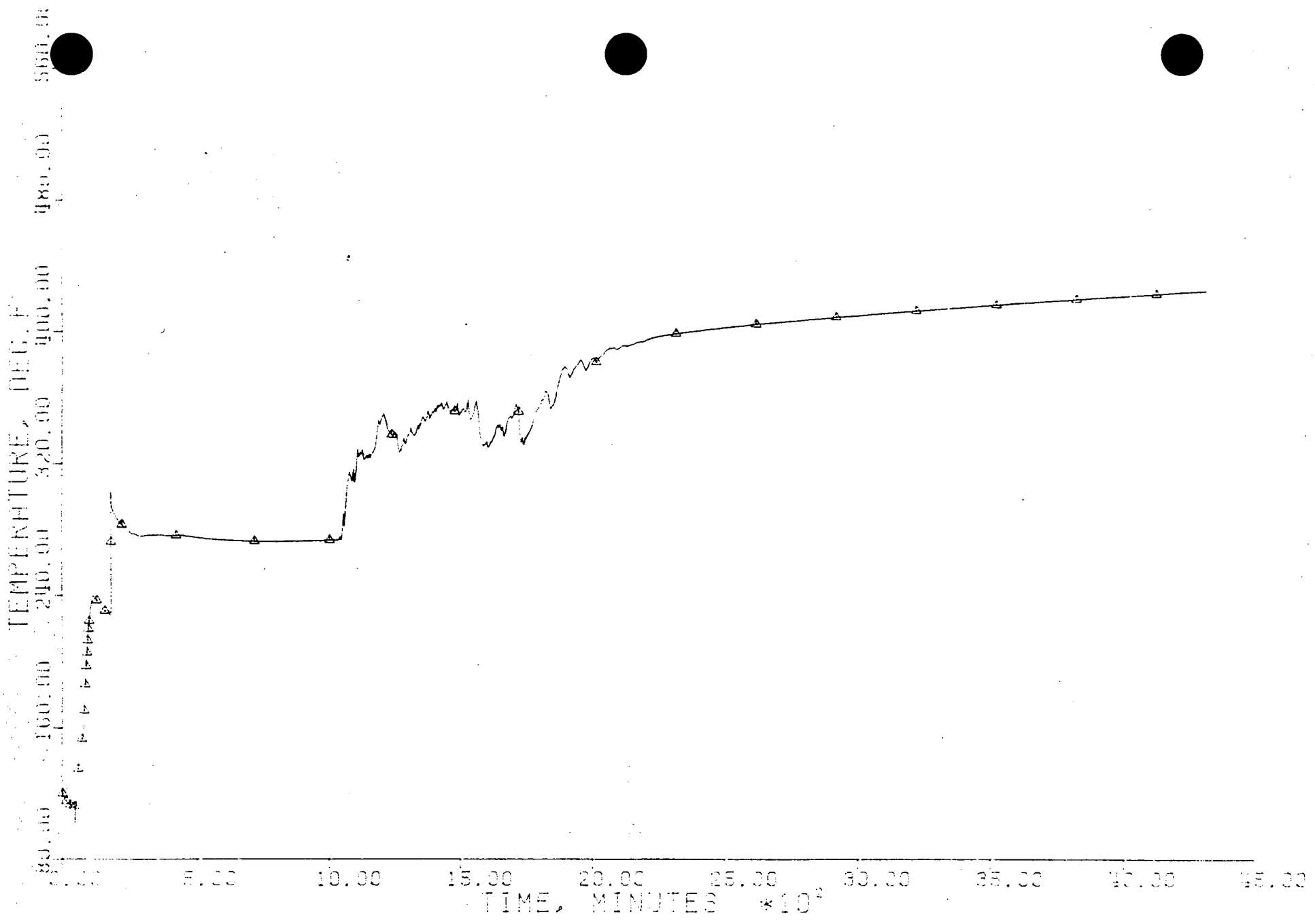
TEMPERATURE, DEG. F
160.00
240.00
320.00
400.00
5.00
10.00
15.00
20.00
25.00
30.00
35.00
40.00
45.00
TIME, MINUTES *10²

FIGURE 5.14

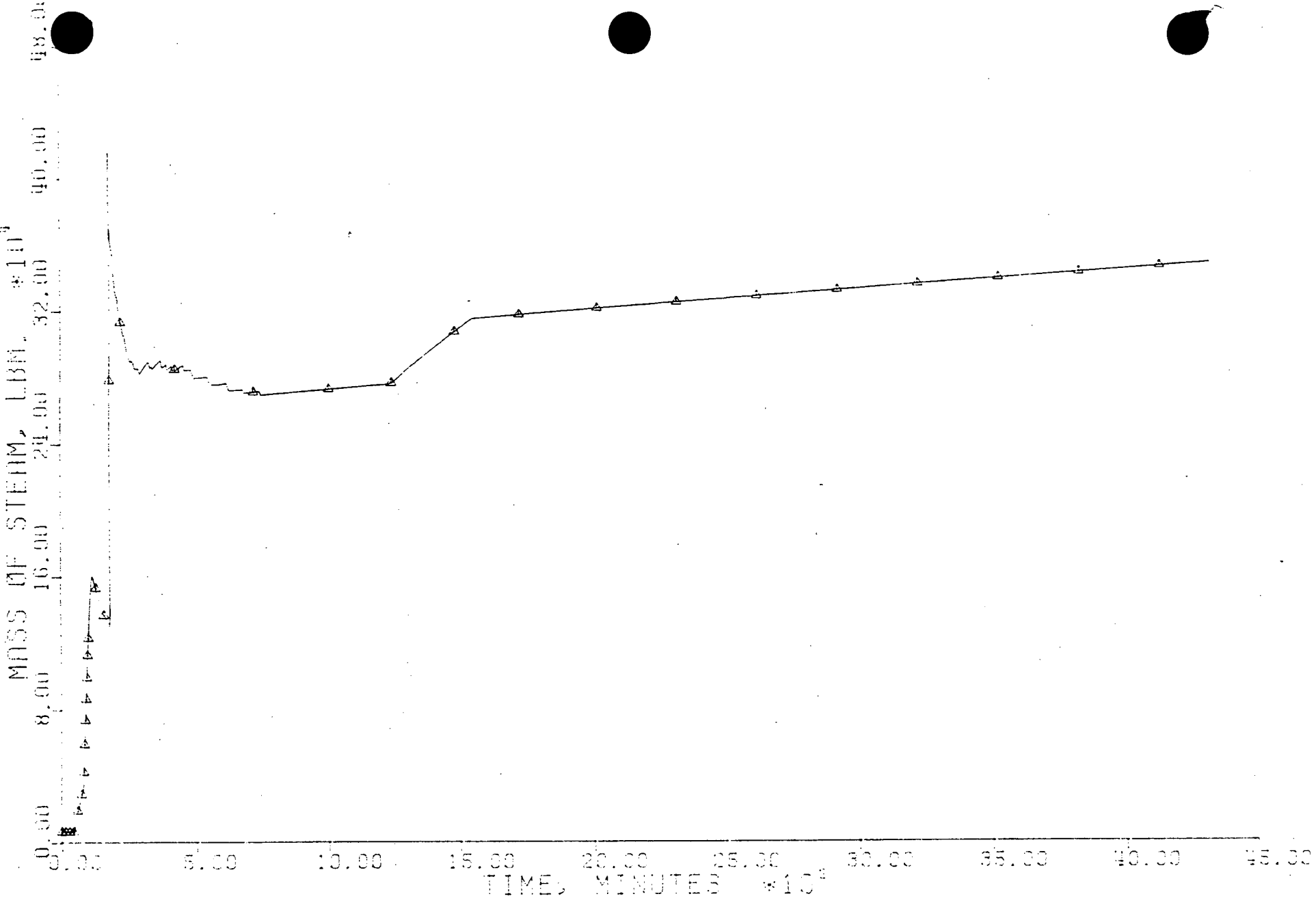
MASS OF STEAM, LBM, *10³
8.000
16.000
32.000
40.000
0.000
5.00
10.00
15.00
20.00
25.00
30.00
35.00
40.00
45.00
TIME, MINUTES *10¹

FIGURE 5.15

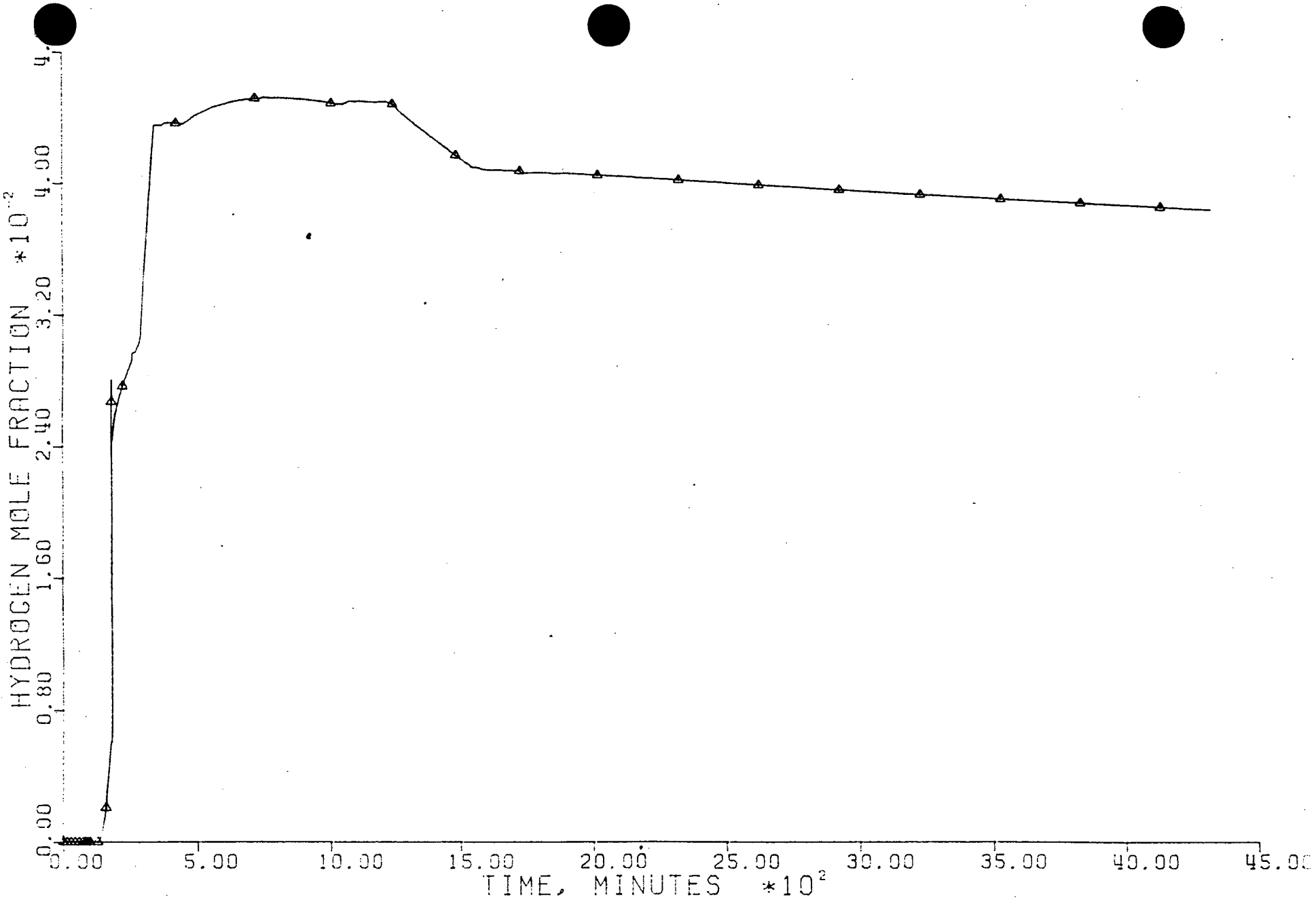
HYDROGEN MOLE FRACTION *10⁻²
0.00
0.80
1.60
2.40
3.20
4.00
4.
0.00
5.00
10.00
15.00
20.00
25.00
30.00
35.00
40.00
45.00
TIME, MINUTES *10²

FIGURE 5.16

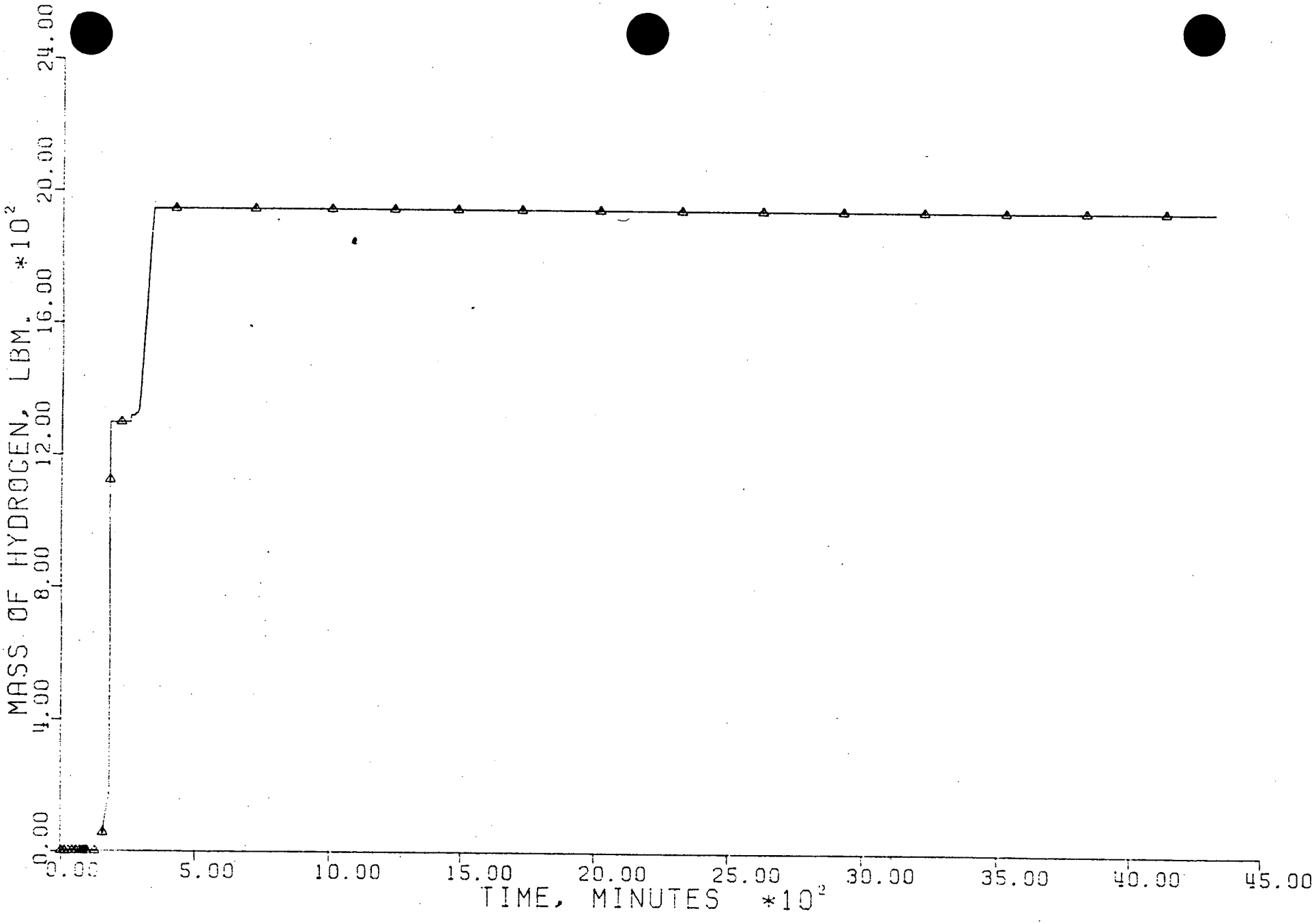
MASS OF HYDROGEN, LBM. *10²
0.00
4.00
8.00
12.00
16.00
20.00
24.00
0.00
5.00
10.00
15.00
20.00
25.00
30.00
35.00
40.00
45.00
TIME, MINUTES *10²

FIGURE 5.17

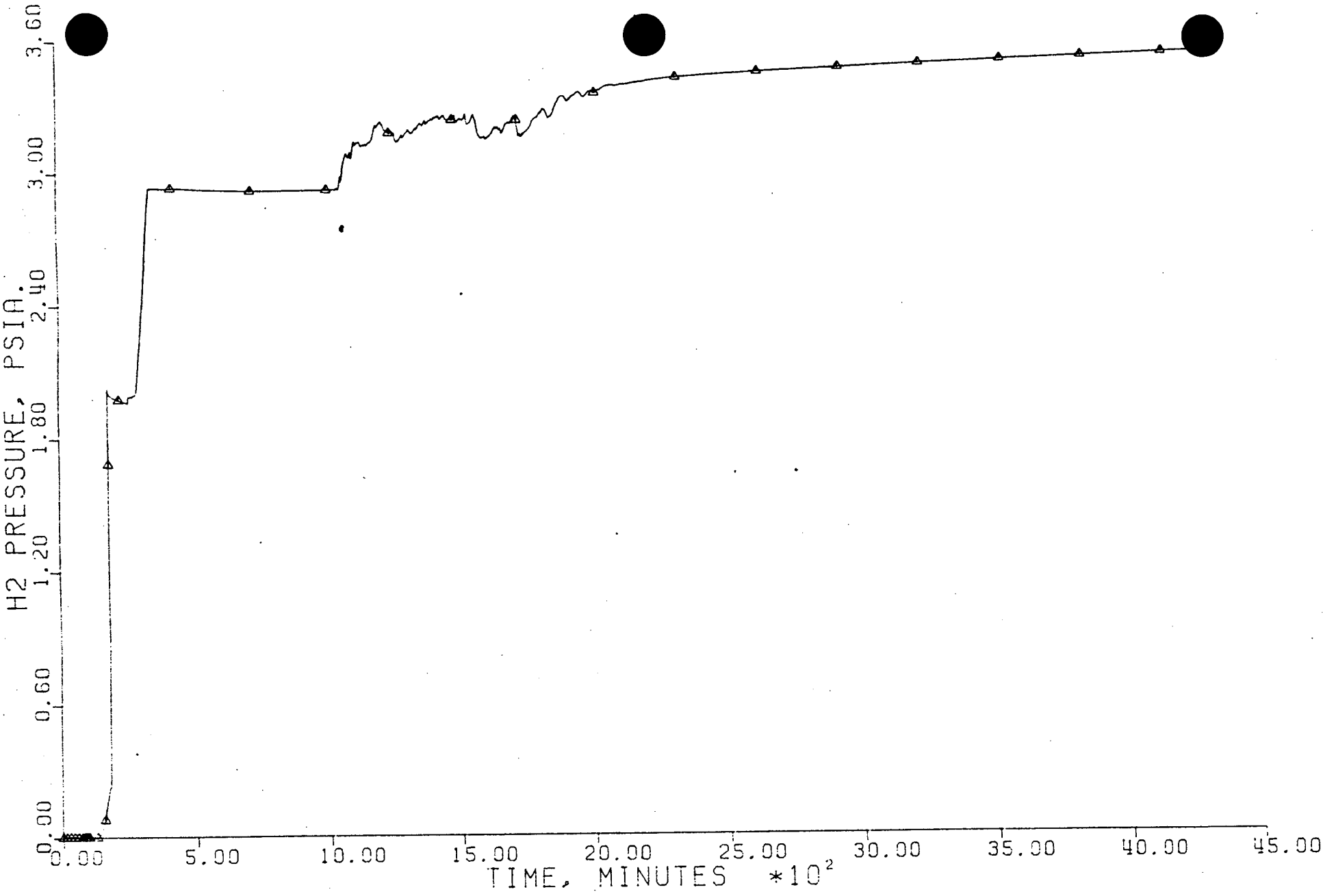
H2 PRESSURE, PSIA.
0.00
0.60
1.20
1.80
2.40
3.00
3.60
0.00
5.00
10.00
15.00
20.00
25.00
30.00
35.00
40.00
45.00
TIME, MINUTES *10²

FIGURE 5.18

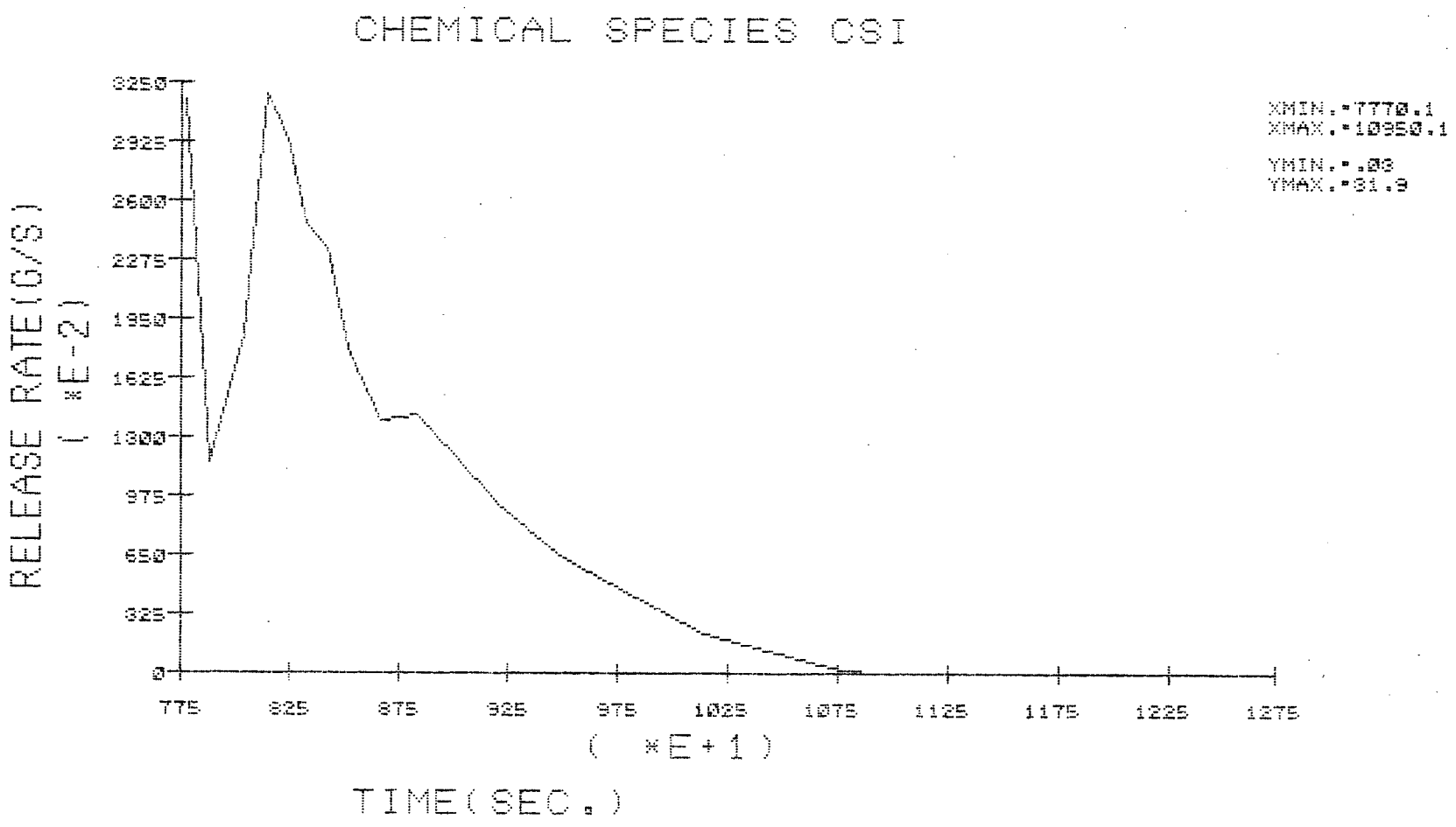
CHEMICAL SPECIES CSI
XMIN.=7770.1
XMAX.=10950.1
YMIN.=.00
YMAX.=31.9
RELEASE RATE(G/S)
(*E-2)
3250
2925
2600
2275
1950
1625
1300
975
650
325
0
775
825
875
925
975
1025
1075
1125
1175
1225
1275
(*E+1)
TIME(SEC.)

FIGURE 5.19

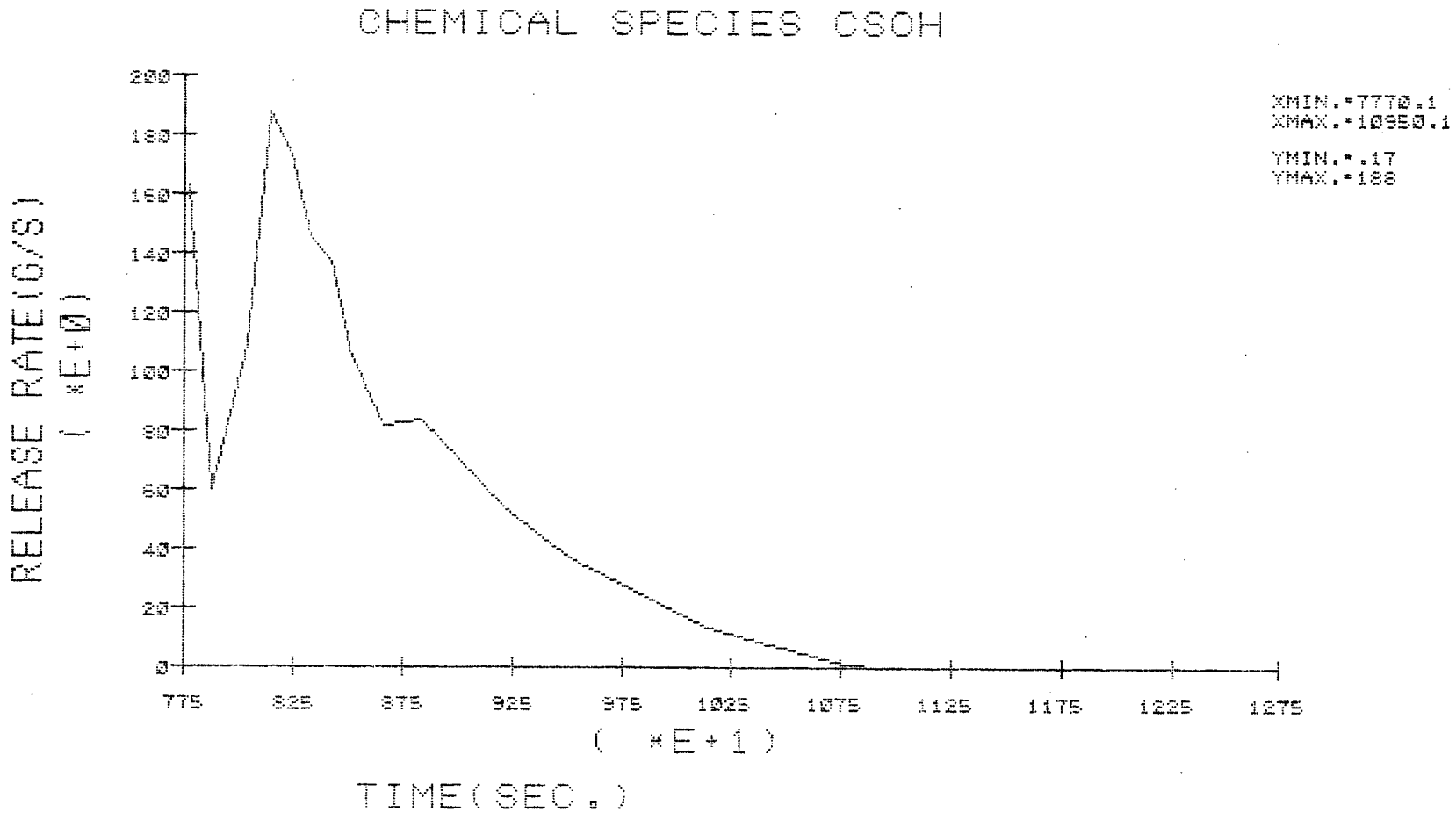
CHEMICAL SPECIES CSOH
XMIN.=7770.1
XMAX.=10950.1
YMIN.=.17
YMAX.=188
RELEASE RATE(G/S)
(*E+0)
200
180
160
140
120
100
80
60
40
20
0
775
825
875
925
975
1025
1075
1125
1175
1225
1275
(*E+1)
TIME(SEC.)

FIGURE 5.20

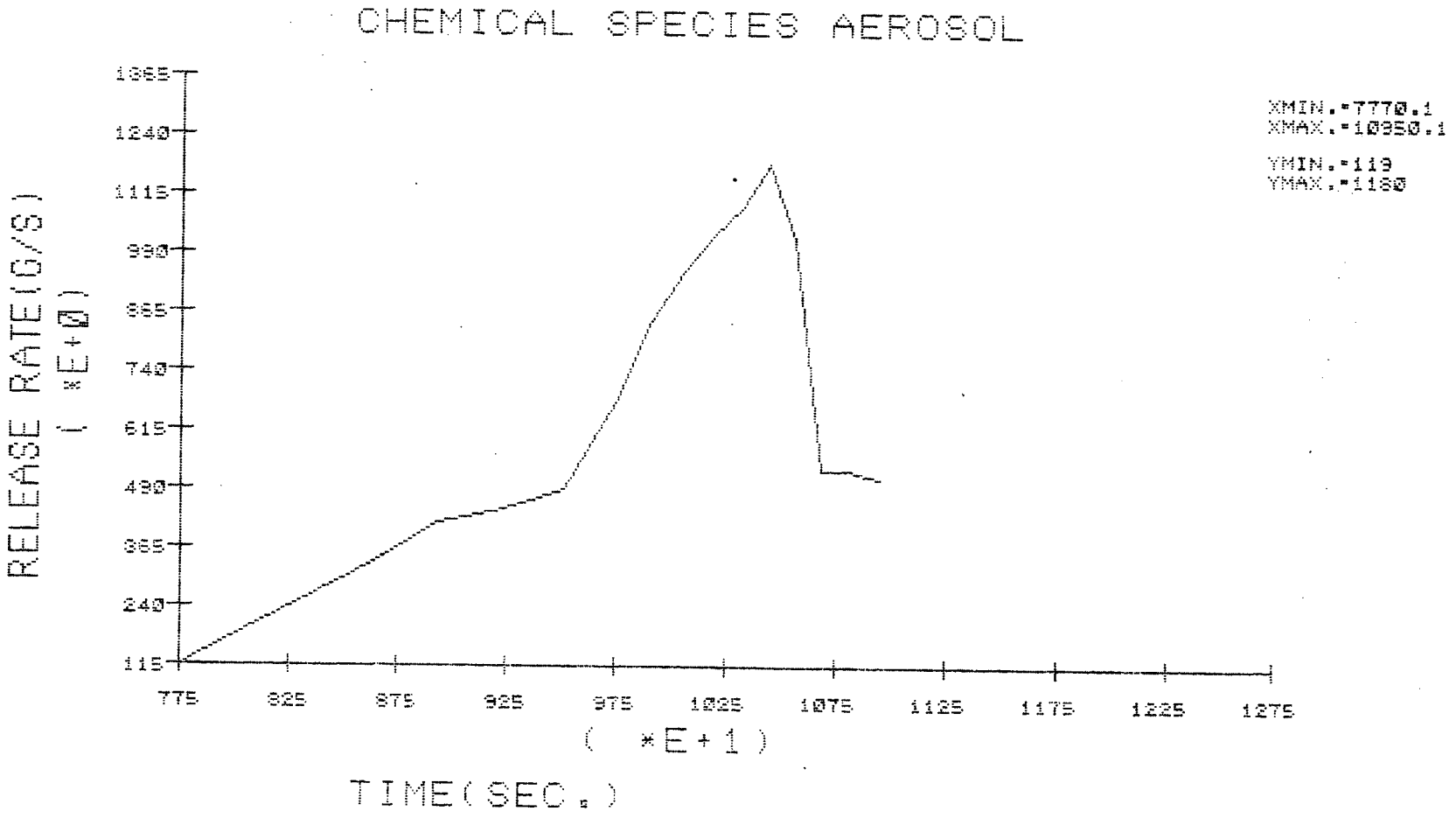
CHEMICAL SPECIES AEROSOL
XMIN.=7770.1
XMAX.=10950.1
YMIN.=119
YMAX.=1180
RELEASE RATE(G/S)
(*E+0)
1365
1240
1115
990
865
740
615
490
365
240
115
775
825
875
925
975
1025
1075
1125
1175
1225
1275
(*E+1)
TIME(SEC.)

FIGURE 5.21

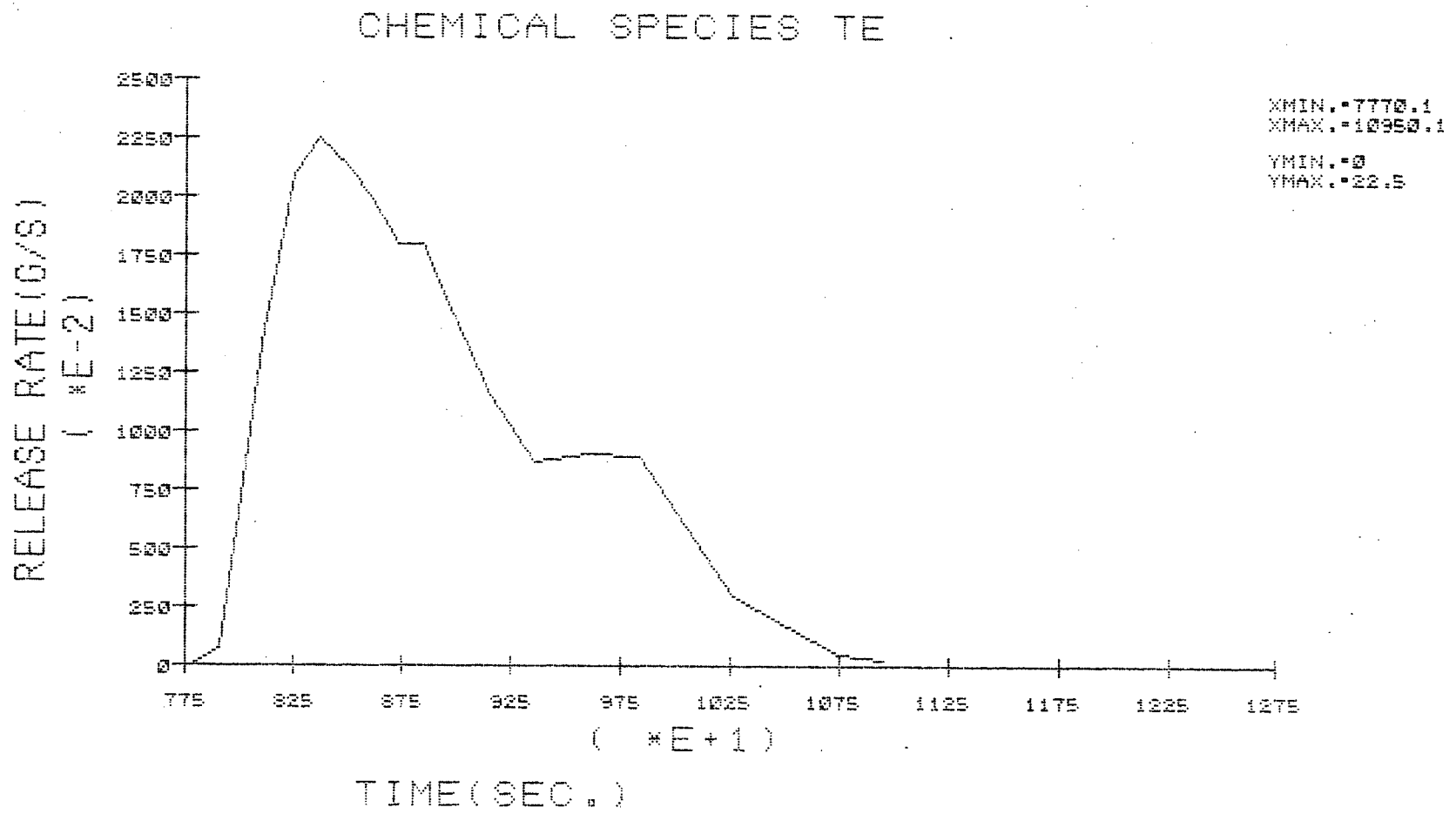
CHEMICAL SPECIES TE
XMIN.=7770.1
XMAX.=10950.1
YMIN.=0
YMAX.=22.5
RELEASE RATE(G/S)
(*E-2)
2500
2250
2000
1750
1500
1250
1000
750
500
250
0
775
825
875
925
975
1025
1075
1125
1175
1225
1275
(*E+1)
TIME(SEC.)

FIGURE 5.22

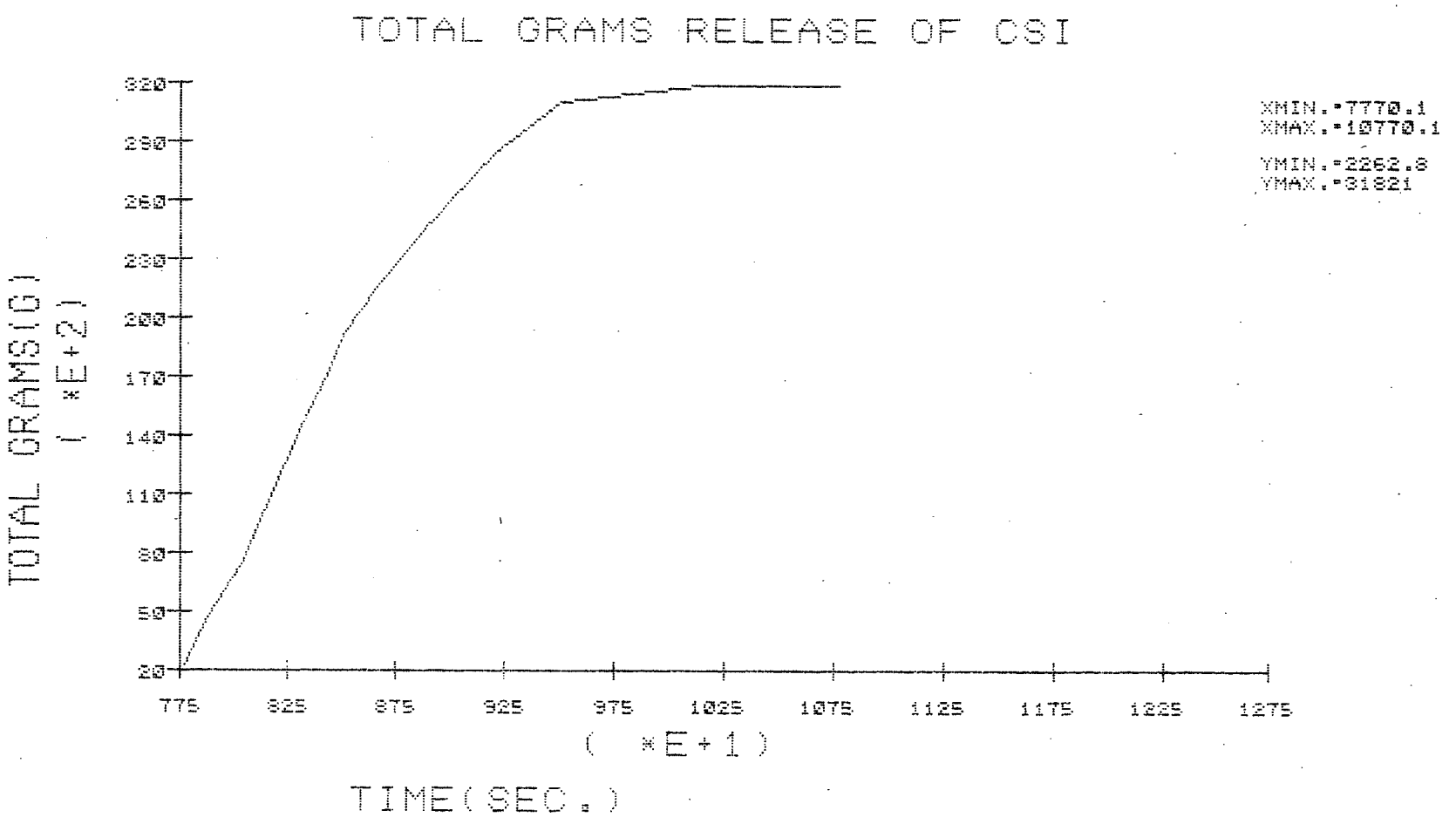
TOTAL GRAMS RELEASE OF CSI
XMIN.=7770.1
XMAX.=10770.1
YMIN.=2262.8
YMAX.=31821
TOTAL GRAMS(G)
(*E+2)
320
290
260
230
200
170
140
110
80
50
20
775
825
875
925
975
1025
1075
1125
1175
1225
1275
(*E+1)
TIME(SEC.)

FIGURE 5.23

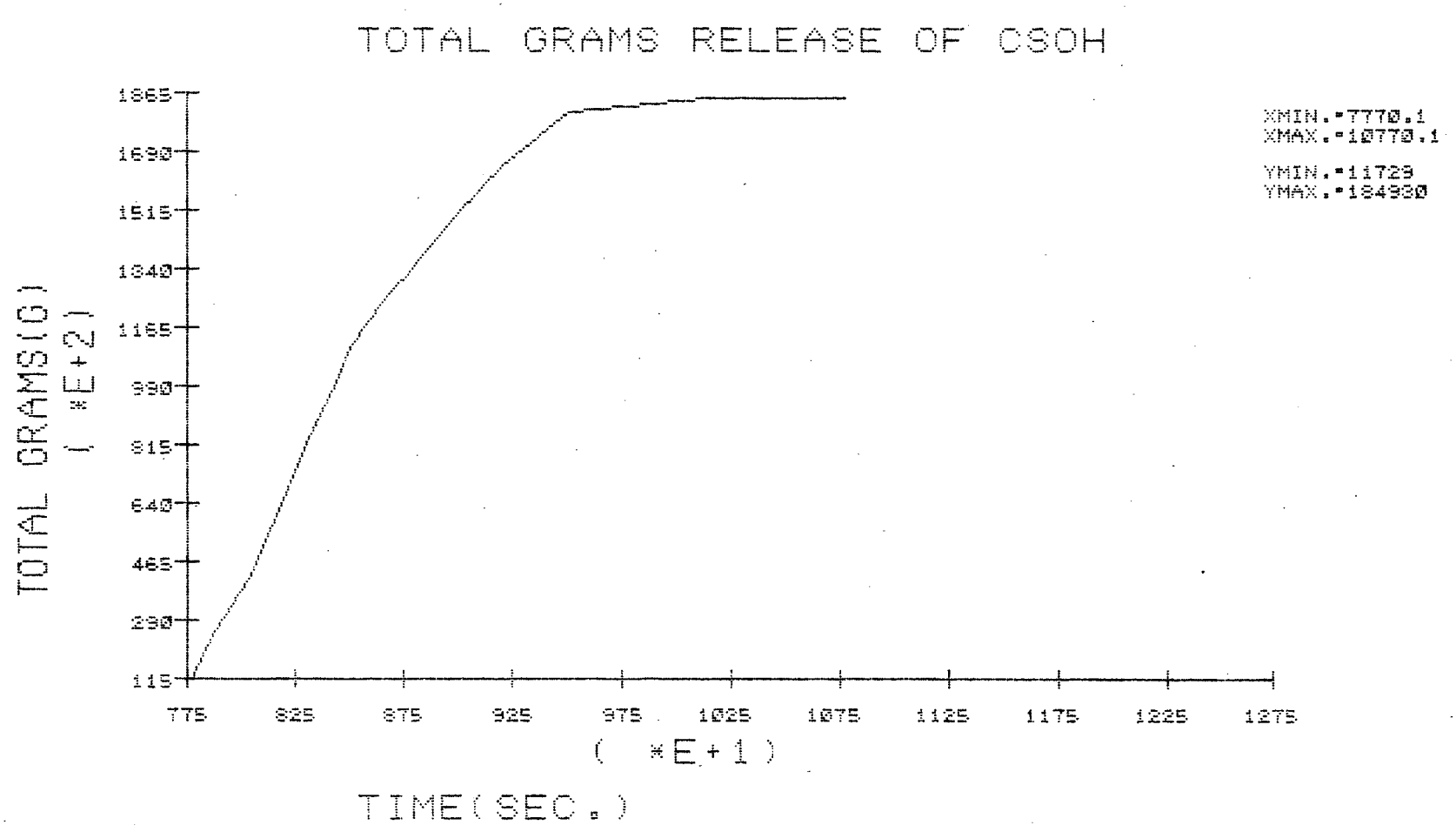
TOTAL GRAMS RELEASE OF CSOH
XMIN.=7770.1
XMAX.=10770.1
YMIN.=11729
YMAX.=184930
TOTAL GRAMS(G)
(*E+2)
1865
1690
1515
1340
1165
990
815
640
465
290
115
775
825
875
925
975
1025
1075
1125
1175
1225
1275
(*E+1)
TIME(SEC.)

FIGURE 5.24

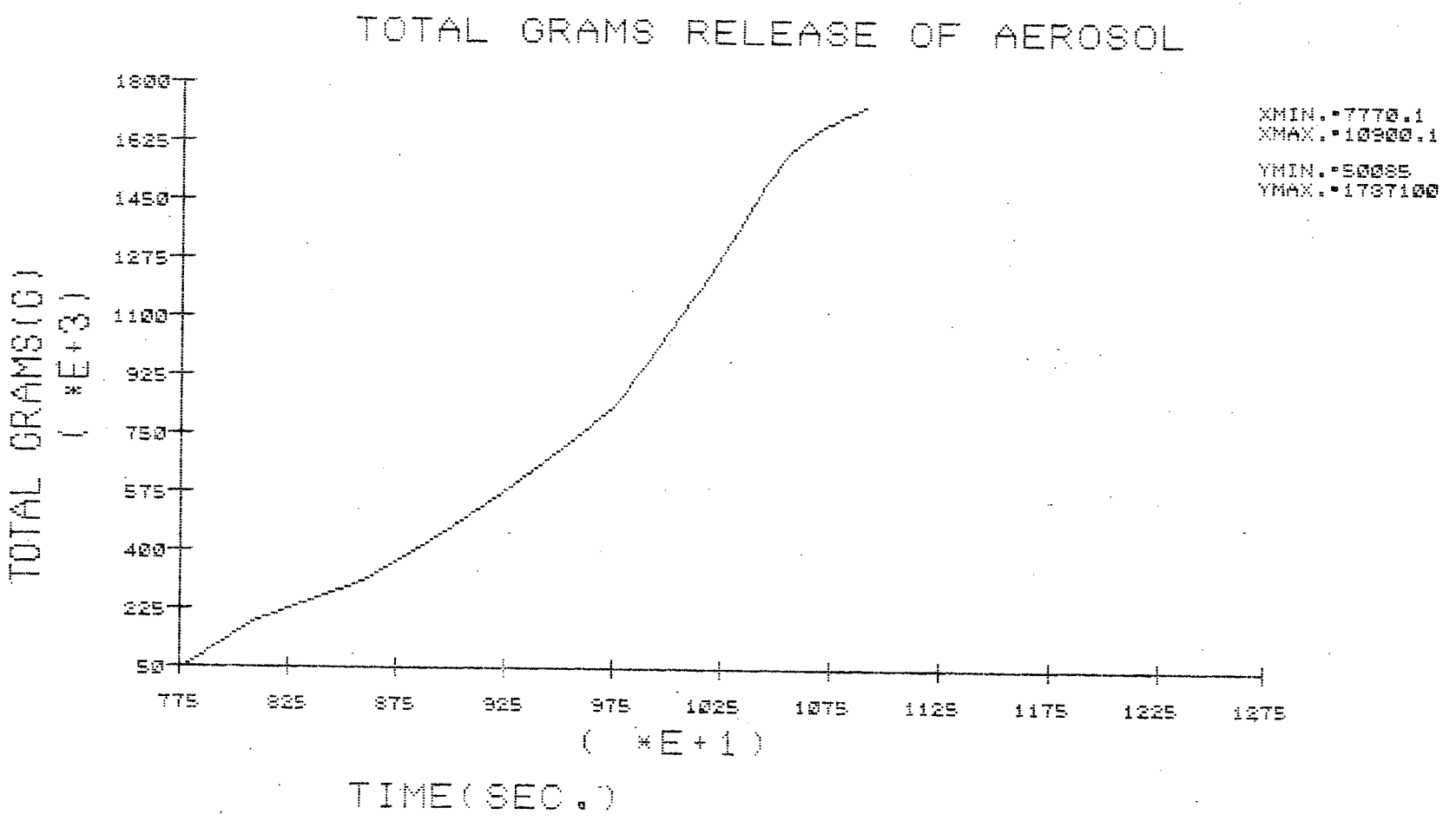
TOTAL GRAMS RELEASE OF AEROSOL
XMIN.=7770.1
XMAX.=10900.1
YMIN.=50085
YMAX.=1737100
TOTAL GRAMS(G)
(*E+3)
1800
1625
1450
1275
1100
925
750
575
400
225
50
775
825
875
925
975
1025
1075
1125
1175
1225
1275
(*E+1)
TIME(SEC.)

FIGURE 5.25

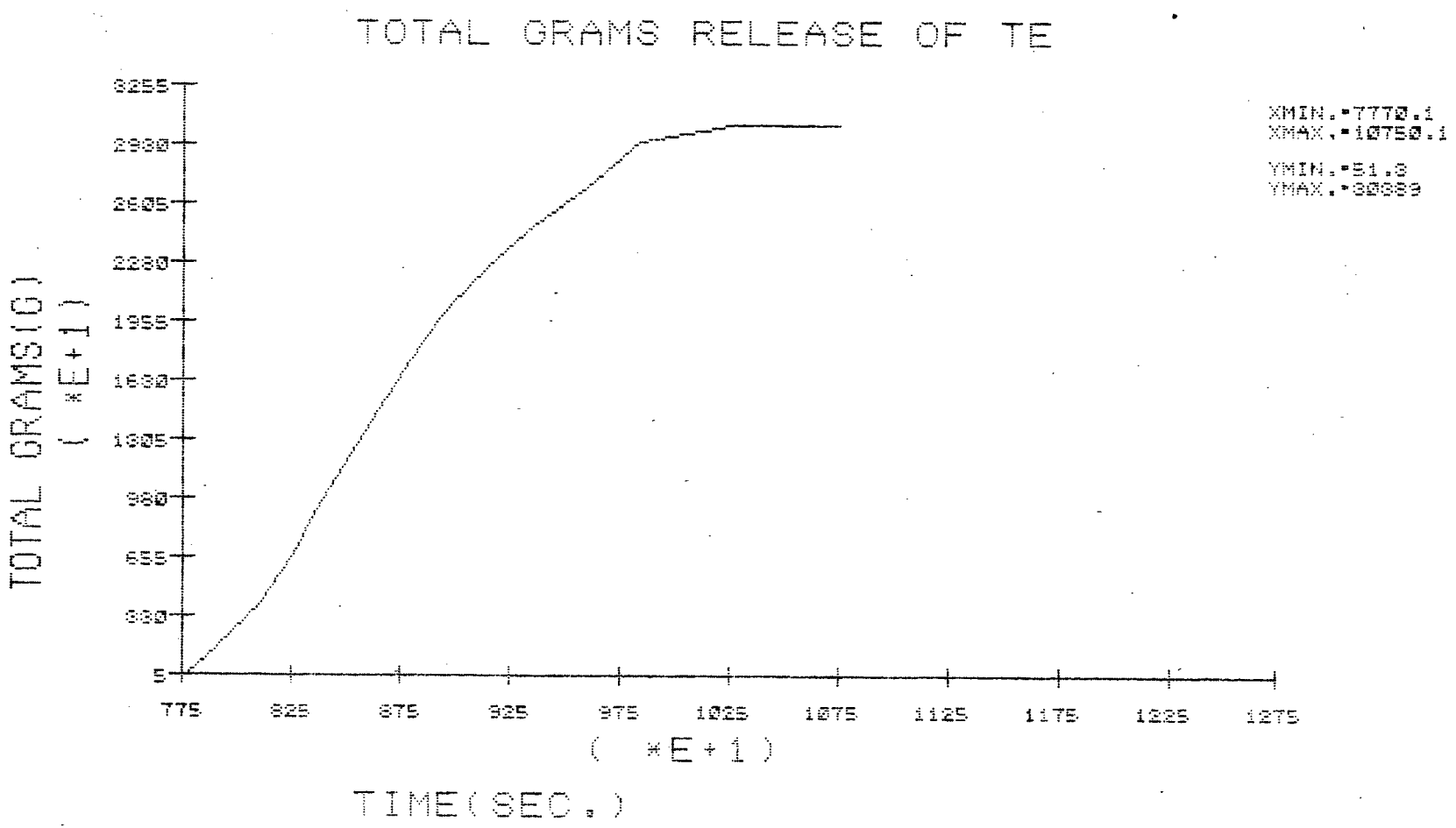
TOTAL GRAMS RELEASE OF TE
XMIN.=7770.1
XMAX.=10750.1
YMIN.=51.3
YMAX.=3000
TOTAL GRAMS(G)
(*E+1)
3255
2930
2605
2280
1955
1630
1305
980
655
330
5
775
825
875
925
975
1025
1075
1125
1175
1225
1275
(*E+1)
TIME(SEC.)

FIGURE 5.26

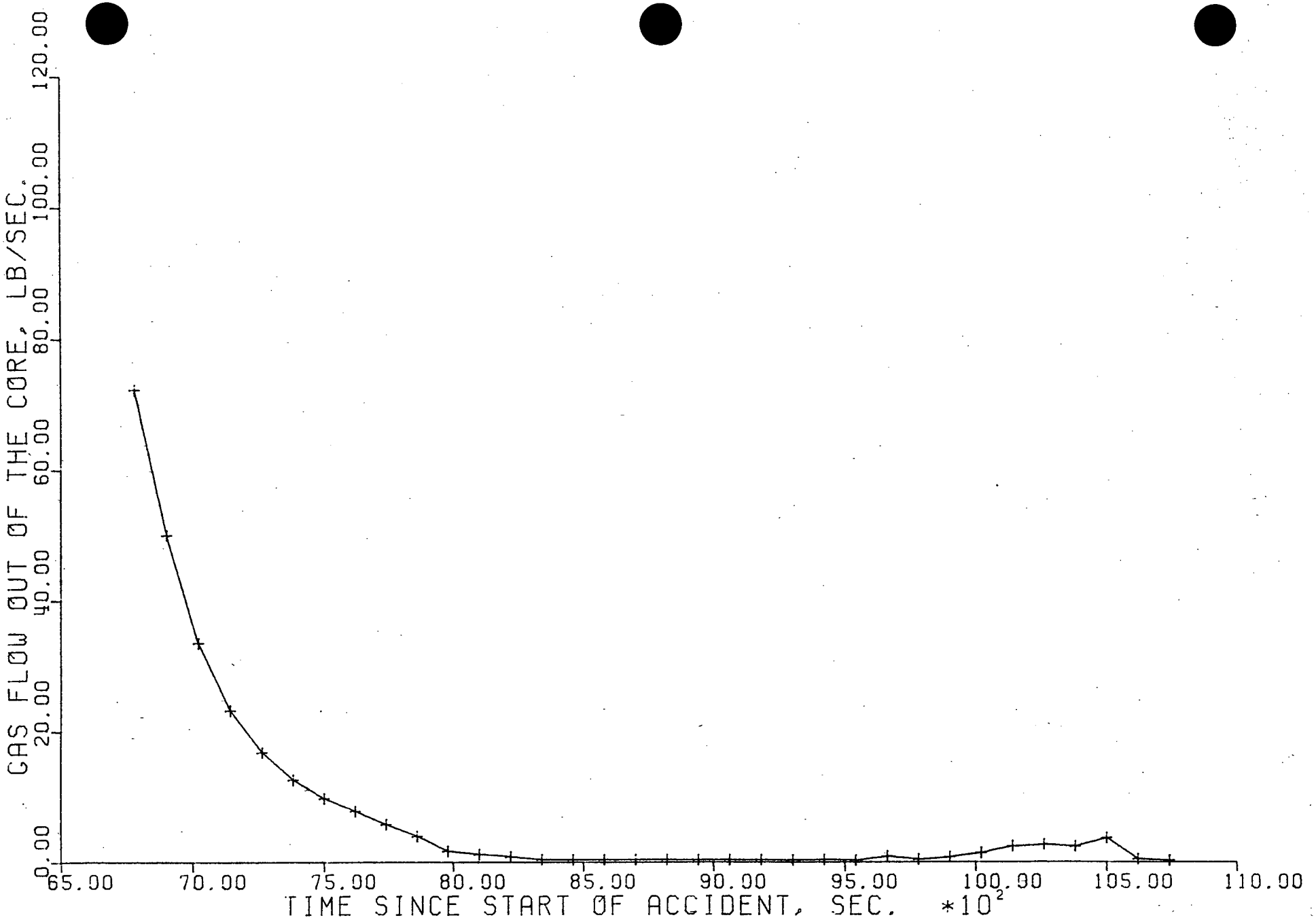
GAS FLOW OUT OF THE CORE, LB/SEC.
0.00
20.00
40.00
60.00
80.00
100.00
120.00
65.00
70.00
75.00
80.00
85.00
90.00
95.00
100.00
105.00
110.00
TIME SINCE START OF ACCIDENT, SEC. *10²

FIGURE 5.27

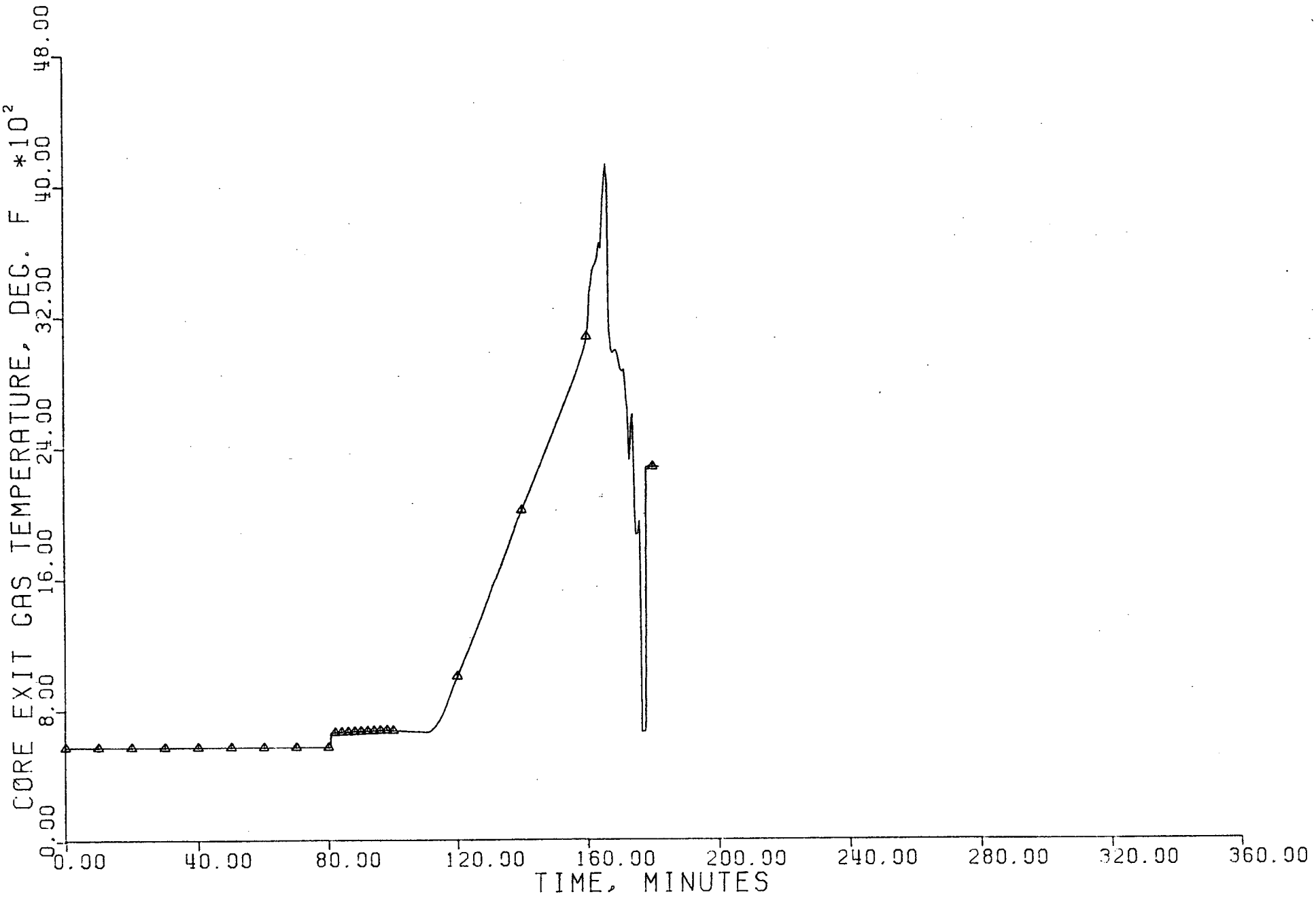
CORE EXIT GAS TEMPERATURE, DEG. F *10²
0.00
8.00
16.00
24.00
32.00
40.00
48.00
0.00
40.00
80.00
120.00
160.00
200.00
240.00
280.00
320.00
360.00
TIME, MINUTES

FIGURE 5.28

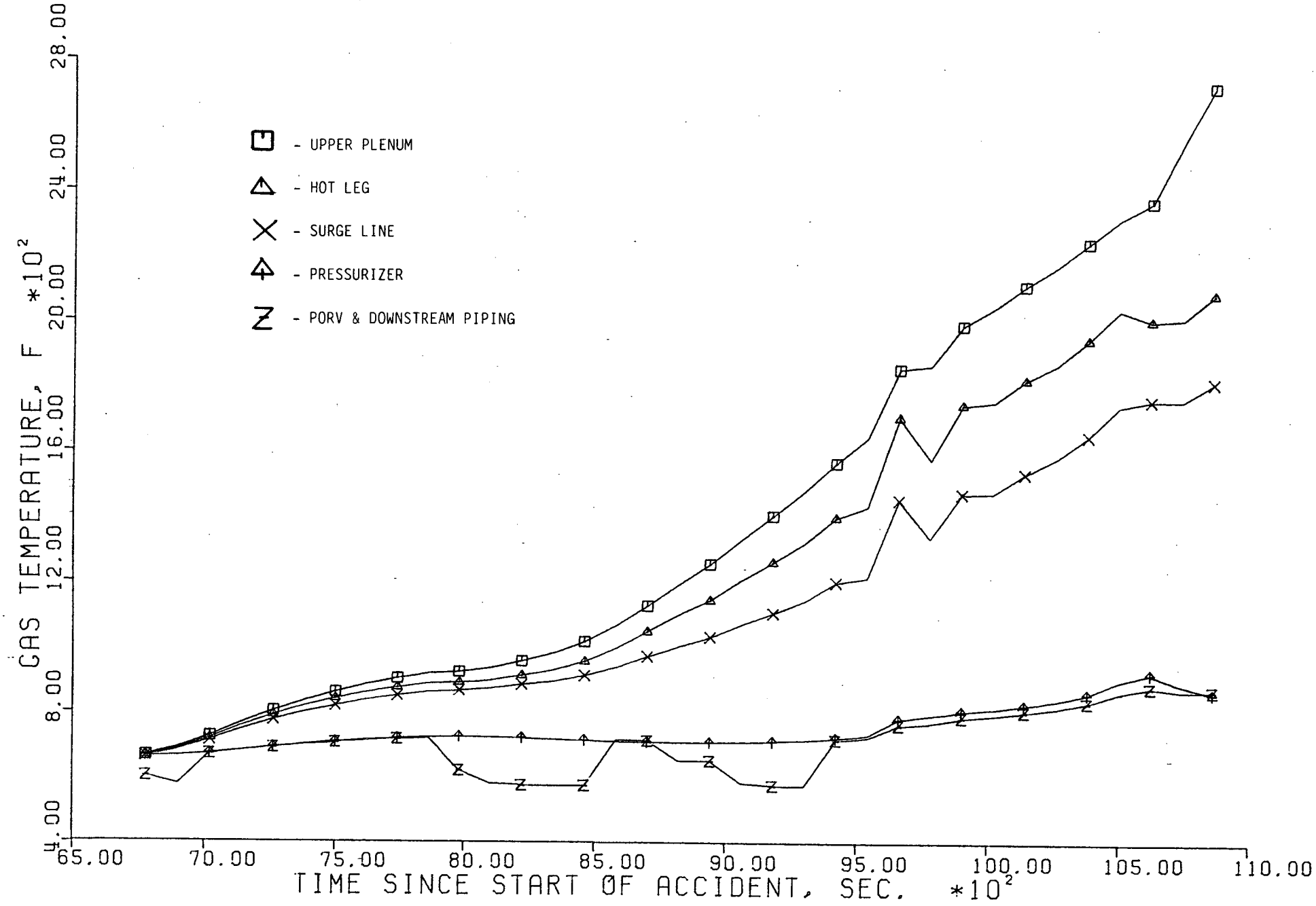
- UPPER PLENUM
- HOT LEG
- SURGE LINE
- PRESSURIZER
- PORV & DOWNSTREAM PIPING
GAS TEMPERATURE, F *10²
4.00
8.00
12.00
16.00
20.00
24.00
28.00
65.00
70.00
75.00
80.00
85.00
90.00
95.00
100.00
105.00
110.00
TIME SINCE START OF ACCIDENT, SEC. *10²

FIGURE 5.29

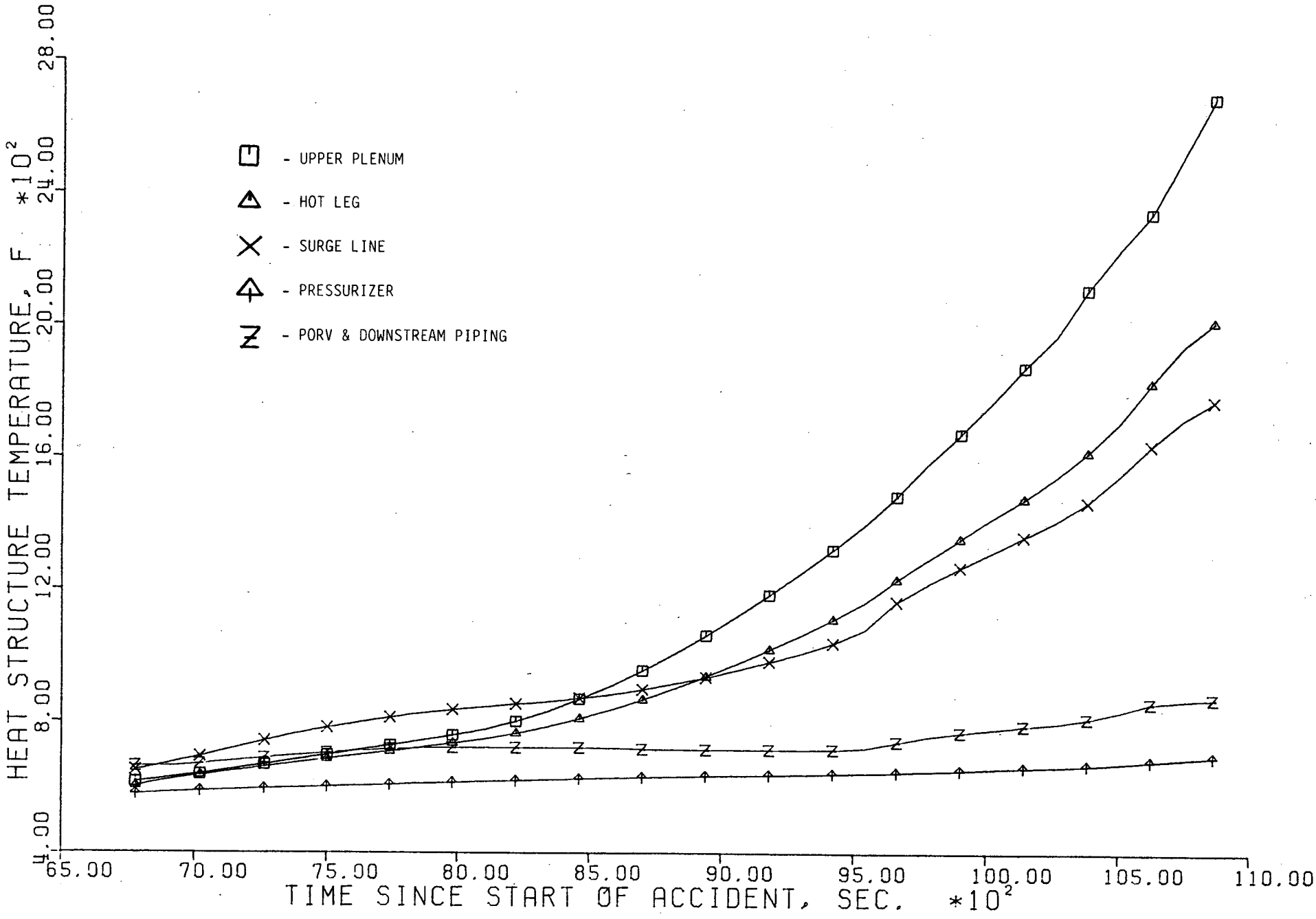
HEAT STRUCTURE TEMPERATURE, F *10²
4.00
8.00
12.00
16.00
20.00
24.00
28.00
- UPPER PLENUM
- HOT LEG
- SURGE LINE
- PRESSURIZER
- PORV & DOWNSTREAM PIPING
65.00
70.00
75.00
80.00
85.00
90.00
95.00
100.00
105.00
110.00
TIME SINCE START OF ACCIDENT, SEC. *10²

FIGURE 5.30

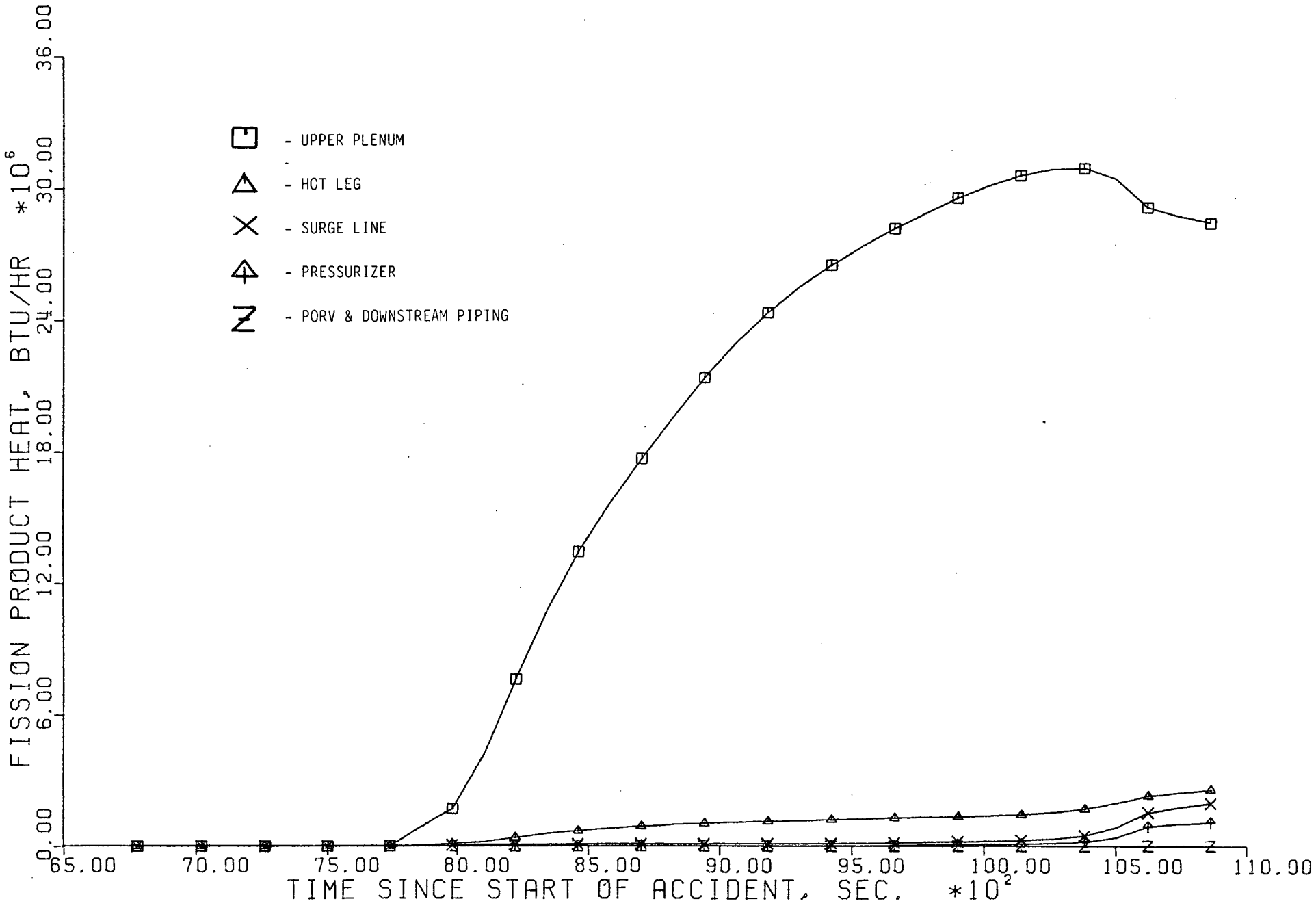
- UPPER PLENUM
- HOT LEG
- SURGE LINE
- PRESSURIZER
- PORV & DOWNSTREAM PIPING
FISSION PRODUCT HEAT, BTU/HR *10^6
0.00
6.00
12.00
18.00
24.00
30.00
36.00
65.00
70.00
75.00
80.00
85.00
90.00
95.00
100.00
105.00
110.00
TIME SINCE START OF ACCIDENT, SEC. *10^2

FIGURE 5.31

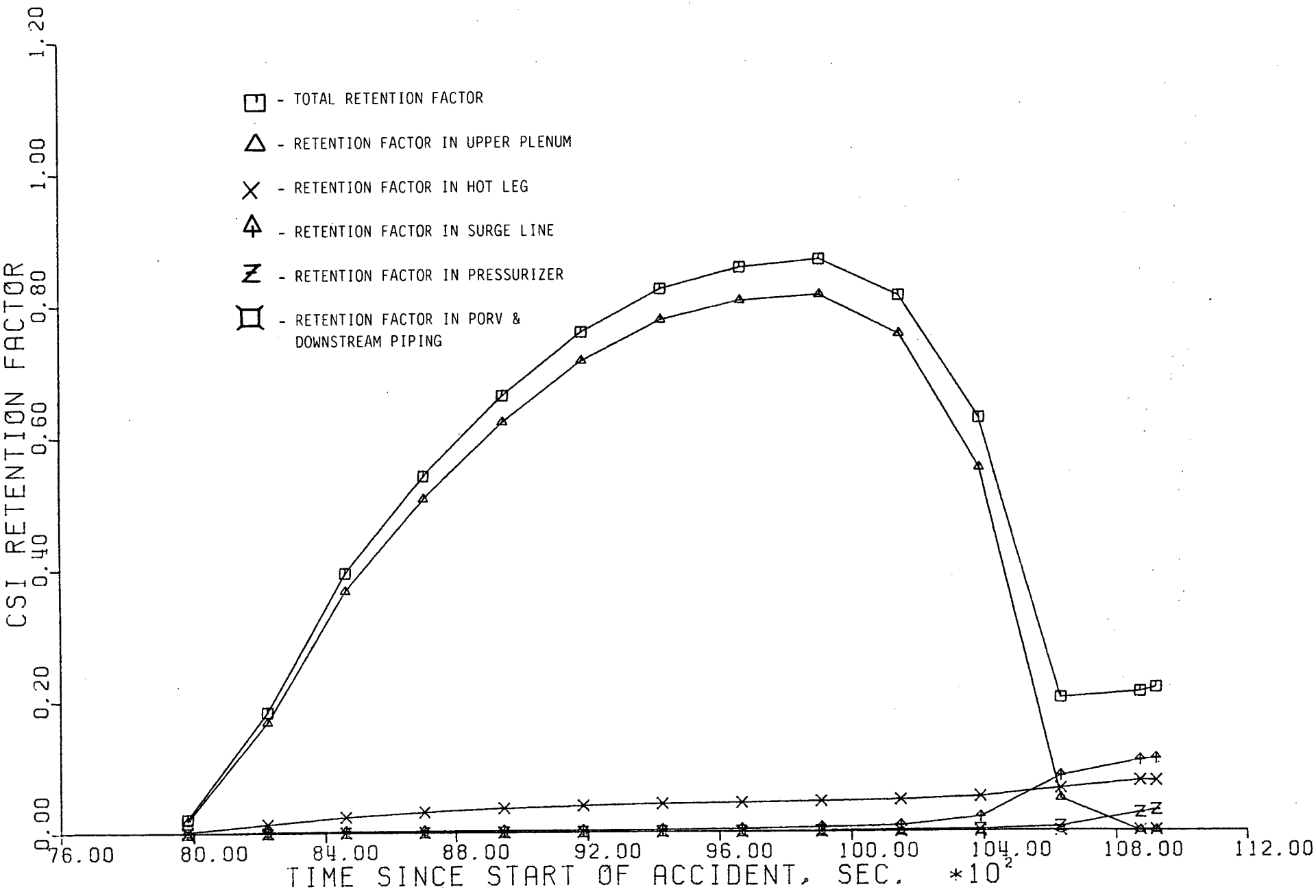
- TOTAL RETENTION FACTOR
- RETENTION FACTOR IN UPPER PLENUM
- RETENTION FACTOR IN HOT LEG
- RETENTION FACTOR IN SURGE LINE
- RETENTION FACTOR IN PRESSURIZER
- RETENTION FACTOR IN PORV & DOWNSTREAM PIPING
CSI RETENTION FACTOR
0.00
0.20
0.40
0.60
0.80
1.00
1.20
76.00
80.00
84.00
88.00
92.00
96.00
100.00
104.00
108.00
112.00
TIME SINCE START OF ACCIDENT, SEC. *10²

FIGURE 5.32

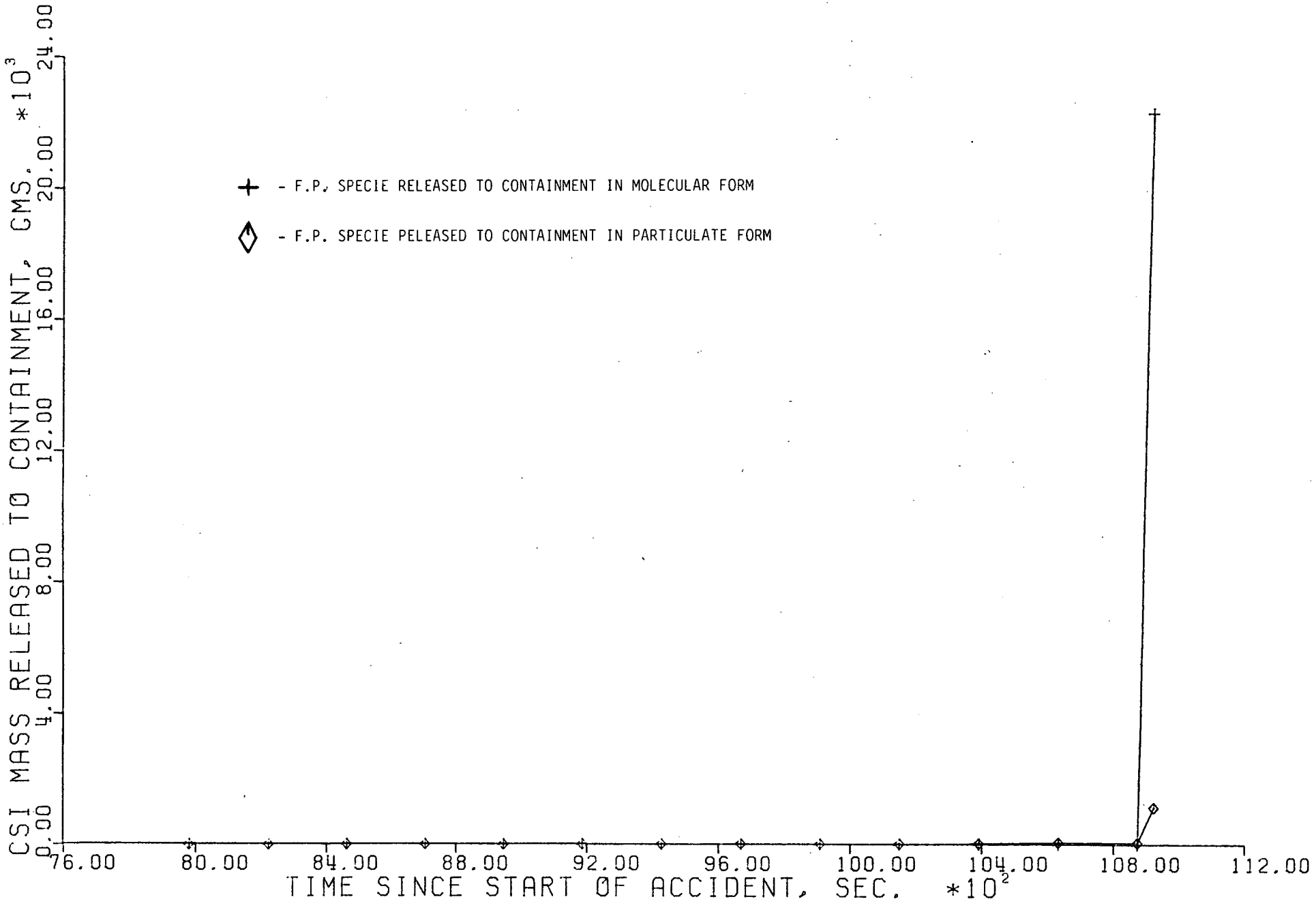
+ - F.P. SPECIE RELEASED TO CONTAINMENT IN MOLECULAR FORM
◇ - F.P. SPECIE PELEASED TO CONTAINMENT IN PARTICULATE FORM
CSI MASS RELEASED TO CONTAINMENT, GMS. *10^3
0.00
4.00
8.00
12.00
16.00
20.00
24.00
76.00
80.00
84.00
88.00
92.00
96.00
100.00
104.00
108.00
112.00
TIME SINCE START OF ACCIDENT, SEC. *10^2

FIGURE 5.33

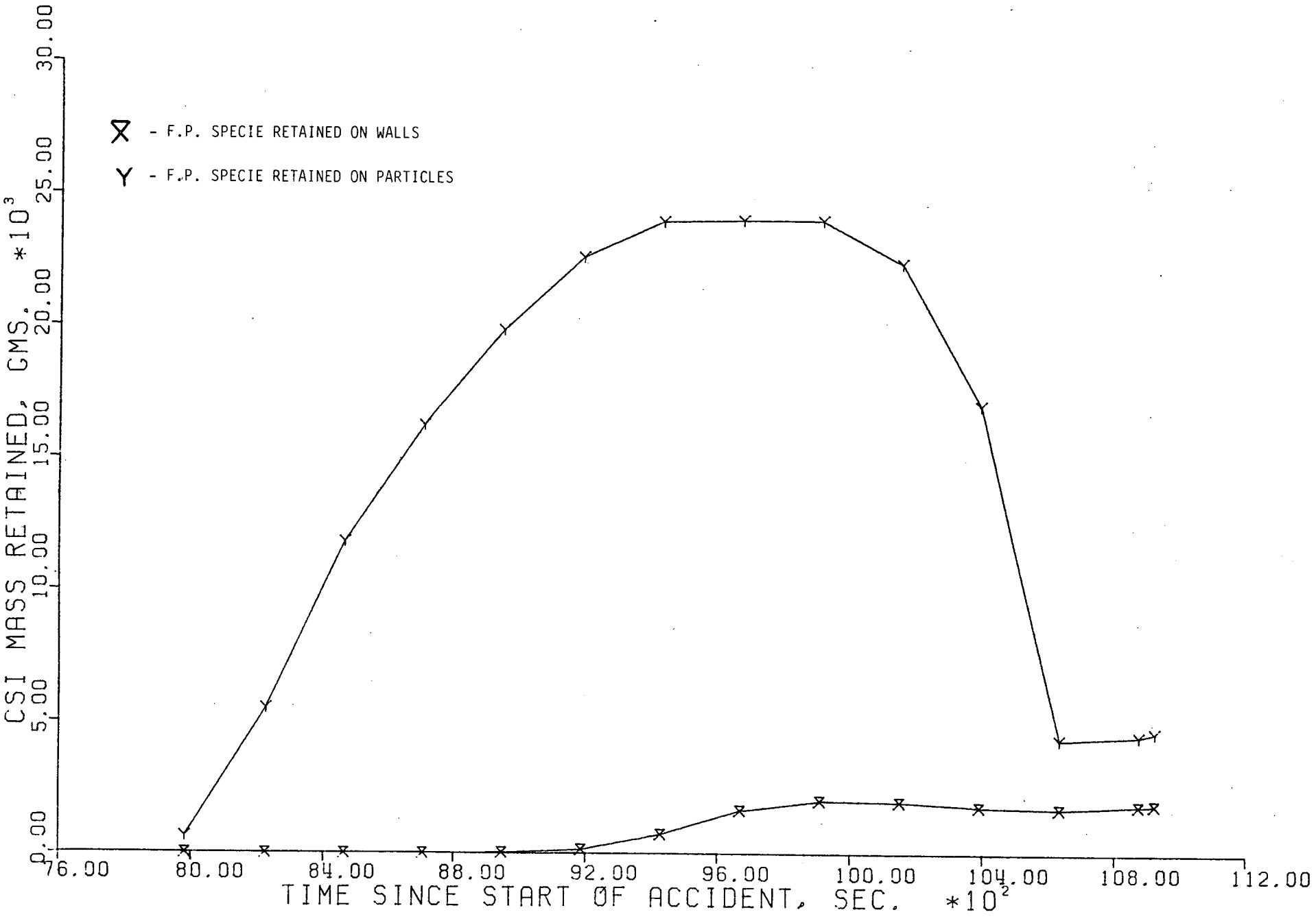
X - F.P. SPECIE RETAINED ON WALLS
Y - F.P. SPECIE RETAINED ON PARTICLES
CSI MASS RETAINED, GMS. *10^3
0.00
5.00
10.00
15.00
20.00
25.00
30.00
76.00
80.00
84.00
88.00
92.00
96.00
100.00
104.00
108.00
112.00
TIME SINCE START OF ACCIDENT, SEC. *10^2

FIGURE 5.34

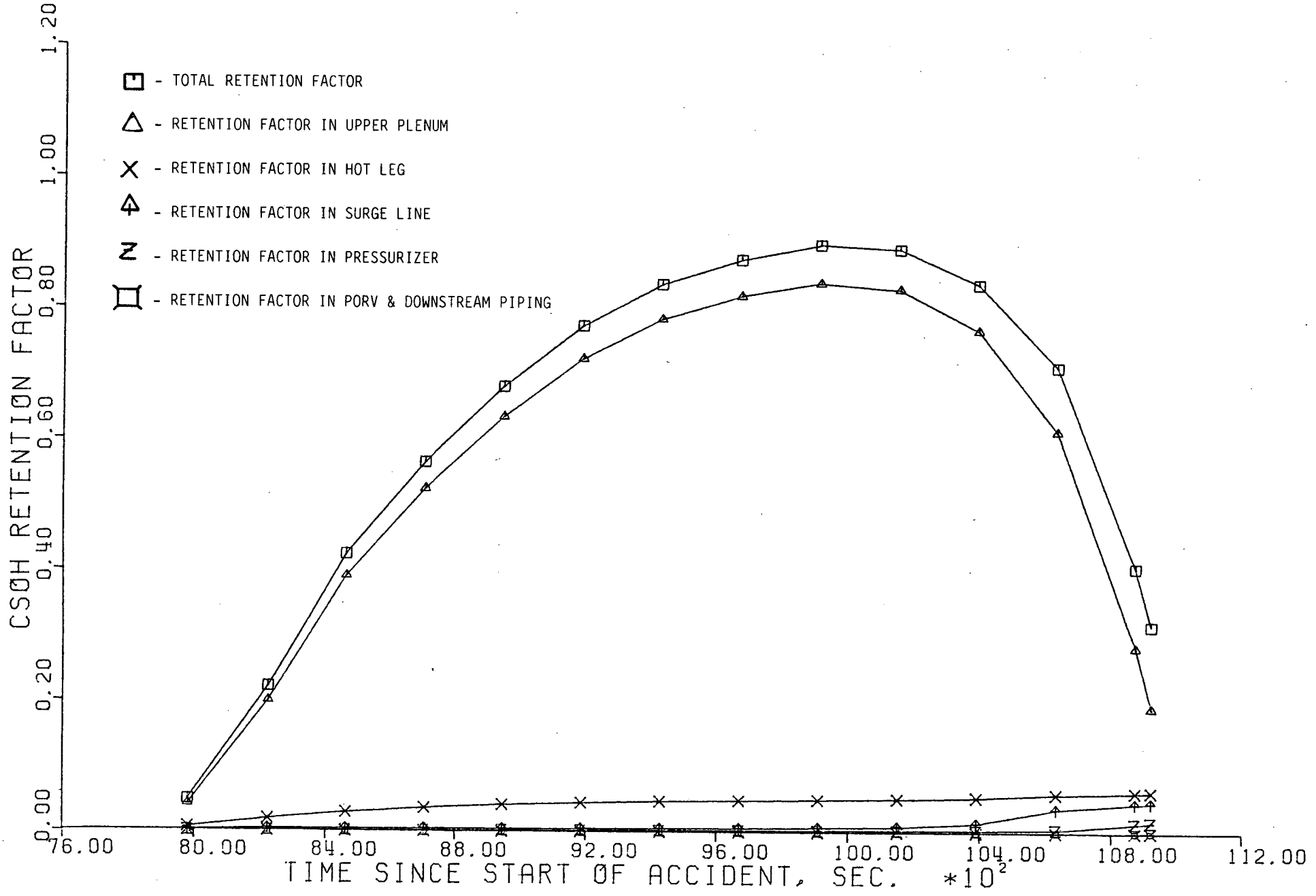
- TOTAL RETENTION FACTOR
- RETENTION FACTOR IN UPPER PLENUM
- RETENTION FACTOR IN HOT LEG
- RETENTION FACTOR IN SURGE LINE
- RETENTION FACTOR IN PRESSURIZER
- RETENTION FACTOR IN PORV & DOWNSTREAM PIPING
CSOH RETENTION FACTOR
0.00
0.20
0.40
0.60
0.80
1.00
1.20
76.00
80.00
84.00
88.00
92.00
96.00
100.00
104.00
108.00
112.00
TIME SINCE START OF ACCIDENT, SEC. *10²

FIGURE 5.35

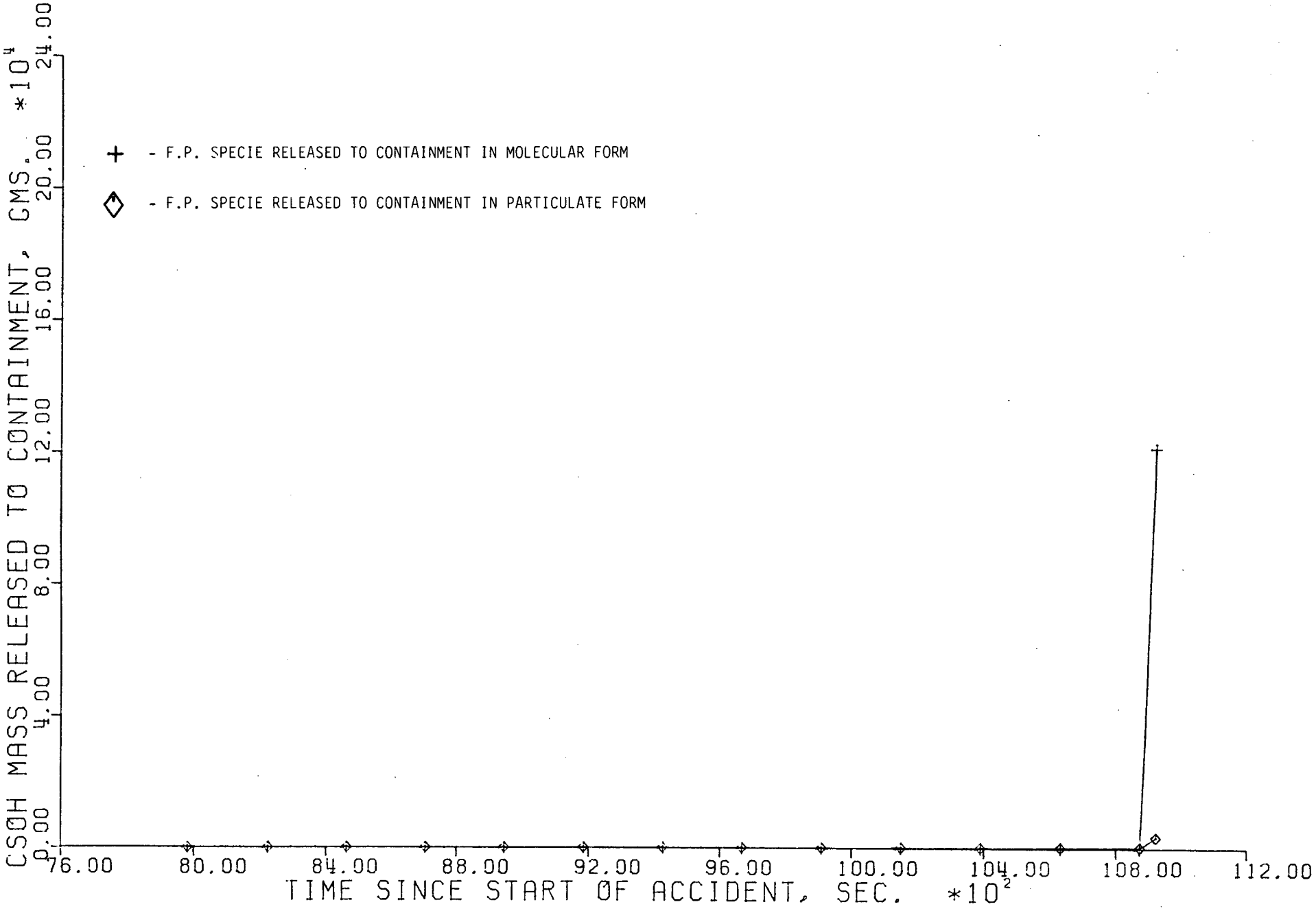
+ - F.P. SPECIE RELEASED TO CONTAINMENT IN MOLECULAR FORM
◇ - F.P. SPECIE RELEASED TO CONTAINMENT IN PARTICULATE FORM
CSOH MASS RELEASED TO CONTAINMENT, GMS. *10^4
0.00
4.00
8.00
12.00
16.00
20.00
24.00
76.00
80.00
84.00
88.00
92.00
96.00
100.00
104.00
108.00
112.00
TIME SINCE START OF ACCIDENT, SEC. *10^2

FIGURE 5.36

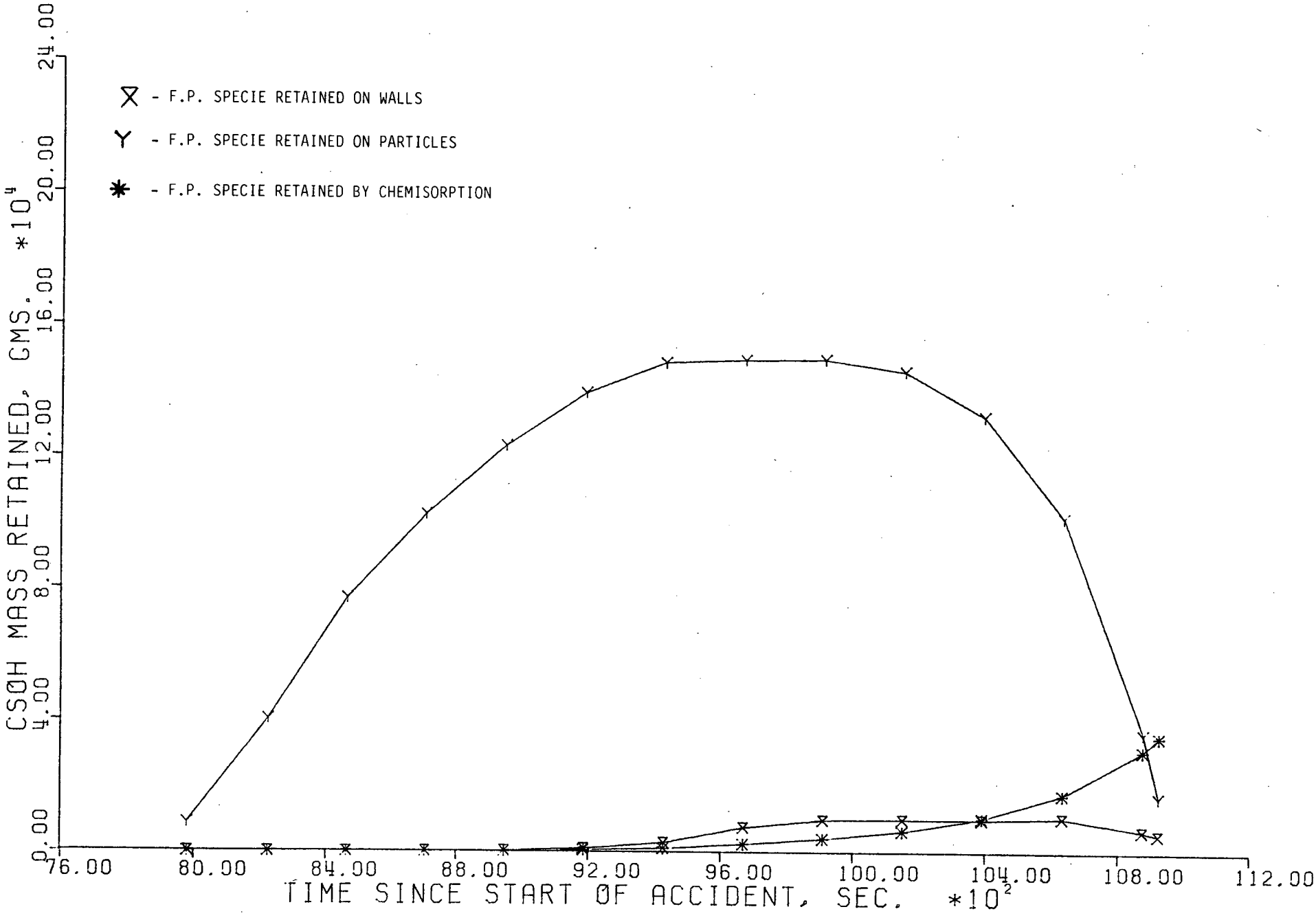
X - F.P. SPECIE RETAINED ON WALLS
Y - F.P. SPECIE RETAINED ON PARTICLES
* - F.P. SPECIE RETAINED BY CHEMISORPTION
CSOH MASS RETAINED, GMS. *10^4
0.00
4.00
8.00
12.00
16.00
20.00
24.00
76.00
80.00
84.00
88.00
92.00
96.00
100.00
104.00
108.00
112.00
TIME SINCE START OF ACCIDENT, SEC. *10^2

FIGURE 5.37

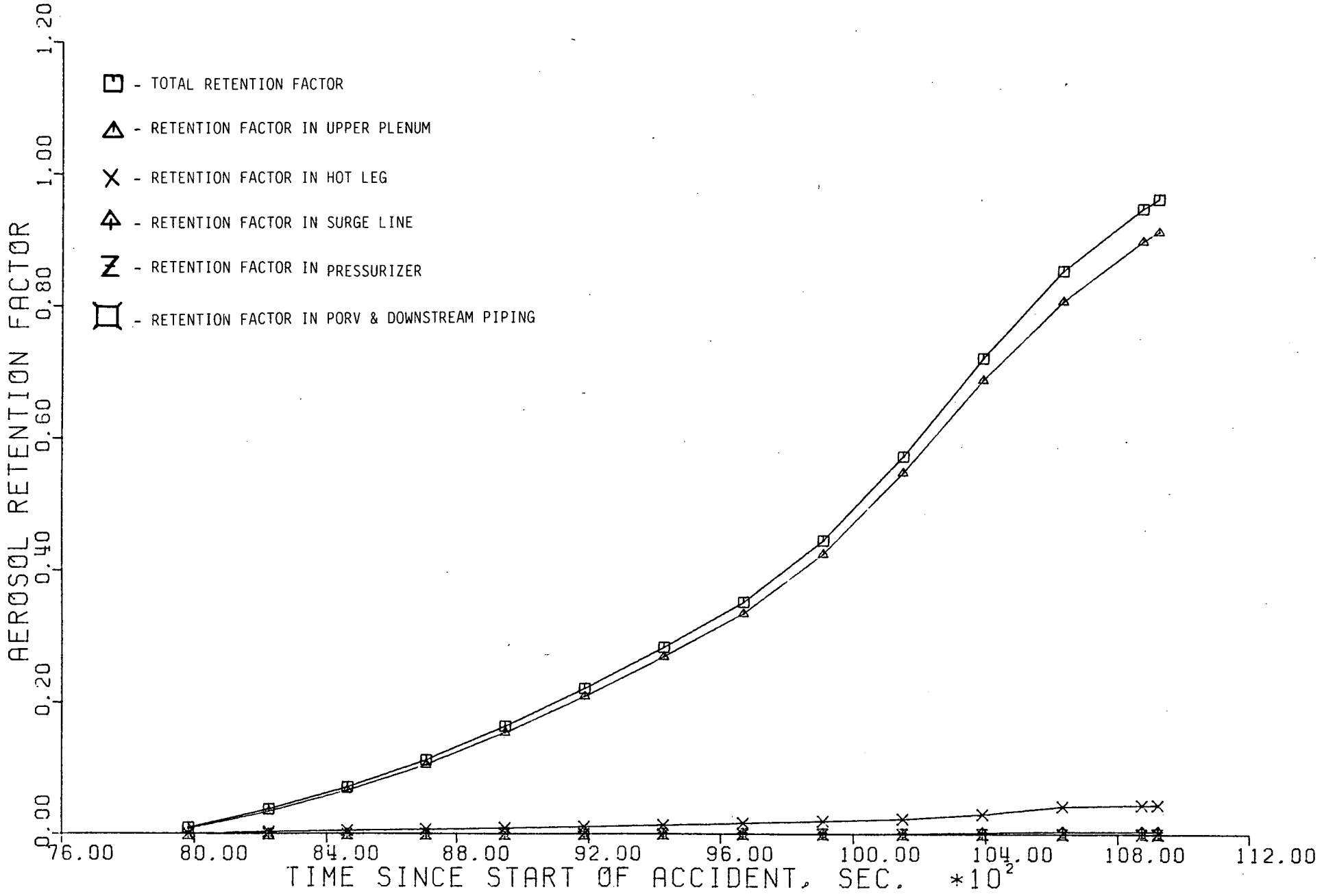
- TOTAL RETENTION FACTOR
- RETENTION FACTOR IN UPPER PLENUM
- RETENTION FACTOR IN HOT LEG
- RETENTION FACTOR IN SURGE LINE
- RETENTION FACTOR IN PRESSURIZER
- RETENTION FACTOR IN PORV & DOWNSTREAM PIPING
AEROSOL RETENTION FACTOR
0.00
0.20
0.40
0.60
0.80
1.00
1.20
76.00
80.00
84.00
88.00
92.00
96.00
100.00
104.00
108.00
112.00
TIME SINCE START OF ACCIDENT, SEC. *10²

FIGURE 5.38

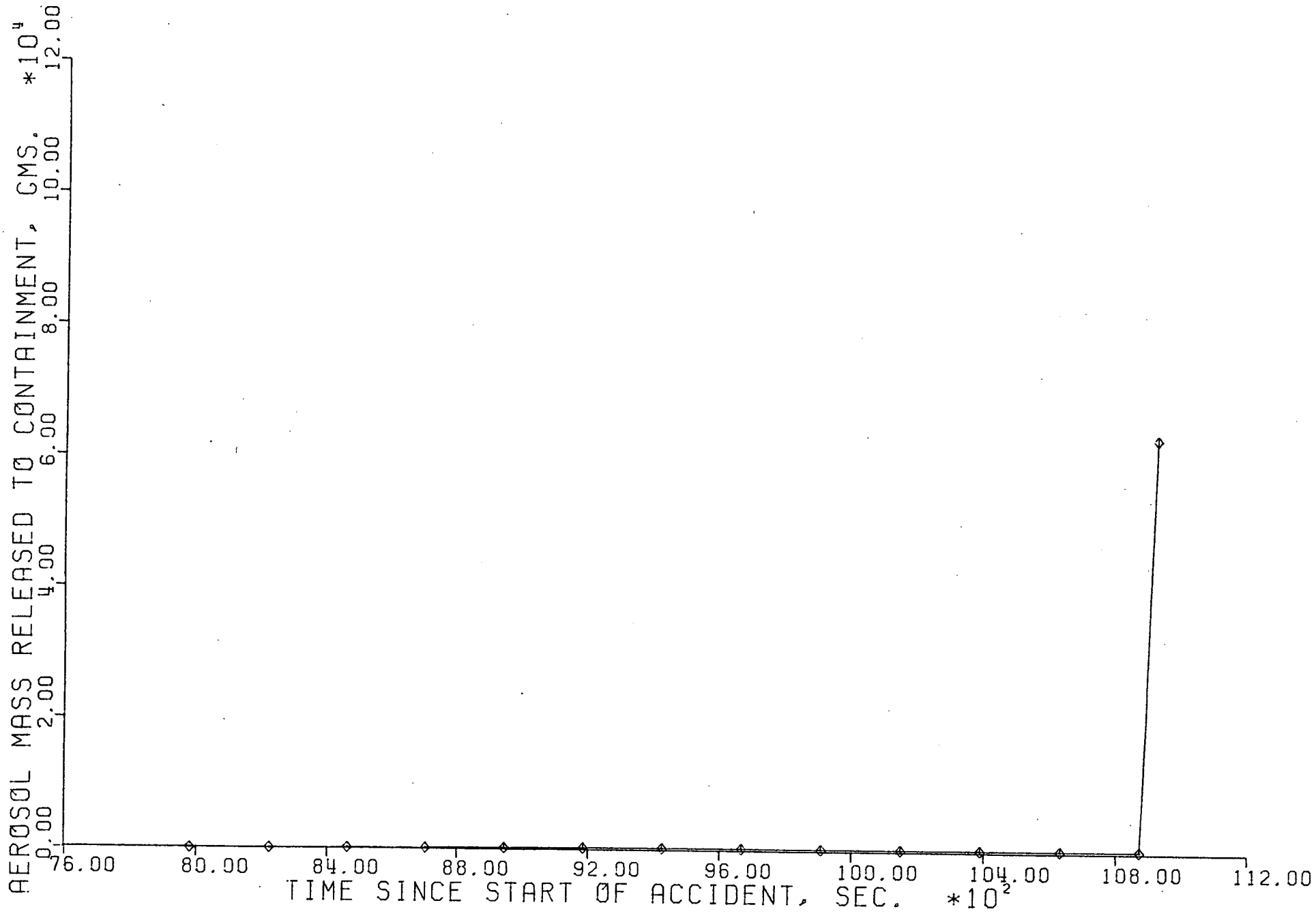
AEROSOL MASS RELEASED TO CONTAINMENT, GMS. *10⁴
0.00
2.00
4.00
6.00
8.00
10.00
12.00
76.00
80.00
84.00
88.00
92.00
96.00
100.00
104.00
108.00
112.00
TIME SINCE START OF ACCIDENT, SEC. *10²

FIGURE 5.39

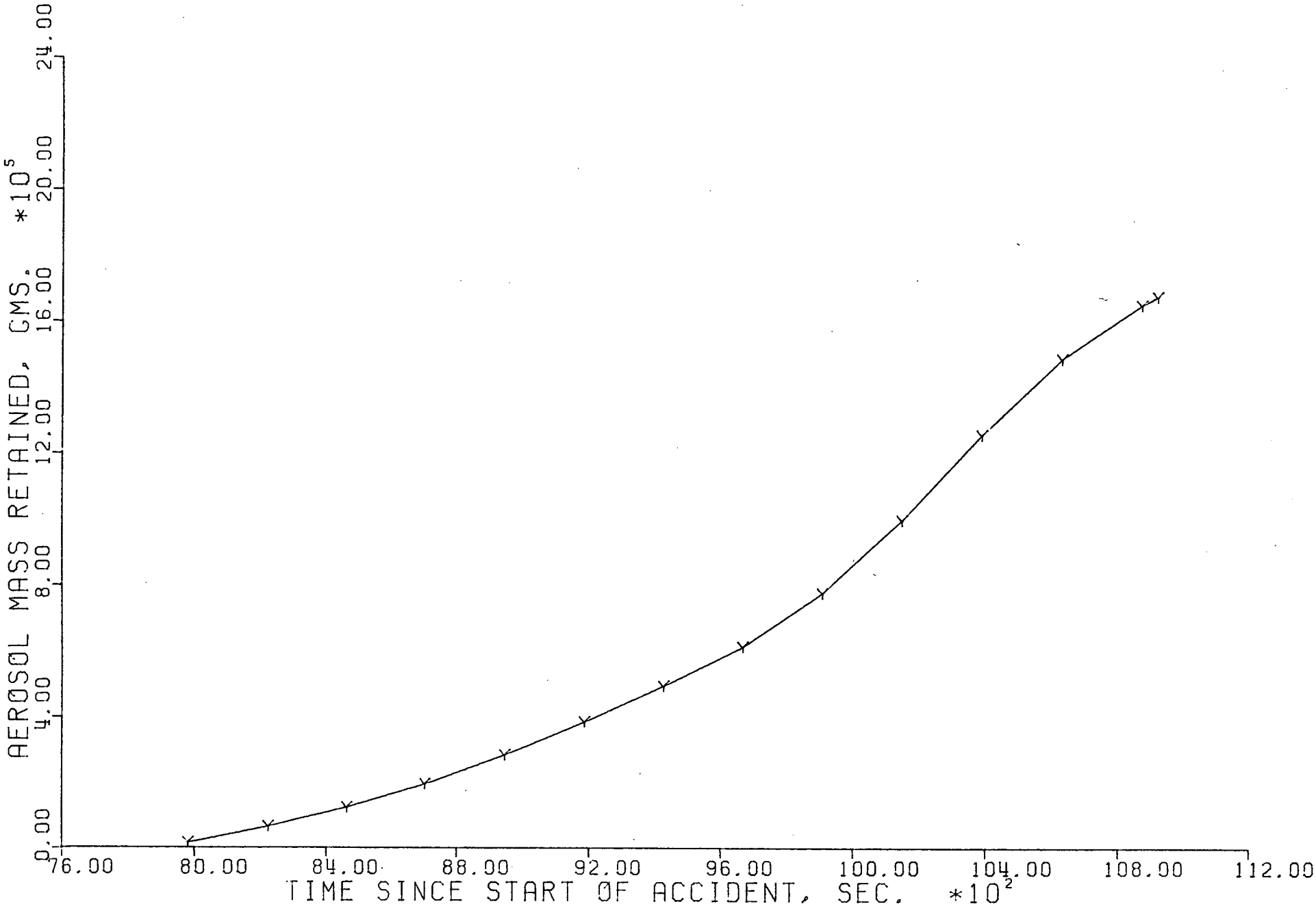
AEROSOL MASS RETAINED, GMS. *10^5
0.00
4.00
8.00
12.00
16.00
20.00
24.00
76.00
80.00
84.00
88.00
92.00
96.00
100.00
104.00
108.00
112.00
TIME SINCE START OF ACCIDENT, SEC. *10^2

FIGURE 5.40

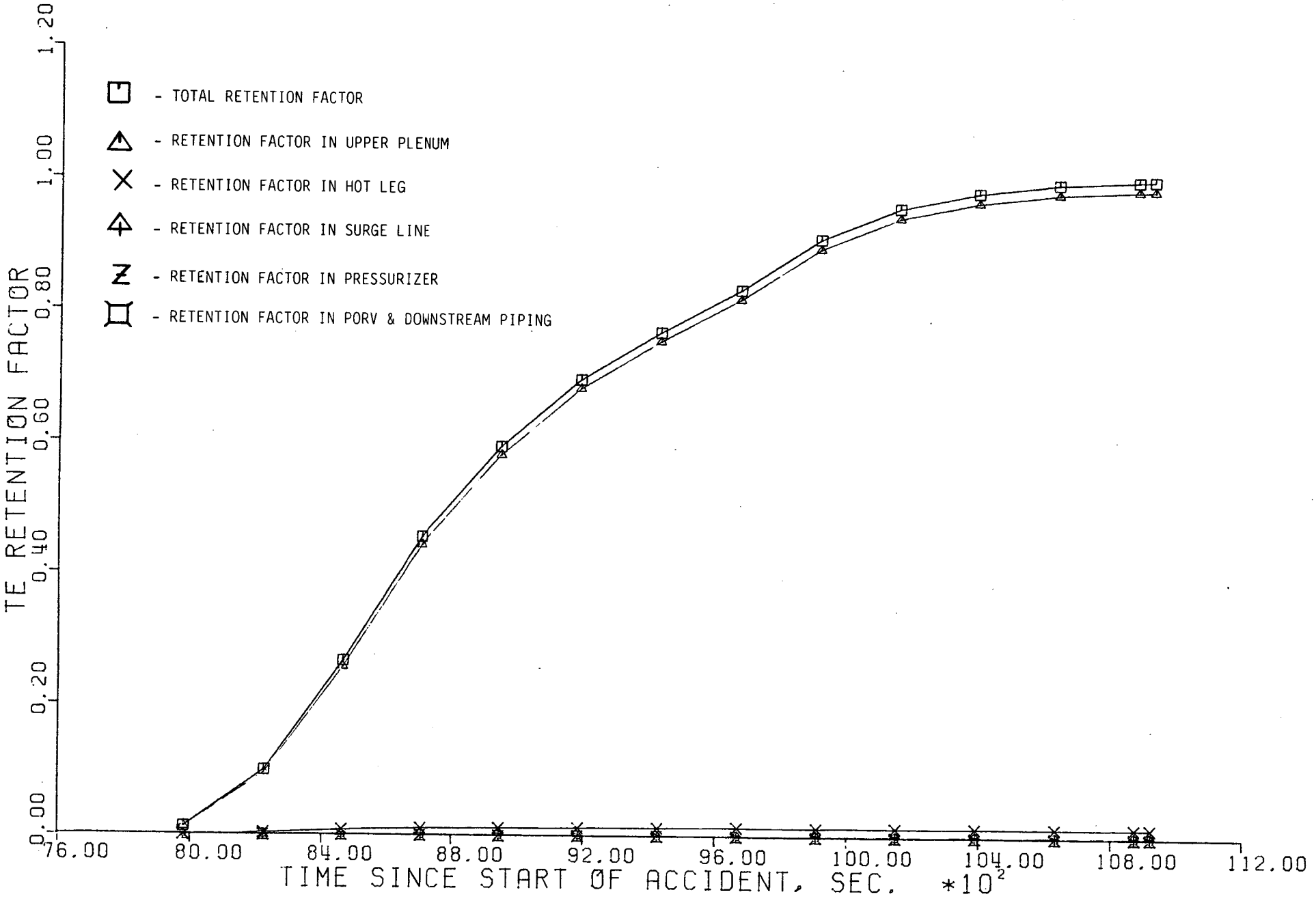
- TOTAL RETENTION FACTOR
- RETENTION FACTOR IN UPPER PLENUM
- RETENTION FACTOR IN HOT LEG
- RETENTION FACTOR IN SURGE LINE
- RETENTION FACTOR IN PRESSURIZER
- RETENTION FACTOR IN PORV & DOWNSTREAM PIPING
TE RETENTION FACTOR
0.00
0.20
0.40
0.60
0.80
1.00
1.20
76.00
80.00
84.00
88.00
92.00
96.00
100.00
104.00
108.00
112.00
TIME SINCE START OF ACCIDENT, SEC. *10²

FIGURE 5.41

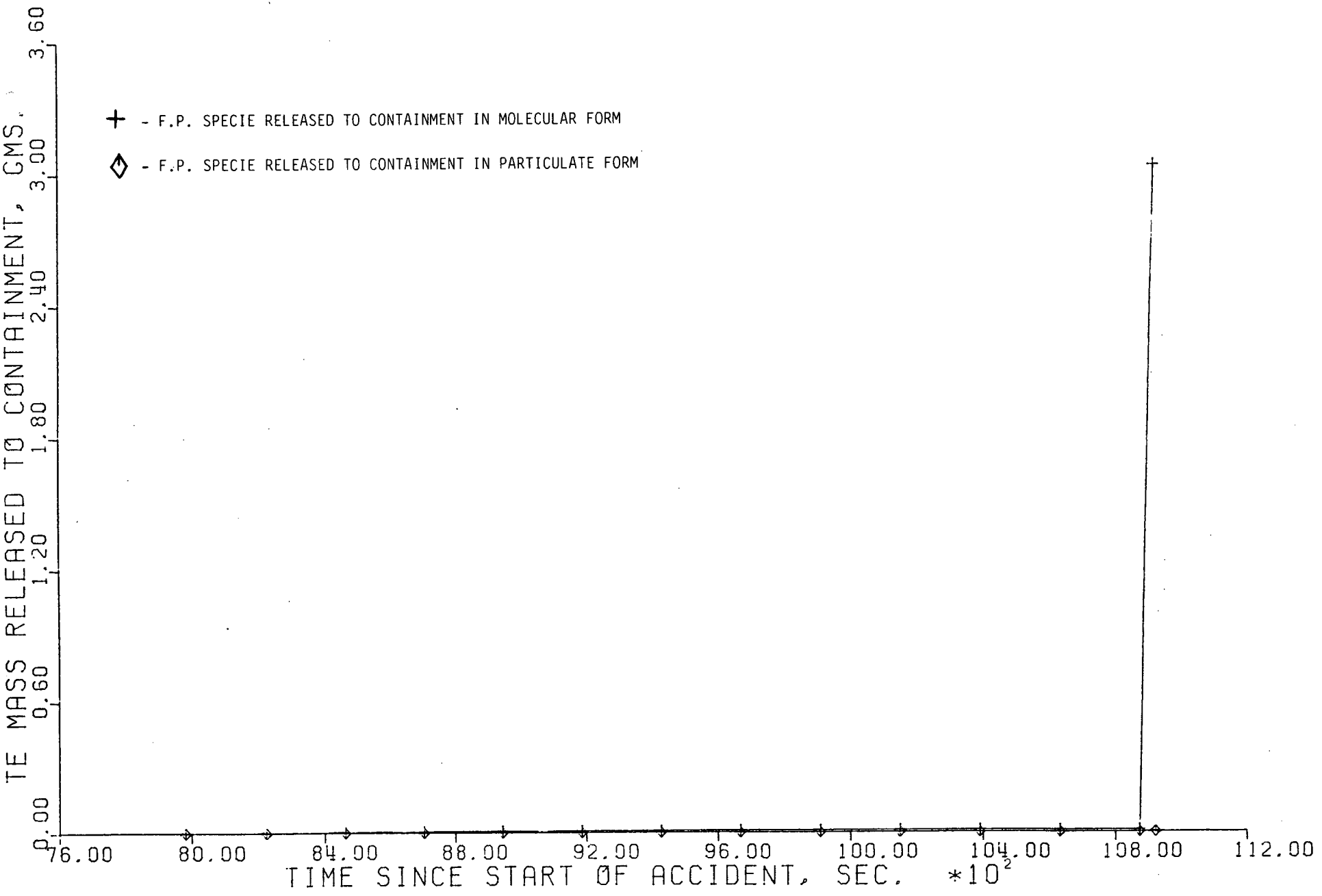
+ - F.P. SPECIE RELEASED TO CONTAINMENT IN MOLECULAR FORM
◇ - F.P. SPECIE RELEASED TO CONTAINMENT IN PARTICULATE FORM
TE MASS RELEASED TO CONTAINMENT, GMS.
0.00
0.60
1.20
1.80
2.40
3.00
3.60
76.00
80.00
84.00
88.00
92.00
96.00
100.00
104.00
108.00
112.00
TIME SINCE START OF ACCIDENT, SEC. *10²

FIGURE 5.42

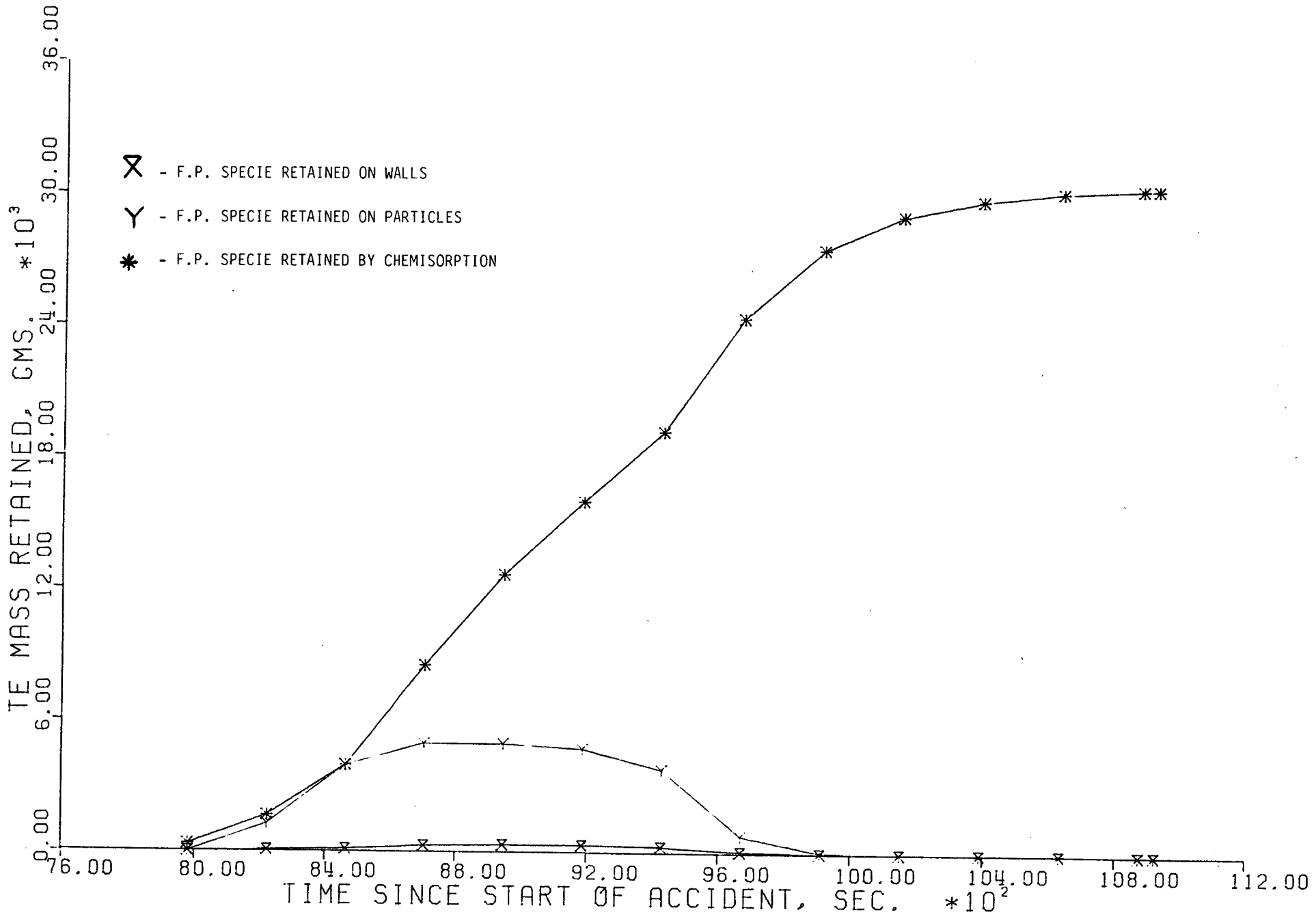
X - F.P. SPECIE RETAINED ON WALLS
Y - F.P. SPECIE RETAINED ON PARTICLES
* - F.P. SPECIE RETAINED BY CHEMISORPTION
TE MASS RETAINED, GMS. *10^3
0.00
6.00
12.00
18.00
24.00
30.00
36.00
76.00
80.00
84.00
88.00
92.00
96.00
100.00
104.00
108.00
112.00
TIME SINCE START OF ACCIDENT, SEC. *10^2

FIGURE 5.43

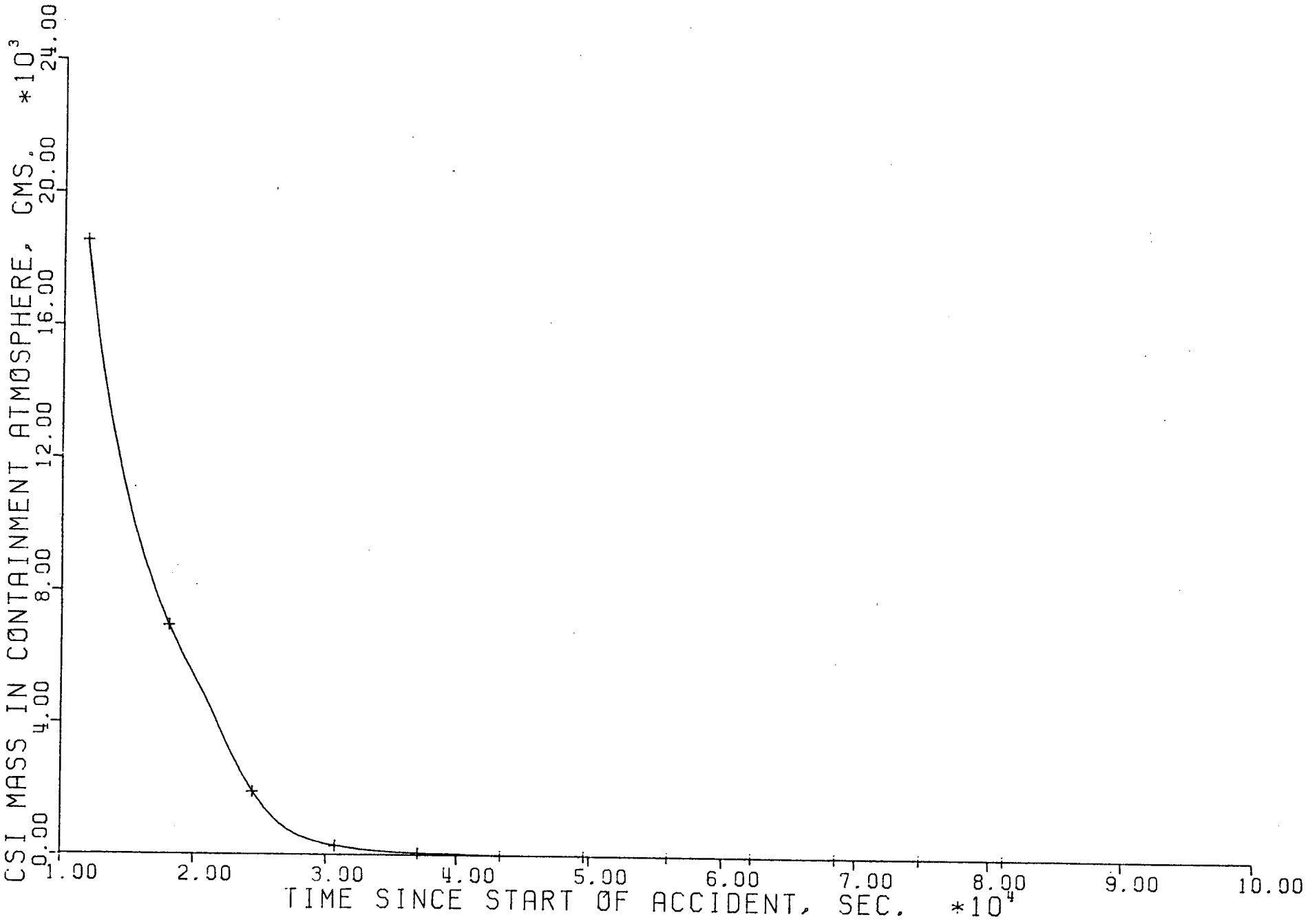
CSI MASS IN CONTAINMENT ATMOSPHERE, GMS. *10^3
0.00
4.00
8.00
12.00
16.00
20.00
24.00
1.00
2.00
3.00
4.00
5.00
6.00
7.00
8.00
9.00
10.00
TIME SINCE START OF ACCIDENT, SEC. *10^4

FIGURE 5.44

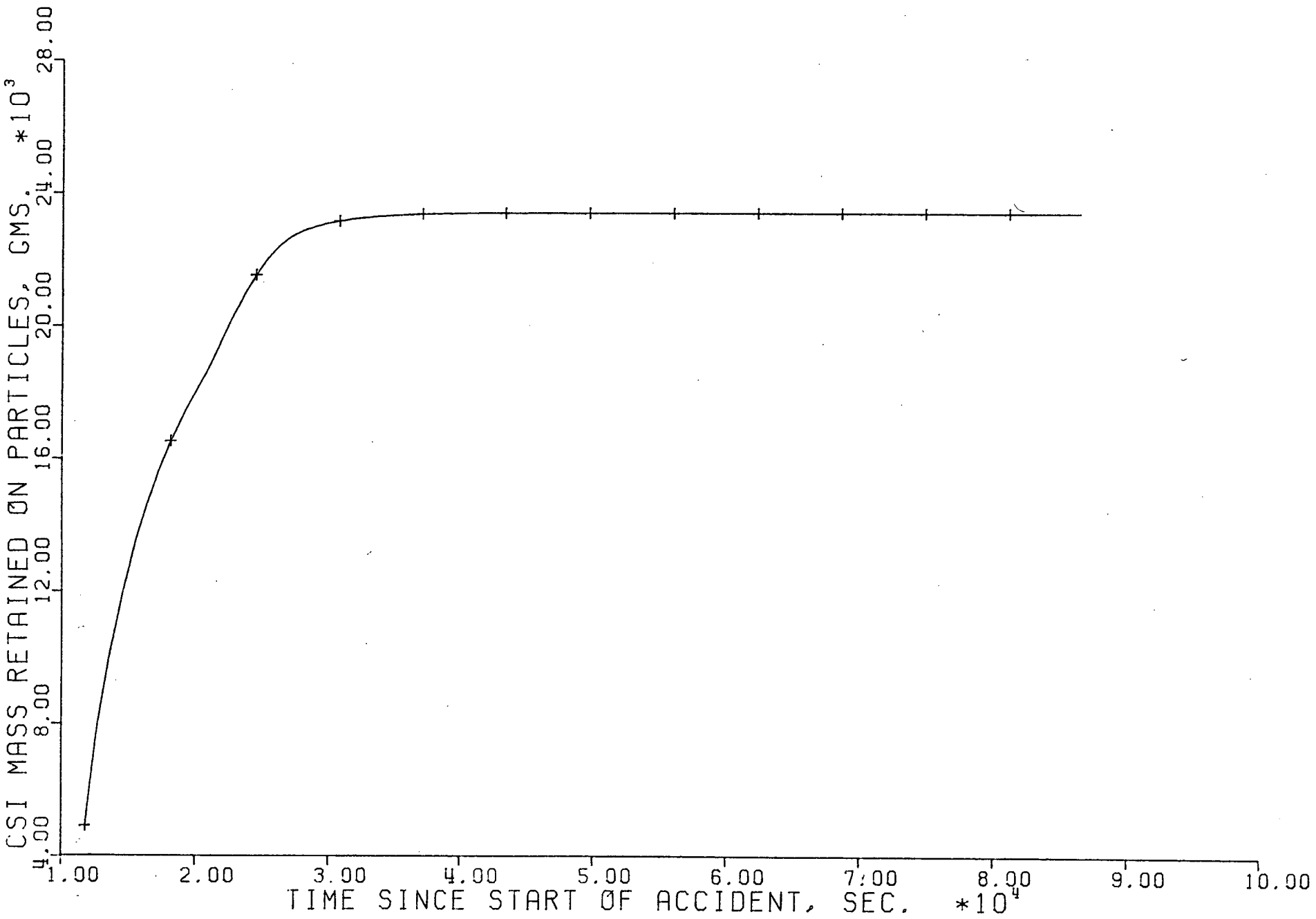
CSI MASS RETAINED ON PARTICLES, GMS. *10^3
4.00
8.00
12.00
16.00
20.00
24.00
28.00
1.00
2.00
3.00
4.00
5.00
6.00
7.00
8.00
9.00
10.00
TIME SINCE START OF ACCIDENT, SEC. *10^4

FIGURE 5.45

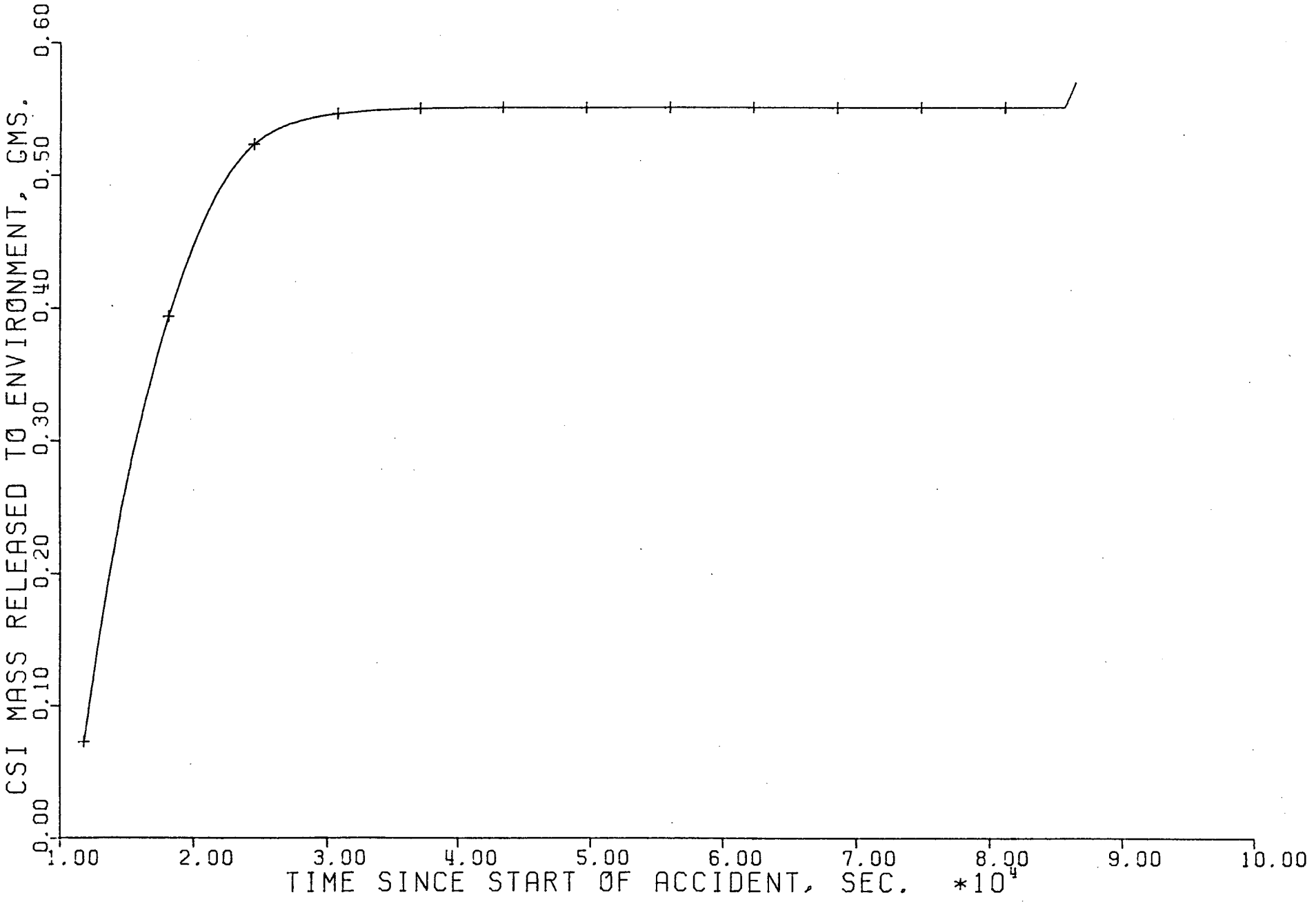
CSI MASS RELEASED TO ENVIRONMENT, GMS.
0.00
0.10
0.20
0.30
0.40
0.50
0.60
1.00
2.00
3.00
4.00
5.00
6.00
7.00
8.00
9.00
10.00
TIME SINCE START OF ACCIDENT, SEC. *10^4

FIGURE 5.46

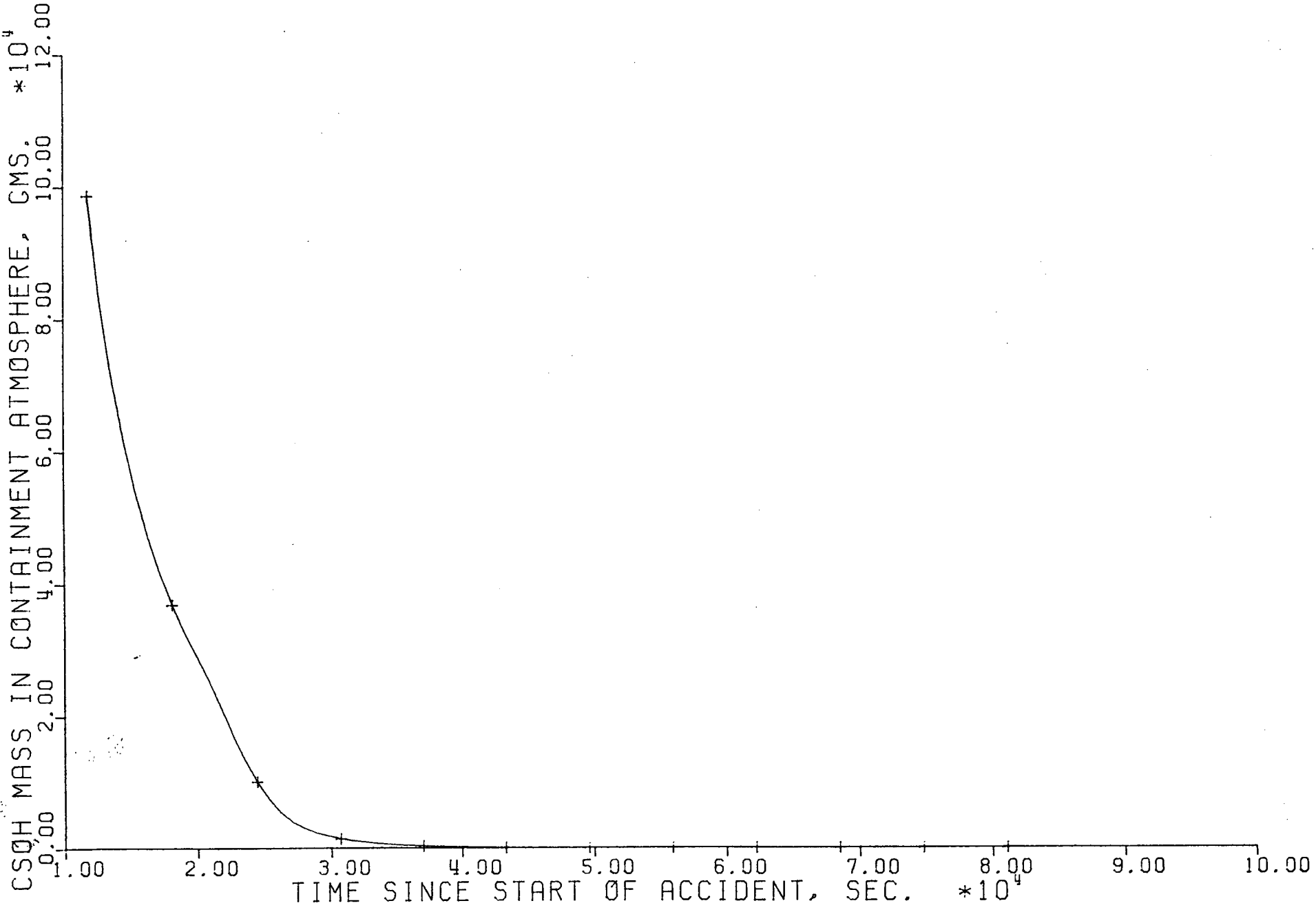
CSOH MASS IN CONTAINMENT ATMOSPHERE, GMS. *10^4
0.00
2.00
4.00
6.00
8.00
10.00
12.00
1.00
2.00
3.00
4.00
5.00
6.00
7.00
8.00
9.00
10.00
TIME SINCE START OF ACCIDENT, SEC. *10^4

FIGURE 5.47

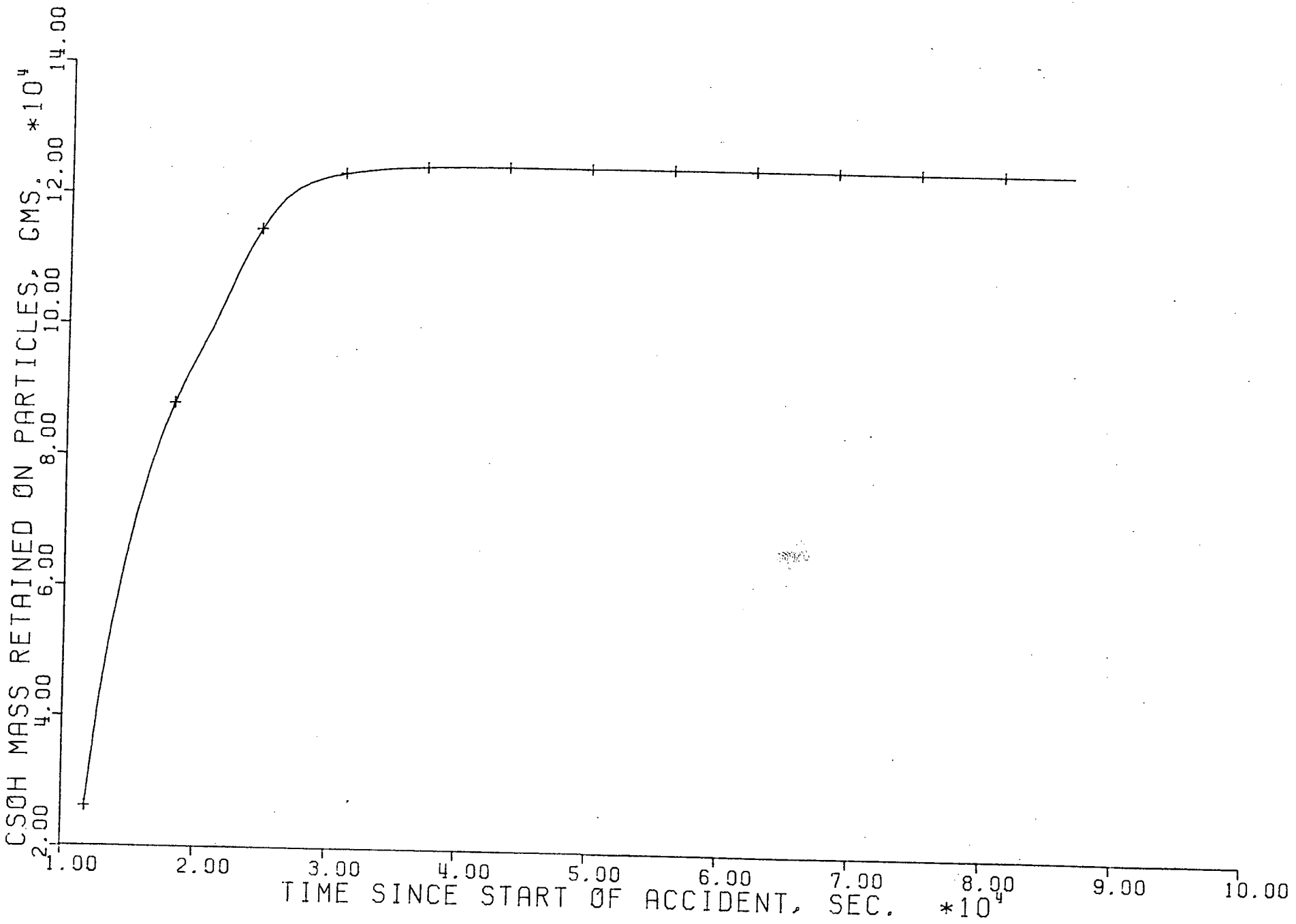
CSOH MASS RETAINED ON PARTICLES, GMS. *10⁴
2.00
4.00
6.00
8.00
10.00
12.00
14.00
1.00
2.00
3.00
4.00
5.00
6.00
7.00
8.00
9.00
10.00
TIME SINCE START OF ACCIDENT, SEC. *10⁴

FIGURE 5.48

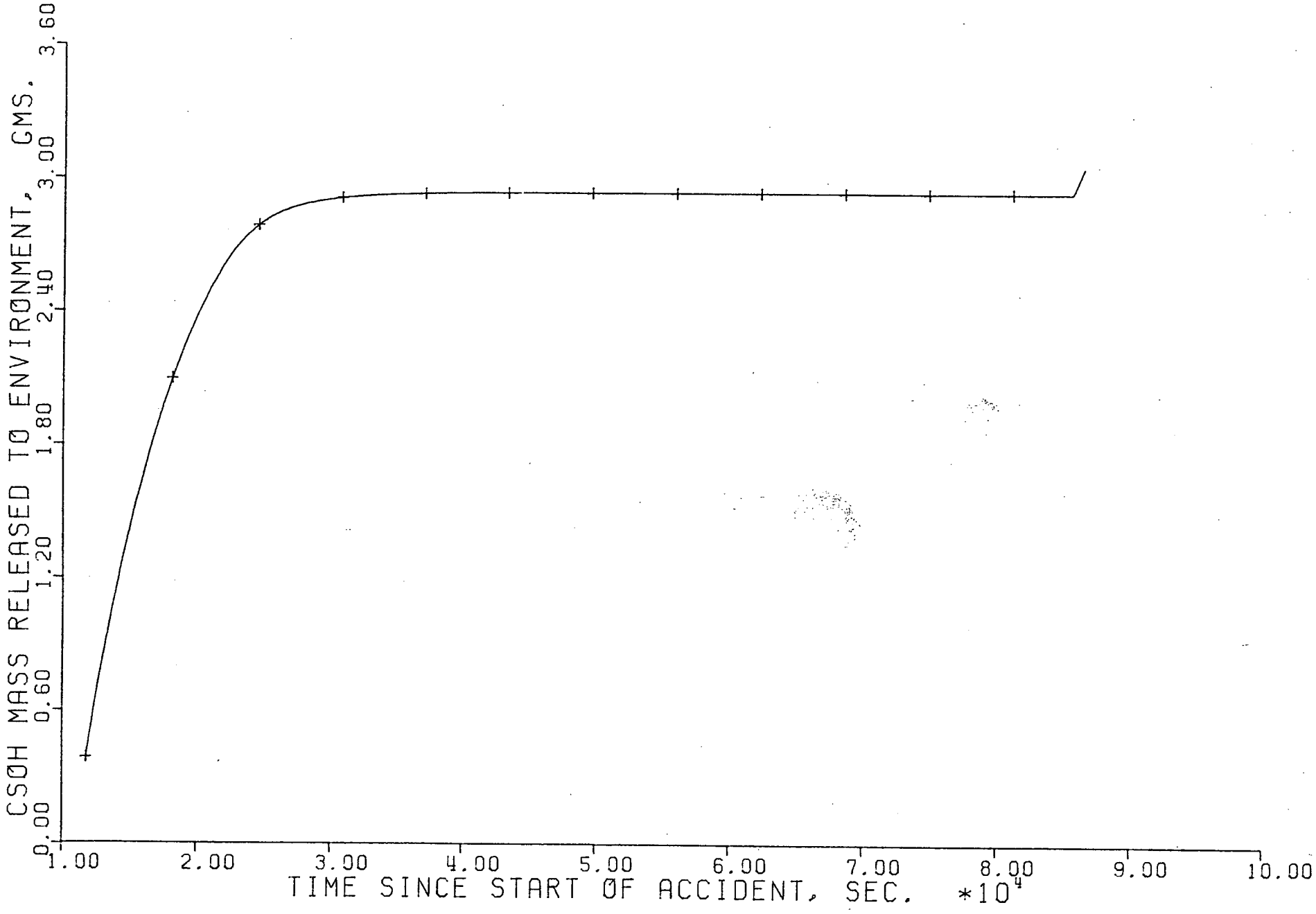
CSØH MASS RELEASED TØ ENVIRØNMENT, GMS.
0.00
0.60
1.20
1.80
2.40
3.00
3.60
1.00
2.00
3.00
4.00
5.00
6.00
7.00
8.00
9.00
10.00
TIME SINCE START ØF ACCIDENT, SEC. *10^4

FIGURE 5.49

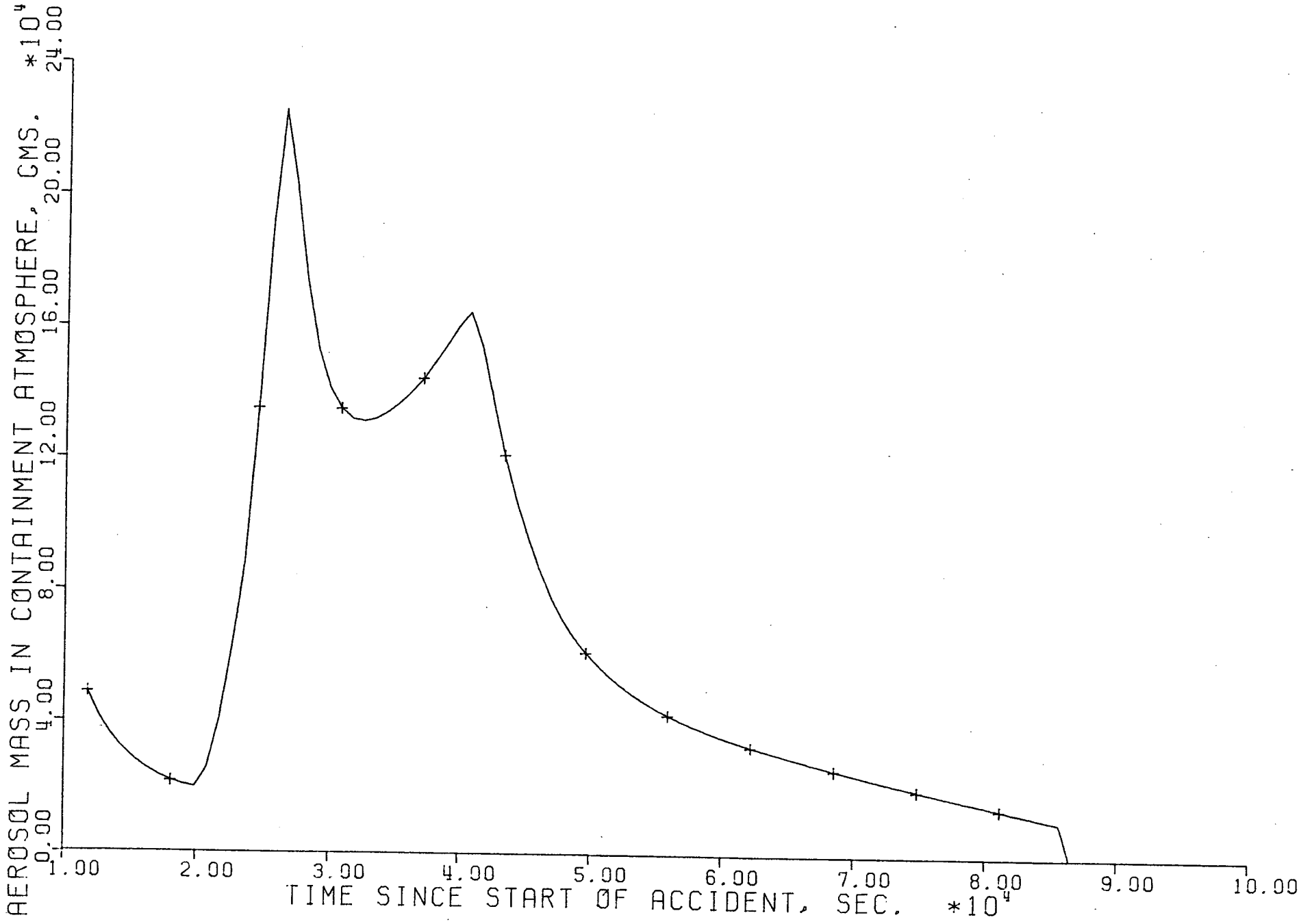
AEROSOL MASS IN CONTAINMENT ATMOSPHERE, GMS. *10⁴
0.00
4.00
8.00
12.00
16.00
20.00
24.00
1.00
2.00
3.00
4.00
5.00
6.00
7.00
8.00
9.00
10.00
TIME SINCE START OF ACCIDENT, SEC. *10⁴

FIGURE 5.50

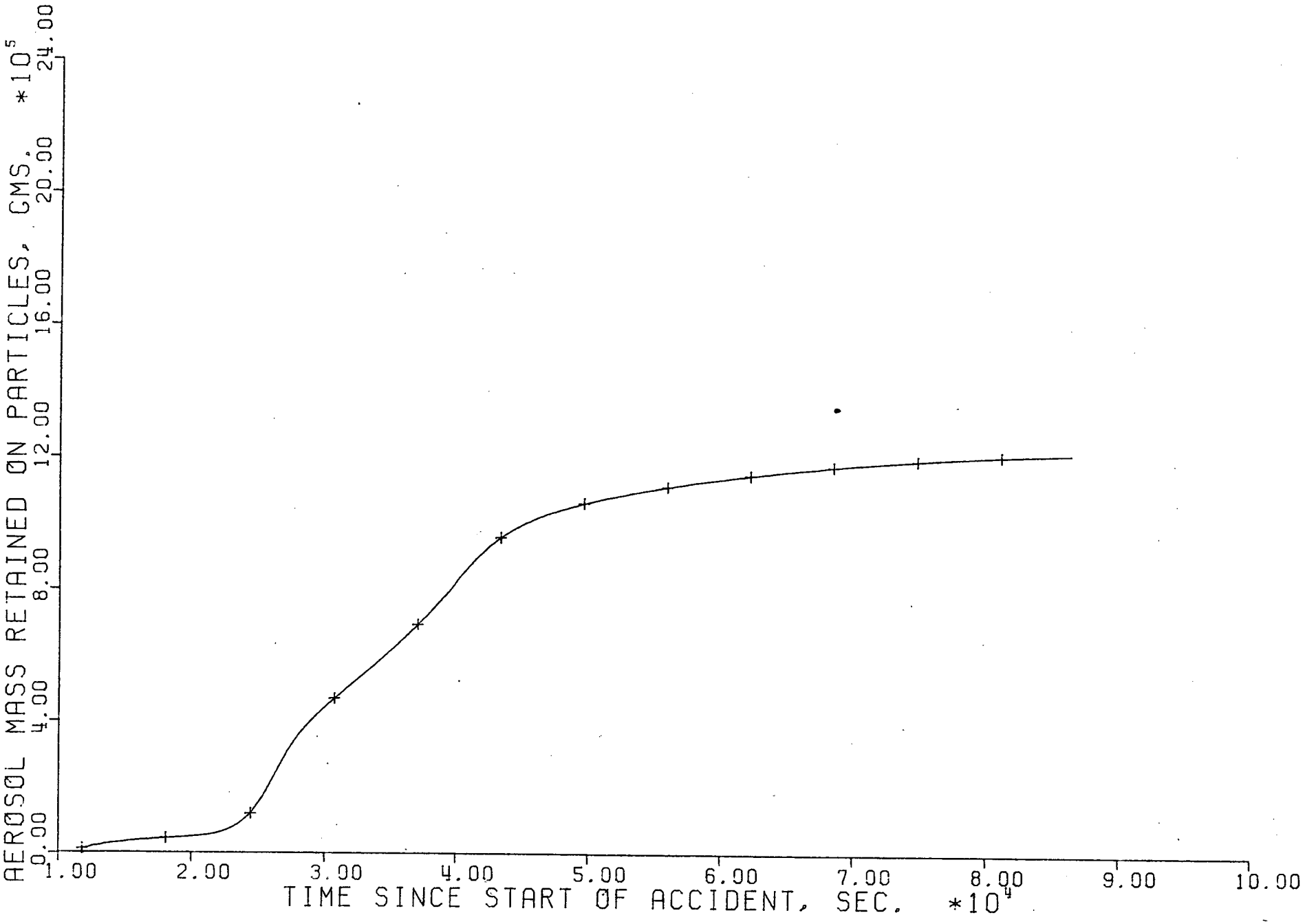
AEROSOL MASS RETAINED ON PARTICLES, GMS. *10^5
0.00
4.00
8.00
12.00
16.00
20.00
24.00
1.00
2.00
3.00
4.00
5.00
6.00
7.00
8.00
9.00
10.00
TIME SINCE START OF ACCIDENT, SEC. *10^4

FIGURE 5.51

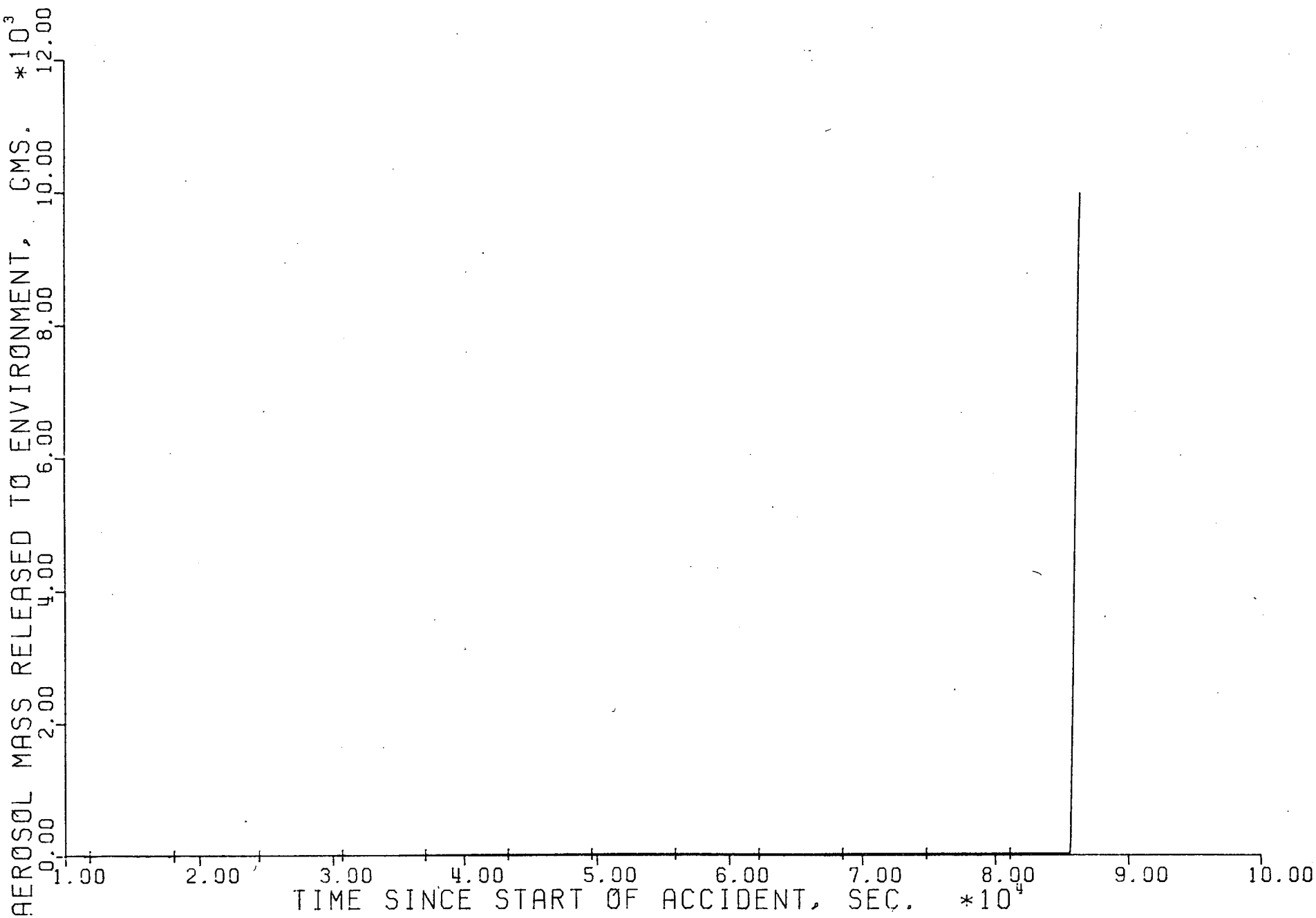
AEROSOL MASS RELEASED TO ENVIRONMENT, CMS. *10^3
0.00
2.00
4.00
6.00
8.00
10.00
12.00
1.00
2.00
3.00
4.00
5.00
6.00
7.00
8.00
9.00
10.00
TIME SINCE START OF ACCIDENT, SEC. *10^4

FIGURE 5.52

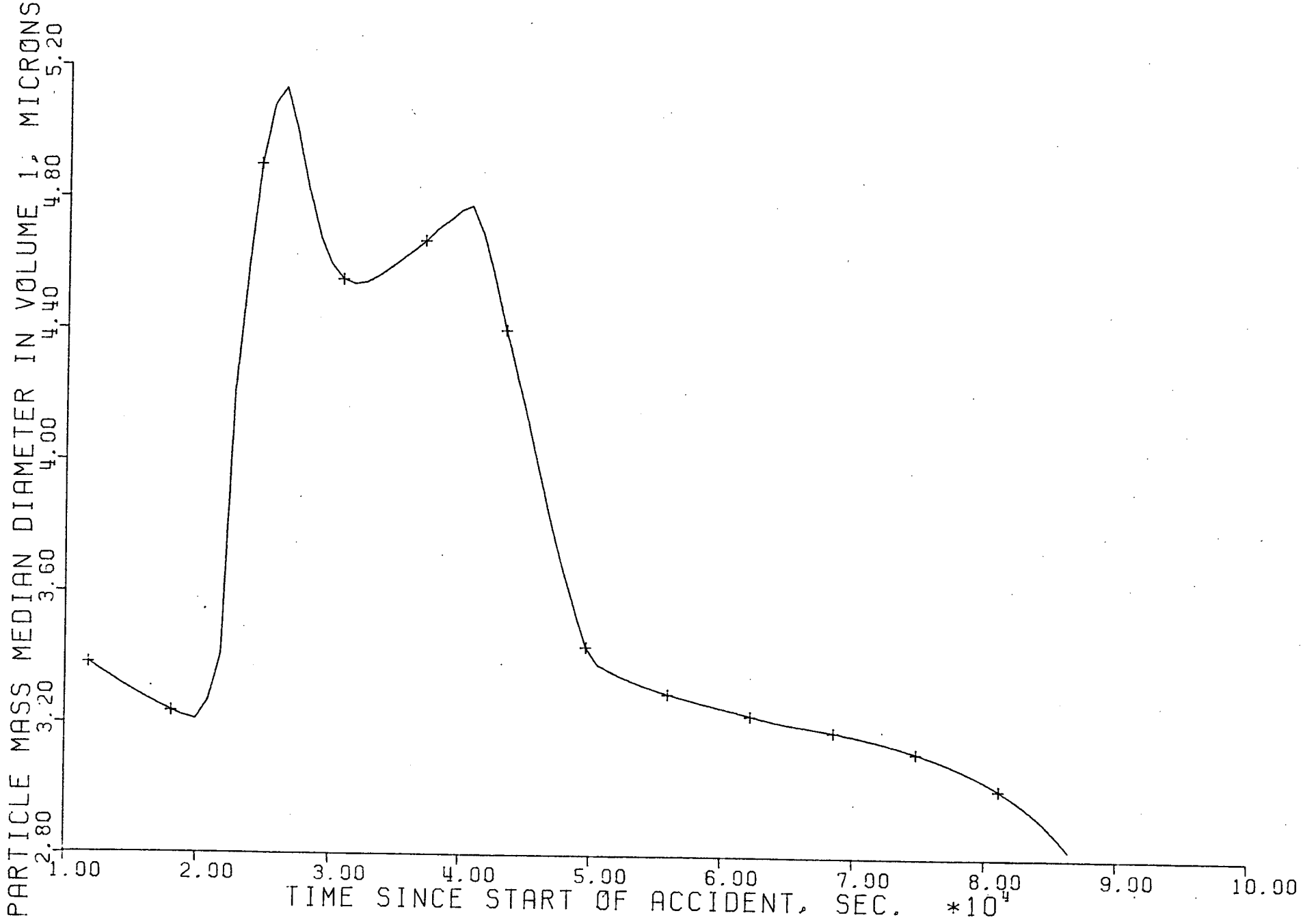
PARTICLE MASS MEDIAN DIAMETER IN VOLUME 1, MICRONS
2.80
3.20
3.60
4.00
4.40
4.80
5.20
1.00
2.00
3.00
4.00
5.00
6.00
7.00
8.00
9.00
10.00
TIME SINCE START OF ACCIDENT, SEC. *10⁴

FIGURE 5.53

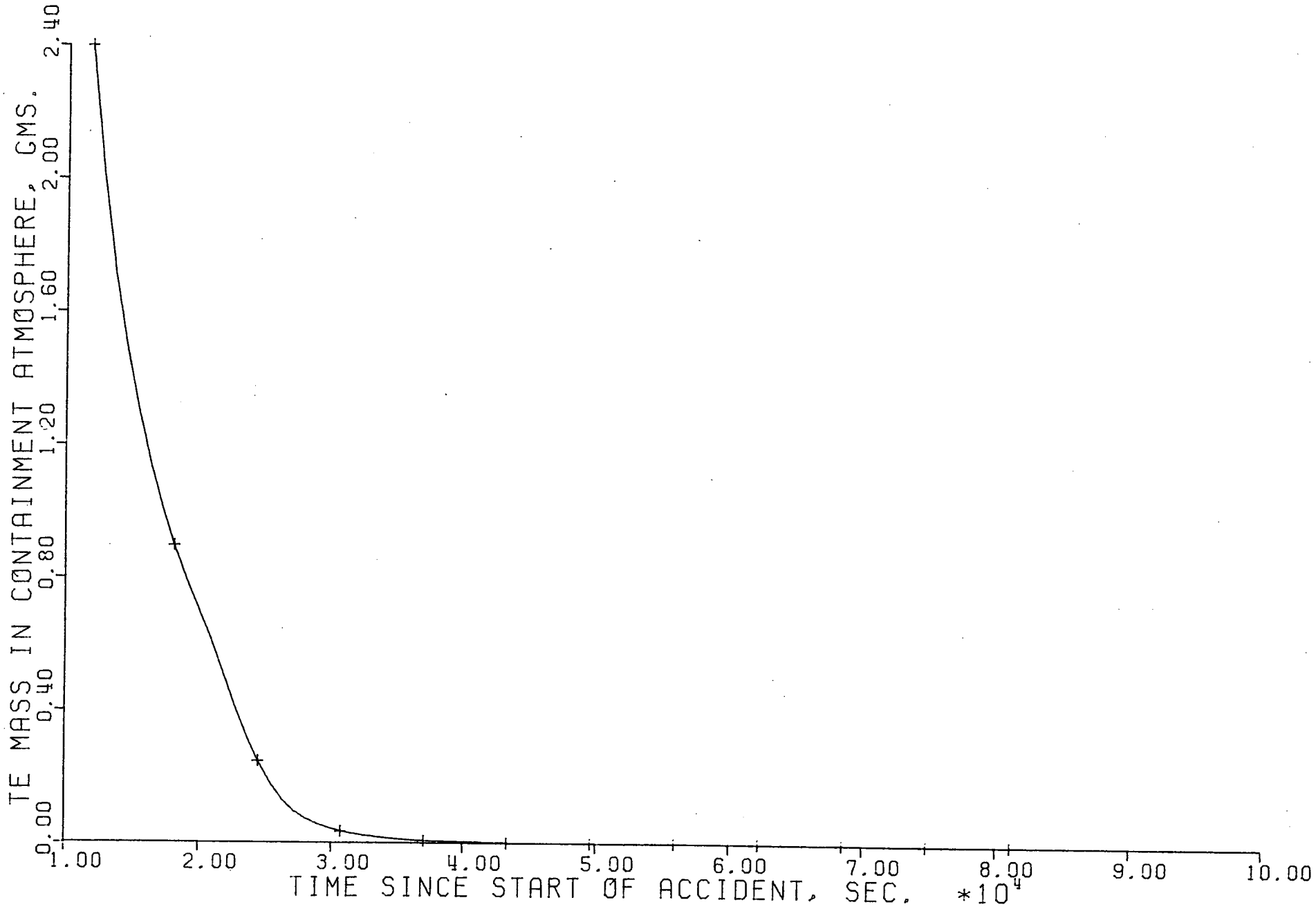
TE MASS IN CONTAINMENT ATMOSPHERE, GMS.
0.00
0.40
0.80
1.20
1.60
2.00
2.40
1.00
2.00
3.00
4.00
5.00
6.00
7.00
8.00
9.00
10.00
TIME SINCE START OF ACCIDENT, SEC. *10^4

FIGURE 5.54

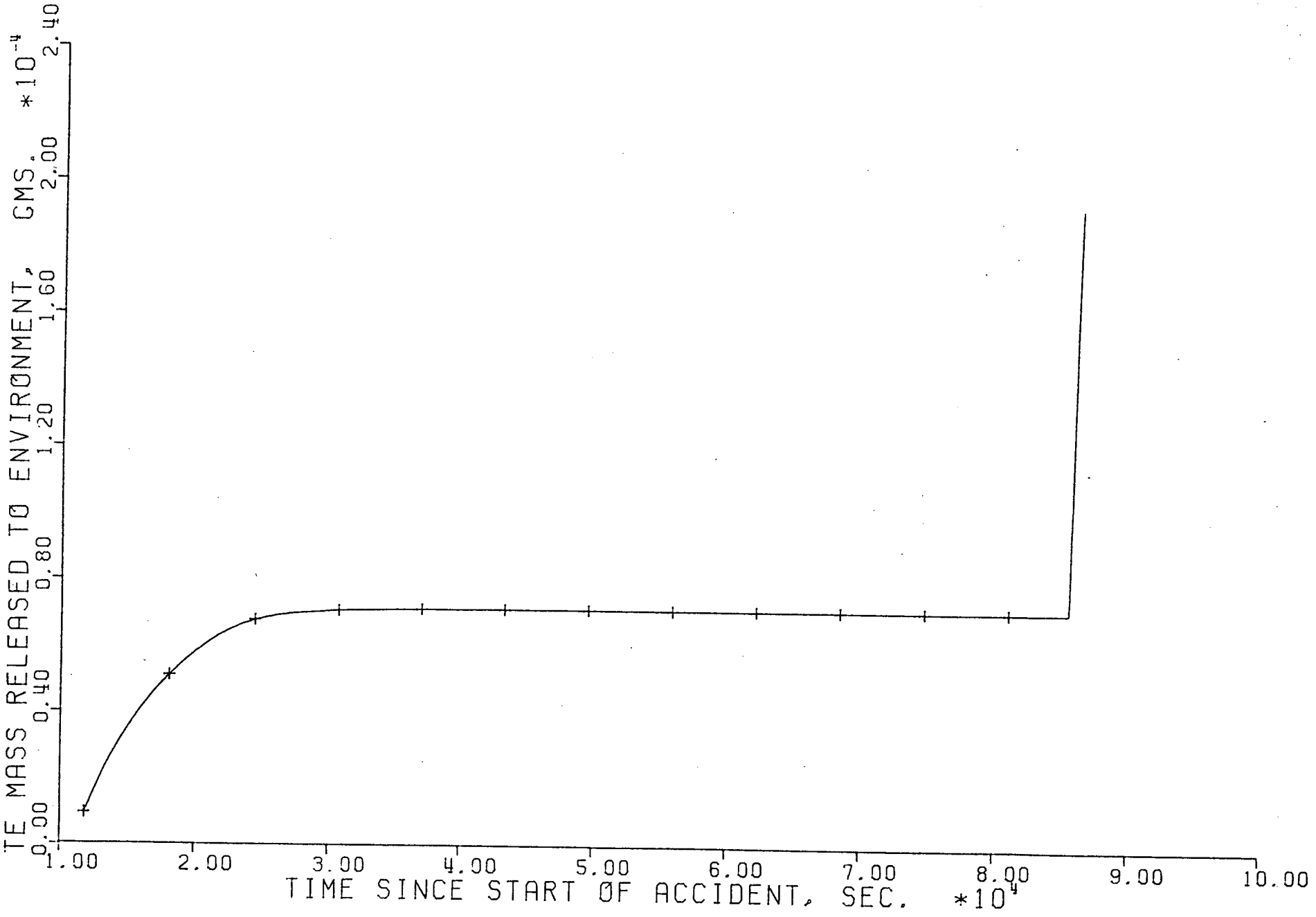
TE MASS RELEASED TØ ENVIRØNMENT, CMS. *10⁻⁴
0.00
0.40
0.80
1.20
1.60
2.00
2.40
1.00
2.00
3.00
4.00
5.00
6.00
7.00
8.00
9.00
10.00
TIME SINCE START ØF ACCIDENT, SEC. *10⁴

FIGURE 5.55

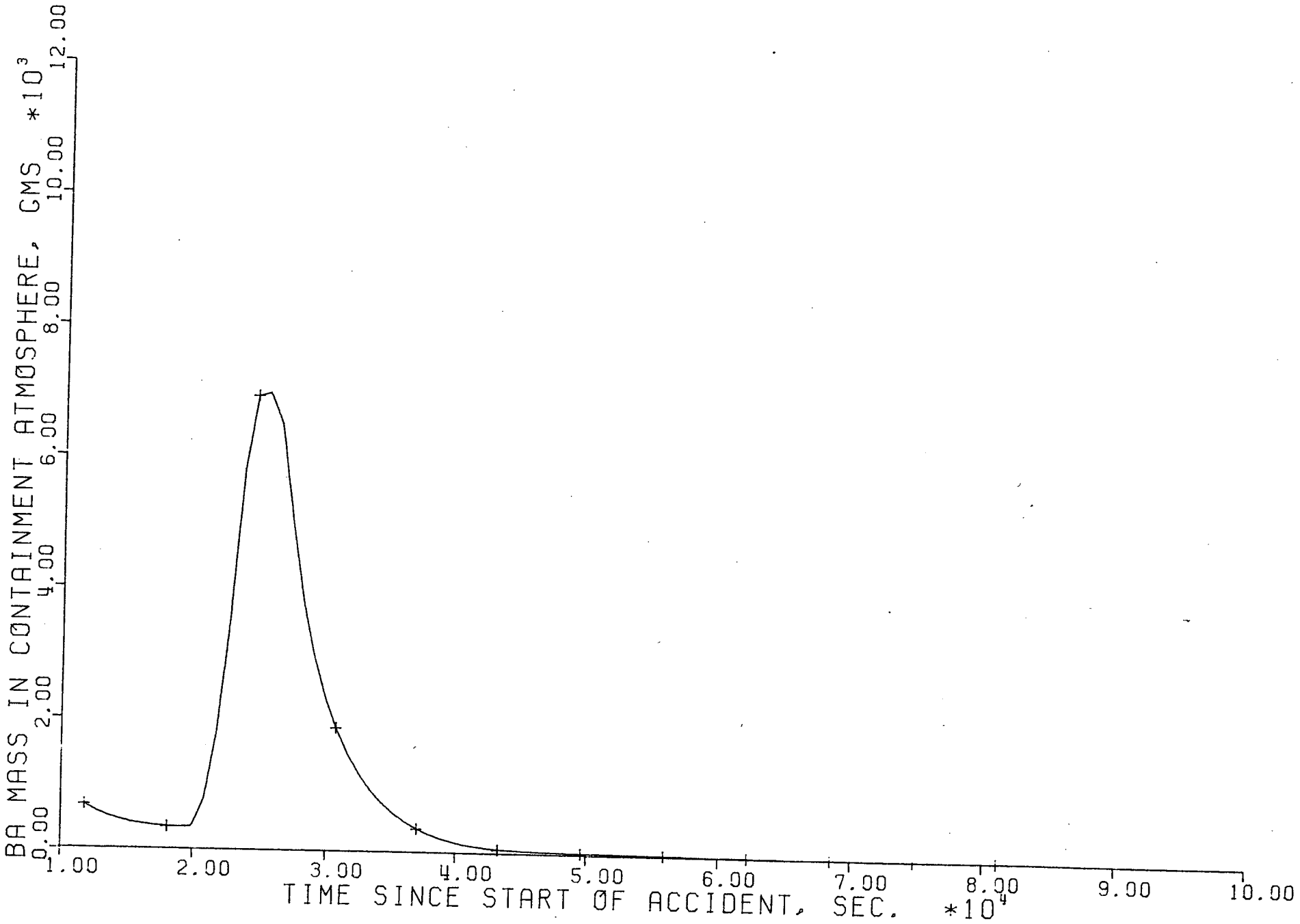
BA MASS IN CONTAINMENT ATMOSPHERE, GMS *10³
0.00
2.00
4.00
6.00
8.00
10.00
12.00
1.00
2.00
3.00
4.00
5.00
6.00
7.00
8.00
9.00
10.00
TIME SINCE START OF ACCIDENT, SEC. *10⁴

FIGURE 5.56

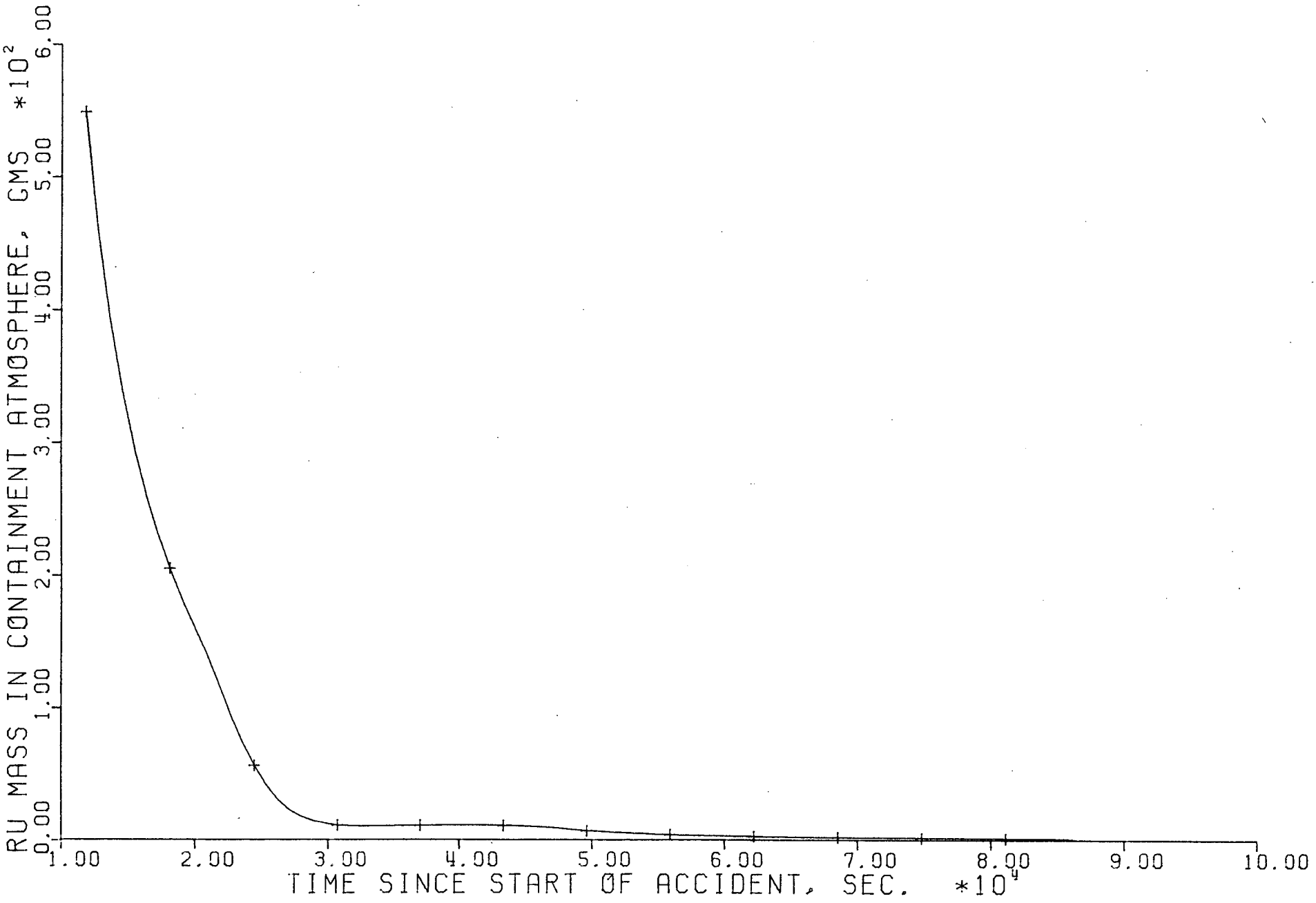
RU MASS IN CONTAINMENT ATMOSPHERE, GMS *10²
0.00
1.00
2.00
3.00
4.00
5.00
6.00
1.00
2.00
3.00
4.00
5.00
6.00
7.00
8.00
9.00
10.00
TIME SINCE START OF ACCIDENT, SEC. *10⁴

FIGURE 5.57

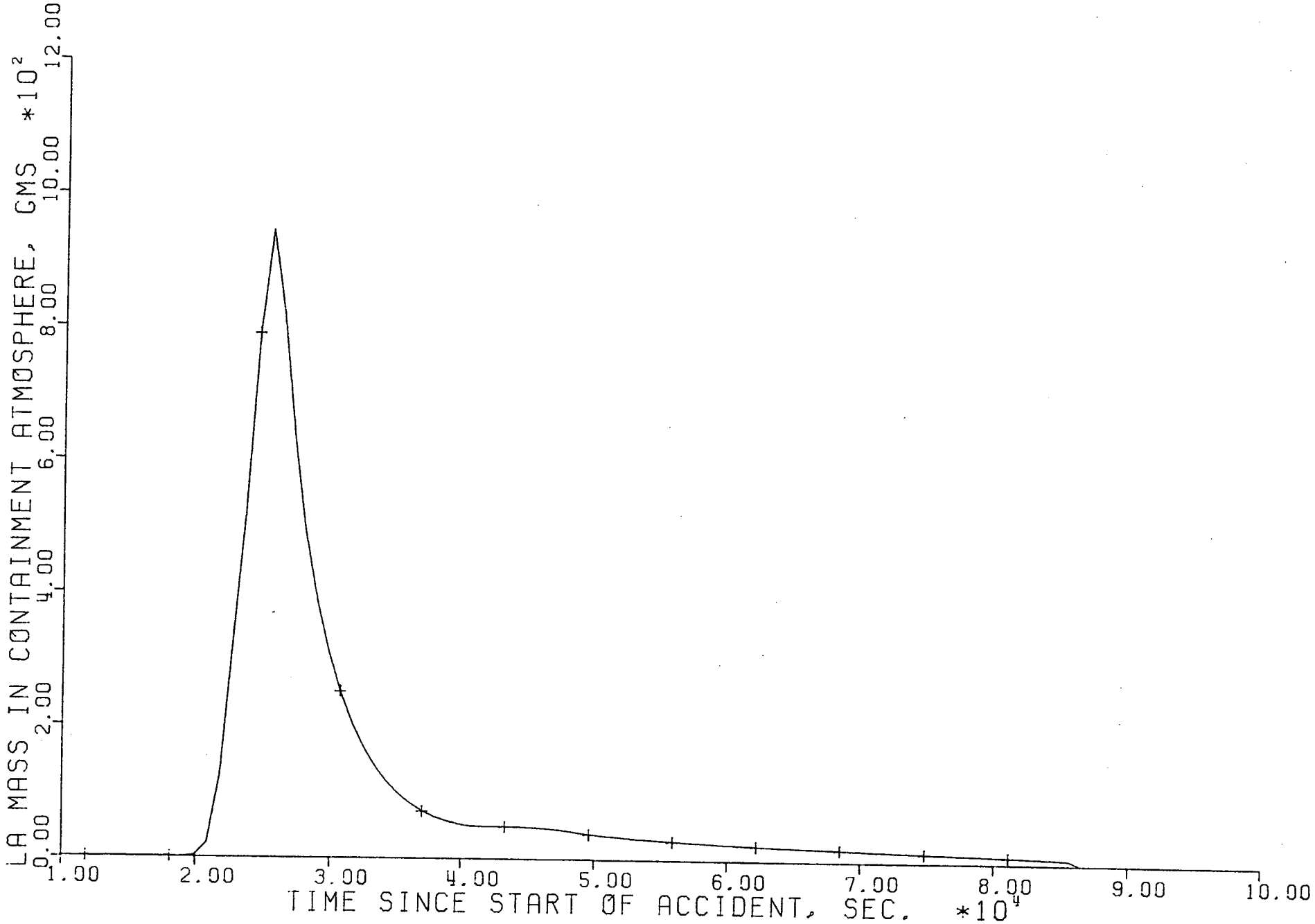
LA MASS IN CONTAINMENT ATMOSPHERE, GMS *10²
0.00
2.00
4.00
6.00
8.00
10.00
12.00
1.00
2.00
3.00
4.00
5.00
6.00
7.00
8.00
9.00
10.00
TIME SINCE START OF ACCIDENT, SEC. *10⁴

FIGURE 5.58

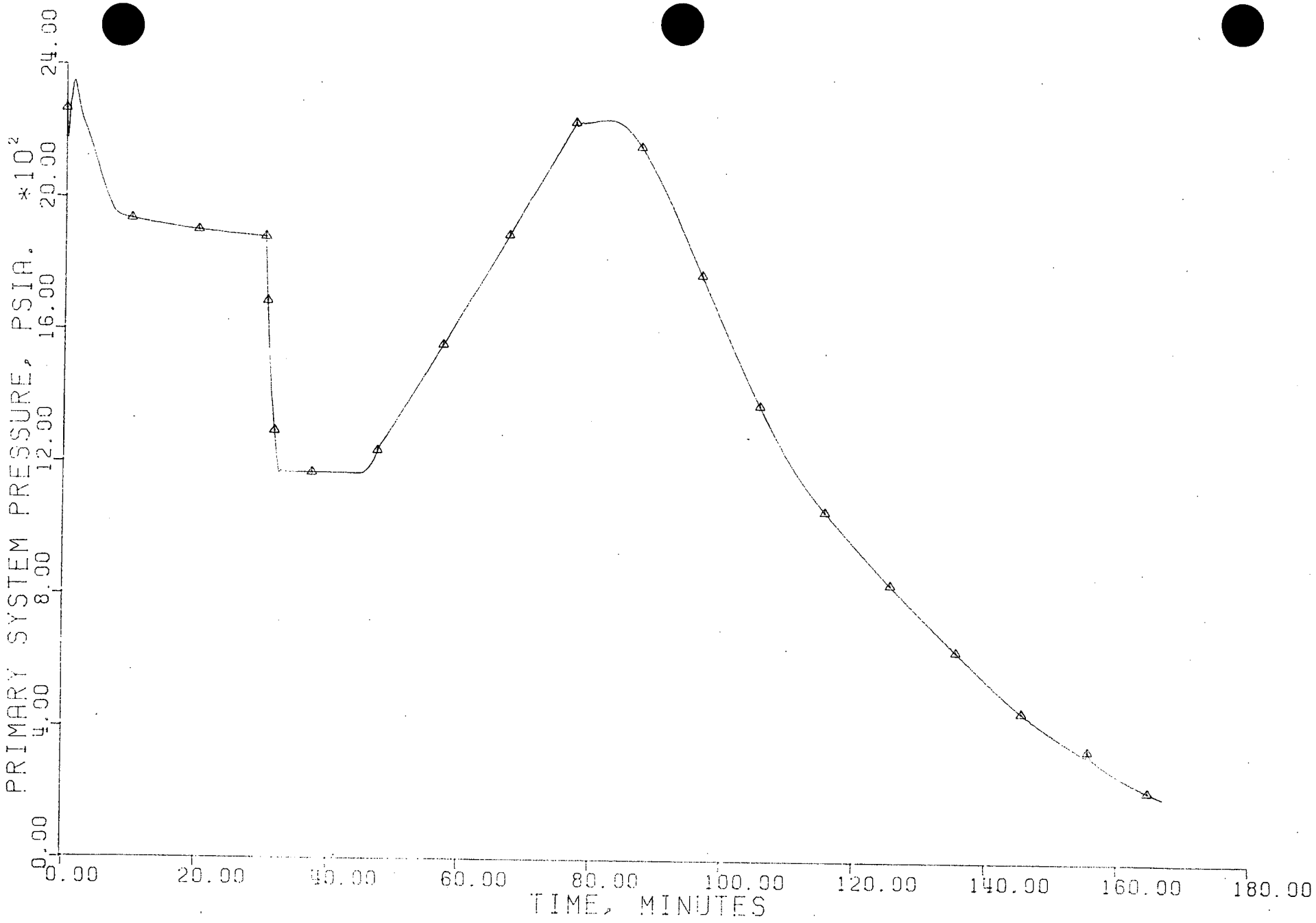
PRIMARY SYSTEM PRESSURE, PSIA. *10²
24.00
20.00
16.00
12.00
8.00
4.00
0.00
0.00
20.00
40.00
60.00
80.00
100.00
120.00
140.00
160.00
180.00
TIME, MINUTES

FIGURE 5.59

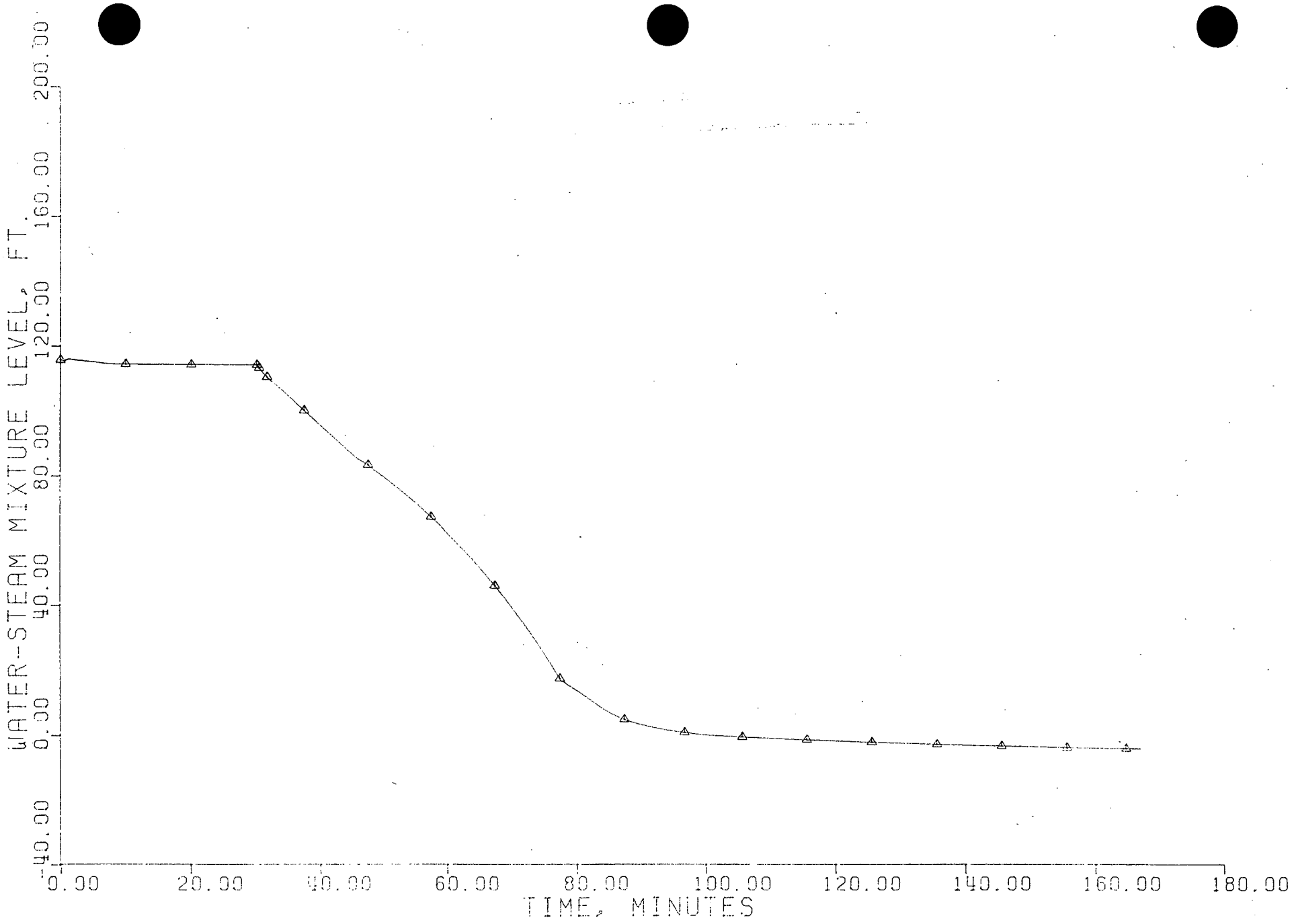
WATER-STEAM MIXTURE LEVEL, FT.
200.00
160.00
120.00
80.00
40.00
0.00
-40.00
0.00
20.00
40.00
60.00
80.00
100.00
120.00
140.00
160.00
180.00
TIME, MINUTES

FIGURE 5.60

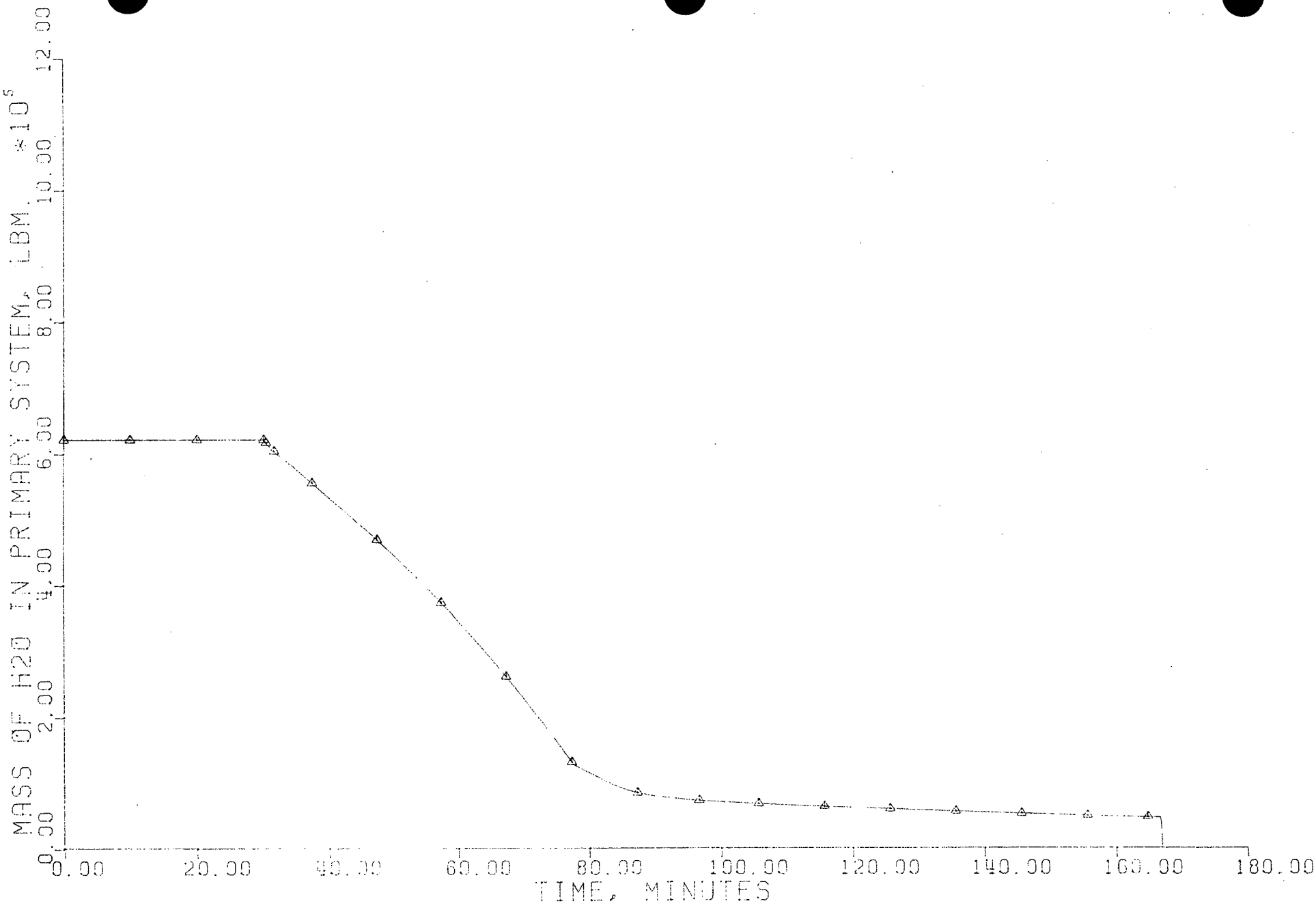
MASS OF H2O IN PRIMARY SYSTEM, LBM. *10^5
0.00
2.00
4.00
6.00
8.00
10.00
12.00
0.00
20.00
40.00
60.00
80.00
100.00
120.00
140.00
160.00
180.00
TIME, MINUTES

FIGURE 5.61

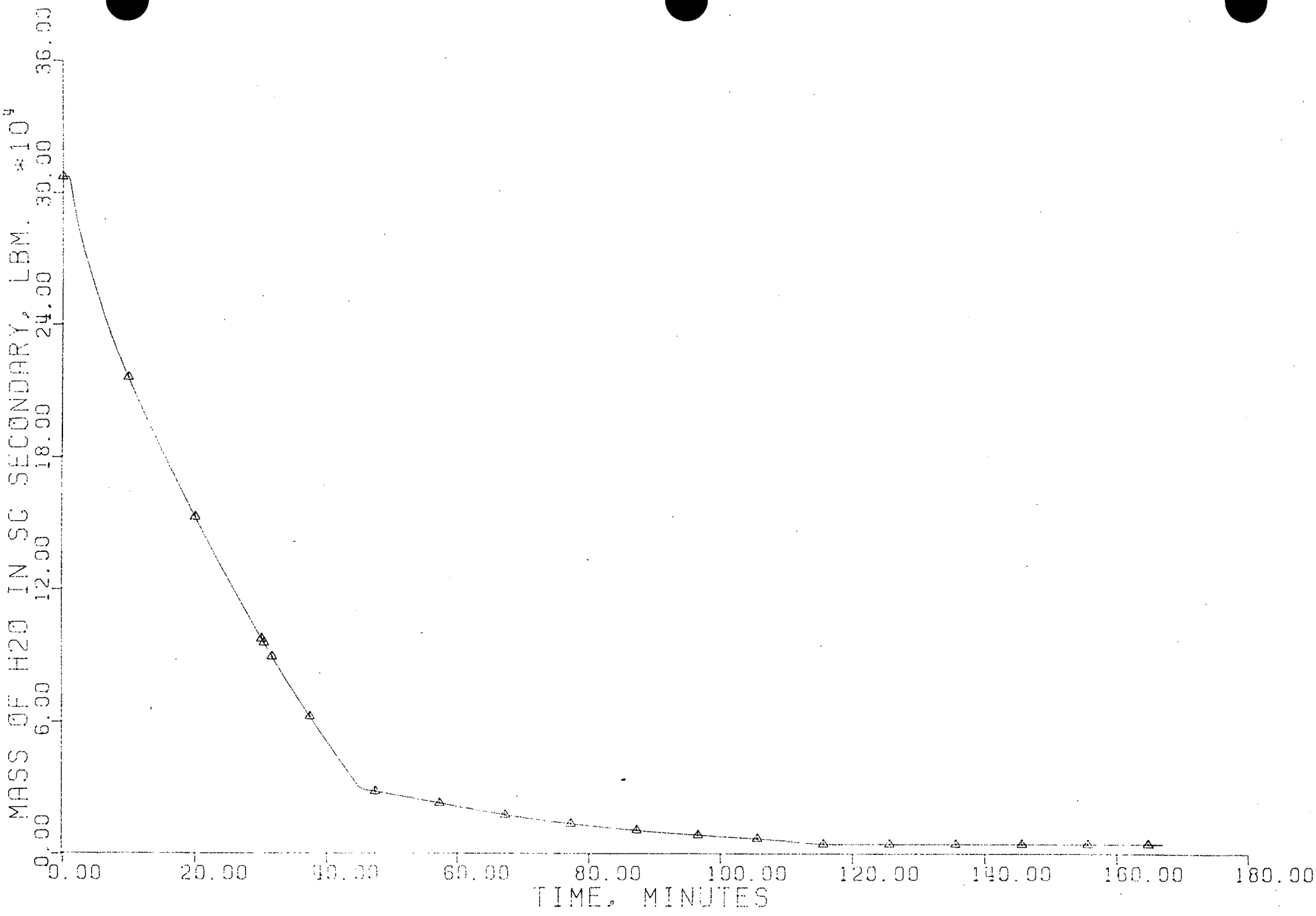
MASS OF H20 IN SC SECONDARY, LBM. *10⁴
0.00
6.00
12.00
18.00
24.00
30.00
36.00
0.00
20.00
40.00
60.00
80.00
100.00
120.00
140.00
160.00
180.00
TIME, MINUTES

FIGURE 5.62

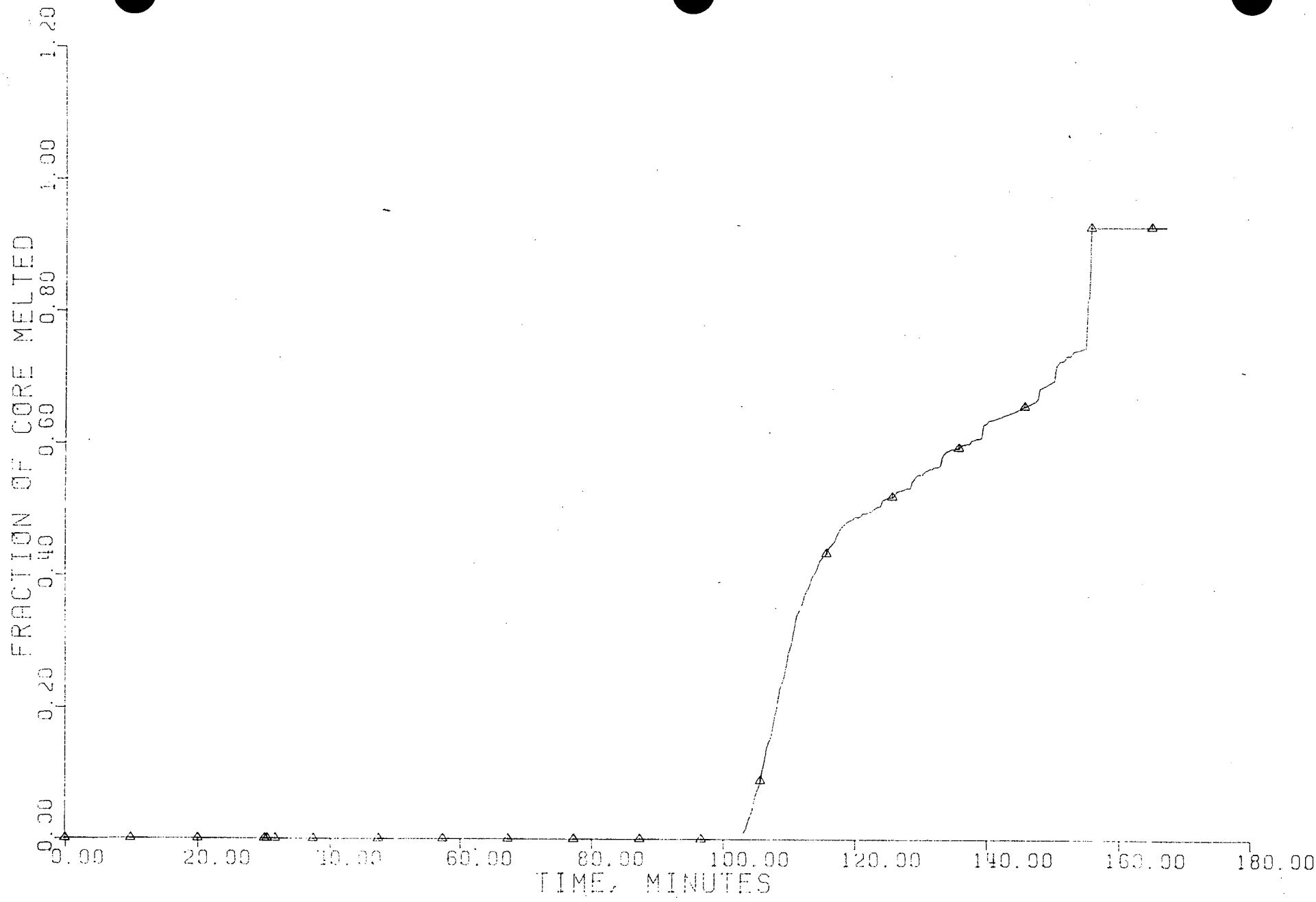
FRACTION OF CORE MELTED
0.30
0.20
0.40
0.60
0.80
1.00
1.20
0.00
20.00
40.00
60.00
80.00
100.00
120.00
140.00
160.00
180.00
TIME, MINUTES

FIGURE 5.63

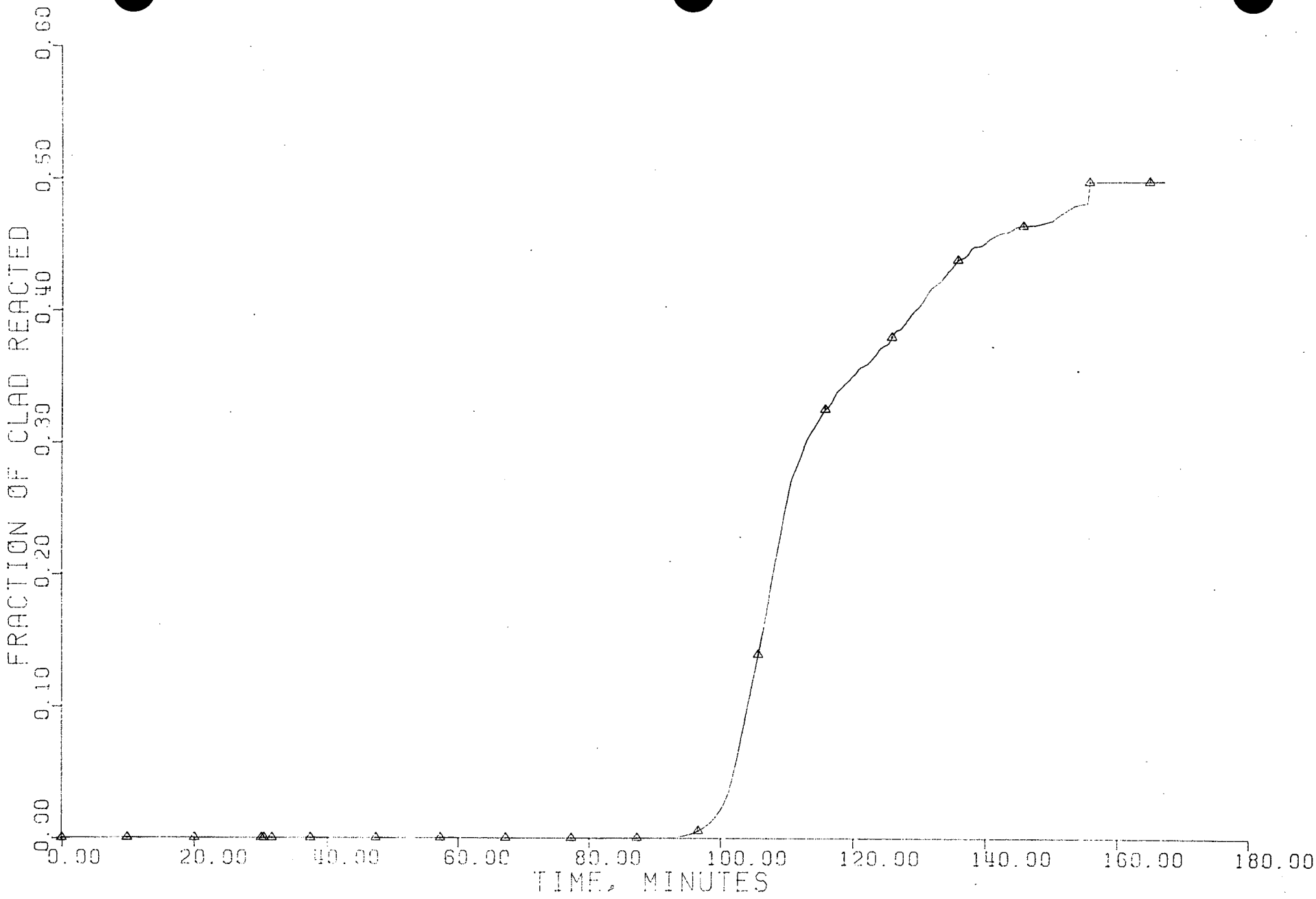
FRACTION OF CLAD REACTED
0.00
0.10
0.20
0.30
0.40
0.50
0.60
0.00
20.00
40.00
60.00
80.00
100.00
120.00
140.00
160.00
180.00
TIME, MINUTES

FIGURE 5.64

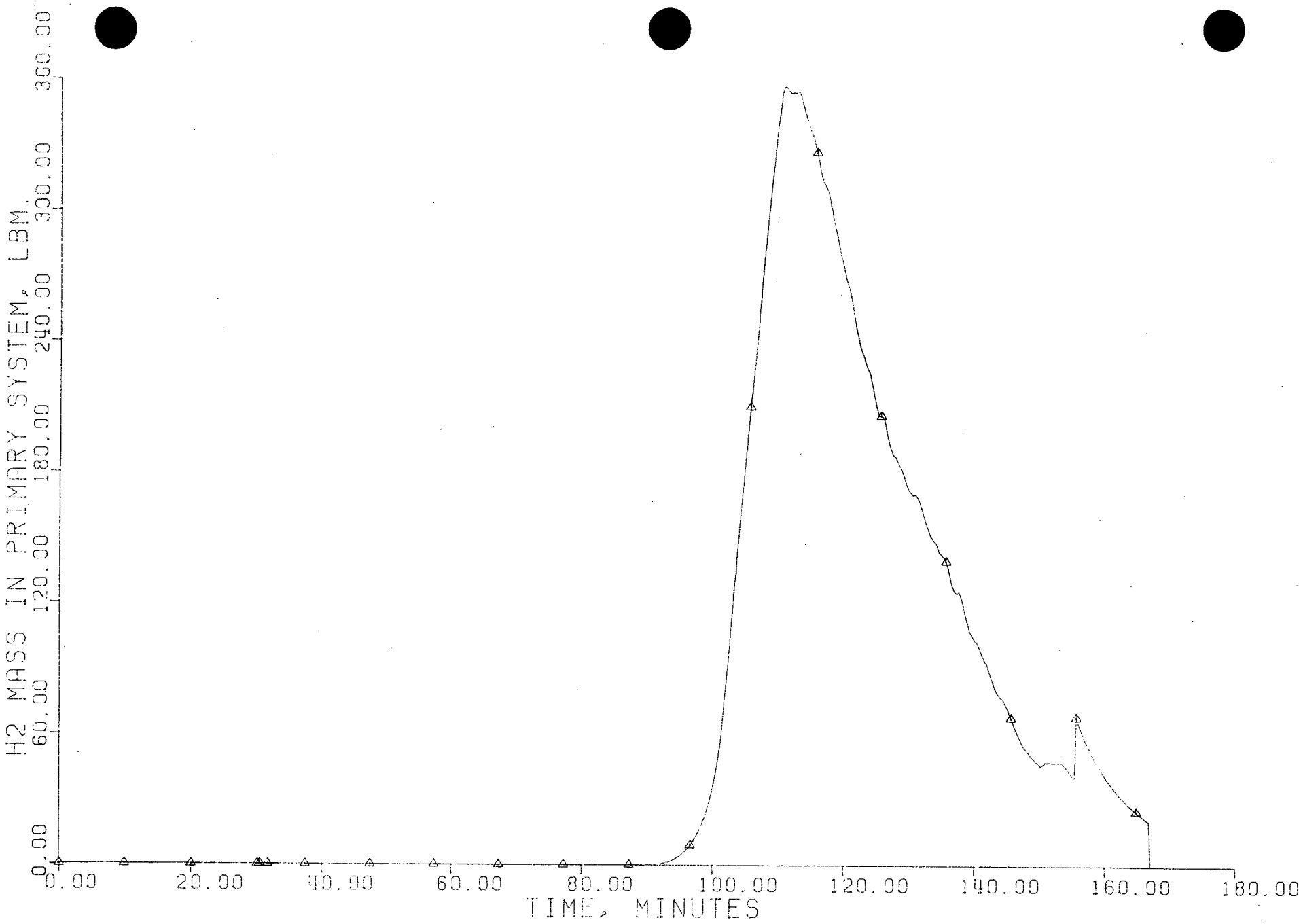
H2 MASS IN PRIMARY SYSTEM, LBM.
0.00
60.00
120.00
180.00
240.00
300.00
300.00
0.00
20.00
40.00
60.00
80.00
100.00
120.00
140.00
160.00
180.00
TIME, MINUTES

FIGURE 5.65

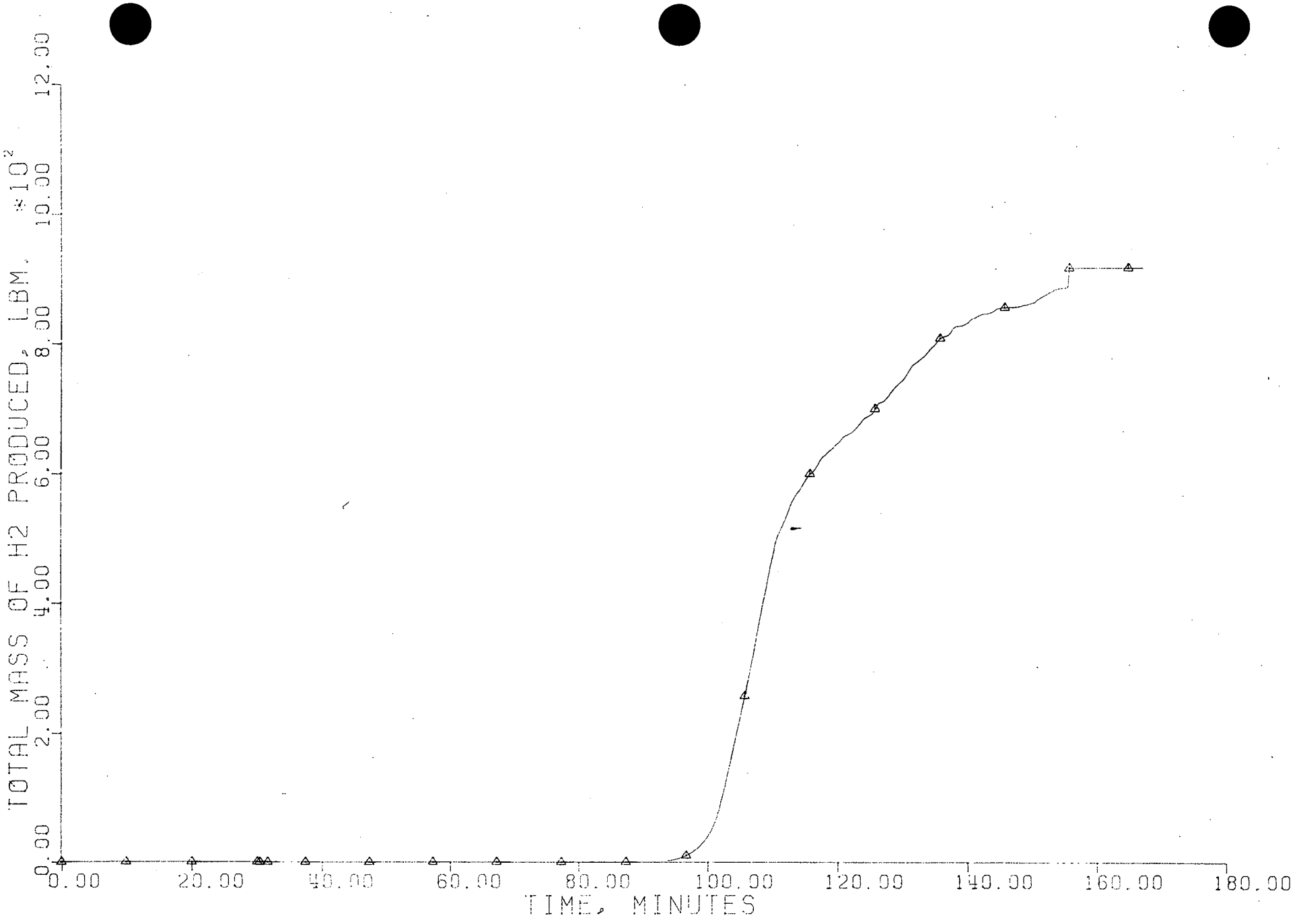
TOTAL MASS OF H2 PRODUCED, LBM. *10²
0.00
2.00
4.00
6.00
8.00
10.00
12.00
0.00
20.00
40.00
60.00
80.00
100.00
120.00
140.00
160.00
180.00
TIME, MINUTES

FIGURE 5.66

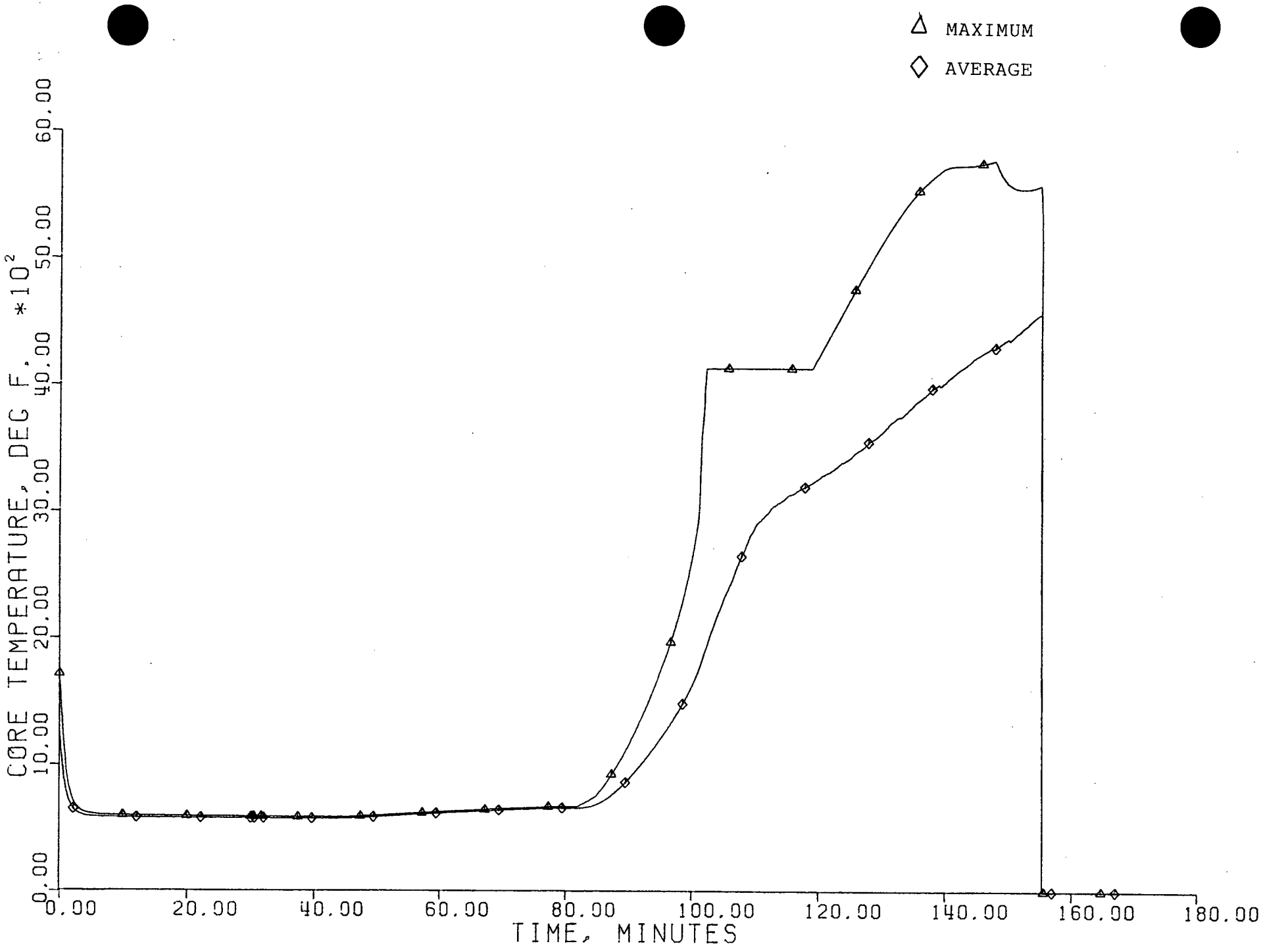
MAXIMUM
AVERAGE
CORE TEMPERATURE, DEG F. *10²
0.00
10.00
20.00
30.00
40.00
50.00
60.00
0.00
20.00
40.00
60.00
80.00
100.00
120.00
140.00
160.00
180.00
TIME, MINUTES

FIGURE 5.67

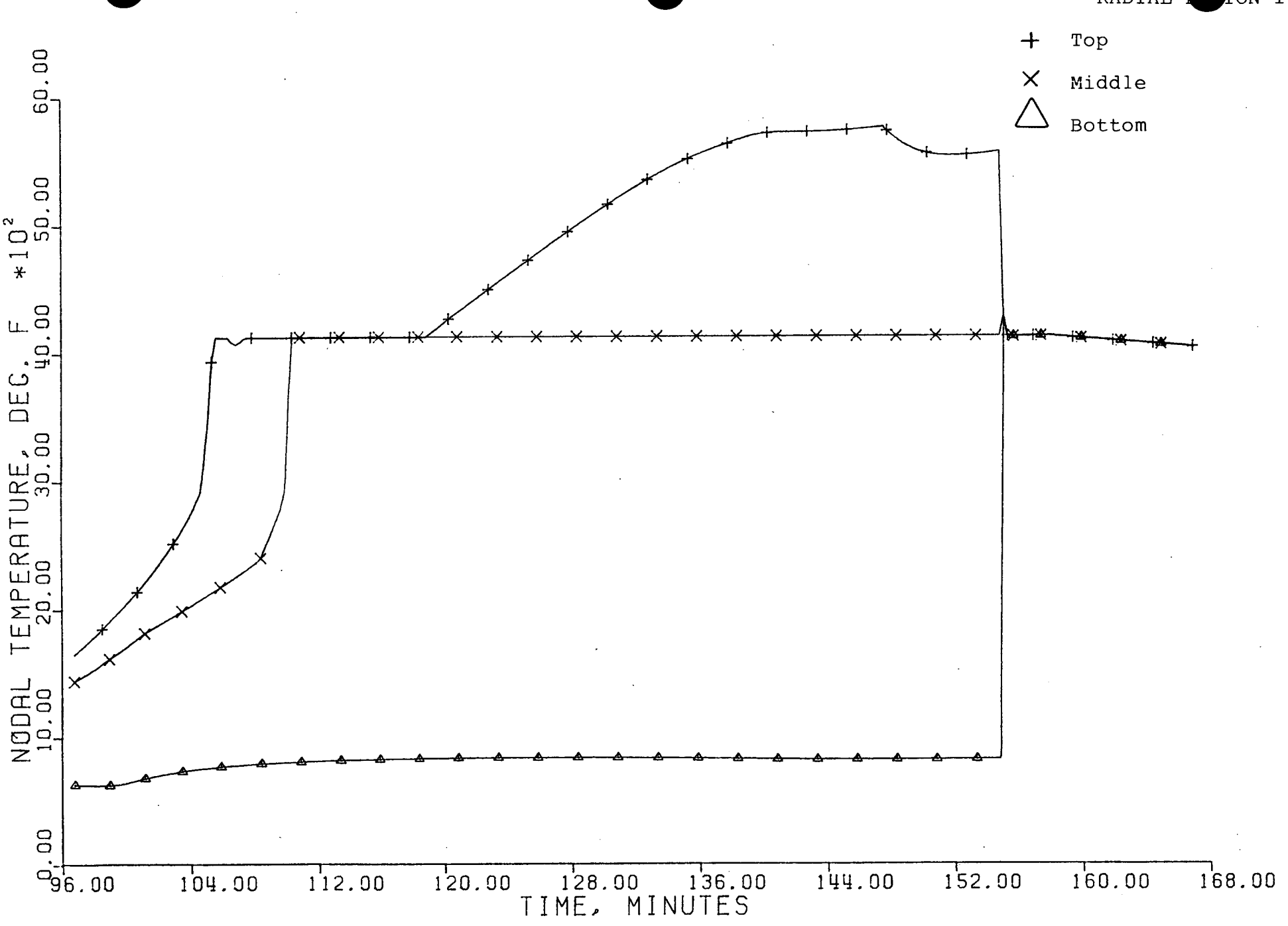
RADIAL ION 1
Top
Middle
Bottom
NODAL TEMPERATURE, DEG. F *10²
0.00
10.00
20.00
30.00
40.00
50.00
60.00
96.00
104.00
112.00
120.00
128.00
136.00
144.00
152.00
160.00
168.00
TIME, MINUTES

FIGURE 5.68

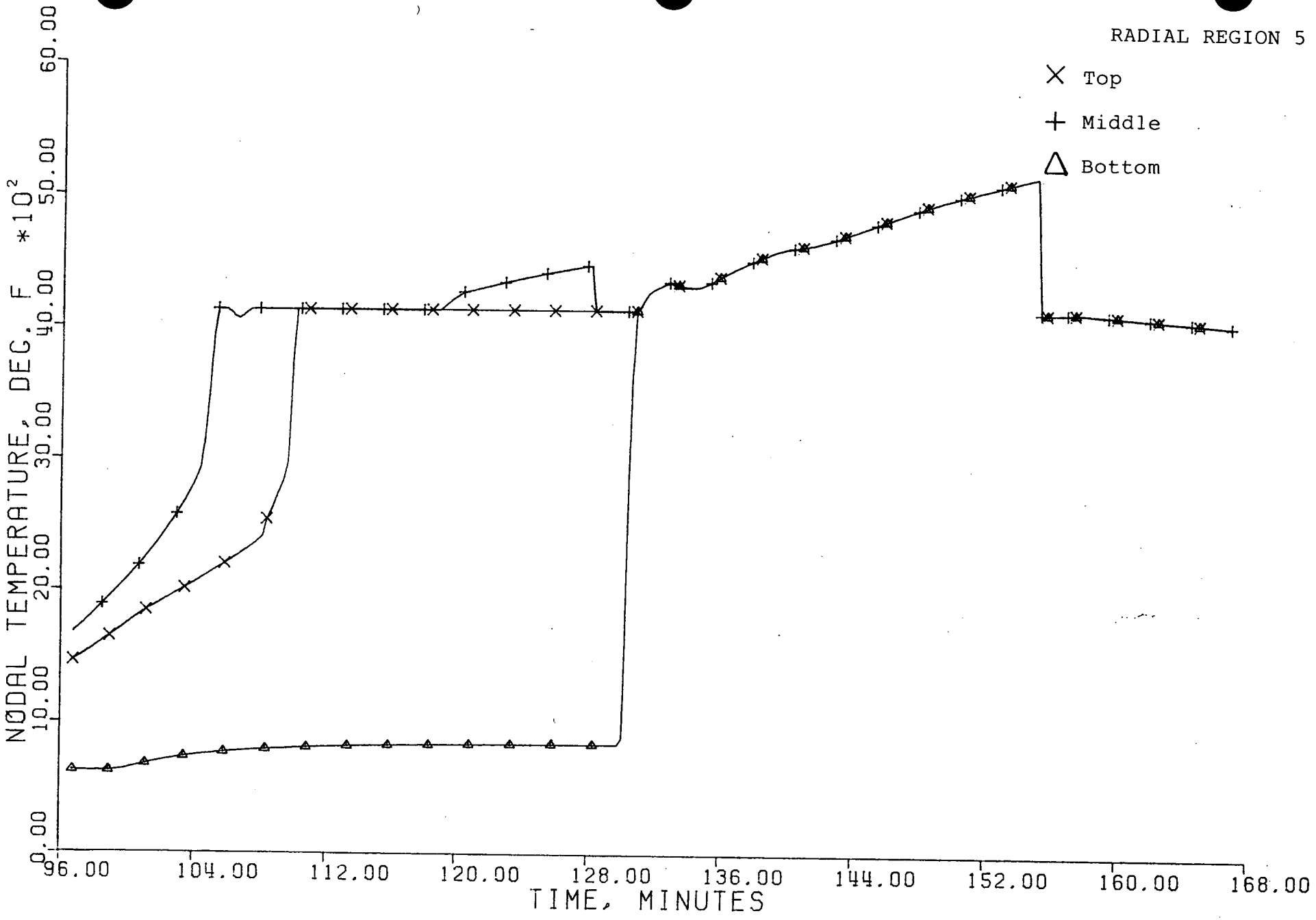
RADIAL REGION 5
Top
Middle
Bottom
NODAL TEMPERATURE, DEG. F *10²
0.00
10.00
20.00
30.00
40.00
50.00
60.00
96.00
104.00
112.00
120.00
128.00
136.00
144.00
152.00
160.00
168.00
TIME, MINUTES

FIGURE 5.69

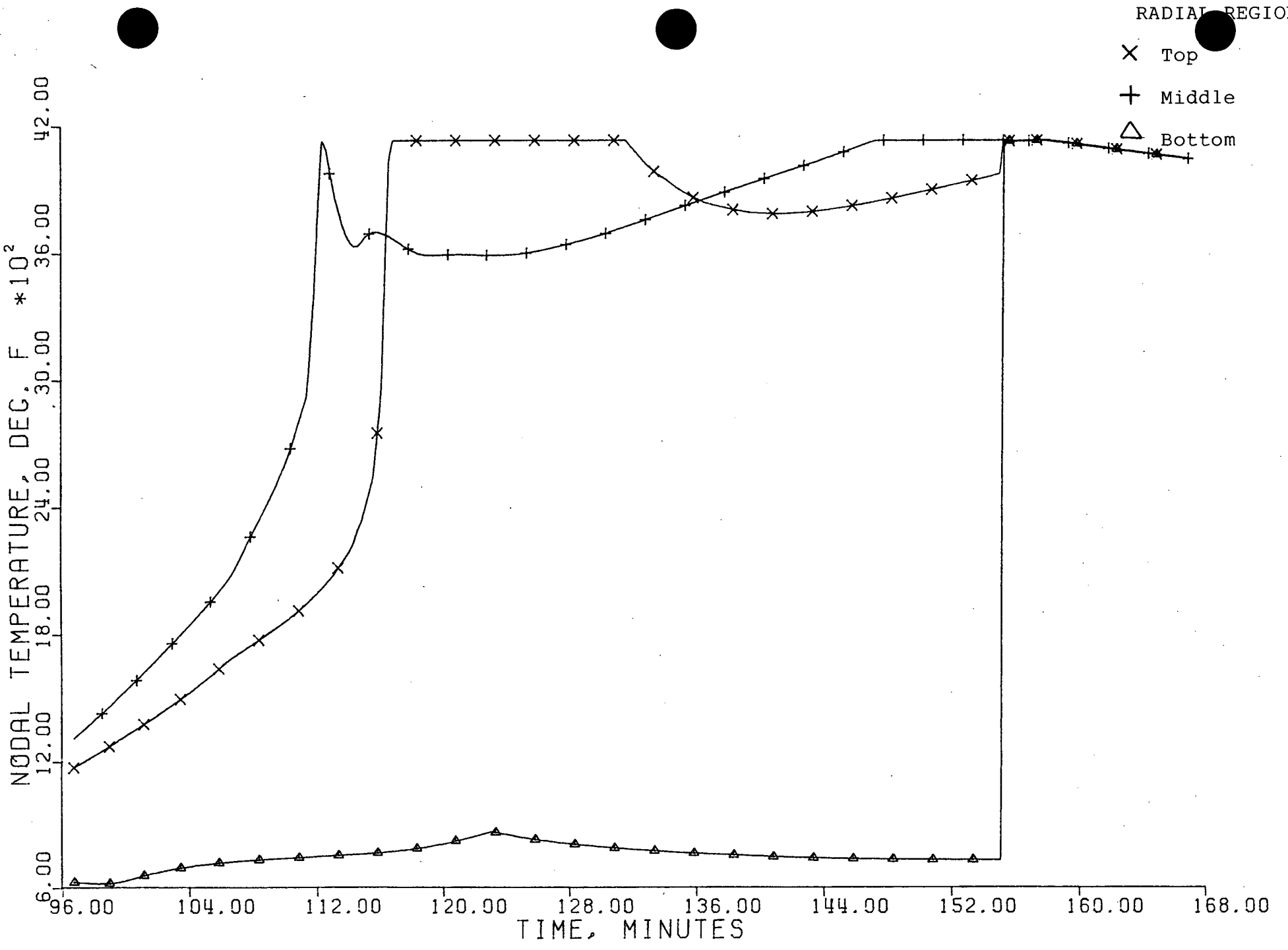
RADIAL REGION1.0
Top
Middle
Bottom
NODAL TEMPERATURE, DEG. F *10²
42.00
36.00
30.00
24.00
18.00
12.00
6.00
96.00
104.00
112.00
120.00
128.00
136.00
144.00
152.00
160.00
168.00
TIME, MINUTES

FIGURE 5.70

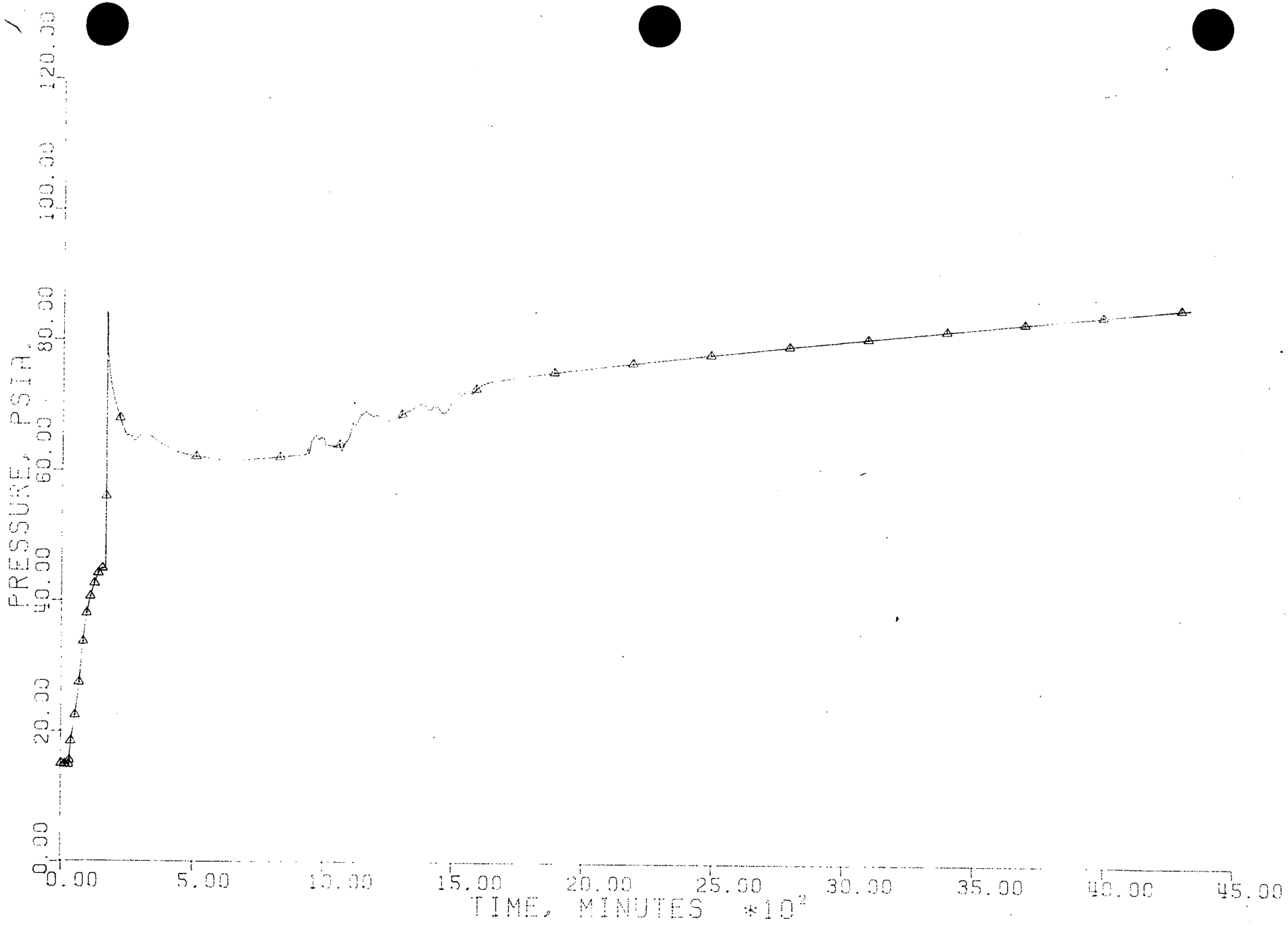
PRESSURE, PSIA
0.00
20.00
40.00
60.00
80.00
100.00
120.00
0.00
5.00
10.00
15.00
20.00
25.00
30.00
35.00
40.00
45.00
TIME, MINUTES *10²

FIGURE 5.71

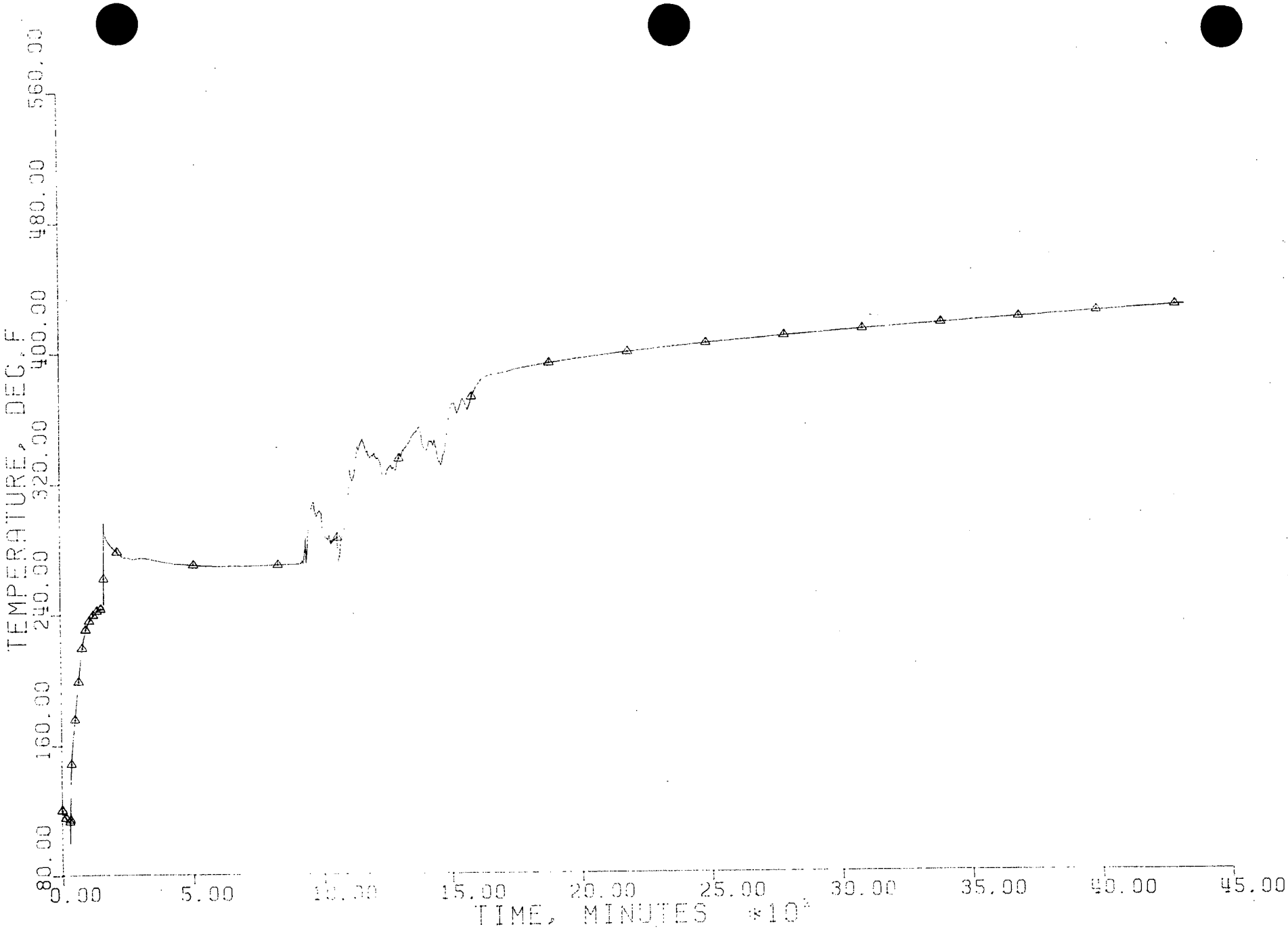
TEMPERATURE, DEG.F
80.00
160.00
240.00
320.00
400.00
480.00
560.00
0.00
5.00
10.00
15.00
20.00
25.00
30.00
35.00
40.00
45.00
TIME, MINUTES *10

FIGURE 5.72

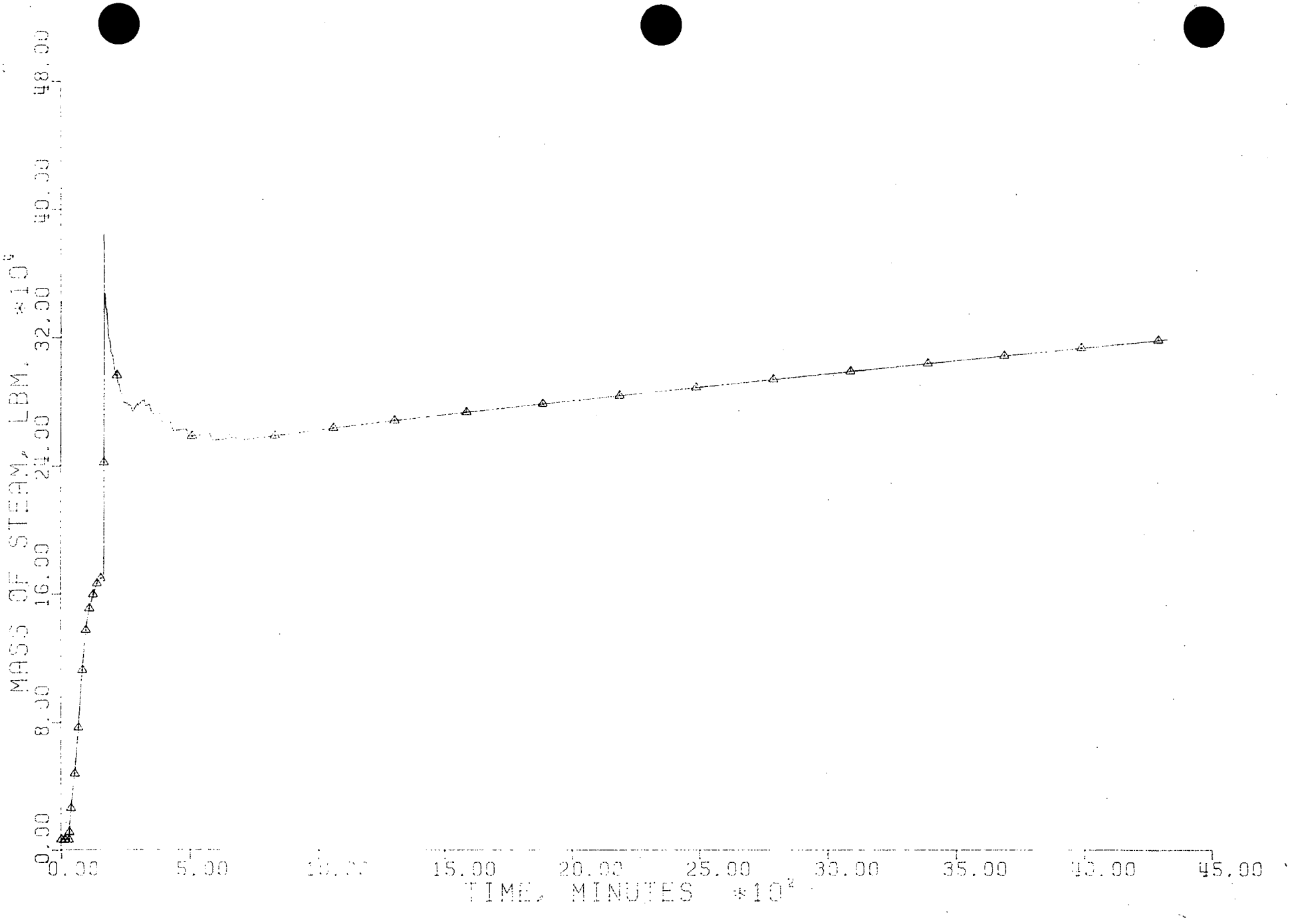
MASS OF STEAM, LBM. *10³
0.00
8.00
16.00
24.00
32.00
40.00
48.00
0.00
5.00
15.00
20.00
25.00
30.00
35.00
40.00
45.00
TIME, MINUTES *10²

FIGURE 5.73

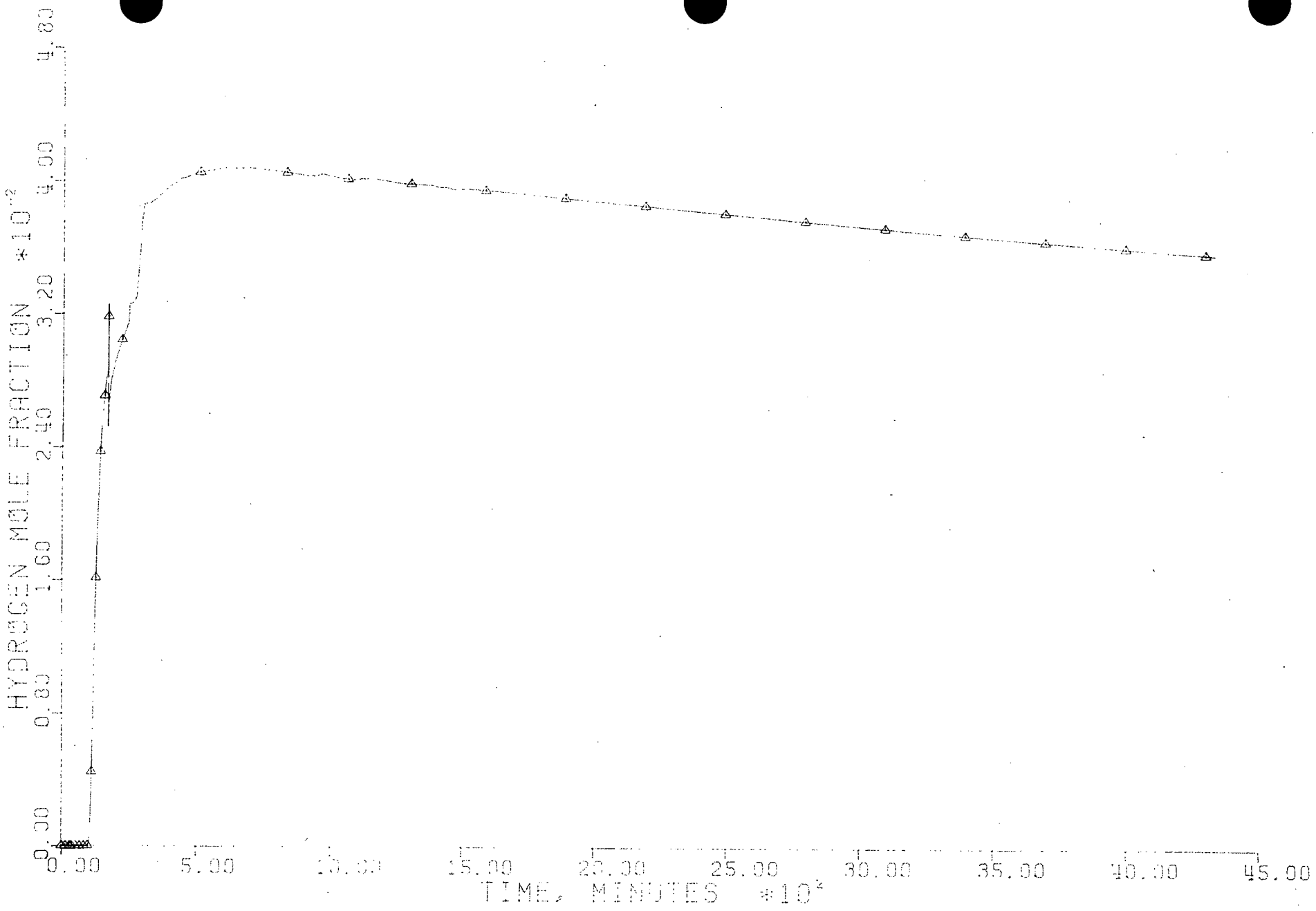
HYDROGEN MOLE FRACTION *10⁻²
4.80
4.00
3.20
2.40
1.60
0.80
0.00
0.00
5.00
15.00
25.00
30.00
35.00
40.00
45.00
TIME, MINUTES *10⁴

FIGURE 5.74

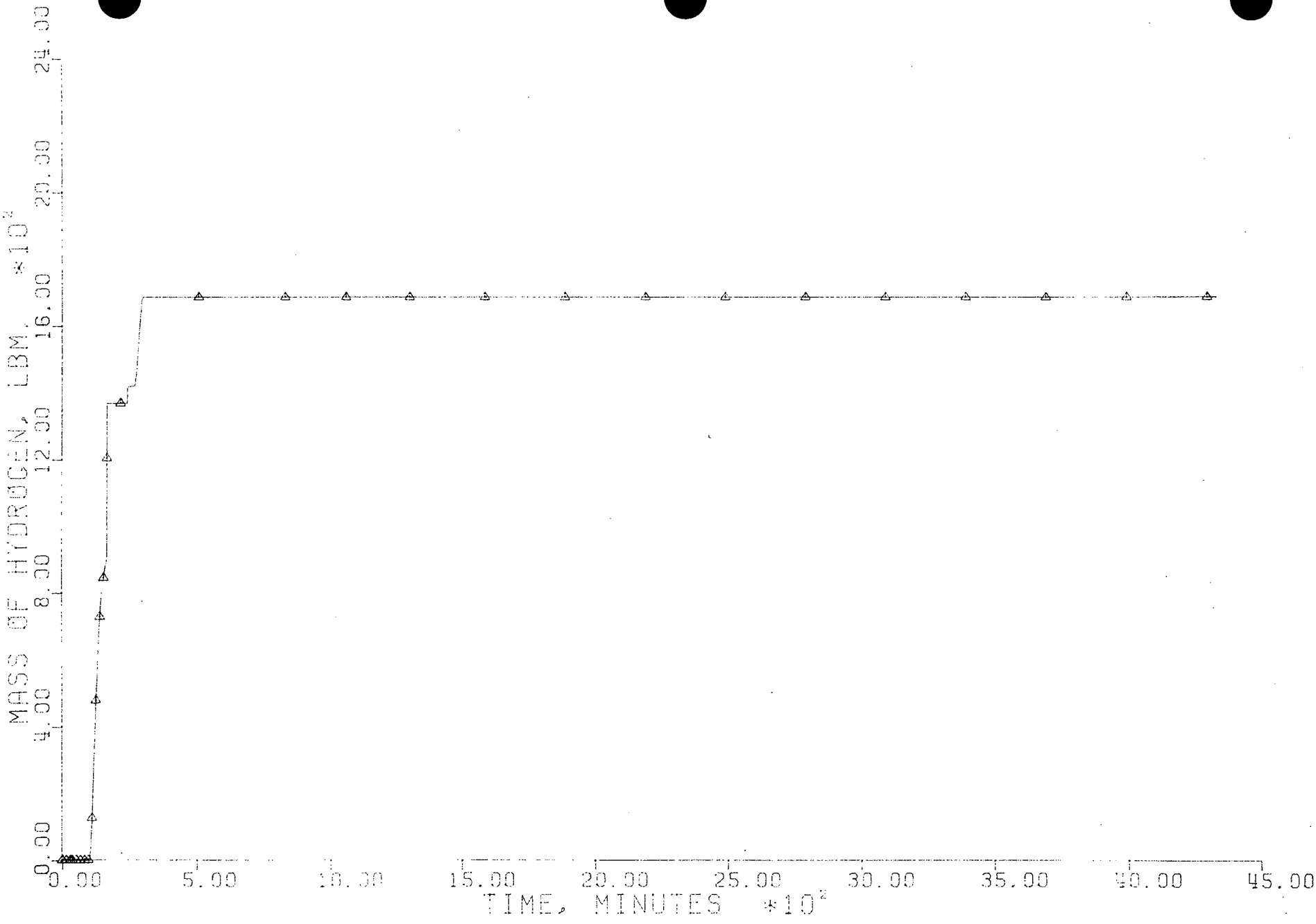
MASS OF HYDROGEN, LBM. *10²
0.00
4.00
8.00
12.00
16.00
20.00
24.00
0.00
5.00
10.00
15.00
20.00
25.00
30.00
35.00
40.00
45.00
TIME, MINUTES *10²

FIGURE 5.75

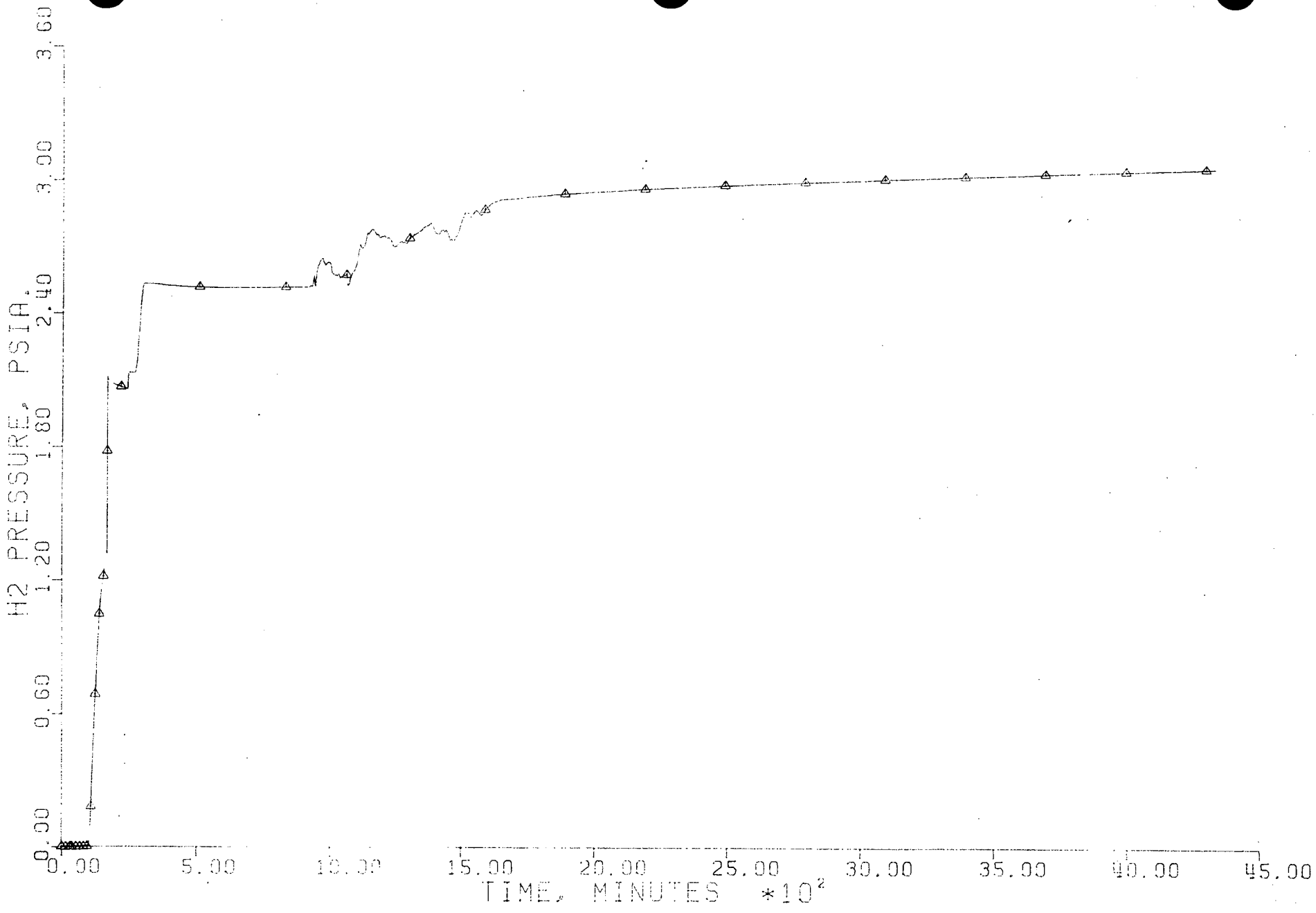
H2 PRESSURE, PSIA.
0.00
0.60
1.20
1.80
2.40
3.00
3.60
0.00
5.00
10.00
15.00
20.00
25.00
30.00
35.00
40.00
45.00
TIME, MINUTES *10²

FIGURE 5.76

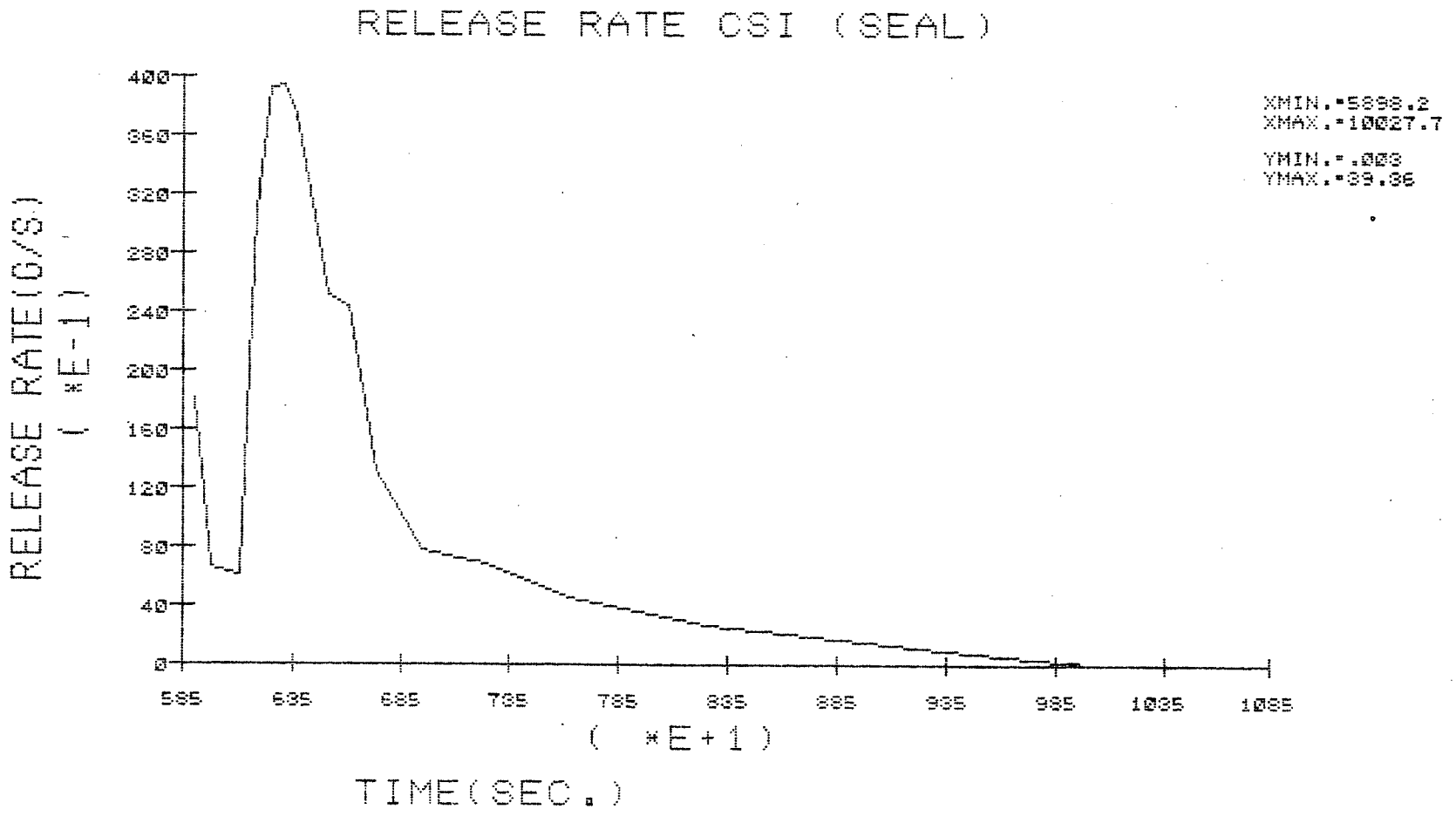
RELEASE RATE CSI (SEAL)
XMIN.=5898.2
XMAX.=10027.7
YMIN.=.003
YMAX.=39.36
RELEASE RATE(G/S)
(*E-1)
400
360
320
280
240
200
160
120
80
40
0
585
635
685
735
785
835
885
935
985
1035
1085
(*E+1)
TIME(SEC.)

FIGURE 5.77

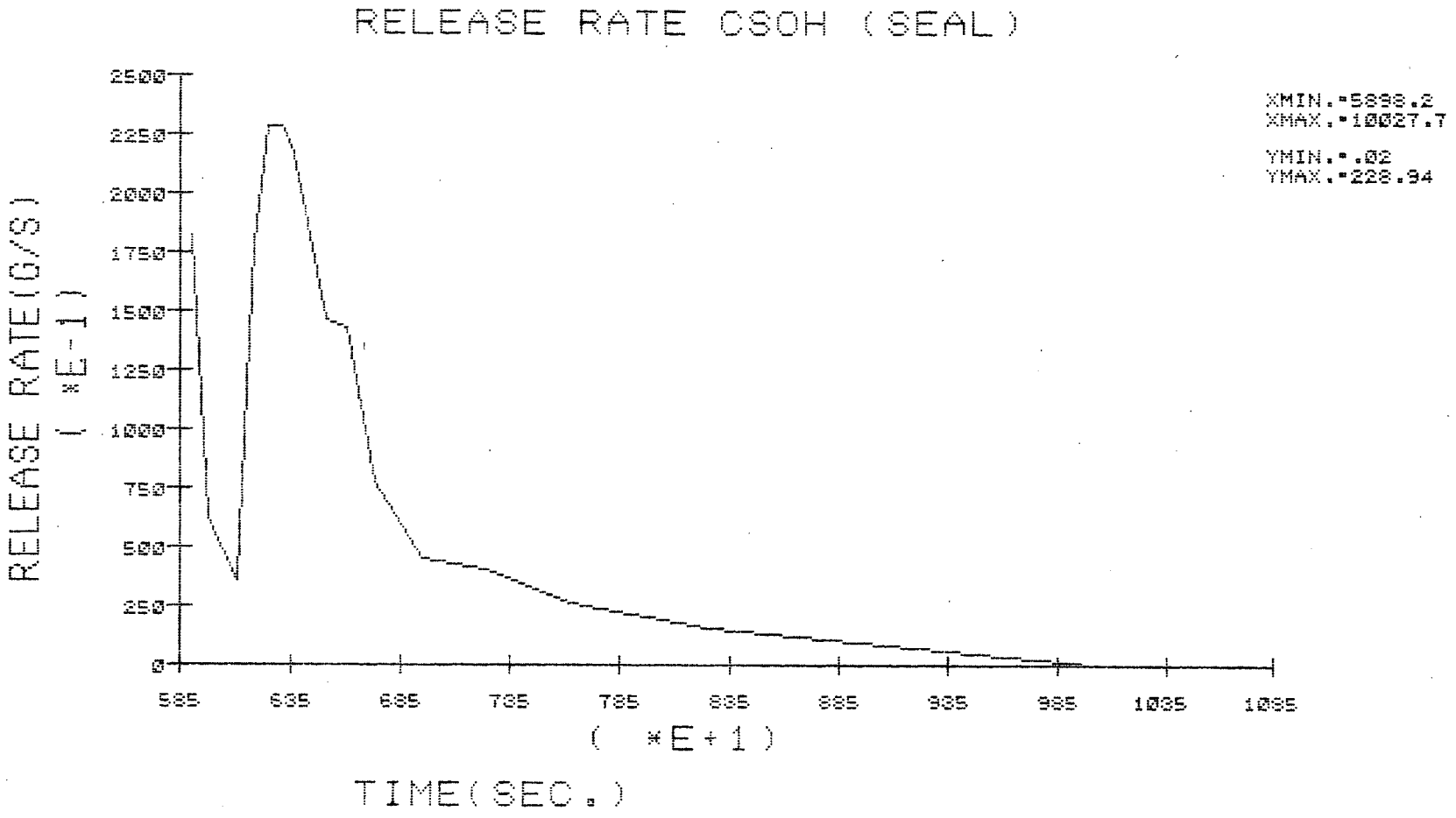
RELEASE RATE CSOH (SEAL)
XMIN.=5898.2
XMAX.=10027.7
YMIN.=.02
YMAX.=228.94
RELEASE RATE(G/S)
(*E-1)
2500
2250
2000
1750
1500
1250
1000
750
500
250
0
585
635
685
735
785
835
885
935
985
1035
1085
(*E+1)
TIME(SEC.)

FIGURE 5.78

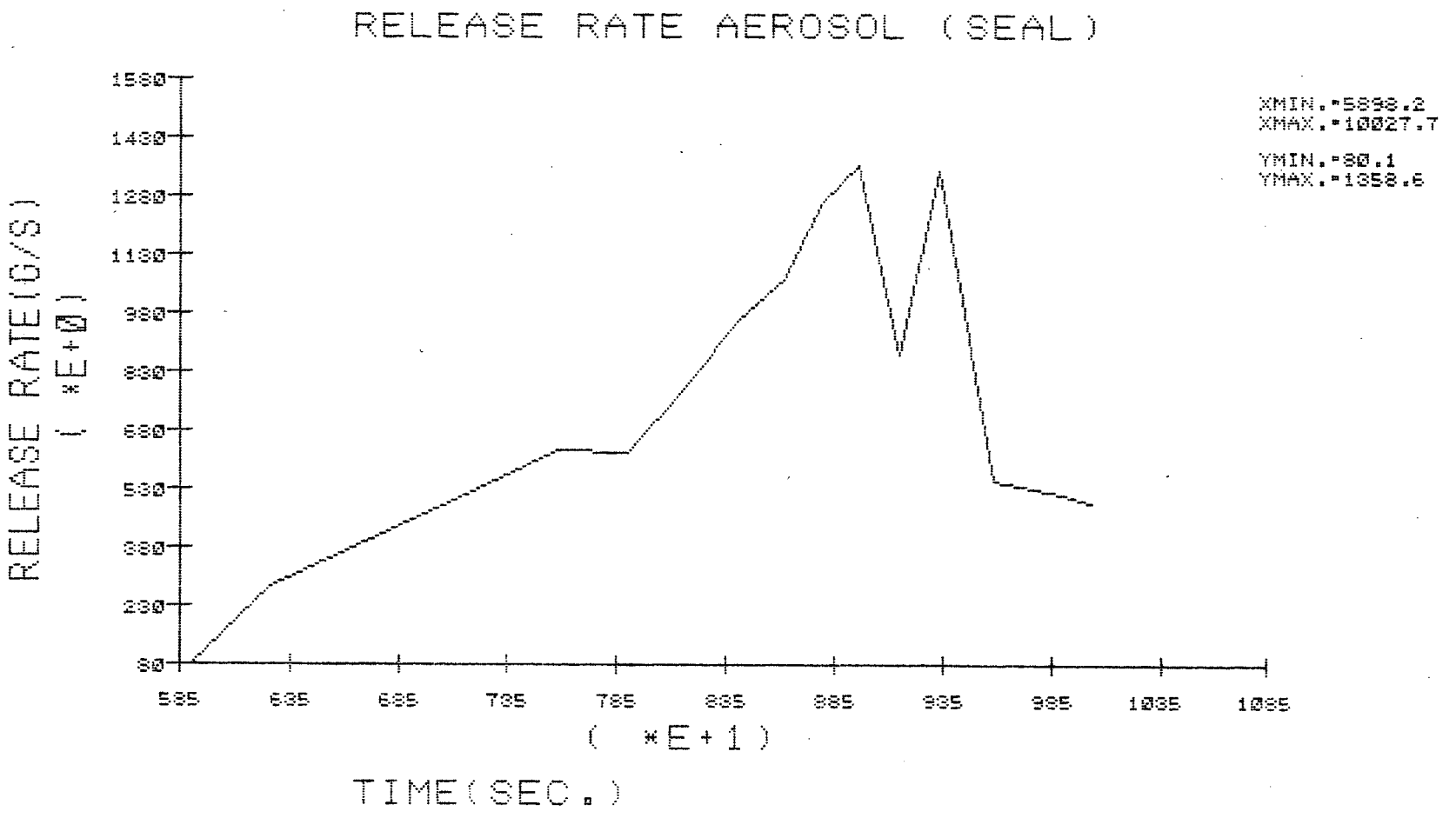
RELEASE RATE AEROSOL (SEAL)
XMIN.=5898.2
XMAX.=10027.7
YMIN.=80.1
YMAX.=1358.6
RELEASE RATE(G/S)
(*E+0)
1580
1430
1280
1130
980
830
680
530
380
230
80
585
635
685
735
785
835
885
935
985
1035
1085
(*E+1)
TIME(SEC.)

FIGURE 5.79

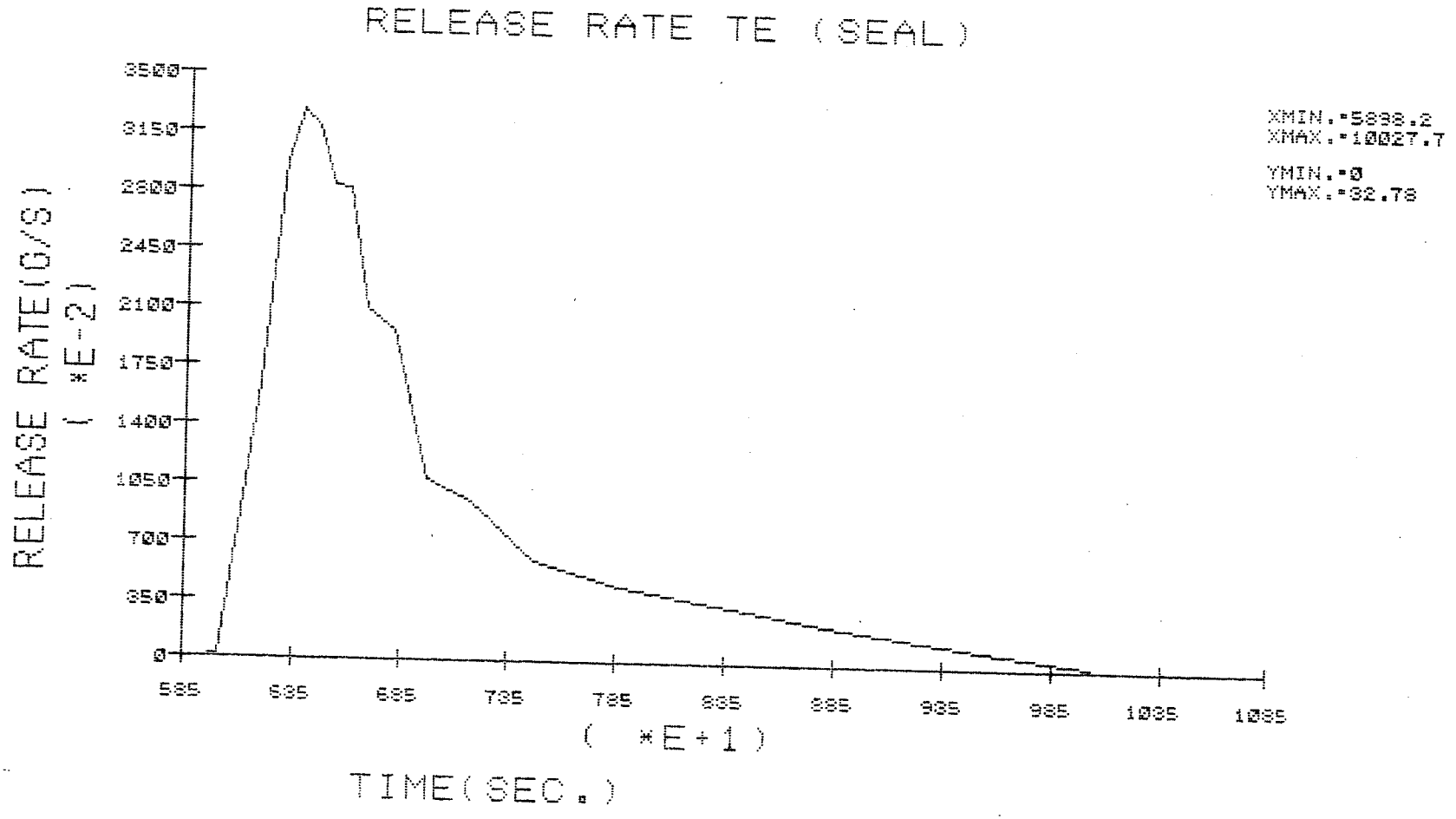
RELEASE RATE TE (SEAL)
XMIN.=5898.2
XMAX.=10027.7
YMIN.=0
YMAX.=32.78
RELEASE RATE(G/S)
(*E-2)
3500
3150
2800
2450
2100
1750
1400
1050
700
350
0
585
635
685
735
785
835
885
935
985
1035
1085
(*E+1)
TIME(SEC.)

FIGURE 5.80

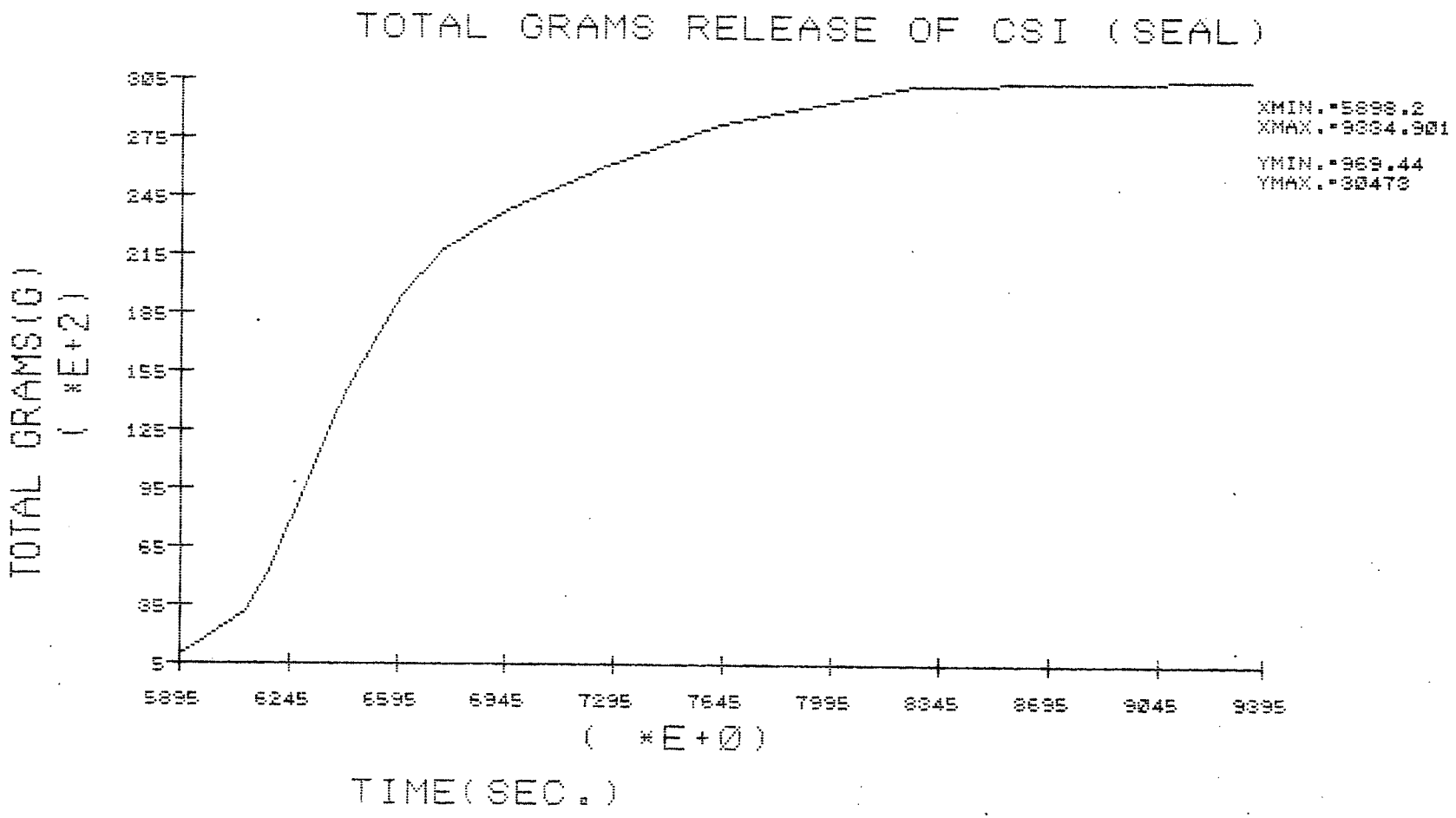
TOTAL GRAMS RELEASE OF CSI (SEAL)
XMIN.=5898.2
XMAX.=9394.901
YMIN.=969.44
YMAX.=30473
TOTAL GRAMS(G)
(*E+2)
305
275
245
215
185
155
125
95
65
35
5
5895
6245
6595
6945
7295
7645
7995
8345
8695
9045
9395
(*E+0)
TIME(SEC.)

FIGURE 5.81

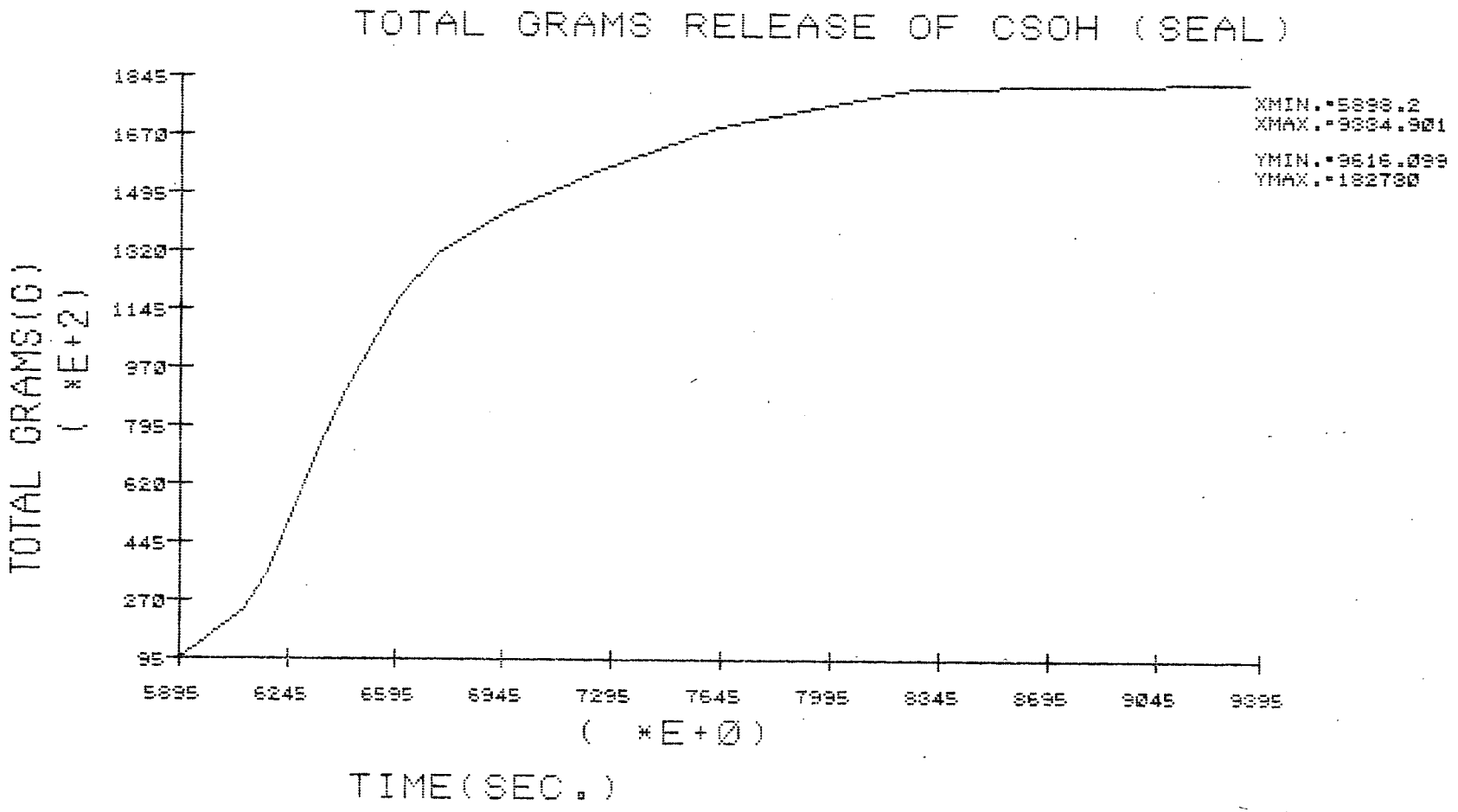
TOTAL GRAMS RELEASE OF CSOH (SEAL)
XMIN.=5898.2
XMAX.=9304.901
YMIN.=9616.099
YMAX.=182730
TOTAL GRAMS(G)
(*E+2)
1845
1670
1495
1320
1145
970
795
620
445
270
95
5895
6245
6595
6945
7295
7645
7995
8345
8695
9045
9395
(*E+0)
TIME(SEC.)

FIGURE 5.82

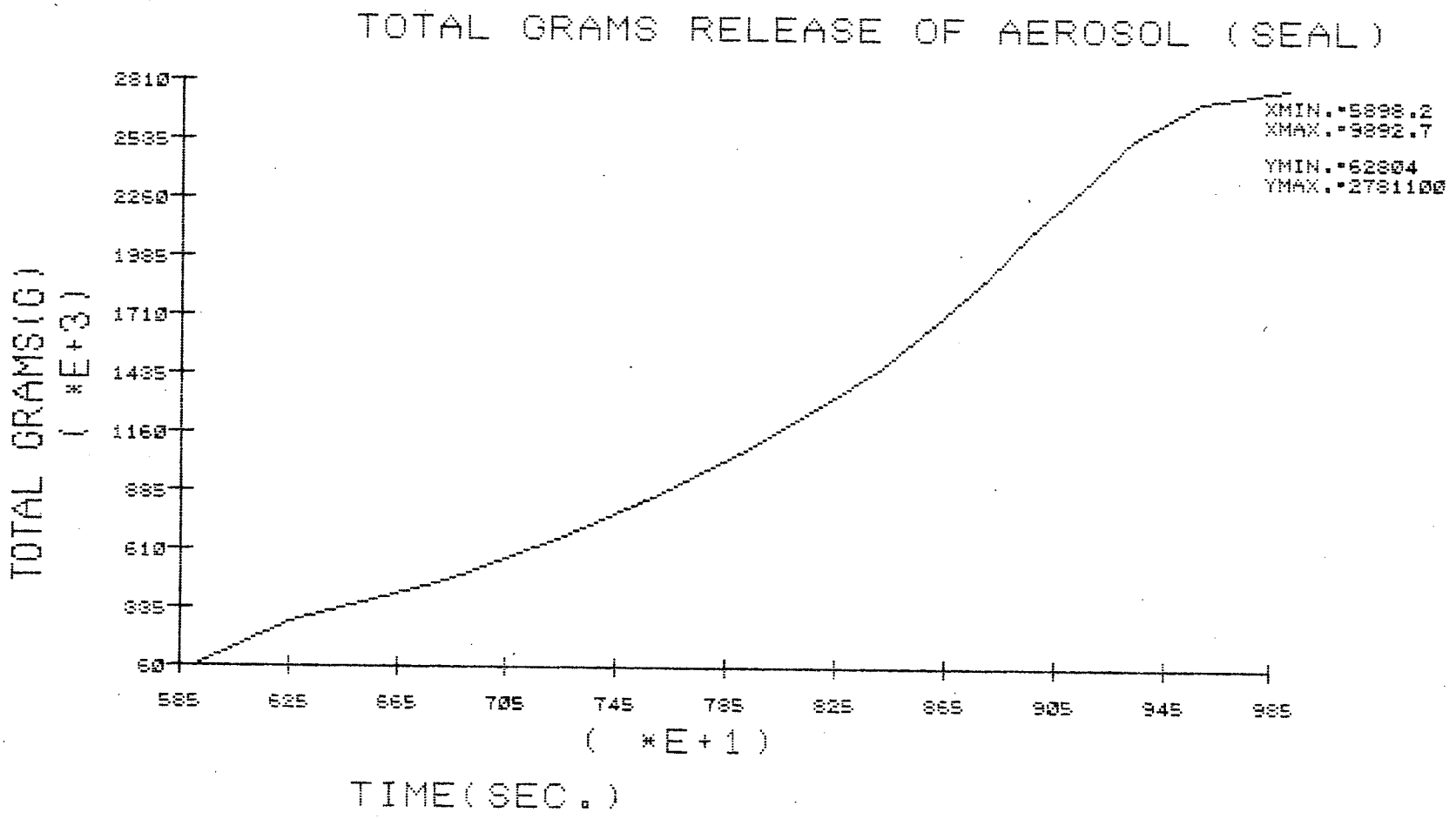
TOTAL GRAMS RELEASE OF AEROSOL (SEAL)
XMIN.=5898.2
XMAX.=9892.7
YMIN.=62804
YMAX.=278110Ø
TOTAL GRAMS(G)
(*E+3)
2810
2535
2260
1985
1710
1435
1160
885
610
335
60
585
625
665
705
745
785
825
865
905
945
985
(*E+1)
TIME(SEC.)

FIGURE 5.83

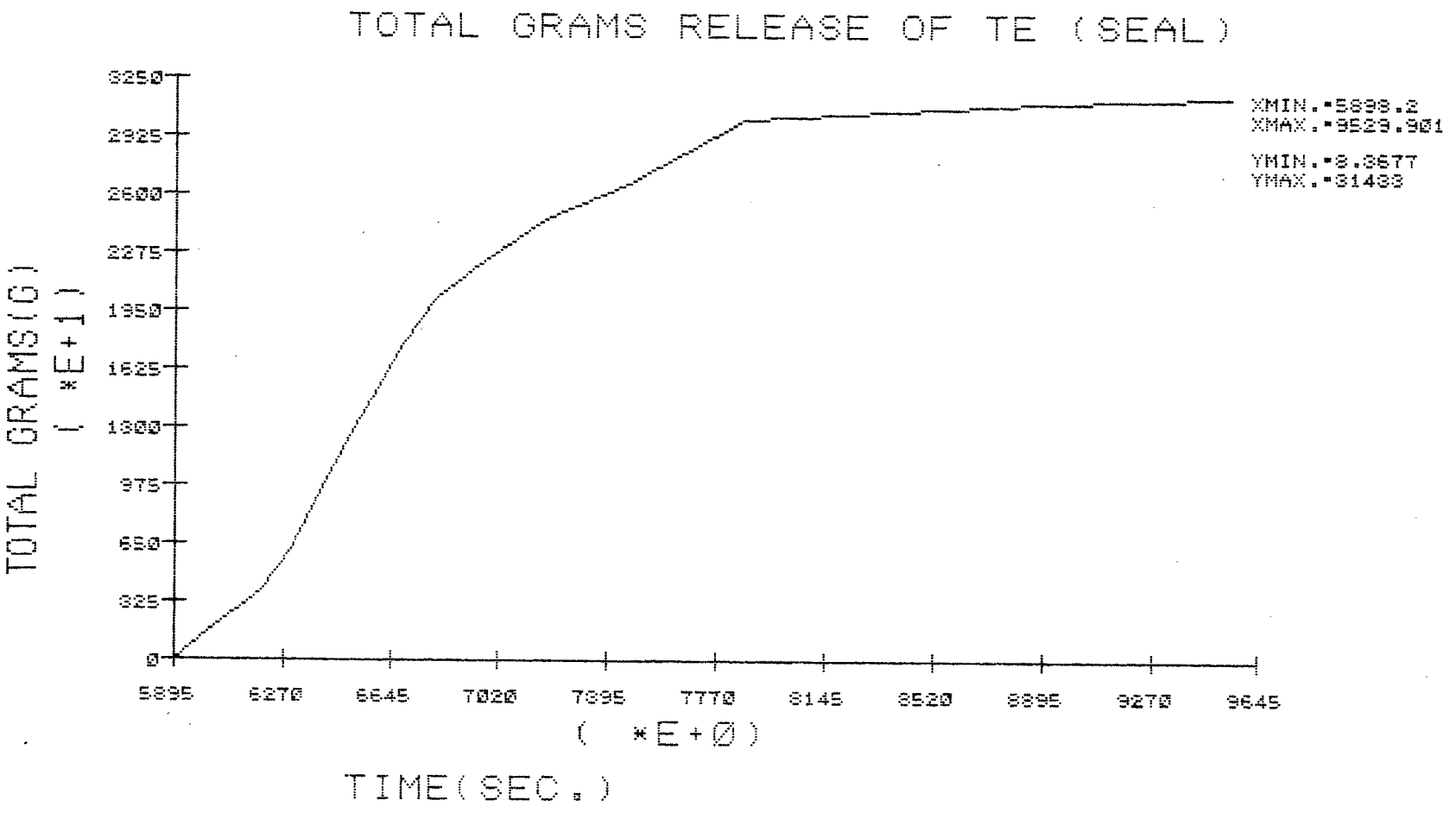
TOTAL GRAMS RELEASE OF TE (SEAL)
TOTAL GRAMS(G)
(*E+1)
3250
2925
2600
2275
1950
1625
1300
975
650
325
0
5895
6270
6645
7020
7395
7770
8145
8520
8895
9270
9645
(*E+0)
TIME(SEC.)
XMIN.=5898.2
XMAX.=9529.901
YMIN.=8.3677
YMAX.=31483

FIGURE 5.84

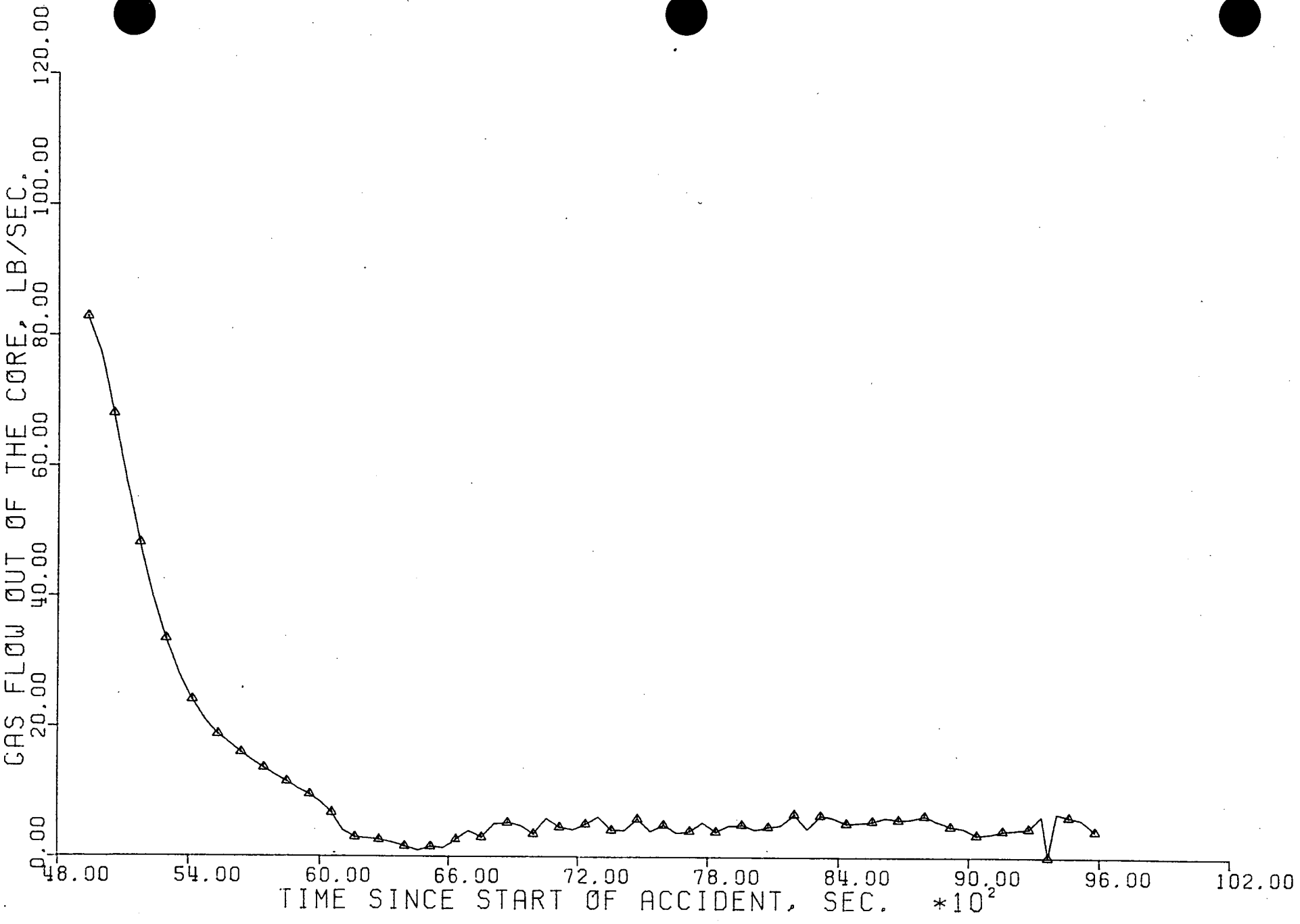
GAS FLOW OUT OF THE CORE, LB/SEC.
0.00
20.00
40.00
60.00
80.00
100.00
120.00
48.00
54.00
60.00
66.00
72.00
78.00
84.00
90.00
96.00
102.00
TIME SINCE START OF ACCIDENT, SEC. *10²

FIGURE 5.85

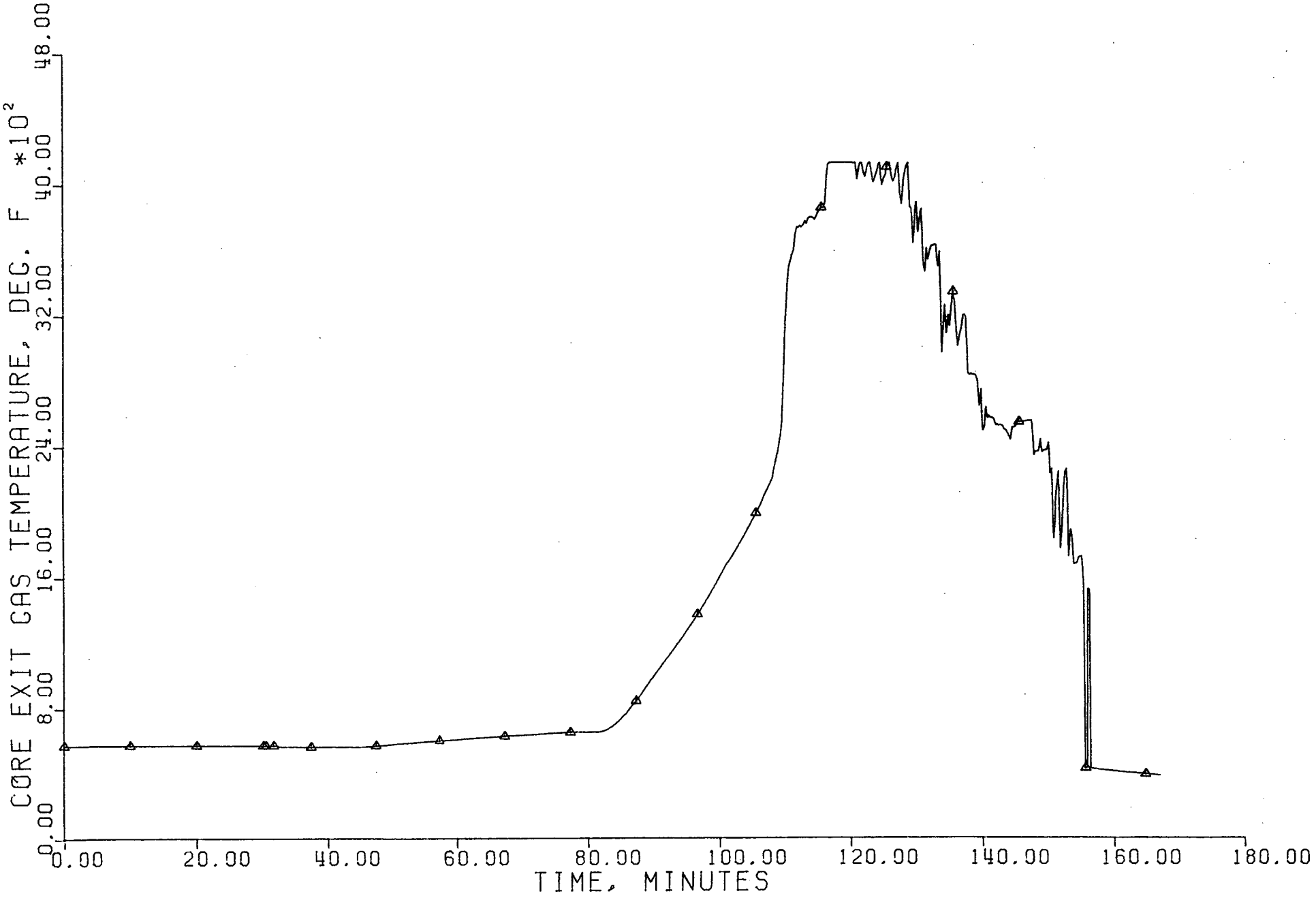
CORE EXIT GAS TEMPERATURE, DEG. F *10²
0.00
8.00
16.00
24.00
32.00
40.00
48.00
0.00
20.00
40.00
60.00
80.00
100.00
120.00
140.00
160.00
180.00
TIME, MINUTES

FIGURE 5.86

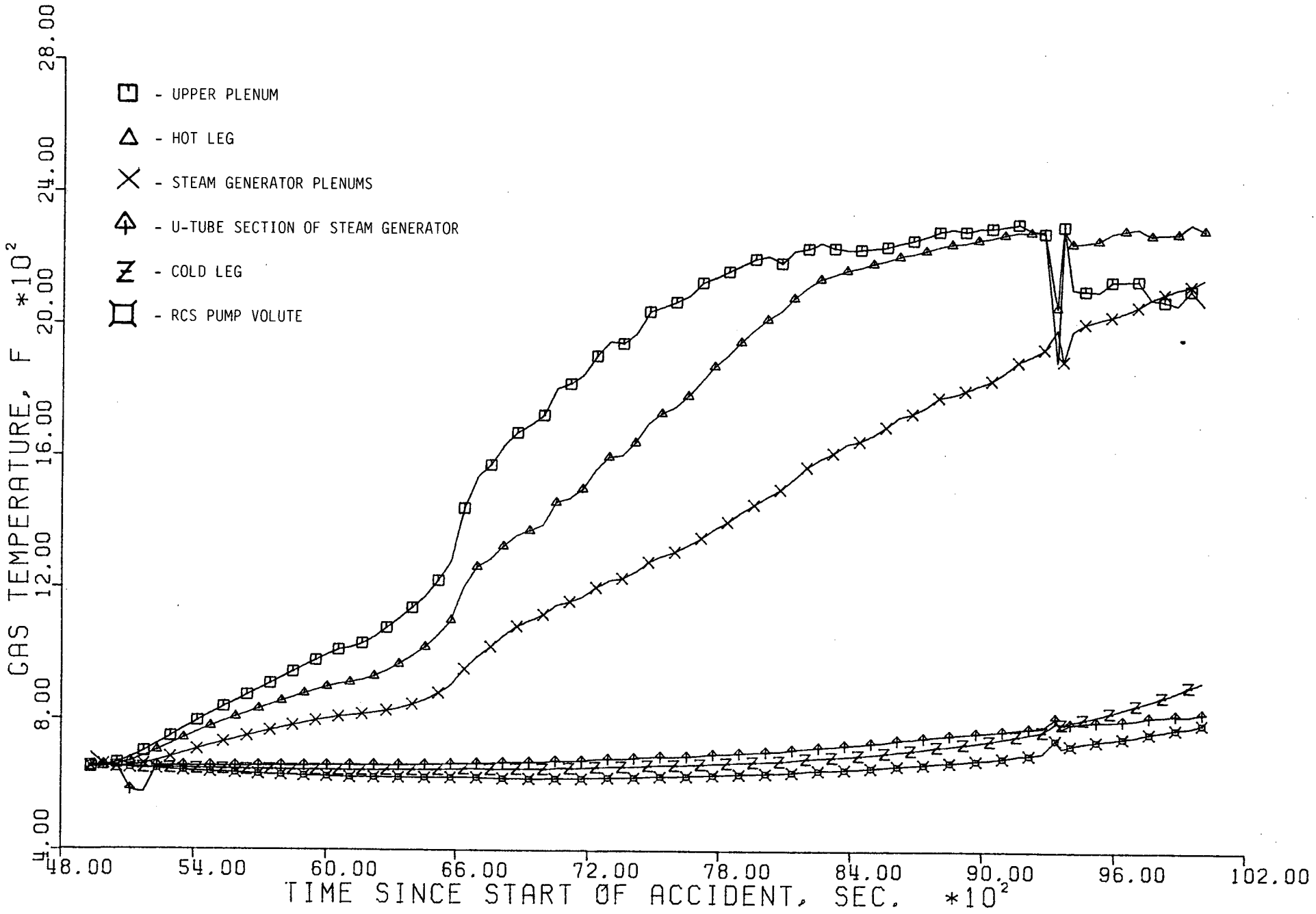
- UPPER PLENUM
- HOT LEG
- STEAM GENERATOR PLENUMS
- U-TUBE SECTION OF STEAM GENERATOR
- COLD LEG
- RCS PUMP VOLUTE
GAS TEMPERATURE, F *10²
4.00
8.00
12.00
16.00
20.00
24.00
28.00
48.00
54.00
60.00
66.00
72.00
78.00
84.00
90.00
96.00
102.00
TIME SINCE START OF ACCIDENT, SEC. *10²

FIGURE 5.87

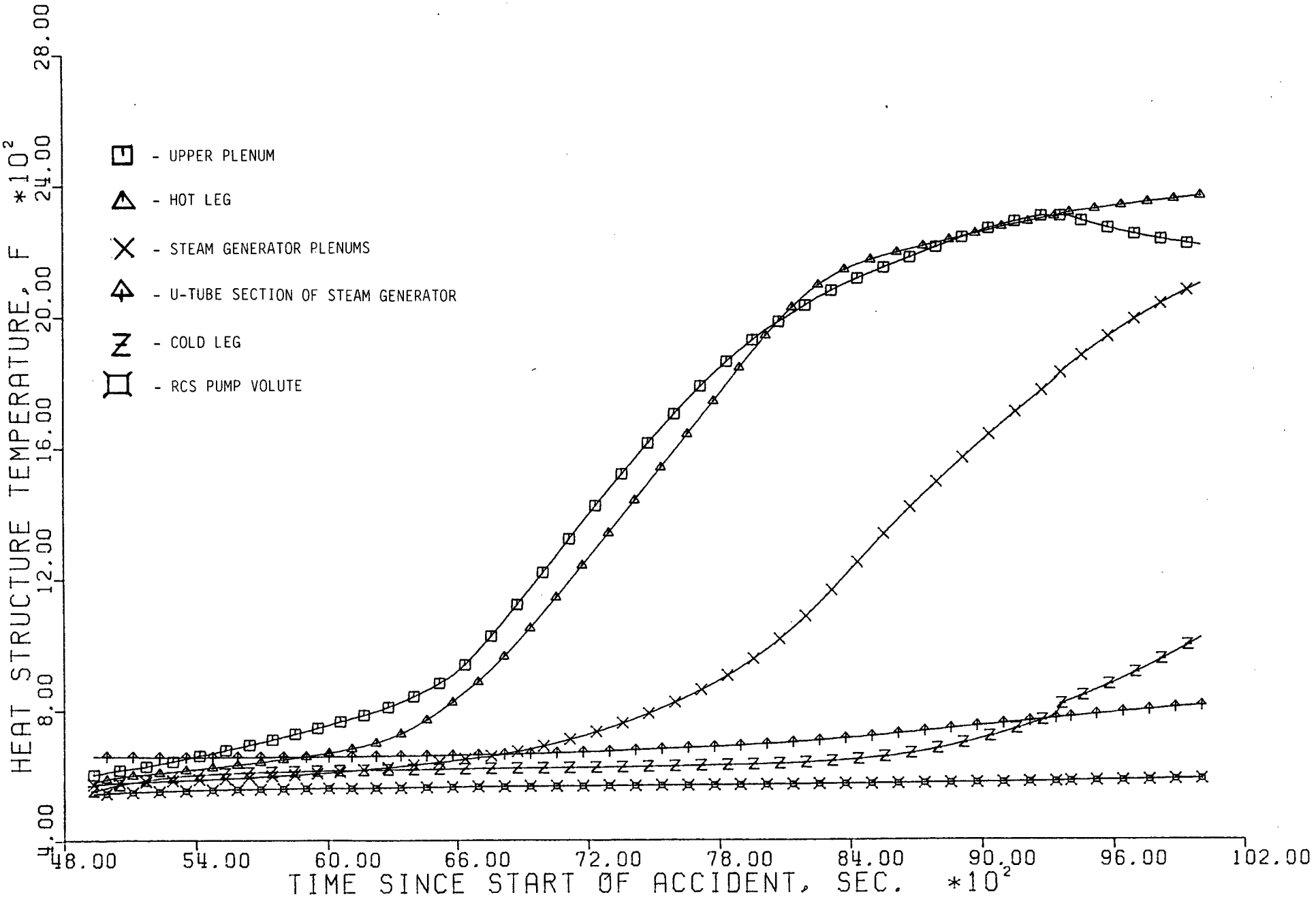
- UPPER PLENUM
- HOT LEG
- STEAM GENERATOR PLENUMS
- U-TUBE SECTION OF STEAM GENERATOR
- COLD LEG
- RCS PUMP VOLUTE
HEAT STRUCTURE TEMPERATURE, F *10²
4.00
8.00
12.00
16.00
20.00
24.00
28.00
48.00
54.00
60.00
66.00
72.00
78.00
84.00
90.00
96.00
102.00
TIME SINCE START OF ACCIDENT, SEC. *10²

FIGURE 5.88

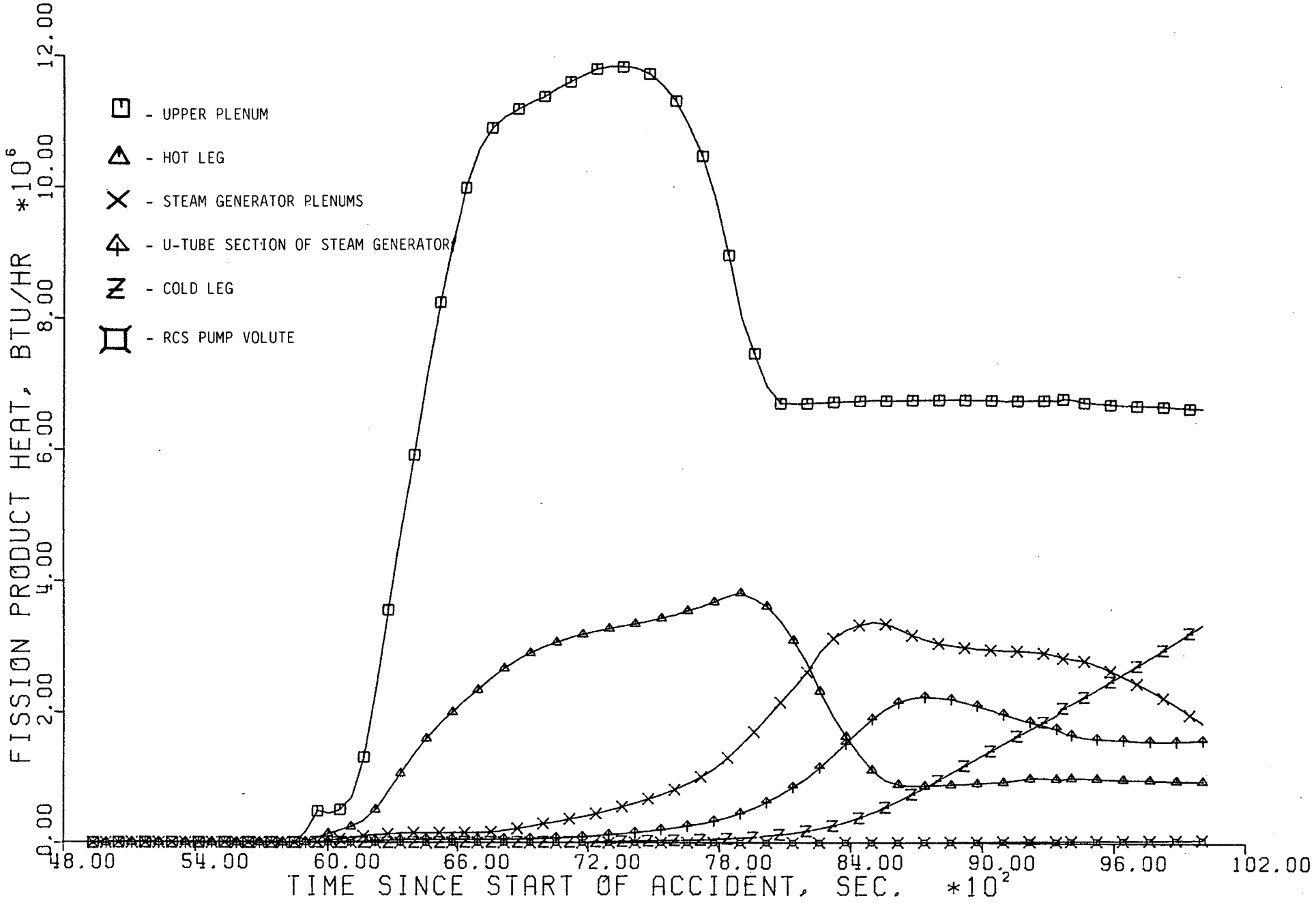
- UPPER PLENUM
- HOT LEG
- STEAM GENERATOR PLENUMS
- U-TUBE SECTION OF STEAM GENERATOR
- COLD LEG
- RCS PUMP VOLUTE
FISSION PRODUCT HEAT, BTU/HR *10^6
0.00
2.00
4.00
6.00
8.00
10.00
12.00
48.00
54.00
60.00
66.00
72.00
78.00
84.00
90.00
96.00
102.00
TIME SINCE START OF ACCIDENT, SEC. *10^2

FIGURE 5.89

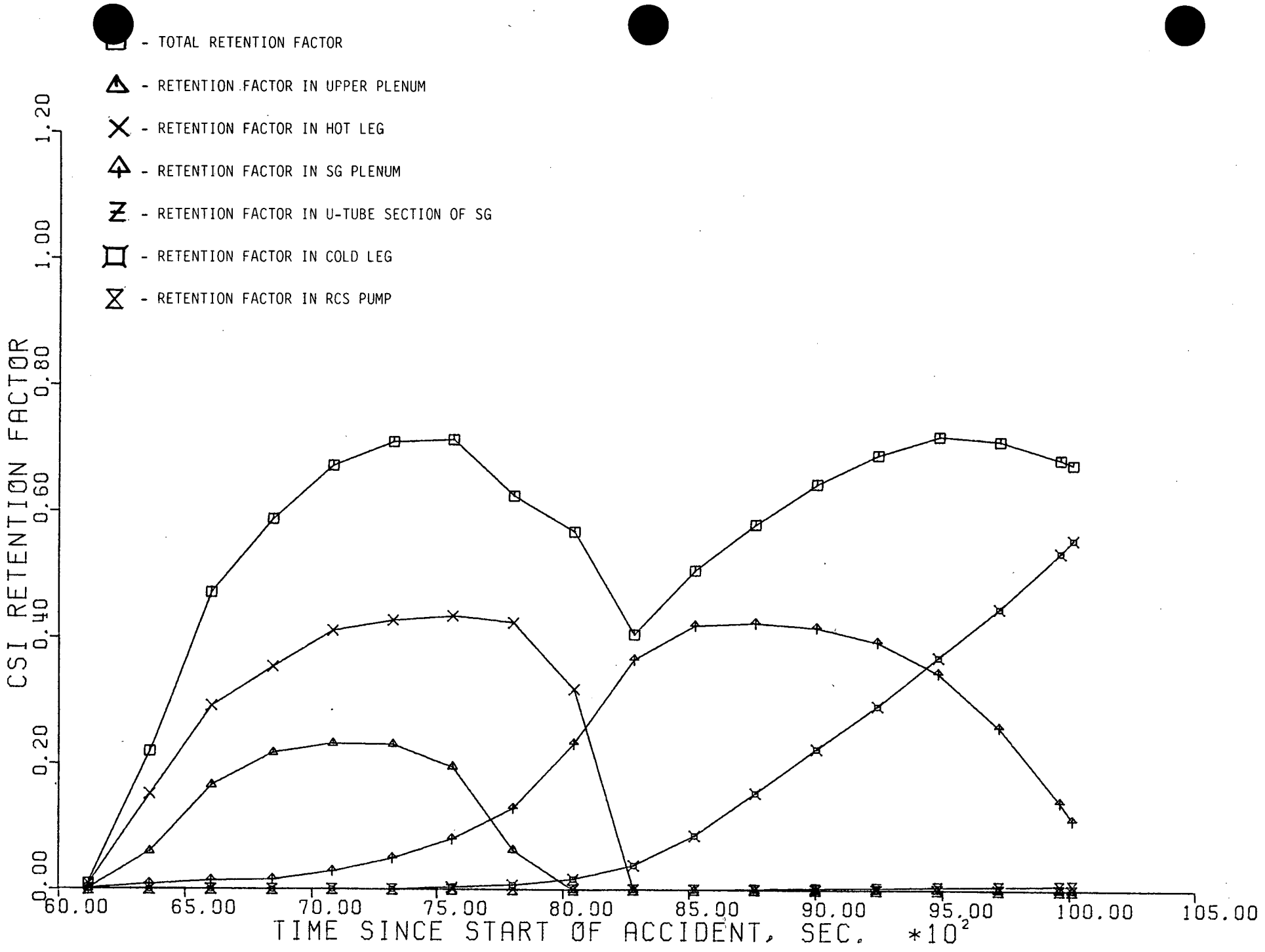
- TOTAL RETENTION FACTOR
- RETENTION FACTOR IN UPPER PLENUM
- RETENTION FACTOR IN HOT LEG
- RETENTION FACTOR IN SG PLENUM
- RETENTION FACTOR IN U-TUBE SECTION OF SG
- RETENTION FACTOR IN COLD LEG
- RETENTION FACTOR IN RCS PUMP
CSI RETENTION FACTOR
0.00
0.20
0.40
0.60
0.80
1.00
1.20
60.00
65.00
70.00
75.00
80.00
85.00
90.00
95.00
100.00
105.00
TIME SINCE START OF ACCIDENT, SEC. *10²

FIGURE 5.90

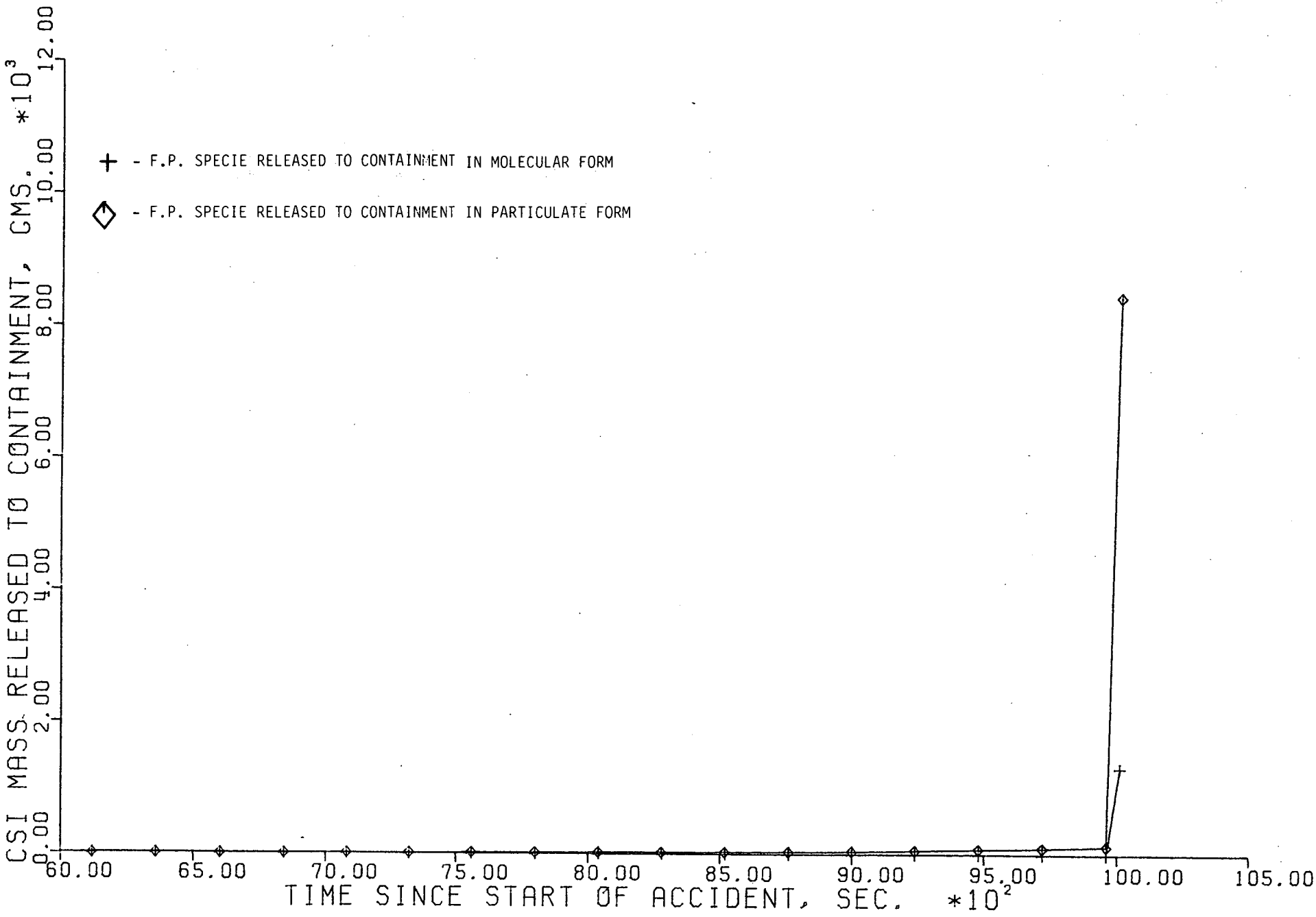
+ - F.P. SPECIE RELEASED TO CONTAINMENT IN MOLECULAR FORM
◇ - F.P. SPECIE RELEASED TO CONTAINMENT IN PARTICULATE FORM
CSI MASS RELEASED TO CONTAINMENT, CMS. *10³
0.00
2.00
4.00
6.00
8.00
10.00
12.00
60.00
65.00
70.00
75.00
80.00
85.00
90.00
95.00
100.00
105.00
TIME SINCE START OF ACCIDENT, SEC. *10²

FIGURE 5.91

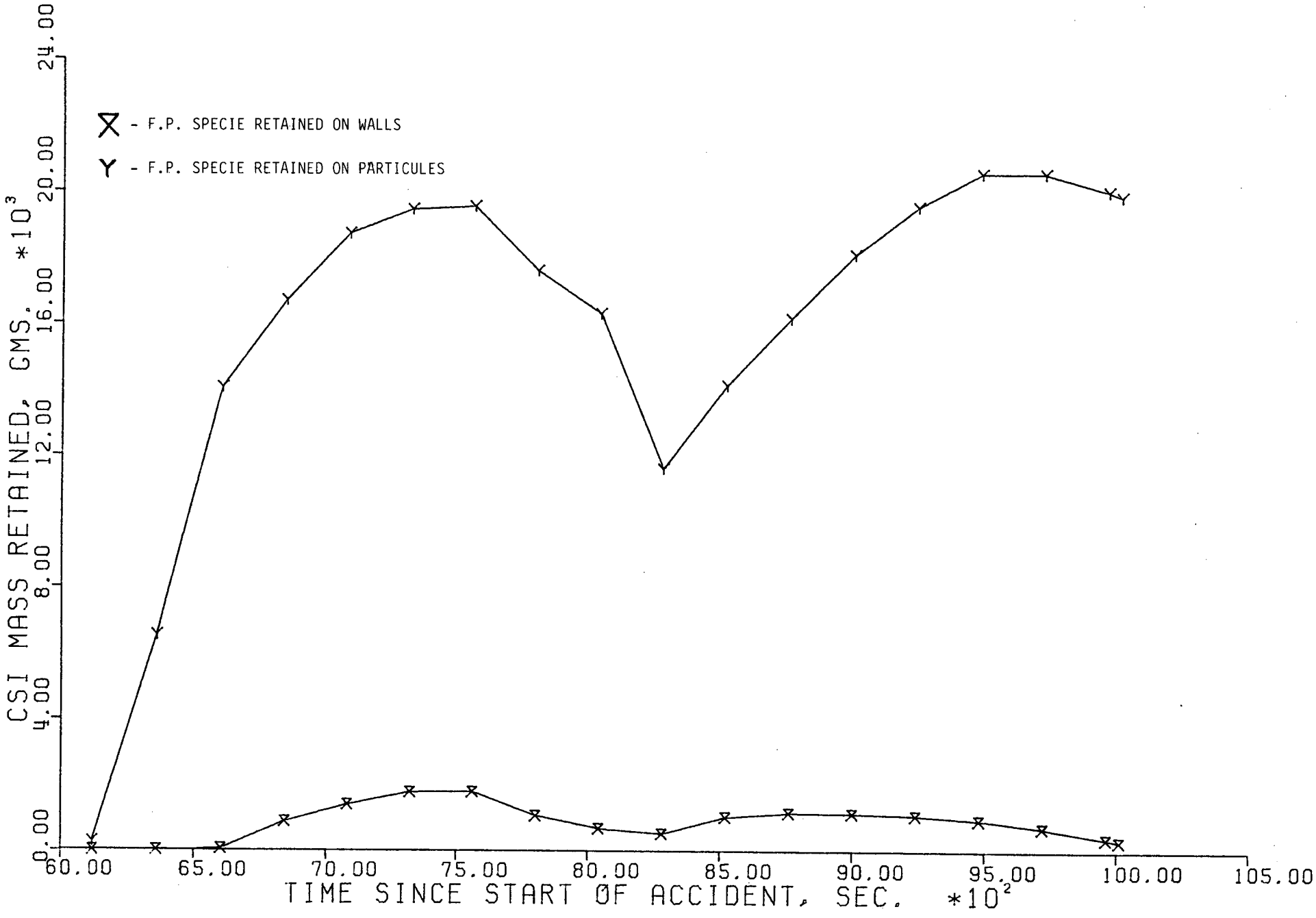
X - F.P. SPECIE RETAINED ON WALLS
Y - F.P. SPECIE RETAINED ON PARTICULES
CSI MASS RETAINED, GMS. *10³
0.00
4.00
8.00
12.00
16.00
20.00
24.00
60.00
65.00
70.00
75.00
80.00
85.00
90.00
95.00
100.00
105.00
TIME SINCE START OF ACCIDENT, SEC. *10²

FIGURE 5.92

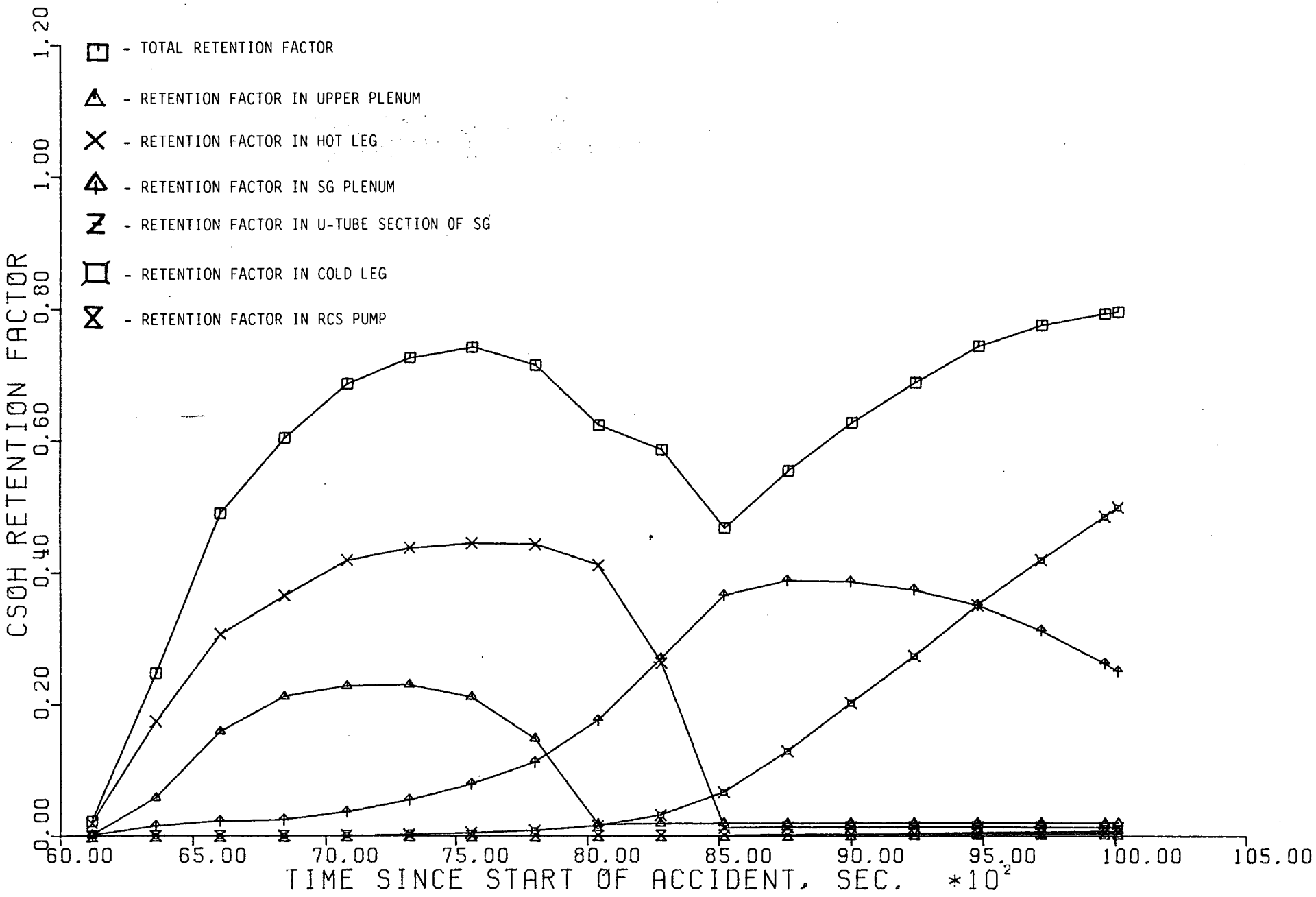
- TOTAL RETENTION FACTOR
- RETENTION FACTOR IN UPPER PLENUM
- RETENTION FACTOR IN HOT LEG
- RETENTION FACTOR IN SG PLENUM
- RETENTION FACTOR IN U-TUBE SECTION OF SG
- RETENTION FACTOR IN COLD LEG
- RETENTION FACTOR IN RCS PUMP
CSOH RETENTION FACTOR
0.00
0.20
0.40
0.60
0.80
1.00
1.20
60.00
65.00
70.00
75.00
80.00
85.00
90.00
95.00
100.00
105.00
TIME SINCE START OF ACCIDENT, SEC. *10²

FIGURE 5.93

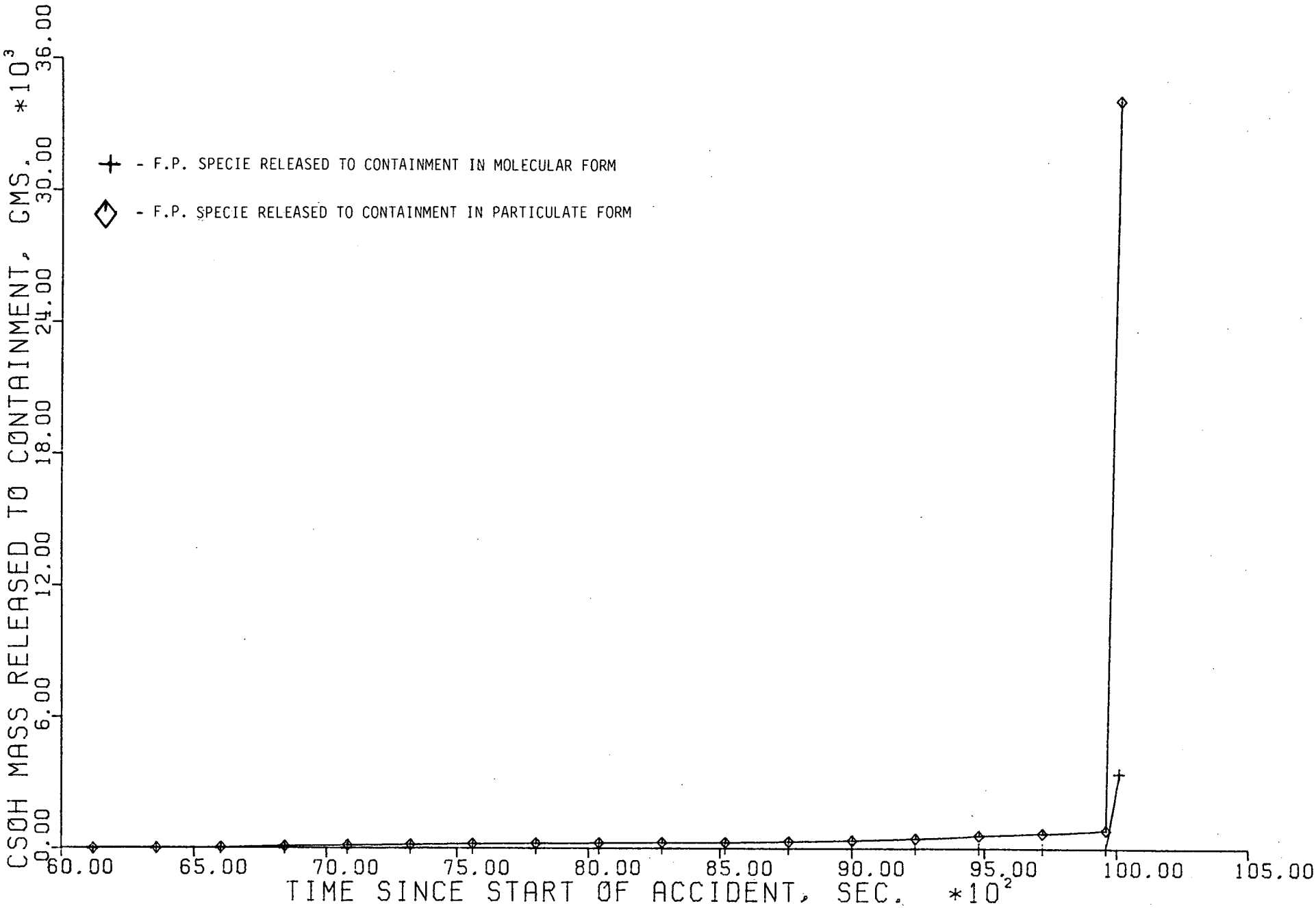
+ - F.P. SPECIE RELEASED TO CONTAINMENT IN MOLECULAR FORM
◇ - F.P. SPECIE RELEASED TO CONTAINMENT IN PARTICULATE FORM
CSOH MASS RELEASED TO CONTAINMENT, GMS. *10^3
0.00
6.00
12.00
18.00
24.00
30.00
36.00
60.00
65.00
70.00
75.00
80.00
85.00
90.00
95.00
100.00
105.00
TIME SINCE START OF ACCIDENT, SEC. *10^2

FIGURE 5.94

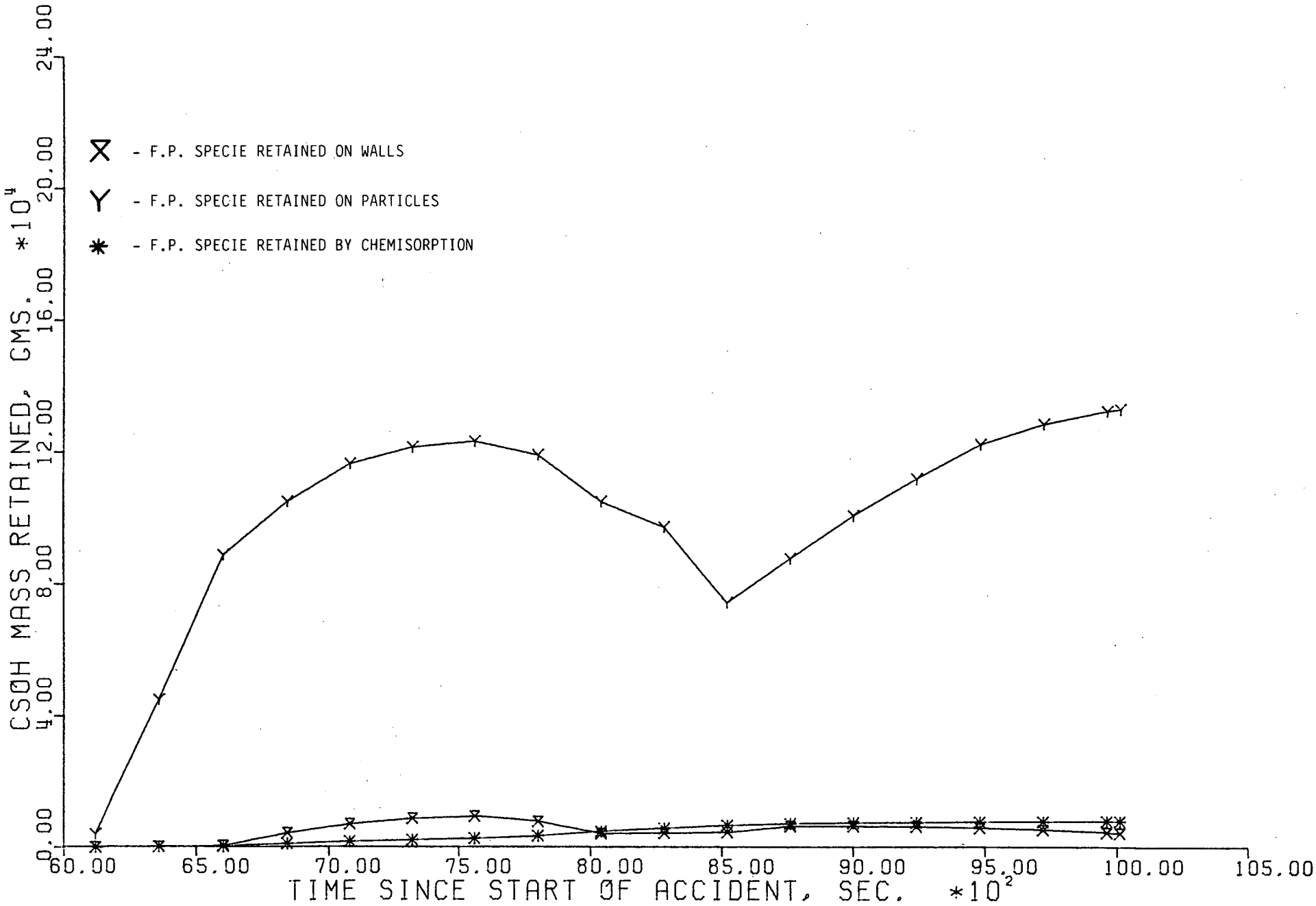
X - F.P. SPECIE RETAINED ON WALLS
Y - F.P. SPECIE RETAINED ON PARTICLES
* - F.P. SPECIE RETAINED BY CHEMISORPTION
CSOH MASS RETAINED, GMS. *10^4
0.00
4.00
8.00
12.00
16.00
20.00
24.00
60.00
65.00
70.00
75.00
80.00
85.00
90.00
95.00
100.00
105.00
TIME SINCE START OF ACCIDENT, SEC. *10^2

FIGURE 5.95

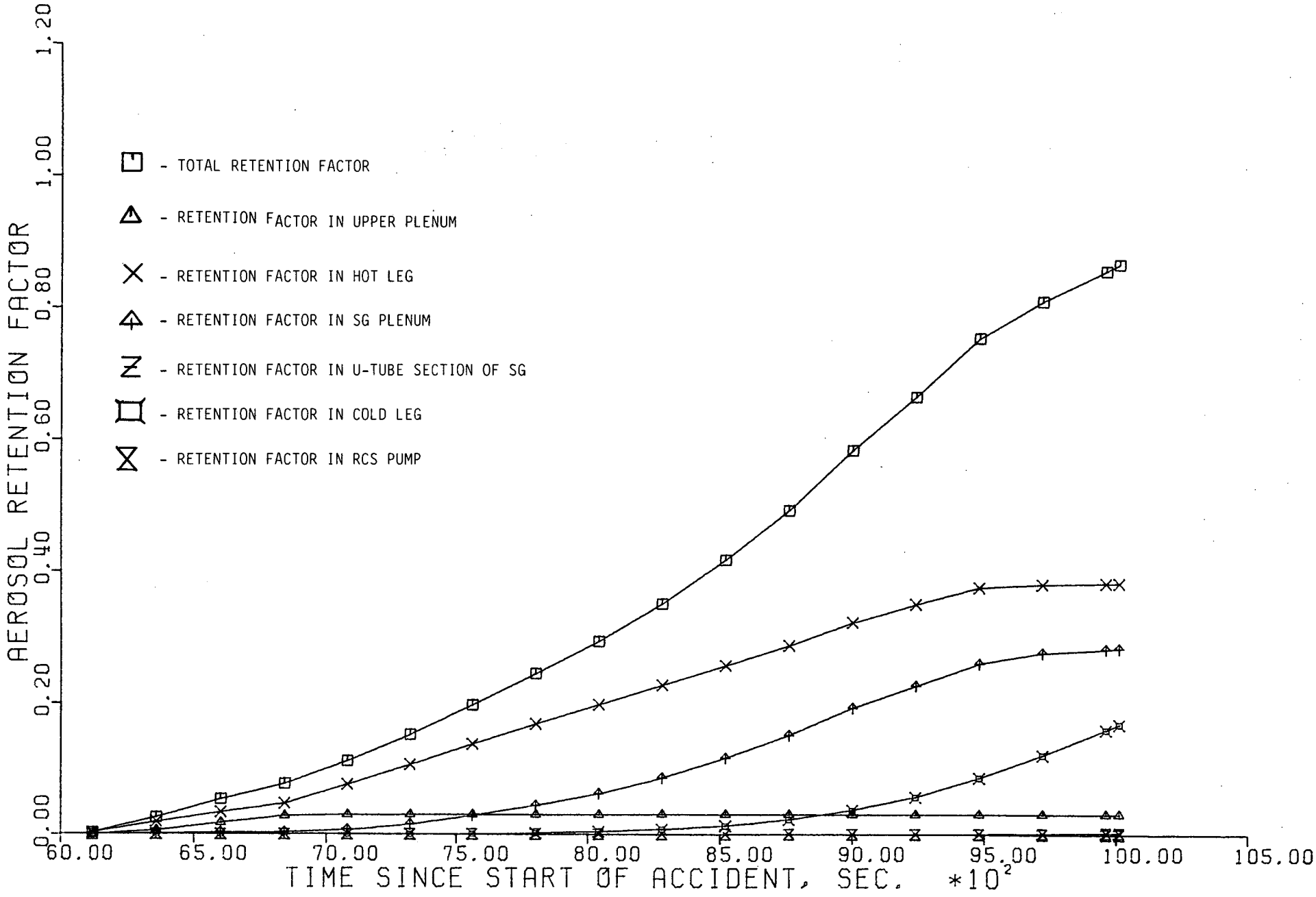
AEROSOL RETENTION FACTOR
0.00
0.20
0.40
0.60
0.80
1.00
1.20
60.00
65.00
70.00
75.00
80.00
85.00
90.00
95.00
100.00
105.00
TIME SINCE START OF ACCIDENT, SEC. *10²
- TOTAL RETENTION FACTOR
- RETENTION FACTOR IN UPPER PLENUM
- RETENTION FACTOR IN HOT LEG
- RETENTION FACTOR IN SG PLENUM
- RETENTION FACTOR IN U-TUBE SECTION OF SG
- RETENTION FACTOR IN COLD LEG
- RETENTION FACTOR IN RCS PUMP

FIGURE 5.96

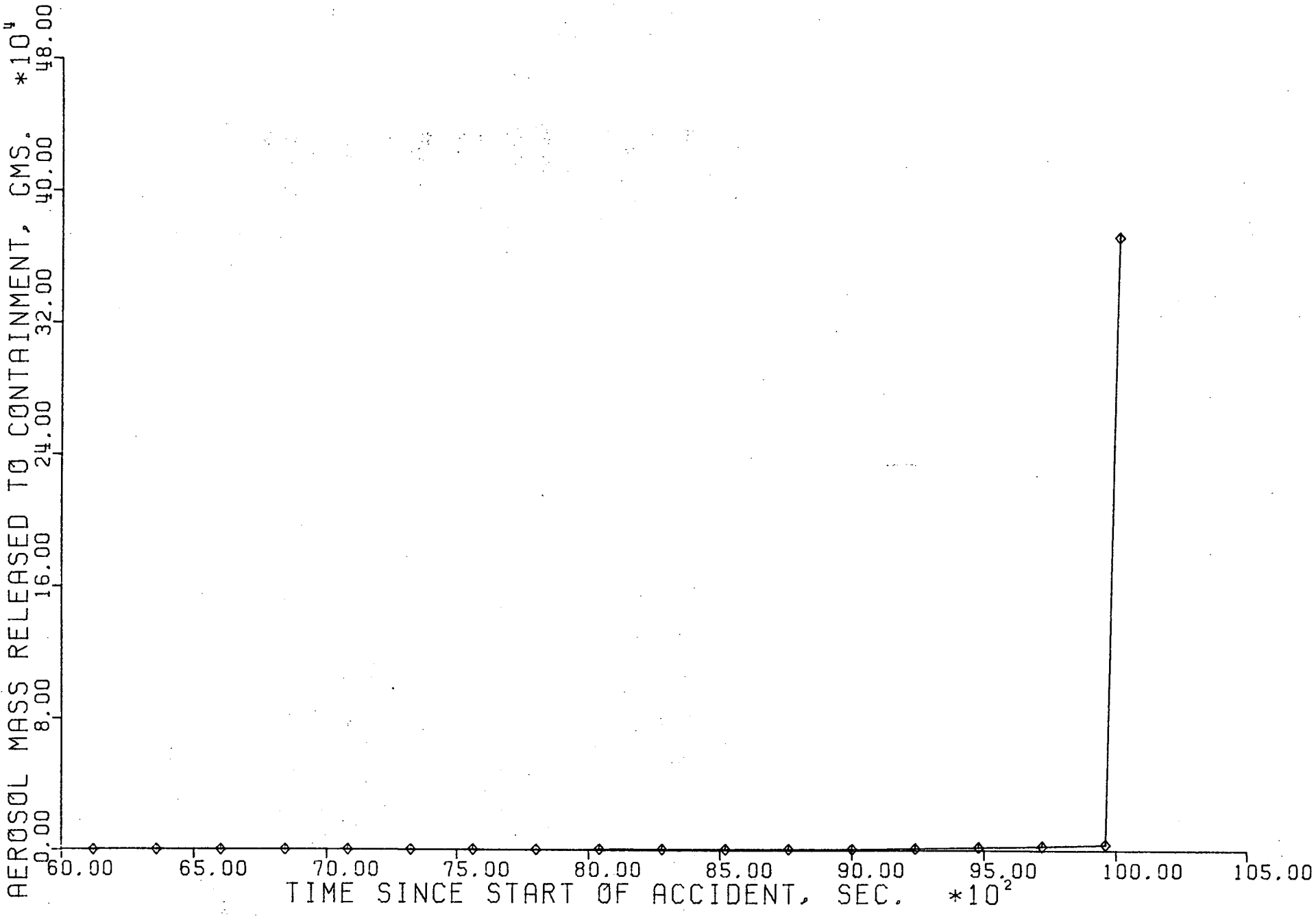
AEROSOL MASS RELEASED TO CONTAINMENT, GMS. *10⁴
0.00
8.00
16.00
24.00
32.00
40.00
48.00
60.00
65.00
70.00
75.00
80.00
85.00
90.00
95.00
100.00
105.00
TIME SINCE START OF ACCIDENT, SEC. *10²

FIGURE 5.97

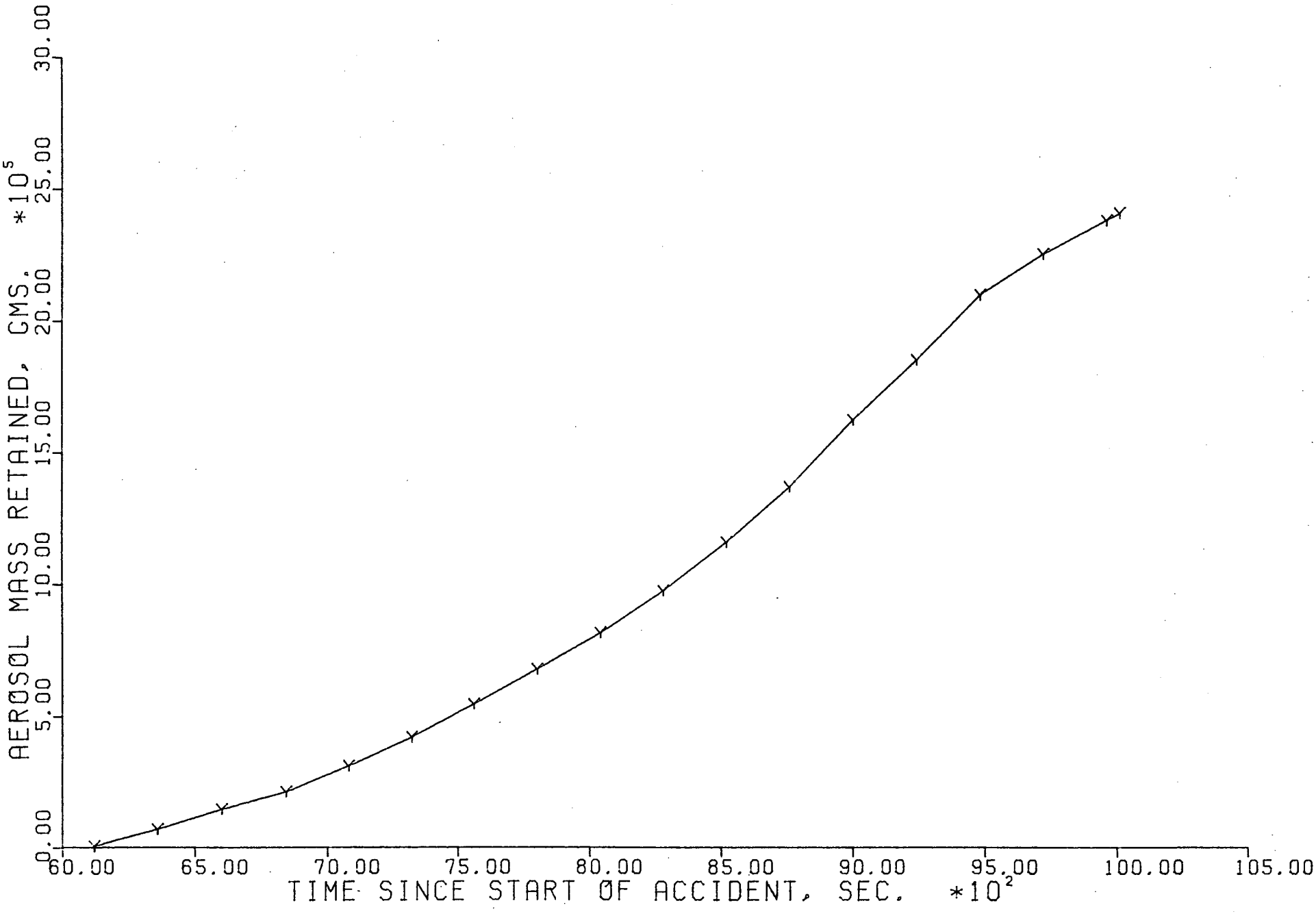
AEROSOL MASS RETAINED, GMS. *10^5
0.00
5.00
10.00
15.00
20.00
25.00
30.00
60.00
65.00
70.00
75.00
80.00
85.00
90.00
95.00
100.00
105.00
TIME SINCE START OF ACCIDENT, SEC. *10^2

FIGURE 5.98

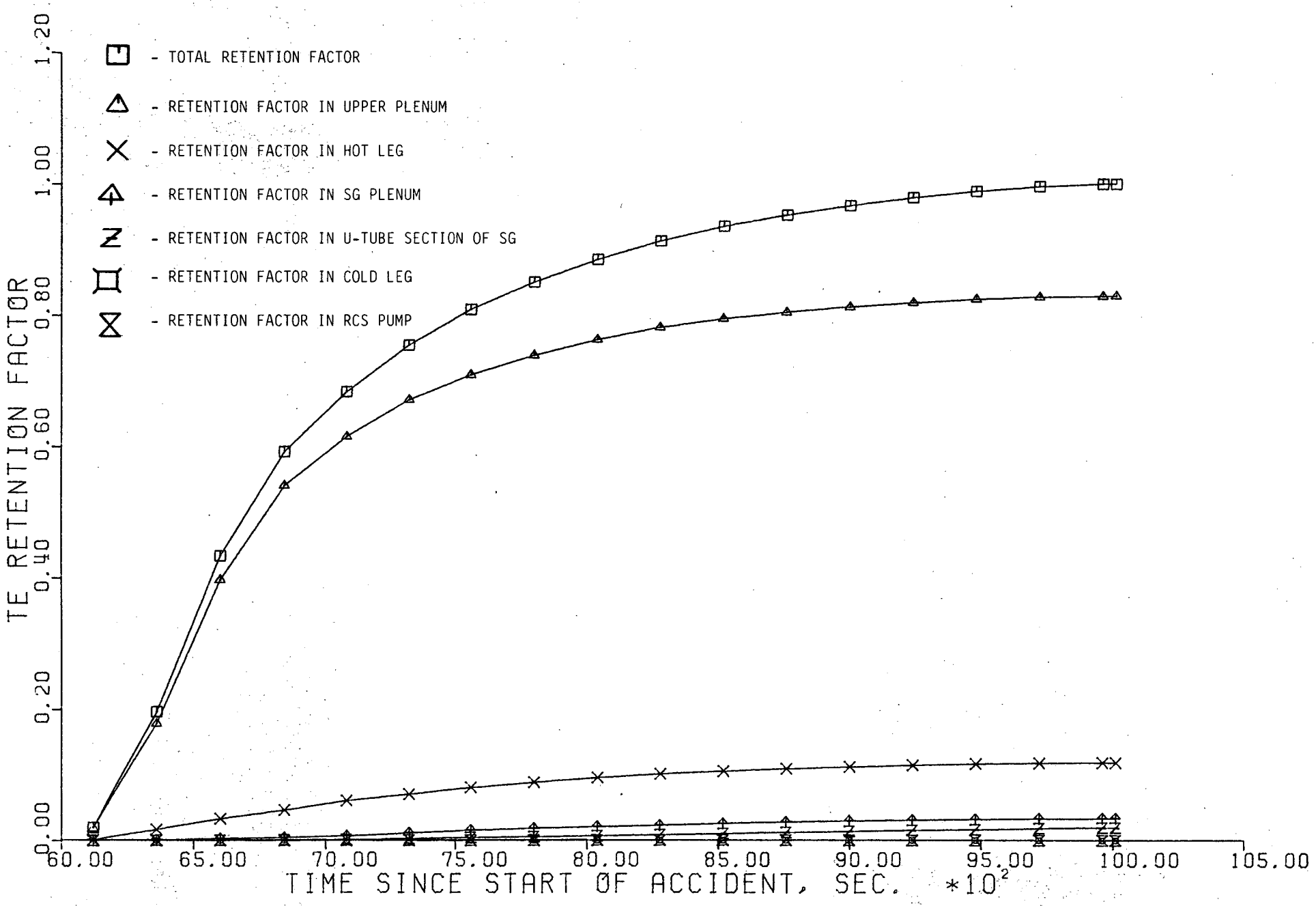
- TOTAL RETENTION FACTOR
- RETENTION FACTOR IN UPPER PLENUM
- RETENTION FACTOR IN HOT LEG
- RETENTION FACTOR IN SG PLENUM
- RETENTION FACTOR IN U-TUBE SECTION OF SG
- RETENTION FACTOR IN COLD LEG
- RETENTION FACTOR IN RCS PUMP
TE RETENTION FACTOR
0.00
0.20
0.40
0.60
0.80
1.00
1.20
60.00
65.00
70.00
75.00
80.00
85.00
90.00
95.00
100.00
105.00
TIME SINCE START OF ACCIDENT, SEC. *10²

FIGURE 5.99

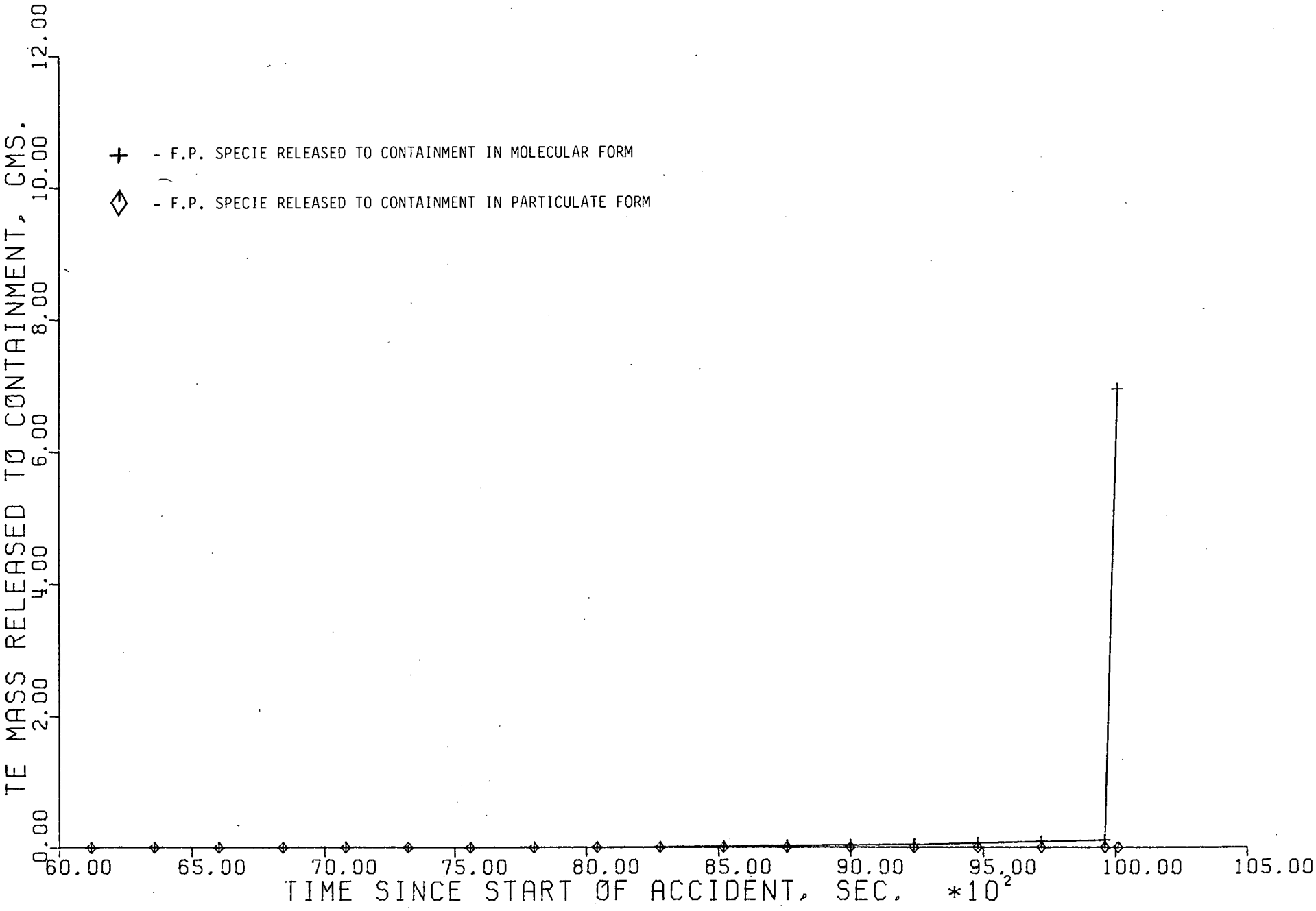
+ - F.P. SPECIE RELEASED TO CONTAINMENT IN MOLECULAR FORM
◇ - F.P. SPECIE RELEASED TO CONTAINMENT IN PARTICULATE FORM
TE MASS RELEASED TO CONTAINMENT, CMS.
0.00
2.00
4.00
6.00
8.00
10.00
12.00
60.00
65.00
70.00
75.00
80.00
85.00
90.00
95.00
100.00
105.00
TIME SINCE START OF ACCIDENT, SEC. *10²

FIGURE 5.100

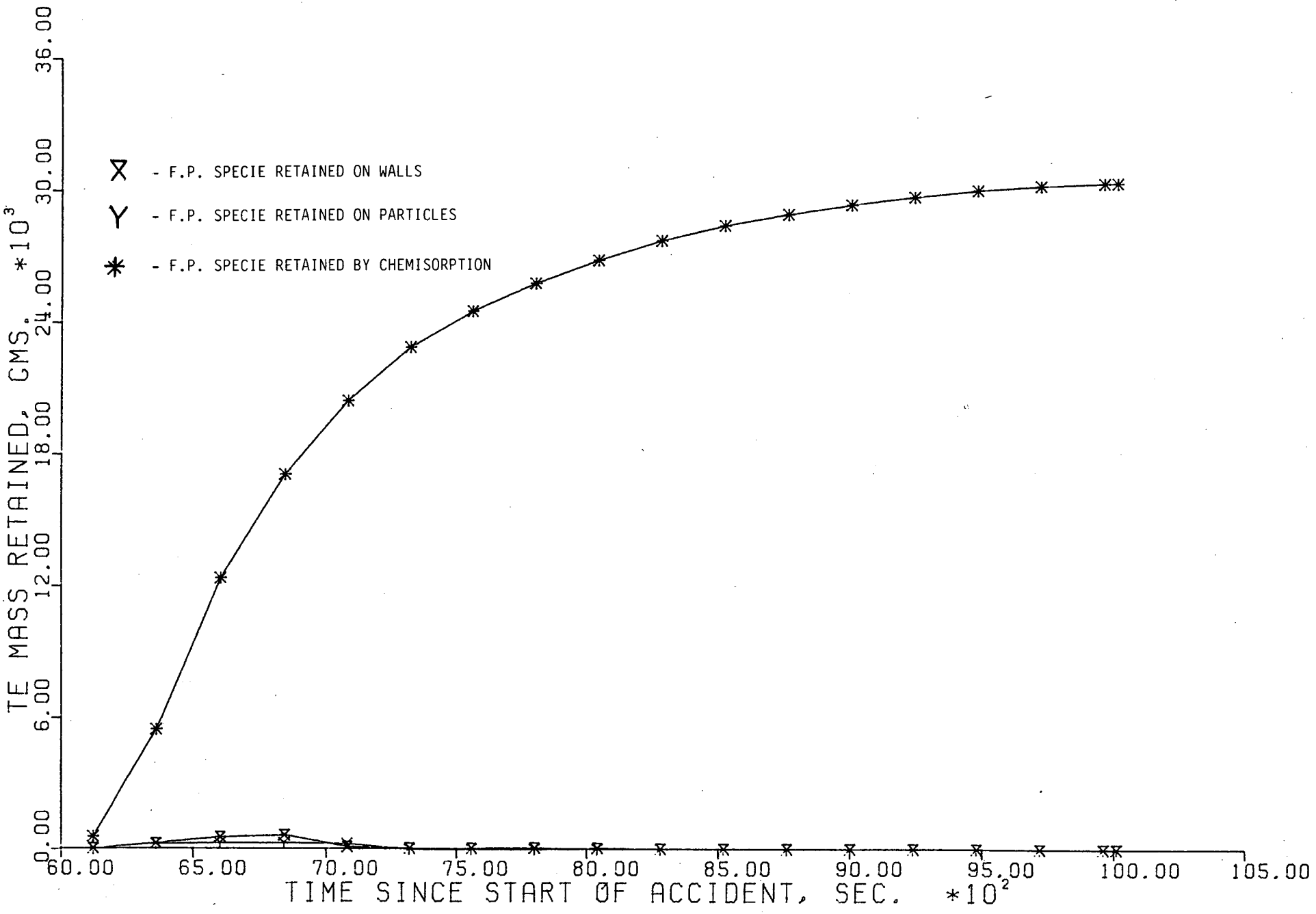
- F.P. SPECIE RETAINED ON WALLS
- F.P. SPECIE RETAINED ON PARTICLES
- F.P. SPECIE RETAINED BY CHEMISORPTION
TE MASS RETAINED, CMS. *10^3
0.00
6.00
12.00
18.00
24.00
30.00
36.00
60.00
65.00
70.00
75.00
80.00
85.00
90.00
95.00
100.00
105.00
TIME SINCE START OF ACCIDENT, SEC. *10^2

FIGURE 5.101

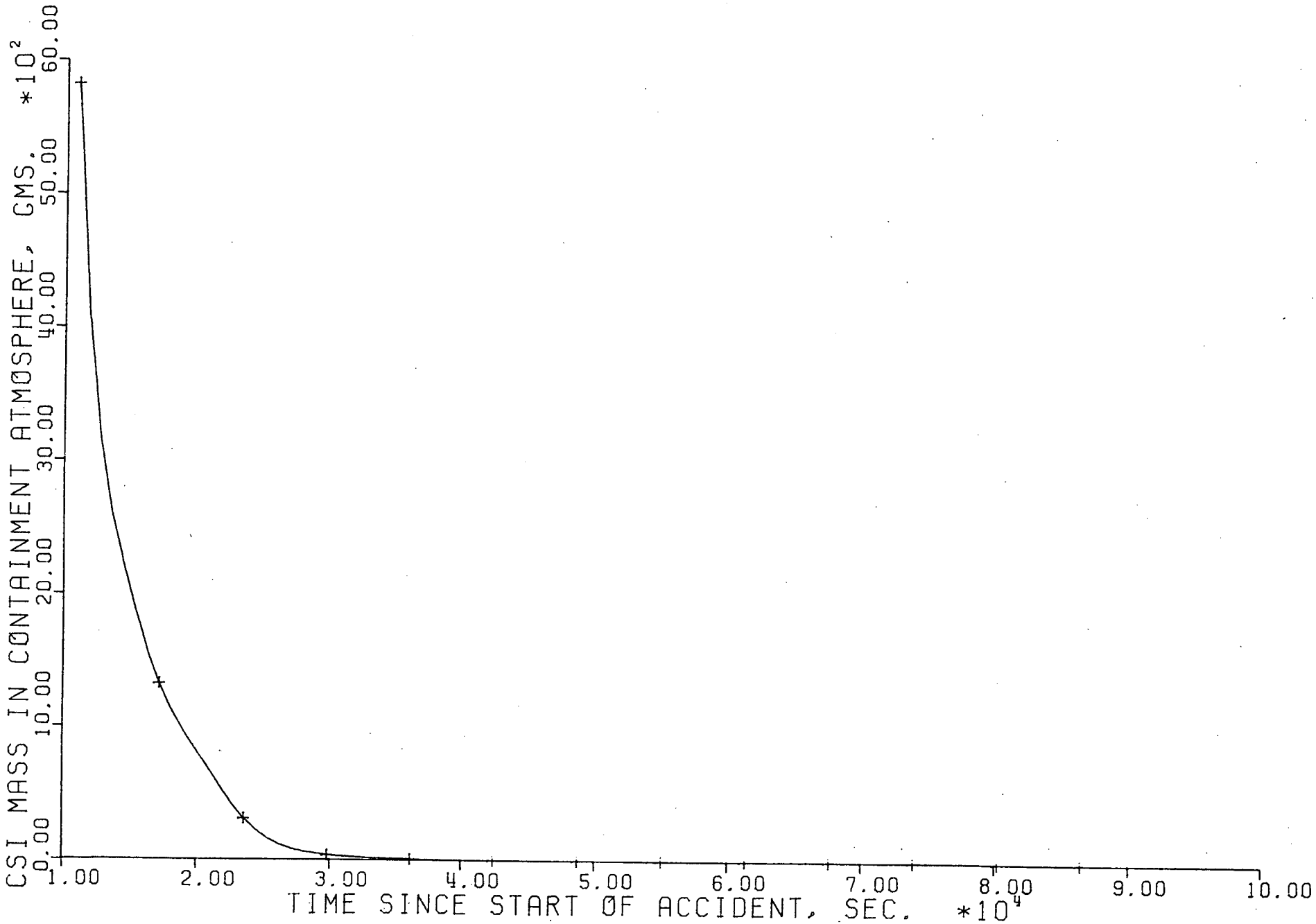
CSI MASS IN CONTAINMENT ATMOSPHERE, GMS. *10²
0.00
10.00
20.00
30.00
40.00
50.00
60.00
1.00
2.00
3.00
4.00
5.00
6.00
7.00
8.00
9.00
10.00
TIME SINCE START OF ACCIDENT, SEC. *10⁴

FIGURE 5.102

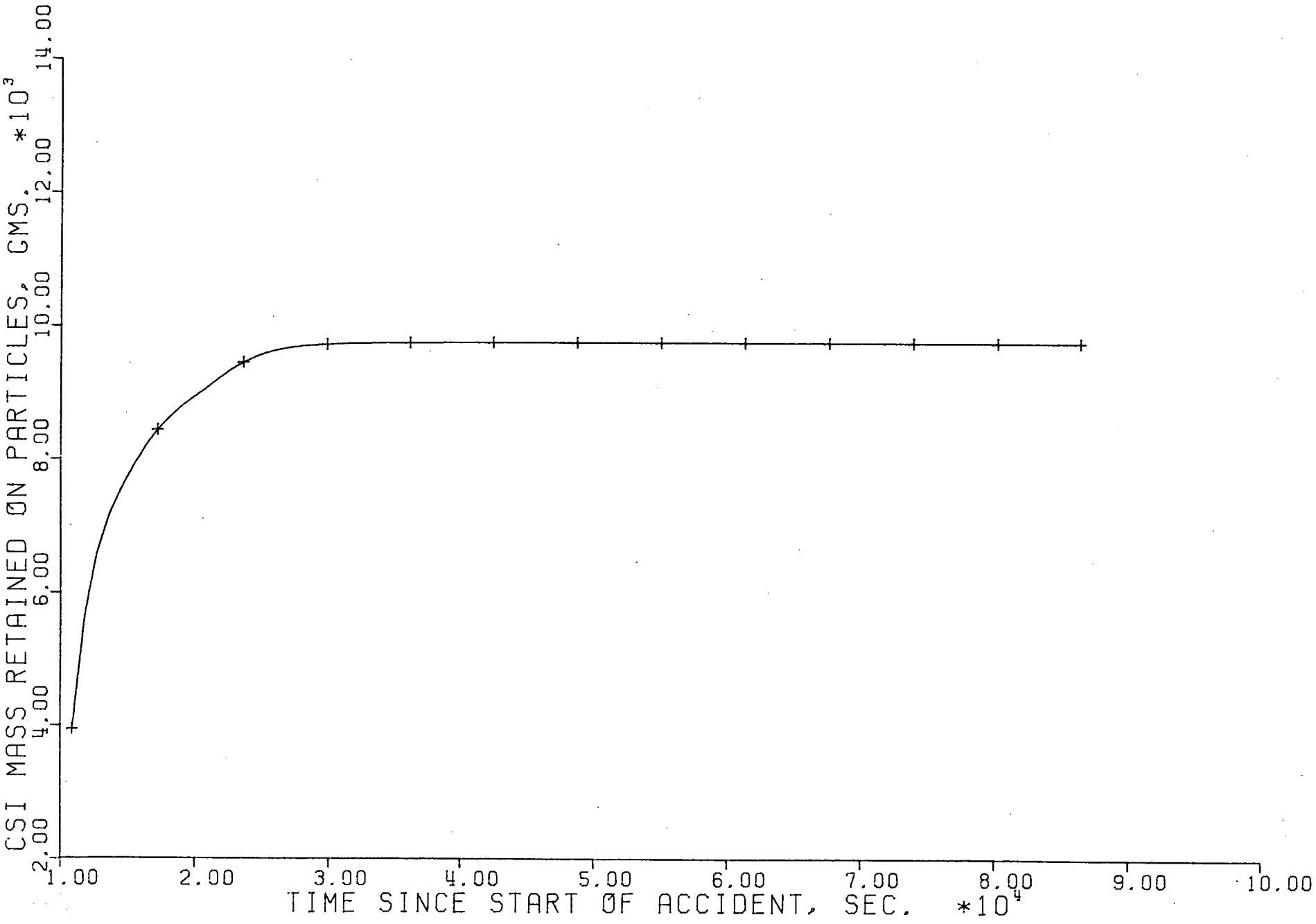
CSI MASS RETAINED ON PARTICLES, GMS. *10^3
2.00
4.00
6.00
8.00
10.00
12.00
14.00
1.00
2.00
3.00
4.00
5.00
6.00
7.00
8.00
9.00
10.00
TIME SINCE START OF ACCIDENT, SEC. *10^4

FIGURE 5.103

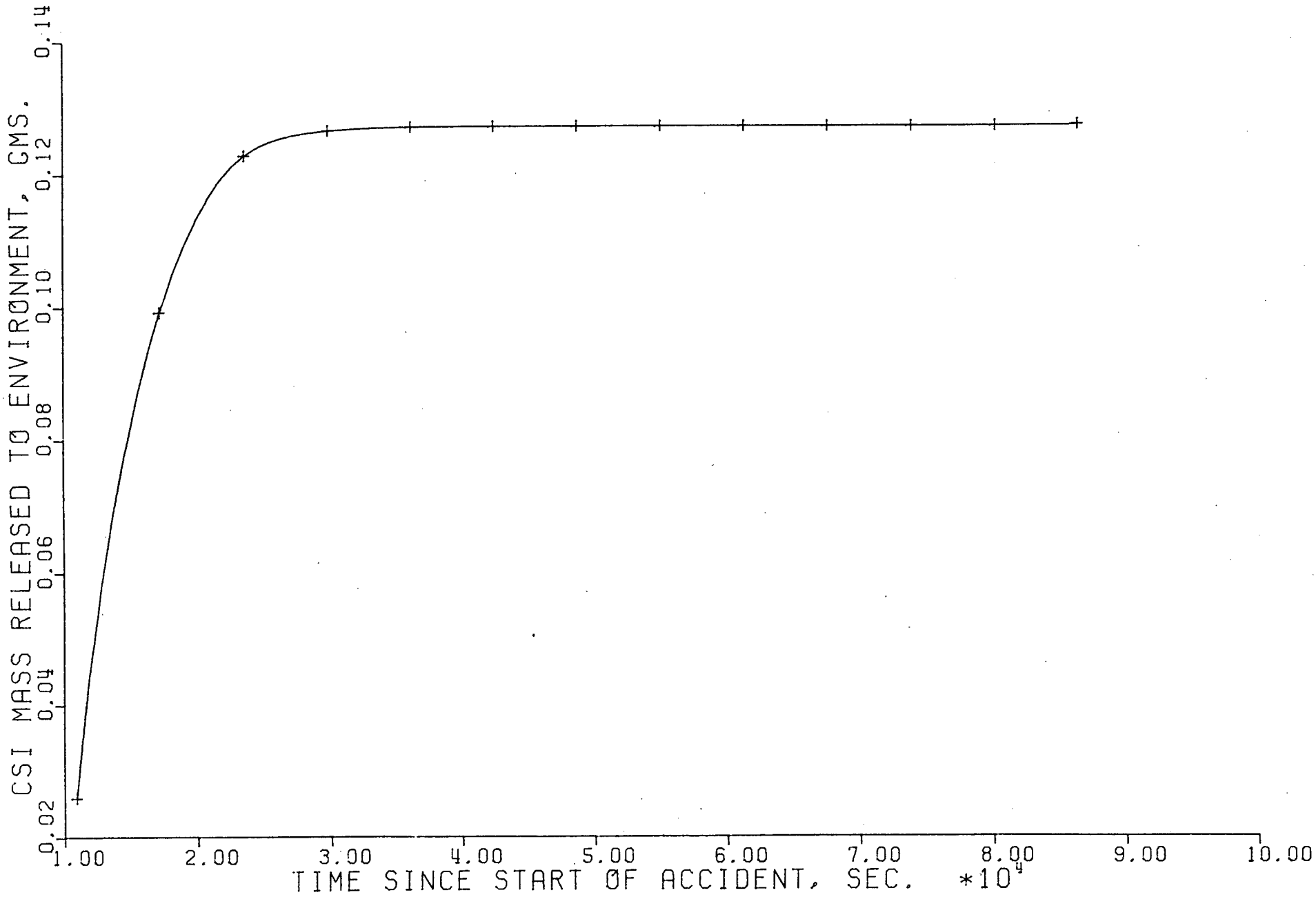
CSI MASS RELEASED TO ENVIRONMENT, CMS.
0.02
0.04
0.06
0.08
0.10
0.12
0.14
1.00
2.00
3.00
4.00
5.00
6.00
7.00
8.00
9.00
10.00
TIME SINCE START OF ACCIDENT, SEC. *10^4

FIGURE 5.104

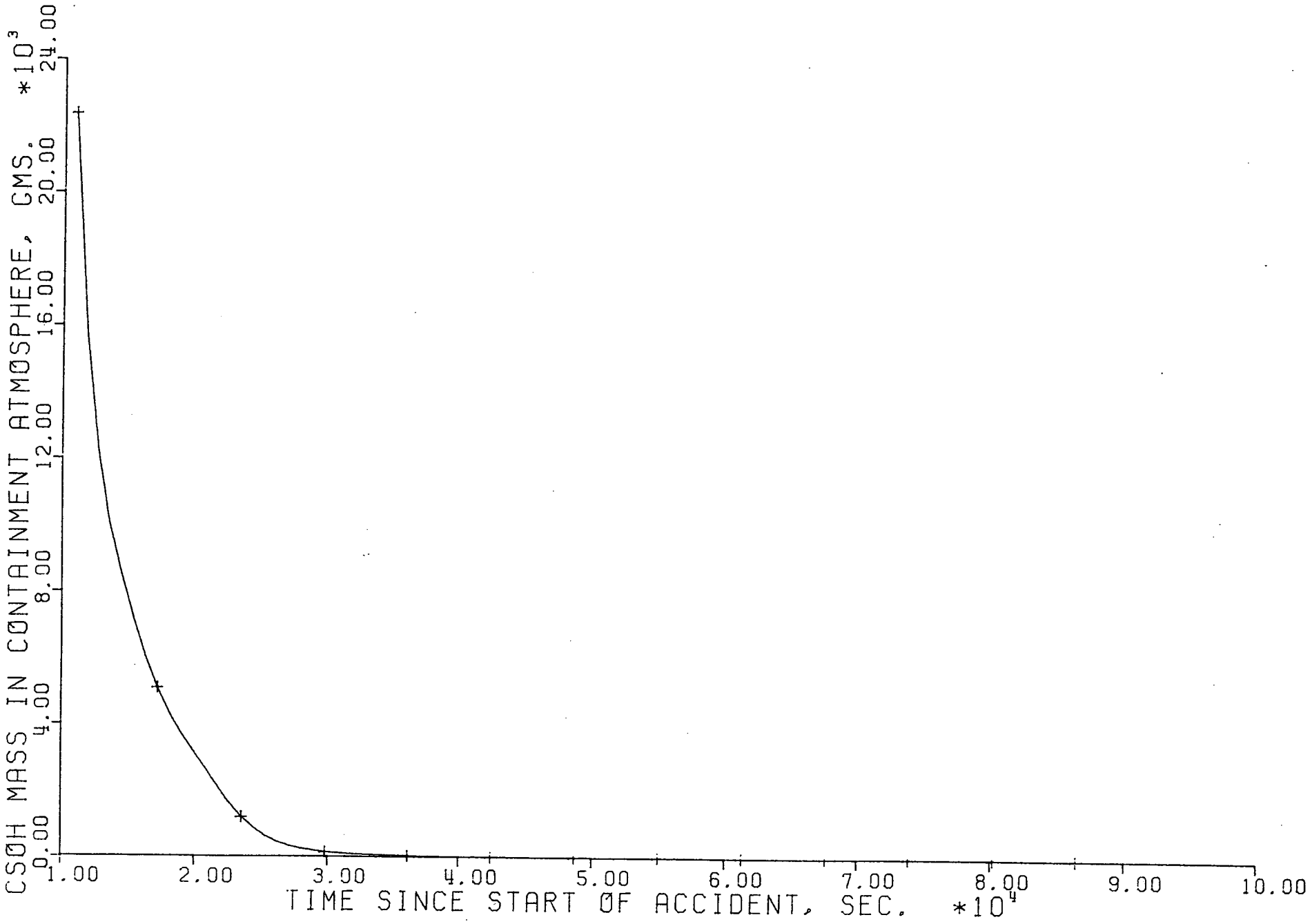
CSOH MASS IN CONTAINMENT ATMOSPHERE, GMS. *10^3
0.00
4.00
8.00
12.00
16.00
20.00
24.00
1.00
2.00
3.00
4.00
5.00
6.00
7.00
8.00
9.00
10.00
TIME SINCE START OF ACCIDENT, SEC. *10^4

FIGURE 5.105

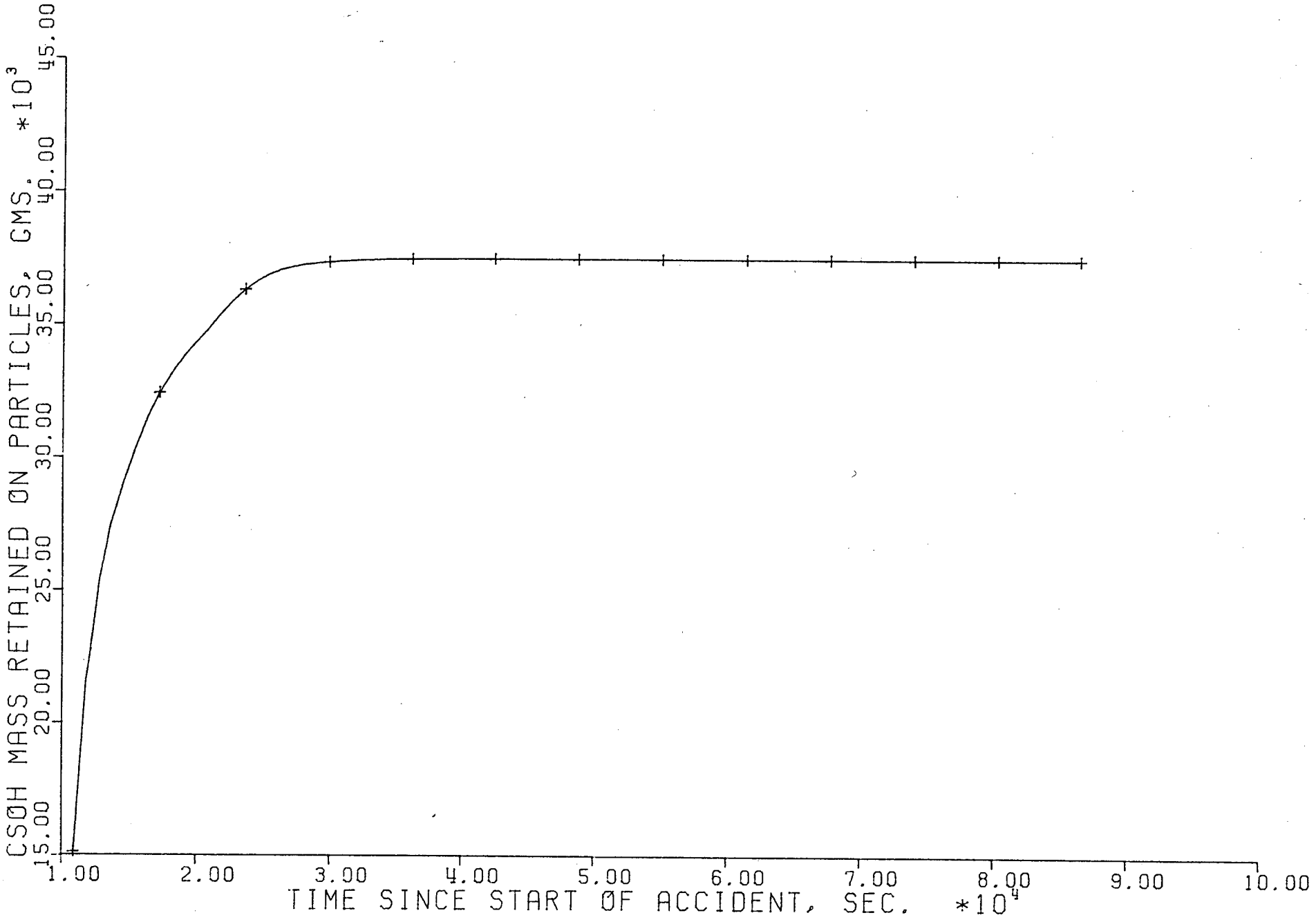
CSØH MASS RETAINED ØN PARTICLES, GMS. *10³
15.00
20.00
25.00
30.00
35.00
40.00
45.00
1.00
2.00
3.00
4.00
5.00
6.00
7.00
8.00
9.00
10.00
TIME SINCE START ØF ACCIDENT, SEC. *10⁴

FIGURE 5.106

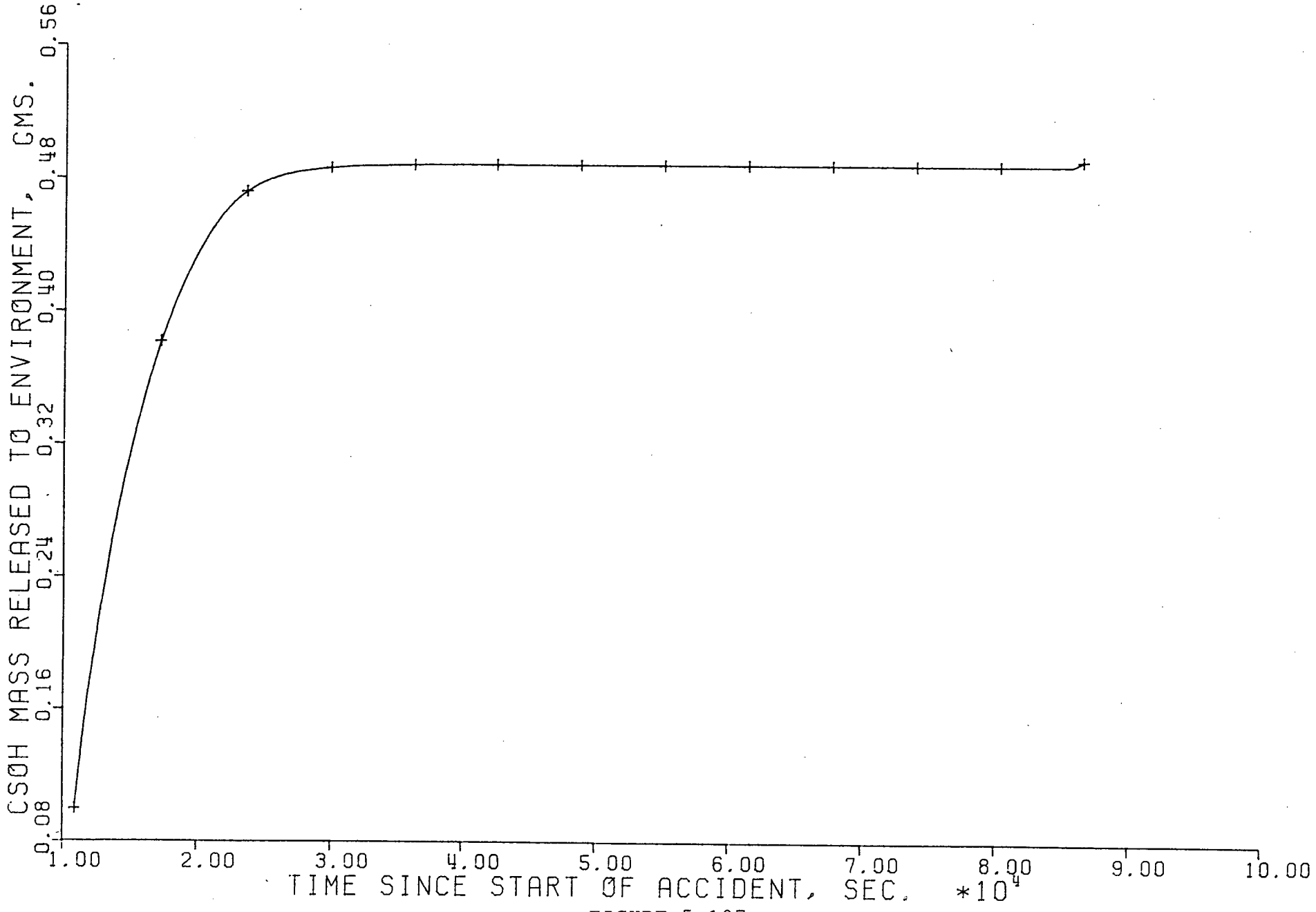
CSOH MASS RELEASED TO ENVIRONMENT, GMS.
0.08
0.16
0.24
0.32
0.40
0.48
0.56
1.00
2.00
3.00
4.00
5.00
6.00
7.00
8.00
9.00
10.00
TIME SINCE START OF ACCIDENT, SEC. *10^4

FIGURE 5.107

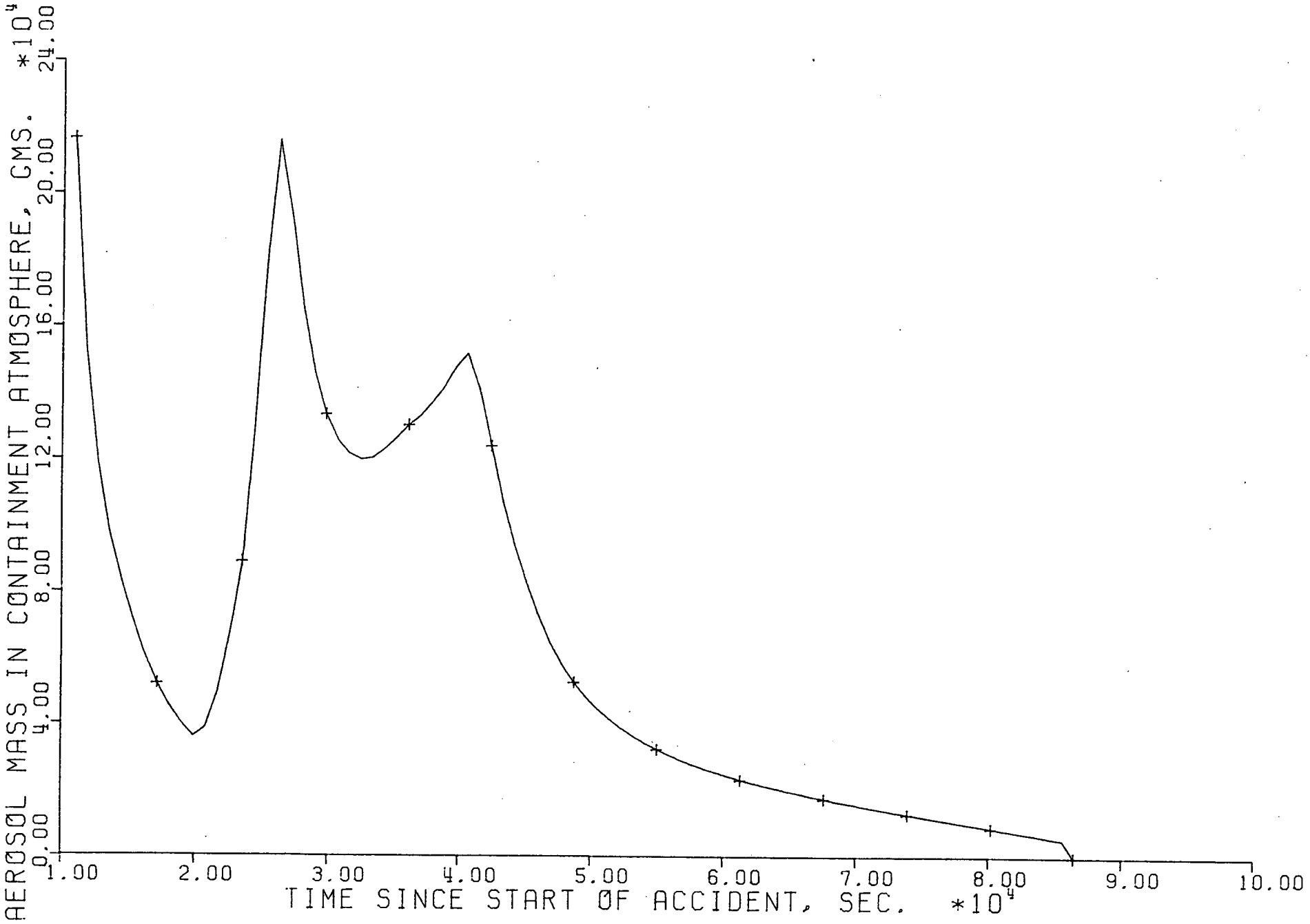
AERØSØL MASS IN CØNTAINMENT ATMØSPHERE, CMS. *10⁴
0.00
4.00
8.00
12.00
16.00
20.00
24.00
1.00
2.00
3.00
4.00
5.00
6.00
7.00
8.00
9.00
10.00
TIME SINCE START ØF ACCIDENT, SEC. *10⁴

FIGURE 5.108

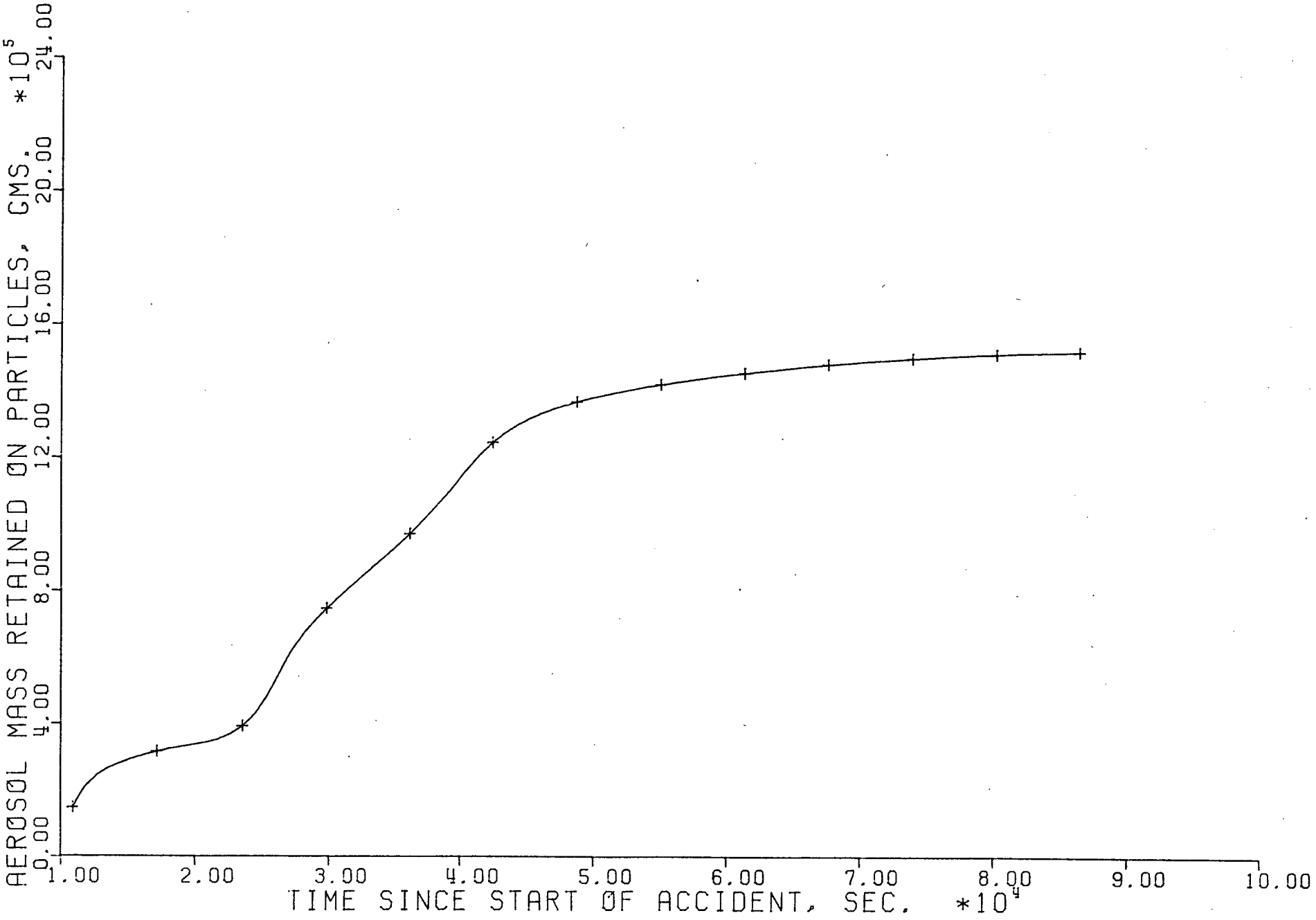
AEROSOL MASS RETAINED ON PARTICLES, GMS. *10^5
0.00
4.00
8.00
12.00
16.00
20.00
24.00
1.00
2.00
3.00
4.00
5.00
6.00
7.00
8.00
9.00
10.00
TIME SINCE START OF ACCIDENT, SEC. *10^4

FIGURE 5.109

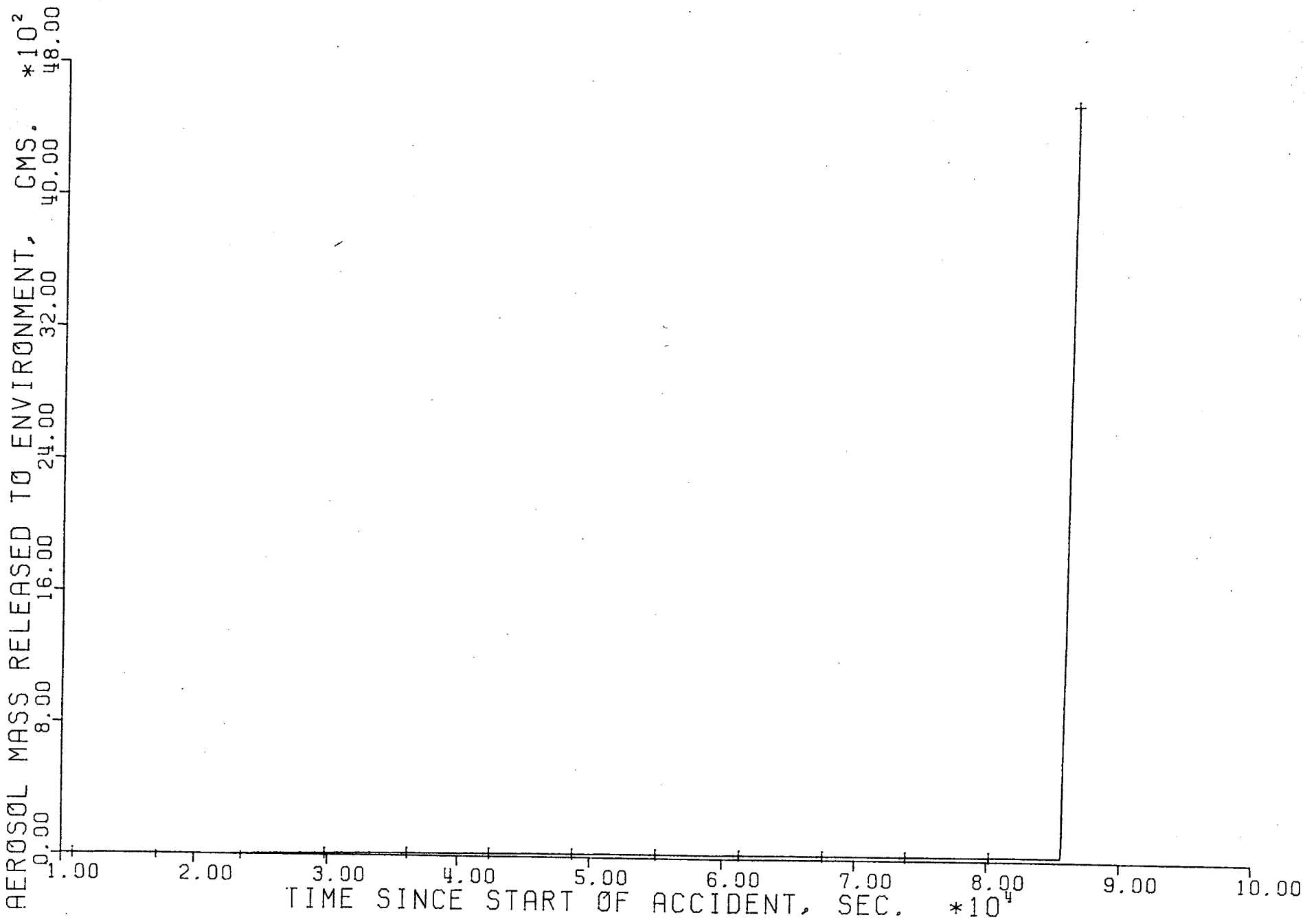
AEROSOL MASS RELEASED TO ENVIRONMENT, CMS. *10²
0.00
8.00
16.00
24.00
32.00
40.00
48.00
1.00
2.00
3.00
4.00
5.00
6.00
7.00
8.00
9.00
10.00
TIME SINCE START OF ACCIDENT, SEC. *10⁴

FIGURE 5.110

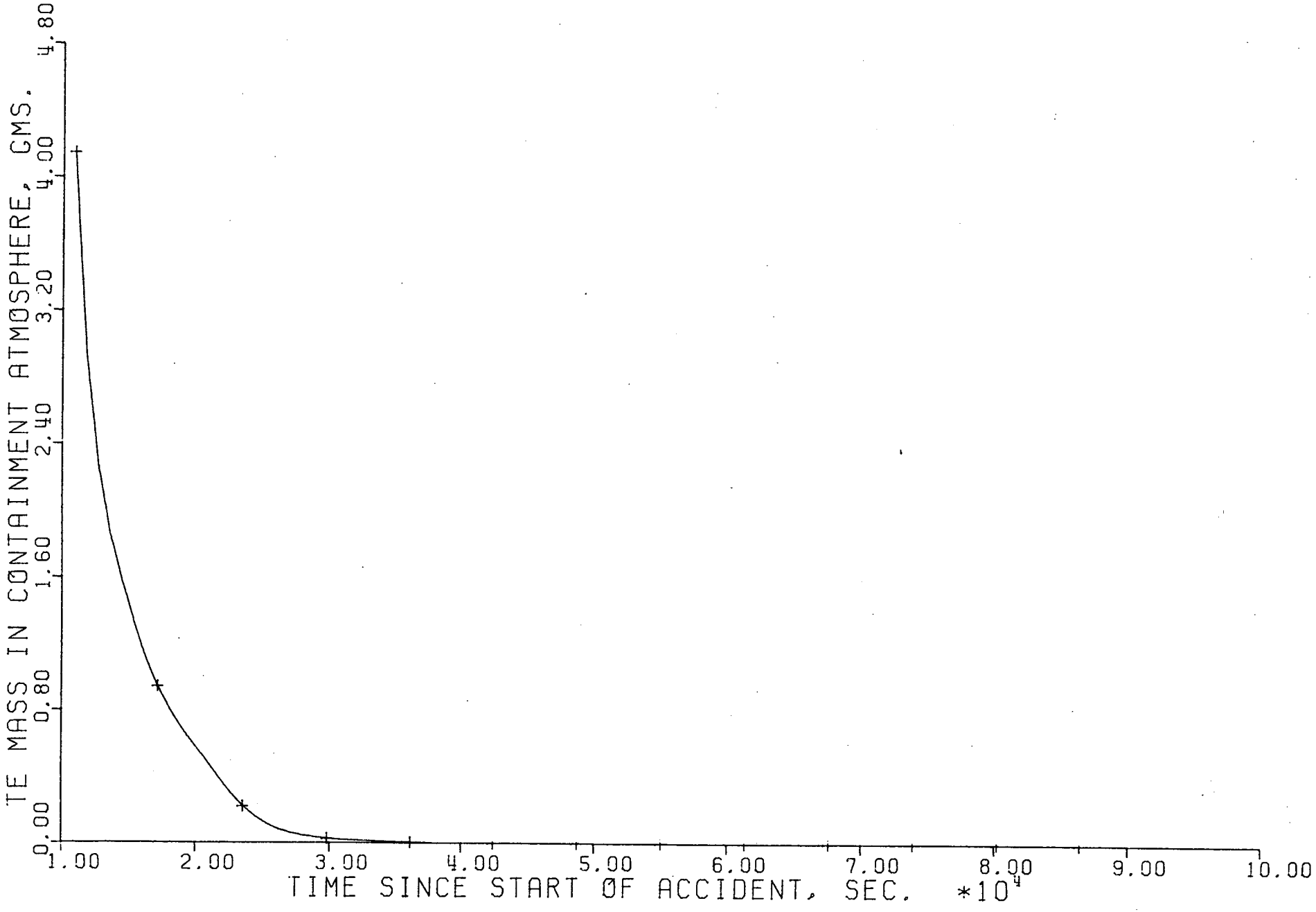
TE MASS IN CONTAINMENT ATMOSPHERE, GMS.
0.00
0.80
1.60
2.40
3.20
4.00
4.80
1.00
2.00
3.00
4.00
5.00
6.00
7.00
8.00
9.00
10.00
TIME SINCE START OF ACCIDENT, SEC. *10^4

FIGURE 5.111

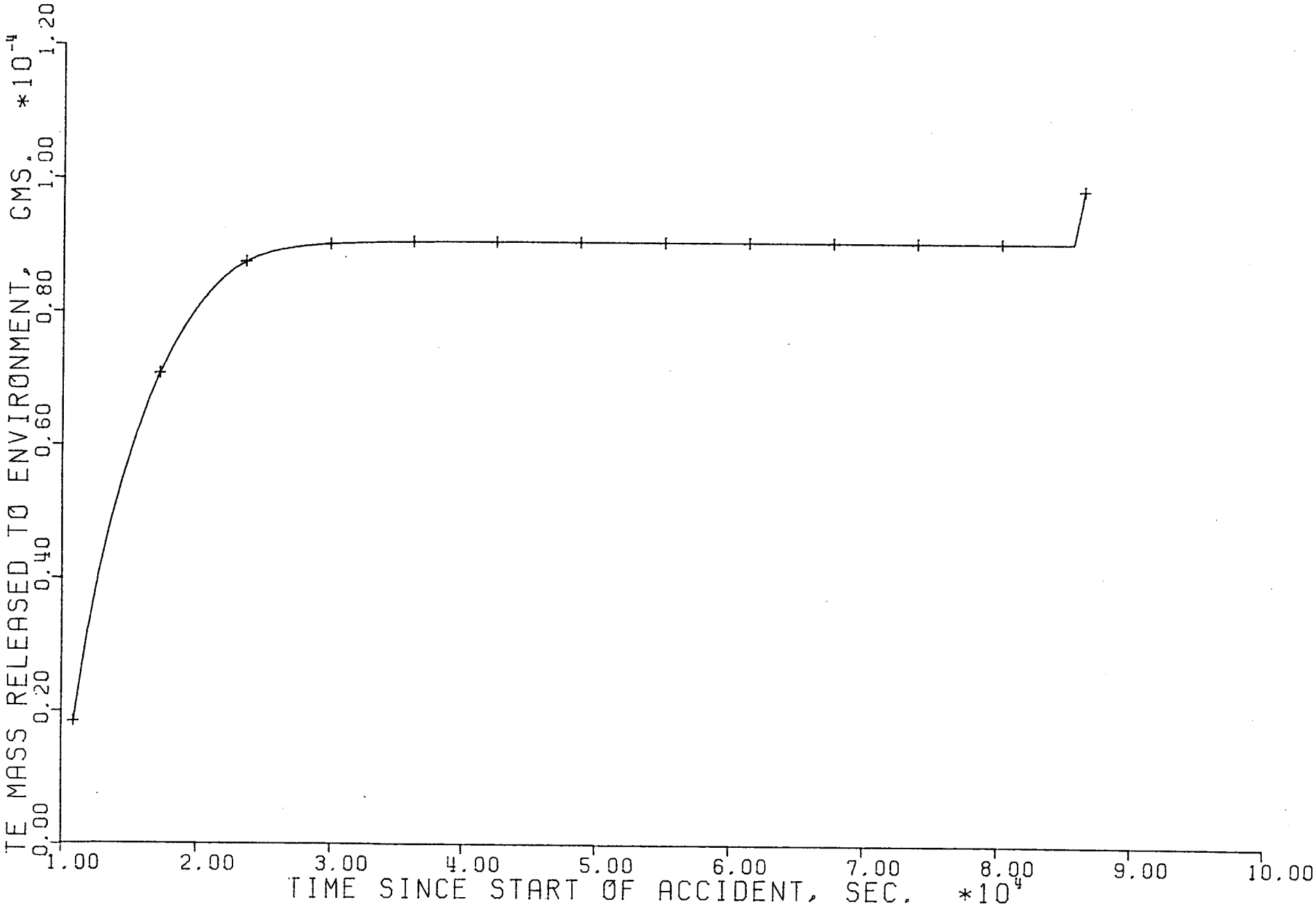
TE MASS RELEASED TO ENVIRONMENT, CMS. *10⁻⁴
0.00
0.20
0.40
0.60
0.80
1.00
1.20
1.00
2.00
3.00
4.00
5.00
6.00
7.00
8.00
9.00
10.00
TIME SINCE START OF ACCIDENT, SEC. *10⁴

FIGURE 5.112

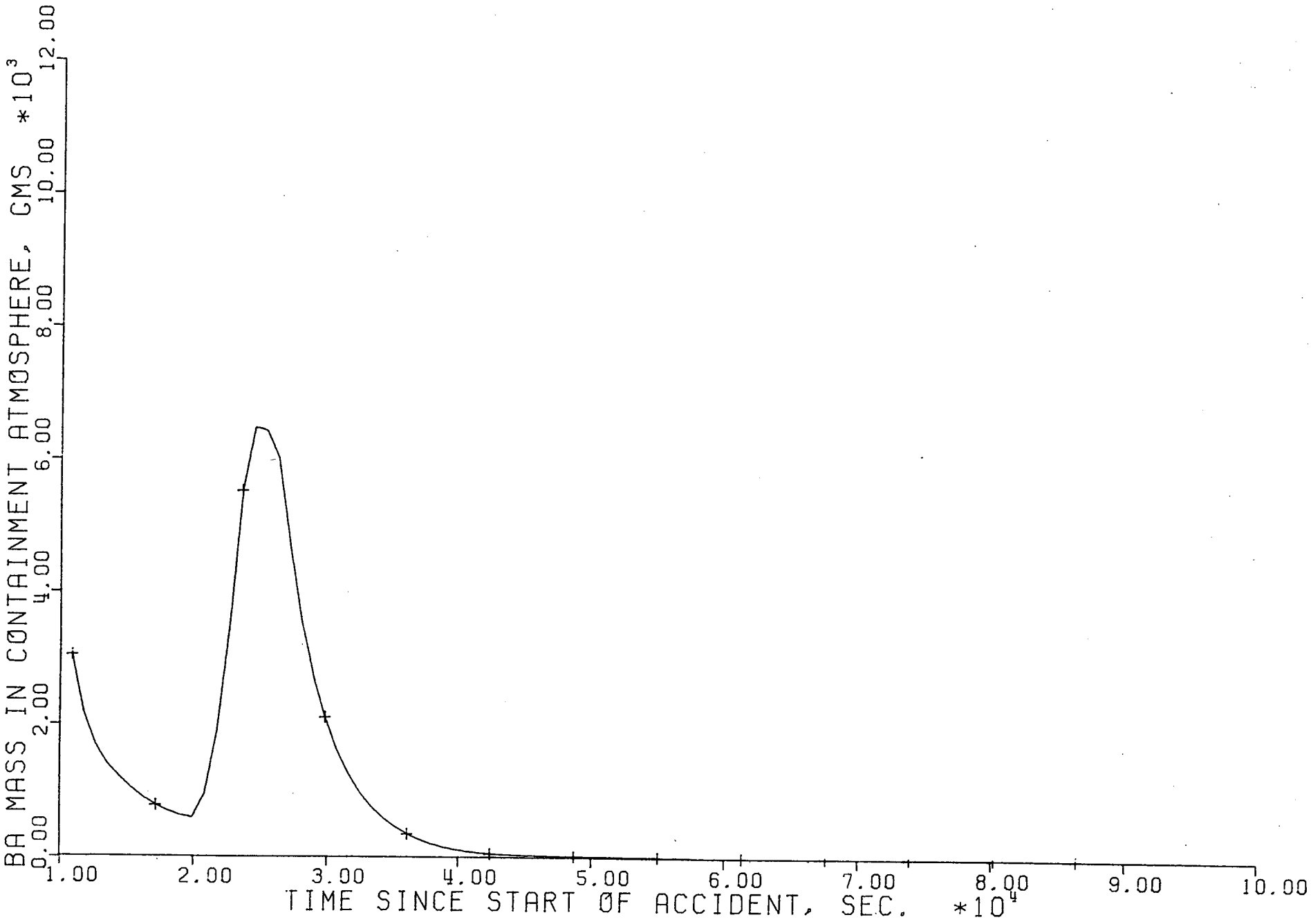
BA MASS IN CONTAINMENT ATMOSPHERE, CMS *10³
0.00
2.00
4.00
6.00
8.00
10.00
12.00
1.00
2.00
3.00
4.00
5.00
6.00
7.00
8.00
9.00
10.00
TIME SINCE START OF ACCIDENT, SEC. *10⁴

FIGURE 5.113

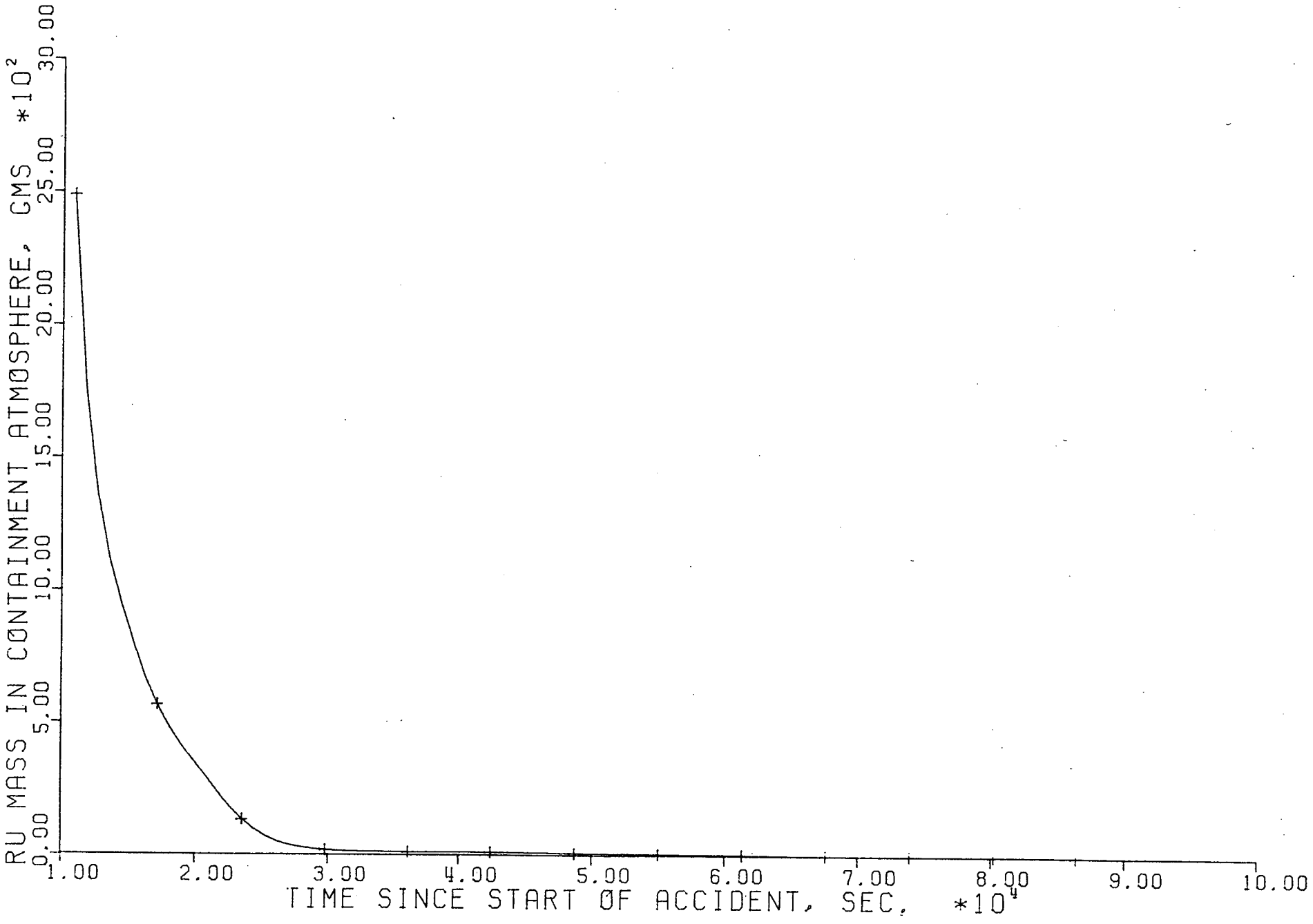
RU MASS IN CONTAINMENT ATMOSPHERE, GMS *10²
0.00
5.00
10.00
15.00
20.00
25.00
30.00
1.00
2.00
3.00
4.00
5.00
6.00
7.00
8.00
9.00
10.00
TIME SINCE START OF ACCIDENT, SEC. *10⁴

FIGURE 5.114

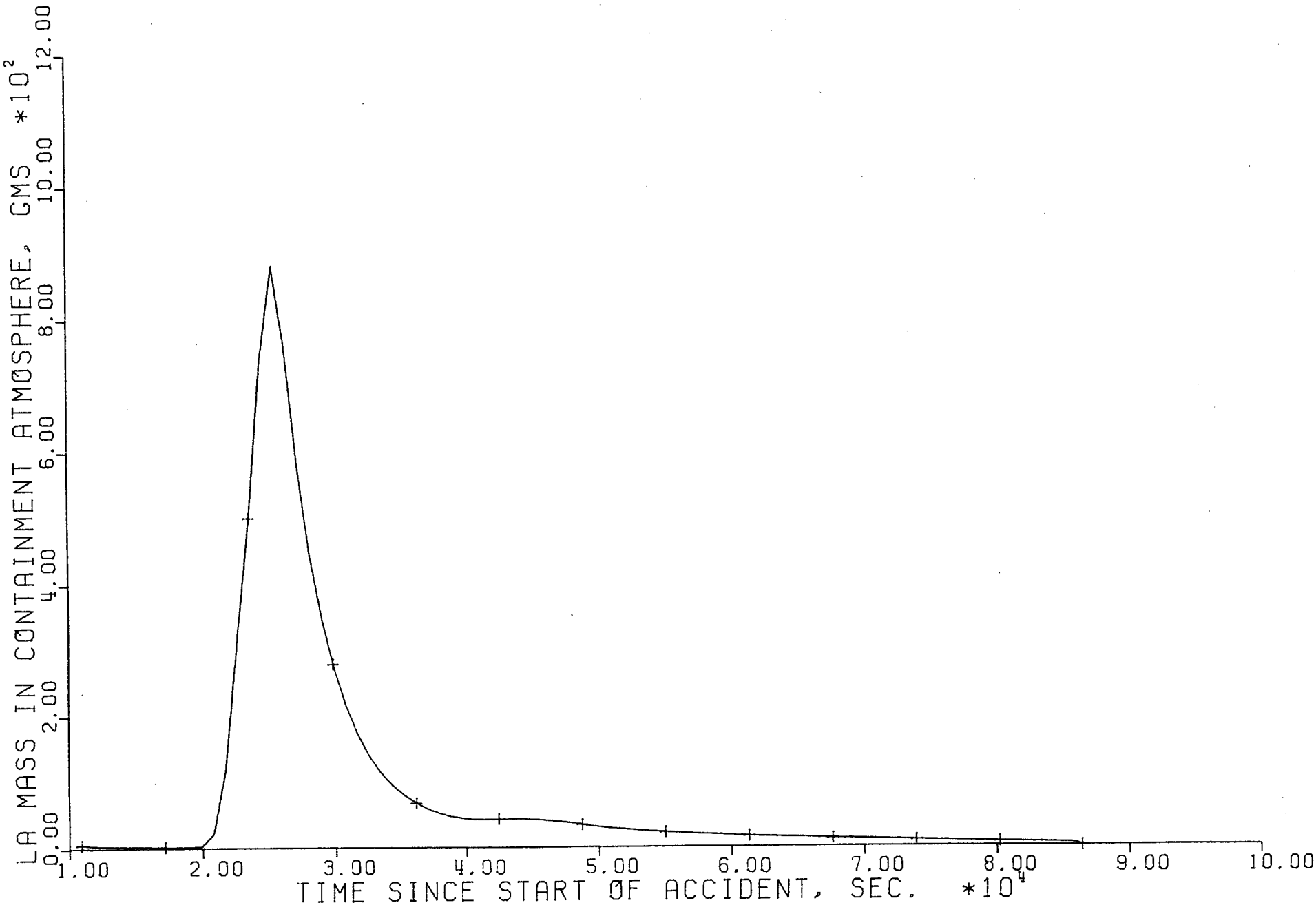
LA MASS IN CONTAINMENT ATMOSPHERE, GMS *10²
0.00
2.00
4.00
6.00
8.00
10.00
12.00
1.00
2.00
3.00
4.00
5.00
6.00
7.00
8.00
9.00
10.00
TIME SINCE START OF ACCIDENT, SEC. *10⁴

FIGURE 5.115

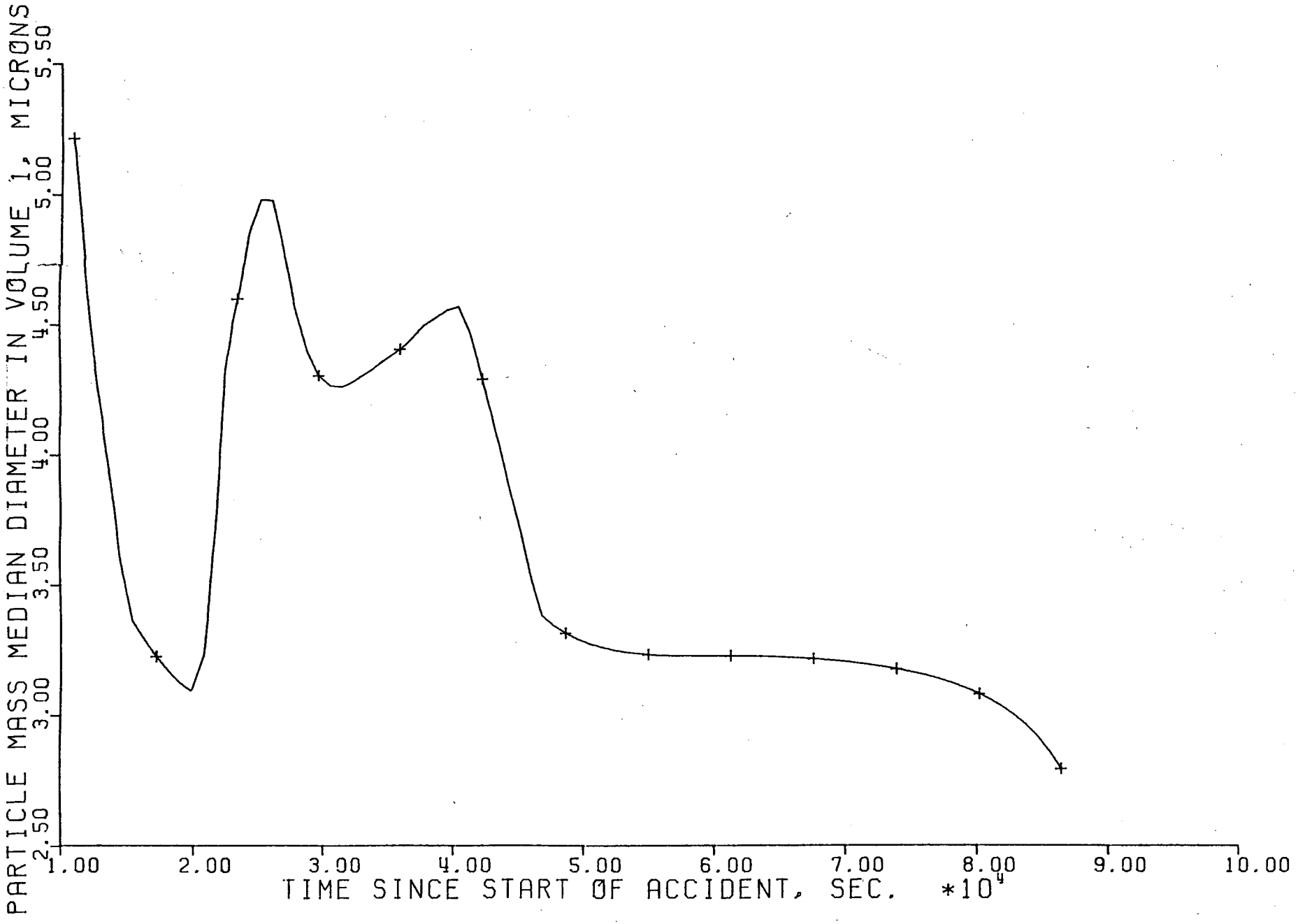
PARTICLE MASS MEDIAN DIAMETER IN VOLUME 1, MICRONS
2.50
3.00
3.50
4.00
4.50
5.00
5.50
1.00
2.00
3.00
4.00
5.00
6.00
7.00
8.00
9.00
10.00
TIME SINCE START OF ACCIDENT, SEC. *10^4

FIGURE 5.116

6.0 CONSEQUENCE ASPECTS

The re-evaluation of source terms as reported in this document can have an important impact on the projected consequences of an accident. To provide a context for these revised source terms, NYPA has calculated the impact of the NYPA source terms on the projected consequences of an accident at IP-3. The results of this calculation demonstrate that the revised source terms could dramatically reduce the projected consequences of an accident.

6.1 CRAC-2 Code*

The source term values calculated in this study and reported in Section 5 for the two accident scenarios were used to evaluate public consequences. These calculations were done with the CRAC-2 computer code.

The consequence analysis is based on Indian Point site-specific data, including meteorology, demography and topography. The analysis assumes that no evacuation efforts would be undertaken to mitigate the consequences of the accident sequences.

Each CRAC-2 run uses a continuous series of measured hourly meteorological conditions. A set of runs with a randomly selected start time is made to form a probability distribution. The calculated health effects, based on simulation of radiation exposure, are combined to form frequency distributions of consequences versus probability for a chosen hypothetical accident sequence. The program is input with libraries of site specific population and meteorological data.

6.2 Discussion of Results

Table 6.1 shows the amount of core inventory available for release to the atmosphere at time of containment failure** for the two accident scenarios.

---

* Calculations of Reactor Accident Consequences Version 2, CRAC-2. NUREG/CR-2326. Sandia National Laboratories, 1983.

** Although the containment does not fail because its calculated pressure is below the failure limit, the calculations performed in the consequence analysis assume containment failure 24 hours after the start of accident. The standard assumption for containment failure is 72 hours.

Table 6.2 makes a comparison of the fraction of core inventory available for release to the environment calculated with MATADOR II for this study with those of WASH-1400. It is observed that the fission product inventory calculated and available for release is generally a factor of 100 lower than WASH-1400, except for noble gases. With source terms at the newly calculated levels, a reduction in risks was hypothesized.

Table 6.3 presents the consequence results for various types of damage indices. The table gives the number of people affected in terms of a conditional probability for the occurrence of the damage.

Table 6.4 presents the WASH-1400 source terms to permit comparison of the differences that accrue from a decrease in released fission products to the environment from the accident.

Early Fatalities

No early fatalities are calculated for either of the sequences studied with NYPA source terms and thus no figures exist for this damage index. This is mainly due to the extremely small amounts of iodine and cesium available in the containment for release in case of containment failure.

The plot of conditional probability of early fatalities versus number of people affected is shown in Figure 6.1 with WASH-1400 source terms. The conditional risk of early fatalities as a function of distance from the plant is shown in Table 6.5 for the WASH-1400 and NYPA source terms. The CRAC-2 calculations compute a zero probability for early fatalities at any distance from the plant with NYPA source terms and a decreasing probability with distance for WASH-1400 source terms. Figure 6.2 shows early fatalities are non-existent with realistic source terms.

Latent Fatalities

Figure 6.3 shows the "conditional consequence curve" for latent fatalities. This curve shows the likelihood of latent fatalities given the specified magnitude of release at containment failure.

The curve shows that there are 10 latent fatalities with a conditional probability of 1.6 percent with the NYPA source terms. By comparison, the

WASH-1400 source terms result in 10 latent fatalities with a conditional probability of 100 percent and 10,000 latent fatalities at a conditional probability of 1.6 percent.

The figure also shows that the conditional probability drops sharply beyond a certain value of the latent fatality.

Bone Marrow Dose

The bone-marrow dose is an equivalent to whole-body dose. In the present study, a plot of the conditional probability for bone marrow dose as a function of distance from the plant is shown in Figure 6.4 for various dose values. The curve shows the bone marrow dose is far below the 200 Rem value. Furthermore, the plot of the bone marrow dose of 5 Rem is seen to fall off markedly beyond distances of 2.5 miles.

Thus the radiation dose likely to be absorbed by the public due to a core melt accident is quite small and even this is confined to a location very close to the plant.

On the same Figure 6.4 a plot of bone marrow dose for 200 Rem and 50 Rem as a function of distance is plotted with WASH-1400 source terms. The 200 Rem plots show a rapid decrease beyond the 10 miles from the plant.

Table 6.6 presents the bone marrow dose as a function of distance from the plant for both NYPA and WASH-1400 source terms. The bone marrow dose with realistic NYPA source terms is very small and decreases rapidly with distance as shown in Figure 6.5.

6.3 Uncertainty in Consequence Calculation

The consequence analysis results for NYPA source terms and WASH-1400 show significant differences because of the extremely low magnitude of the fission product released to the environment with NYPA source terms. It should be noted that these calculations were done with no evacuation and therefore no uncertainty is associated with evacuation models.

However, recognizing that the introduction of uncertainties given the large number of variables present in the consequence model can

significantly impact the results, one of the study tasks was to establish the degree to which uncertainties in the source term calculations would affect the consequence results. Accordingly, a CRAC-2 computer code run was performed with NYPA source terms increased by a factor of 100, resulting in a still extremely low probability of early fatalities. Table 6.7 presents the consequence results for the arbitrary increase of a factor of 100 in the calculated source terms.

6.4 Conclusions

1. No early fatalities occur due to the low amount of fission products released into the environment at containment failure. This is true even with factors of uncertainty added to the calculated source terms. The calculations were done with no evacuation.

2. The bone marrow dose with NYPA source terms is less than 5 Rem beyond 2.5 miles. The EPA protective actions guides suggest evacuation for doses greater than 5 Rem.

3. The number of latent fatalities with NYPA source terms is about a factor of 1,000 less than that calculated with the WASH-1400 source terms.

TABLE 6.1

FRACTION OF CORE INVENTORY AVAILABLE FOR RELEASE

E.P. SPECIES	FRACTION OF INVENTORY	
	TMLB EVENT	PUMP SEAL LOCA
Iodine	2.0×10^{-5}	4.5×10^{-6}
Cesium	1.6×10^{-5}	3.1×10^{-6}
Tellurium	6.5×10^{-9}	3.3×10^{-9}
Barium/Strontium	3.1×10^{-6}	2.4×10^{-6}
Ruthenium	1.5×10^{-6}	7.7×10^{-7}
Lanthanum	5.4×10^{-6}	2.5×10^{-6}
Noble Gases	0.90	0.90

TABLE 6.2

FRACTION OF CORE INVENTORY AVAILABLE

FOR RELEASE TO ENVIRONMENT

F.P. SPECIES	MATADOR II CALC.	WASH-1400 STUDIES	RATIO OF MATADOR II TO WASH-1400
Iodine	0.20×10^{-4}	0.70	2.8×10^{-3}
Cesium	0.16×10^{-4}	0.50	3.2×10^{-3}
Tellurium	0.65×10^{-8}	0.30	2.1×10^{-8}
Barium/Strontium	0.31×10^{-5}	0.06	5.1×10^{-5}
Ruthenium	0.15×10^{-5}	0.20×10^{-1}	7.5×10^{-5}
Lanthanum	0.54×10^{-5}	0.40×10^{-2}	1.35×10^{-3}
Noble Gases	0.90	0.90	1.0

* TMLB Accident Sequence

** PWR-2 Release Category

TABLE 6.3

CRAC-2 Results with NYPA Source Terms*

No. of People Affected	CONDITIONAL PROBABILITY Early Fatalities	Latent Fatalities
1	0	0.991
2	0	0.763
5	0	0.339
10	0	1.6×10^{-1}
20	0	6.4×10^{-2}
50	0	9.6×10^{-3}
100	0	0
200	0	0

*TMLB Accident Sequence

TABLE 6.4

CRAC-2 Results with WASH-1400 Source Terms

No. of People Affected	CONDITIONAL PROBABILITY Early Fatalities	Latent Fatalities
1	.998	1.0
2	.995	.999
5	.994	.999
10	.986	.999
20	.979	.996
50	.958	.982
100	.929	.976
200	.784	.957
500	.672	.946
1000	.587	.900
2000	.375	.773
10000	.137	1.59×10^{-1}
30000	1.0×10^{-3}	3.71×10^{-3}

TABLE 6.5

Conditional Probability for Early Fatality

Distance (Miles)	NYPA* Source Term	WASH-1400** Source Term
0.5	0	1.2×10^{-1}
1.0	0	7.2×10^{-2}
2.0	0	4.9×10^{-2}
2.5	0	4.2×10^{-2}
3.0	0	3.5×10^{-2}
4.0	0	2.0×10^{-2}
5.0	0	1.3×10^{-2}
7.0	0	7.5×10^{-3}
9.0	0	3.6×10^{-3}
10.0	0	2.8×10^{-3}

*TMLB Accident Sequence

**PWR-2 Release Category

TABLE 6.6

CRAC-2 Results on Bone Marrow Dose (Rem)

Distance (Miles)	NYPA* Source Term	WASH-1400** Source Term
0.5	9.65	6.4×10^{3}
2.5	1.76	6.02×10^{2}
4.0	9.0×10^{-3}	2.34×10^{2}
7.0	4.56×10^{-1}	1.0×10^{2}
9.0	3.4×10^{-1}	6.15×10^{1}
10.0	1.2×10^{-1}	1.75×10^{1}

*TMBL Accident Sequence

**PWR-2 Release Category

TABLE 6.7

CRAC Results into NYPA Source Terms

Increased by a Factor of 100

No. of People Affected	CONDITIONAL PROBABILITY Early Fatalities	Latent Fatalities
1	5.3×10^{-3}	1.0
2	3.9×10^{-3}	0.99
5	2.7×10^{-3}	0.99
10	1.5×10^{-3}	0.98
20	3.4×10^{-4}	0.97
50	0	0.68
100	0	0.40

FIGURE 6.1

NUMBER OF EARLY FATALITIES vs. CONDITIONAL PROBABILITY *

WASH 1400 SOURCE TERMS

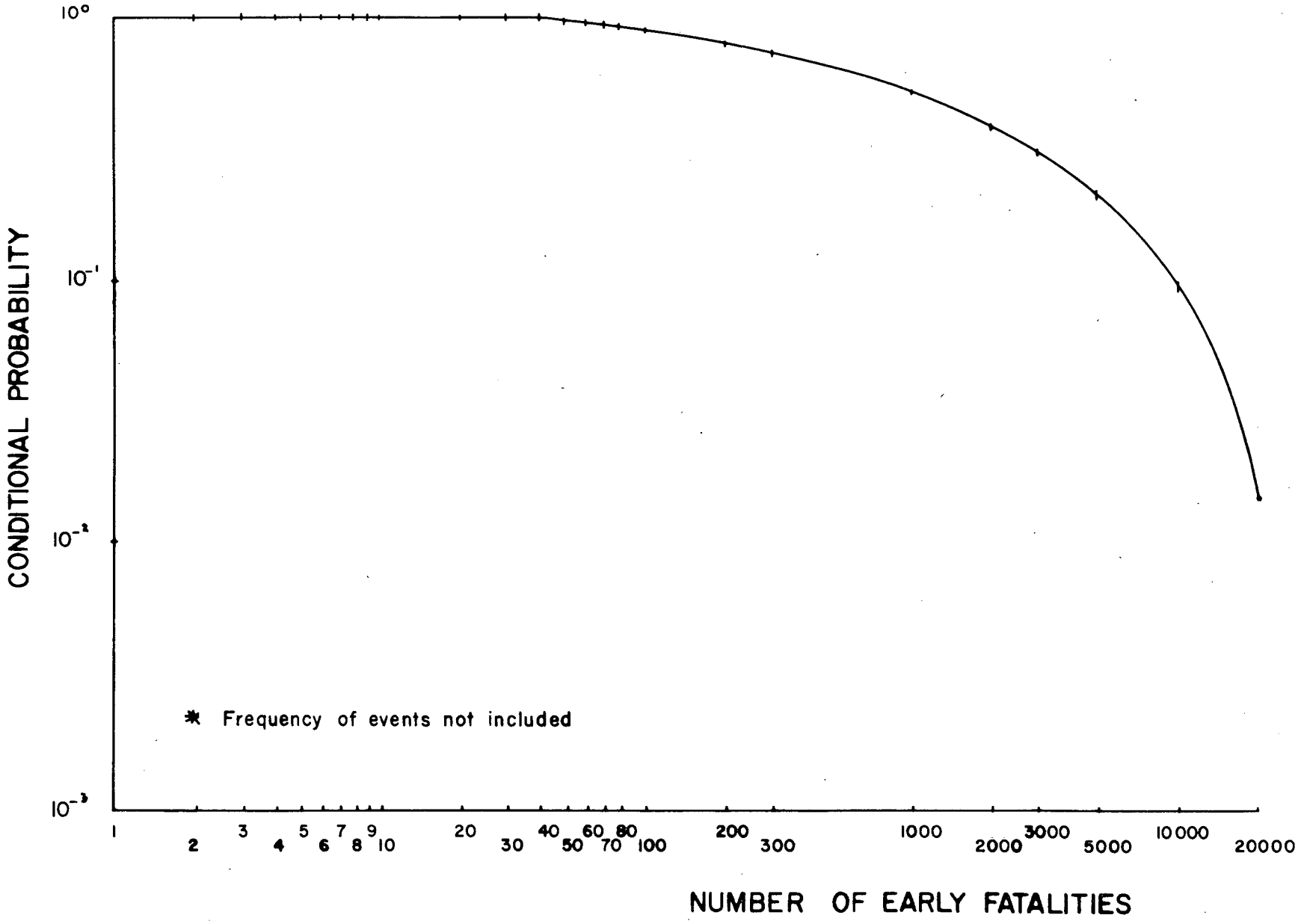

FIGURE 6.2

WASH 1400 SOURCE TERMS

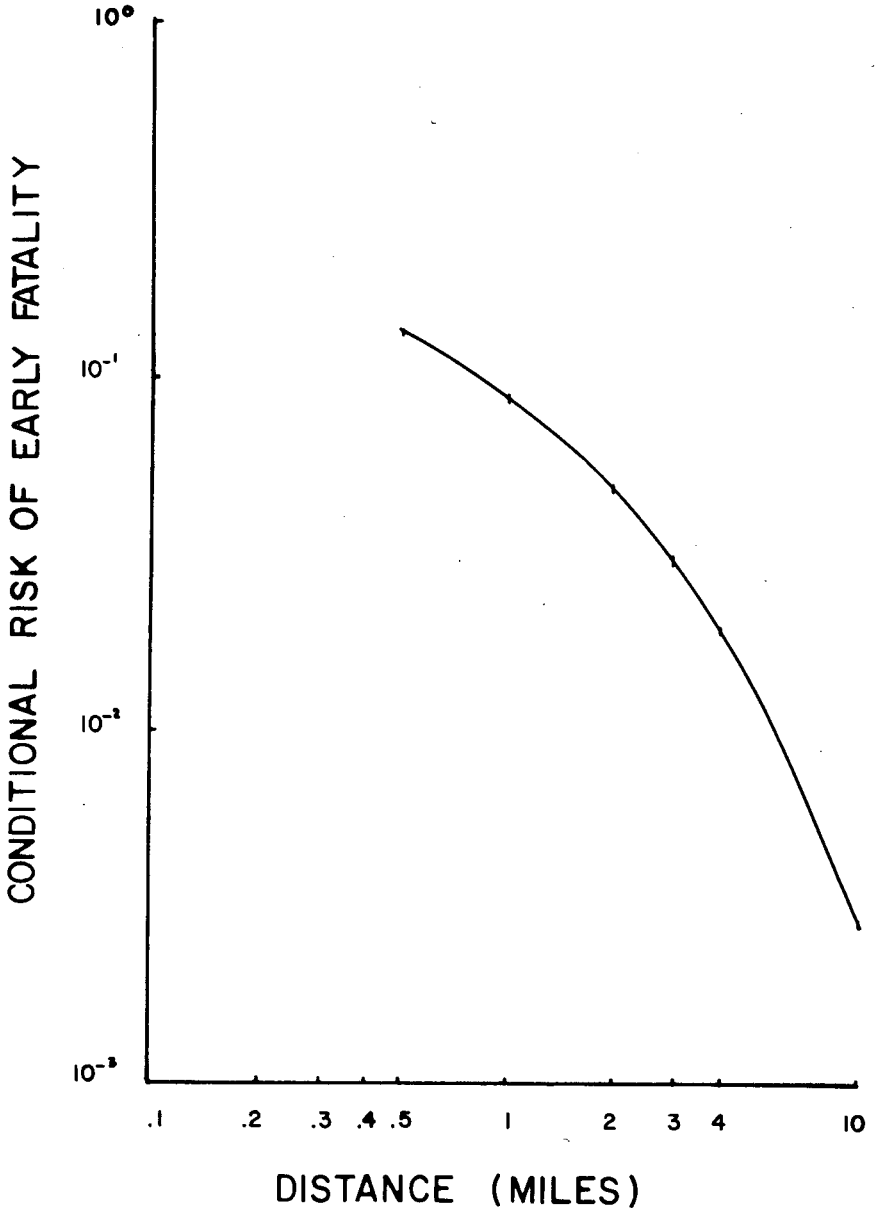

Note: No Curve for NYPA Source Terms as no Early Fatalities are Calculated

FIGURE 6.3

NUMBER OF LATENT FATALITIES vs. CONDITIONAL PROBABILITY *

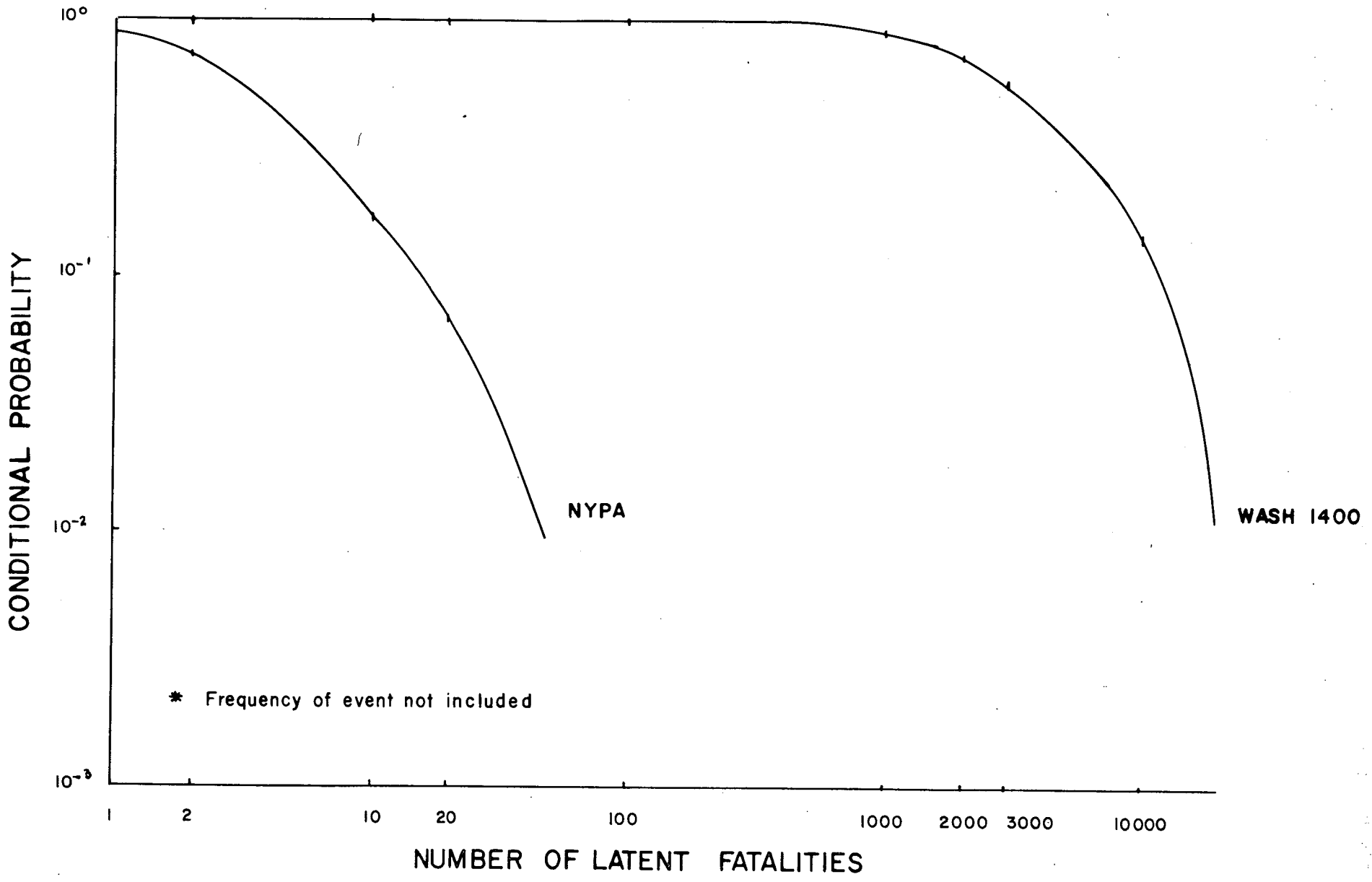

FIGURE 6.4

CONDITIONAL PROBABILITY vs. DISTANCE FOR BONE MARROW* DOSE (REM)

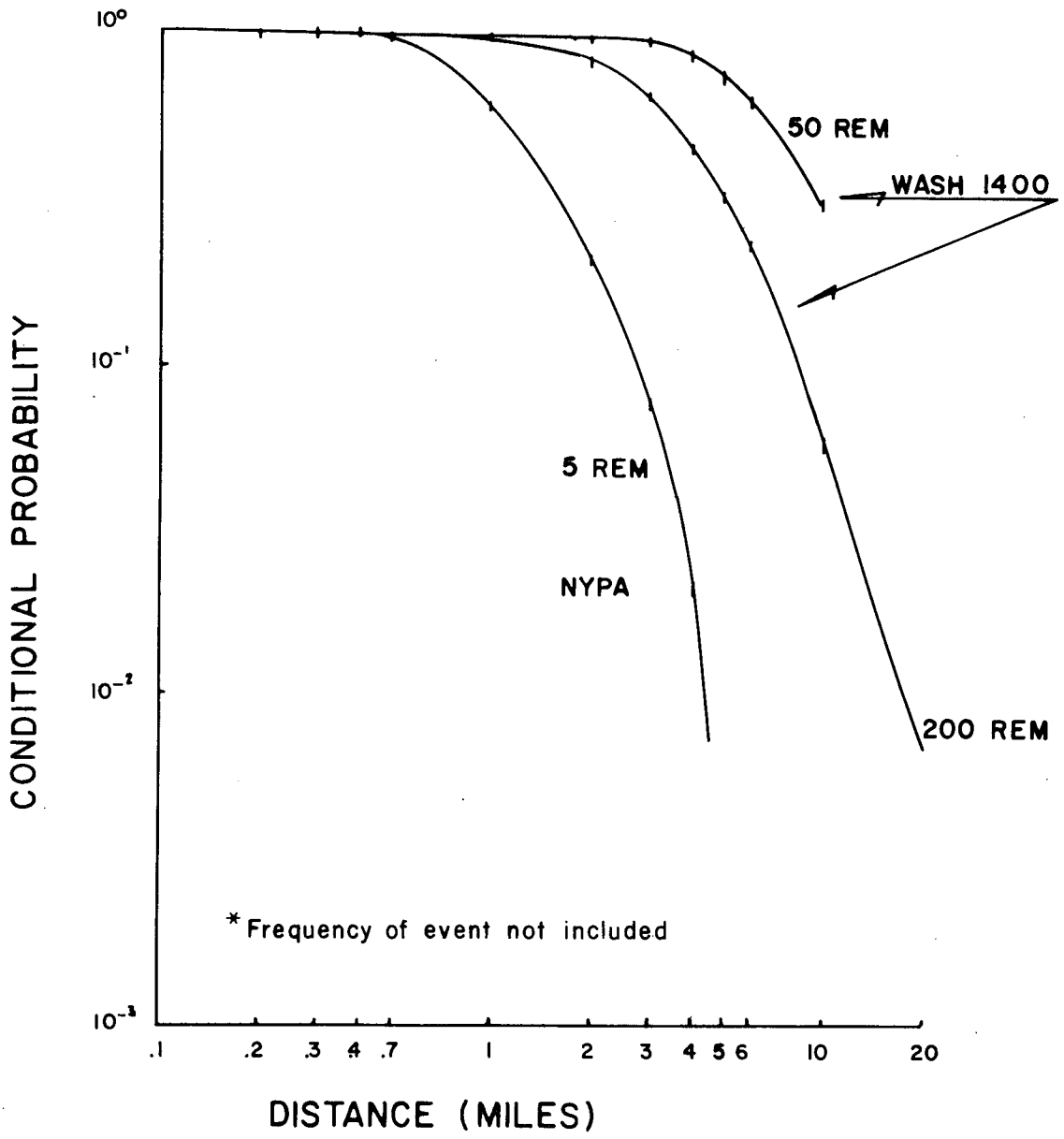

MEAN BONE MARROW DOSE vs. DISTANCE

FIGURE 6.5

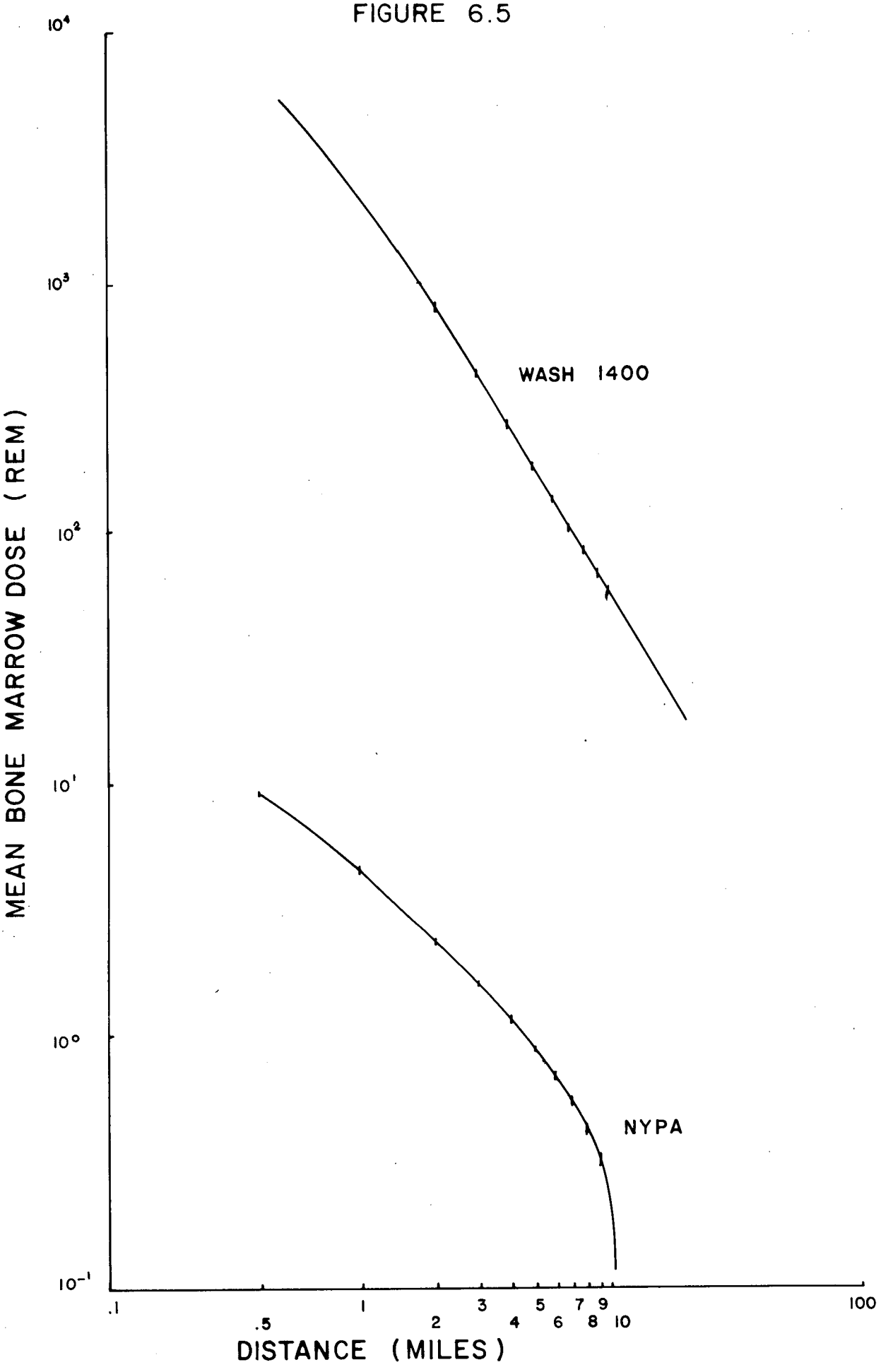

LEGEND

- Total Retention Factor
- Retention Factor in Upper Plenum
- Retention Factor in Hot Leg
- Retention Factor in Surge Line
- Retention Factor in Pressurizer
- Retention Factor in PORV & downstream piping
- F.P. Specie Released to Containment in Molecular Form
- F.P. Specie Released to Containment in Particulate Form
- F.P. Specie Retained on Walls
- F.P. Specie Retained on Particles
- F.P. Specie Retained by Chemisorption

Figure 1- Composite Result, Primary System
TMLB Accident Sequence

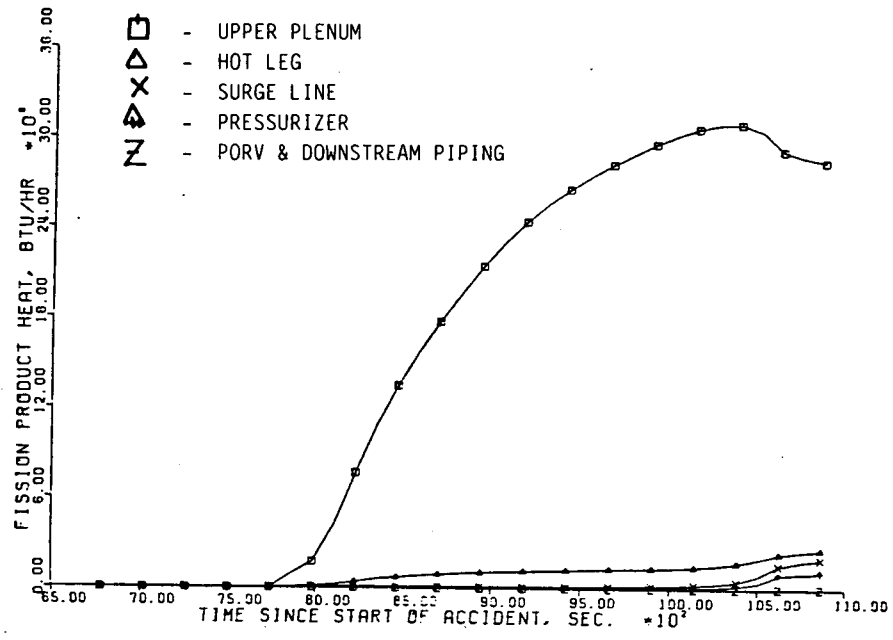

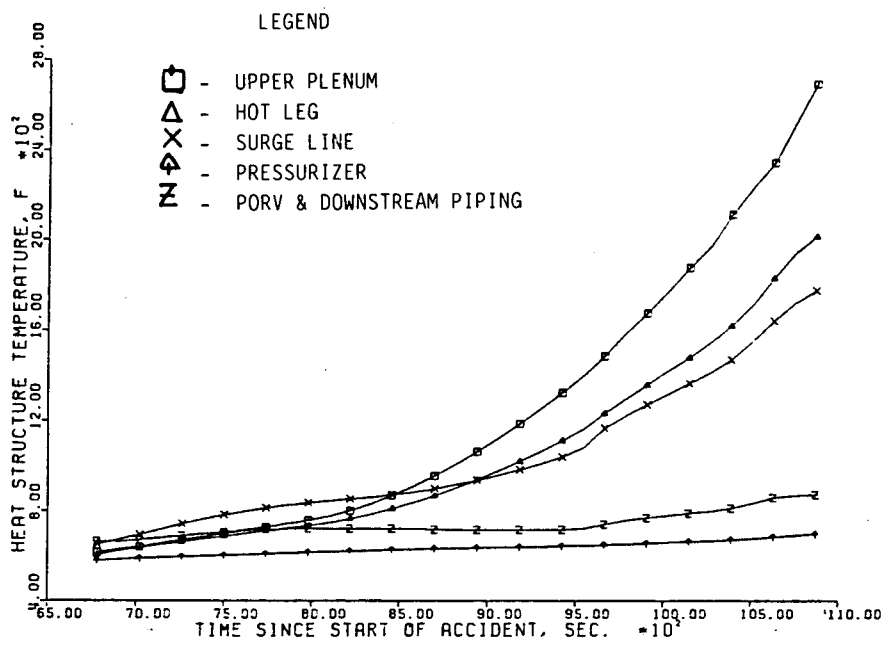

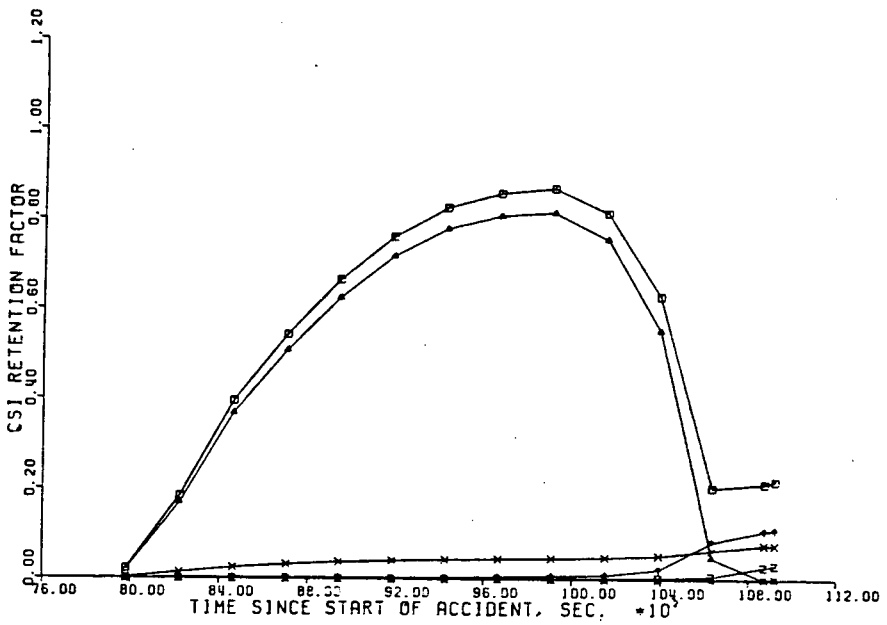

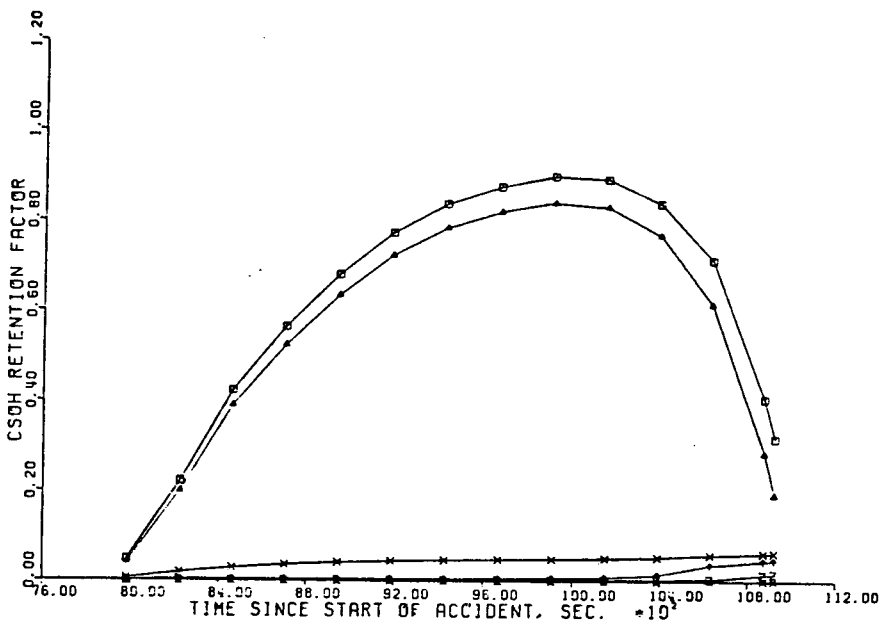

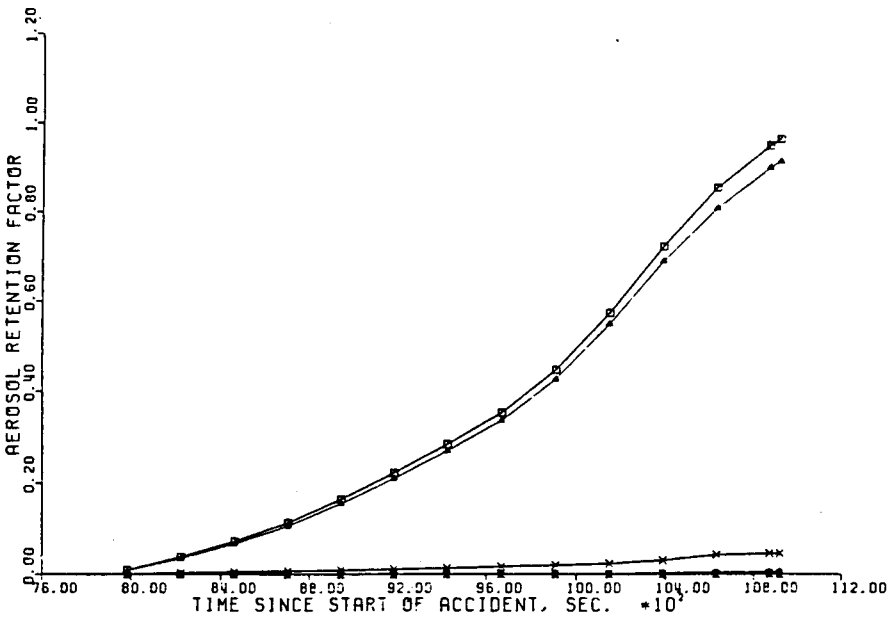

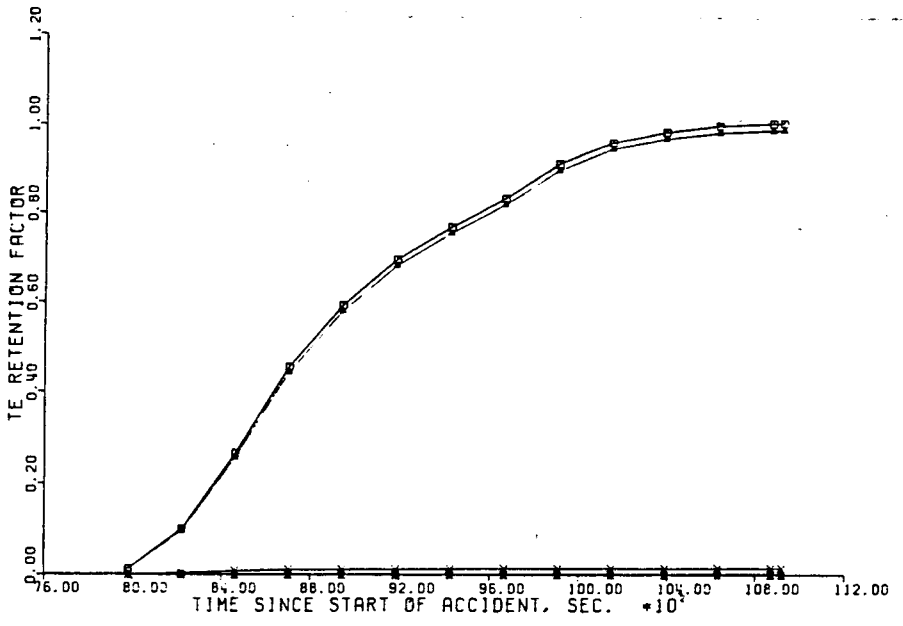

8706030335-01

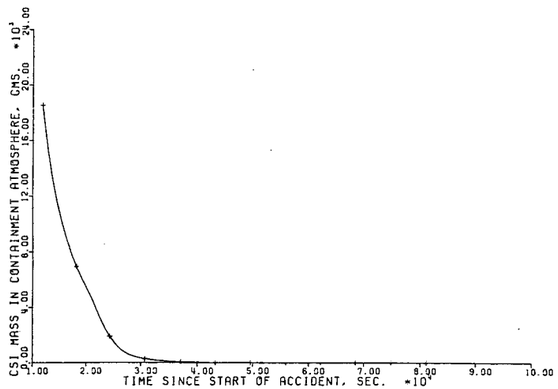

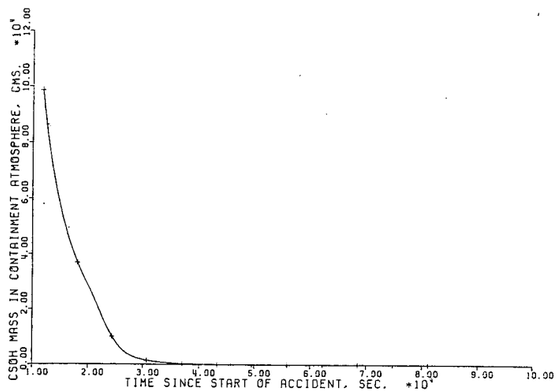

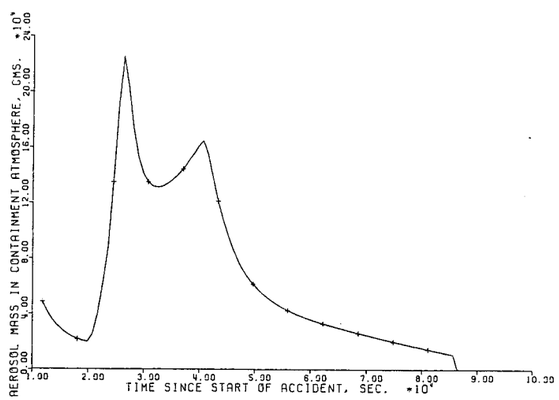

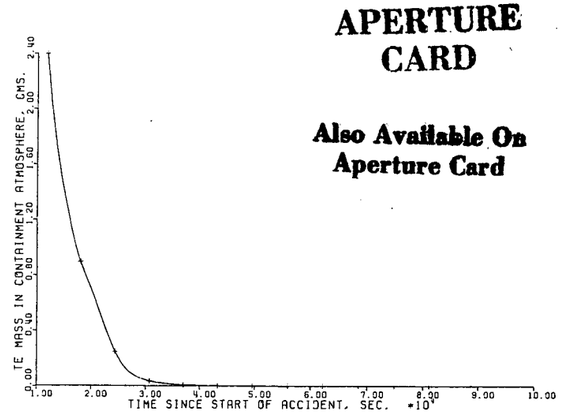

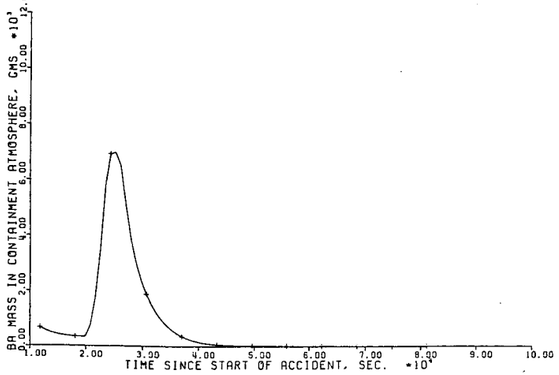

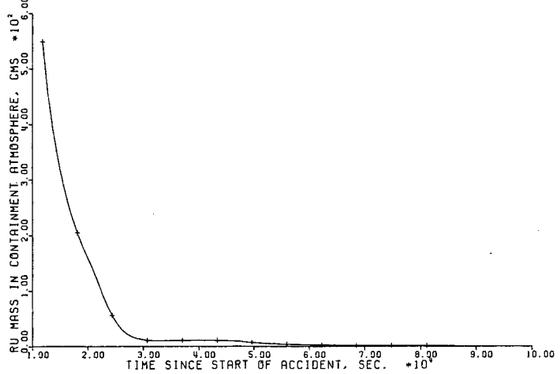

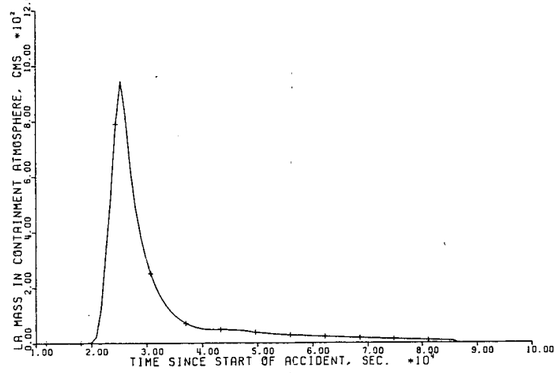

Figure 2- Composite Results, Containment
TMLB Accident Sequence

Figure 3- composite Results, Primary System
Pump Seal Loca Sequence

LEGEND

- Total Retention Factor
- Retention Factor in Upper Plenum
- Retention Factor in Hot Leg
- Retention Factor in SG Plenum
- Retention Factor in U-tube Section of SG
- Retention Factor in Cold Leg
- Retention Factor in RCS Pump
- F.P. Specie Released to Containment in Molecular Form
- F.P. Specie Released to Containment in Particulate Form
- F.P. Specie Retained on Walls
- F.P. Specie Retained on Particles
- F.P. Specie Retained by Chemisorption

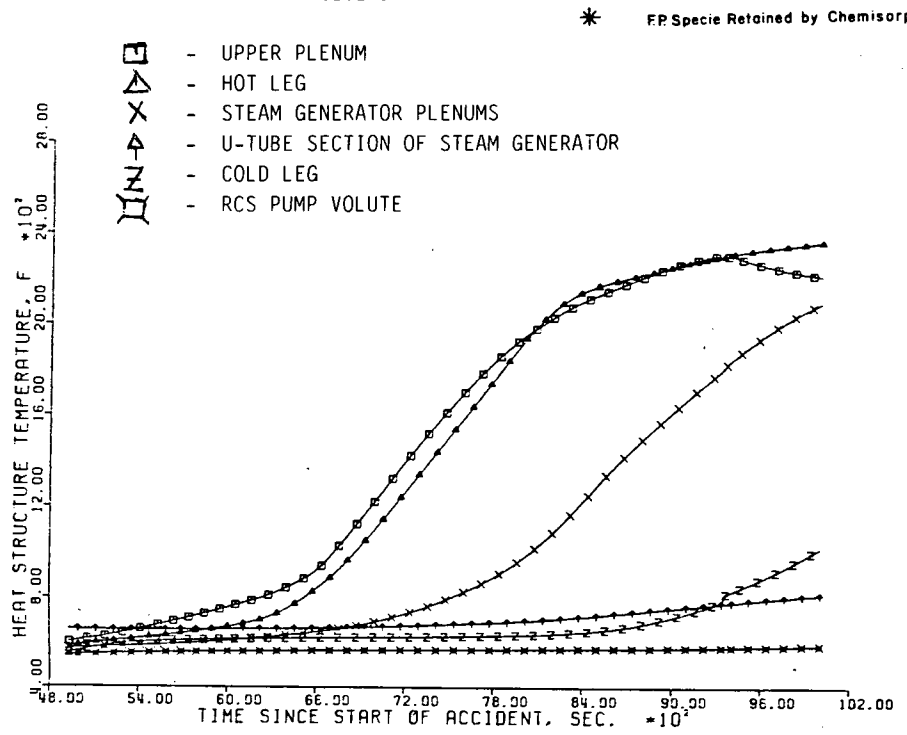

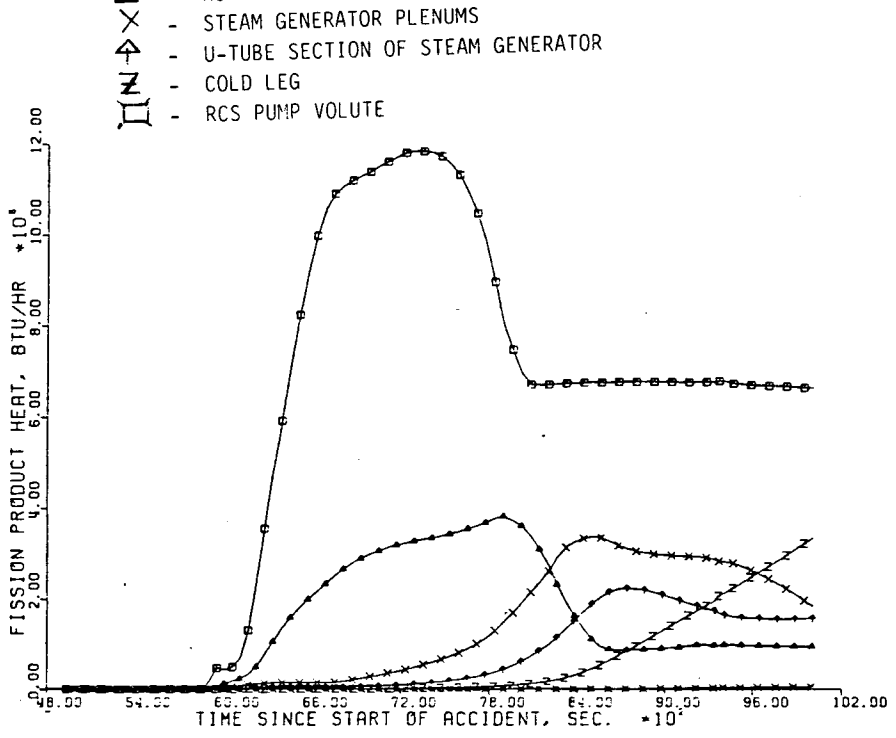

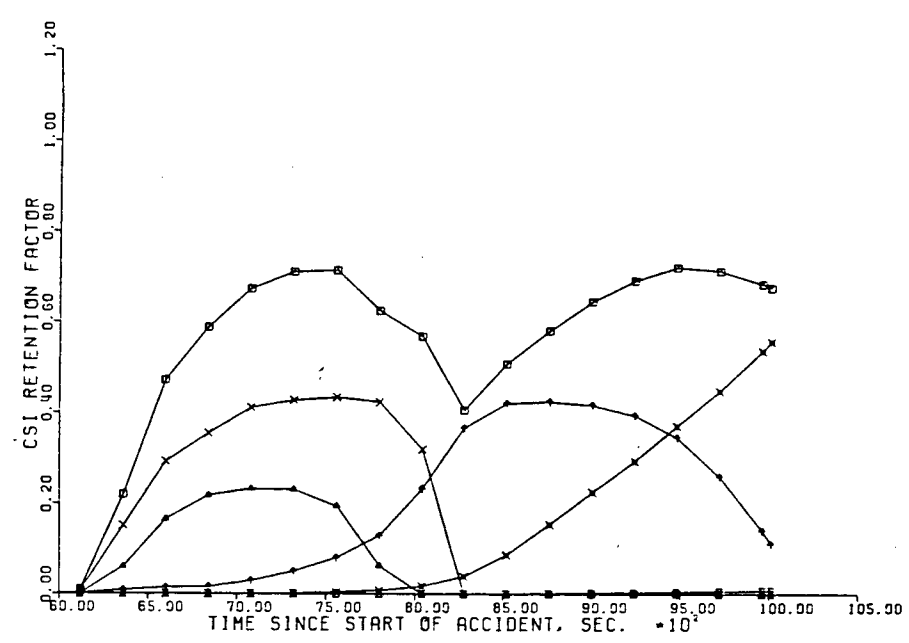

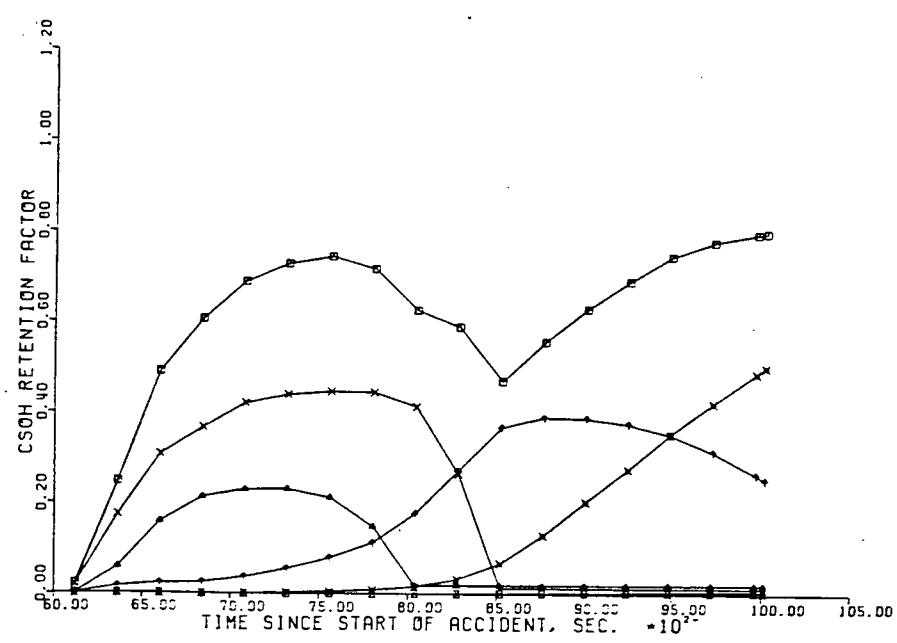

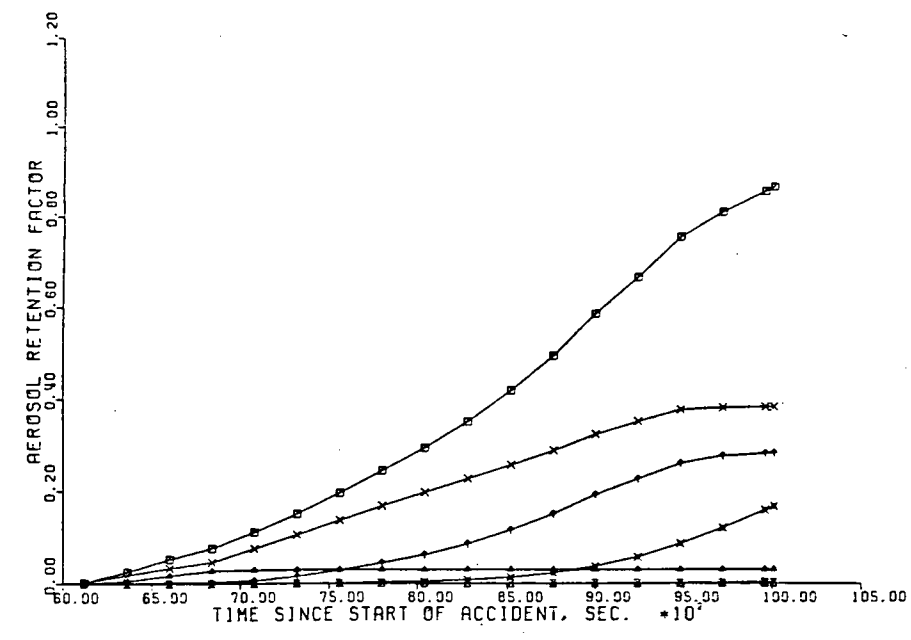

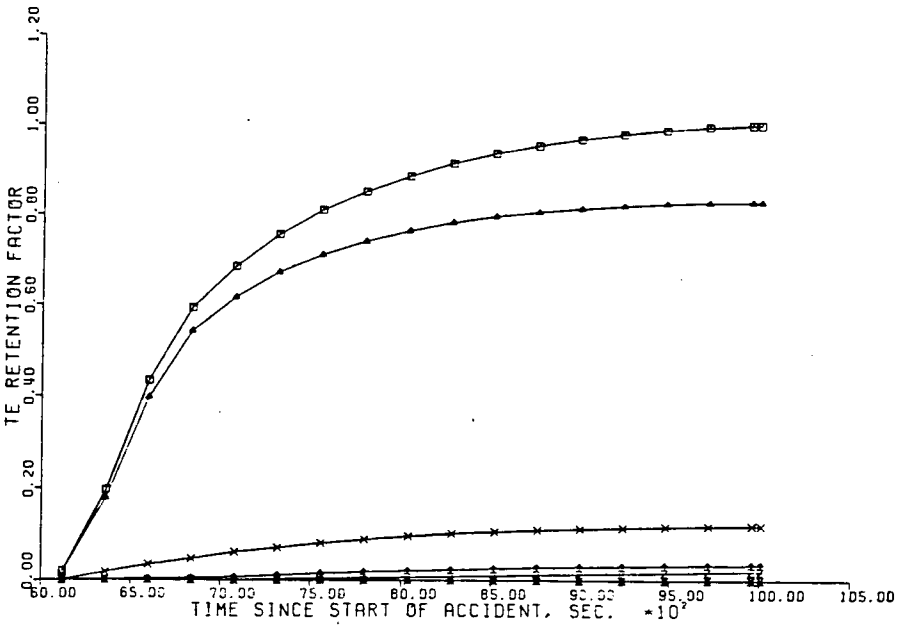

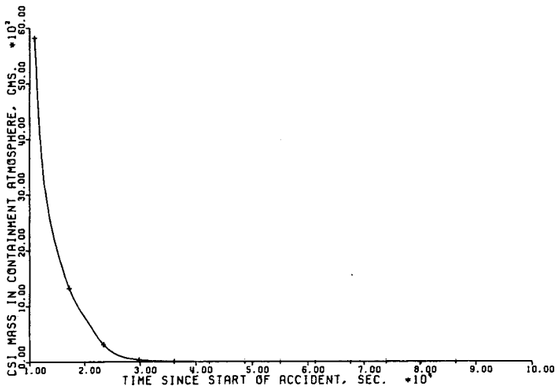

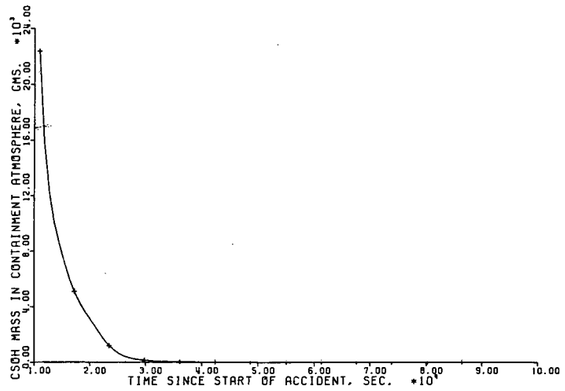

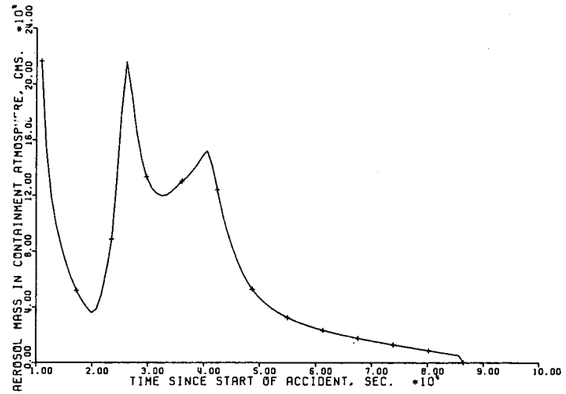

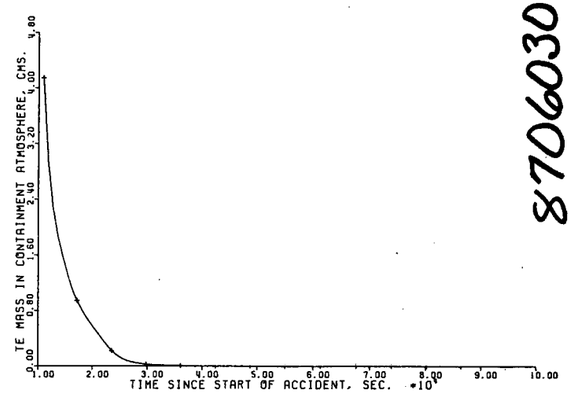

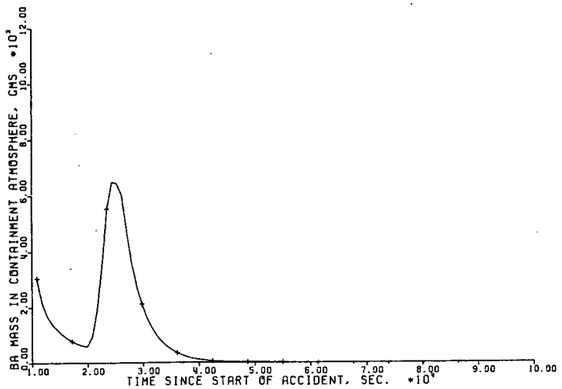

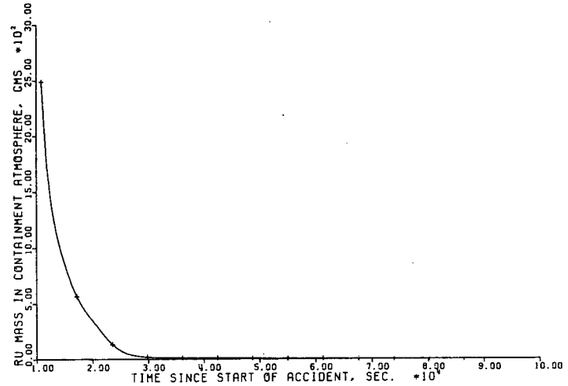

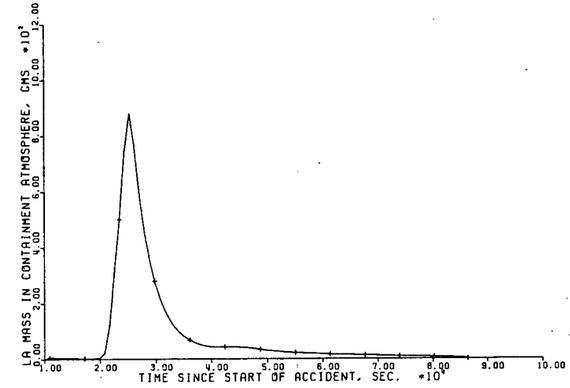

Figure 4- Composite Results, Containment
Pump Seal Loca Sequence

Source Term Safety Assessment

Indian Point 3 Nuclear Power Plant

New York Power Authority

Risk Management Associates and
New York Power Authority

Volume 2 of 2

Volume 2

SOURCE TERM
SAFETY ASSESSMENT
FOR THE
INDIAN POINT 3 NUCLEAR POWER PLANT

CONTENTS

Appendix A

ANALYSES OF THE V-SEQUENCE AT INDIAN POINT 3

APPENDIX A

An accident sequence of great interest in LWR's is the "V" sequence or interfacing systems LOCA.[1] Pressurized water reactors have both high pressure and low pressure piping systems. When the plants are producing power, the water that is used to directly cool the core is all within a high pressure system, because typical power operating pressures are above 2000 psi. However, when the plant is shutdown the pressures are significantly reduced for certain other activities, such as refueling. When in a low pressure regime, the valves that separate the high and low pressure piping systems can be opened. A concern that arises then is could the isolation valves that separate the high pressure and low pressure systems fail while the plant is at power. To do so could mean that the low pressure system might burst, leading to a loss of coolant accident. Further, much of the low pressure piping is outside of the containment structure. Such a LOCA would not only challenge the core, it could simultaneously bypass the containment if the break were outside of the containment. In addition, since the loss of water would be outside of the containment, there could eventually be such a loss of water inventory, that there would not be sufficient water to recirculate from the containment sumps for long-term cooling. After the initial injection phase was over and cooling water from the accumulators and refueling water storage tank had passed through the core and then through the break outside the containment, core melting would commence with a fairly direct path to the environment. This possible severe accident has long been recognized and designs purposely make it very unlikely. In the IPPSS[2], the mean frequency of the interfacing systems LOCA was only about

4×10^{-7}/Reactor year. Although this low probability event contributed about 1/2% to the core melt frequency, it was responsible for some 97% of the early fatality risk.

Because of the V-sequence dominance of the early fatality risk, it was decided to look more closely at both the assumptions and the analyses that produced these results. Several observations were made:

(1) The frequency of such an event is highly design dependent.

(2) The impact on the early fatality risk could be made much smaller if;

(a) No failures of the isolation valves that separate the high and low pressure piping systems would lead to a break outside of the containment,

or

(b) There were a break outside of the containment, the subsequent mass flow rate would be low enough (i.e. break size small enough) so that operator action could be taken to prevent core uncovery,

or

(c) Various radionuclides would be trapped along the pathway between the core and the point of entry to the environment, e.g., a smaller source term.

NYPA investigations therefore started with a closer examination of the integrity of various elements of the high and low pressure boundaries. The Indian Point Units (2 & 3) have an attractive design in that there are very few high-pressure/low-pressure pathways that penetrate the containment. The most important of these pathways or lines is the 14" Residual Heat Removal (RHR) suction line (see Figure 1). The major conclusions of analyzing this line are:

(1) Results of structural analysis show that with the strengthening of the one overstressed support outside the containment building, any break in the RHR piping is most likely to occur inside the containment.

(2) Leakage from Valve 732 based on Anchor Darling communications is low enough to give the operators ample time to prevent core uncovery, with the recommended modifications made to this valve.

(3) An ample amount of time (hours) is available for the operators, to take mitigative action to minimize/terminate the incident.

(4) The "V" sequence is a non-event and not important to risk.

Another path, the cold leg (discharge) lines, exists where a "V" sequence can be postulated has also been analyzed and included in this Appendix.

The major conclusion regarding the cold leg (discharge) line is:

The thermal hydraulic analysis for the event showed that core uncovery occurred in hours, during which time the operator can take proper steps to isolate the line without degrading any safety system.

Because of the above design configuration and capabilities, a closer examination of the IP3 "V" sequence shows that this can no longer be considered a major risk contributor.

With this introduction, details of the "V" sequence analysis are now presented.

Details of Analysis

A description of the RHR Suction path is shown in Figure 1. As a result of this design, the high-pressure/low-pressure valves are located inside

the containment building. In almost all other PWR systems, these valves are located outside the containment building. This is primarily because in other plants the low pressure recirculation pumps also serve as the RHR pumps. It is important to note that at IP3 the RHR pumps are NOT necessary to provide primary low-pressure recirculation. The RHR pumps provide a backup system only to the recirculation system. IP3 also has a relief valve in the low pressure piping after the two boundary valves which is within the containment building. The IP3 RHR suction path which, when postulated to fail during a classical V-sequence, accounts for approximately 90% of the total early fatality risk for the plant.

In the classical V-sequence the initiating event is assumed to be a break in the low-pressure piping beyond the boundary valves. Therefore, it is critical to know exactly where the break location is for the IP3 design, since these boundary valves are located inside the containment building. If it can be shown by detailed analysis that the break does in fact occur inside the containment building, the V-sequence would reduce to a less severe, standard DBA LOCA, which all nuclear power plants are designed to withstand. The approach taken in this analysis was as follows:

(1) Determine the system response and hydrodynamic loads placed on the system due to a postulated V-sequence.

(2) Perform an in-depth structural analysis based on the fluid transient forcing functions calculated in (1) above. Quantify all pipe stresses and pipe support loading. Then, attempt to determine the

break location as accurately as possible based on structural analysis and structural theory.

(3) Determine what passive mitigation features could and should be made to the system if the break is found to be outside the containment building.

(4) Review what effective active mitigation response (i.e., operator actions) would and could have on the results.

(5) Lastly, determine if any other leakage paths exist (i.e., cold leg injection path) that could result in a postulate V-sequence for IP3.

In the classical V-sequence, as applied to IP3, the high-pressure isolation valves are MOV-731 and MOV-730, with MOV-730 being the pressure boundary between Class 2501R (Sch 140) and Class 601R (Sch 40) piping. MOV-731 is assumed left open, MOV-730 is assumed to fail instantaneously, and Valve 732 is closed. All piping is assumed to be filled with water, the pressure upstream at MOV-730 is 2250 psia and downstream is 50 psia initially, which is the case during normal operations. Since pressure waves propagating in the water in the piping system will result in a pressure shock to the system, RELAP 5 MOD1[3] was used to calculate the system hydrodynamic response. Initial conditions for the analysis are as follows:

(1) Failure time for the disc in MOV-730 is 10 milliseconds.

(2) All piping walls are to be considered rigid.

(3) The hot leg is a large source relative to the RHR system piping.

(4) Upstream of MOV-730 the pressure is 2250 psia and the temperature 605°F.

(5) Downstream of MOV-730 the pressure is 50 psia and the temperature 120°F.

Some results of the RELAP 5 analysis and the nodalization of the RHR system are shown in Figures 2 through 22. The maximum pressure in the piping occurs behind the reflected shock wave at approximately 80 milliseconds, the magnitude being 4010 psia and duration being 5 milliseconds near Valve 732 and systematically dropping in the upstream direction. Duration for maximum pressure, measured above the steady-state pressure of 2250 psia, at any point in the piping is approximately 20 milliseconds. The situation of MOV-731 instantaneously failing and MOV-730 being assumed open was also addressed. The resulting pressure wave and hydrodynamic forces were similar to those of the other case. Another important result from the RELAP 5 analysis was that the relief valve (RV1896) had no immediate effect on the pressure wave spikes. This is because the time constant for the relief valve is approximately one second, and the maximum pressure wave spikes occur prior to .16 seconds. Therefore, the waves have dissipated prior to the relief valve opening.

According to the initial conditions, the system is flooded and the significant loading on the system is due directly to the internal pipe pressure wave propagation, with no fluid flow occurring. The only unbalanced forces are those due to the pressure differential in the pipe for 20 milliseconds. Therefore significant stresses in the piping are the hoop and axial stresses due to the pressure wave only. Forcing functions developed in the RELAP 5/FORCE analysis were then utilized as input to a fully dynamic structural analysis using the ANSYS[4] computer code. Possible failures of the RHR line were analyzed with respect to both

ductile rupture and brittle fracture of the pipe wall. The support system for the RHR pipe was also analyzed along with possible failure modes of Valve 732. Specifically, the following locations were considered for possible failure:

(1) Straight pipe sections

(2) Elbow pipe sections

(3) Branch piping sections

(4) Piping supports

(5) The penetration

(6) Valve 732

Detailed results of the dynamic structural analysis and the nodalization model used are shown in Figures 23 through 26 and Tables 1 through 5. The analysis shows that failure of the piping will most likely occur from the unbalanced transient fluid forces produced on the piping and not the peak or steady state pressure. If failure were to occur, it would most likely occur at the high-stress areas in the piping. These high-stress points are at certain elbows (see Tables 1 & 2) inside the containment.

Ductile rupture from a bursting pressure viewpoint was also considered. Analysis shows that a sustained pressure of 4693 psia is required to burst the pipe under consideration. Since the fluid transient analysis shows a peak pressure of 4010 psia at 100°F, the pipe can be considered to be under the bursting limit.

Also, possible failure locations in the piping are influenced by the results that show the piping supports are overloaded and will most likely

fail (see Table 4). In particular, overloading or failure of the supports allows the piping to deflect significantly during the pressure wave transients.

In addition, the containment piping penetration was also evaluated for failure. Yielding or possible failure of the penetration outside or inside containment would be possible mainly from the large deflections that occur in piping due to the piping supports that fail. Since all supports inside containment and only one support outside containment is overloaded (Table 4), the penetration would have a higher probability of failure inside containment.

Taking all of the above into consideration, one can conclude that a failure of the piping itself is most likely to occur inside the containment. However, if the one overloaded support outside containment is modified to resist the transient loads, then the possibility of failure outside containment would be virtually eliminated.

Anchor Darling, the valve manufacturer of valve 732, was contacted to determine the effect a pressure spike of 4000 psi for approximately 5 milliseconds followed by a steady state pressure of 2250 psi would have on the valve. Mr. J. Chapple of Anchor Darling[5] indicated he had witnessed the effects of overpressure on these type valves and would predict the following:

> "The upstream disc would lift off the seat allowing pressure to enter the bonnet chamber. Leakage would occur in the body to bonnet-bolted joint and the steam packing due to internal pressure. The downstream

disc would bow and seat leakage (small) would occur due to possible stellite cracking. At hydro pressure of 1100 psi, the disc material is at 90% of yield. No catastrophic failure and no significant damage to the valve body is anticipated".

Further calculations[6] were performed to estimate the amount of leakage through and out of value 732. It was determined that the peak leakage would be no more than 500 gpm, if certain modifications are made to this valve.

Leakage of 500 gpm at 2250 psia and 605°F is equivalent to approximately a one-inch break. Adding to this the two-inch relief line (RV 1896) leakage, the equivalent break size would be three inches. Small break analysis previously done for TMI Lessons Learned (NUREG-0578)[7] requirements show that the primary system would be below 600 psia in approximately 45 minutes for a three-inch break. The importance of determining the approximate leakage rates and time of primary system depressurization to below 600 psia on the results will be made apparent in the subsequent conclusions.

Based on the results obtained in the analysis, the V-sequence is a non-event and will have minimal impact on plant risk at IP3. Justification for this statement is borne out by (1) the structural analysis results; (2) the functional mitigative capabilities of the IP3 plant specific design; and (3) diverse combinations of possible mitigative operator actions.

(1) Results of the structural analysis show that with the strengthening of

the one overstressed support outside the containment building, any break in the RHR piping is most likely to occur inside the containment. This would reduce the V-sequence to a less-severe DBA-LOCA, which is a licensing requirement for all nuclear power plants.

(2) If no break in the piping occurs, only leakage through valve 732 has to be contended with. As stated earlier, the maximum leakage of Valve 732 is less than 500 gpm, with modificatioins to the valve. The minimal safety injection pump flow rate is 465 gpm[8]. There is also an additional 90 gpm being added to the reactor coolant system (RCS) via the charging pumps. Since these minimal pump flow rates are larger than the possible maximum leakage (555 gpm in versus 500 gpm out), and the integrated leakage from Valve 732 would be substantially less than the 500 gpm maximum due to depressurization of the RCS, no core uncovery will occur. Furthermore, leakage flow through the relief valve (RV 1896) would be available for recirculation. It should be noted that the above conditions would only persist until the RCS is below 600 psia (approximately 45 minutes). Recirculation would be established at that time, and since the RHR system is independent from the recirculation system, any break and/or leakage in the RHR system would not preclude long term cooling of the reactor core. Most classic V-sequences cannot be mitigated because in most situations the pipe where the break occurs is an integral part of the recirculation system, thus precluding establishment of a long-term cooling mode. This is not the case with the IP3 design. Water inventories available for making up the leakage from Valve 732 are large enough so that no operator action to replenish these inventories would be necessary for at least six hours.

The time frame involved here is important. Note that it is hours and not minutes.

(3) A sizeable amount of active mitigation (operator action) can be accomplished when a time frame of hours is involved. Firstly, the source of leakage can be determined. Once this is done and the RCS is below 600 psia, the interlocks on the two high pressure boundary valves (MOV-730 and MOV-731) are inhibited. The operator could try cycling the valves to attain closure, thus isolating the line. If closure of either valves could not be achieved, the refueling water storage tank (RWST) could be replenished using the city water system on-site. This would guarantee sufficient inventory for an almost indefinite duration. When the RCS is adequately cool, the leaking Valve 732 and/or the RHR line could be isolated, freeze-plugged, and/or repaired. The primary heat removal mechanism during this time period would be via the steam generators and the auxiliary feedwater system.

Figure 27 shows that another path exists where a V-sequence could be postulated. This path would involve a break in line 60 outside of containment. A break inside containment would not result in a V-sequence for the same reasons stated earlier in the suction line case. To evaluate the impact of the outside containment break, a MARCH 2.0 run was made to determine the core uncovery time. It was found that core uncovery occurred at approximately 538 minute (almost 9 hours). Again, the time frame involved is of the order of hours, <u>not</u> minutes. Further, given that length of time, the operator could close MOV-1869A and MOV-1869B to isolate the line. This isolation would <u>not</u> degrade any required safety system.

The only effect this isolation would have, would be to obviate a back-up mode option to the existing safety injection system where either the RHR pumps or recirculation pumps act as booster pumps to the high head safety injection pumps.

Calculation of public risk from postulated degraded core events at nuclear power plants should be based on that plant's specific system design to ensure credibility of results. In this study of a postulated V-sequence, it was shown that if a failure were to occur for the RHR suction path case, it would almost certainly occur inside containment. Leakage from Valve 732 can be tolerated because diversity of the IP3 systems and the specific design of the RHR system allows for various mitigative actions to be taken. Mitigative action is also plausible because the time frame involved is on the order of hours, not minutes for both leakage path cases. Therefore, it is concluded that a postulated V-sequence is a non-event and will have minimal impact on plant risk at IP3.

REFERENCES

1) "Reactor Safety Study", WASH-1400, U. S. Nuclear Regulatory Commission, October, 1975.

2) "Indian Point Probabilistic Safety Study", New York Power Authority, March, 1982.

3) "MAINSTREAM-EKS ANSYS Code Manual", Volumes 1 & 2, Boeing Computer Services Company.

4) "MAINSTREAM-EKS ANSYS Code Manual", Volumes 1 & 2, Boeing Computer Services Company.

5) IUP-6096, Letter from United Engineers & Constructors to New York Power Authority, dated 10/8/82.

6) Calculations done by Anchor Darling, June, 1984.

7) Report on Small Break Accidents for Westinghouse NSSS System WCAP-9600, Westinghouse Electric Corporation, dated June, 1979.

8) Indian Point Unit FSAR, dated July, 1982.

9) "As Built Stress Report", RHR System, Line Number 10 - Problem #408 & 423, Job Order 6604-168, UE & C.

10) Calculation Set Numbers 6604-199-02.1 & 6604-199-02.2, UE & C.

11) ASME Boiler & Pressure Vessel Code, Section III, Division 1, Appendices, 1983 Edition.

12) ASME Boiler & Pressure Vessel Code, Section III, Sub-section NB, 1980 Edition.

TABLE 1 STRESS SUMMARY FOR OUTSIDE CONTAINMENT

PIPING OF LINE NO. 10

NODAL POINT	POSTULATED EVENT: PEAK PRES(1)	POSTULATED EVENT: STRESS INTENSITY DUE TO UNBALANCED FORCES(2)	TOTAL (3) MAXIMUM STRESS DUE TO DWT + OBE	TOTAL ASME (4) CODE STRESS (NB.3642) EQ. 9	LEVEL D (5) SERVICE ALLOWABLE STRESS
	(PSIA)	(KSI)	(KSI)	(KSI)	(KSI)
4	4010	7.90	2.37	37.41	60.0
1		7.55		41.96	
3		7.29		37.18	
5		7.14		37.12	

NOTES:

(1) From output of RELAP 5 MOD1run

(2) From output of ANSYS run

(3) From Ref. 10

(4) Loading combination: DWT + OBE + Transient Load (Press + Moment)

(5) 3Sm but not greater than 2Sy (NB - 3656 of ASME Code (Ref. 12)
Sm = 20 KSI For material SA 312 Type 304 at 120°F
(Ref. 11)

TABLE 2 STRESS SUMMARY FOR INSIDE CONTAINMENT PIPING OF LINE NO. 10

NODAL POINT	POSTULATED EVENT: PEAK PRES. (1)	POSTULATED EVENT: STRESS INTENSITY DUE TO UNBALANCED FORCES (2)	TOTAL (3) MAXIMUM STRESS DUE TO DWT + OBE	TOTAL ASME (4) CODE STRESS (NB.3652) EQ. 9	LEVEL IS (5)3 SERVICE ALLOWABLE STRESS	REMARK
	(PSIA)	(KSI)	(KSI)	(KSI)	(KSI)	
42	3800	55.85	2.32	82.94	60.0	OVERSTRESS
43		45.38		67.90		OVERSTRESS
44		17.63		50.31		
48		16.06		48.81		

NOTES:

(1) From output of RELAP 5 MOD1 run

(2) From output of ANSYS run

(3) From Ref. 10

(4) Loading combination: DWT + OBE + Transient Load (Press + Moment)

(5) $3S_m$ but not greater than $2S_y$ (NB - 3656 of ASME Code (Ref. 12)
S_m = 20 KSI For material SA 312 Type 304 at 120°F (Ref. 11)

TABLE 3

SUPPORT LOADS FOR

OUTSIDE CONTAINMENT PIPING SYSTEM

OF LINE NO. 10

SUPPORT MARK NO.	POSTULATED[1] EVENT LOAD (KIPS)	ORIGINAL[2] DESIGN LOAD (KIPS)
AC-H-10-11-R	± 24.16	- 7.578
AC-R-10-12-H	± 1.49	± 2.588
AC-R-10-13-H	± 4.85	± 3.910
AC-H-10-14-S	± 4.28	- 4.607

NOTES:

(1) From the output of ANSYS run

(2) From Ref. 9

TABLE 4 SUPPORT LOADS FOR

INSIDE CONTAINMENT PIPING SYSTEM

OF LINE # 10

SUPPORT MARK NO.	POSTULATED[1] EVENT LOAD (KIPS)	ORIGINAL[2] DESIGN LOAD (KIPS)
AC-H-10-1-R	± 45.46	- 6.755
AC-H-10-1-R	± 33.09	- 2.980
AC-H-10-3-R	± 30.43	- 3.745
AC-H-10-4-R	± 38.91	- 5.603
AC-R-41-H	±102.90	+ 4.255
AC-R-40-H	± 36.56	± 2.54
AC-H-10-5-R	± 17.54	- 4.686
AC-H-10-6-R	± 4.74	- 5.829
AC-H-10-7-R	± 51.84	- 1.079

NOTES:

(1) From the output of ANSYS runs

(2) From Ref. 9

TABLE 5: LOADS OF PENETRATION K DUE TO THE POSTULATED EVENT

LOAD	(1) Axial (Kips)	Shear (Kips)	Torsion (K-in)	Bending Moment (K-in)
From Outside Containment	186.90	11.01	15.0	463.78
From Inside Containment	145.10	19.60	221.0	1000.00
(2) Envelop Results	186.90	19.60	221.0	1000.00
(3) Design Load for Emergency Cond.	-5.16	7.63	-53.8	406.0

NOTES:

(1) Shear & Moment are combined vectorially from Y & Z Components

(2) The maximum values occur at a different instant. Hence, the envelop values instead of absolute sum were used for the estimation.

(3) From UE&C penetration calculation J.O. 6604.168, Ref. 9.

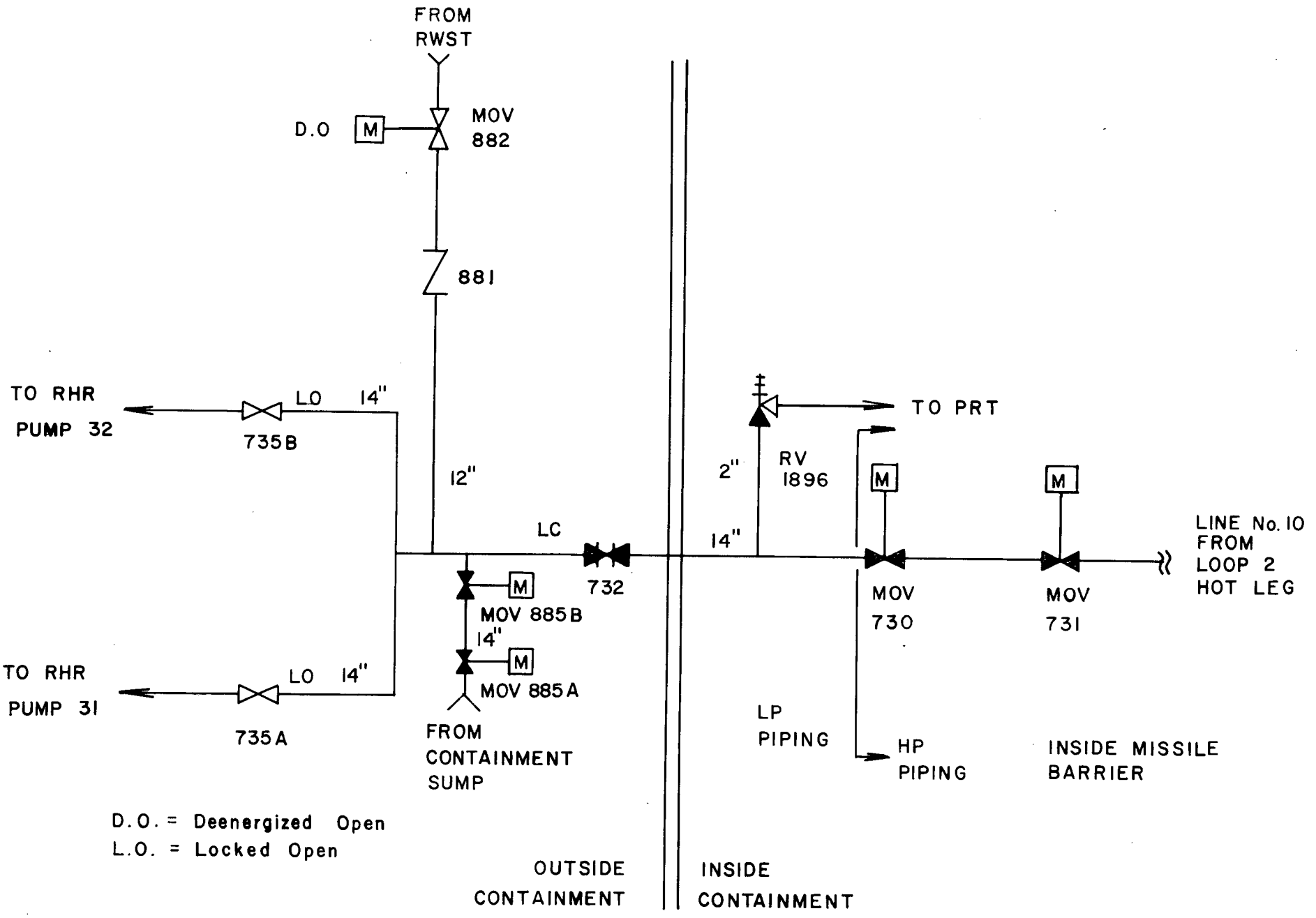

FIGURE 1 Indian Point 3 RHR Suction Path

V-SEQUENCE TRANSIENT OF RHR LINE No. 10

INDIAN POINT UNIT No. 3

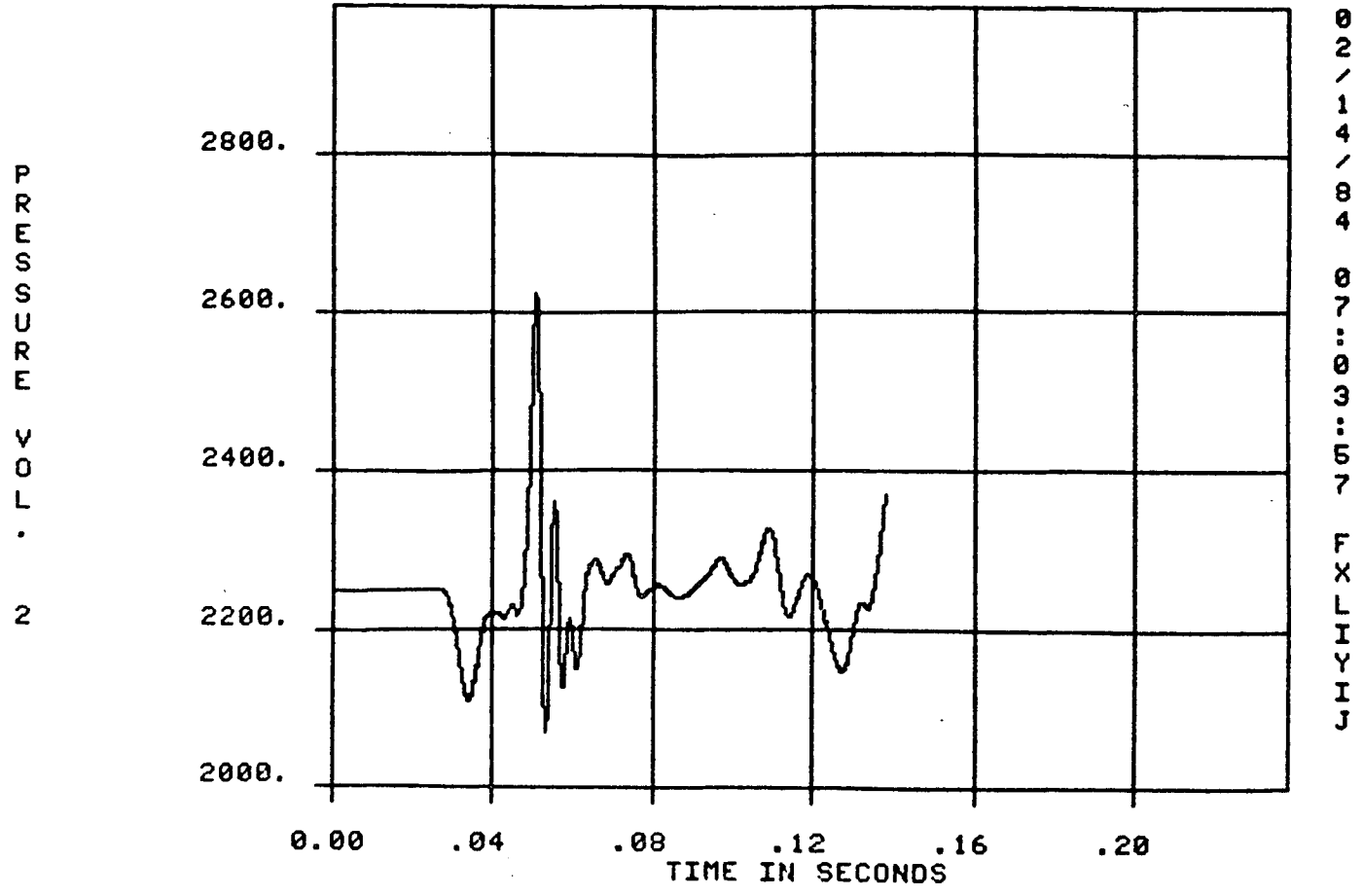

FIGURE 2

V-SEQUENCE TRANSIENT OF RHR LINE No.10

INDIAN POINT UNIT No.3

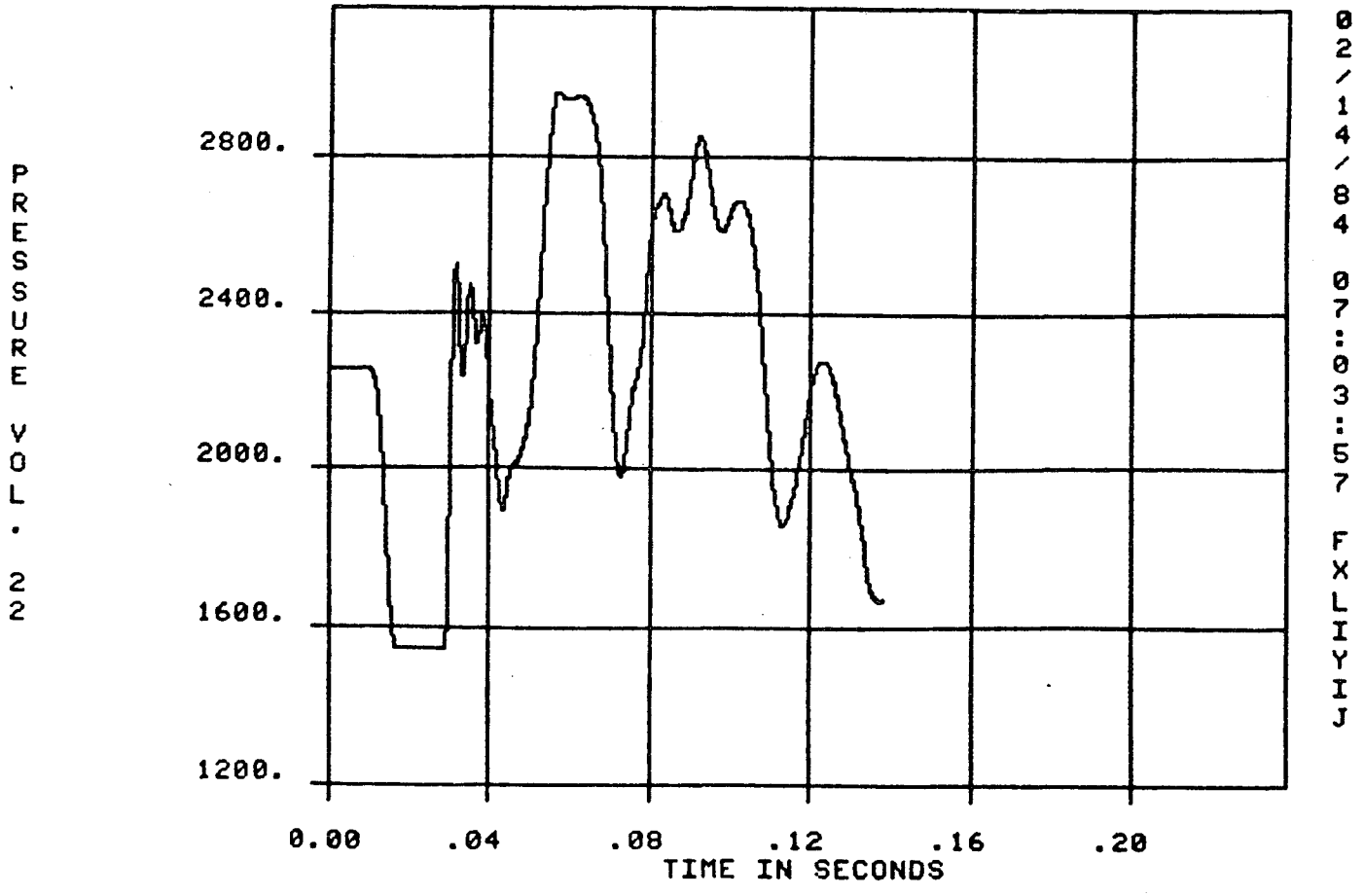

FIGURE 3

V-SEQUENCE TRANSIENT OF RHR LINE No. 10

INDIAN POINT UNIT No. 3

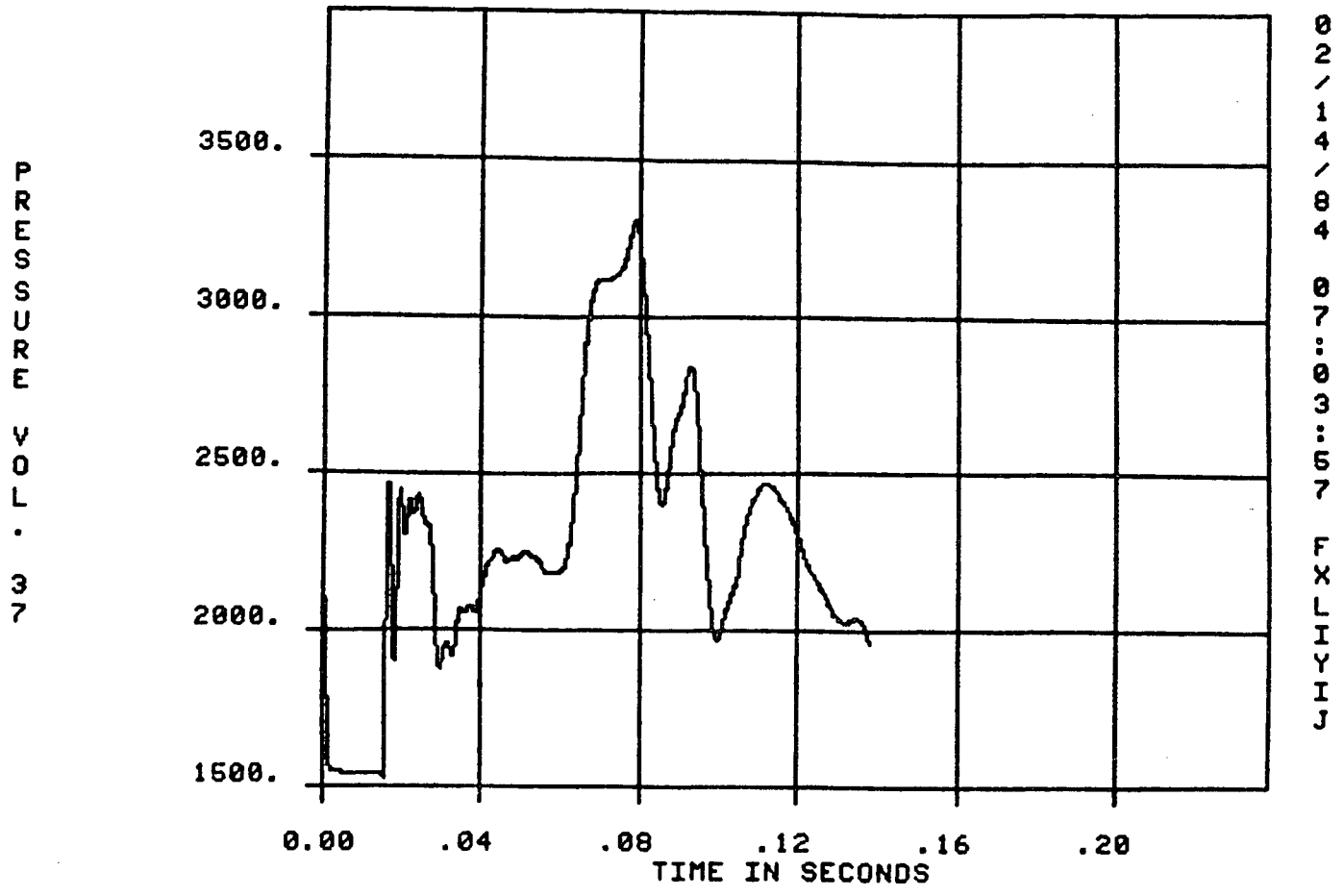

FIGURE 4

V-SEQUENCE TRANSIENT OF RHR LINE No. 10

INDIAN POINT UNIT No.3

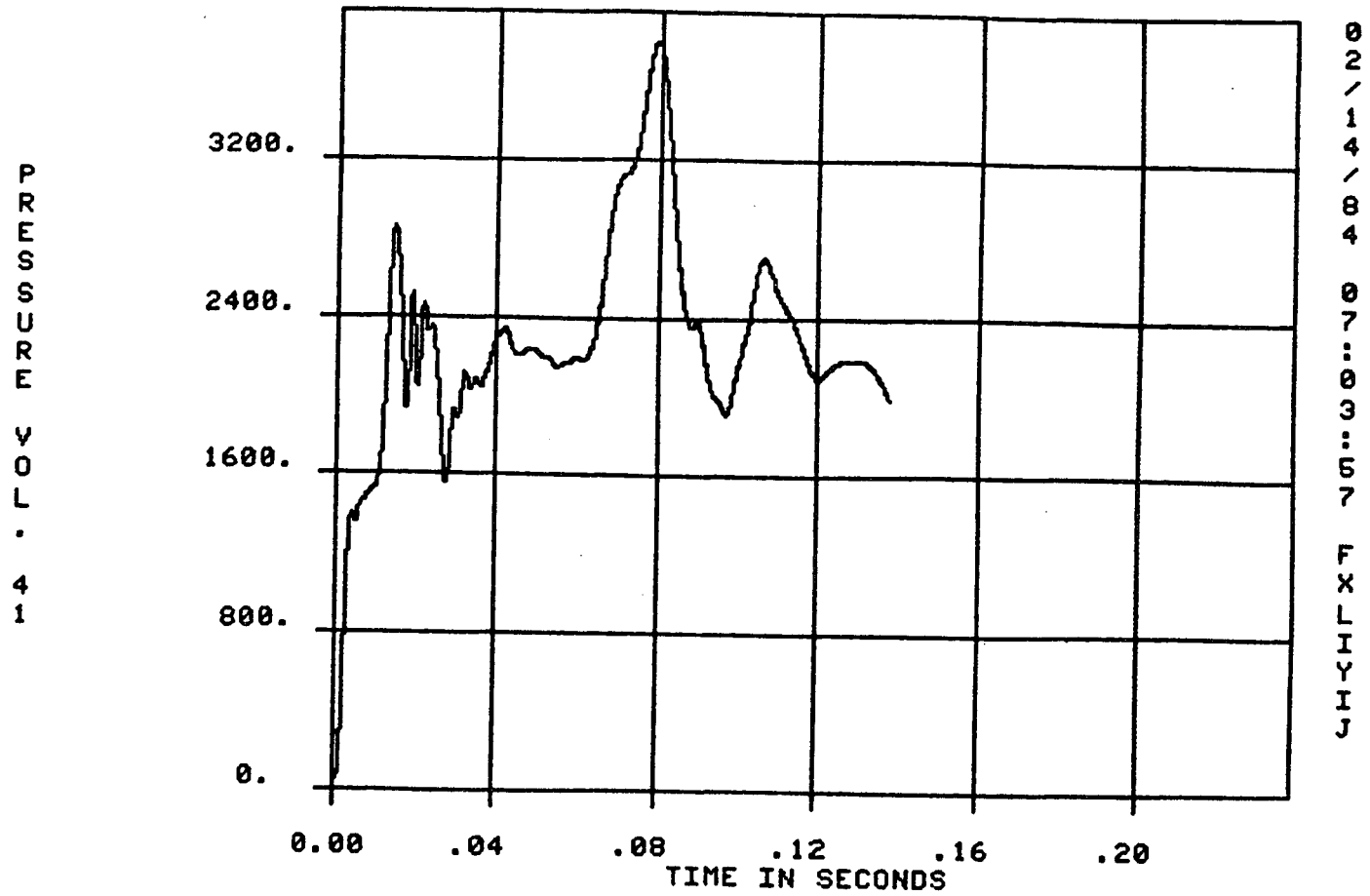

FIGURE 5

V-SEQUENCE TRANSIENT OF RHR LINE No. 10

INDIAN POINT UNIT No. 3

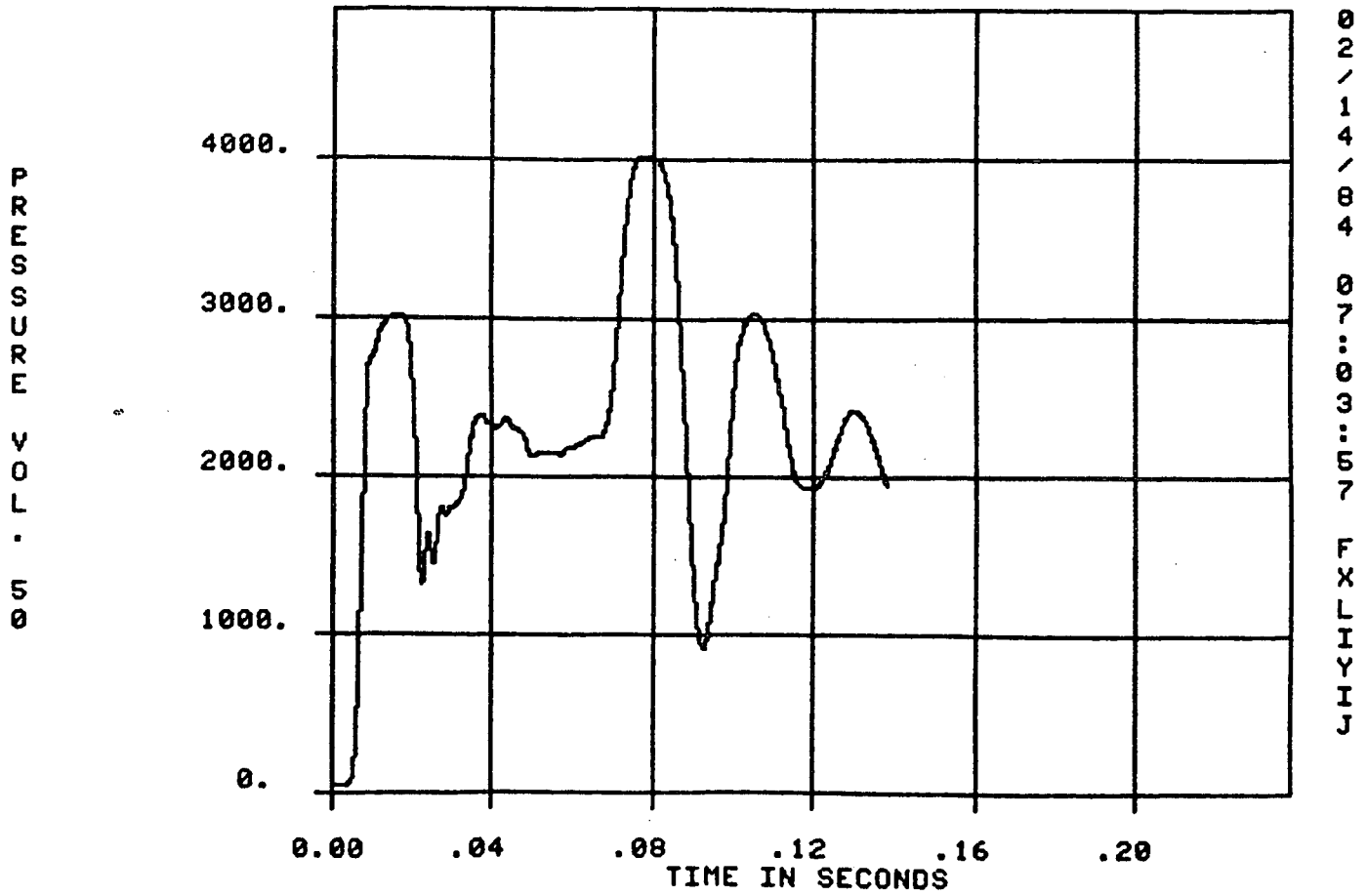

FIGURE 6

V-SEQUENCE TRANSIENT OF RHR LINE No. 10

INDIAN POINT UNIT No.3

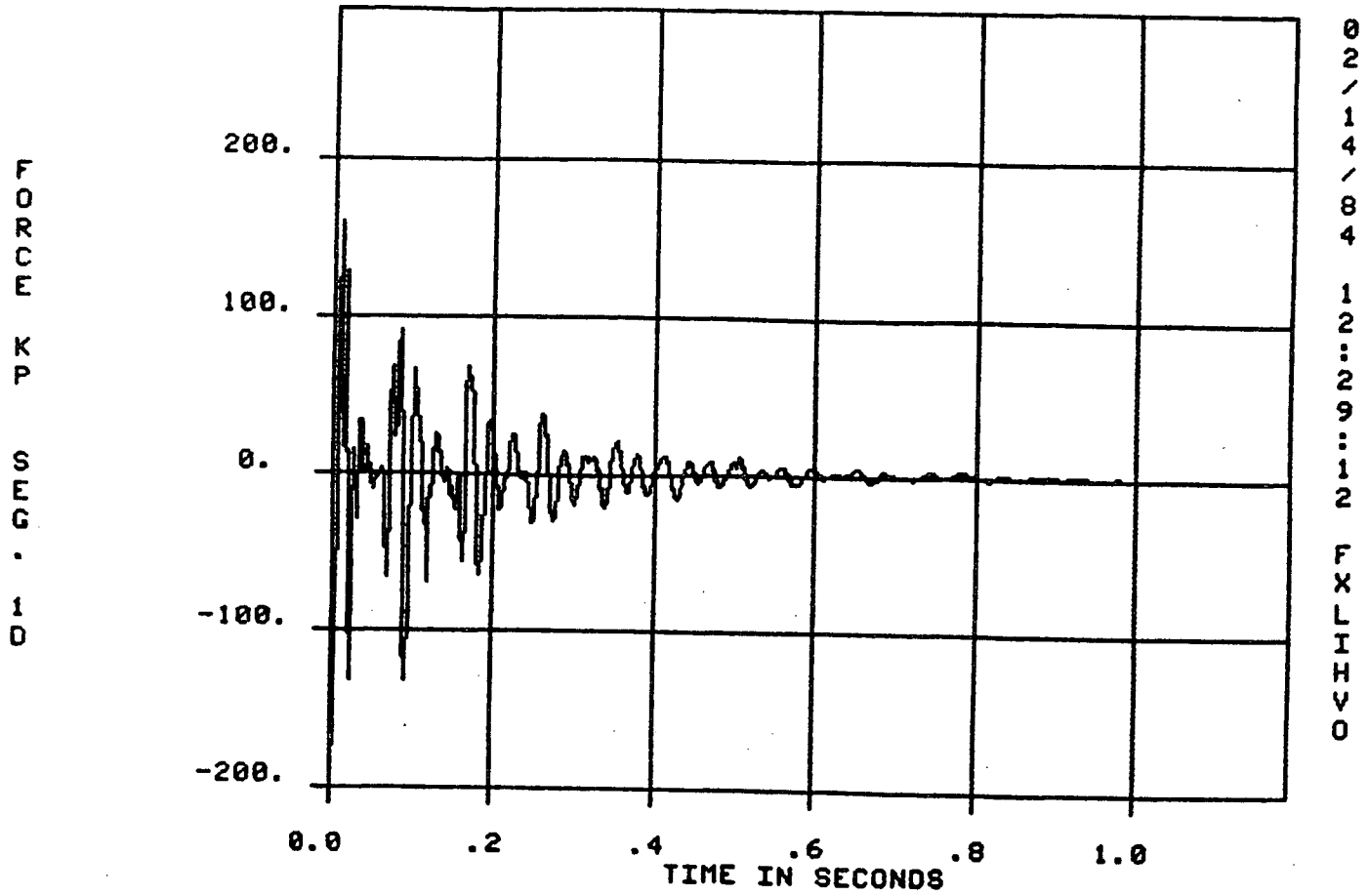

FIGURE 7

V-SEQUENCE TRANSIENT OF RHR LINE No. 10

INDIAN POINT UNIT No. 3

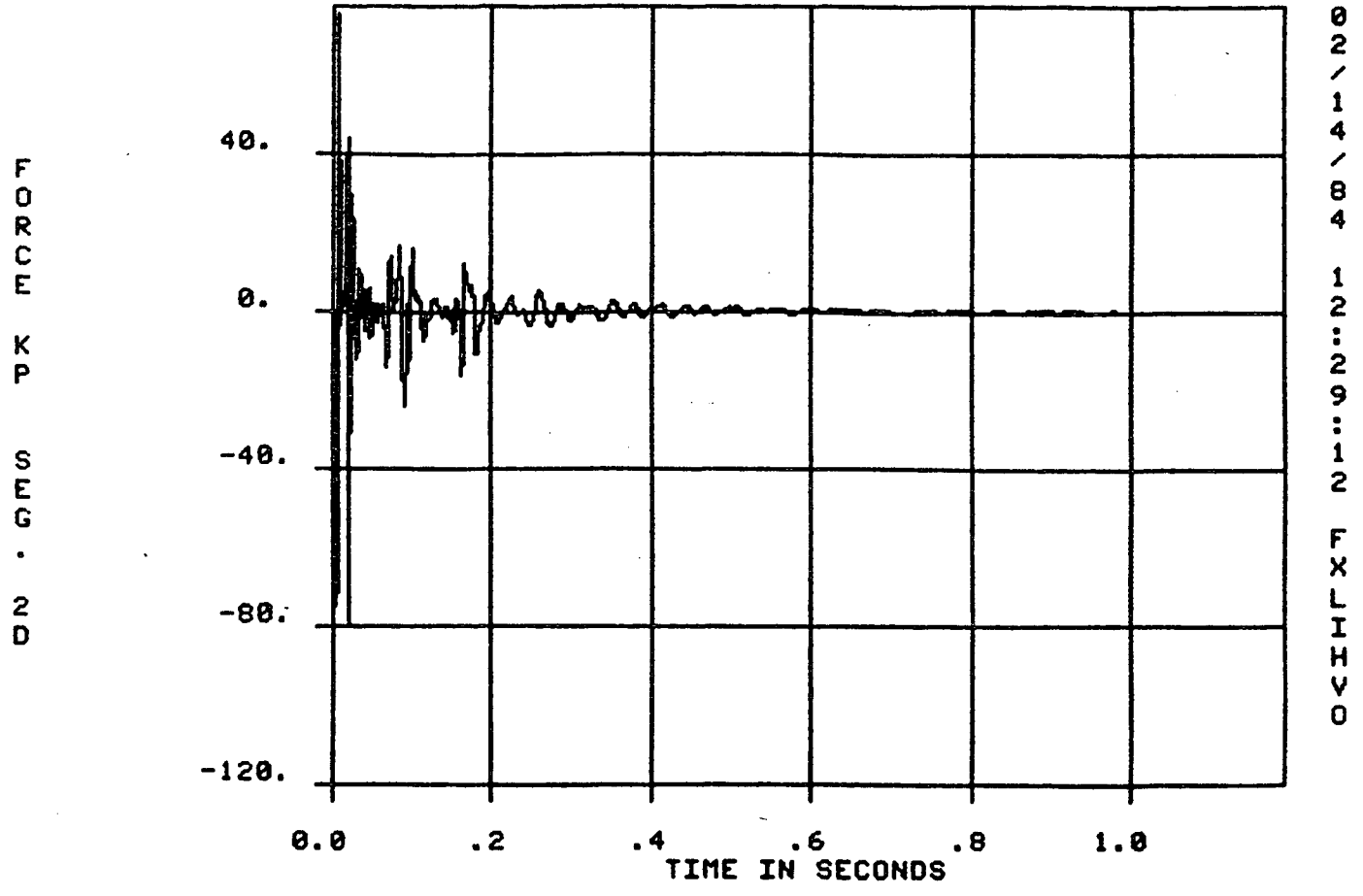

FIGURE 8

V-SEQUENCE TRANSIENT OF RHR LINE No. 10

INDIAN POINT UNIT No. 3

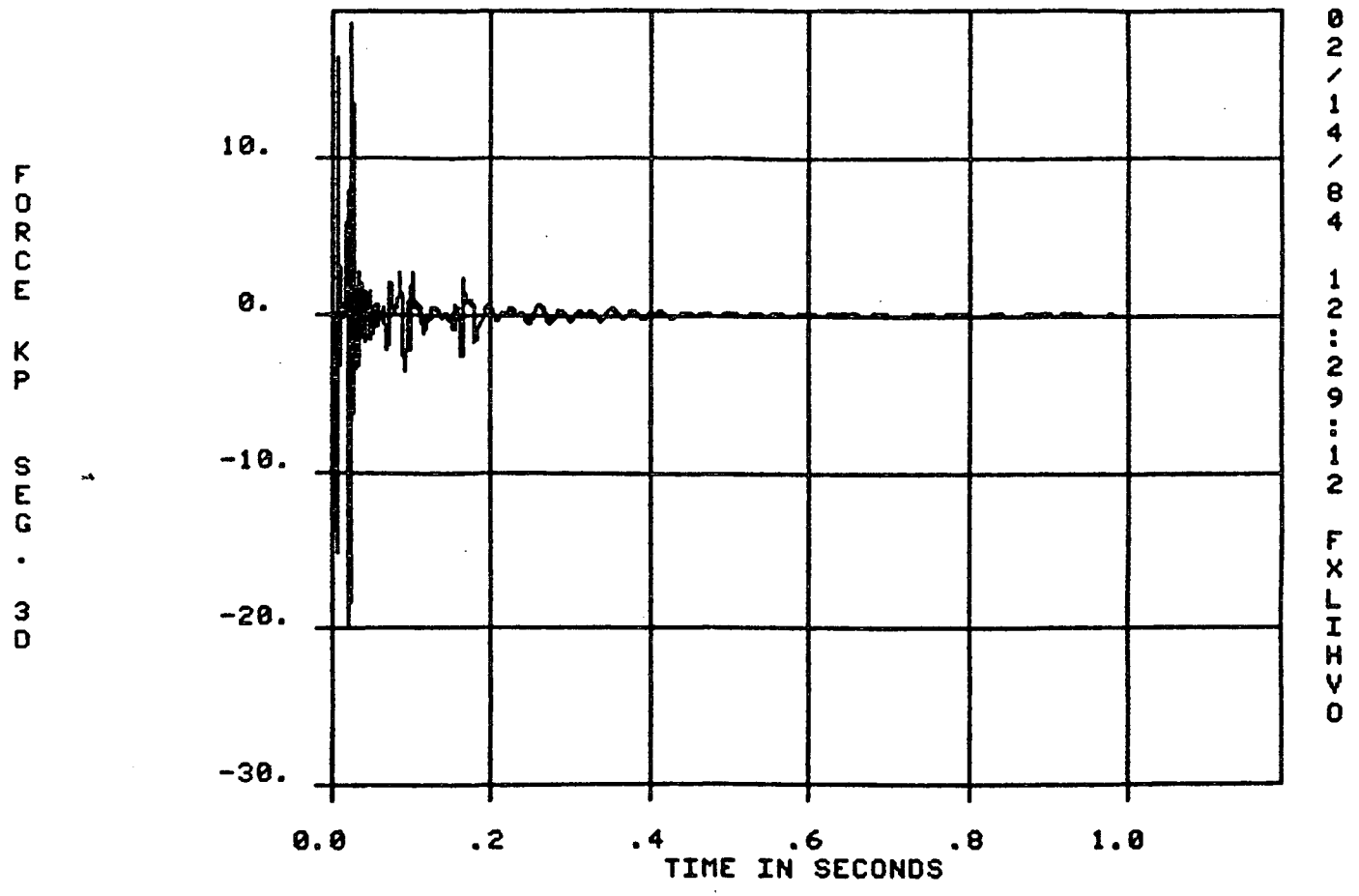

FIGURE 9

V-SEQUENCE TRANSIENT OF RHR LINE No. 10

INDIAN POINT UNIT No. 3

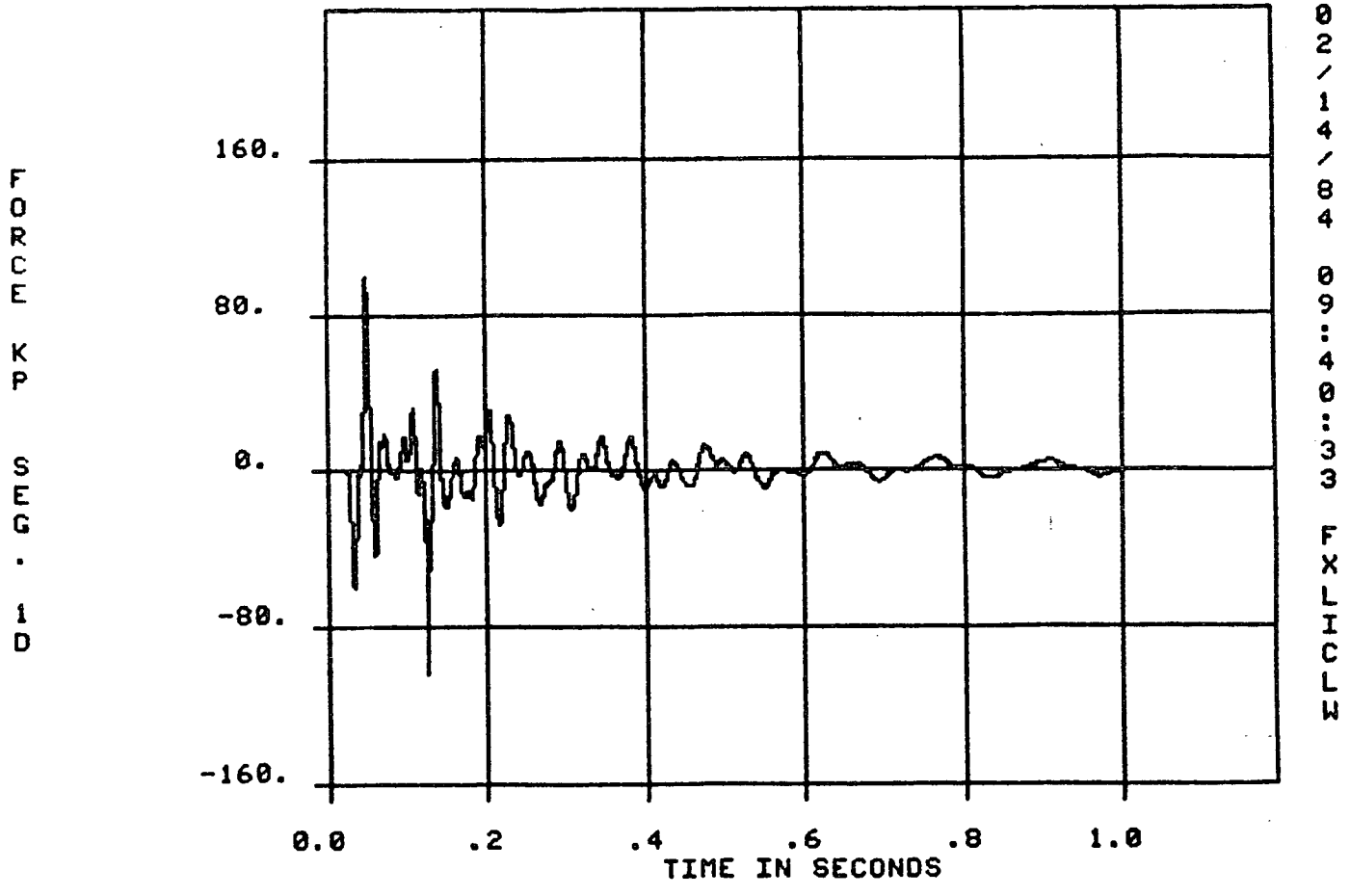

FIGURE 10

V-SEQUENCE TRANSIENT OF RHR LINE No. 10

INDIAN POINT UNIT No. 3

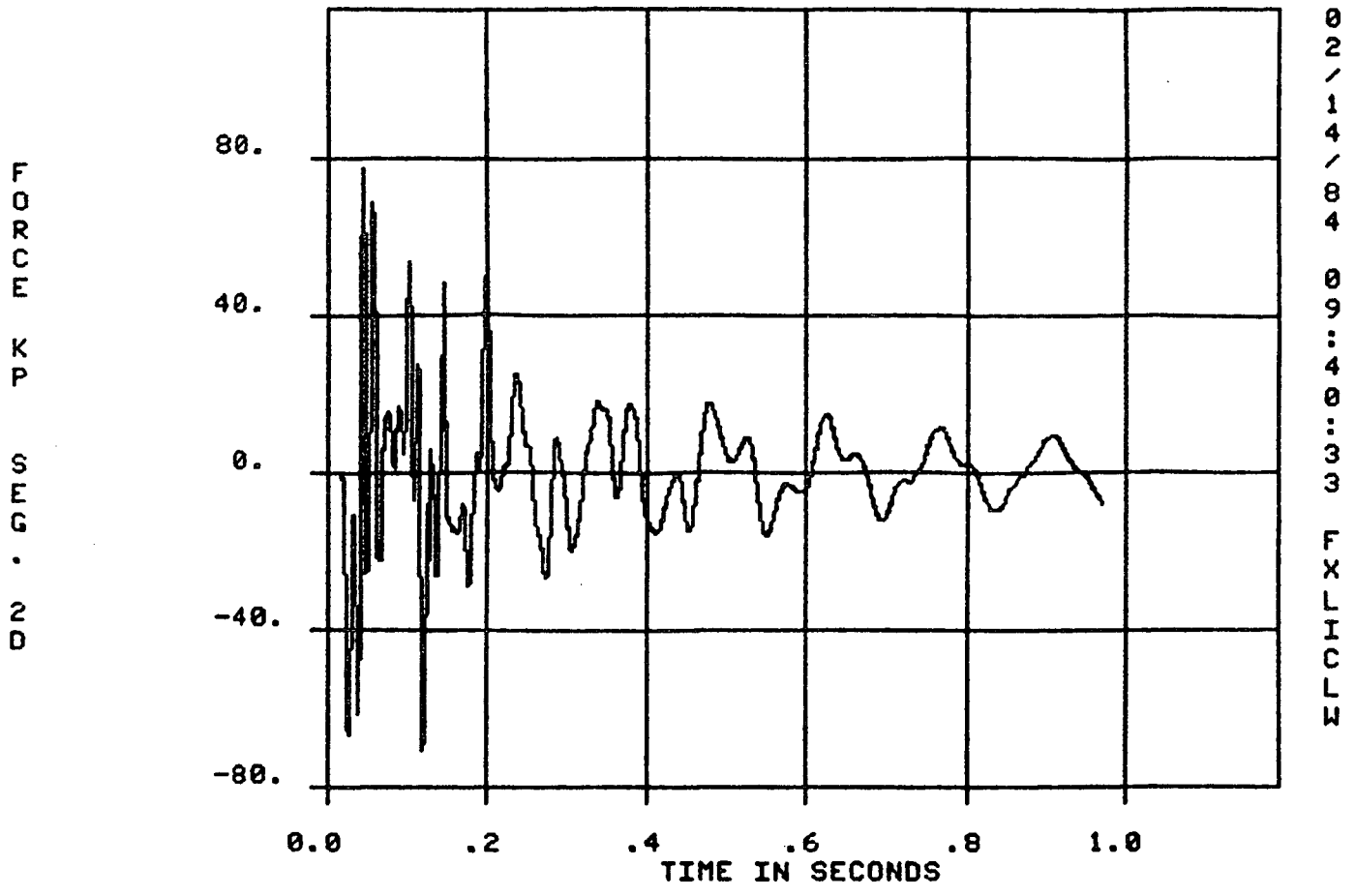

FIGURE 11

V-SEQUENCE TRANSIENT OF RHR LINE No. 10

INDIAN POINT UNIT No.3

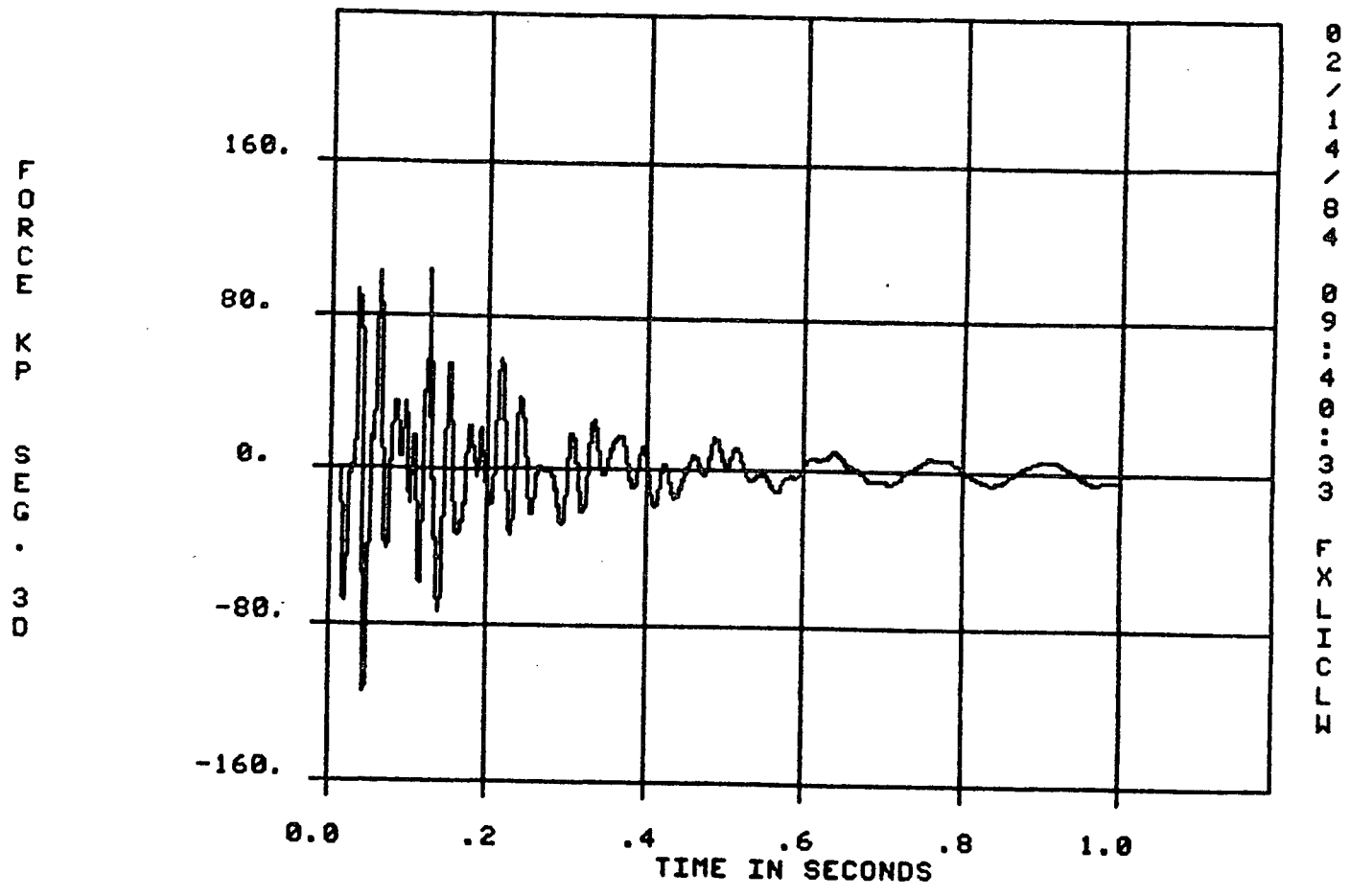

FIGURE 12

V-SEQUENCE TRANSIENT OF RHR LINE No. 10

INDIAN POINT UNIT No.3

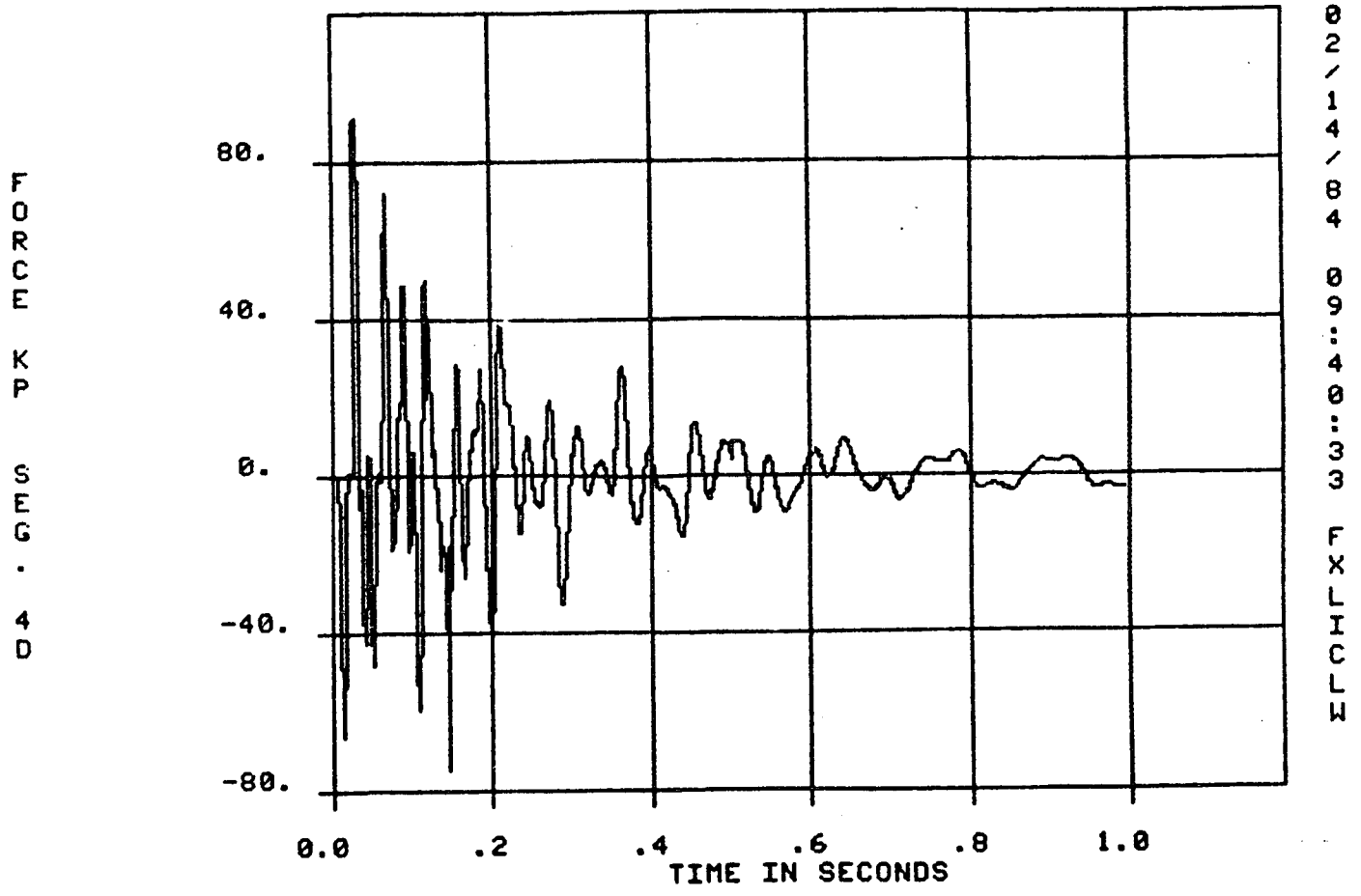

FIGURE 13

V-SEQUENCE TRANSIENT OF RHR LINE No. 10

INDIAN POINT UNIT No. 3

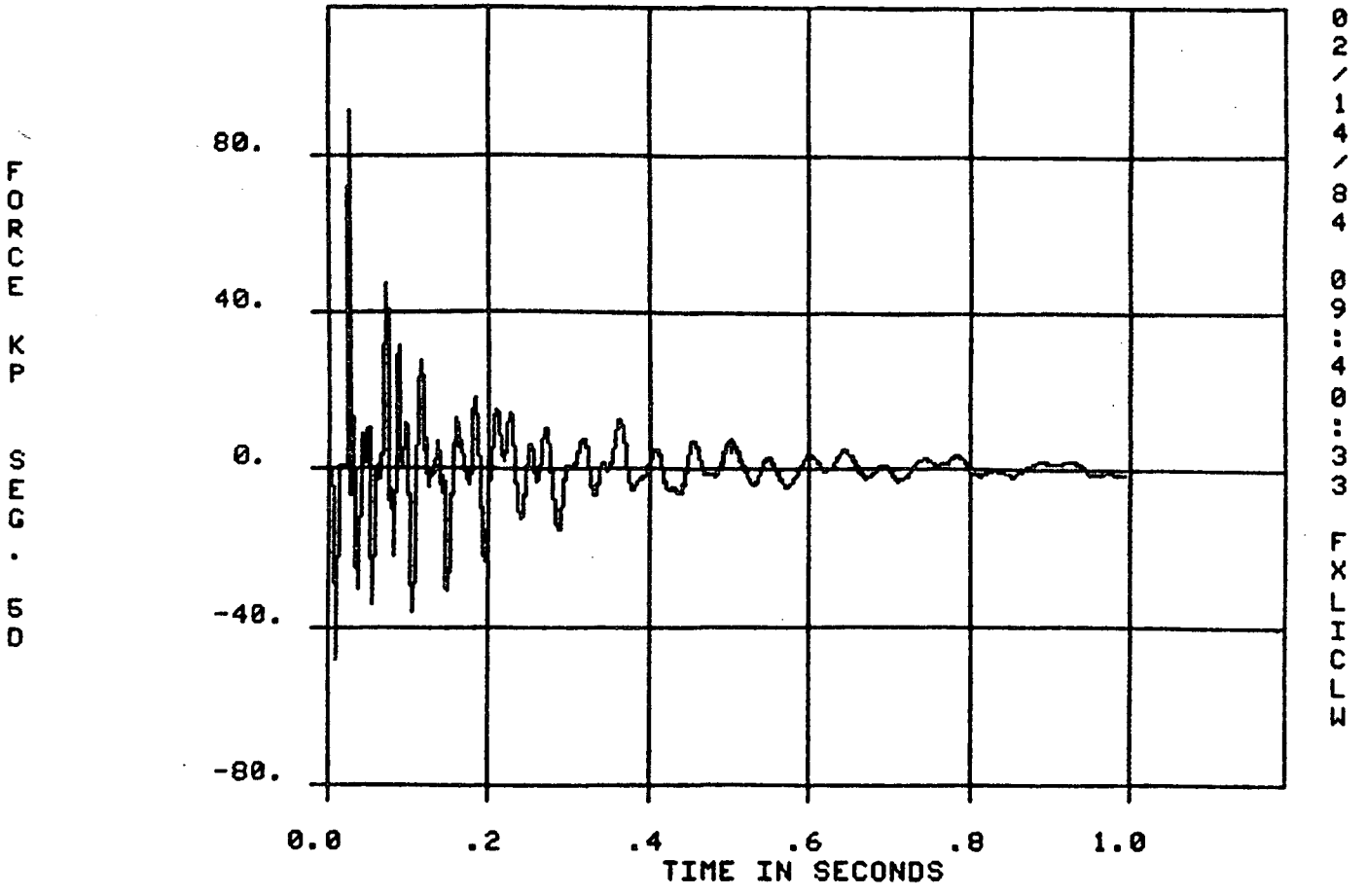

FIGURE 14

V-SEQUENCE TRANSIENT OF RHR LINE No. 10

INDIAN POINT UNIT No. 3

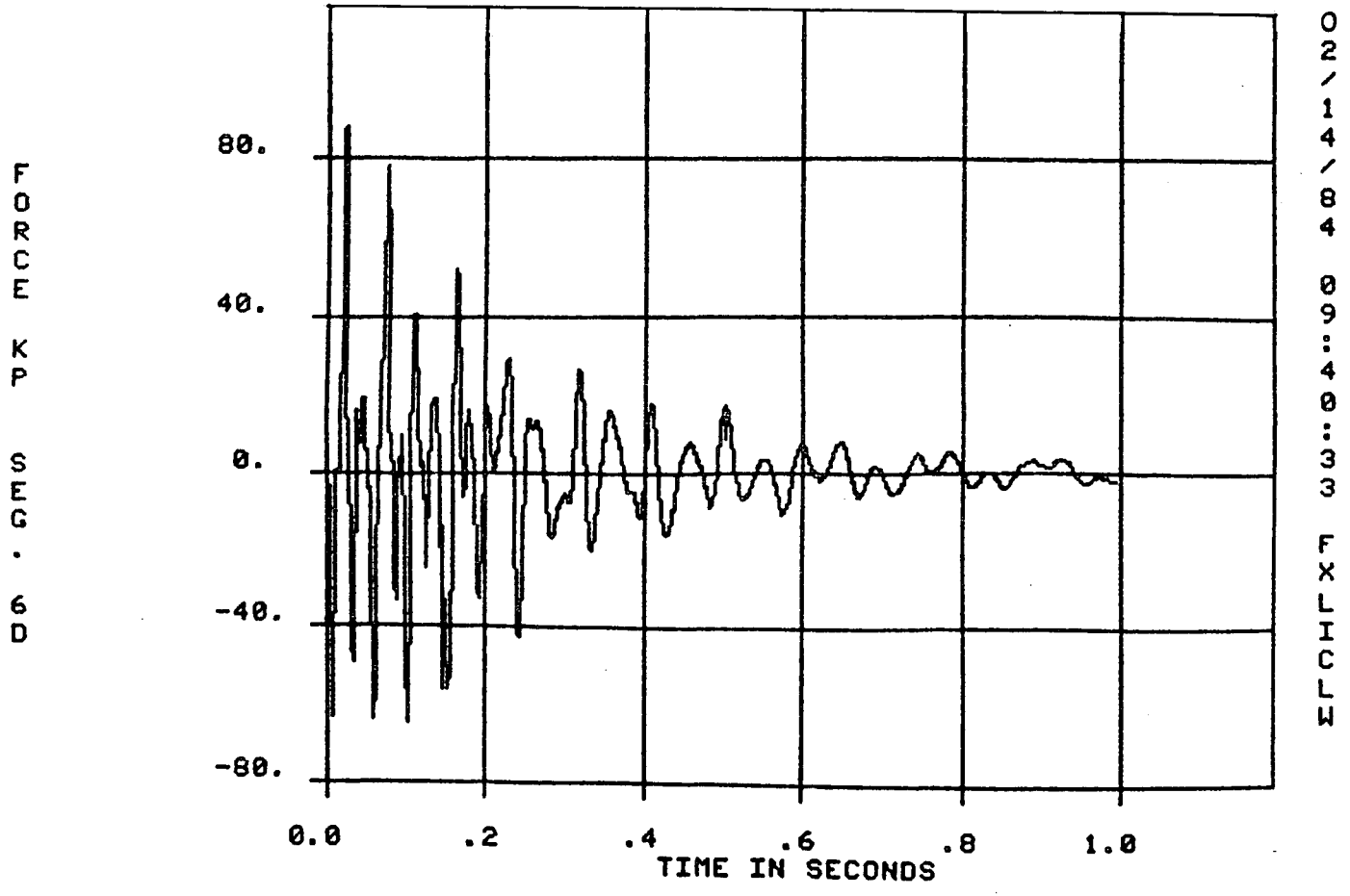

FIGURE 15

V-SEQUENCE TRANSIENT OF RHR LINE No. 10

INDIAN POINT UNIT No. 3

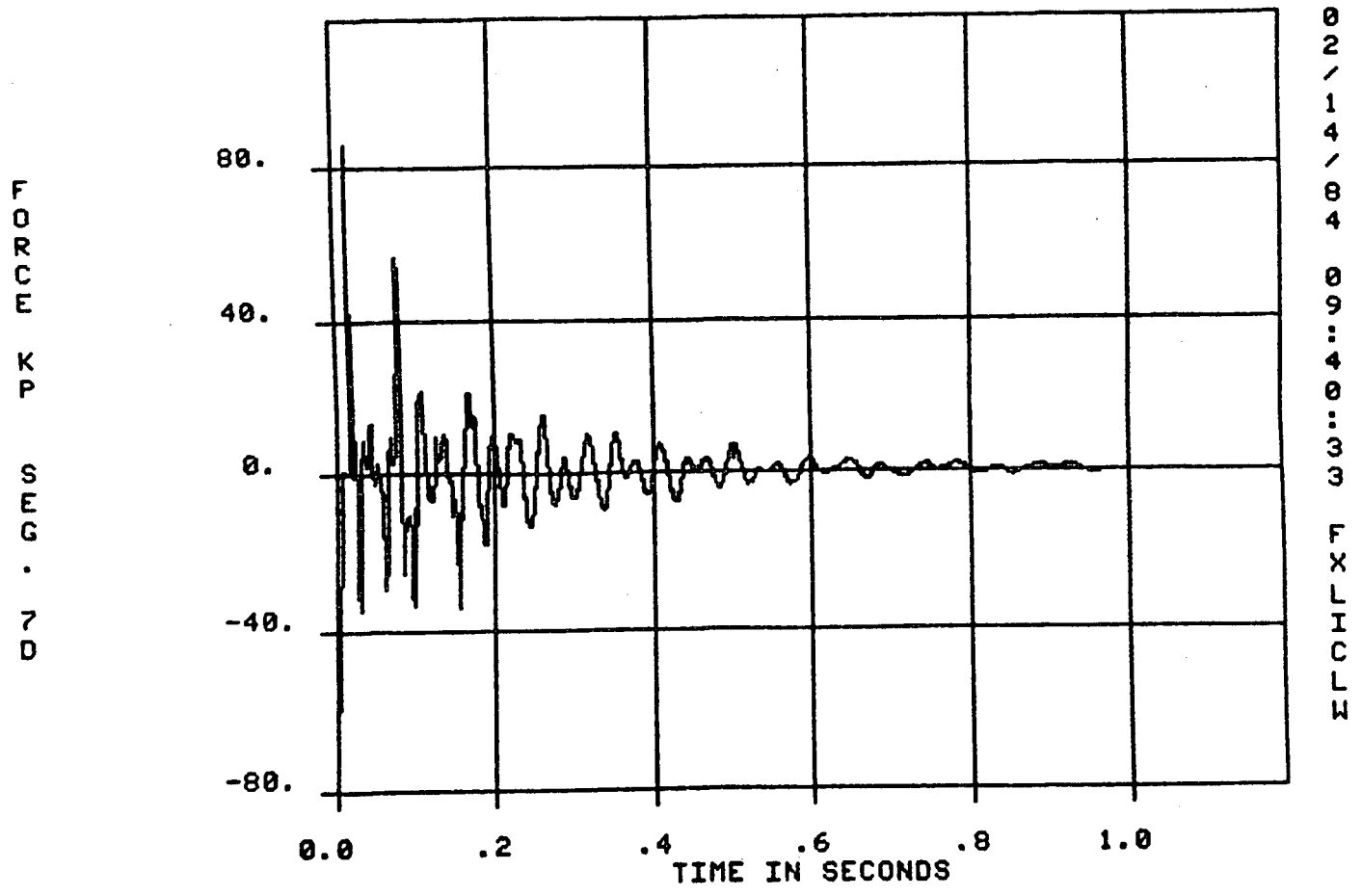

FIGURE 16

V-SEQUENCE TRANSIENT OF RHR LINE No. 10

INDIAN POINT UNIT No. 3

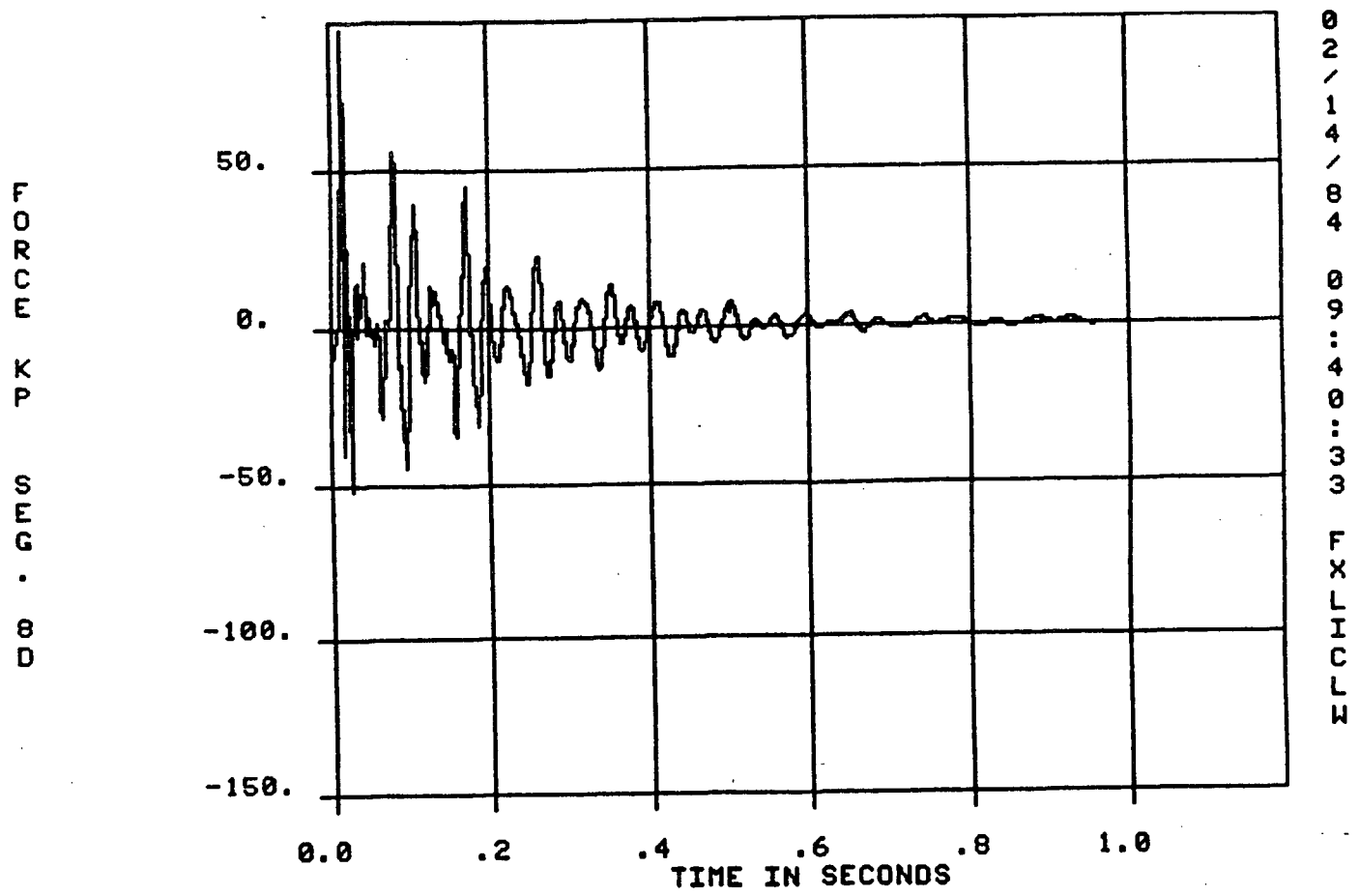

FIGURE 17

V-SEQUENCE TRANSIENT OF RHR LINE No. 10

INDIAN POINT UNIT No. 3

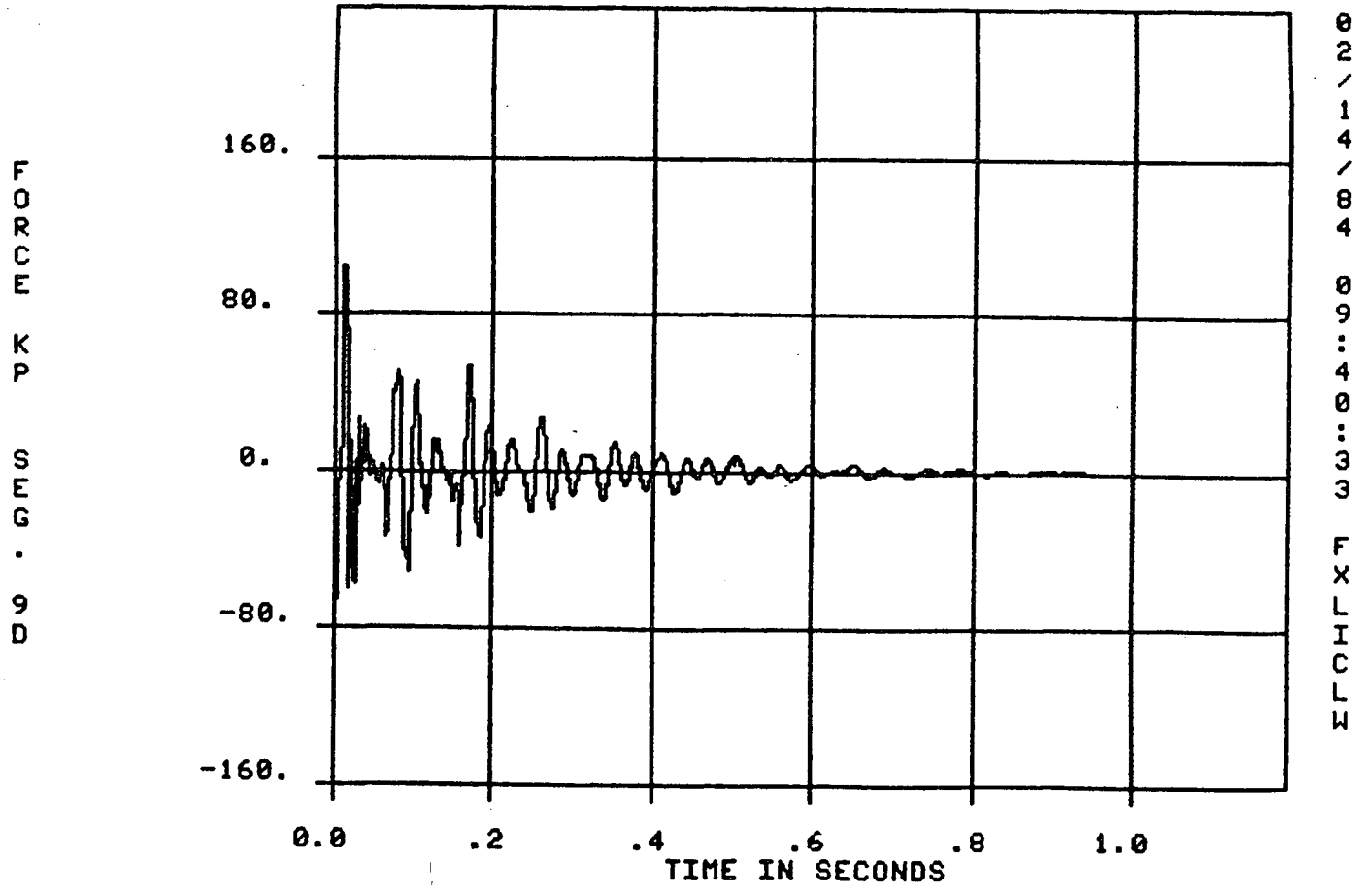

FIGURE 18

V-SEQUENCE TRANSENT OF RHR LINE No. 10

INDIAN POINT UNIT No. 3

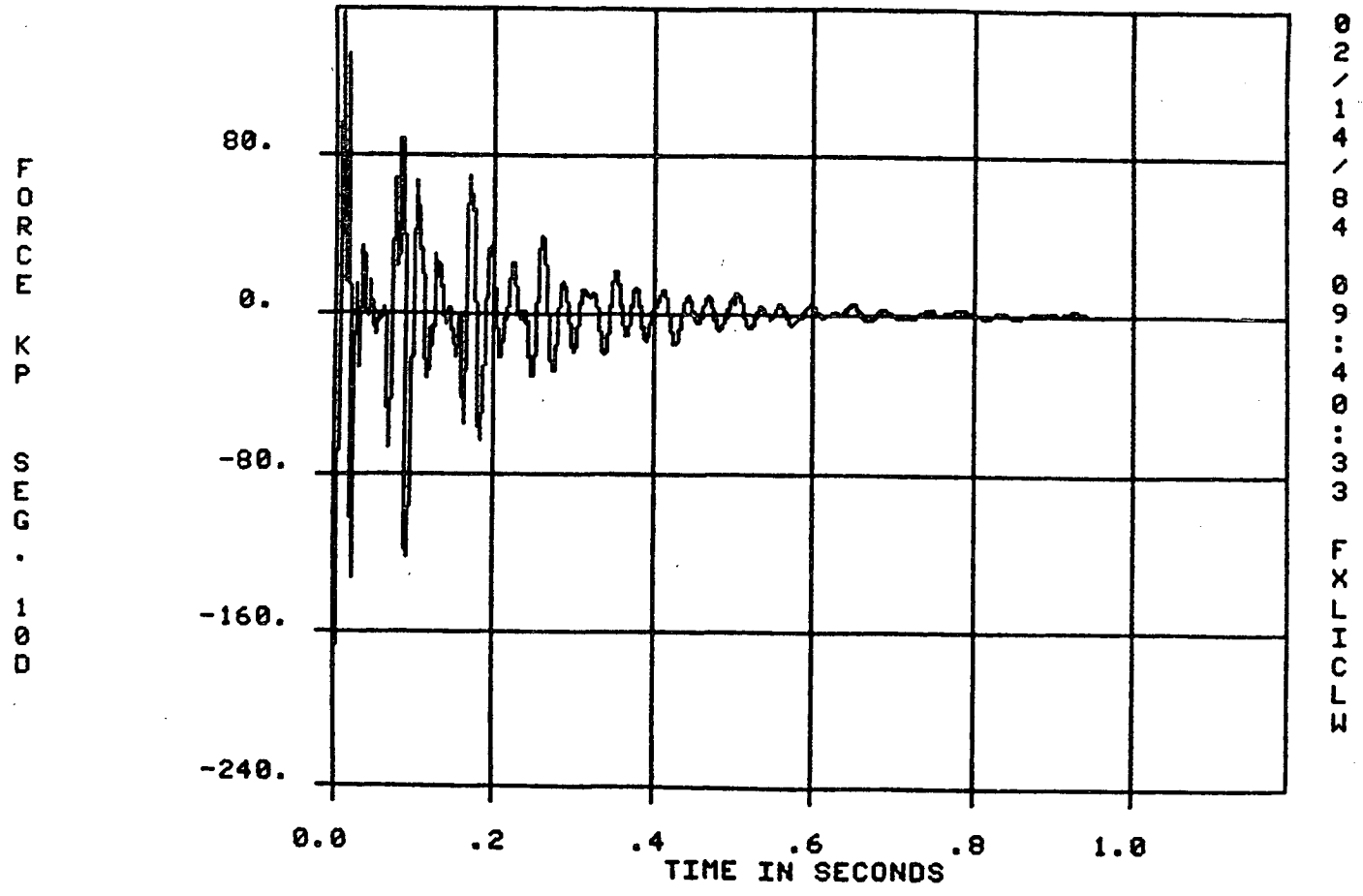

FIGURE 19

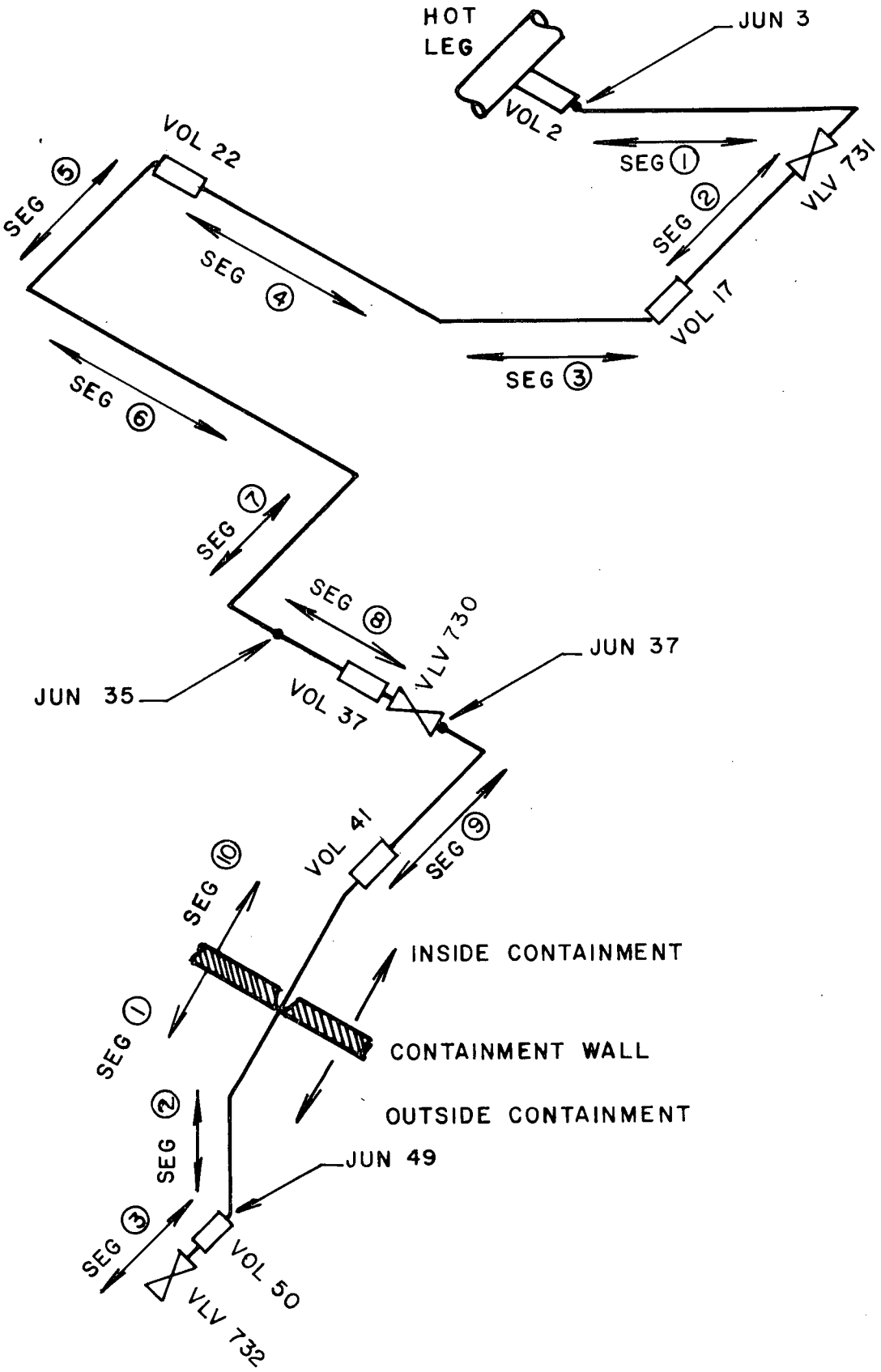

FIGURE 20

Line #10 Configuration for Volume
&
Pipe Segment Identification

RELAP MATH MODEL

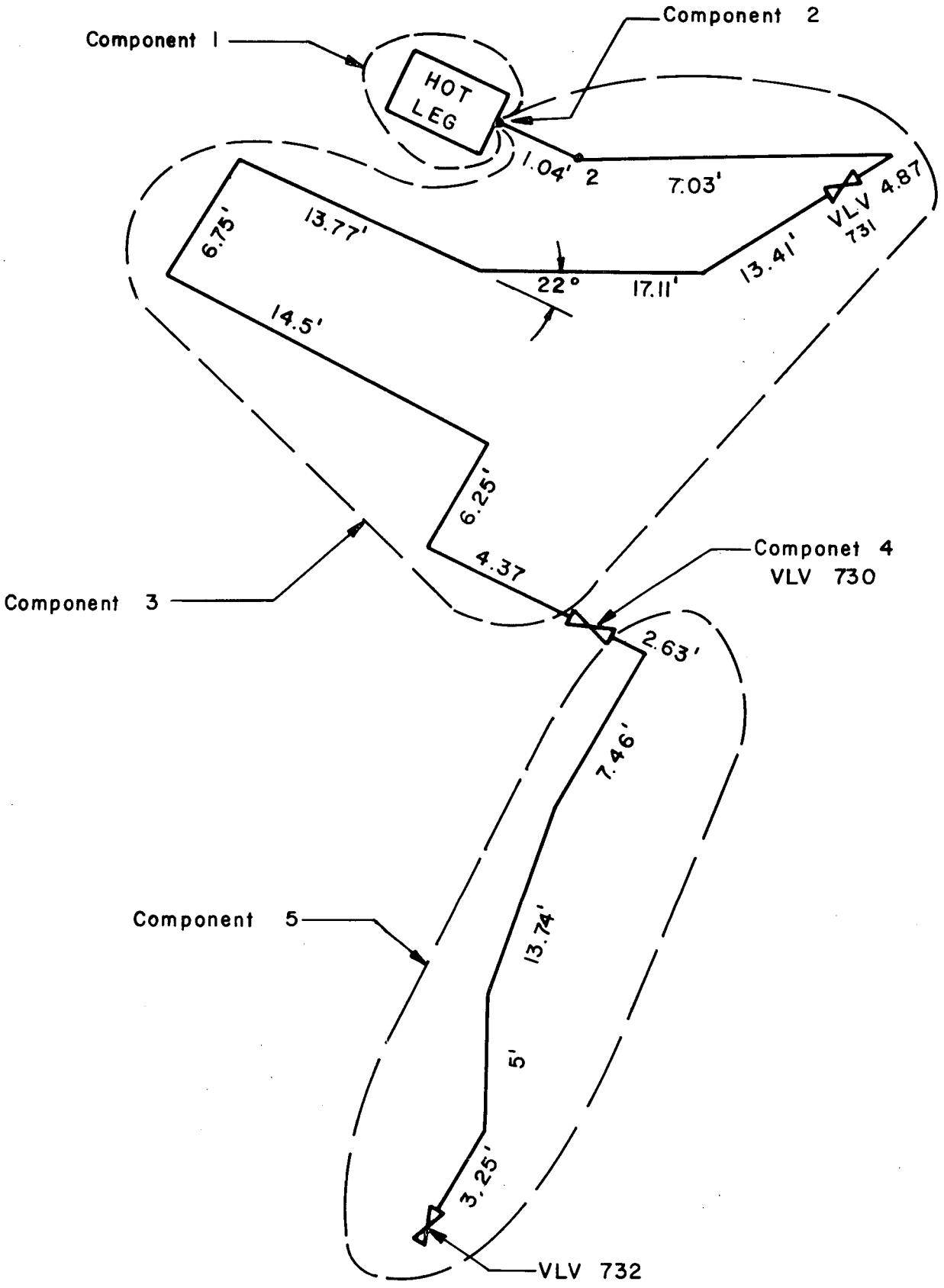

FIGURE 21

DETAIL OF COMPONENT 3

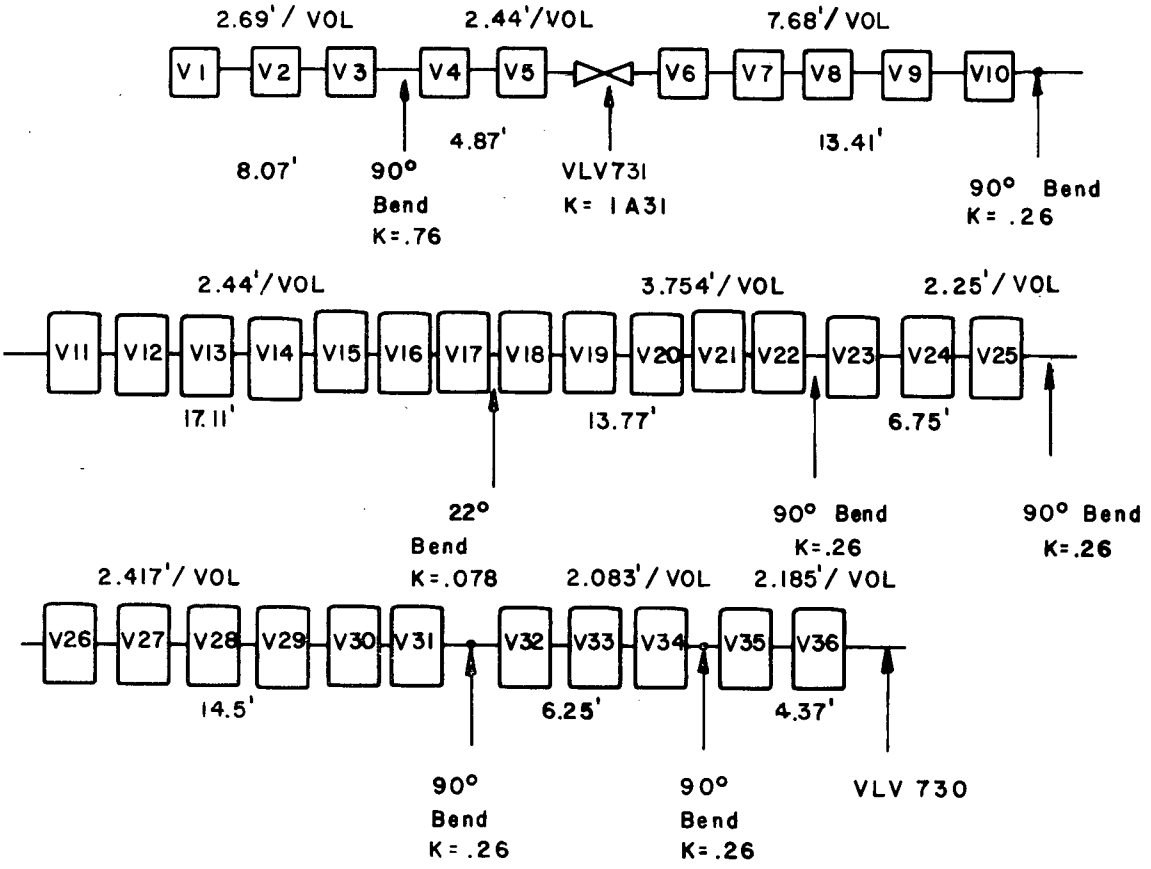

DETAIL OF COMPONENT 5

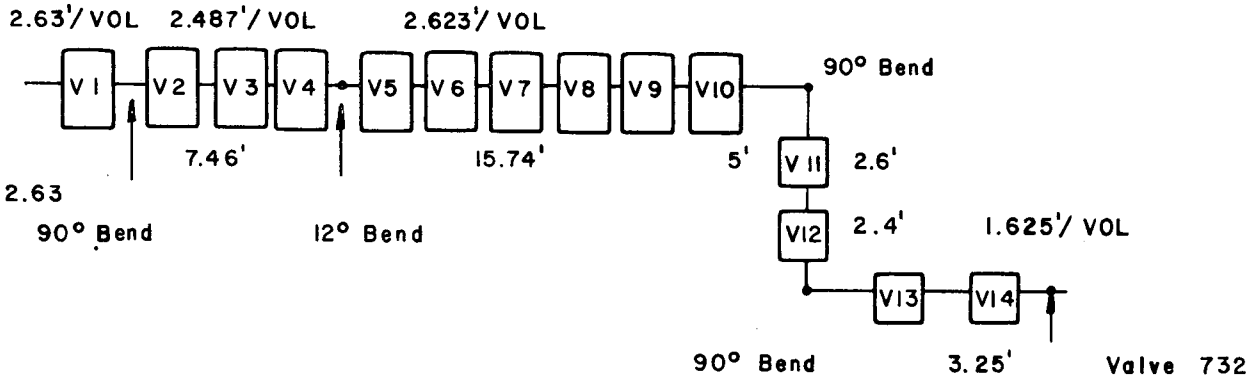

FIGURE 22

INDIAN POINT UNIT No. 3 RHR SYSTEM

NODAL POINT PLOT OF LINE No. 10

(OUTSIDE CONTAINMENT)

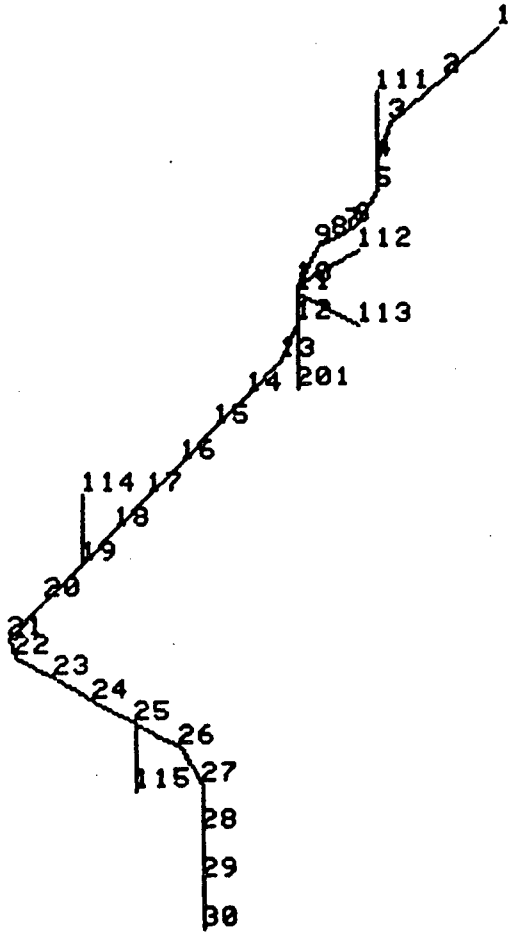

FIGURE 23

ELEMENT PLOT OF LINE No. 10
(OUTSIDE CONTAINMENT)
IP No.3, RHR SYSTEM

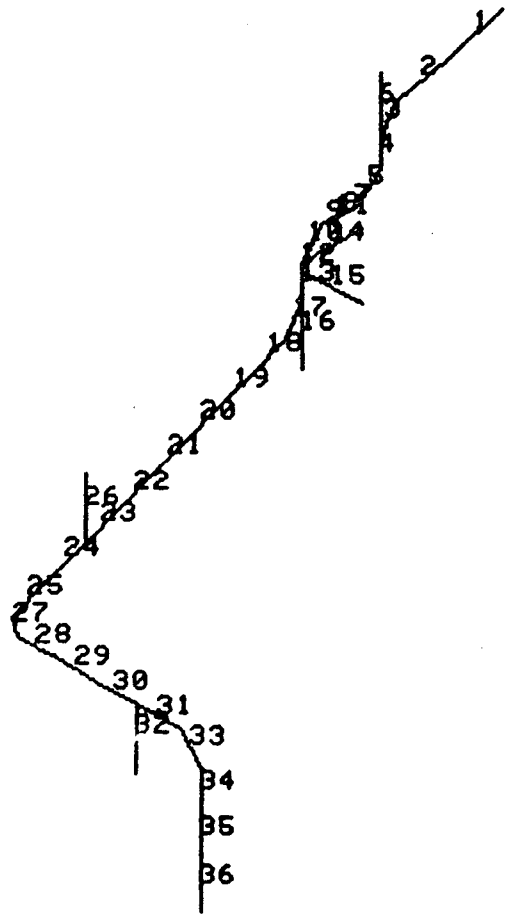

FIGURE 24

NODAL POINT PLOT OF LINE No 10

(INSIDE CONTAINMENT)

IP No.3, RHR SYSTEM

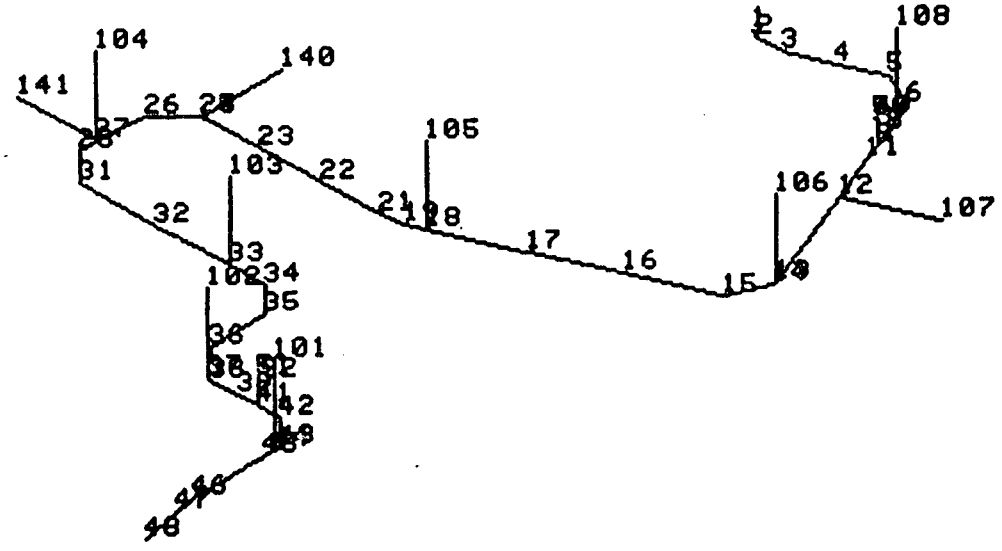

FIGURE 25

ELEMENT PLOT OF LINE No. 10

(INSIDE CONTAINMENT)

IP No.3, RHR SYSTEM

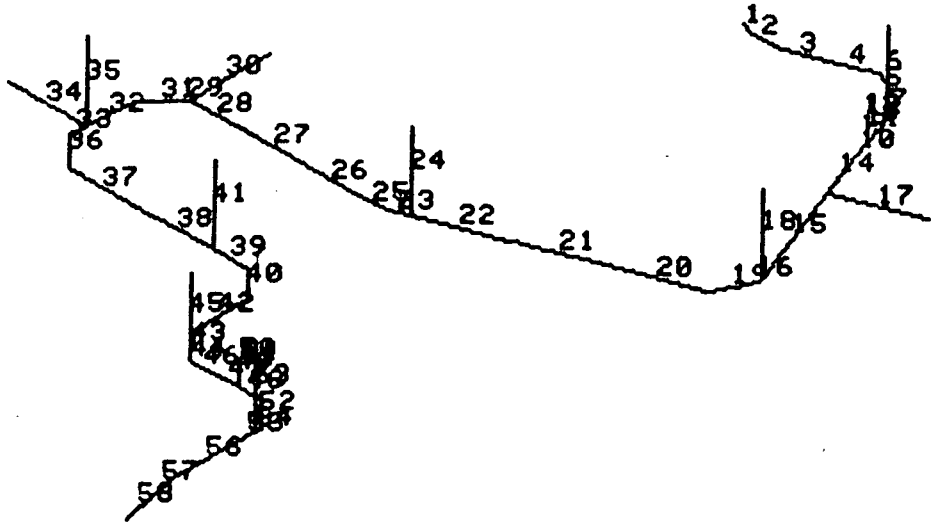

FIGURE 26

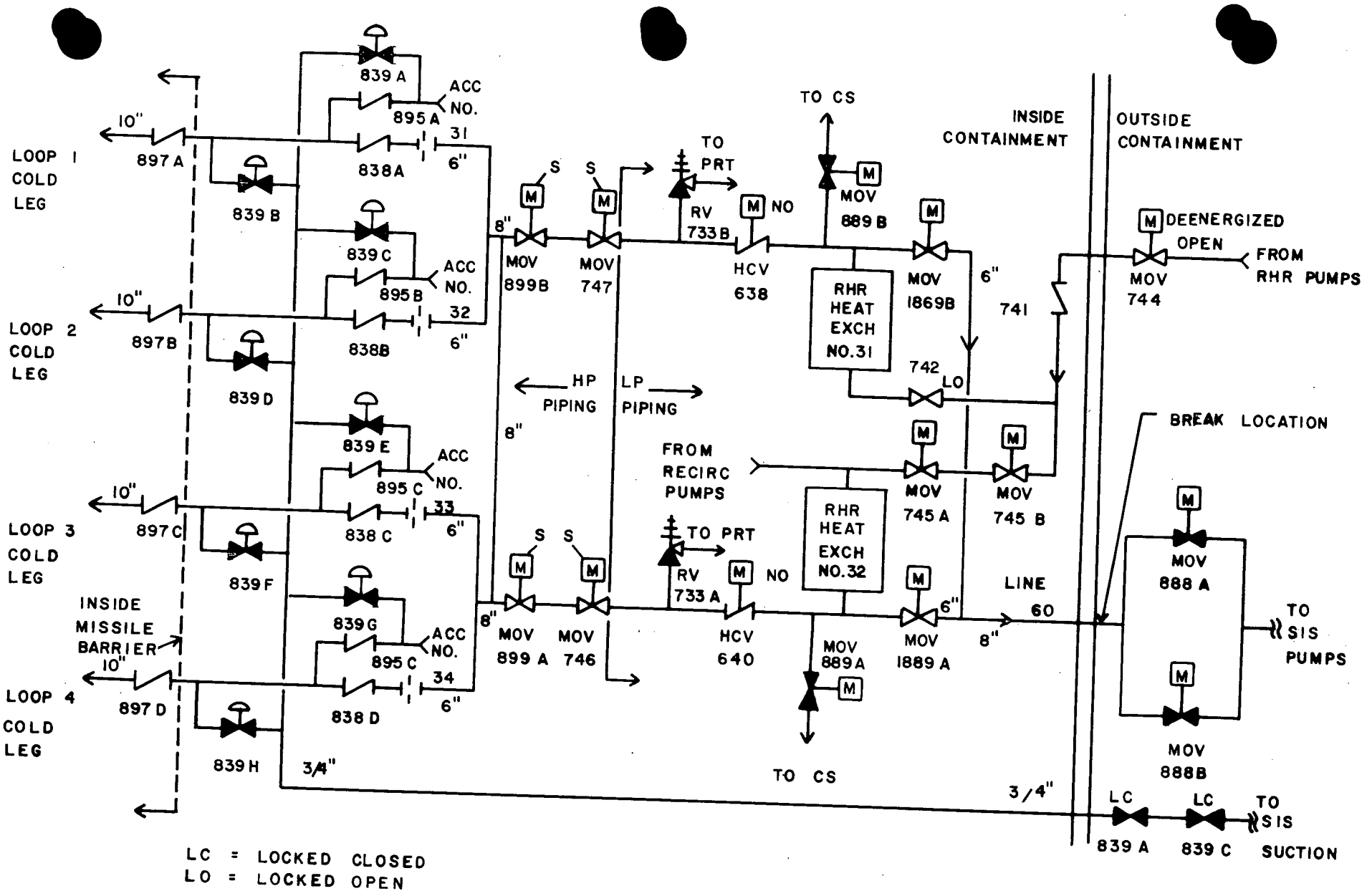

FIGURE 27

INDIAN POINT 3 COLD LEG INJECTION PATH

Appendix B

M-C-T USER'S GUIDE

1.0 Introduction

M-C-T is a computer program for simulating the release and subsequent behavior of fission products inside the primary system during a severe accident. The computer code consists of three modules, M, C, and T. The first module, M, processes the MARCH 2.0 output and calculates the temperatures of the surfaces in the primary system. The second module, C, calculates the release rates of the fission product species, based on the temperature-time histories of the fuel nodes, as calculated by MARCH 2.0. The third module, T, evaluates the retention extent of the fission products in the primary system and calculates the release rates of the fission products out of the primary system.

The overall program flow is shown in Figure 1. The analysis commences with the execution of the M module in its first mode (run 1) in order to process the MARCH 2.0 input data. This initial run is necessary to develop the necessary input information for the execution of the M module in its second mode (run 2). Run 2 will result in the generation of the primary system surface temperatures needed in the execution of the T module. Module M is executed in this mode until core uncovery is reached at which time modules M and T are executed concurrently in order to account for fission product heating.

The C module calculates the release rates of the fission product species from the fuel during the progression of the accident. The necessary input for the execution of this module is obtained from output of the MARCH 2.0 analyses, and it consists of the temperature-time histories of the fuel nodes, as defined by MARCH 2.0. The output of the C module execution

consists of time histories of the release rates of fission product species, as well as other materials such as core structural materials. This output is saved for input in the T module. The T module is executed concurrently with the M module, as mentioned earlier; and it analyzes the retention capability of the primary system based on the temperatures supplied by run 2 of the M module and the volatile and aerosol release rates supplied by the C module. Moreover, the T module calculates the release rate-history of the primary system volatile and aerosol inventory.

2.0 M-C-T CODE DESCRIPTION

The M-C-T code can be executed one of two ways. The first one is a serial mode in which the M module is executed first and its output is used to manually enter thermal hydraulic data into the T module. In its parallel mode the M and T modules are executed in parallel such that a feedback loop between fission product depositon and structural heatup is established.

In addition, capability exists in the M-C-T code to execute each module separately. The discussion which follows focuses on the recommended parallel execution of the M-C-T code.

2.1 M Module Description

The M module is an interface computer code which utilizes data generated by MARCH 2.0 and fission products deposited during a given time step to calculate thermal-hydraulic data for input to the T module for use in the next time step. The code employs MARCH 2.0 output parameters to perform a gas-to-structures heat transfer analysis and converts its calculations into a form compatible as input to the T module.

Typically, two M module runs are performed. The first run simply reads the MARCH 2.0 output file from TAPE 20 and lists it, identifying each time step and its associated parameters of interest, by a time step index. Based on this first run, the user selects the MARCH 2.0 time step index at which core uncovery occurs and at which fuel heat up commences. The second run of the M module performs gas-to-structure calculations at each MARCH 2.0 time step in conjunction with T module calculation.

The M module gas-to-structure heat transfer analysis calculates thermal-hydraulic data for control volumes in the core exit gas flow path. To account for escape from the primary system through pipe breaks, a fictitious control volume is added to represent the outer containment, auxiliary building, or the outside environment. Flow between control volumes is identified in a control volume flow matrix which consists of source volumes to indicate flow exiting a volume and receiver volumes to indicate flow entering a volume. The control volume flow matrix is input to show the path of the gas from source volume J to control volume I. A value of 1 or 0 is assigned to each matrix member to indicate flow/no flow from J to I. Each row and column in the matrix is summed and the values are used as limits for the number of flow paths to/from each control volume.

Required geometric data for each control volume include heat transfer area, cross-flow area, hydraulic diameter, length along line of flow, and vertical height. Additional required inputs include initial control volume gas and wall temperatures, heat capacities, number of heat transfer structures within a control volume, and percentage of flow entering each volume. For a control volume containing more than one structure, each structure must be identified with its own geometry, wall temperature, and heat capacity. For a control volume with a change in flow percentage, a flag must be set (e.g., FLAG2=.TRUE.). If this flag has been set to change, the time at which the change occurs (e.g., FTIME(2)) and the new flow percentage to the volume (e.g., FF(2)) are required inputs.

Figure 2.1 shows the sequential flow of the calculations in the M module. It should be noted that calculations begin at the start of core melt and end at failure of the reactor pressure vessel. A description of each subroutine in the M module is given below.

Subroutine EXITQ

In the M module, the subroutine EXITQ and its associated subroutines analyze the thermal-hydraulic processes. EXITQ is the main subroutine for the gas-to-structure heat transfer analysis and is the largest subroutine in the M module.

The approach used in solving for the thermal-hydraulic conditions in each volume involves an explicit finite difference solution to the flow equations. Conditions within each volume are obtained by moving consecutively from volume to volume downstream of the core. In each case the data for a particular volume are the initial gas temperature, mass, ratio of hydrogen to steam, and rate of heat addition to structures. Also known from the MARCH 2.0 calculation are the total pressure, the temperature of the gases leaving the core, the ratio of hydrogen to steam of these gases, and the mass flow rate. For each volume, the unknown variable is the flow rate out of the volume. The equations that must be solved are conservation of mass and conservation of energy. It is also assumed that the hydrogen and steam in a volume have the same temperature and that each obeys an appropriate equation of state. Conservation of momentum is not imposed since it is assumed that at a particular time step, all volumes have the total pressure predicted by the MARCH 2.0 code. These equations can then be solved iteratively by varying the outlet flow until

the total pressure is equal to the input MARCH 2.0 calculated pressure while satisfying the conservation equations and the equations of state. In practice, this approach is time consuming. Instead, an approximate method is used in the M module to estimate the flow out of the volume assuming that the gases act as an ideal gas over the time step. This allows an analytic solution for the flow out of the volume to be given by:

$$W_n = \frac{H_n 0 + W_{n-1}\,t(h_{n-1} + 460C_0 - C_1 - C_0 PV_n/R}{(h_n + 460\,C_0 - C_1)\Delta t}$$

$$+ \frac{M_{totn}(460C_0 - C_1) - Q + (P - P_0)V_n}{(h_n + 460\,C_0 - C_1)\Delta t}$$

where:

W_n = flow out of volume n,

W_{n-1} = flow out of volume n-1,

H^0_n = total enthalpy of gases in volume n at beginning of time step,

h_n = specific enthalpy of gases in volume n,

h_{n-1} = specific enthalpy of gases in volume n-1,

M_{totn} = total mass of gases in volume n,

Δt = time step,

P = pressure,

P_0 = pressure of gases in volume n at beginning of time step,

V_n = gas volume in control volume n,

Q = heat transferred between volume gas and wall,

and it is assumed that

$$h_n = C_0 T + C_1$$

where

T = temperature in F,

C_0, C_1 = coefficients recalculated at each time step based on the equations of state for steam and hydrogen.

Given the estimated value of the outflow, the gases are then required to satisfy realistic equations of state for steam and hydrogen. The result of the approximation is to yield a slightly different value of the pressure at the end of the time step than the MARCH 2.0 calculated value. Because of the crudeness of the one-volume solution that led to the MARCH 2.0 calculated pressure, this discrepancy is considered minor.

It should be noted that this subroutine also regulates control volume flow by dividing the MARCH 2.0 time steps into subintervals in order to prevent the total evacuation of the mass in a volume within a time step. The subinterval time steps are determined by first examining each control volume to obtain the one having the least gas volume; second, treating the mixture exiting the top of the core as an ideal gas to determine an appropriate volumetric flow rate; and third, subdividing the MARCH 2.0 time step until the volumetric flow rate times the subinterval time is less than or equal to 10% of the volume having the least gas volume. The heat transfer analysis is completed for each control volume over the MARCH 2.0 time step, and thus, all subintervals, before proceeding to the analysis for the next control volume at the same MARCH 2.0 time step.

The Newton-Raphson method of iteration is then employed to solve for control volume steam temperature, pressure, and enthalpy. The following three simultaneous equations are used:

$$HST = (HH - H2M*HH2)/STMM$$

$$T = F(PSTM, HST)$$

$$\gamma = f(PSTM, HST)$$

where:

HST = specific enthalpy of steam in the control volume, BTU/lbm,

T = temperature of steam in the control volume, F,

γ = specific volume of steam in the control volume, ft^3/lbm,

PSTM = partial pressure of steam in the control volumes, psia,

HH2 = specific enthalpy of hydrogen in the control volume, BTU/lbm,

HH = total enthalpy of the steam hydrogen mixture in the control volume, BTU,

H2M = mass of hydrogen in the control volume, lbm,

STMM = mass of steam in the control volume, lbm.

The method uses initial guesses of steam temperature, pressure and enthalpy to calculate new values of each. This iterative process continues until values are found to satisfy the three equations. Once solutions to the simultaneous equations have been found, a heat balance between the gas and each structure within the control volume is performed. The heat transferred from the steam-hydrogen mixture exiting the top of the core to each control volume is calculated through an internally calculated heat transfer coefficient.

In determining the heat transfer coefficient between the gas and the structure, the Reynolds Number is first calculated and depending on whether the flow is in the laminar or turbulent regime the coefficient is calculated as:

Laminar

$$h_c = k_m Nu_d / d \quad , \text{BTU/hr/ft}^2\text{/F}$$

Turbulent

$$h_c = 0.0144\ C_{pm} G^{0.8} / d^{0.2} \quad , \text{BTU/hr/ft}^2\text{/F}$$

where:

k_m = thermal conductivity of the gas mixture, BTU/hr/ft^2/F

$$Nu_d = 3.66 + \frac{0.0668(d/L)Re_d Pr}{1 + 0.04((d/L)Re_d Pr)^{2/3}}$$

d = hydraulic diameter, ft

C_{pm} = specific heat of the gas mixture, BTU/lb/F

G = mass velocity, lb/hr/ft^2

A natural convection coefficient is also calculated depending on the Rayleigh Number regime:

for $\bar{X} < 10^9$

$$h_c = 0.59\ k/L\ X^{0.25} \quad , \text{BTU/hr/ft}^2\text{/F}$$

for $\bar{X} > 10^9$

$$h_c = 0.10\ k/L\ X^{0.33} \quad , \text{BTU/hr/ft}^2\text{/F}$$

where:

k_m = thermal conductivity of the gas mixture, BTU/hr/ft^2/F

L = length, ft

$\bar{X}$ = Rayleigh Number

The larger of the natural and forced convection coefficients is used in the analysis.

The first control volume above the core also receives radiation heat transfer from the top of the core. The inlet gas temperature for this volume is the gas temperature exiting the top of the core. For other volumes, the inlet temperature is the gas temperature at the outlet of the previous control volume.

Subroutine EXITQ also calculates the energy addition due to fission products deposited during previous T module time step and the energy losses through the control volume insulation.

A flow diagram showing the calculations in subroutine EXITQ is given in Figure 2.2. It should be noted that for a control volume with inlet gas-wall temperature difference of five degrees or less, the calculations are skipped. Thus, the outlet gas and wall temperatures of the control volume remain unchanged and the outlet flow rate is equated to the inlet flow rate.

Subroutine ALTER

Subroutine ALTER saves control volume thermal-hydraulic data as a function of time step index N. It also serves to redefine output parameters for total mass flow rates less than 10^{-10} lb/sec. For any time step index, if the flow meets this criterion: (1) total, hydrogen, and steam mass flow rates are set to zero, and (2) control volume inlet, outlet, and wall temperatures remain unchanged.

Subroutine STASH (serial mode)

Subroutine STASH stores M module output data required by the T module in a flow parameter matrix for each volume. In addition, it sums input flow rates and averages temperatures for control volumes with more than one source.

Subroutine AVERAGE (serial mode)

Subroutine AVERAGE is a numerical averaging routine used to reduce the M module input data from MARCH 2.0 code. It gives a sequence of up to 20 values at preselected event time step indexes of all MARCH 2.0 parameters required for the heat transfer analysis. These interval values are stored on M module output file TAPE9.

Subroutine ENDS (serial mode)

Subroutine ENDS stores the M-module input data from the MARCH 2.0 code at the first and final time step indexes.

Subroutine REDUCE (serial mode)

Subroutine REDUCE uses a numerical averaging routine to reduce the flow parameter matrices created in subroutine STASH into a form acceptable for input to the T-module. It uses the preselected event indexes to generate 20 intervals of matrix data for each control volume.

Subroutine TAPE (serial mode)

Subroutine TAPE writes the reduced flow parameter matrix of each volume on an output file labelled TAPE2. The file is cataloged for later use in the T-module.

Subroutine ENDPTS (serial mode)

Subroutine ENDPTS stores the flow parameter matrix values for all control volumes at the first and final time step indexes.

Subroutine ENTHAL

Subroutine ENTHAL uses an empirical equation to express hydrogen specific heat and, thus, the specific enthalpy of hydrogen as a function of temperature. The relationship may be adequately approximated throughout the range of temperatures from 80 F to 5840 F with a maximum error of 0.60%. The subroutine additionally uses empirical equations to express specific enthalpy of saturated liquid or saturated vapor as a function of pressure. The relationships may be adequately approximated throughout the range of pressures from 1.1 psia to the critical pressure of 3208.2 psia (PCRIT).

Subroutine TEMP

Subroutine TEMP approximates the temperature of the steam as a function of pressure and specific enthalpy. The empirical relationship employed in the subroutine is valid for pressure less than 3208.2 psia and specific enthalpy equal to or greater than saturated vapor enthalpy at pressure.

Subroutine SPVOL

Subroutine SPVOL approximates the specific volume of steam as a function of pressure and specific enthalpy. The critical pressure value is 3208.2 psia and the specific enthalpy boundary is enthalpy greater than or equal to saturated vapor enthalpy at pressure.°

Subroutine PART

Subroutine PART calculates the partial derivatives of temperature and specific volume with respect to both steam pressure and enthalpy for use in the Newton-Raphson iterative calculations. The subroutine differentiates the empirical relationships previously established for temperature and specific volume.

Subroutine SUBTIME

Subroutine SUBTIME stores time subinterval M-module control volume source parameters for later use as inputs to the receiver volumes at corresponding time intervals.

Subroutine HRSTM

Subroutine HRSTM calculates steam emissivity by using the product of steam partial pressure and control volume hydraulic diameter in conjunction with a plot of gas emissivity versus gas temperature given in McAdam°s Figure 4-15. The resulting emissivity is used to calculate a radiant heat transfer coefficient between the control volume gas and wall surface.

Subroutine PROP

Subroutine PROP evaluates hydrogen and water properties. The routine is specifically used in the M-module code to obtain hydrogen and steam specific heats, conductivities, and viscosities for use in the gas-to-structures heat transfer analysis.

Subroutine INTERP

Subroutine INTERP is used in conjunction with subroutine PROP and performs required properties' interpolation.

2.2 C MODULE DESCRIPTION

C module is a correlative code which provides estimates of aerosol and fission product release rates from the core during the period of core melting in a light water reactor. Quantifying the aerosol and fission product release from the core region is an important first step in the determination of radionuclide source term for the containment during a hypothetical severe core damage accident. The timing of the release of various materials is an important influence on their retention in the reactor coolant system. This is because the timing of release determines which specie emanating from the core will be available for interaction. The timing also determines the residence time of the released materials and the temperatures which they encounter in the RCS, since these are both dynamic parameters. Simplistic source terms, such as constant or linearly increasing release rates with concurrent releases for all radionuclides, may therefore lead to unreleastic estimates of radionuclide transport behavior.

The C module computes fission product and structural material release from the core as a function of time and temperature. The code is capable of considering up to 10 radial and 24 axial divisions of the core for a total of 240 nodes and 16 separate species. The initial inventories of various fission products are obtained from the program ORIGEN or a similar source and, in this study, are apportioned among 240 core regions specified by axial height according to the radial and axial power profile. In an actual PWR the distribution would vary both axially and radially and would change with time. Typically in a PWR, fuel is shifted between three radial zones during its irradiation history. In order to flatten the

power distribution across the core the freshest fuel is placed in the outside zone of the core and the most highly burned up fuel is placed in the central region. An abrupt change in the spatial distribution of radionuclides occurs therefore at the time of refueling but then continues to shift during the cycle as the fissile inventory is preferentially depleted in the regions of higher flux.

Alternate distributions of fission products can be used in the C module and the effect on the fission product release rates of the "flat-tube" assumption can be quantitatively assessed by examination of the results of parametric studies. It is expected that uncertainties in the release rate coefficients will have a more significant effect on release rates than will the assumptions regarding fission product distribution among core regions.

Temperatures at each of the nodes are obtained from the MARCH 2.0 code for each number of time steps beginning at the start of the accident and continuing to a user specified time. An average temperature is computed over each time span during core heatup and melting, and if the temperature is less than 900 C for any node, no release will occur before failure of the cladding of a fuel rod. When any axial position in a fuel bundle achieves a temperature of 900 C, a gap release of certain volatile fission products is calculated by the code for all of the fuel rods in that radial zone. This is intended to simulate the gap release accompanying the bursting of individual fuel rods. This release occurs due to accumulation in the gap between fuel and cladding of certain fission products caused by migration within the fuel. The amount of the gap release is taken to be 5

percent of the initial amount present for cesium, 1.7 percent for iodine, 3 percent for the noble fission gases, .01 percent for tellurium and antimony, and .0001 percent for barium and strontium. Since this emission is very small in comparison with the melt release, and is concurrent with the melt release, it is not treated separately in any of the transport analyses. Clearly, the gap release would require more careful analysis if less severe hypothetical accident conditions were considered.

Subsequent mass release as the nodes progress towards melting is calculated on a nodal basis as the product of the amount of each species remaining, the release rate coefficient, and the time interval of integration. The mass released is then summed over all the nodes in the core for each species to give a total mass released during the time step. It should be noted that the MARCH 2.0 code predictions for core temperatures do not take into account the heat of vaporization of materials released from the core.

The computation of the fractional release rate coefficients for fission products is based on empirical correlations derived from experiments performed by Lorenz, Parker, Albrecht, and others. The data from these experiments were graphed and curves developed as depicted in Figure 2.4. A fractional release rate coefficient, K(T), is derived for each species by fitting an equation of the form:

$$K(T) = Ae^{BT}$$

to correspond to each of these curves. The resulting values of A and B for three different temperature regions of the graph are given in

Table 2.1. It should be noted that the fractional release rate is a function of temperature and elemental species only, and any effects of pressure and specific surface area of the melt on the release rate are not considered. Additionally, details of complex phase interactions of various components within the melting core are, for the most part, not known quantitatively and hence the release rates are valid only to the extent that the experiments upon which the release rates are based adequately modeled a core meltdown situation.

There are several uncertainties associated with the C-module predictions which are not immediately apparent. These uncertainties most strongly impact the predicted aerosol release rates, rather than the more volatile materials whose releases are less sensitive. One difficulty in predicting aerosol release is due to the fact that as core melting progresses, the temperatures increase throughout the core until, eventually, a loss of geometry would be expected to occur. There is no means currently available to predict the manner in which this will occur. The assumption used in the MARCH 2.0 code is that the entire core slumps at the time 75 percent of the nodes in the core are molten. The core is presumed to be quenched by the water remaining in the lower plenum at this time, resulting in a very much reduced rate of aerosol generation. In the C-module this phenomenon is simply simulated by halting the release of all materials at the time of core slumping. No subsequent release is considered in these analyses until the core-concrete interactions begin.

The behavior of the control rods during core melting is also a source of uncertainty with respect to aerosol generation. In the sequences modeled here, the rods are fully inserted into the core, and it is assumed that

these rods are at the same temperatures as the core node in which they reside. Thus, the release of control rod materials is simulated in the C module by the addition of the tin, steel, cadmium, silver and indium to the inventory of materials available for release as aerosols. Because of the low melting point of silver, it was assumed that silver would solidify in the core region and thus would not participate in the aerosol. In addition, 40% of the other* materials comprising the aerosol were assumed to be retained in the core region. The boron poison present in the rods is not considered as a source of aerosol material though it is understood that it may play a role in aerosol formation.

One further point regarding the calculation of release rate coefficients should be noted here. During core melting, the MARCH 2.0 code predicts instances of core nodal temperatures above the UO_2 melting point which are not regarded as being realistic. The use of these high values in the expression for the release rate coefficients would lead to excessively high estimates of release rates for the lower volatility materials. The release rates calculated in this work therefore are calculated using a temperature value of 2760 C in place of any values predicted by MARCH 2.0 in excess of this value. This selection of a maximum temperature was based upon the approximate UO_2 melting temperature of 2880 C. The "Technical Bases Report", NUREG-0772 states that the melting point of UO_2 may be lowered by up to 300 C with the addition of ZrO_2, and even lower with other compounds, such as control rod material. Thus, it is not clear at present what this maximum achievable temperature should be. Below is a brief description of the C module subroutines:

*All materials other than the noble gases, iodine, cesium and tellurium.

Subroutine CORSOR

This is the main subroutine which drives the analysis process.

Subroutine INVENT

Defines the initial inventories of fission products, core materials and control rod materials. Furthermore, INVENT1 distributes fission products according to an axial and radial power distribution. Core materials are distributed radially according to the core volume fraction for each radial region. Control rod material is distributed equally over the radial and axial nodes defined by the fuel nodalization scheme.

Subroutine CONROD

Calculates the release of control rod alloy material based on the fuel nodes time-temperature history provided by MARCH 2.0.

Subroutine CORTEM

Reads MARCH 2.0 core nodal temperature data.

Subroutine EMIT1

Calculates, emission rates according to Table 2.1 constants, and the remaining amount of fission products at each of a user specified number of nodes in a core. Time steps and temperatures are obtained from the MARCH 2.0 code. Initial fission product inventories are obtained from INVENT1.

Subroutine RATE

Calculates, writes and stores release rates needed by the T-module.

2.3 T MODULE DESCRIPTION.

Essentially, the T module considers a system of an arbitrary number of control volumes that are connected by fluid flow in an arbitrary way. In each control volume a radionuclide species can reside on at least two carriers, either in particle (liquid or solid) or vapor form. Combining the phase of the fission product species with the concept of carrier, one can describe four states in which the species may reside:

- steam-molecular
- steam-particle
- walls-molecular
- walls-particle.

This list of states is not necessarily exhaustive (for instance, for two-phase flow, the carrier water must be considered) and the logic of the code has been chosen to readily accept an arbitrary number of states. It must be realized, however, that the addition of extra states increases computer running times.

2.3.1 Transport Rate Equations

Radionuclide transport can occur among the four states of an individual control volume or between certain states of different control volumes if they are connected by fluid flow. The former types of transport are generally limited by molecular effects and are modeled and correlated in the code itself. Transport of the fission products between control volumes is assumed to occur in phase with fluid transport. This transport is imposed by time-dependent thermal-hydraulic data read into the code in subroutine INPUT.

It is important to consider the types of flow or extent of mixing expected, and to specify criteria for their evaluation. Transverse mixing is approximated by turbulent or convective flow. Longitudinal mixing does not occur and is only approximated, provided fractional deposition within a control volume is small. This criterion can be quantified for the simple situation of a single control volume in which only particle deposition with deposition velocity, v_d, occurs. Then analysis of the homogeneously mixed case gives at steady state:

$$\frac{n}{n_o} = \frac{1}{1 + (A_d/A_c)\, v_d/v} \qquad (1)$$

where

n = final particle concentration

n_o = initial particle concentration

v = flow velocity

A_d = deposition area

A_c = cross flow area

while the more accurate differential flow analyses gives, again for steady state:

$$\frac{n}{n_o} = \exp[-(A_d/A_c)(v_d/v)] \qquad (2)$$

The two expressions agree approximately, provided

$$A_d v_d / A_c v << 1 \qquad (3)$$

If one defines

$$T_f = L/v \quad = \text{residence time for flow}$$

$$= V/A_d v_d \quad = \text{residence time for deposition,}$$

where

L = length of volume along with flow direction
V = volume,

then the criterion that the completely mixed control volume approach used in the T module be adequate is

$$\frac{T_f}{T_d} << 1 \qquad (4)$$

and the criterion that steady state be reached is

$$t >> \left(\frac{1}{T_f} + \frac{1}{T_d}\right)^{-1} \qquad (5)$$

Based on considerations of the above criteria, it is assumed in the T module that a given LWR primary system can be subdivided into a sufficient number of control volumes such that the radionuclide population in each of these is expected to be well mixed. It is further assumed that the transport rates of a radionuclide between states of a given control volume are proportional to the amount of the fission product in the state from which transport occurs. This latter assumption is equivalent to the concept of a mass transfer coefficient or deposition velocity. Working with the mass of a given radionuclide specie rather than its symmetrical treatment, the underlying transport equations of the T module code are:

$$\frac{dM^k_{lm}}{dt} = S^k_{lm} + \sum_{n\neq m} {}^{m}\beta^k_{lm}\, M^k_{ln} - \sum_{n\neq m} {}^{n}\beta^k_{lm}\, M^k_{lm} + \sum_{j\neq l} {}^{l}F_{jm}\, M^k_{jm} - \sum_{j\neq l} {}^{j}F_{lm}\, M^k_{lm} \qquad (6)$$

Here

M^k_{lm} = mass of radionuclide specie k in volume l and state m

S^k_{lm} = source rate of specie k in volume l and state m

${}^{n}\beta^k_{lm}$ = transfer coefficient for transport of specie k in volume l from state m to state n

${}^{j}F_{lm}$ = transfer coefficient for transport of fission product in state m from volume l to volume j.

Equation (6) may be rewritten as

$$\frac{dM^k_{lm}}{dt} = S^k_{lm} + \sum_{n\neq m} {}^{m}\beta^k_{ln} M^k_{ln} + \sum_{j\neq l} {}^{l}F_{jm} M^k_{jm} + E^k_{lm} M^k_{lm} \qquad (7)$$

where

$$E^k_{lm} = -\left[\sum_{n\neq m} {}^{m}\beta^k_{lm} + \sum_{j\neq l} {}^{j}F_{lm}\right]$$

If m signifies a surface state, ${}^{n}\beta^k_{lm}$ represents a mass release rate P; if m signifies a volume state, ${}^{n}\beta^k_{lm}$ represents a deposition

velocity, v_d, multiplied by the area available for deposition, A_l, and divided by the volume, V_l, of the control volume. Thus,

$$ {}^{n}\beta k_{lm} = v_d(m,n,l,k)\frac{A_l}{V_l} \qquad m = \text{volume state} \qquad (8) $$

$$ = P(m,n,l,k) \qquad m = \text{surface state} $$

Both v_d and P are, in general, strongly dependent upon on the thermal-hydraulic conditions existing in the given control volume. Since these in turn are time dependent, v_d and P are themselves functions of time. This time dependence places conditions on the technique used in solving Equation (6). These are considered in the subsequent section.

To permit flexibility in transport analyses of a variety of systems, the β coefficients are developed in a separate subroutine, BETV, (discussed in some detail in Section 2.3.2.2.). A separate subroutine FF, is reserved for the development of the transfer coefficients, F, for transport between volumes. This subroutine is discussed in Section 2.3.2.1.

T module does not account for chemical reaction kinetics. This implies that Equation (6) separates with respect to explicit dependence on k. Implicitly, coupling with respect to k remains through joint radionuclide transport on mixed aerosol particles. This coupling can, however, be accounted for by simultaneous time translation of Equation (6) for each k for each time step. For simplicity, the superscript k can therefore be dropped in the following.

To simplify the logic and to decrease running time of the code the two-dimensional matrix M_{Im} is linearized by a mapping subroutine, MAPV, from a two-dimensional array into a linear array. MAPV joins the rows of M_{Im} head-to-tail in the linear array M as exemplified in the following simple FORTRAN example which maps the matrix X(10,10) into the linear array Y(100):

```
      DO 1 I = 1,10
    1 MAPV(I) = (I - 1)*10 .
```

X(I,J) and ((MAPV(I)+J) are now in a one to one relationship.
The elements ${}^{m}\beta_{In}, {}^{I}F_{Jm}$ of Equation (6) can then be combined in a two-dimentional matrix A such that Equation (6) can formally be written

$$\frac{dM}{dt} = S + AM \qquad (9)$$

Note that S and M are one-dimensional matrices, or vectors. The elements of A are developed in the subroutine MATRIX.

2.3.1.1 Solution Technique

While a formal solution to Equation(9) can be written for a general time dependent source vector S and a general time dependent transport matrix A, this cannot, in general, be done in closed form. That is, the formal solution involves exponential series of integrals that must be evaluated numerically. For this reason, as well as for difficulties associated with the mass transfer coefficient approach in connection with some transport processes, Equation (9) is solved under the assumption that both S and A are essentially independent of time for the duration of a time step. In fact, the size of each time step is chosen specifically to fulfill this requirement.

With the assumption of time independent S and M, the solution to Equation (9) is found by iteration:

Noting from Equation (9) that the higher derivatives of M obey the recursion relation

$$M^{(n+1)} = AM^{(n)} ,$$

The Taylor expansion for M

$$M = M_o + M_o^{(1)}t + M_o^{(2)}t^2/2! + \ldots\ldots\ldots$$

becomes

$$M = M_o + (S_o + AM_o)t + A(S_o + AM_o)t^2/2! + \ldots\ldots\ldots$$

which may be written as

$$M = M_o + (1 + z/2! + z^2/3! + \ldots\ldots)(AM_o + S_o)t \quad (10)$$

where $z = At$.

Equations analogous to (9) and (10) are encountered in the computer code CORRAL where z is manipulated as a two-dimientional array, which permits the use of a scaling procedure to ensure rapid convergence. In order to do so efficiently, however, powers of z are evaluated, which implies that the solution algorithm is rather time consuming (computation time is dependent on the third power of the order of z).

Since the very much larger order of the z matrices employed in the present codes make the CORRAL solution algorithm impractical, a faster solution technique was sought. Instead of working with powers of z, an iterative scheme is used which is illustrated by rewriting Equation (10) as

$$M = M_o + (AM_o + S)t + z/2\,(AM_o + S)t + z/3\,[z/2\,(AM_o + S)t] + \ldots\ldots \qquad (11)$$

That is, each successive term (after the second) is found from the preceding terms by multiplication with the factor z/n, where n is one minus the number of the term. Thus, powers of z are never evaluated and the running time for this solution algorithm depends on the second power of the order of z. It is therefore substantially faster than the CORRAL algorithm for problems involving large z matrices.

Summation of the series solution (11) is cut off when the addition of a following term of the series produces a relative change in M whose absolute value is less than a predetermined amount. Since scaling is not employed, this may require successive evaluations of the solution for short time intervals t in order to ensure convergence within a reasonable number of iterations. An additional constraint on the time interval arises from the requirement that the vectors S and M be approximately constant over the time interval under consideration. This is assured by requiring the absolute values of relative changes of the elements of S and M to be less than a predetermined value over the given time interval.

The solution as expressed by Equation (11) is programmed in the subroutine MATSA.

2.3.1.2 Structure and Linearization of the A Matrix

Each element of the A matrix is identified by the subscripts I and J (volumes) and m and n (states). The linearization of the M_{Im} vector casts the A matrix into the form given below, where the location of each subarray or block is defined by the values of I and J. Thus, off-diagonal sub-blocks describe intervolume transport between volumes I and J while diagonal sub-blocks describe intravolume transport for volume I. The location of any elements within each sub-block is defined by m and n.

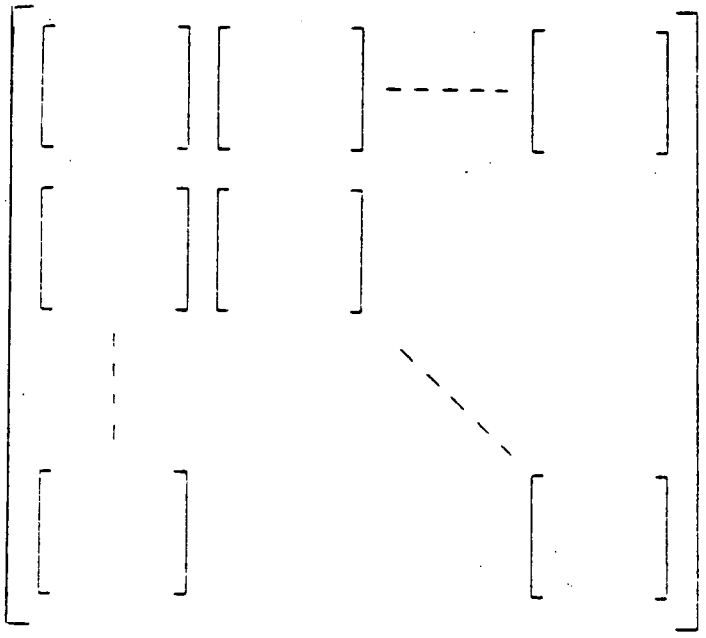

Off-diagonal sub-blocks contain the $^{J}F_{Im}$ coefficients while diagonal sub-blocks contain the^{n} k_{Im} coefficients (Equation 6). This is illustrated for a three state, three volume case below:

$$
\begin{bmatrix}
\begin{bmatrix} E_{11} & {}^{1}\beta_{12} & {}^{1}\beta_{13} \\ {}^{2}\beta_{11} & E_{12} & {}^{2}\beta_{13} \\ {}^{3}\beta_{11} & {}^{3}\beta_{12} & E_{13} \end{bmatrix} &
\begin{bmatrix} {}^{1}F_{21} & & \\ & {}^{1}F_{22} & \\ & & {}^{1}F_{23} \end{bmatrix} &
\begin{bmatrix} {}^{1}F_{31} & & \\ & {}^{1}F_{32} & \\ & & {}^{1}F_{33} \end{bmatrix} \\
\begin{bmatrix} {}^{2}F_{11} & & \\ & {}^{2}F_{12} & \\ & & {}^{2}F_{13} \end{bmatrix} &
\begin{bmatrix} E_{21} & {}^{1}\beta_{22} & {}^{1}\beta_{23} \\ {}^{2}\beta_{21} & E_{22} & {}^{2}\beta_{23} \\ {}^{3}\beta_{21} & {}^{3}\beta_{22} & E_{23} \end{bmatrix} &
\begin{bmatrix} {}^{2}F_{31} & & \\ & {}^{2}F_{32} & \\ & & {}^{2}F_{33} \end{bmatrix} \\
\begin{bmatrix} {}^{3}F_{11} & & \\ & {}^{3}F_{12} & \\ & & {}^{3}F_{13} \end{bmatrix} &
\begin{bmatrix} {}^{3}F_{21} & & \\ & {}^{3}F_{22} & \\ & & {}^{3}F_{23} \end{bmatrix} &
\begin{bmatrix} E_{31} & {}^{1}\beta_{32} & {}^{1}\beta_{33} \\ {}^{2}\beta_{31} & E_{32} & {}^{2}\beta_{33} \\ {}^{3}\beta_{31} & {}^{3}\beta_{32} & E_{33} \end{bmatrix}
\end{bmatrix}
$$

Note that only the diagonal elements of the off-diagonal blocks are non-zero and that these in turn are only non-zero when a flow connection exists for flow from volume j to volume i. For reactor primary systems, the number of flow connections per volume does not often exceed 2. Most of the possible off-diagonal block elements are in fact zero.

The diagonal elements of the diagonal blocks E_{im}, represent fission product transport from volume i and state m. Because fission product mass must be converted, they can be expressed as sums over β and F elements residing elsewhere in the complete A matrix (Equation (7)).

In order to conserve computer storage space, and to greatly reduce the long running times associated with the manipulation of such large matrices, the matrix A is itself linearized by again employing a mapping vector scheme. In addition, such a scheme readily permits the deletion of the zero elements of A.

The storage array for the A matrix is filled at the beginning of each time step by calling up the subroutine BETV, which constructs the β's, or intra-volume transfer coefficients, and by calling up FF which constructs the F's, or intervolume transfer coefficients. The procedure is to first develop the off-diagonal blocks and the off-diagonal elements of the diagonal blocks. These are then used to evaluate the diagonal elements of the diagonal blocks. This process is repeated in turn for each chemical specie considered. Since the intervolume transfer coefficients are independent of the particular specie under consideration, these are evaluated for the initial specie only.

2.3.2 MODEL FEATURES

2.3.2.1 Intervolume Mass Transfer

Transport of radionuclides between volumes is assumed to occur solely by convection. Considering only superheated steam flow, it thus occurs only for the states steam-molecular, and steam-particle.

Thermal-hydraulic data and the steam mass flow rates are read into the code from the M module calculations.

Since each control volume is assumed well mixed, the rate of nuclide transport out of a volume is just the fractional rate of change of mass of the carrier (steam):

$$J_{F_{lm}} = \frac{FXS(l,j)}{\rho_s(l)V(l)} \qquad (12)$$

where

FXS(l,j) = steam mass flow rate from volume l to volume j

$\rho_s(l)$ = density of steam in volume l

V(l) = volume of volume l.

Here, ρ_s is determined from correlations related to temperatures and pressures. Thus, the convective exchange of matter between control volumes is driven by the input values for steam production rates. However, the exchange of material between control volumes used to describe the upper plenum regions should be driven by the sum of the net steam flows and the natural convection flows which seem to be much greater than the steam flows in many cases. Consideration must also be given to the non-unidirectional nature of the natural convection flow patterns.

In the RCS and in particular in the upper plenum of the primary vessel, the T module is applied in such a way that the transport between control volumes is treated as if it were given by the net steam production rates as calculated by MARCH 2.0/M module. However, for a number of the sequences analyzed, thermal driving forces are calculated to be large enough to produce natural convection currents that are much stronger than the steam evolution rates from the core. Such natural convection should enhance material transport among connected flow volumes, and so enhance the mixing between control volumes. In essence, then, the conditions expected to exist for concentration of aerosols and vapors may actually be in closer agreement with the "well-mixed" assumption than one would be led to believe by the MARCH 2.0/M module developed input flows between control volumes.

The M and T modules both attempt to account for enhanced heat and mass transport coefficients resulting from natural convection. However, the application of the calculated heat and mass transport coefficients in conjunction with the inherent uni-directionality of the control volume approach used in the T module seems to be a questionable approach. It is the area of inappropriate and non-unified thermal hydraulics and mass transport within the primary reactor vessel that is seen as being the major shortcoming of the T module.

2.3.2.2 Intravolume Mass Transfer

Thermal hydraulic modeling in the T module is very important, because a number of the key deposition mechanisms modeled in the code rely on internal thermal-hydraulic calculations to determine parameters important to deposition. Models that rely on thermal-hydraulic calculations include, among others, those for vapor condensation onto walls and aerosol deposition onto walls by thermophoresis.

In the development of the the T module, it was acknowledged that forced-flow conditions might not always exist in the RCS; that is, that natural convection flow might be dominant under some conditions. To account for the influence of natural convection, the T module calculates an "effective" Reynold's number using the following formulation:

$$Re_{ef} = (Gr/70)^{0.5} \qquad \text{for } Gr > 10^7$$

$$Gr = [g(\Delta T)\ D^3]/\gamma^2 T$$

where

Re_{ef} = effective Reynold's number

Gr = Grashof number

g = gravitational acceleration

D = control-volume hydraulic diameter

ΔT = gas-wall temperature difference

T = gas temperatures,

γ = kinematic viscosity of steam

When the effective flow Re is greater than the Re calculated using the input steam production rates, then the effective Re is used to calculate condensation mass transfer coefficients and thermal gradients used in thermophoresis calculations.

At present, there has been no reference identified to document the basis for the correlation used to calculate an effective Reynold's number for conditions where natural convection dominates.

The correlation used in the T module to calculate an effective boundary layer thickness, and so an effective wall thermal gradient for thermophoresis calculations, is

$$Nu = hD/k = D/\delta = 0.021\ Re^{0.8}$$

where

Nu = Nusselt member, Re = Reynold's number

k = gas thermal conductivity

h = k/δ = heat-transfer coefficient

δ = boundary-layer thickness

D = control-volume hydraulic diameter

This is a heat-transfer correlation for turbulent flow conditions, which may not always exist in the RCS. In addition, the correlation is for fully-developed flow conditions, which may not exist through much of the upper plenum. If, for example, flow Reynold's numbers varied between 100 and 1000, then the so-called entrance length for full-developed flow in the upper plenum would vary from 6 to 60 hydraulic diameters downstream of the lower end of the upper plenum. Assuming an upper plenum hydraulic diameter of 4 inches, for these assumed Reynold's numbers, fully-developed flow would not occur within 2 to 20 feet of the upper plenum lower section. Nusselt numbers calculated for fully-developed flow conditions are typically less than those occurring in the flow entrance region.

Effective wall heat transfer coefficients would be under-estimated by assuming fully-developed flow by a factor of three or more.

The correlation used in the T module to model condensation mass transfer to wall surfaces is:

$$Sh = k_w D/D_g = 0.023\ Re^{0.83}\ Sc^{0.33}$$

where

Sh = Sherwood number, Sc = Schmidt number

Re = Reynold's number

k_w = condensation mass transfer coefficient (cm/s)

D = hydraulic diameter, D_g = vapor diffusion coefficient

This is again a correlation purely for turbulent, fully-developed flow conditions, and so the same criticism relevant to the calculation of Nusset numbers applies.

2.3.2.2.1 Condensation of Vapor Onto and Evaporation from Aerosols and RCS Surfaces

The condensation/evaporation of CsI, CsOH, and Te onto/from particle and wall surfaces is modeled in the T module using the following formulations:

$$\frac{dC_s}{dt} = -\frac{A_w k_w}{V}\left(C_s - C^s_w\right) - \frac{\langle A_p k_p \rangle}{V}\left(C_s - C^s_p\right)$$

$$\frac{dM_w}{dt} = A_w k_w \left(C_s - C^s_p\right)$$

$$\frac{dM_p}{dt} = A_p k_p \left(C_s - C^s_p\right)$$

where

C_s = M_s/V = concentration of the nuclide vapor in steam

M_s = Total mass of the nuclide vapor in steam

V = Volume of the control volume

M_w = Total mass of nuclide vapor condensed on walls

Mp = Total mass of nuclide vapor condensed on aerosol particles

C^s_w = Equilibrium vapor concentration of the nuclide at the temperature of the wall surfaces (assumed independent of pressure)

C^s_p = Equilibrium vapor concentration of the nuclide at the temperature of the steam (assumed independent of pressure and particle surface curvature)

A_w = Area of wall surfaces

A_p = Surface area of aerosol particle

k_w = Mass transfer coefficient for nuclilde transfer between steam and wall surfaces-steam interface

k_p = Mass transfer coefficient for nuclide transfer between steam and particle surface-steam interface

The correlations used for k_w and k_p are:

k_w= condensation mass transfer coefficient (cm/s)

$k_p = D_g/r$

where

D_g = vapor diffusion coefficient
r = particle radius

Possible inaccuracies related to the formulations used in the T module for condensation/evaporation include the following:

1. The correlation for k_w is applicable to well-developed turbulent flow conditions only; turbulent flow does not exist in the RCS for all accident sequences.

2. No account is taken for the possible influence of non-condensable gases on vapor condensation. Also, no account is taken for vapor pressure suppression at particle surfaces or due to multi-specie vapor solutions. Including these effects would lead to reductions in calculated vapor condensation rates.

3. The mass transport coefficient, k_w, used is one for steady-state transport in a fully-developed flow regime. For most sequences the flow can be characterized as being "quasi-steady" for the majority of time up to pressure vessel rupture. However, as discussed previously, fully-developed flow conditions are not likely to exist in the upper plenum for most accident sequences; including this effect would tend to increase the calculated vapor condensation rates.

2.3.2.2.2 Vapor "Sorption" Onto Wall Surfaces

The T module assumes that vapor sorption onto walls can be modeled using a "deposition velocity" model that can be expressed as:

$$\frac{dM}{dt} = - V_d \left(\frac{A}{V}\right) M$$

where

M = mass of vapor species airborne in control volume

v_d = vapor species deposition velocity (cm/s)

A = control volume surface area

V = volume in control volume

It is assumed in the T module that all "sorption" onto surfaces is irreversible. In addition, sorption onto aerosol particles is not accounted for. The deposition velocities used for I_2, CsI, CsOH, and Te are given below:

Specie	V_d(cm/s)
I_2	$9(10^{-8})\ e^{8100/RT}$
CsI	0
CsOH	0.01
Te	1.0

The deposition velocity model as used in the T module is empirical. Modeling sorption deposition velocities can hide complex mechanisms that might be occurring in the sorption process such as transport in the vapor phase, sorption/desorption at the surface, chemical reactions with the surface materials, and diffusion into the bulk of the surface or through a surface layer. Using vapor deposition velocity models would be appropriate if the system conditions are such that surface reactions are rate-limiting (that is, they dominate the transport mechanisms), if surface saturation effects do not occur, and if the empirical values are obtained under these conditions using appropriate materials, species, temperatures, and mass loadings. This is generally a very difficult assignment.

Some comments related to the accuracy of the values of deposition velocities used in the T module are presented below:

1. The correlation used for I_2 deposition velocity is based on the data from Genco et al. These tests were performed at temperatures between 150 and 550 C, and the agreement of the correlation with the data, in that for higher temperatures - more like those expected in the RCS - would seem to result in errors, based on measurements made by Battelle, of about a factor of two.

2. The deposition velocity used for CsI is zero. Data contained in a Battelle report indicates CsI deposition velocities less than 0.001 were measured for the temperature range relevant to the RCS; these are small values and provide some justification for the assumption of no CsI deposition by sorption.

3. The deposition velocities used for CsOH and Te were based on "Phase 1" deposition velocity measurements made for these species at Sandia Laboratories. Discussions with Sandia staff involved in the work indicate that the level of confidence one should have in these measurements is an order of magnitude, because the Phase 1 experiments were performed simply to get some scoping-type answers. The "Phase 2" experiments now being performed at Sandia will be performed over a range of temperatures (this was not done for the Phase 1 experiments), and the data to be obtained from those tests is expected to be more accurate.

The modeling of CsOH and Te sorption onto surfaces by the T module is limited by the fact that there is a very sparse data base available. The present efforts at Sandia, and also the effort starting at ORNL have the best likelihood of producing data that will permit better estimation of sorption processes for more species over a wider range of temperatures.

2.3.2.3 Aerosol Behavior

The underlying assumption of the aerosol model equations, one that is made by most present aerosol behavior codes, is that the aerosol can be viewed as a homogeneous mixture, except for narrow surface boundary layers through which mass transport of the particulate phase takes place. This assumption was tested for the special case of sodium pool fire aerosols with a model that sub-compartmentalizes the containment into three individually mixed zones connected by fluid flow and found to be adequate after the fire ceases and conservative during the burn period. It permits model equations that are independent of spatial coordinates and thus makes their numerical solution practicable.

The second, fundamental assumption is that the expected non-sphericicity and fluffiness of the aerosol agglomerates can be modeled using just two size independent correction factors -- the dynamic shape factor and the collision shape factor. These will be treated below. Their size independence is not an inherent requirement of the code but a convenient assumption in lieu of experimental data to the contrary.

Given these assumptions, the general equation of aerosol behavior is:

$$\frac{dn(x,t)}{dt} = S(x,t) - R(x,t)n(x,t) - L(x,t)n(x,t) - F(x,t)n(x,t)$$
$$+ 1/2 \int_0^x K(x',x-x')n(x',t)n(x-x',t)dx' - n(x,t) \int_0^\infty K(x,x')n(x',t)dx'$$

Here

$n(x,t)dx$	=	number of particles of mass x in dx at time t per unit volume
$S(x,t)dx$	=	number of particles of mass x in dx uniformly introduced into the aerosol system per unit time per unit volume
$R(x,t)n(x,t)dx$	=	number of particles of mass x in dx uniformly removed from the aerosol system per unit time per unit volume by deposition
$L(x,t)n(x,t)dx$	=	number of particles of mass x in dx uniformly removed from the aerosol system per unit time per unit volume by leaks
$F(x,t)n(x,t)dx$	=	number of particles of mass x in dx uniformly removed from the aerosol system per unit time per unit volume by filters
$K(x,x')n(x)n(x')dxdx'$	=	number of collisions between particles of mass x in dx and x' in dx' per unit time per unit volume.

2.3.2.3.1 Natural Removal Terms

Natural removal by sedimentation diffusion and thermophoresis are considered. This is described in general by a deposition velocity, $v(x,t)$ such that

$$R(x,t) = v(x,t) \frac{A_I}{V}$$

where

A_I = surface area available for deposition due to mechanism I
V = control volume.

v is taken as the steady state velocity $v = B(x)* F(x.t)$ with $B(x)$ the mobility of a particle of mass x and $F(x,t)$ the applied force. The mobility is given by

$$B(x) = \frac{1}{\chi\, 6\pi\mu r_e} \left\{1 + AKn + QKn\,[\exp(-\,b/Kn)]\right\}$$

with

χ = dynamic shape factor

μ = viscosity of gas

$r_e = [3x/(4\pi\rho_p)]^{1/3}$

ρ_p = particle material density

Kn = Knudsen number of particle

A = 1.246, Q = 0.42, b = 0.87

Here the Knudsen-Weber-Cunningham correction constants are those of Millikan for oil drops. Their precise values depend on the particle constituents, but do not effect sensitivity in typical code predictions.

2.3.2.3.1.1 Sedimentation

For particle Reynold's numbers less than one, the Stoke's settling velocity

$$v(x,t) = 4\pi/3\,[r_e^3\,\rho_p g B(x)]$$

holds. For some severe accident scenarios, however, the T module predicts a large fraction of the suspended mass to reside on particles whose diameter exceeds 100 μm. For these, the above equation no longer holds and may in fact be off by as much as a factor of two. The T module therefore uses empirical data in the form of a correction factor for particles whose Reynold's number is greater than one and less than 1259. For Reynold's numbers in excess of this value, no empirical values of v are known. As a compromise, the correction value for R_e = 1259 is used here as well.

To account for particle nonsphericity, it is assumed that a correction factor, f, exists such that

$$fC_F = \frac{F_D}{\pi r_e^2 \gamma^2 (\rho_g/2)\, v^2}$$

where

γ = collision shape factor

C_F = Fanning friction factor for spheres

F_D = actual drag force on particle

From the limit requirement that

$$F_D = 6\pi\chi x r_e v$$

and

$$v = \frac{2}{9}\frac{\rho_g g r_e^2}{\mu x}$$

in the Stoke's regime, one can determine f to be equal to x/γ. The collision shape factor, γ, was initially introduced to account for a collision cross-section of nonspherical particles that depends on a collision radius, r_c, different than r_e. Thus r_c was taken as proportional to r_e: $r_c = \gamma r_e$. γ has never been measured but approximate values have been inferred by backfitting computer codes. Unfortunately, γ has also been shown, along with χ, to be the most sensitive code parameter.

To avoid the introduction of further parameters of comparable sensitivity, γ is also used in the T module as a proportionality factor between some geometric particle radius, r, of an agglomerated, nonspherical, particle and its mass equivalent radius: $r = \gamma r_e$. Then all data correlated on spherical particles is written in terms of γr_e. Thus, in particular, $Kn = \lambda/\gamma r_e$, where λ is the gas phase mean free path.

2.3.2.3.1.2 Diffusion

$$v(x,t) = \frac{D(x)}{\delta_D}$$

where

$D(x)$ = $B(x)kT$

k = Boltzmann's constant

T = absolute temperature

δ_D = diffusion boundary layer thickness.

δ_D is known to depend on the momentum boundary layer thickness, δ_o, of the flowing gas-wall interface and on particle size through its dependence on D(x) via

$$\delta_D = \delta_o Sc^{-1/3}$$

where

Sc = $(\rho_g D)$

ρ_g = density of gas phase

Nevertheless, D is assumed an input constant since experimental evidence to the contrary is scarce and, more importantly, since diffusive deposition appears to play a minor role in reactor accident calculations.

2.3.2.3.1.3 Thermophoresis

Thermophoresis is driven by temperature gradients. These are usually not well known everywhere so that considerable uncertainty in code output exists for cases in which thermophoresis is significant. Because of this uncertainty, great precision in the expression for the thermophoretic deposition velocity is not necessary. The code uses an expression, developed by Brock, that agrees within a factor of two with available data:

$$F_{thermophoresis} = \frac{-9\pi\mu^2 r_e}{\rho_p} \Phi \frac{\Delta T}{\Delta T \delta_{TH}}$$

where

$$= \frac{1}{1 + 3C_m Kn} \quad \frac{k_g k_p + C_t Kn}{1 + 2k_g/k_p + 2C_t Kn}$$

T = temperature difference between wall surface and gas over the thermal boundary layer thickness, δ_{TH}.

C_m = momentum accommodation coefficient, taken as 1.0.

C_t = thermal accommodation coefficient, taken as 2.49

k_g = thermal conductivity of the gas phase

k = thermal conductivity of a particle

Since the Brock expression for the thermophoretic force is based on spherical particles, γr_e is used wherever a particle radius is referenced.

The values of C_m and C_t indicated are those that result in the best fit of the above expression with data for NaCl aerosol. Measurements on dry Na_2O_2 particles have yielded values of C_t between 1.9 and 2.5, with the former value based on the assumption that $k_g/k_p = 0.01$, the latter on kg/kp = 1.0. For fluffy agglomerates, the thermal conductivity, k_p, as used in the expression, probably does not correspond to the particle's material thermal conductivity. It is likely that k_p approaches k_g with increase in fluffiness, but no independent measurements of k_p are known.

It should be noted that for severe accident scenarios, most of the airborne mass is associated with particles whose Knudsen number is small. In this case,

$$\Phi \rightarrow \frac{1}{2 + k_p/k_g}$$

and is thus essentially independent of C_t, and C_m, but a strong function of the unknown, k_p. Its uncertainty is comparable, in effect, to that in the average thermal gradient at interior surfaces.

2.3.2.3.2 Coagulation

Of the multitude of mechanisms that can contribute to particle collisions (and therefore coagulation) only two appear to play a significant role in passive aerosol systems: Brownian and gravitational coagulation. The T module includes these and turbulent coagulation since the latter may play a role in situations where natural convection becomes severe enough to result in significant turbulent energy dissipation.

(I) Brownian Coagulation

$$K_B(x,x') = 4\pi kT\gamma[\, B(x) + B(x')](r_e + r'_e)$$

(II) Gravitational Coagulation

$$K_G(x,x') = \epsilon(x,x')\frac{2\pi g \rho_g \gamma^2}{9\mu\chi}\left|r_e^2 - r'^2_e\right|(r_e + r'_e)^2$$

where

$\epsilon(x,x')$ = collision efficiency.

The collision efficiency can be viewed as that factor which makes the general equation of aerosol behavior correct. Most recent experimental and theoretical investigations into this factor have yielded data tables that

have been employed in the T module on large scale sodium fire simulation runs. The results of these runs are surprisingly similar to ones using the simple expression

$$\epsilon(x,x') = 1.5[\, r/(r + r')^2$$

where x', r' refer to the larger particle. This expression strictly holds for inertialess particles and r'>>r only. Its use for all values of r' and r yields satisfactory agreement with simulation experiments to date.

2.3.2.3.2.1 Turbulent Coagulation

An expression for turbulent coagulation was added to the T module in the expectation that sufficient turbulence would exist to make this mechanism significant. Pressure simulation experiments suggest that it plays a noticeable, but minor, role.

The two most widely used theoretical treatments of turbulent coagulation are probably those of Saffman and Turner and Levich. Both are based on the hypothesis that microscale turbulence is essentially isotopic and that the particles are smaller than microscale. Both also invoke the same conceptualization of the turbulent collision process: relative particle motion due to entrainment in a variable fluid velocity field and relative particle motion due to differences in inertial response to fluid acceleration. It is not surprising therefore that, since quantification of isotropic microscale turbulence is based on dimensional analysis, the two approaches result in identical expressions except for multiplicative constants. By the same token, these multiplicative constants must be considered indeterminate until experimentally determined.

The T module expression for turbulent coagulation is based on Saffman and Turner's, including their multiplicative constants. Their expressions have been modified to include a collision efficiency for particle motion relative to the fluid and the shape factors for non-spherical particles discussed above. While the collision efficiency for particles colliding due to their motion with a variable fluid velocity field may not be unity, it was assumed as such in the T module. Thus

$$K_{T+G}(x,x') = 2(2\pi)^{1/2}\gamma^2(r_e + r'_e)^2[\epsilon(x,x')^2(\tau_1-\tau_2)^2 1.3E^{3/2}/\nu^{1/2} + 1/3\ \epsilon(x,x')^2(\tau_1-\tau_2)^2 g^2 + 1/9\gamma^2(r_e+r'_e)^2 E/\nu]^{1/2}$$

where

τ = $2r_e^2\rho_p/(9\mu\chi)$ = particle time response

ν = kinematic viscosity of the gas

E = turbulent dissipation energy density

Note that, following Saffman and Turner, the gravitational coagulation mechanism is incorporated into K_{T+G}.

Finally, the assumption is made that

$$K(x,x') = K_B(x,x') + K_{T+G}(x,x').$$

Since K_B and K_{T+G} are of equal magnitude over a narrow particle size range only, this approach is not expected to result in significant error.

2.3.2.3.2.2 Laminar Coagulation

The influence of aerosol deposition due to laminar flow is modeled in T module using the relation:

$$\frac{dC}{dt} = - V_{d,lam}(A/V)C$$

$V_{d,lam}$ = laminar flow deposition velocity

Aerosol deposition from laminar flow for any particle size can be calculated accurately. An expression developed by Gormley and Kennedy for the fractional number of particles deposited in flows in circular pipes is:

$$N/N_o = 0.8191e^{-7.314h} + 0.0975e^{-44.6h} + 0.0325e^{-114h}$$

$$n > 0.0156$$

$$N/N_o = 1 - 4.07h^{2/3} + 2.4h + 0.446h^{4/3}$$

$$n < 0.0156$$

where

N = number of particles that reach the end of the pipe length L.

N_o = number of particles that enter the pipe (distributed uniformly over the cross section)

$h = LD/2va^2$

a = pipe radius

A fictitious deposition velocity for an equivalent, completely mixed system can be derived from these expressions as follows:

Letting n be the concentration of particles in the completely mixed volume and n_o the concentration of particles entering the volume, the deposition velocity, v_d, across a boundary layer is defined by the expression

$$\frac{dn}{dt} = - v_d \frac{A}{V} n$$

where

A = surface area
V = volume

for $v_d/v = <<1$, therefore,

$$n - n_o = v_d(A/V)(L/v)n = - v_d(2/a)(L/v)n$$

or

$$v_{d,lam} = (n_o/n - 1)av/2L = (N_o/N - 1)\ av/2L$$

2.3.2.4 Missing Phenomena

In the T module as in most codes, there may be phenomena that have been left out; or implied assumptions and approximations due to the particular application that could be important to the overall assessment of the validity of the code for given applications. Some items that could possibly fit into this category are discussed below.

2.3.2.4.1 2-Dimensional Thermal Hydraulics

The control volume formalism used in the T module does not lend itself easily to the presence of the presumed essentially 2-dimensional recirculating flow patterns in the primary reactor vessel, especially if these flow patterns penetrate the "boundaries" chosen for the control volumes.

2.3.2.4.2 Resuspension of Deposited Aerosols

There are presently provisions in the T module to account for resuspension of aerosols from surfaces due to the high flows that might occur at core slumping or pressure-vessel melt-through. However, this option has not been exercised in this study.

2.3.2.4.3 Chemical Reactions of Deposited Materials With Surfaces

The chemical species of the fission product forms assumed to be liberated from the core are input to the T module. The fission products that deposit onto surfaces are assumed to stay in the same chemical form. If the chemical form of the deposited materials were to change due to interactions with surface materials, the deposited fission products would either be more or less volatile in terms of their potential for re-evolution from the surface.

2.3.2.4.4 Aerosol Impaction

Because of the nature of the flow patterns and geometry of the upper-plenum regions it would appear that direct impaction of aerosols onto the surfaces could be a significant aerosol removal mechanism not presently modeled in the T module.

2.3.3 Flow Chart and Brief Description of Subroutines

To help the reader grasp the overall interactions of the various mechanisms and phenomenological models in the T module, an "influence diagram" is shown in Figure 2.5. This influence diagram is designed to present in compact form a detailed picture of what phenomena are treated by the code and how these phenomena interact with each other. If a

particular phenomenon has a direct influence on another (i.e., if the value of the key variable associated with that phenomenon enters explicitly into the mathematical model expressing the "influenced" phenomenon behavior) then this is indicated by a connecting line with an arrow showing the direction of the interaction. For example, as seen on Figure 2.5, gravitational deposition is treated in the code and is indicated to depend directly on only the particle size distribution and the aerosol concentration (it also, however, depends directly on the control volume geometry which is indicated on the diagram as an input by placing it in a square box).

In addition to being influenced by the concentrations and particle size distributions, gravitational deposition, in turn, directly influence the concentration (by removing material) and the size distribution (by selectively removing larger particles at a faster rate). Consequently, the connections showing the interactions among these items are given as two lines with arrows going both ways.

Items outlined by the dashed lines are intended to demonstrate that there may be phenomena that could have an influence but are not explicitly treated in the code.

Figures 2.6 and 2.7 show the main logic of the T module. Moreover, each subroutine is described briefly below.

It should be emphasized that the general dynamics of the steam-nuclide system of a LWR primary system during meltdown have been divided into

three categories, each with its own response time. These are: phase transitions (treated in ADHOC), particle deposition and agglomeration (treated in COCALL) and vapor deposition and flow (treated in BETV, FF, MATRIX, and MATSA). The response times are such that it appears plausible to treat phase transitions with the remaining system at psuedo steady state and again to treat agglomeration with flow and deposition of nuclides at psuedo steady state.

The solution of the total dynamics of the system is therefore carried out sequentially rather than simultaneously by first performing phase change transitions, then flow and vapor deposition transitions over a time step during which agglomeration causes only small changes in particle size parameters. Finally, the size distribution is changed by agglomeration and particle deposition, taking flow, deposition, and source of particles into account.

Subroutine INPUT

All input to the T module is read into the code in INPUT in engineering units and immediately written out in those units. These are then converted to the working cgs-Kelvin units of the code, except for the particle radius (μm), particle geometric mean radius (μm), and particle geometric mean radius cubed (μm^3)

INPUT is subdivided by the subheadings

- Control Data and Program Constants
- Sensitivity Multipliers
- Geometric Data
- Thermal-hydraulic Data
- Initial Conditions
- Source Data

Subroutine ADHOC

ADHOC solves the mass transfer equations for vapor-to-liquid transitions of species such as I_2 or CsOH over the time step determined by TSTEP.

The change of particle radius due to condensation and evaporation of a nuclide specie is calculated in ADHOC. To do so, the average change in particle mass is used to calculate a new value of the geometric mean radius. The average particle density read in as input is used.

Subroutine BETV

The deposition velocity elements, ${}^{n}\beta^{k}_{lm}$ Equation (6), are developed in BETV which is organized so that new expressions can readily be inserted as they become available.

Subroutine CDIFF

Calculates necessary derivatives for analytical solutions of DC/DT = S+AC in MATSA.

Subroutine CFORM

The nuclide mass of each state of the system is stored in the vectors C and CO. C is a temporary storage variable employed in MATSA. To conserve computer memory, C and CO are overwritten as each new specie is considered.CFORM is used to transfer each specie dependent image of CO to external core storage and to retrieve these images as needed.

Subroutine COCALL

COCALL is the interface subroutine between the T module and the aerosol behavior subroutines provided by QUICK.

Subroutine DEPO

Calculates the cumulative mass removed by diffusion, themophoresis, sedimentation, filtration, and leakage. The rate of mass loss for each size interval for each removal mechanism is calculated and the lost mass is determined by a simple Eulerian integration in order to optimize code running time.

Subroutine DIFFUN

Computes the rate of change of the number of particles in each size interval, required by the fifth-order Runga Kutta solver routine. The first portion of the routine handles coagulation by two particle collisions. The second portion of the routine includes the effects of the source and removal terms.

DIFFUN uses the next to last and the last channel to accumulate the number and mass, respectively, of particles which grow beyond the range of particle size being considered. The number of channels in this range is NS-1. (See INIT and SOURCE for a discussion of the development of NS.) As the particle size distribution widens, NS is increased to include larger particles in the system of equations. (See EXTEND for a description of the channel extension procedure.)

Subroutine DROP

Does the opposite of EXTEND described subsequently.

Subroutine EMOVE

Transfers the contents of one vector into another and vice versa.

Subroutine EXTEND

When coagulation necessitates the inclusion of an additional channel in the distribution, subroutine EXTEND performs the required operations. The solver routine is restarted with a reduced Δt, and NS is incremented by 1.

The lost number and mass channel numbers are also incremented by 1 to maintain a running total for number and mass lost from the end of the distribution.

Subroutine FF

FF calculates the flow terms JF_{lm} of Equation (6). These are simply the mass flow rate of steam through junction lj divided by the mass of steam in volume l.

Subroutine FINDY

FINDY is a general linear interpolation routine for arbitrary spacing of arguments. It is used principally for interpolating input tables of data.

Subroutine FLUID

Fluid properties, dimensionless groups, and particle-fluid properties are calculated in FLUID for all volumes over a given time. These are as follows:

- steam velocity
- steam viscosity
- steam Reynold's number
- the turbulent energy dissipation rate for steam
- the temperature gradient at the wall surfaces using the Dittus-Boelter correlation for the heat transfer coefficient for pipe flow together with input data on temperature differences between bulk flow and wall surfaces
- the friction velocity of the steam
- the mean free path of the steam
- the Knudsen number of an average particle
- the slip correction factor for an average particle
- the diffusion coefficient of an average particle

Subroutine INIT

Three initial distributions are selected. Two of these distributions are used when checking against special analytic solutions to the aerosol equation. The third distribution is the log normal distribution used for most aerosol work. INIT initializes the distribution for the selected case. In conjunction with the BMIN1 code control parameter, INIT determines NS which determines the number of channels which are considered by DIFFUN.

Subroutine KERN

Three forms of the coagulation kernel are available in KERN. The three are Brownian, gravitational and turbulent coagulation. If turbulent coagulation stops during the problem, KERN is recalled to recompute the kernel without turbulent coagulation.

Subroutine MATRIX

MATRIX sets up the matrix elements of the A Matrix.

Subroutine MATSA

MATSA sums the series solution of Equation (9) to convergence given the time step developed in TSTEP.

Subroutine MESH

MESH determines the nodal spacing of the mass channels. The mass of each channel is taken to be the geometric mean of the left and right nodes of each channel except for the first channel where the arithmetic mean is used. For the general case, the spacing is equal on the logarithm of particle size.

Subroutine NSTOKE

NSTOKE corrects for the non-Stokesian behavior of aerosol particles. An array VPLUS(I) is calculated which contains the ratio of the non-Stokesian over Stokesian settling velocity. SETTLE is used to determine the non-Stokesian settling velocity.

Subroutine PSOURCE

PSOURCE determines the value of the source coefficient used in the aerosol equation assuming a log normal source particle distribution. PSOURCE determines the value of NS for cases which have no initial aerosol concentration. It is called by COCALL to evaluate the source coefficients at the start of the problem.

Subroutine REMOVE

The removal rate coefficients for diffusional, gravitational and themophoretic deposition are calculated in REMOVE. These coefficients are used in DEPO and DIFFUN.

Subroutine SETTLE

SETTLE determines the non-Stokesian settling velocities used by NSTOKE. As discussed elsewhere in this report, empirical values of settling velocities for particle Reynold's numbers in excess of 1259 are not available. Above this Reynold's number, the correction at Re = 1259 is used.

Subroutine SFORM

The table of mass source rate as a function of time for each volume is stored in the fields SE and SET. To conserve computer memory, these

fields are overwritten for each new specie considered. SFORM is used to transfer each specie dependent image of SE and SET to external core storage and to retrieve these as needed.

Subroutine SOURCE

SOURCE is used to calculate the source rate, S, in a given volume at a given time using the interpolation routine FINDY on the source data tables SE and SET.

Subroutine SPART

SPART utilizes the input source particle distribution parameters PSE(I,J) and corresponding times PSET(I,J) for each volume, and determines the distribution parameters PS(L) for each volume source at time t.

Subroutine SPSCALC

Performs specie specific calculations for ADHOC.

Subroutine STOR

Sums the masses of the steam-particle state and source rate over all species.

Subroutine THDATA

THDATA develops the following thermal-hydraulic data for a given time:

- steam mass flow rate through each junction
- steam temperature
- steam pressure
- steam density
- wall surface temperature

Subroutine TSTEP

TSTEP develops the appropriate time step for each iteration. At present, because of the sequential solution technique employed, the time step is read in as estimated from trial runs on the criterion that transport of nuclides per time step not proceed through more than three or four volumes. For typical meltdown scenarios this criterion is sufficient to ensure adequacy of the solution technique employed in MATSA. Expected particle concentrations are sufficiently low to ensure that the particle dynamics and the general mass transfer dynamics are interfaced adequately in the T module if this criterion is met. More mathematically rigorous criteria are envisioned for TSTEP as development of the T module leads to more rigorous treatment of the complete dynamics of the system.

Subroutine XDP

XDP determines the channel of the particle resulting from the collision of any two particles in the system. The mass of the resultant particles is apportioned between two channels so that mass is conserved in the system. The results of the calculations by XDP are used by the coagulation portion of DIFFUN.

Subroutine OUTPUT

OUTPUT is called at DIV subdivisions of the meltdown time interval to be calculated. DIV is read into the code in the main program. It prints out all parameters of interest and is discussed in detail in a separate section.

3.0 DESCRIPTION OF INPUT TO M-C-T CODE

A list of input cards for M-C-T is schematically given below. The listed parameters are described in detail. Additionally, any special clarifying comments or cautions are also included. Note that all input to M-C-T is unformatted. That requires that at least one blank (space) be placed between each number entered as input.

1. ICALL — Determines which M-C-T modules will be executed. If ICALL=1, M and T modules will be executed. If ICALL=2, C and T modules will be excuted. If ICALL =0, only T module will be executed. If ICALL<0, all modules will be executed.

2. IFIRST — Control parameter used together with ICALL=1 or ICALL=2 to execute only the M module or the C module, respectively. If IFIRST≠0 and ICALL=1 only the M module is executed. If IFIRST≠0 and ICALL=2, only the C module is executed.

3. IAUTO — Parameter which determines if T module inputs are read in manually, IAUTO=0 or generated internally in the M and C modules and entered into the T module through common block. When analyses are performed which account for fission product heating IAUTO≠0.

4. XLOOP — A parameter used in conjunction with analyses which model, more than one fission product flow path as one equivalent path. For example, in the case of a Seal Loca in all four RCS pumps, the fission product path is modeled as consisting of all four loops. In the M module calculation, the thermal response is calculated for only one loop. Thus, XLOOP value should be 0.25.

The following series of inputs assume that ICALL=-1 thus executing all M-C-T modules.

M-Module Input

5. IMER1
6. IMER2 — Parameters which determine Run Mode of the M module. If IMER1=1 and IMER2=0 Run Mode 1 of M module is chosen and MARCH 2.0 data is listed for examination and preparation of input to items 8, 47 and 48 below. When choosing Run Mode 1 the user should set IFIRST=0 and ICALL=1. If IMER1=0 and IMER2=1, Run Mode 2 of M module is chosen and all calculations in the M module are performed. When choosing Run Mode 2 the user should set IFIRST=0 and ICALL=-1 unless it is the intention of the user to execute only the M module in its Run Mode 2.

7. NSTEP — An increment parameter used to control listing of the M module input data. NSTEP=2 would allow listing of every other record, beginning with the first, from MARCH 2.0 output data sets. This number is read in only if IMER1=1 and IMER2=0.

8.	NUNCV	Time step index from Run Mode 1 listing, at which analysis is begun.
9.	NSW	Time step index at which first fission product releases occur. Obtained by examining echo print of TAPE25 from MARCH 2.0 which will identify the time step index at which TAPE25 was started.
10.	IPR	Debugging print options. If IPR=1 or IPR1=1,
11.	IPR1	detailed printouts will result. If IPR=0 and IPR1=0, no extended printouts will result.
12.	NPRT	Cycle number to start print if, print options have been selected.
13.	NLAST	Last averaging interval completed. Used to re-start M module analysis, (not used).
14.	IVOL	Number of control volumes. In order to account for escape from the primary system, a control volume is included to represent the containment. The value of IVOL does <u>not</u> include the core which is control volume 1.
15.	ISG	Steam generator control volume number. Note that for a BWR, ISG=0.

16. ITRAN — Parameter differentiating the types of accident sequences being analyzed. If ITRAN=0, large break ITRAN=1; transients and small pipe breaks; ITRAN=2, transients with ECCS recirculation inoperable. Note that for ITRAN=0 for a PWR, the steam generator structure temperature is reduced to the saturation temperature of the steam generator secondary.

The following data refer to volumes above the core in the exit gas stream. Note that I=1 identifies the core and the values are <u>not</u> read in, Parameters 17 through 30 are read in IVOL times.

17. TT(I) — Initial control volume wall surface temperature, F

18. GG(I) — Initial control volume gas temperature, F

19. VOL(I) — Gas volume for the control volume, ft^3

20. LL(I) — Length of control volume, ft.

21. HGT(I) — Vertical height of control volume, ft.

22. ISTR(I) — Number of structures within a control volume

23. CM1(I) — Product of mass and specific heat of a control volume, BTU/F. For steam generators, CM1 should include water in secondary.

24. DELX(I) — Thickness of a control volume, ft.

25. AH1(I) — Heat transfer area of a control volume, ft^2

26. DD1(I) — Flow hydraulic diameter of control volume, ft.

27. AR1(I) — Flow area of a control volume, ft^2

28. CONTEM — Containment temperature used for insulation heat losses, ^oF

29. INS — Type of insulation for control volume I. INS=1, the insulation is THERMAL-12; INS=2, the insulation is a mirror type; INS=0, the control volume is assumed to be adiabatic.

30. THICK(I) — Insulation thickness, in.

The following parameters pertain to the structures identified in 22 above. A set of values should be read in for each structure in each volume for which ISTR(I)=1.

31. TTS(I,M) — Initial structure wall temperature in a control volume, F.

32. CM(I,M) — Product of mass and specific heat of a structure in a control volume, BTU/F.

33. AH(I,M) — Heat transfer area of a structure in a control volume, ft^2.

34. DD(I,M) — Flow hydraulic diameter for a structure in a control volume, ft.

35. AR(I,M) — Flow area for a structure in a control volume, ft.

36. LL1(I,M) — Length for a structure in a control volume, ft.

37. DELX1(I,M) — Thickness of structure in a control volume, ft.

38. TOTM1(I) — Total gas mass in control volume, lbm.

39. H2M(I) — Hydrogen gas mass in control volume, lbm

40. W(I) — Mass flow rate from control volume, lbm/sec.

41. PSTART — System pressure at restart time, psia.

Parameters 38, 39, and 40 are entered as non-zero values <u>only</u> if RESTART is excercised. In such a case, values at the last completed averaging interval are input.

42. NCV(I,J) — Flow/no flow matrix indicating no flow, NCV(I,J)= 0 or flow NCV(I,J)=1 from source volume J to control volume I. For each J source volume (IVOL volumes)

no flow/flow information should be provide for I (IVOL+1) control volumes.

43. FF(I+1) — The percentage of total source flow rate entering control volume I+1.

44. FLAG(I) — Parameter indicating whether a change occurs in the percentage of total mass flow rate, FF(I+1) or not. If FLAG(I)=1, a change occurs; FLAG(I)=0 no change takes place. IVOL values of FLAG(I) should be read in. Thus FLAG(2) =0 indicates no change in flow from source volume to control volume 2. Note that the core is control volume 1 and is not included in the IVOL value. No input for FLAG(1) is needed.

45. FTIME(I) — The time at which the change in percentage of total mass flow rate from source volume to control volume I occurs. Read in <u>only</u> if FLAG(I)=1.

46. FF2(I) — The new value of the percentage of total source flow rate entering control volume I at FTIME(I). Read in <u>only</u> if FLAG(I)=1.

47. NINT — The number of intervals for data averaging. A maximum of 18 intervals is allowed. These intervals are obtained from the examination of the data

listing resulting from the M module in Run Mode 1. This parameter and the next one are used only if IAUTO=0. If IAUTO=0, NINT can be set equal to 2 and any three values for INT(N) supplied below.

48. INT(N) — Endpoints of the chosen NINT intervals to be used for the averaging technique. A maximum of 19 endpoints are permitted and are expressed in terms of time step indexes as established from the start of calculations, i.e., time step index 1 on Run Mode 1 listing.

The values in the following parameters are intended to selectively replace values of parameters listed in Run Mode, 1 if these are suspect or if one desires to analyze the sensitivity of the Run Mode 2 results to certain MARCH 2.0 output parameters.

49. NBDPT — Number of time step indexes at which changes to parameters will be made. Normally NBDPT=0. If NBDPT=0 input the additional parameter values.

50. NBPT(I) — Time step index at each parameter change. NBDPT values should be input.

51. STMBD(I) — Changed steam flow rate for each time step index, NBPT, lbm/min.

52. H2BD(I) Changed hydrogen flow rate for each time step index NBPT, lbm/min.

53. PRESBD(I) Changed primary system pressure for each time step index NBPT, psia.

54. TGASBD(I) Core exit gas temperature for each time step index NBPT, F.

55. HSUMT Total release of hydrogen gas, lbm

56. QZERO Reactor power, BTU/hr.

57. TAP Time at power, minutes.

QZERO and TAP should be set equal to 0 if no fission product heating analyses are to be performed and the following parameters should be read in if QZERO and TAP=0.

58. NTIM Number of times at which fission product group distributions are input

59. NGP Number of fission product group.

60. TDK(I) Times at which fission product group distributions are input. NTIM values are entered.

61. QFCT(J,I) Fraction of decay heat generated by each fission product group NGP. NTIM values are input for each NGP group.

62. Z(MM) Elevation of each flow junction MM. For future use in evaluating natural convection terms. IVOL +1 values should be entered.

The following parameters are read in next from TAPE 20, generated by MARCH 2.0.

63. N time step index number.

64. TIME Accident time from start of core melt, min.

65. TRMAX Maximum core temperature, F.

66. TCORE Average core temperature, F.

67. TSAT Primary system saturation temperature, F.

68. TGEX Core exit gas temperature, F.

69. PRES Primary system pressure, psia.

70. STMEXC Core exit steam flow rate, lbm/min.

71. H2EXC — Core exit hydrogen flow rate, lbm/min.

72. DTMN — Time differential, min.

73. FCM — Fraction of core melted.

74. HSAT — Primary system saturation enthalpy, BTU/lbm.

75. TMAXSG — Maximum temperature in steam generator secondary, F.

76. HFGSG — Heat of vaporization in steam generator secondary, BTU/lbm.

77. WTRSG — Weight of water in steam generator secondary, lbm.

78. RADT — Heat radiated to grid plate above core, BTU/hr.

C Module Input

79. TSTRT — Time at which C module analysis is to start, min., obtained from MARCH 2.0 tapes. TAPE25 should be examined to see at which time and time step index MARCH 2.0 commenced writing the tape. TSTART should then be set equal to that time.

80. TFAIL — Time at which reactor vessel failure occurs, min., obtained from MARCH 2.0.

81.	SMLT	Time at which melting of the core commences, min., should be set equal to TSTART.
82.	NRAD	Number of radial regions in the core.
83.	NAX	Number of axial nodes in the core.
84.	NST	Number of radial regions for use in distributing non-fission product inventories.
85.	RADDIS(I)	Radial peaking factors. NRAD values should be entered.
86.	AXDIS(I)	Axial power distribution.NAX values should be entered.
87.	STDIS(I)	Fraction of core volume in radial regions. NST values should be entered.

The following input parameters refer to initial reactor inventories of different species in kg.

88.	TCS	Cesium
89.	TI2	Iodine
90.	TXE	Xenon
91.	TKR	Krypton
92.	TTE	Tellurium
93.	TAG	Silver not contained in control rods
94.	TSB	Antimony
95.	TBA	Barium
96.	TSN	Tin
97.	TRU	Ruthenium
98.	TUO2	Uranium Dioxide

99.	TZRC	Zirconium-cladding
100.	TZR	Zirconium-fission product
101.	TFE	Iron
102	TMO	Molybdenum
103.	TSR	Strontium
104.	TAGR	Silver-control rods
105.	TCDR	Cadmium-control rods
106.	TINR	Indium-control rods

T Module Input

107.	TITLE	Title, up to 80 characters in length.
108.	CPMAX	Central processor time (seconds) allowed for the problem before dumping to restart.
109.	DIV	Divides the time interval over which the code is to run into DIV equal subintervals. OUTPUT is called at the end of each subinterval.

110. KOMAD — If KOMAD = 1, comments are printed from ADHOC that give information on total evaporation of a nuclide species from either particles or walls.

111. NRES — If NRES = 1, the T module restarts from a previously interrupted run using initial values previously stored on the NTAP file; only this and the previous card are read in.

112. T, TMAX, DELTM — T is the initial time of problem start, sec. TMAX is the time in seconds over which the calculation is to run. This time is equal to (TFAIL-TSTRT) x 60. A few seconds should be subtracted to assure that the source rates generated in the C module overlap the problem time span. DELTM is the time step to be taken per iteration. Its value is discussed in the description of TSPEP.

113. REL, ET41, ETA2 — REL is the convergence criterion for the series expansion of the solution of Equation (9). It gives the upper bound to the ratio of the relative magnitude of the last included term to the partial sum up to that term. ETA1 and ETA2 are used in subroutine TSTEP to control the problem time step.

114. NK, NV, NS, NDP — NK, (<10), is the number of species to be considered. NV, (<10), is the number of control volumes considered. NS is the number of states. This number must be 5 unless minor modifications in BETV are undertaken. NDP is the number of particle parameters considered. This value must be 2 at present.

115. SN(I) — Are read in on one card 10(A8) format. Each SN is the character name of a species (A format). Must be read in the following order: I_2, CsI, CsOH, Aer,Te.

116. NCC — Contains the flow connections of the control volumes. The first digit contains all flow connections to the first volume. If flow occurs to the first volume from the second volume, a 1 must appear as the second digit, and so on.

117. NBET — Gives the number of control flags in BETV. There are at present three of these.

118. NB — Contains the control flags of BETV for each volume. Each digit represents the control for the volume whose number corresponds to the sequence number in the input stream. The first digit must be 0 if I_2 adsorption is to be inhibited in that volume. The second digit must be 0 if particle

deposition is to be inhibited in that volume. The third digit allows particle settling either against flow (digit set equal to 0), or across the flow, (digit set equal to 1).

119. NHOC — Gives the number of control flags in ADHOC. There is only one of these at present.

120. ND — Coded control digits for ADHOC. The organization is identical to that of NB. If ND = 0 no condensation is allowed in the corresponding volume.

121. NOCOG — The n^{th} digit corresponds to the n^{th} volume. If coagulation is to be suppressed in this volume this digit is set equal to 0.

122. VPM — Arbitrary multiplier of all vapor pressure terms. Can be used to measure code sensitivity to uncertainties in vapor pressure correlations.

123. FRM — Arbitrary multiplier of the steam mass flow rates in all volumes. Can be used to measure code sensitivity to changes in flow rate.

124. STM — Arbitrary multiplier of surface temperature in all volumes. Can be used to measure code sensitivity to uncertainties in surface temperatures.

125.	SRM	Arbitrary multiplier of the I_2 adsorption velocity. Can be used to gauge code sensitivity to uncertainty in this parameter.
126.	THDM	Arbitrary multiplier of the thermophoretic deposition velocity. Can be used to measure code sensitivity to uncertainty in this expression.
127.	TDM	Arbitrary multiplier of the deposition velocity due to particle deposition from turbulent flow. Can be used to gauge code sensitivity to uncertainty in this velocity.
128.	VTM	Arbitrary multiplier of the vapor mass transfer coefficients used in ADHOC. Can be used to gauge code sensitivity to uncertainty in these.
129.	NTCOAG	If not equal to 1, turbulent coagulation is ignored in all volumes.
130.	LENGTH, DIAME, AREA, ASED, HEIGHT	The five geometric parameters are read in English units, (per control volume). LENGTH is the length, DIAME the equivalent of diameter, AREA the crossflow area, ASED the surface area available to sedimentation of aerosol particles, HEIGHT the vertical length of the control volume.

NOTE: Data in 131 through 135 are provided to the T module internally, if IAUTO=0.

131. NTST — Number of entries in the time flow data table for the junction flow of a given junction.

TF — Time data (in seconds) corresponding to the flow data. These are listed chronologically with up to 20 entries.

F — Steam mass flow rate (lb/sec) corresponding to the time data above. Again, up to 20 entries may be used.

NOTE: Junctions must be entered in a specific way. Their data are entered in 131 above in this numbered sequence. The numbering scheme is as follows. Look at Volume 1 first. Next scan all volumes in their numbered sequence.

Assign the junction number 1 to the junction between volume 1 and the first volume encountered that has flow to volume 1, and so on.

132. NTST — Number of entries in the time-pressure data table.

TF — Time data (in seconds) corresponding to the pressure data.

	F	Steam pressure (psia) data.
		NOTE: This set of cards is repeated for each volume, in sequence.
133.	NTST	Number of entries in the time-wall surface temperature data table.
	TF	Time data (seconds) corresponding to the temperature data.
	T	Wall surface temperature (F) data.
		NOTE: This set of cards is repeated for each volume, in sequence.
134.	NOCO	If the n^{th} digit from the left is 1, specie n has initial mass present.
135.	CO	Is filled by the initial masses in all states, in the sequence: volume 1, steam-molecule; steam-particle; wall-molecule, wall-particles; volume 2, etc. If NOCO indicates that the given nuclide specie has no mass present in the system initially, these cards are skipped.
		NOTE: This set of cards is repeated for each specie that has mass in the system initially.

136. NOSOV — If the n^{th} digit is 1, source data exists for the state n.

NOSOS — If the n^{th} digit is 1, source data exists for the state n.

NOTE: Data for NTST, SET and SE are provided to the T module internally, if IAUTO=0.

NTST — Number of entries in the source rate-time data table.

SET — Time data (seconds) corresponding to the source rate data.

SE — Source rate (g/sec) data.

NOTE: NTST, SET, SE are repeated for each state in each volume that has a source. The sequence in which they are read in is: states of the first volume, starting with the first state. Then the second volume, and so on. Volumes and states that have no source are skipped.

All cards in Item 136 are repeated for each specie considered.

137. NOSPV — If the n^{th} digit is 1, the source rate of state steam-particle of volume n has the lognormal size distribution parameters σ_g and r_g read in.

NTST — Number of entries in the $\sigma_g(r_g)$-time data table.

PSET — Time data (seconds) corresponding to the $\sigma_g(r_g)$ data.

PSE — $\sigma_g(r_g)$ data.

NOTE: NTST, PSET, PSE are read in first for σ_g, then for r_g. These two sets are repeated for each volume with a steam-particle source, in sequence.

138. PDEN — Gives the (uniform) particle density in each volume. By permitting change in density as a function of control volume, it is hoped that gross changes in particle constitution can be approximated.

4.0 M-C-T CODE OUTPUT

M-C-T code output is divided into three portions, M, C, and T module outputs. The essential output of the M module consists of records of control volume temperatures (gas inlet, gas outlet, and wall surface) and mass flow rates (total and hydrogen) over time for each control volume. In addition, control volume geometries and the control volume flow matrix along with several correlated parameters from the MARCH 2.0 accident analysis are output.

The M module stores the thermal-hydraulic data of each control volume in the accident sequence on output data file TAPE2 for use by the T module or passes information to the T module through a common block depending on the execution mode of M-C-T. The data in order of storage is as follows: TPARM(K) - time of data output; FLOP (K,I,5) - total mass flow rate exiting each control volume I; TPARM (K), PRESOUT(K) - control volume pressure; TPARM(K), FLOP (K,I,6) - average control volume gas temperature; and TPARM (K), FLOP(K,I,7) - contol volume wall surface temperature. The variable K denotes the time interval index. Additionally, the code stores an output data file TAPE1, the M module input data from the MARCH 2.0 code. These parameters as output from MARCH can be listed as user-specified intervals if the Run Mode 1 is selected.

The output of the C module consists of the listing of the release rates of the specified isotopic species for up to twenty time intervals. This information is also saved on TAPE4 for subsequent use in the T module execution or passed to the T module through a common block, depending on

the execution mode of M-C-T. Additionally, the C module provides a listing of the total releases for the different isotopic species and their cumulative releases versus time.

The essential output of the T module consists of a record of all nuclide masses in all states and all volumes at the desired time (contents of the C vector). To account for escape from the primary system through pipe breaks, a fictitious control volume is added to represent the containment. All deposition mechanisms are switched off (by means of NHOC and NBET) in this volume.

The particle number concentration (particles/cm^3), the geometric standard deviation and the geometric mean radius of the particle size distribution are listed at the end of OUTPUT for each volume.

Finally, those parameters that aid in an understanding of the phenomena described in the T-module are listed at the beginning of OUTPUT for each volume; these are as follows:

Steam	Steam bulk flow velocity
STEAM, RE	Steam flow Reynolds number
GRAS., RE	Equivalent Reynolds number due to thermal convection

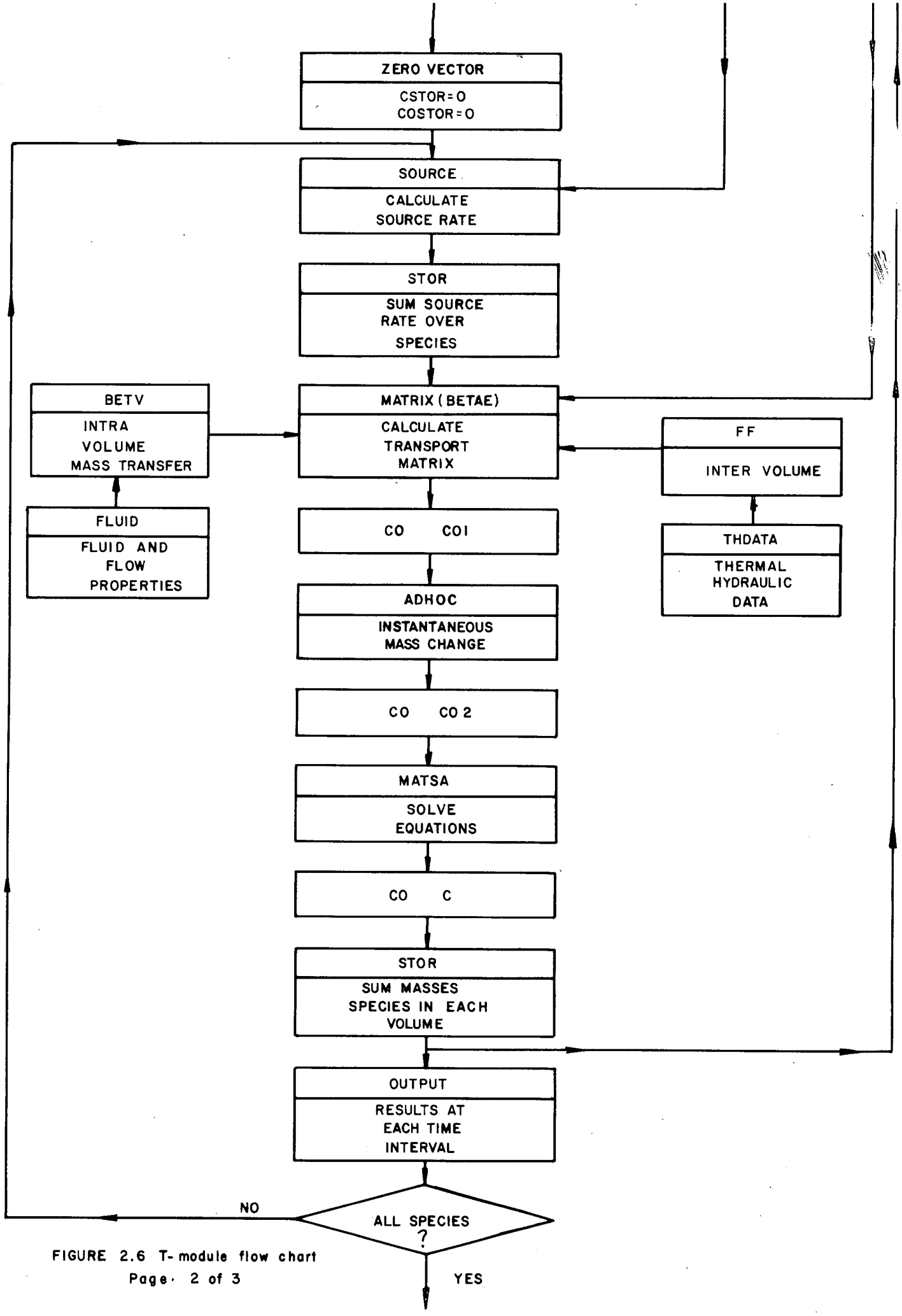

FIGURE 2.6 T-module flow chart

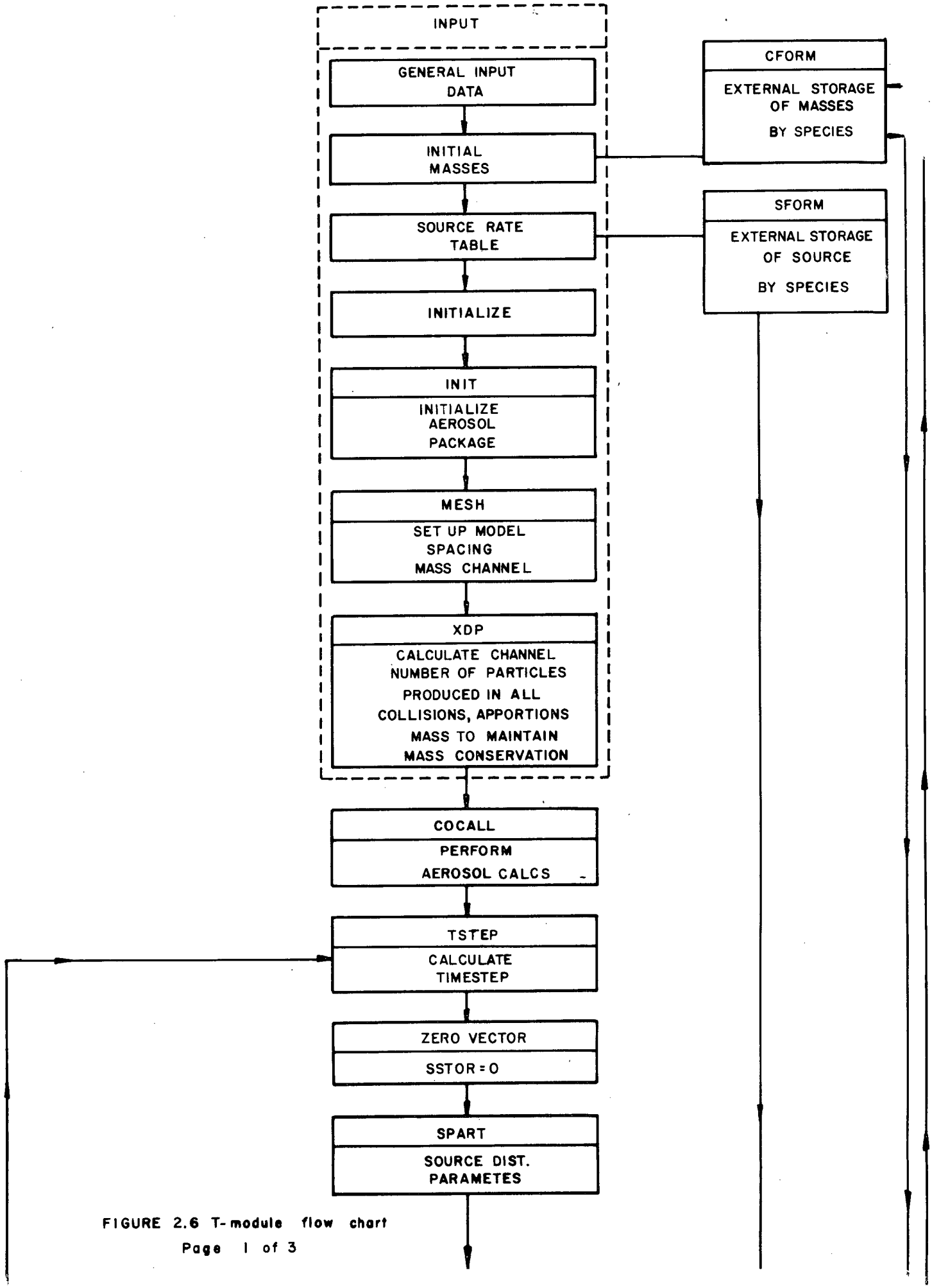

FIGURE 2.6 T-module flow chart

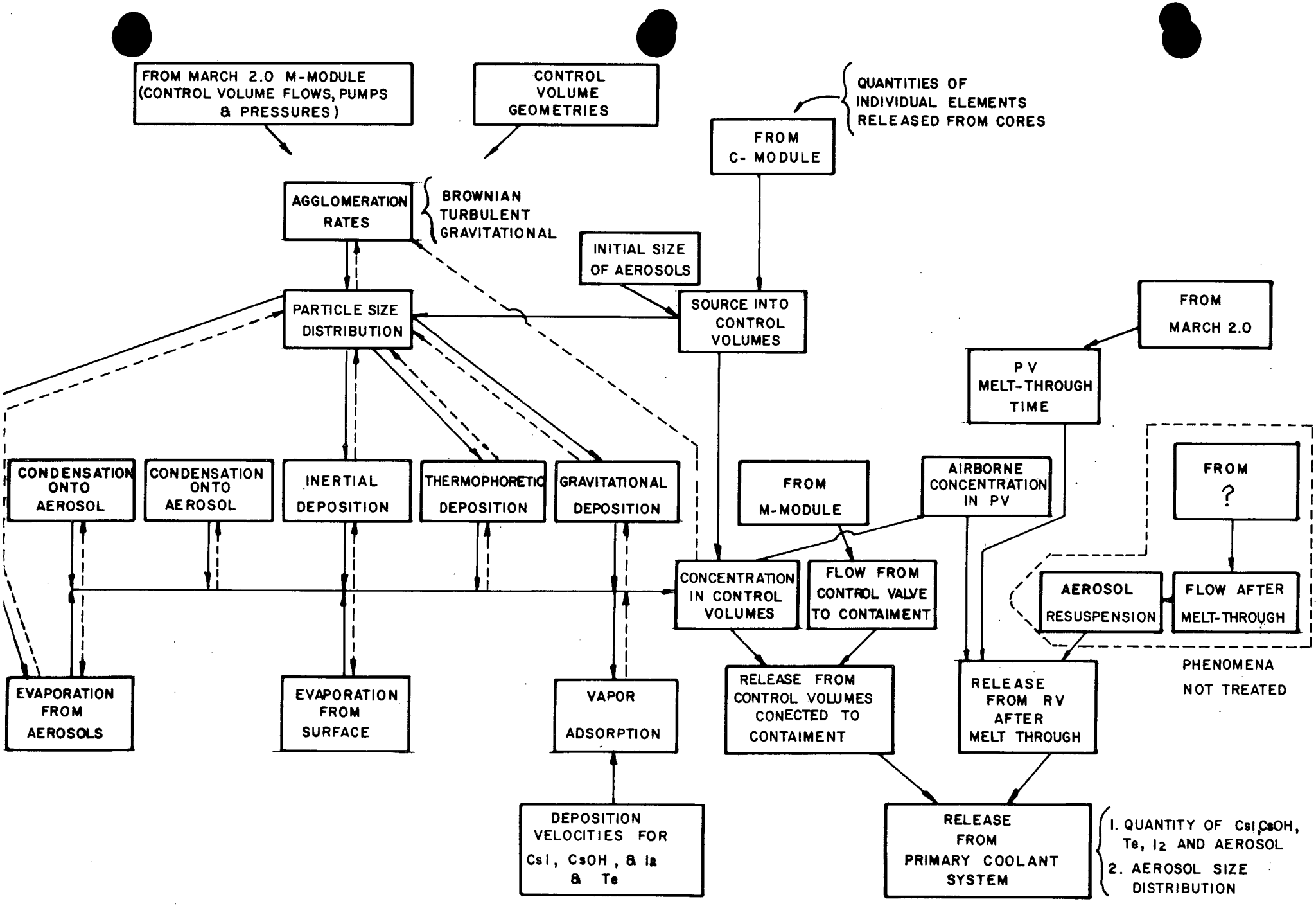

FIGURE 2.5 T- module INFLUENCE DIAGRAM.

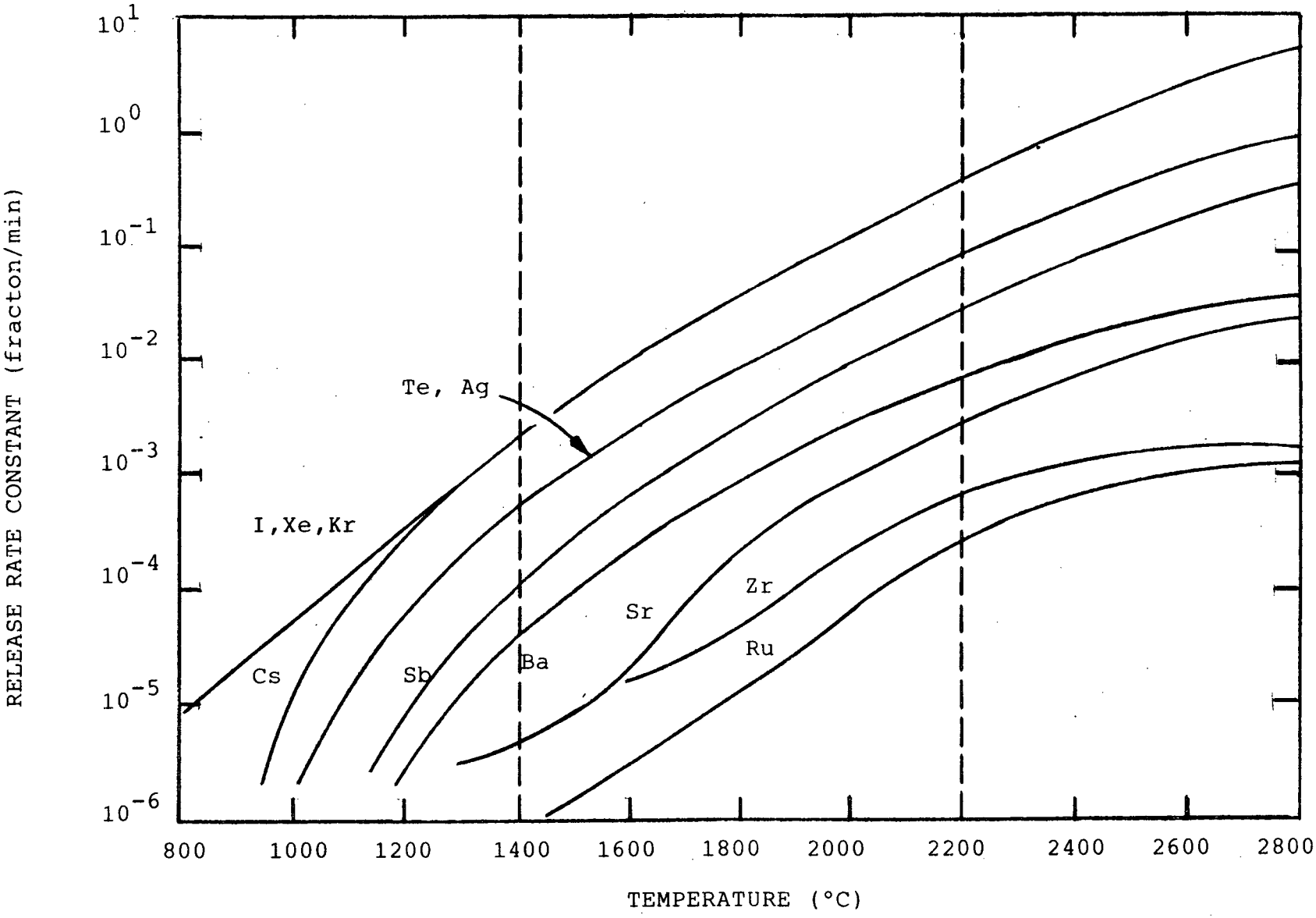

FIGURE 2.4 FISSION PRODUCT RELEASE RATE CONSTANTS FROM FUEL-SMOOTHED CURVES (Courtesy of R. Wichner, Oak Ridge National Laboratory)

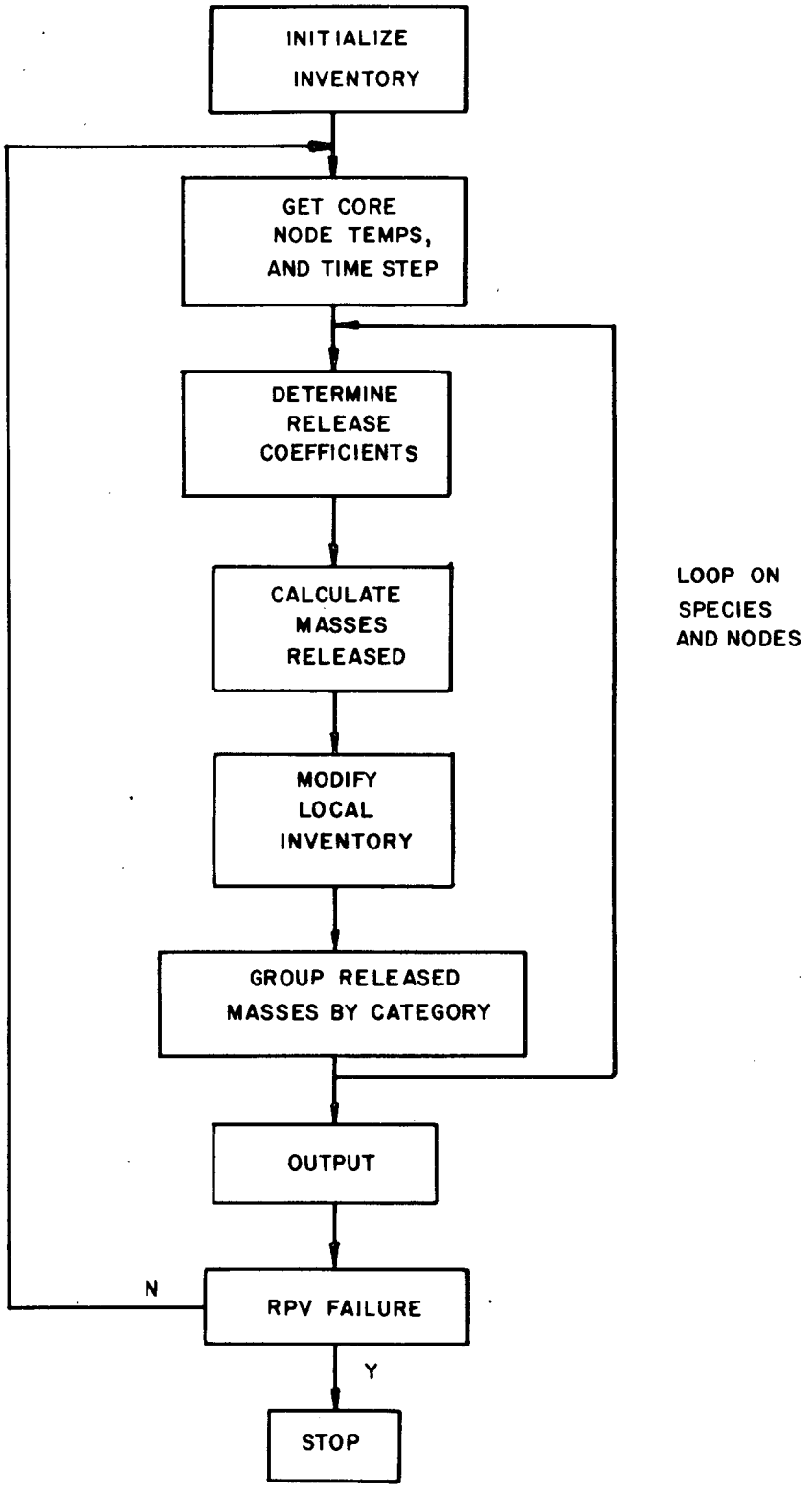

FIGURE 2.3 FLOW CHART OF THE CORSOR PROGRAM

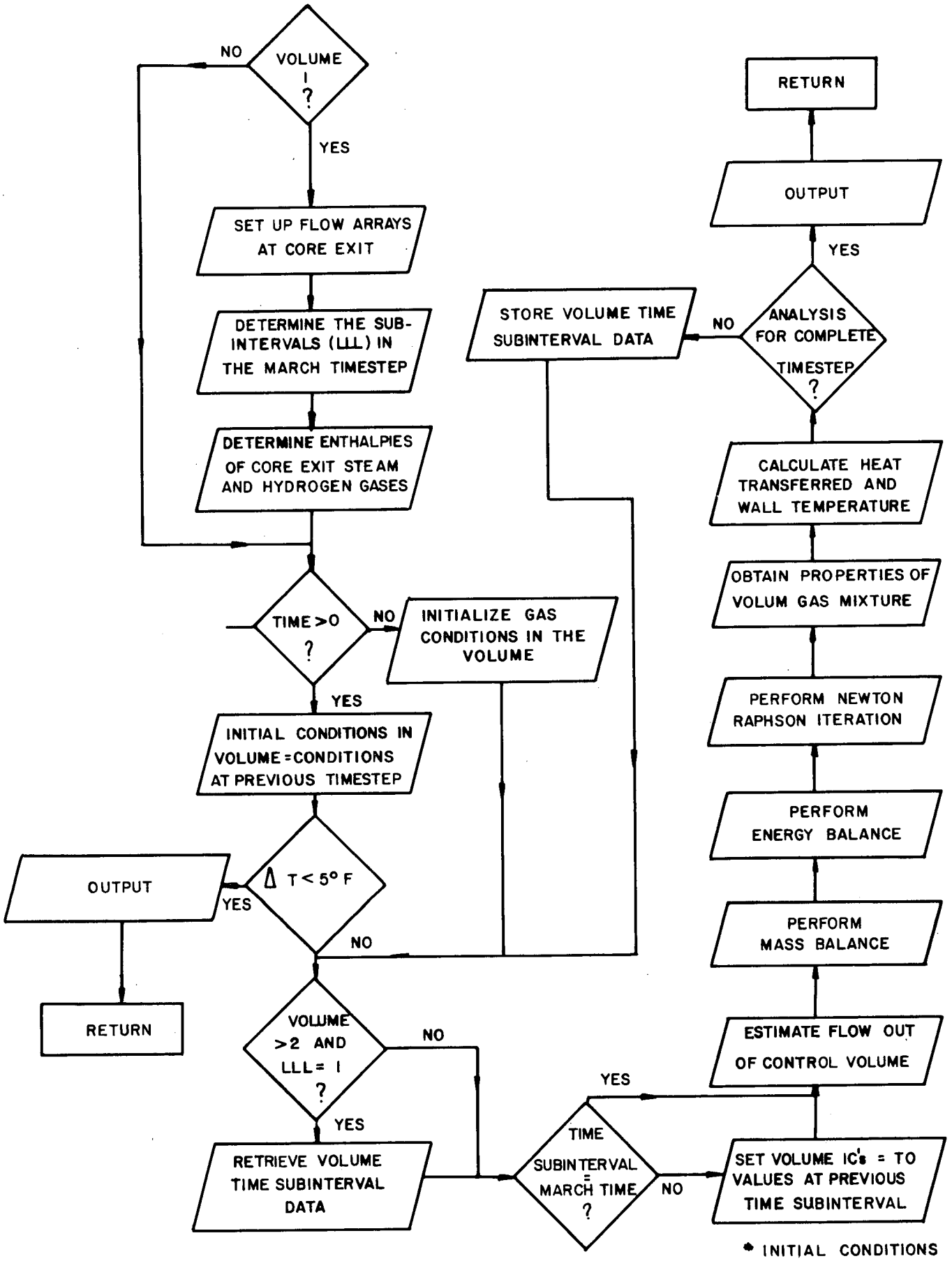

FIGURE 2.2 FLOW CHART SUBROUTINE EXITQ

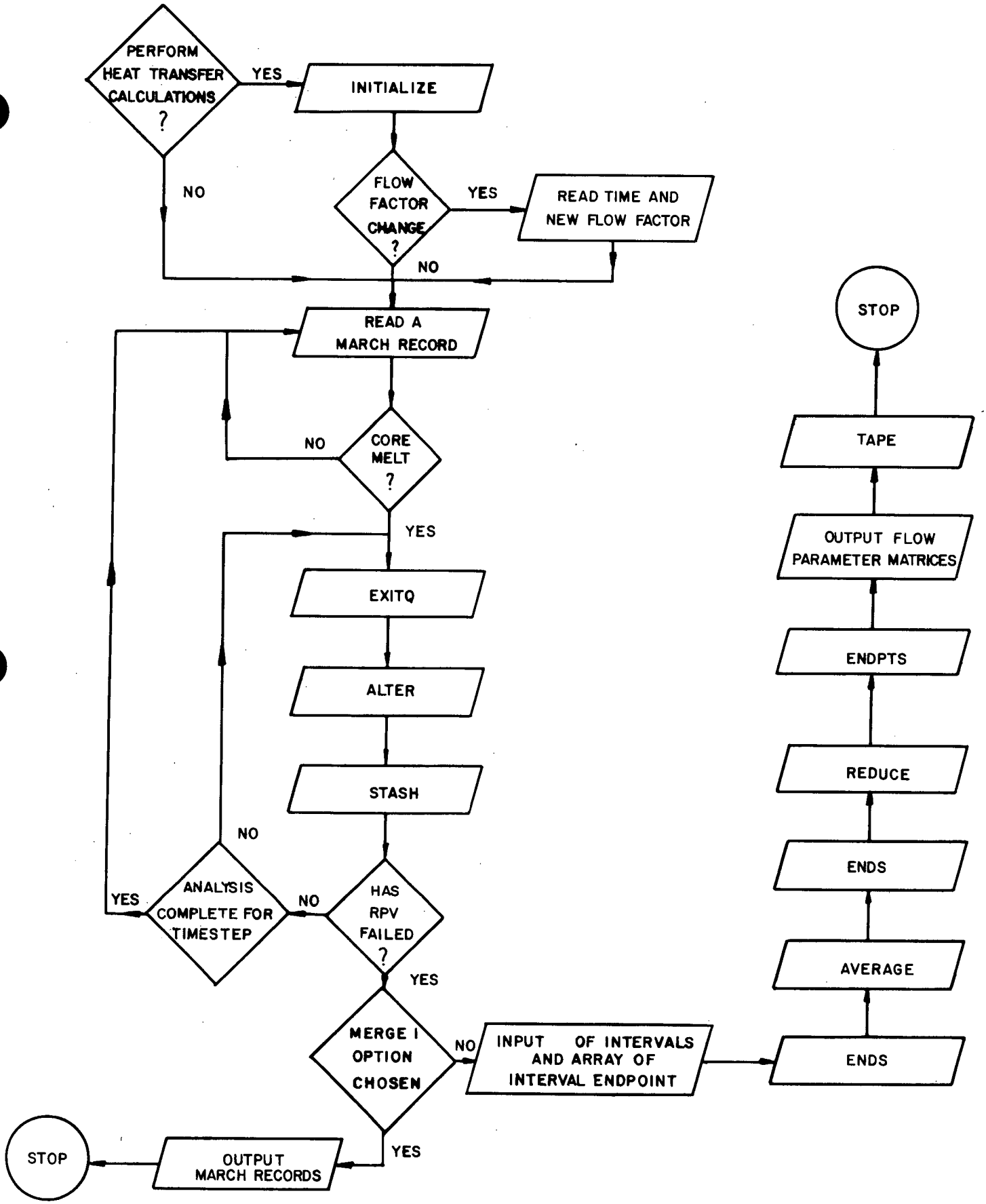

FIGURE 2.1 FLOW CHART OF THE MERGE CODE

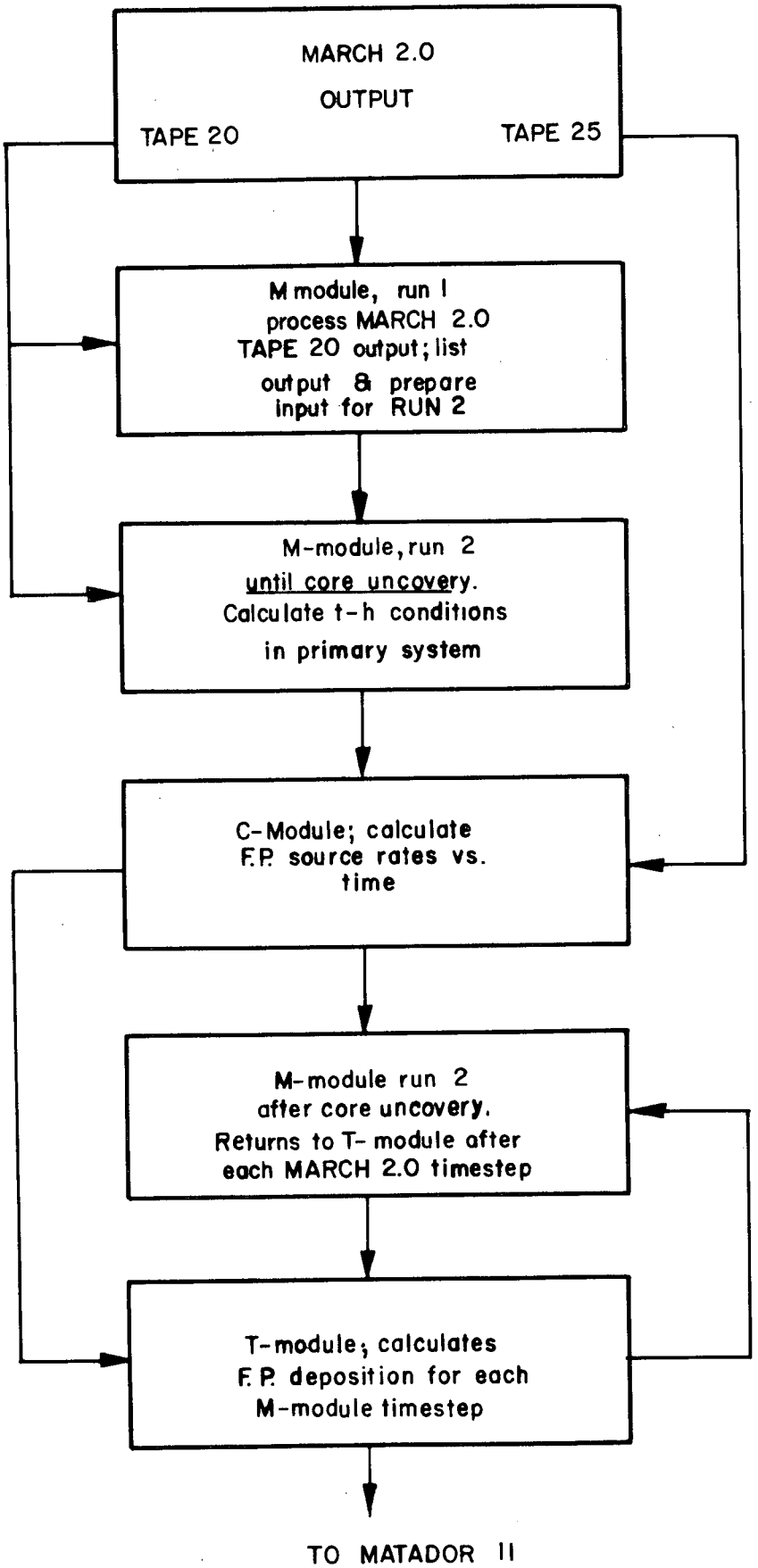

Figure 1 M-C-T Program flow

VTU	Particle deposition velocity due to particle inertia
VDT	Particle deposition velocity due to diffusion from turbulent flow
VDL	Particle deposition velocity due to diffusion from laminar flow
VTH	Particle deposition velocity due to thermophoresis
VDI	Deposition velocity of I_2 vapor
VSE	Deposition velocity due to gravitational settling

Fission	800C<T<=1400C		1400C<T<=2200C		T>2200C	
Product Group	A	B	A	B	A	B
I, Xe, Kr	7.02E-09	0.00886	2.02E-07	0.00667	1.74E-05	0.00460
Cs	7.53E-12	0.0142	2.02E-07	0.00667	1.74E-05	0.00460
Te, Ag	3.88E-12	0.0135	9.39E-08	0.00630	1.18E-05	0.00411
Sb	1.90E-12	0.0128	5.88E-09	0.00708	2.56E-06	0.00426
Ba	7.50E-14	0.0144	8.26E-09	0.00631	1.38E-05	0.00290
Mo	5.01E-12	0.0115	5.93E-08	0.00523	3.70E-05	0.00200
Sr	2.74E-08	0.0036	2.78E-11	0.00853	9.00E-07	0.00370
Zr	6.64E-12	0.00631	6.64E-12	0.00631	1.48E-07	0.00177
Ru	1.36E-11	0.00768	1.36E-11	0.00768	1.40E-06	0.00248
Fuel	5.00E-13	0.00768	5.00E-13	0.00768	5.00E-13	0.00768
Cladding-Zr	6.64E-12	0.00631	6.64E-12	0.00631	1.48E-07	0.00177
Cladding-Sn	1.90E-12	0.01280	5.88E-09	0.00708	2.56E-06	0.00426
Structure	6.64E-10	0.00631	6.64E-10	0.00631	1.48E-05	0.00177

Table 2.1 Values used for the constants A and B in the approximation of the release rate coefficients, $K(T) = Ae^{BT}$

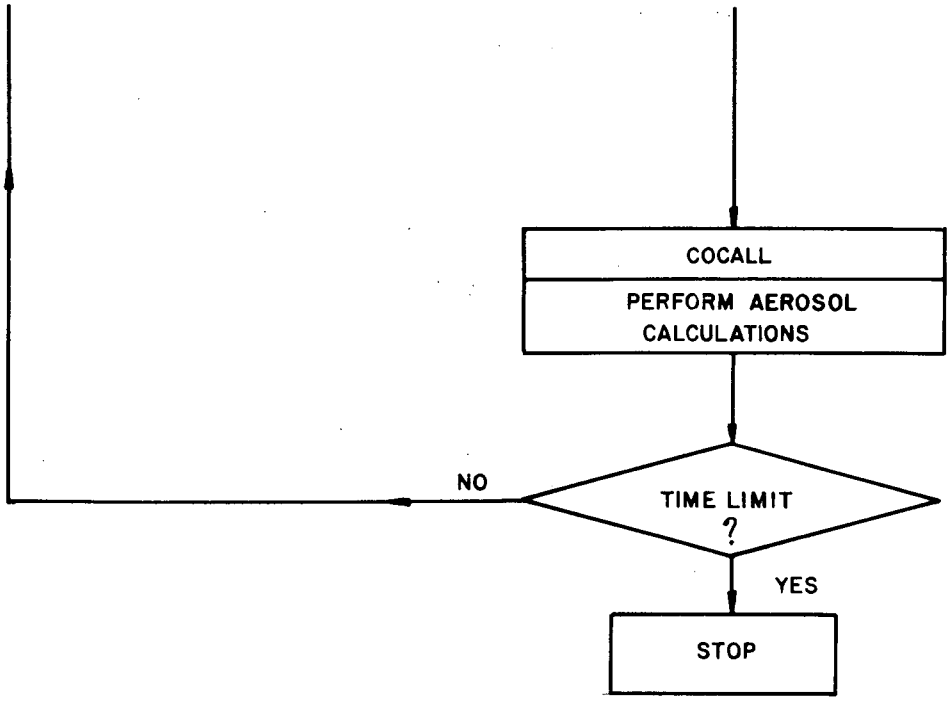

FIGURE 2.6 T-module flow chart

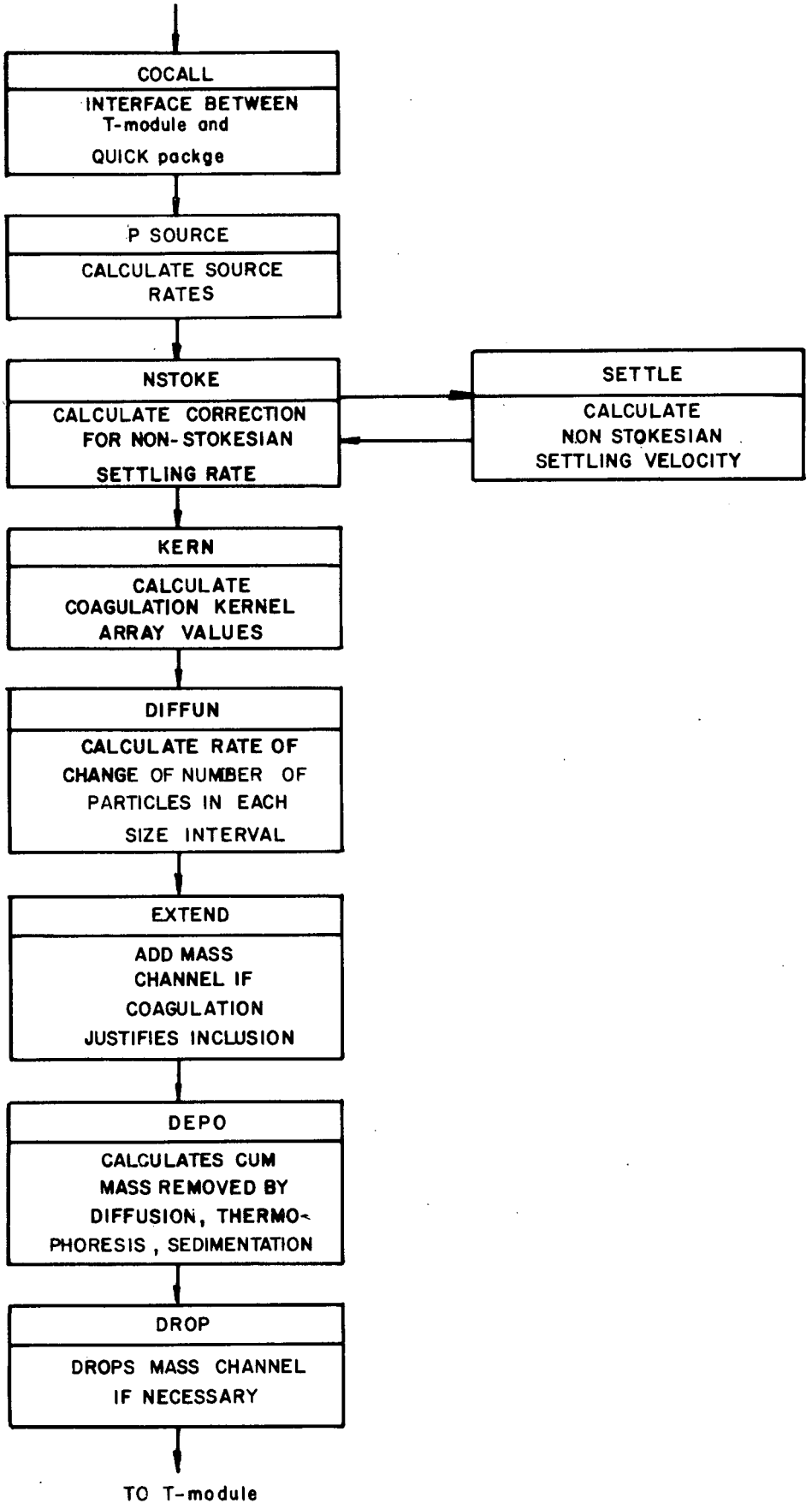

FIGURE 2.7- AEROSOL BEHAVIOR CALCULATIONS

Appendix C

MATADOR II USER'S GUIDE

1.0 Introduction

The MATADOR II code is used to analyze the behavior of radionuclides in light water reactor containments during and after severely degraded core accidents. The code is capable of analyzing the behavior of radionuclides existing both as vapor and aerosol. The radionuclides that exist as aerosols are grouped by dividing the size range over which aerosols can exist into 20 or fewer intervals and placing each aerosol into the appropriate interval according to its size. Radionuclides can exist in five states; vapor, condensed on suspended particles, condensed on structural walls, deposited by particle settling and chemisorbed. In addition, the radionuclides can be picked up by spray water droplets and be located in bulk water in the sump or on the containment floor. Radionuclides can also be picked up and collected by other engineered safety systems besides sprays such as filters, ice condensers, pressure supression pools, etc. The transfer and removal of radionuclides by these systems (called DF transfers) are achieved by the use of decontamination factors and do not enter into the rate equations.

2.1 MATADOR II DESCRIPTION.

Essentially, MATADOR II considers a system of an arbitrary number of control volumes that are connected by fluid flow in an arbitrary way. In each control volume a radionuclide specie can reside on at least two carriers either in particle (liquid or solid) or vapor form. Combining the phase of the fission product specie with the concept of carrier, one can describe four states in which the specie may reside:

- steam-molecular
- steam-particle
- walls-molecular
- walls-particle.

In addition, radionuclides can be picked up by spray water droplets and be located in bulk water in the sump or on the containment floor. Radionuclides can also be picked up and collected by other engineered safety systems besides sprays, such as filters, ice condensers, pressure suppression pools, etc. This list of states is not necessarily exhaustive (for instance, for two-phase flow, the carrier water must be considered) and the logic of the code has been chosen to readily accept an arbitrary number of states. It must be realized, however, that the addition of extra states increases computer running times.

2.1.1 Transport Rate Equations

Radionuclide transport can occur among the several states of an individual control volume or between certain states of different control volumes if these are connected by fluid flow. The former types of transport are generally limited by molecular effects and are modeled and correlated in the code itself. Transport of the fission products between control volumes

is assumed to occur in phase with fluid transport. This transport is imposed by time-dependent thermal-hydraulic data read into the code.

It is important to consider the types of flow or extent of mixing expected, and to specify criteria for their evaluation. Transverse mixing is approximated by turbulent or convective flow. Longitudinal mixing does not occur and is only approximated, provided fractional deposition within a control volume is small. This criterion can be quantified for the simple situation of a single control volume in which only particle deposition with deposition velocity, v_d, occurs. Then analysis of the homogeneously mixed case gives at steady state:

$$\frac{n}{n_o} = \frac{1}{1 + (A_d/A_c)\, v_d/v} \qquad (1)$$

where

n = final particle concentration

n_o = initial particle concentration

v = flow velocity

A_d = deposition area

A_c = cross flow area

while the more accurate differential flow analyses gives, again for steady state:

$$\frac{n}{n_o} = \exp[-(A_d/A_c)(v_d/v)] \qquad (2)$$

The two expressions agree approximately, provided

$$A_d v_d / A_c v << 1 \qquad (3)$$

If one defines

$$\tau_f = L/v \quad = \text{residence time for flow}$$

$$= V/A_d v_d \quad = \text{residence time for deposition,}$$

where

L = length of volume along with flow direction
V = volume,

then the criterion that the completely mixed control volume approach used in MATADOR II be adequate is

$$\frac{\tau_f}{\tau_d} << 1 \qquad (4)$$

and the criterion that steady state be reached is

$$t >> \left(\frac{1}{\tau_f} + \frac{1}{\tau_d}\right)^{-1} \qquad (5)$$

Based on considerations of the above criteria, it is assumed in MATADOR II that a given system can be subdivided into a sufficient number of control volumes such that the radionuclide population in each of these is expected to be well mixed. It is further assumed that the transport rates of a radionuclide between states of a given control volume are proportional to the amount of the fission product in the state from which transport occurs. This latter assumption is equivalent to the concept of a mass transfer coefficient or deposition velocity. Working with the mass of a given radionuclide specie rather than its symmetrical treatment, the underlying transport equations of MATADOR II are:

$$\frac{dM^k_{lm}}{dt} = S^k_{lm} + \sum_{n\neq m} {}^{m}\beta^k_{lm}\, M^k_{ln} - \sum_{n\neq m} {}^{n}\beta^k_{lm}\, M^k_{lm} + \sum_{j\neq l} {}^{l}F_{jm}\, M^k_{jm} - \sum_{j\neq l} {}^{j}F_{lm}\, M^k_{lm} \qquad (6)$$

Here

M^k_{lm} = mass of radionuclide specie k in volume l and state m

S^k_{lm} = source rate of specie k in volume l and state m

${}^{n}\beta^k_{lm}$ = transfer coefficient for transport of specie k in volume l from state m to state n

${}^{j}F_{lm}$ = transfer coefficient for transport of fission product in state m from volume l to volume j.

Equation (6) may be rewritten as

$$\frac{dM^k_{lm}}{dt} = S^k_{lm} + \sum_{n\neq m} {}^{m}\beta^k_{ln} M^k_{ln} + \sum_{j\neq l} {}^{l}F_{jm} M^k_{jm} + E^k_{lm} M^k_{lm} \qquad (7)$$

where

$$E^k_{lm} = -\left[\sum_{n\neq m} {}^{m}\beta^k_{lm} + \sum_{j\neq l} {}^{j}F_{lm}\right]$$

If m signifies a surface state, ${}^{n}\beta^k_{lm}$ represents a mass release rate P; if m signifies a volume state, ${}^{n}\beta^k_{lm}$ represents a deposition

velocity, v_d, multiplied by the area available for deposition, A_l, and divided by the volume, V_l, of the control volume. Thus,

$$n\beta k_{lm} = v_d(m,n,l,k)\frac{A_l}{V_l} \qquad m = \text{volume state} \qquad (8)$$

$$= P(m,n,l,k) \qquad m = \text{surface state}$$

Both v_d and P are, in general, strongly dependent upon on the thermal-hydraulic conditions existing in the given control volume. Since these in turn are time dependent, v_d and P are themselves functions of time. This time dependence places conditions on the technique used in solving Equation (6). These are considered in the subsequent section.

To permit flexibility in transport analyses of a variety of systems, the β coefficients are developed in a separate subroutine, BETV, (discussed in some detail in Section 2.1.2.2.). A separate subroutine FF, is reserved for the development of the transfer coefficients, F, for transport between volumes. This subroutine is discussed in Section 2.1.2.1.

MATADOR II does not account for chemical reaction kinetics. This implies that Equation (6) separates with respect to explicit dependence on k. Implicitly, coupling with respect to k remains through joint radionuclide transport on mixed aerosol particles. This coupling can, however, be accounted for by simultaneous time translation of the set of Equation (6) for each k for each time step. For simplicity, the superscript k can therefore be dropped in the following.

To simplify the logic and to decrease running time of the code the two-dimensional matrix M_{lm} is linearized by a mapping, MAPV from a two-dimensional array onto a linear array. MAPV joins the rows of M_{lm} head-to-tail in the linear array M as exemplified in the following simple FORTRAN example which maps the matrix X(10,10) onto the linear array Y(100):

```
      DO 1 I = 1,10
    1 MAPV(I) = (I - 1)*10 .
```

X(I,J) and ((MAPV(I)+J) are now in a one to one relationship. The elements ${}^{m}\beta_{ln}, {}^{l}F_{jm}$ of Equation (6) can then be combined in a two-dimentional matrix A such that Equation (6) can formally be written

$$\frac{dM}{dt} = S + AM \qquad (9)$$

Note that S and M are one-dimensional matrices, or vectors. The elements of A are developed in the subroutine MATRIX.

2.1.1.1 Solution Technique

While a formal solution to Equation(9) can be written for a general time dependent source vector S and a general time dependent transport matrix A, this cannot, in general, be done in closed form. That is, the formal solution involves exponential series of integrals that must be evaluated numerically. For this reason, as well as for difficulties associated with the mass transfer coefficient approach in connection with some transport processes, Equation (9) is solved under the assumption that both S and A are essentially independent of time for the duration of a time step. In fact, the size of each time step is chosen specifically to fulfill this requirement.

With the assumption of time independent S and M, the solution to Equation (9) is found by iteration:

Noting from Equation (9) that the higher derivatives of M obey the recursion relation

$$M^{(n+1)} = AM^{(n)} ,$$

The Taylor expansion for M

$$M = M_o + M_o^{(1)}t + M_o^{(2)}t^2/2! + \ldots\ldots\ldots$$

becomes

$$M = M_o + (S_o + AM_o)t + A(S_o + AM_o)t^2/2! + \ldots\ldots\ldots$$

which may be written as

$$M = M_o + (1 + z/2! + z^2/3! + \ldots\ldots)(AM_o + S_o)t \quad (10)$$

where $z = At$.

Equations analogous to (9) and (10) are encountered in the computer code CORRAL where z is manipulated as a two-dimientional array, which permits the use of a scaling procedure to ensure rapid convergence. In order to do so efficiently, however, powers of z are evaluated, which implies that the solution algorithm is rather time consuming (computation time is dependent on the third power of the order of z).

Since the very much larger order of the z matrices employed in the present codes make the CORRAL solution algorithm impractical, a faster solution technique was sought. Instead of working with powers of z, an iterative scheme is used which is illustrated by rewriting Equation (10) as

$$\begin{aligned} M = M_o &+ (AM_o + S)t \\ &+ z/2\ (AM_o + S)t \\ &+ z/3\ [z/2\ (AM_o + S)t] \\ &+ \ldots\ldots\ldots \end{aligned} \quad (11)$$

That is, each successive term (after the second) is found from the preceding terms by multiplication with the factor z/n, where n is one minus the number of the term. Thus, powers of z are never evaluated and the running time for this solution algorithm depends on the second power of the order of z. It is therefore substantially faster than the CORRAL algorithm for problems involving large z matrices.

Summation of the series solution (11) is cut off when the addition of a following term of the series produces a relative change in M whose absolute value is less than a predetermined amount. Since scaling is not employed, this may require successive evaluations of the solution for short time intervals t in order to ensure convergence within a reasonable number of iterations. An additional constraint on the time interval arises from the requirement that the vectors S and M be approximately constant over the time interval under consideration. This is assured by requiring the absolute values of relative changes of the elements of S and M to be less than a predetermined value over the given time interval.

The solution as expressed by Equation (11) is programmed in the subroutine MATSA.

2.1.1.2 Structure and Linearization of the A Matrix

Each element of the A matrix is identified by the subscripts I and J (volumes) and m and n (states). The linearization of the M_{Im} vector casts the A matrix into the form given below, where the location of each subarray or block is defined by the values of I and J. Thus, off-diagonal sub-blocks describe intervolume transport between volumes I and J while diagonal sub-blocks describe intravolume transport for volume I. The location of any elements within each sub-block is defined by m and n.

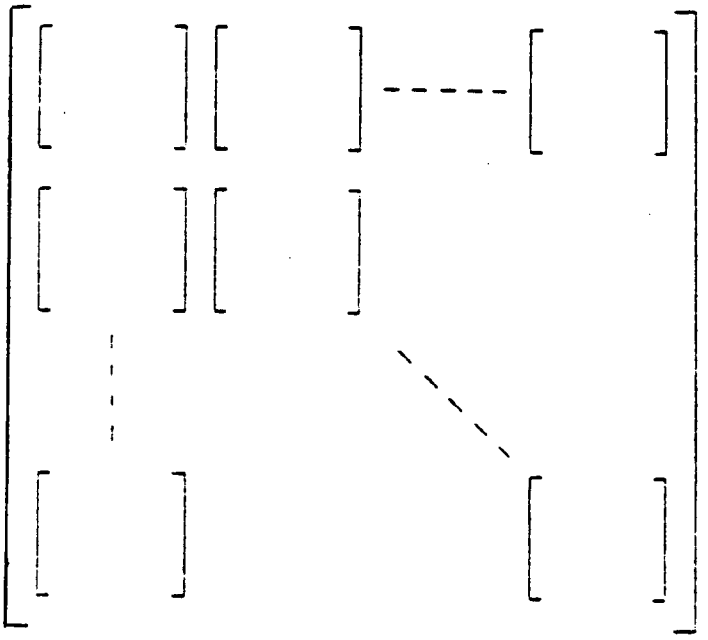

Off-diagonal sub-blocks contain the $^{J}F_{Im}$ coefficients while diagonal sub-blocks contain the^{n} k_{Im} coefficients (Equation 6). This is illustrated for a three state, three volume case below:

$$\begin{bmatrix}
\begin{bmatrix} E_{11} & {}^{1}\beta_{12} & {}^{1}\beta_{13} \\ {}^{2}\beta_{11} & E_{12} & {}^{2}\beta_{13} \\ {}^{3}\beta_{11} & {}^{3}\beta_{12} & E_{13} \end{bmatrix} & \begin{bmatrix} {}^{1}F_{21} & & \\ & {}^{1}F_{22} & \\ & & {}^{1}F_{23} \end{bmatrix} & \begin{bmatrix} {}^{1}F_{31} & & \\ & {}^{1}F_{32} & \\ & & {}^{1}F_{33} \end{bmatrix} \\
\begin{bmatrix} {}^{2}F_{11} & & \\ & {}^{2}F_{12} & \\ & & {}^{2}F_{13} \end{bmatrix} & \begin{bmatrix} E_{21} & {}^{1}\beta_{22} & {}^{1}\beta_{23} \\ {}^{2}\beta_{21} & E_{22} & {}^{2}\beta_{23} \\ {}^{3}\beta_{21} & {}^{3}\beta_{22} & E_{23} \end{bmatrix} & \begin{bmatrix} {}^{2}F_{31} & & \\ & {}^{2}F_{32} & \\ & & {}^{2}F_{33} \end{bmatrix} \\
\begin{bmatrix} {}^{3}F_{11} & & \\ & {}^{3}F_{12} & \\ & & {}^{3}F_{13} \end{bmatrix} & \begin{bmatrix} {}^{3}F_{21} & & \\ & {}^{3}F_{22} & \\ & & {}^{3}F_{23} \end{bmatrix} & \begin{bmatrix} E_{31} & {}^{1}\beta_{32} & {}^{1}\beta_{33} \\ {}^{2}\beta_{31} & E_{32} & {}^{2}\beta_{33} \\ {}^{3}\beta_{31} & {}^{3}\beta_{32} & E_{33} \end{bmatrix}
\end{bmatrix}$$

Note that only the diagonal elements of the off-diagonal blocks are non-zero and that these in turn are only non-zero when a flow connection exists for flow from volume J to volume I. For reactor primary systems the number of flow connections per volume does not often exceed 2. Most of the possible off-diagonal block elements are in fact zero.

The diagonal elements of the diagonal blocks E_{Im}, represent fission product transport from volume I and state m. Because fission product mass must be conserved, they can be expressed as sums over β and F elements residing elsewhere in the complete A matrix (Equation (7)).

In order to conserve computer storage space, and to greatly reduce the long running times associated with the manipulation of such large matrices, the matrix A is itself linearized by again employing a mapping vector scheme. In addition, such a scheme readily permits the deletion of the zero elements of A.

The storage array for the A matrix is filled at the beginning of each time step by calling up the subroutine BETV, which constructs the β's, or intra-volume transfer coefficients, and by calling up FF which constructs the F°s, or intervolume transfer coefficients. The procedure is to first develop the off-diagonal blocks and the off-diagonal elements of the diagonal blocks. These are then used to evaluate the diagonal elements of the diagonal blocks. This process is repeated in turn for each chemical specie considered. Since the intervolume transfer coefficients are independent of the particular specie under consideration, these are evaluated for the initial specie only.

2.1.2 MODEL FEATURES

2.1.2.1 Intervolume Mass Transfer

Transport of radionuclides between volumes is assumed to occur solely by convection. Considering only superheated steam flow, it thus occurs only for the states steam-molecular, and steam-particle.

Thermal-hydraulic data and the steam mass flow rates are read into the code from the MARCH 2.0 calculations.

Since each control volume is assumed well mixed, the rate of nuclide transport out of a volume is just the fractional rate of change of mass of the carrier (steam):

$$JF_{Im} = \frac{FXS(I,J)}{\rho_S(I)V(I)} \qquad (12)$$

where

FXS(I,J) = steam mass flow rate from volume I to volume J

$\rho_S(I)$ = density of steam in volume I

V(I) = volume of volume I.

Here ρ_S is determined from correlations related to temperatures and pressures. Thus the convective exchange of matter between control volumes is driven by the input values for steam production rates.

2.1.2.2 Intravolume Mass Transfer

Thermal hydraulic modeling in MATADOR II is very important, because a number of the key deposition mechanisms modeled in the code rely on internal thermal-hydraulic calculations to determine parameters important to deposition. Models that rely on thermal-hydraulic calculations include, among others, those for vapor condensation onto walls and aerosol deposition onto walls by thermophoresis.

In the development of MATADOR II, it was acknowledged that forced-flow conditions might not always exist; that is, that natural convection flow might be dominant under some conditions. To account for the influence of natural convection, MATADOR II calculates an "effective" Reynold's number using the following formulation:

$$Re_{ef} = (Gr/70)0.5 \qquad \text{for } Gr > 107$$

$$Gr = [g(\Delta T)\ D^3]/\nu^2 T$$

where

Re_{ef} = effective Reynold's number

Gr = Grashof number

g = gravitational acceleration

D = control-volume hydraulic diameter

ΔT = gas-wall temperature difference

T = gas temperatures,

ν = kinematic viscosity of steam

When the effective flow Re is greater than the Re calculated using the input steam production rates, then the effective Re is used to calculate condensation mass transfer coefficients and thermal gradients used in thermophoresis calculations.

At present, there has been no reference identified to document the basis for the correlation used to calculate an effective Reynold's number for conditions where natural convection dominates.

The correlation used in MATADOR II to calculate an effective boundary layer thickness, and so an effective wall thermal gradient for thermophoresis calculations, is

$$Nu = hD/k = D/\delta = 0.021\ Re^{0.8}$$

where

Nu = Nusselt member, Re = Reynold's number

k = gas thermal conductivity

h = k/δ = heat-transfer coefficient

δ = boundary-layer thickness

D = control-volume hydraulic diameter

This is a heat-transfer correlation for turbulent flow conditions, which may not always exist. In addition, the correlation is for fully-developed flow conditions, which may also not exist. For example, flow Reynold's numbers varied between 100 and 1000, then the so-called entrance length for full-developed flow in the control volume would vary from 6 to 60 hydraulic diameters downstream of the lower end of the control volume. Assuming a hydraulic diameter of 4 inches, for these assumed Reynold°s numbers, fully-developed flow would not occur within 2 to 20 feet on the lower end of the volume. Nusselt numbers calculated for fully-developed flow conditions are typically less than those occurring in the flow entrance region.

Effective wall heat transfer coefficients would be under-estimated by assuming fully-developed flow by a factor of three or more.

The correlation used in MATADOR II to model condensation mass transfer to wall surfaces is:

$$Sh = k_w D/D_g = 0.023\ Re^{0.83}\ Sc^{0.33}$$

where

Sh = Sherwood number, Sc = Schmidt number

Re = Reynold's number

k_w = condensation mass transfer coefficient (cm/s)

D = hydraulic diameter, D_g = vapor diffusion coefficient

This is again a correlation purely for turbulent, fully-developed flow conditions, and so the same criticism relevant to the calculation of Nusset numbers applies.

2.1.2.2.1 Condensation of Vapor Onto and Evaporation from Aerosols and Structural Surfaces

The condensation/evaporation of CsI, CsOH, and Te onto/from particle and wall surfaces is modeled in MATADOR II using the following formulations:

$$\frac{dC_s}{dt} = -\frac{A_w k_w}{V}\left(C_s - C^s_w\right) - \frac{\langle A_p k_p \rangle}{V}\left(C_s - C^s_p\right)$$

$$\frac{dM_w}{dt} = A_w k_w \left(C_s - C^s_p\right)$$

$$\frac{dM_p}{dt} = A_p k_p \left(C_s - C^s_p\right)$$

where

$C_S = M_S/V$ = concentration of the nuclide vapor in steam

M_S = Total mass of the nuclide vapor in steam

V = Volume of the control volume

M_W = Total mass of nuclide vapor condensed on walls

Mp = Total mass of nuclide vapor condensed on aerosol particles

C^S_W = Equilibrium vapor concentration of the nuclide at the temperature of the wall surfaces (assumed independent of pressure)

C^S_p = Equilibrium vapor concentration of the nuclide at the temperature of the steam (assumed independent of pressure and particle surface curvature)

A_W = Area of wall surfaces

A_p = Surface area of aerosol particle

k_W = Mass transfer coefficient for nuclide transfer between steam and wall surfaces-steam interface

k_p = Mass transfer coefficient for nuclide transfer between steam and particle surface-steam interface

The correlations used for k_W and k_p are:

k_W condensation mass transfer coefficient (cm/s)

$k_p = D_g/r$

where

D_g = vapor diffusion coefficient
r = particle radius

Possible inaccuracies related to the formulations used in MATADOR II for condensation/evaporation include the following:

1. The correlation for k_W is applicable to well-developed turbulent flow conditions only; turbulent flow does not exist in the containment for all accident sequences.

2. No account is taken for the possible influence of non-condensable gases on vapor condensation. Also, no account is taken for vapor pressure suppression at particle surfaces or due to multi-specie vapor solutions. Including these effects would tend to lead to reductions in calculated vapor condensation rates.

3. The mass transport coefficient, k_w, used is one for steady-state transport in a fully-developed flow regime. For most sequences the flow can be characterized as being "quasi-steady" for the majority of time. However, as discussed previously, fully-developed flow conditions are not likely to exist for most accident sequences. Including this effect would tend to increase the calculated vapor condensation rates.

2.1.2.2.2 Vapor "Sorption" Onto Wall Surfaces

The T module assumes that vapor sorption onto walls can be modeled using a "deposition velocity" model that can be expressed as:

$$\frac{dM}{dt} = - V_d \left(\frac{A}{V}\right) M$$

where

M = mass of vapor species airborne in control volume

v_d = vapor species deposition velocity (cm/s)

A = control volume surface area

V = volume in control volume

It is assumed in MATADOR II that all "sorption" onto surfaces is irreversible. In addition, sorption onto aerosol particles is not accounted for. The deposition velocities used for I_2, CsI, CsOH, and Te are given below:

Specie	V_d(cm/s)
I_2	$9(10^{-8})\ e^{8100/RT}$
CsI	0
CsOH	0.01
Te	1.0

The deposition velocity model as used in MATADOR II is empirical. Modeling sorption deposition velocities can hide complex mechanisms that might be occurring in the sorption process such as transport in the vapor phase, sorption/desorption at the surface, chemical reactions with the surface materials, and diffusion into the bulk of the surface or through a surface layer. Using vapor deposition velocity models would be appropriate if the system conditions are such that surface reactions are rate-limiting (that is, that they dominate the transport mechanisms), if surface saturation effects do not occur, and if the empirical values are obtained under these conditions using appropriate materials, species, temperatures, and mass loadings. This is generally a very difficult assignment.

Some comments related to the accuracy of the values of deposition velocities used in MATADOR II are presented below:

1. The correlation used for I_2 deposition velocity is based on the data from Genco et al. These tests were performed at temperatures between 150 and 550 C.

2. The deposition velocity used for CsI is zero. Data contained in a Battelle report indicates CsI deposition velocities less than 0.001 were measured for the temperature range relevant to the containment; these are small values and provide some justification for the assumption of no CsI deposition by sorption.

3. The deposition velocities used for CsOH and Te were based on "Phase 1" deposition velocity measurements made for these species at Sandia Laboratories. Discussions with Sandia staff involved in the work indicate that the level of confidence one should have in these measurements is an order of magnitude, because the Phase 1 experiments were performed simply to get some scoping-type answers. The "Phase 2" experiments now being performed at Sandia will be performed over a range of temperatures (this was not done for the Phase 1 experiments), and the data to be obtained from those tests is expected to be more accurate.

The modeling of CsOH and Te sorption onto surfaces by MATADOR II is limited by the fact that there is a very sparse data base available. The present efforts at Sandia, and also the effort starting at ORNL have the best likelihood of producing data that will permit better estimation of sorption processes for more species over a wider range of temperatures.

2.1.2.3 Aerosol Behavior

The underlying assumption of the aerosol model equations, one that is made by most present aerosol behavior codes, is that the aerosol can be viewed as a homogeneous mixture, except for narrow surface boundary layers through which mass transport of the particulate phase takes place. This assumption was tested for the special case of sodium pool fire aerosols with a model that sub-compartmentalizes the containment into three individually mixed zones connected by fluid flow and found to be adequate after the fire ceases and conservative during the burn period. It permits model equations that are independent of spatial coordinates and thus makes their numerical solution practicable.

The second, fundamental assumption is that the expected non-sphericicity and fluffiness of the aerosol agglomerates can be modeled using just two size independent correction factors -- the dynamic shape factor and the collision shape factor. These will be treated below. Their size independence is not an inherent requirement of the code but a convenient assumption in lieu of experimental data to the contrary.

Given these assumptions, the general equation of aerosol behavior is:

$$\frac{dn(x,t)}{dt} = S(x,t) - R(x,t)n(x,t) - L(x,t)n(x,t) - F(x,t)n(x,t)$$
$$+ 1/2 \int_0^x K(x',x-x')n(x',t)n(x-x',t)dx' - n(x,t) \int_0^\infty K(x,x')n(x',t)dx'$$

Here

$n(x,t)dx$	=	number of particles of mass x in dx at time t per unit volume
$S(x,t)dx$	=	number of particles of mass x in dx uniformly introduced into the aerosol system per unit time per unit volume
$R(x,t)n(x,t)dx$	=	number of particles of mass x in dx uniformly removed from the aerosol system per unit time per unit volume by deposition
$L(x,t)n(x,t)dx$	=	number of particles of mass x in dx uniformly removed from the aerosol system per unit time per unit volume by leaks
$F(x,t)n(x,t)dx$	=	number of particles of mass x in dx uniformly removed from the aerosol system per unit time per unit volume by filters
$K(x,x')n(x)n(x')dxdx'$	=	number of collisions between particles of mass x in dx and x' in dx' per unit time per unit volume.

2.1.2.3.1 Natural Removal Terms

Natural removal by sedimentation diffusion and thermophoresis are considered. This is described in general by a deposition velocity, $v(x,t)$ such that

$$R(x,t) = v(x,t) \frac{A_I}{V}$$

where

A_I = surface area available for deposition due to mechanism I

V = volume of containment.

v is taken as the steady state velocity $v = B(x)* F(x,t)$ with $B(x)$ the mobility of a particle of mass x and $F(x,t)$ the applied force. The mobility is given by:

$$B(x) = \frac{1}{\chi 6\pi\mu r_e} \left\{1 + AKn + QKn\,[\exp(-\,b/Kn)]\right\}$$

with

χ = dynamic shape factor
μ = viscosity of gas

$$r_e = [3x/(4\pi\rho_p)]^{1/3}$$

ρ_p = particle material density
Kn = Knudsen number of particle
A = 1.246, Q = 0.42, b = 0.87

Here the Knudsen-Weber-Cunningham correction constants are those for Millikan oil drops. Their precise values depend on the particle constituents but do not enter sensitively into typical code predictions.

2.1.2.3.1.1 Sedimentation

For particle Reynold's numbers less than one, the Stoke's settling velocity

$$v(x,t) = 4/3\,[r_e^3\,{}_p g B(x)]$$

holds. For some severe accident scenarios, however, MATADOR II predicts a large fraction of the suspended mass to reside in particles whose diameter exceeds 100 μm. For these, the above equation no longer holds and may in fact be off by as much as a factor of two. MATADOR II therefore uses empirical data in the form of a correction factor to the above expression for particles whose Reynold's number is greater than one and less than 1259. For Reynold's numbers in excess of this value, no empirical values of v are known. As a compromise, the correction value for R_e = 1259 is used here as well.

To account for particle nonsphericity, it is assumed that a correction factor, f, exists such that

$$fC_F = \frac{F_D}{\pi r_e^2 \gamma^2 (\rho_g/2)\, v^2}$$

where

γ = collision shape factor
C_F = Fanning friction factor for spheres
F_D = actual drag force on particle

From the limit requirement that

$$F_D = 6\pi\chi x r_e v$$

and

$$v = \frac{2}{9} \frac{\rho_g g r_e^2}{\mu x}$$

In the Stoke's regime, one can determine f to be equal to x/γ. The collision shape factor, γ, was initially introduced to account for a collision cross-section of nonspherical particles that depends on a collision radius, r_c, different than r_e. Thus r_c was taken as proportional to r_e: $r_c = \gamma r_e$. γ has never been measured but approximate values have been inferred by backfitting computer codes. Unfortunately, γ has also been shown, along with χ, to be the most sensitive code parameter.

To avoid the introduction of further parameters of comparable sensitivity, γ is also used in MATADOR II as a proportionality factor between some geometric particle radius, r, of an agglomerated, nonspherical, particle and its mass equivalent radius: $r = \gamma r_e$. Then all data correlated on spherical particles is written in terms of γr_e. Thus, in particular, $Kn = \lambda/\gamma r_e$, where λ is the gas phase mean free path.

2.1.2.3.1.2 Diffusion

$$v(x,t) = \frac{D(x)}{\delta_D}$$

where

$D(x) = B(x)kT$

k = Boltzmann's constant

T = absolute temperature

δ_D= diffusion boundary layer thickness.

δ_D is known to depend on the momentum boundary layer thickness, δ_o, of the flowing gas-wall interface and on particle size through its dependence on D(x) via

$$\delta_D = \delta_o Sc^{-1/3}$$

where

$Sc = \mu/\rho_g D)$

ρ_g = density of gas phase

Nevertheless, δ_D is assumed an input constant since experimental evidence to the contrary is scarce and, more importantly, since diffusive deposition appears to play a minor role in reactor accident calculations.

2.1.2.3.1.3 Thermophoresis

Thermophoresis is driven by temperature gradients. These are usually not well known everywhere so that considerable uncertainty in code output exists for cases in which thermophoresis is significant. Because of this uncertainty, great precision in the expression for the thermophoretic deposition velocity is not necessary. The code uses an expression, developed by Brock, that agrees within a factor of two with available data:

$$F_{thermophoresis} = \frac{-9\pi\mu^2 r_e}{\rho_p} \Phi \frac{\Delta T}{\Delta T \delta_{TH}}$$

where

$$= \frac{1}{1 + 3C_m Kn} \quad \frac{k_g k_p + C_t Kn}{1 + 2k_g/k_p + 2C_t Kn}$$

T = temperature difference between wall surface and gas over the thermal boundary layer thickness, δ_{TH}.

C_m = momentum accommodation coefficient, taken as 1.0.

C_t = thermal accommodation coefficient, taken as 2.49

k_g = thermal conductivity of the gas phase

k = thermal conductivity of a particle

Since the Brock expression for the thermophoretic force is based on spherical particles, γr_e is used wherever a particle radius is referenced.

The values of C_m and C_t indicated are those that result in the best fit of the above expression with data on NaCl aerosol. Measurements on dry Na_2O_2 particles have yielded values of C_t between 1.9 and 2.5, with the former value based on the assumption that $k_g/k_p = 0.01$, the latter on kg/kp = 1.0. For fluffy agglomerates, the thermal conductivity, k_p, as used in the expression probably does not correspond to the particle's material thermal conductivity. It is likely that k_p approaches k_g with increase in fluffiness, but no independent measurements of k_p are known.

It should be noted that for severe accident scenarios, most of the airborne mass is associated with particles whose Knudsen number is small. In this case,

$$\Phi \rightarrow \frac{1}{2 + k_p/k_g}$$

and is thus essentially independent of C_t, and C_m, but a strong function of the unknown, k_p. Its uncertainty is comparable, in effect, to that in the average thermal gradient at interior surfaces.

2.1.2.3.2 Coagulation

Of the multitude of mechanisms that can contribute to particle collisions (and therefore coagulation) only two appear to play a significant role in passive aerosol systems: Brownian and gravitational coagulation. MATADOR II includes these and turbulent coagulation since the latter may play a role in situations where natural convection becomes severe enough to result in significant turbulent energy dissipation.

(I) Brownian Coagulation

$$K_B(x,x') = 4\pi kT\gamma[\, B(x) + B(x')](r_e + r'_e)$$

(II) Gravitational Coagulation

$$K_G(x,x') = (x,x')\frac{2\pi g \rho_g^{\,2}}{9\mu\chi}\left|r_e^2 - r'^2_e\right|(r_e + r'_e)^2$$

where

$\epsilon(x,x')$ = collision efficiency.

The collision efficiency can be viewed as that factor which makes the general equation of aerosol behavior correct. Most recent experimental and theoretical investigations into this factor have yielded data tables

that have been employed in MATADOR II on large scale sodium fire simulation runs. The results of these runs are surprisingly similar to ones using the simple expression

$$\epsilon(x,x') = 1.5[\, r/(r + r')^2$$

where x', r' refer to the larger particle. This expression strictly holds for inertialess particles and r'>>r only. Its use for all values of r' and r yields satisfactory agreement with simulation experiments to date.

2.1.2.3.2.1 Turbulent Coagulation

An expression for turbulent coagulation was added to MATADOR II in the expectation that sufficient turbulence would exist to make this mechanism significant. Pressure simulation experiments suggest that it plays a noticeable, but minor, role.

The two most widely used theoretical treatments of turbulent coagulation are probably those of Saffman and Turner and Levich. Both are based on the hypothesis that microscale turbulence is essentially isotopic and that the particles are smaller than microscale. Both also invoke the same conceptualization of the turbulent collision process: relative particle motion due to entrainment in a variable fluid velocity field and relative particle motion due to differences in inertial response to fluid acceleration. It is not surprising therefore that, since quantification of isotropic microscale turbulence is based on dimensional analysis, the two approaches result in identical expressions except for multiplicative constants. By the same token, these multiplicative constants must be considered indeterminate until experimentally determined.

The MATADOR II expression for turbulent coagulation is based on Saffman and Turner's, including their multiplicative constants. Their expressions have been modified to include a collision efficiency for particle motion relative to the fluid and the shape factors for non-spherical particles discussed above. While the collision efficiency for particles colliding due to their motion with a variable fluid velocity field may not be unity, it was assumed as such in MATADOR II. Thus

$$K_{T+G}(x,x') = 2(2\pi)^{1/2}\gamma^2(r_e + r'_e)^2[\epsilon(x,x')^2(\tau_1-\tau_2)^2 1.3E^{3/2}/\nu^{1/2} + 1/3\ \epsilon(x,x')^2(\tau_1-\tau_2)^2 g^2 + 1/9\gamma^2(r_e+r'_e)^2 E/\nu]^{1/2}$$

where

$\tau = 2r_e^2\rho_p/(9\mu\chi)$ = particle time response

ν = kinematic viscosity of the gas

E = turbulent dissipation energy density

Note that, following Saffman and Turner, the gravitational coagulation mechanism is incorporated into K_{T+G}.

Finally, the assumption is made that

$$K(x,x') = K_B(x,x') + K_{T+G}(x,x').$$

Since K_B and K_{T+G} are of equal magnitude over a narrow particle size range only, this approach is not expected to result in significant error.

2.1.2.3.2.2 Laminar Coagulation

The influence of aerosol deposition due to laminar flow is modeled in MATADOR II using the relation:

$$\frac{dC}{dt} = - V_{d,lam}(A/V)C$$

$V_{d,lam}$ = laminar flow deposition velocity

Aerosol deposition from laminar flow for any particle size can be calculated accurately. An expression developed by Gormley and Kennedy for the fractional number of particles deposited in flows in circular pipes is:

$$N/N_o = 0.8191e^{-7.314h} + 0.0975e^{-44.6h} + 0.0325e^{-114h}$$

$$n > 0.0156$$

$$N/N_o = 1 - 4.07h^{2/3} + 2.4h + 0.446h^{4/3}$$

$$n < 0.0156$$

where

N = number of particles that reach the end of the pipe length L.

N_o = number of particles that enter the pipe (distributed uniformly over the cross section)

$h = LD/2va^2$

a = pipe radius

A fictitious deposition velocity for an equivalent, completely mixed system can be derived from these expressions as follows:

Letting n be the concentration of particles in the completely mixed volume and n_o the concentration of particles entering the volume, the deposition velocity, v_d, across a boundary layer is defined by the expression

$$\frac{dn}{dt} = - v_d \frac{A}{V} n$$

where

A = surface area

V = volume

for $v_d/v = <<1$, therefore,

$$n - n_o = v_d(A/V)(L/v)n = - v_d(2/a)(L/v)n$$

or

$$V_{d,lam} = (n_o/n - 1)av/2L = (N_o/N - 1)\ av/2L$$

2.1.2.4 Removal by Engineered Safety Systems

The removal of iodine by the containment sprays is modeled in CORRAL as a mass transfer process. The mass transfer coefficients for iodine in the gas phase and within the liquid droplet were calculated using standard correlations. They were then used in calculating a deposition coefficient ($\lambda_{vapor,\ spray}$) in terms of the volume of the sprayed compartment, the flow rate of the sprayed liquid, and the terminal velocity of the spray droplets. The model used is:

$$\lambda_{vapor,\ spray} = \frac{FH}{V}\left(1 - \exp\left(\frac{-6k_g t_e}{d(H + (k_g/k_f))}\right)\right)$$

where

F = spray flow rate, cm^3/sec = gm/sec if ρ_{spray} = 1 gm/cc,

H = equilibrium Henry's Law constant for iodine (ratio of liquid phase concentration to gas phase concentration of iodine at equilibrium),

V = volume of sprayed compartment,

d = diameter of sprayed droplets,

t_e = fall time (height of fall of drop/terminal velocity of droplet, V_t)

D_f = diffusivity of iodine in the droplet

k_g = gas phase mass transfer coefficient of iodine

$$= \frac{D_g}{d}\left(2.0 + 0.6\ Re^{1/2}\ Sc^{1/3}\right), \text{ and}$$

k_f = liquid phase mass transfer coefficient of iodine = $6.38\ D_f/d$.

The value of V_t is found by matching the velocity independent dimensionless number:

$$f_D Re^2 = 4 \rho (\rho_f - \rho) d^3 g / 3u^2$$

with the appropriate range of Reynolds' number. For $10<Re<100$, $f_D Re^2 = 15.71\ Re^{1.417}$ and for $100<Re<700$, $f_D Re^2 = 6.477\ Re^{1.609}$. ρ_f is the density of the liquid droplets and Re is defined by:

$$Re = d \rho V_t / \mu$$

This model for calculating the rate of iodine vapor removal by the containment sprays is believed to be adequate. It was developed on the basis of observations in the Containment System Experiments, and the data show that the model describes the actual behavior of iodine very well. It was therefore decided that no major modification to this model was necessary and it has been retained in MATADOR II.

Removal by other engineered safety features such as filters, ice condensers, and suppression pools are modeled in CORRAL-2 utilizing the concept of a decontaimination factor (DF). Attenuation of the concentration of iodine vapor due to passage through the filters or the suppression pool is not modeled as a rate process; rather the value of the DF is used to take out some of the iodine and deposit it in the filter or the suppression pool. The value of this factor is input to the code.

The decontamination factor approach has been retained in MATADOR II for treating vapor removal by the filters, ice condensers, suppression pool, containment cracks, etc. These processes are called "DF" processes and they alter the airborne mass of vapors in a containment volume in the following way. If, at the beginning of timestep Δt, the airborne mass in

volume s is C_{so} and in volume r is C_{ro}, and if the DF process takes its inlet from volume s and releases its output to volume r, then the airborne masses of the radionuclide in volumes s and r are changed over the timestep Δt according to

$$C_s = C_s \left(1 - \frac{F \Delta t}{V_s}\right)$$

$$C_r = C_{ro} + C_{so} \frac{F \Delta t}{V_s D_{cf}}$$

where C_s and C_r are the airborne masses of the radionuclide in volumes s and r at the end of the time step, F is the volume flow rate from volume s to volume r through the DF process under consideration, V_s is the volume of volume s, and D_{cf} is the decontaimination factor. In the code, D_{cf}'s are input as a function of time for each DF process and for each chemical specie. The source and receiver volumes s and r could be the same volume, in which case the function of the DF process is simply to take out some of the airborne radionuclide mass from that volume.

There are several reasons for modeling some vapor removal processes using decontamination factors rather than rate expressions. In the case of suppression pool scrubbing, there is not, at present, sufficient experimental data available to provide a sound basis for developing models to estimate vapor removal rates by the pool water. In the case of the filters and the ice condensers, the decontamination factor approach probably models the actual removal process more realistically than a rate expression. This is because the process of radionuclide removal by these systems probably cannot be modeled as a first-order process for inclusion in the transport and deposition equations. It is approriate to point out here that all designs of the filters and pools can be modeled using this

treatment. In all instances, the value of the decontamination factor is input to MATADOR II as a function which depends on both time and radionuclide specie.

Several other processes not included in CORRAL-2 could contribute to radionuclide removal and thereby reduce the levels of radioactivity released to the environment during an accident. These processes include filtration by ice condensers, vent filters, and containment cracks. The MATADOR II code provides for modeling these processes by using decontamination factors. A more mechanistic approach was not practical at this time due to lack of experimental data.

2.1.1.5 Iodine Equilibrium

When airborne molecular iodine is depleted by either sprays or deposition on the water, the depletion rate becomes independent of these mechanisms when the concentration falls below about 1 percent of the initial value plus the sum of sources up to that time [1,2]. At concentrations below this level, an apparent equilibrium situation exists where the concentrations in liquid and gas phases are related by an equilibrium distribution constant, $H = C_f/C_g$. H is a function of time (probably due to slow liquid phase chemical reaction) and has been experimentally determined. In MATATOR II it has been possible to incorporate $H = H(t)$ when equilibrium conditions exist. This treatment is similar to that in CORRAL.

To get the equilibrium described quantitatively, an equivalent lambda for depletion of gas phase I_2 had to be developed. Since the value of H

increases with increasing time, the gas phase is being depleted as time goes on. To get this equivalent lambda, a mass balance can be written for I_2. If C_{go} is the initial airborne concentration, then

$$C_{go}V_g = C_f V_f + C_g V_g$$

or

$$\frac{C_g}{C_{go}} = \frac{C_g V_g}{C_f V_f + C_g V_g} = \frac{1}{\frac{C_f V_f}{C_g V_g} + 1} = \frac{1}{H\frac{V_f}{V_g} + 1}$$

Then for $H = H(t)$, the removal rate of I_2 can be writtenby

$$d\left(\frac{C_g/C_{go}}{dt}\right) = -\frac{1}{\left(H\frac{V_f}{V_g} + 1\right)^2}\left(\frac{V_f}{V_g}\right)\frac{dH}{dt}$$

where the equivalent lambda is

$$\frac{dC_g}{C_g} = -\left[\frac{1}{\left(H\frac{V_f}{V_g} + 1\right)^2}\frac{V_f}{V_g}\frac{dH}{dt}\right] dt = \lambda\, dt$$

$$\frac{dC_g}{C_g} = -\lambda\, dt$$

$$C_g(t) = C_{go}\, e^{-\lambda t}$$

where C_{go} is the concentration of airborne molecular iodine that would have existed if there were no iodine depletion.

Data shows that $H\, V_f/V_g >> 1$ for boric acid and caustic solutions in equilibrium with I_2, so that

$$\lambda = \frac{1}{H}\frac{dH}{dt}$$

Typical data for sprays are shown in Tables 2.1 and 2.2.

2.1.2.6 Removal by Engineered Safety Systems

Removal of particles by sprays is currently modeled in CORRAL using the data obtained in the Containment System Experiments[2]. An analysis of this data allows the calculation of a deposition rate coefficient, λ, for particulate removal by sprays using the equation

$$\lambda_{\text{spray, particles}} = \frac{3FEh}{2Vd}$$

where

F = spray flow rate

h = spray fall height

d = spray drop diameter

V = compartment volume, and

E = spray collection efficiency.

The functional dependence of E on (Ft/V) was arrived at from an examination of the results of the Containment Systems Experiments and is given as

$$E = \begin{cases} -15.825\ (Ft/V) - 0.055;\ 0<Ft/V<0.002 \\ 0.04125 - [0.08626 + 42.68\ (Ft/V)]^{1/2}/21.34;\ 0.002<Ft/V<0.0193 \\ 0.0015;\ Ft/V>0.0193 \end{cases}$$

This treatment of particle attenuation by sprays is modified somewhat in the MATADOR II code.

The loss rate coefficient for aerosol removal due to water spraying is as follows for more than one particle size:

$$\lambda_{Is} = \frac{3Fh}{2d} \frac{\epsilon_I}{V}$$

where

The important consideration now is to describe the collection efficiency, ϵ_I, as a function of aerosol and drop sizes. Because of hydrodynamic interaction between the two particles, only a certain fraction of those in the "sweep out area" of a large particle will actually be contacted. If the "sweep out area" is defined as the area of a circle with the radius of the larger particle, then the collision efficiency, ϵ, is defined as the fraction of the small particles in the sweep out area which are collected. Furthermore, the smaller particle must stick to the larger one to complete the collision process. Here, the sticking or attachment probability is assumed to be unity, since this value is likely and very little theoretical or experimental evidence concerning this phenomenon exists.

In general, there are two major pertinent collision mechanisms which enable a particle to overcome the hydrodynamic repulsion and collide with the water drop. The first mechanism is inertial impaction, which accounts for the deviation of a particle from a streamline due to its inertia. The

other mechanism is called the interception effect, which takes into account the increase of collision probability due to the finite extent of small particles. Thus, we write

$$\epsilon_l = \epsilon_{1l} + \epsilon_{2l}$$

where ϵ_1 is the collision efficiency due to particle inertia and ϵ_2 is the collision efficiency due to interception.

For relatively low particle velocities an empirical formula for the efficiency of enertially caused particle collisions is reported by Fuchs [3] and is given by:

$$\epsilon_1 = \left[1 + \frac{0.75 \ln (2\,Stk)}{Stk - 1.214}\right]^{-2}$$

Here, Stk is the Stokes number defined by

$$Stk = \frac{2(V_g - V_{gl})r_l \rho_{pl}}{9\,R}$$

where ρ_p is the particle density, V_g is the settling velocity of the water drop, V_{gl} that of the particle, r_l and R the radii of particle and water droplet, respectively. The efficiency ϵ_1 is taken as zero when Stk $\leq$1.214.

For viscous flow about a spherical collector, Lee and Gieseke [20] present an equation for the interceptional collision efficiency which is valid for small values of the ratio r_r/R:

$$\epsilon_2 \simeq \frac{3}{2} \frac{(r_l/R)^2}{(1 + r_l/R)^{1/3}}$$

It is clear from the expressions for ϵ_1 and ϵ_2 that separate efficiences are calculated for each particle size in MATADOR II.

Removal by the other engineered safety features like the filters and ice condensers are treated in the new code using the concept of decontamination factors. Decontamination by the containment cracks and vent filters are also modeled. This treatment is similar to that used for vapor species. The only difference is that different decontamination factors are used for different size particles.

2.2 INTERFACES WITH OTHER CODES

MATADOR II requires a variety of thermal-hydraulic parameters to perform the radionuclide transport and deposition calculations. These parameters are all functions of time and are calculated by the MARCH 2.0 code. However, MARCH 2.0 takes hundreds, or even thousands, of timesteps to determine these quantities. Because of computer storage space limitations, a user must choose at most twenty values of these parameters for input to MATADOR II so as to provide an adequate linear approximation to the function.

An algorithm which was originally written for the CORRAL-2 code provides the necessary rules for picking the appropriate values from the output of the MARCH 2.0 code. If we denote the thermal-hydraulic parameter by P and let p represent the vector of parameter values at each MARCH timestep, i.e.,

$$\overline{p} = (P_1, P_2, \ldots, P_m = f(t)$$

then we wish to devise an algorithm for defining a vector c

$$\overline{c} = (C_1, C_2, \ldots, C_N = g(t)$$

where

$$2 \leq N \leq 20$$

and

$$C_I \in \bar{P}_I$$

The functions f(t) and g(t) are discrete, however, and we make them continuous by connecting each successive point with a straight line. The problem is to choose the vector c such that f(t) and g(t) are approximately equal. In order to do this we define a linear operator, L_t,

$$L_t(\cdot) = {}_0\int^t (\cdot)\, dt$$

Next, being at the initial time step, we must calculate a least squares fit of a linear function to this and the successive point. Denoting this function Y(t) we have

$$Y_1(t) = a_1 t_1 + D_1 \quad , \; I = 1,2$$

Finally we calculate a function R(t) as

$$R(t_2) = \frac{L_{t_1} f(t) - L_{t_2} Y_1(t)}{L_{t_2} f(t)} \quad , \; t_1 < t < t_2$$

If R(t) is greater than R_o which is supplied by the user, the program choses t_2 as its first point. If R(t) is less than R_o as it must be for the first time step) then a third point is added and we have

$$R(t_3) = \frac{L_{t_3} f(t) - L_{t_3} Y_2(t)}{L_{t_3} f(t)}$$

This procedure is continued until the program reaches the final value in the p vector. If more than twenty points are chosen before the time t_I reaches t_m, the value of R_o is increased by 10 percent and the

algorithm is restarted. At the end of the calculations two arrays are returned to the main program:

$$XR = (T_1, T_2, \ldots, T_N, 2 \leq N \leq 20$$

$$YR = (Y(T_1), Y(T_2), \ldots, Y(T_N)).$$

The user has the option of requesting integral values rather than point values, in which case the YR array is given by:

$$YR = {}^{L}T_1 (Y_1(t)), \; L_{T2} (Y_2(t)), \ldots, L_N (Y_N(t)))$$

An example of this procedure is shown in Figure 2.1. In this figure, the containment temperature during an accident sequence is shown. The solid boxes indicate the points chosen from this curve by the algorithm when the convergence criterion, R_o reaches one percent. When using the MATADOR II code, the user has the option of either selecting to input thermal-hydraulic data or to allow the code to read a tape on which output from the MARCH code has been written, use the algorithm just described to select an appropriate number of them and use them for input.

The source rates of the various radionculides that enter the containment through the breach or release point in the reactor primary system have for most accidents been assumed to be equal to the release rate from the fuel with no allowance made for primary system deposition. Recent calculations performed using the TRAP code have indicated, however, that the assumption of negligible primary system deposition is not always justified,

particularly for the less volatile radionuclides [4]. It therefore becomes important that, in future calculations, the source term reflect radionuclide depletion during transport through the reactor primary system. The MATADOR II code has been written such that it can directly accept source terms calcualted by such codes as TRAP.

The output of the MATADOR II code consists of environmental radionuclide release fractions for each of the radionuclide groups. These releases can then be used in a radiological consequence code such as CRAC to calculate the health effects of reactor accidents. CRAC, in its present version, performs atmospheric diffusion calculations using burst releases, whereas MATADOR II, predicts radionuclide releases to the environemnt over several hours. Different approaches to modify these output data into a form suitable for input to CRAC will have to be evaluated before an interface with the health effects code can be constructed. A better approach would be to suitably modify CRAC to treat continuous releases of radioactivity to the environment since burst releases would not be expected to occur in all possible accidents.

2.3 DESCRIPTION OF INPUT TO MATADOR II CODE

A list of input cards for MATADOR II is schematically given below. The listed parameters are described in detail. Additionally, any special clarifying comments or cautions are also included. Note that all input is unformatted. That requires that at least one blank (space) be placed between each number entered is input.

1. IESF — Parameter which specifies if any engineered safety features are operational, IESF = 1. If IESF = 0 the code assumes no ESF's.

2. IKI2 — specie number for molecular iodine. If IKI2 is a negative number, thermal-hydraulic data input will be read from the MARCH 2.0 generated tape, TAPE7, and processed through subroutine MARTHA.

3. CUTOFF — the fraction CI2/COI2, where CI2 is the molecular iodine concentration in state ISI2M at the current accident time, and COI2 is the molecular iodine concentration that would have existed in the same state if there were no iodine depletion from the containment atmosphere. CUTOFF is usually equal to 0.01. For CI2/COI2 values below CUTOFF, equilibrium conditions prevail between the iodine in gaseous state and iodine in liquid water.

4. IEQLV — number of data pairs in TI2EL array on the following card

5. TI2EL(I,1) — time (sec)

6. TI2EL(I,2) — molecular iodine equilibrium at the time given by TI2EL(I,1)

$$\lambda = \frac{1}{H}\frac{dH}{dt}$$

Appendix VII of reference 1. Time is measured from the instant the molecular iodine equilibrium conditions are established in the containment.

NOTE: Parameters in 7 through 19 should be entered <u>only</u> if IESF = 0.

7. NFLTV — number of vapor filters employed

8. NFLTP — number of particle filters employed

9. ISPOOL =1 — there is a pressure suppression pool to be considered

   =0 — there is no suppression pool

10. ICE =1 — there is an ice condenser to be considered

    =0 — there is no ice condenser

11. ICRACK =1 — there is a containment crack to be considered

    =0 — there is no crack in containment

12. IBWRA =1 there is a BWR annulus to be considered

=0 there is no BWR annulus.

The total number of processes to be considered is IHOC = NFLTV + NFLTP + ISPOOL + ICE + ICRACK + IBWRA

13. ISOR(IH) the source volume number for the DF transfer IH

14. IREC(IH) the receiver volume number for the DF transfer IH

Repeat 13 and 14 for IHOC times. The DF processes are ordered in the manner shown in the parameter list of 7 through 12, i.e., first give the data for the vapor filters, next the particle filters, next suppression pool, etc.

15. NDF the number of table entries for the DF processes

16. (TFLW(IH,J), = 1, NDF) time entries for the flow rates of the DF transfer IH (sec)

17. (FRATE(IH,J), J = 1, NDF) volumetric flow rates (cm^3/sec) for the DF transfer IH at times given by TFLW(IH,J)

Repeat 16 and 17 together IHOC times

18.	(TDF(IK, IH, J),J=1,NDF) NDF)	time entries for the decontamination factor table for the chemical species IK for the adhoc process IH (sec)
19.	(DF(IK, IH, JP, J), J=1, NDF)	the decontamination factors at the times given on 18 for the DF process IH and the chemical specie NK.

For processes that decontaminate vapors only, input 19 once.
For processess that decontaminate particles only, input Card 19, 20 times (20 particle classes allowed). For processes that decontaminate both vapors and particles, input Card 19, 21 times, the first one of which is for vapor and the next 20 are for particles. For particles, start from the smallest particle size and go to the largest.

For a given chemical specie NK repeat procedures of Cards 18 and 19 IHOC times.

Then repeat the above procedure (Cards 18 and 19) for each chemical specie, i.e., NK times.

20.	P	the equilibrium Henry's Law constant for iodine
21.	SDD	the diameter of spray droplets (cm)

22. ADIAMI — Inside diameter for a BWR annulus (ft)

23. ADIAMO — outside diameter for a BWR annulus (ft)

Skip 22 and 23 if the analysis is not for a BWR (i.e., if IBWRA = 0)

24. TITLE — Title, less than 80 characters in length.

25. CPMAX — Central processor time (seconds) allowed for the problem before dumping for restart.

26. DIV — Divides the time interval over which the code is to run into DIV equal subintervals. OUTPUT is called at the end of each subinterval.

27. KOMAD — If KOMAD = 1, comments are printed from ADHOC that give information on total evaporation of a nuclide species from either particles or walls.

28. NRES — If NRES = 1, MATADOR II restarts from a previously interrupted run using initial values previously stored on the NTAP file; only this and the previous card are read in.

29.	T, TMAX, DELTM	T is the initial time of problem start, sec. TMAX is the time in seconds over which the calculation is to run. DELTM is the time step to be taken per iteration. Its value is discussed in the description of TSPEP.
30.	REL, ET41, ETA2	REL is the convergence criterion for the series expansion of the solution of Equation (9). It gives the upper bound to the ratio of the relative magnitude of the last included term to the partial sum up to that term. ETA1 and ETA2 are used in conjunction with timestep calculations.
31.	NK, NV, NS, NDP	NK, (<10), is the number of species to be considered. NV, (<10), is the number of control volumes considered. NS is the number of states. This number must be 5 unless minor modifications in BETV are undertaken. NDP is the number of particle parameters considered. This value must be 2 at present.

32. SN(I) — Are read in one card 10(A8) format. Each SN is the character name of a species (A format). Must be read in the following order: I_2, CsI, CsOH, Aer,Te.

33. NCC — Contains the flow connections of the control volumes. The first digit contains all flow connections to the first volume. If flow occurs to the first volume from the second volume, a 1 must appear as the second digit, and so on.

34. NBET — Gives the number of control flags in BETV. There are at present three of these.

35. NB — Contains the control flags of BETV for each volume. Each digit represents the control for the volume whose number corresponds to the sequence number in the input stream. The first digit must be 0 if I_2 adsorption is to be inhibited in that volume. The second digit must be 0 if particle deposition is to be inhibited in that volume. The third digit allows particle settling either against flow, digit set equal to 0, or across the flow, digit set equal to 1.

36.	NHOC	Gives the number of control flags in ADHOC. There is only one of these at present.
37.	ND	Coded control digits for ADHOC. The organization is identical to that of NB. If ND = 0 no condensation is allowed in the corresponding volume.
38.	NOCOG	The n^{th} digit corresponds to the n^{th} volume. If coagulation is to be suppressed in this volume this digit is set equal to 0.
39.	VPM	Arbitrary multiplier of all vapor pressure terms. Can be used to measure code sensitivity to uncertainties in vapor pressure correlations.
40.	FRM	Arbitrary multiplier of the steam mass flow rates in all volumes. Can be used to measure code sensitivity to changes in flow rate.
41.	STM	Arbitrary multiplier of surface temperature in all volumes. Can be used to measure code sensitivity to uncertainties in surface temperatures.

42.	SRM	Arbitrary multiplier of the I_2 adsorption velocity. Can be used to gauge code sensitivity to uncertainty in this parameter.
43.	THDM	Arbitrary multiplier of the thermophoretic deposition velocity. Can be used to measure code sensitivity to uncertainty in that expression.
44.	TDM	Arbitrary multiplier of the deposition velocity due to particle deposition from turbulent flow. Can be used to gauge code sensitivity to uncertainty in this velocity.
45.	VTM	Arbitrary multiplier of the vapor mass transfer coefficients used in ADHOC. Can be used to gauge code sensitivity to uncertainty in these.
46.	NTCOAG	If not equal to 1, turbulent coagulation is ignored in all volumes.
47.	LENGTH, DIAME, AREA, ASED, HEIGHT	The five geometric parameters are read in English units, (per control volume). LENGTH is the length, DIAME the equivalent of diameter, AREA the crossflow area, ASED the

surface area available to sedimentation of aerosol particles, HEIGHT the vertical length of the control volume.

Parameters 48 through 50 are not read in if IKI2 is negative.

48. NTST — Number of entries in the time flow data table for the junction flow of a given junction.

TF — Time data (in seconds) corresponding to the flow data. These are listed chronologically with up to 20 entries.

F — Steam mass flow rate (lb/sec) corresponding to the time data above. Again, up to 20 entries may be used.

NOTE: Junctions must be entered in a specific way. Their data are entered in 48 above in this numbered sequence. The numbering scheme is as follows. Look at Volume 1 first. Next scan all volumes in their numbered sequence.

Assign the junction number 1 to the junction between volume 1 and the first volume encountered that has flow to volume 1, and so on.

49.	NTST	Number of entries in the time-pressure data table.
	TF	Time data (in seconds) corresponding to the pressure data.
	F	Steam pressure (psia) data.
		NOTE: This set of cards is repeated for each volume, in sequence.
50.	NTST	Number of entries in the time-wall surface temperature data table.
	TF	Time data (seconds) corresponding to the temperature data.
	T	Wall surface temperature (F) data.
		NOTE: This set of cards is repeated for each volume, in sequence.
51.	NOCO	If the n^{th} digit from the left is 1, specie n has initial masses present.

52. CO — Is filled by the initial masses in all states, in the sequence: volume 1, steam-molecule; steam-particle; wall-molecule, wall particles; volume 2, etc. If NOCO indicates that the given nuclide specie has no masses present in the system initially, these cards are skipped.

NOTE: This set of cards is repeated for each specie that has masses in the system initially.

53. NOSOV — If the n^{th} digit is 1, source data exists for the state n.

NOSOS — If the n^{th} digit is 1, source data exists for the state n.

NTST — Number of entries in the source rate-time data table.

SET — Time data (seconds) corresponding to the source rate data.

	SE	Source rate (g/sec) data.

NOTE: NTST, SET, SE are repeated for each state in each volume that has a source. The sequence in which they are read in is: states of the first volume first, starting with the first state. Then the second volume, and so on. Volumes and states that have no source are skipped.

All cards in item 53 are repeated for each specie considered.

55.	NOSPV	If the n^{th} digit is 1, the source rate of state steam- particle of volume n has the lognormal size distribution parameters σ_g and r_g read in.
	NTST	Number of entries in the $\sigma_g(r_g)$-time data table.
	PSET	Time data (seconds) corresponding to the $\sigma_g(r_g)$ data.
	PSE	$\sigma_g(r_g)$ data.

NOTE: NTST, PSET, PSE are read in first for σ_g, then for r_g. These two sets are repeated for each volume with a steam-particle source, in sequence.

57. PDEN — Gives the (uniform) particle density in each volume. By permitting change in density as a function of control volume, it is hoped that gross changes in particle constitution can be approximated.

REFERENCES

[1] "Reactor Safety Study, An Assessment of Accident Risks In U.S. Commercial Nuclear Power Plants", WASH-1400 (October, 1975).

[2] Hilliard, R. K., et al., "Removal of Iodine and Particles by Sprays In the Containment Systems Experiment", Nuclear Technology, 10, pp 499-519 (1971).

[3] Fuchs, N. A., "The Mechanics of Aerosols", The MacMillan Company, New York (1964).

[4] Baybutt, P., Gieseke, J. A., Jordan, H., and Raghuram, S., "An Assessment of LWR Primary System Radionuclide Retention In Meltdown Accidents Using the TRAP Computer Code", paper presented at the ANS/ENS Topical Meeting on Thermal Reactor Safety, Knoxville, Tennessee (April, 1980).

TABLE 2.1

EQUILIBRIUM DATA FOR I_2 WITH BORIC ACID SPRAYS [2]

time, min	H	C_g/C_{go}
0	2676	0.01
100	1.5×10^4	1.8×10^{-3}
500	4.0×10^4	6.75×10^{-4}
1000	7.0×10^4	3.86×10^{-4}
2000	1.5×10^{-5}	1.8×10^{-4}
4000	5×10^{-5}	5.4×10^{-5}
> 7000	1×10^6	2.7×10^{-5}

TABLE 2.2

EQUILIBRIUM DATA FOR I_2 WITH CAUSTIC SPRAYS [2]

time, min	H	C_g/C_{go}
0-100	Constant H, = 0	0.01
100-1000	Variable H, = .095 hr^{-1}	
1000	7.0×10^4	3.86×10^{-4}
2000	1.5×10^5	1.8×10^{-4}
4000	5×10^5	5.4×10^{-5}
7000	1×10^6	2.7×10^{-5}

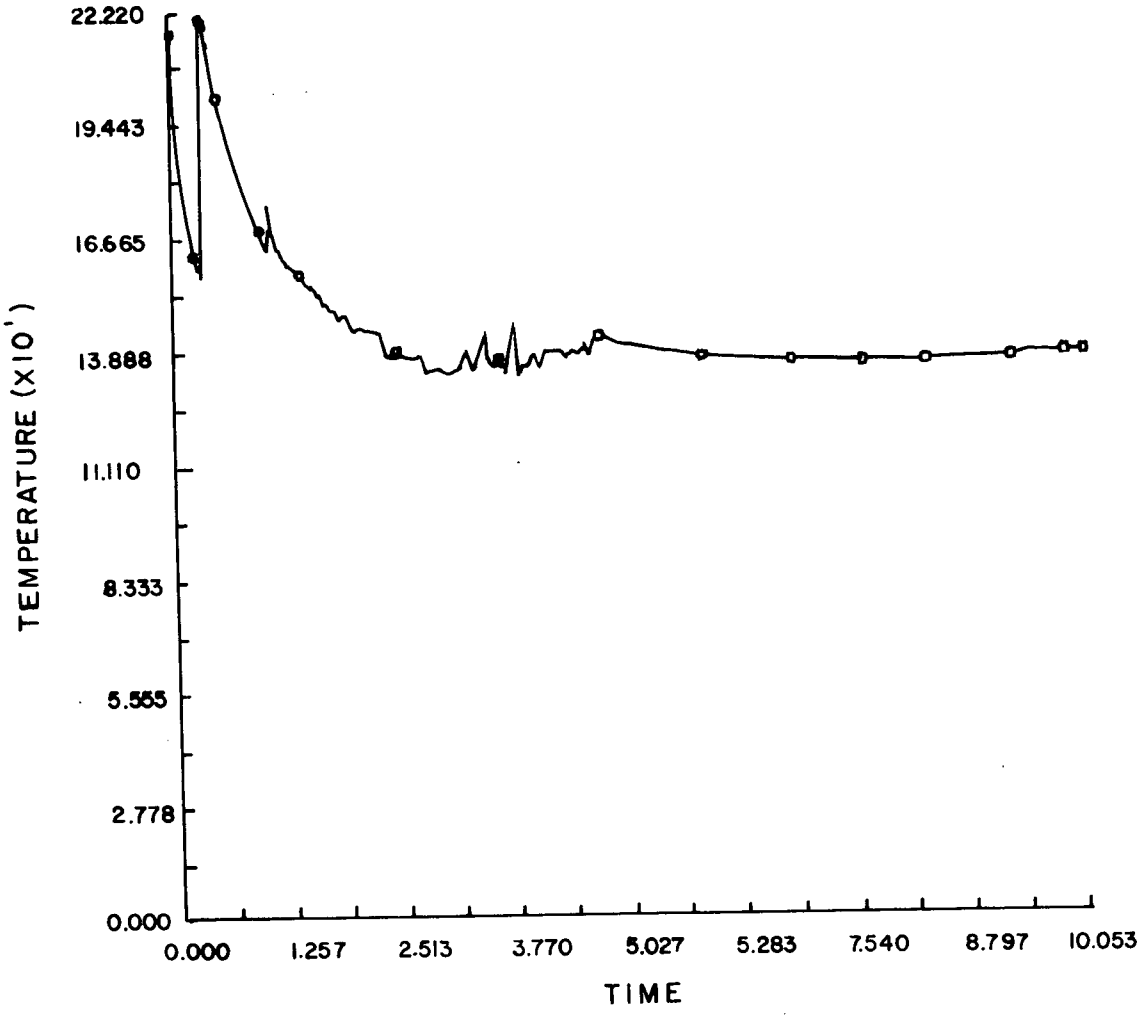

FIGURE 2.1 EXAMPLE OF FITTING MARCH CODE OUTPUT

APPENDIX D

Individual plots of multi-plot Figures in Section 5

Section 5.1 Figures

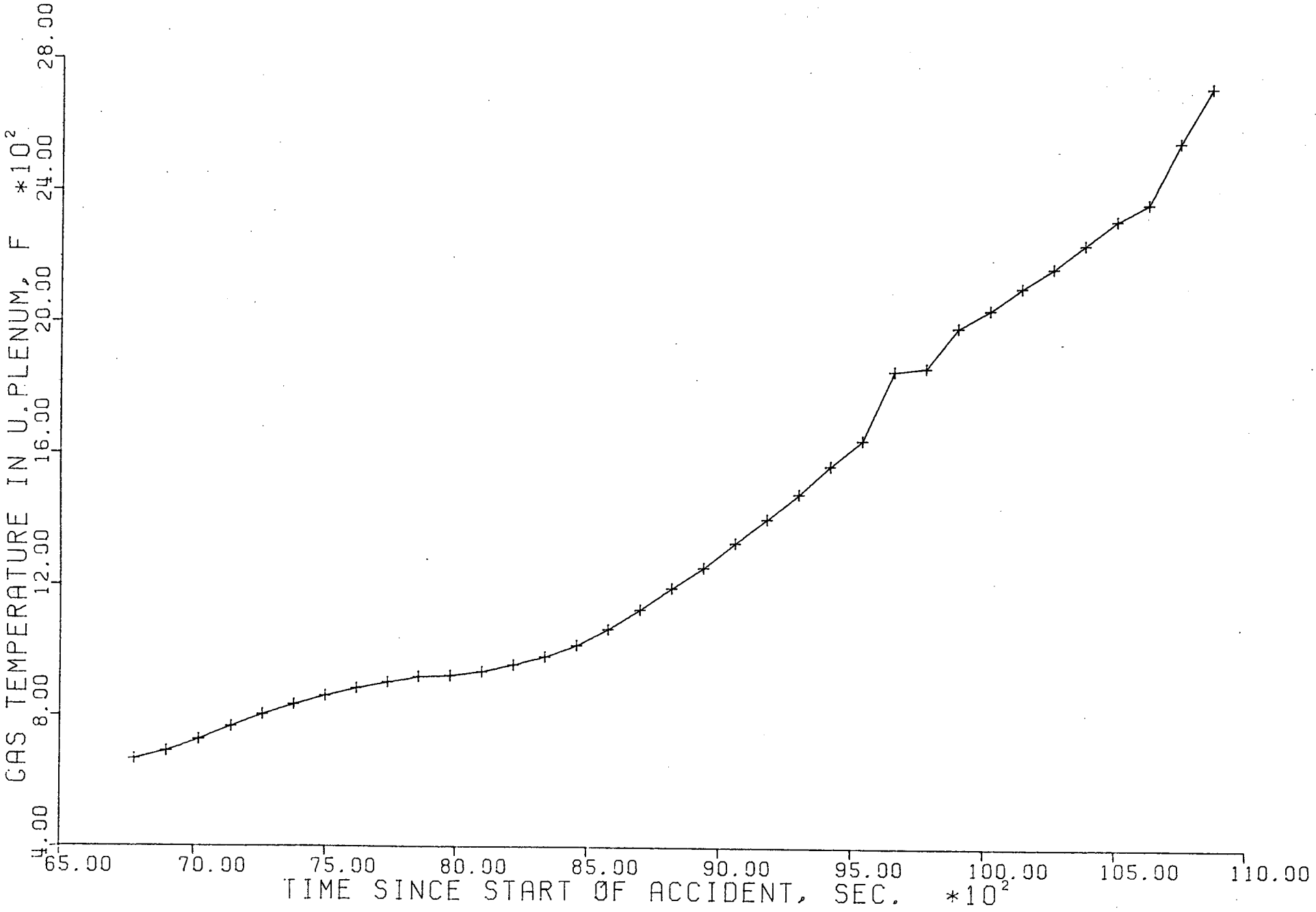
GAS TEMPERATURE IN U.PLENUM, F *10²
4.00
8.00
12.00
16.00
20.00
24.00
28.00
65.00
70.00
75.00
80.00
85.00
90.00
95.00
100.00
105.00
110.00
TIME SINCE START OF ACCIDENT, SEC. *10²

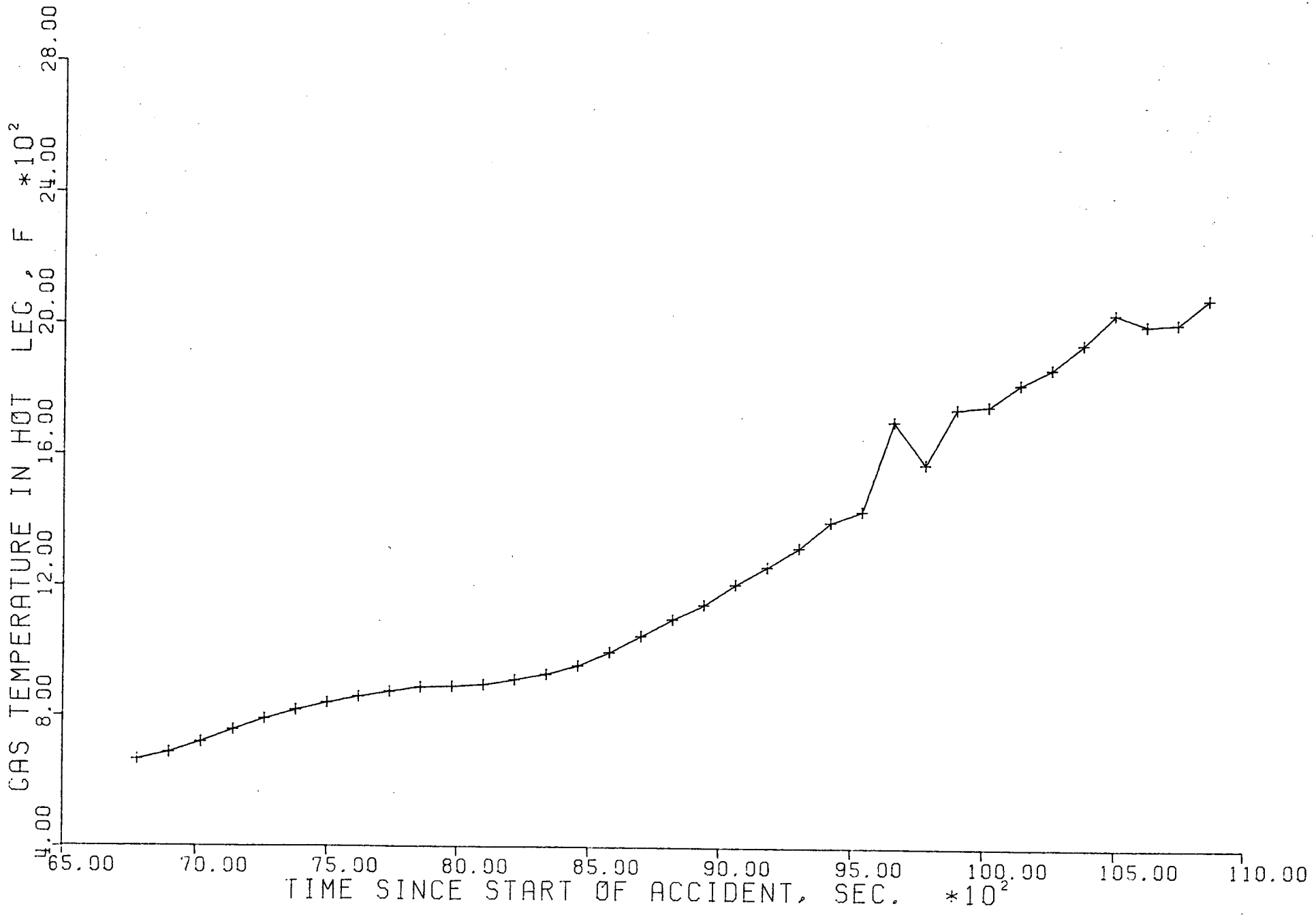
GAS TEMPERATURE IN HOT LEG, F *10²
4.00
8.00
12.00
16.00
20.00
24.00
28.00
65.00
70.00
75.00
80.00
85.00
90.00
95.00
100.00
105.00
110.00
TIME SINCE START OF ACCIDENT, SEC. *10²

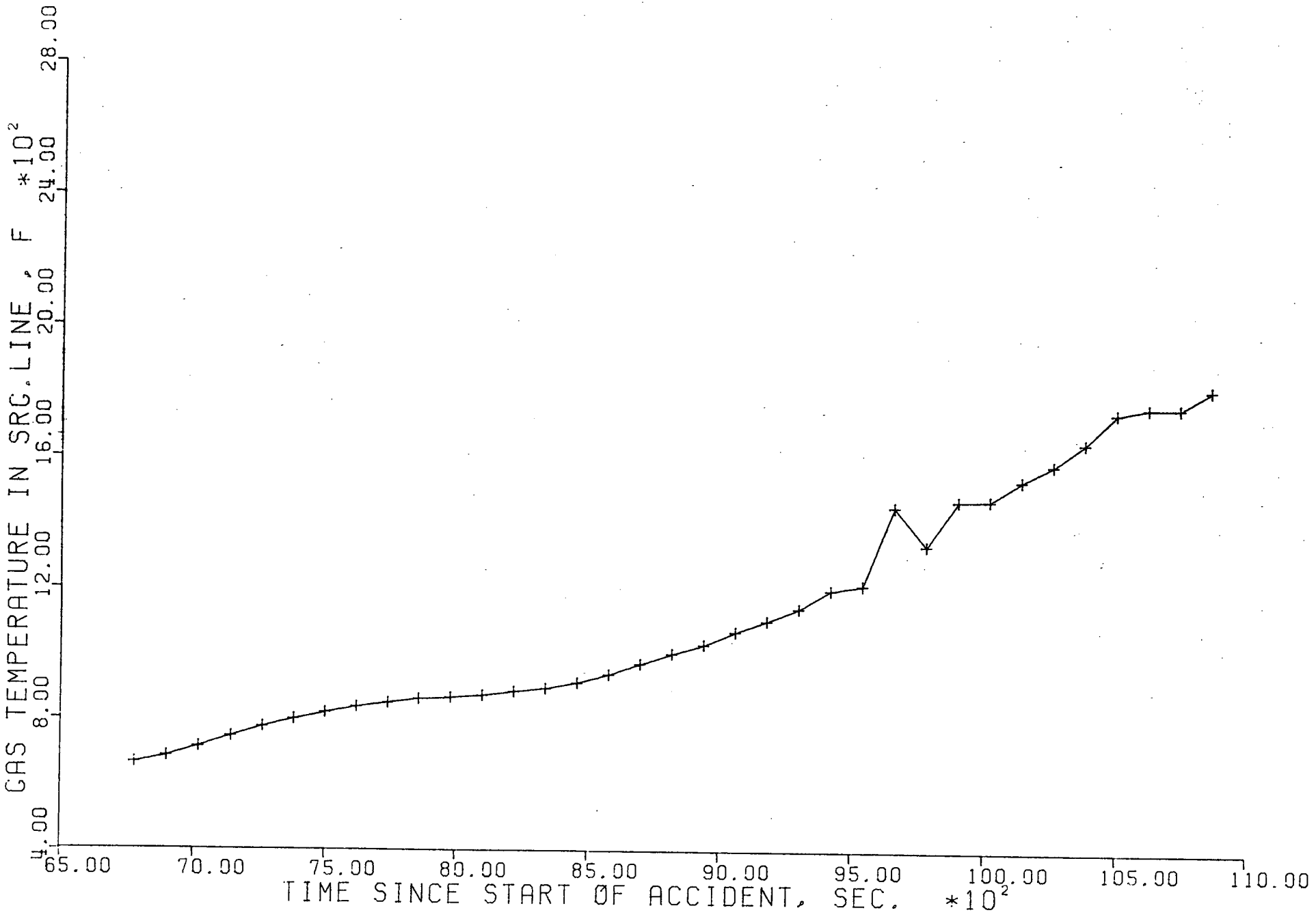
GAS TEMPERATURE IN SRC. LINE, F *10²
4.00
8.00
12.00
16.00
20.00
24.00
28.00
65.00
70.00
75.00
80.00
85.00
90.00
95.00
100.00
105.00
110.00
TIME SINCE START OF ACCIDENT, SEC. *10²

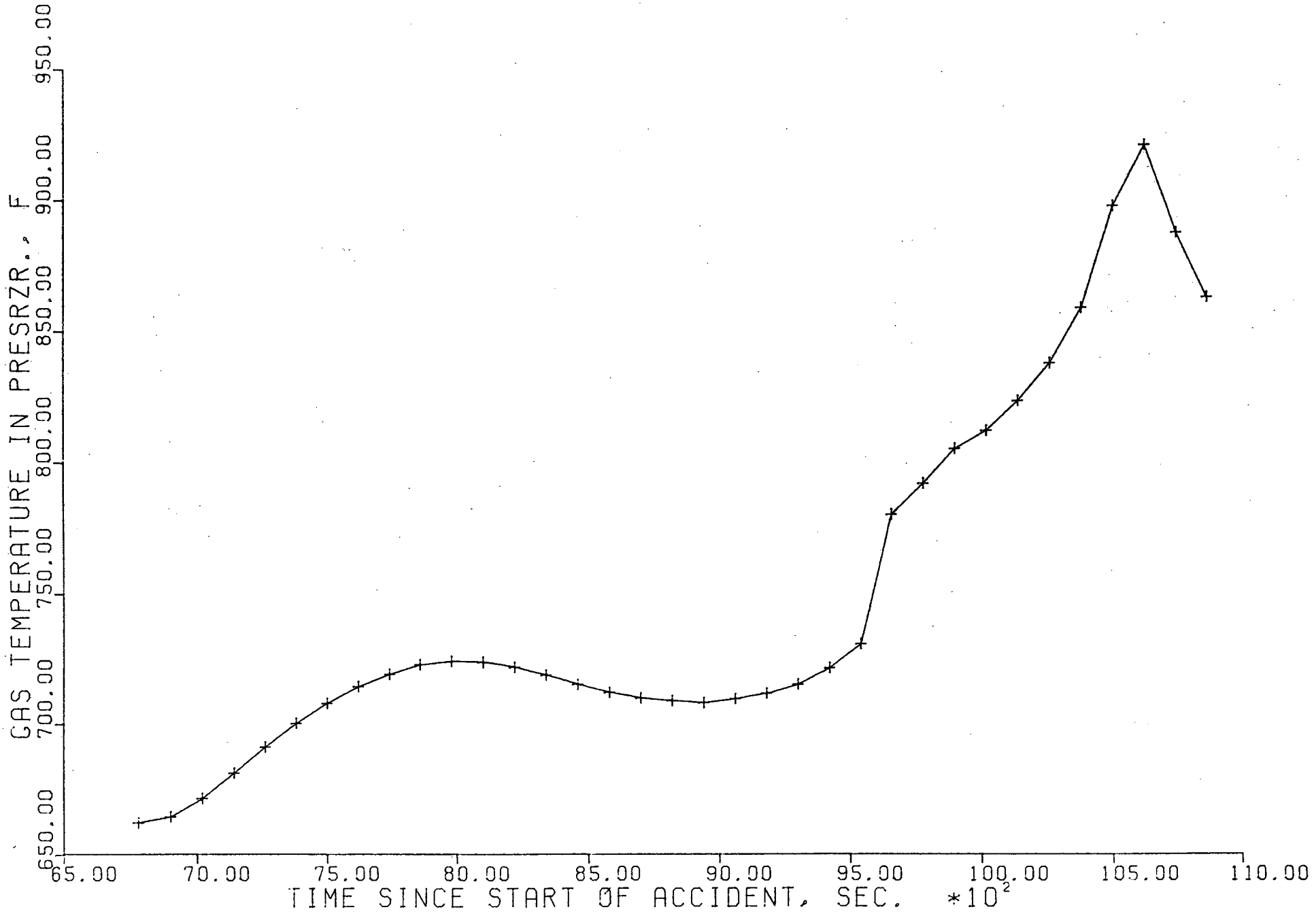
GAS TEMPERATURE IN PRESRZR., F
650.00
700.00
750.00
800.00
850.00
900.00
950.00
65.00
70.00
75.00
80.00
85.00
90.00
95.00
100.00
105.00
110.00
TIME SINCE START OF ACCIDENT, SEC. *10²

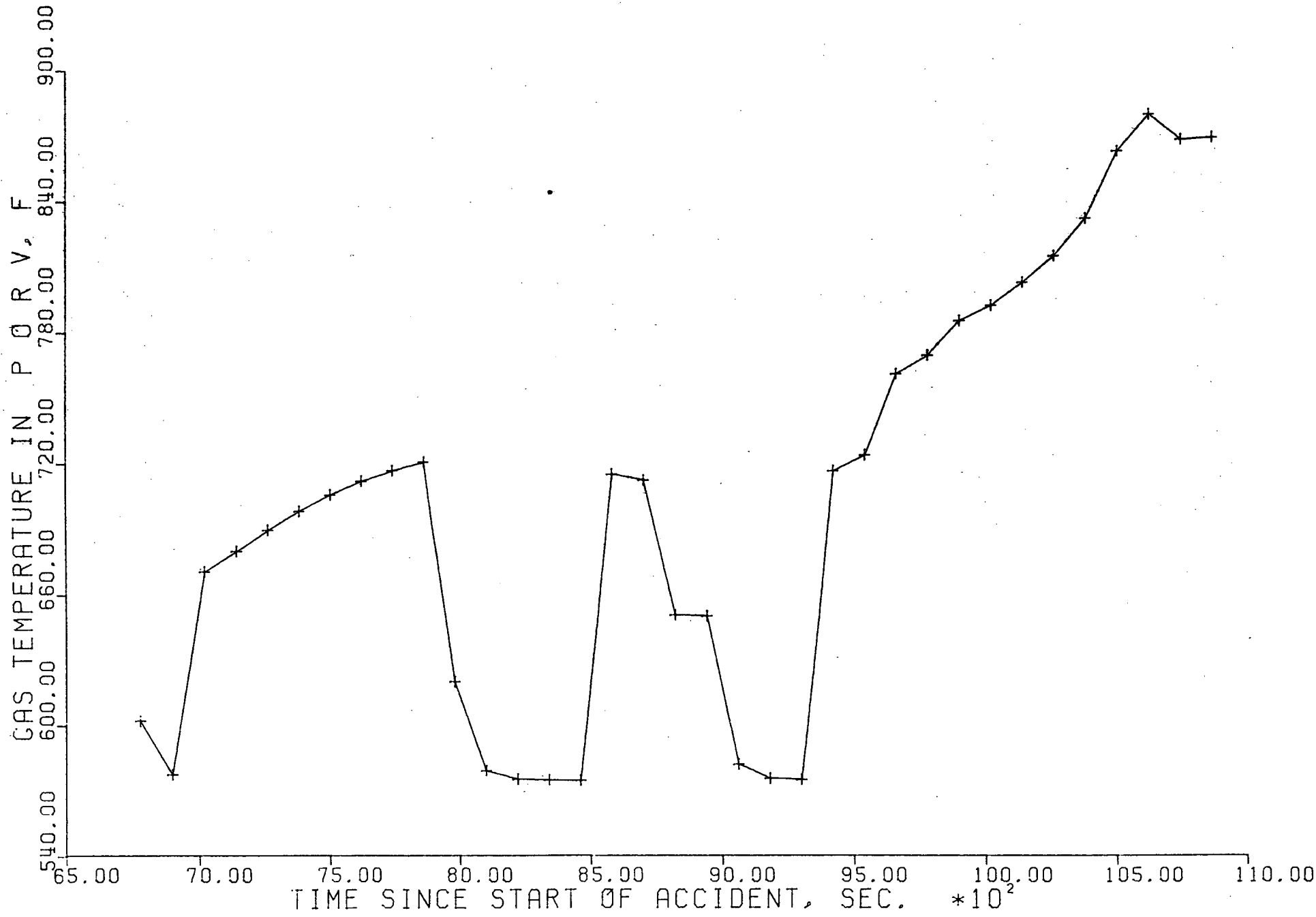
GAS TEMPERATURE IN P Ø R V, F
900.00
840.00
780.00
720.00
660.00
600.00
540.00
65.00
70.00
75.00
80.00
85.00
90.00
95.00
100.00
105.00
110.00
TIME SINCE START ØF ACCIDENT, SEC. *10²

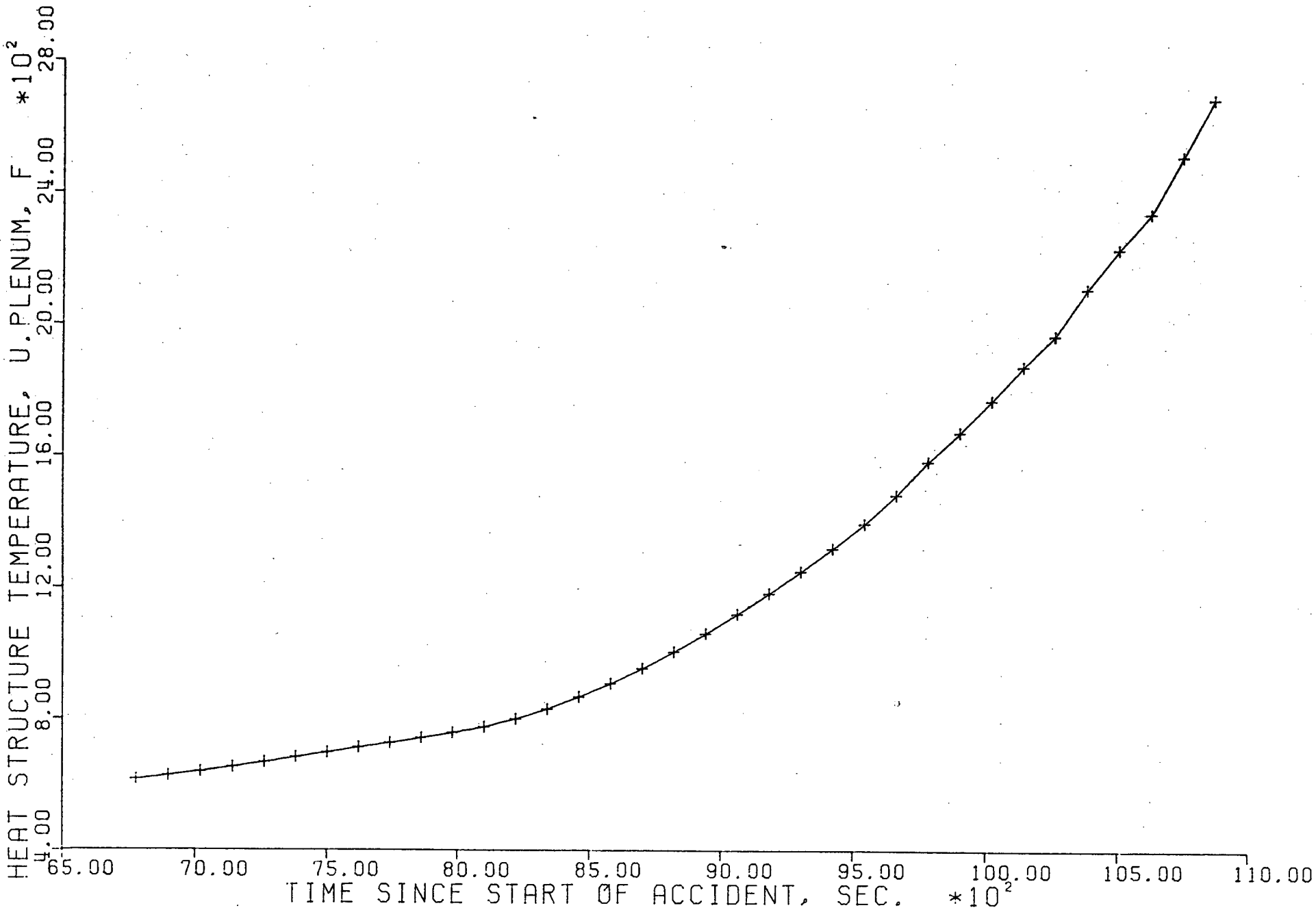
HEAT STRUCTURE TEMPERATURE, U.PLENUM, F *10²
4.00
8.00
12.00
16.00
20.00
24.00
28.00
65.00
70.00
75.00
80.00
85.00
90.00
95.00
100.00
105.00
110.00
TIME SINCE START OF ACCIDENT, SEC. *10²

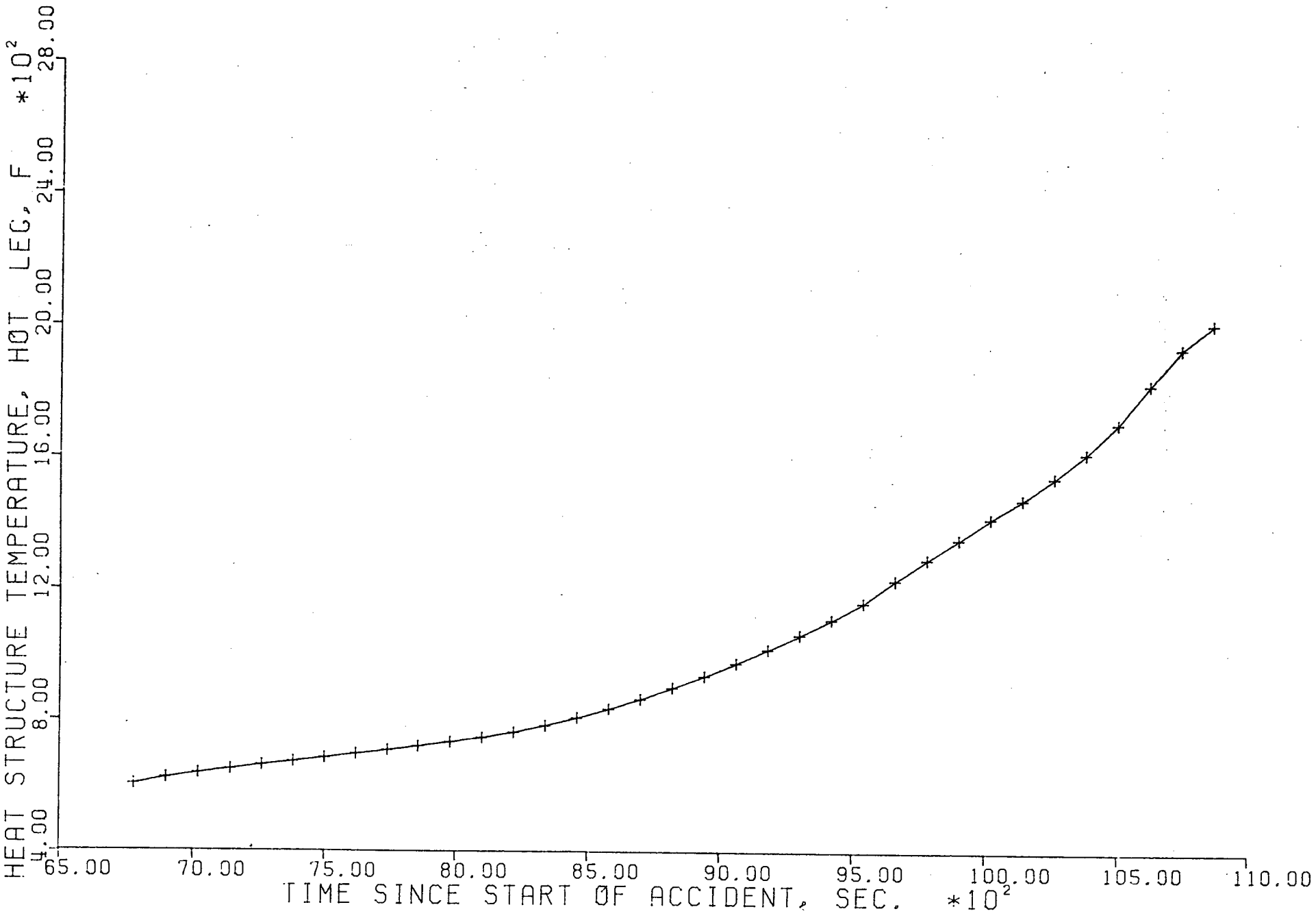
HEAT STRUCTURE TEMPERATURE, HOT LEG, F *10²
4.00
8.00
12.00
16.00
20.00
24.00
28.00
65.00
70.00
75.00
80.00
85.00
90.00
95.00
100.00
105.00
110.00
TIME SINCE START OF ACCIDENT, SEC. *10²

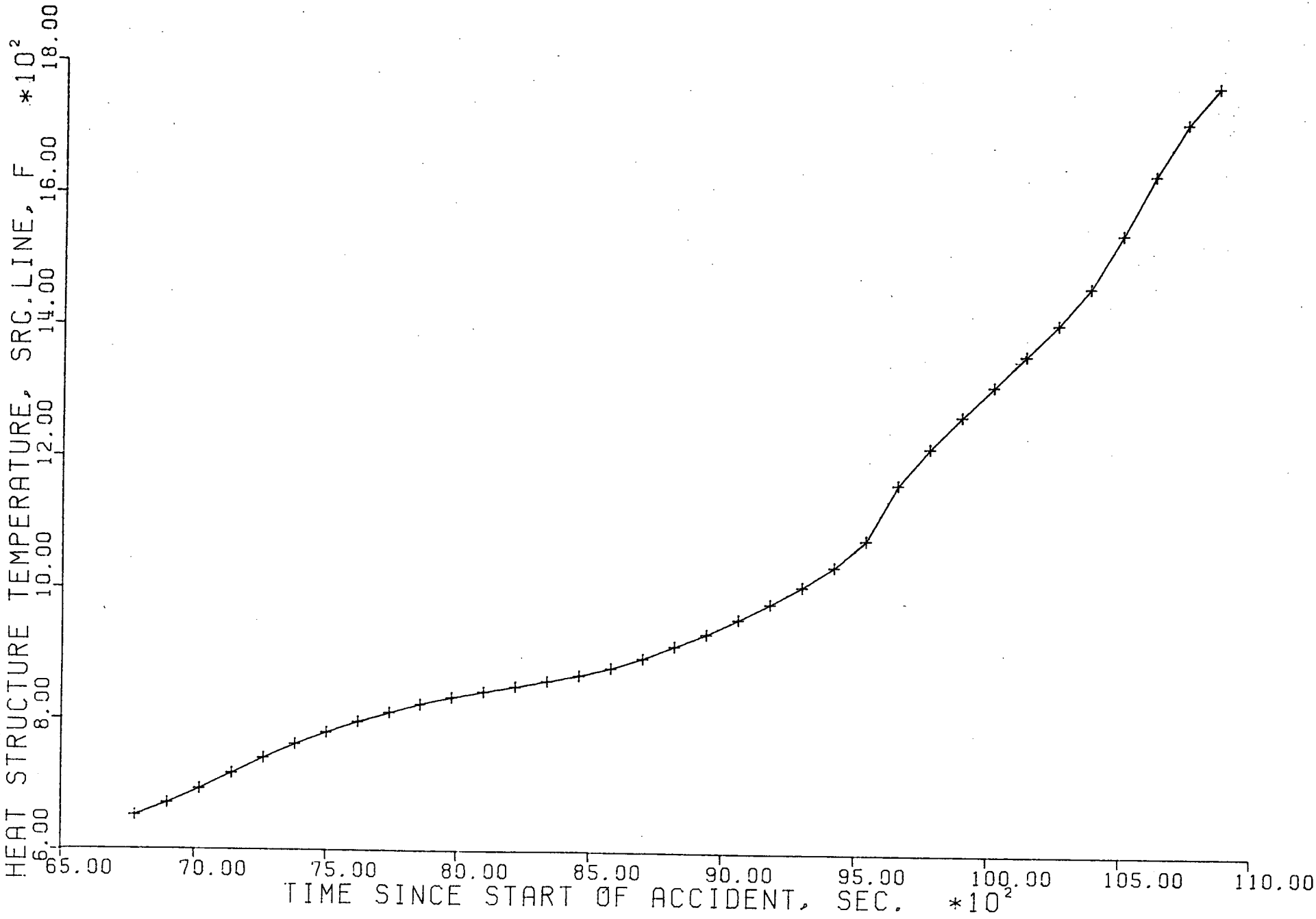
HEAT STRUCTURE TEMPERATURE, SRC.LINE, F *10²
6.00
8.00
10.00
12.00
14.00
16.00
18.00
65.00
70.00
75.00
80.00
85.00
90.00
95.00
100.00
105.00
110.00
TIME SINCE START OF ACCIDENT, SEC. *10²

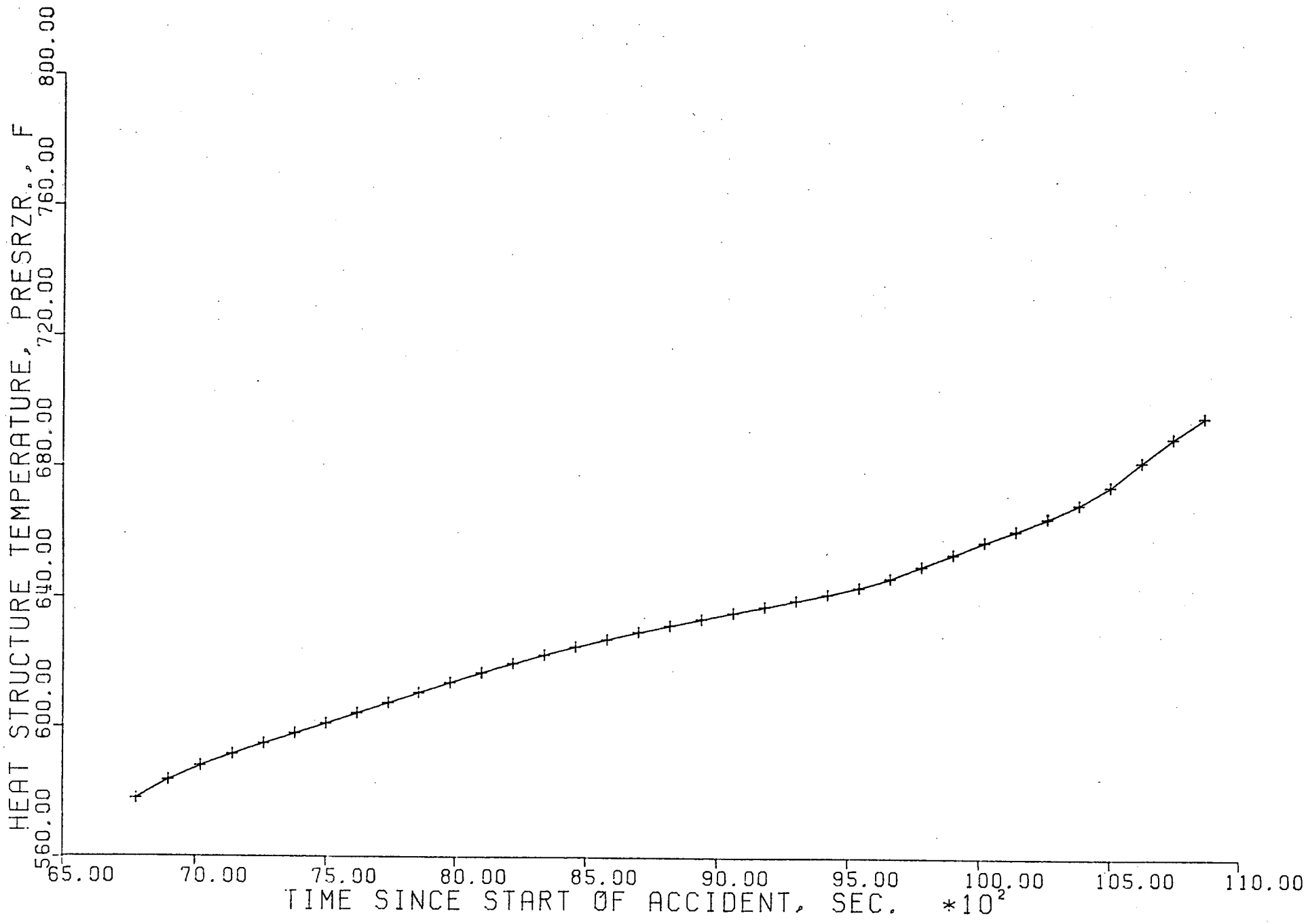
HEAT STRUCTURE TEMPERATURE, PRESRZR., F
800.00
760.00
720.00
680.00
640.00
600.00
560.00
65.00
70.00
75.00
80.00
85.00
90.00
95.00
100.00
105.00
110.00
TIME SINCE START OF ACCIDENT, SEC. *10²

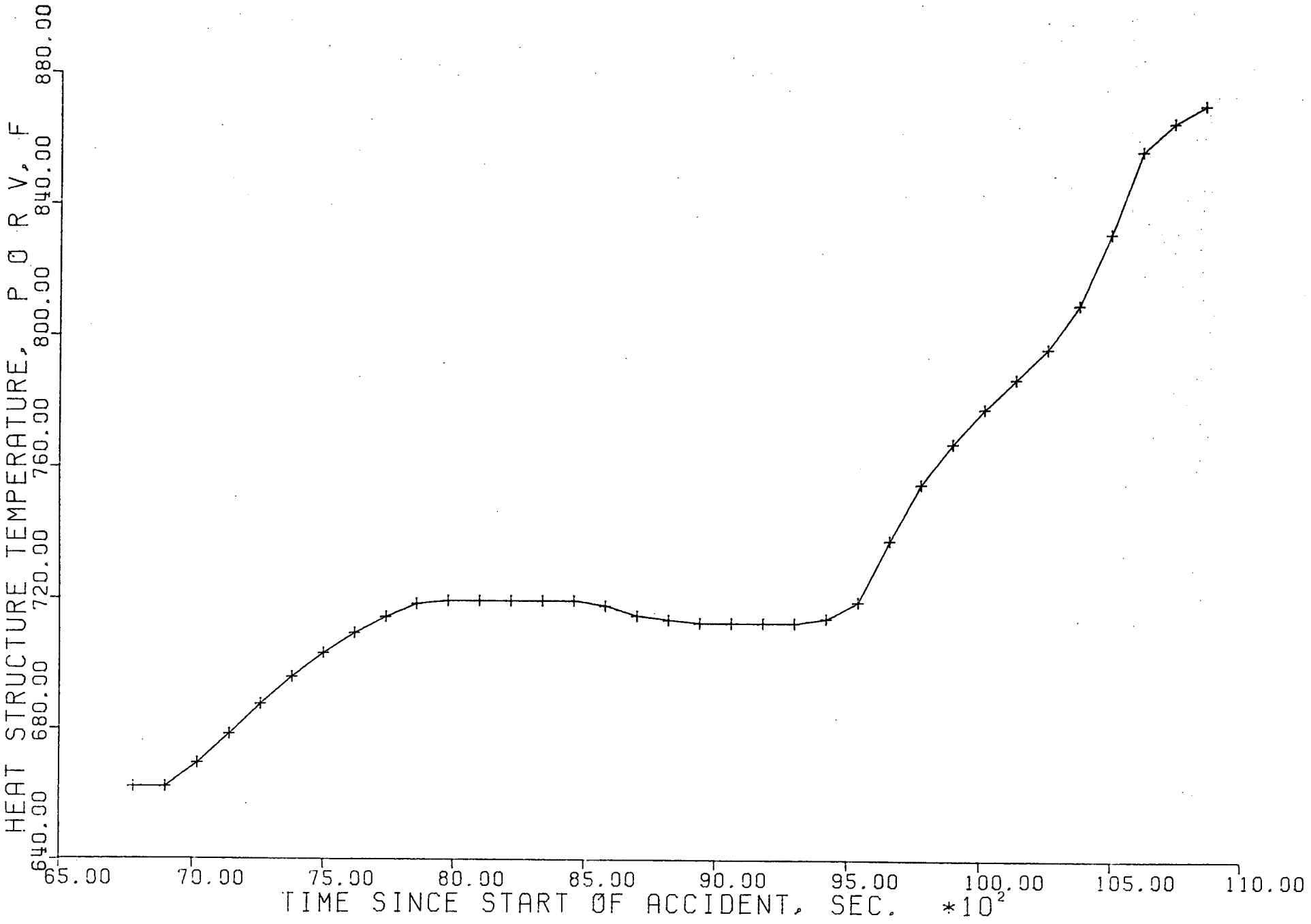
HEAT STRUCTURE TEMPERATURE, P Ø R V, F
640.00
680.00
720.00
760.00
800.00
840.00
880.00
65.00
70.00
75.00
80.00
85.00
90.00
95.00
100.00
105.00
110.00
TIME SINCE START ØF ACCIDENT, SEC. *10²

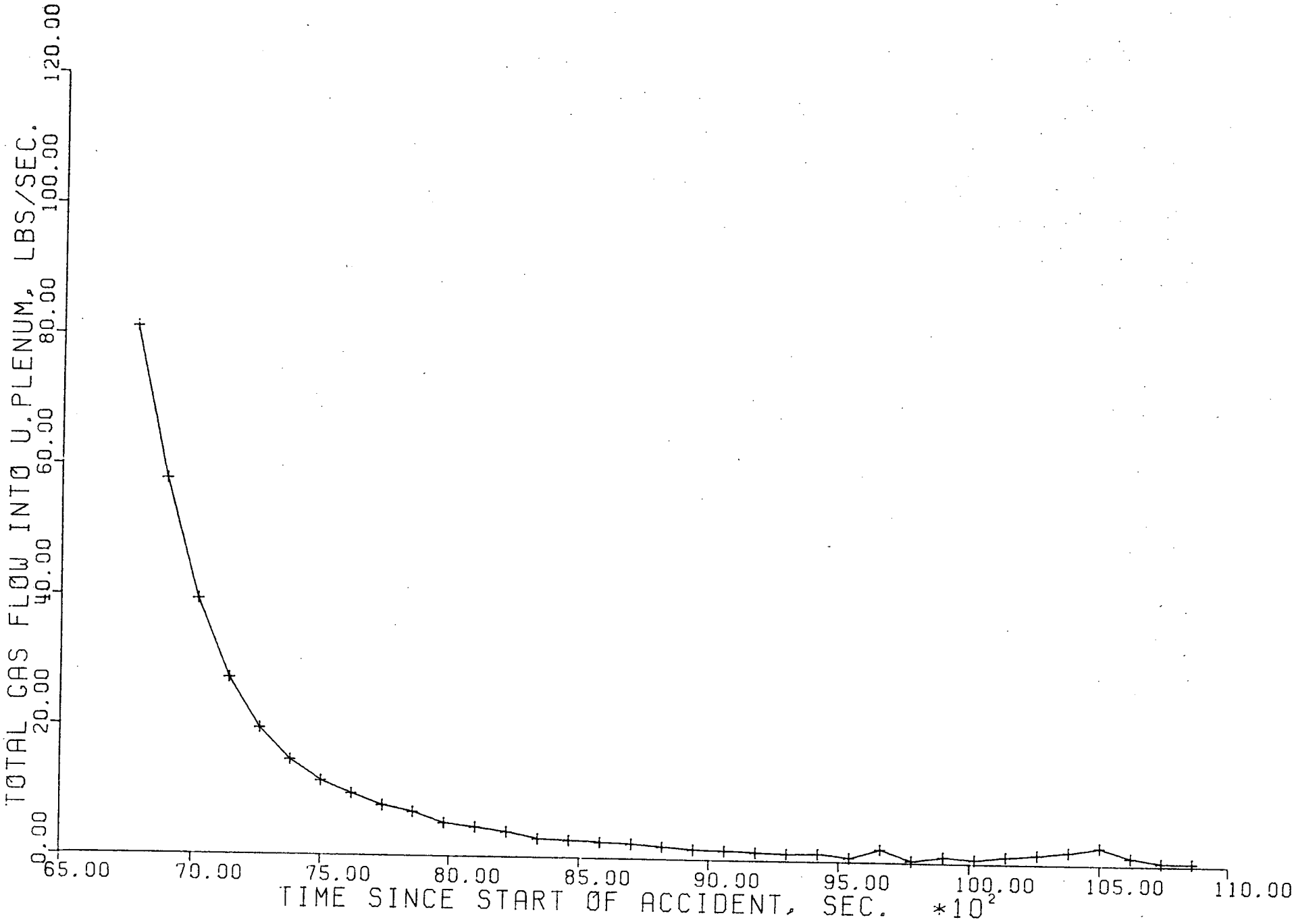
TOTAL GAS FLOW INTO U.PLENUM, LBS/SEC.
0.00
20.00
40.00
60.00
80.00
100.00
120.00
65.00
70.00
75.00
80.00
85.00
90.00
95.00
100.00
105.00
110.00
TIME SINCE START OF ACCIDENT, SEC. *10²

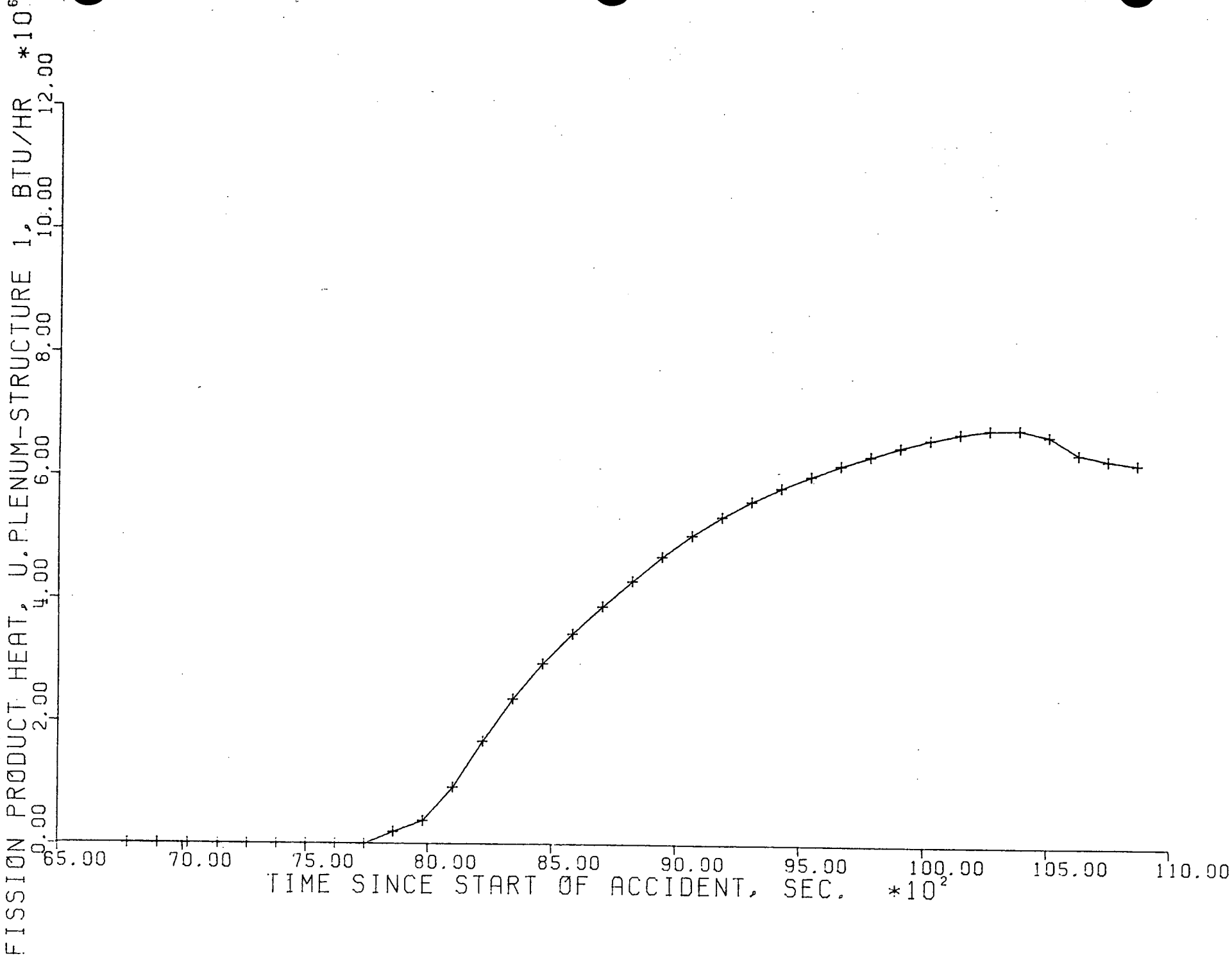
FISSION PRODUCT HEAT, U.PLENUM-STRUCTURE 1, BTU/HR *10^6
0.00
2.00
4.00
6.00
8.00
10.00
12.00
65.00
70.00
75.00
80.00
85.00
90.00
95.00
100.00
105.00
110.00
TIME SINCE START OF ACCIDENT, SEC. *10^2

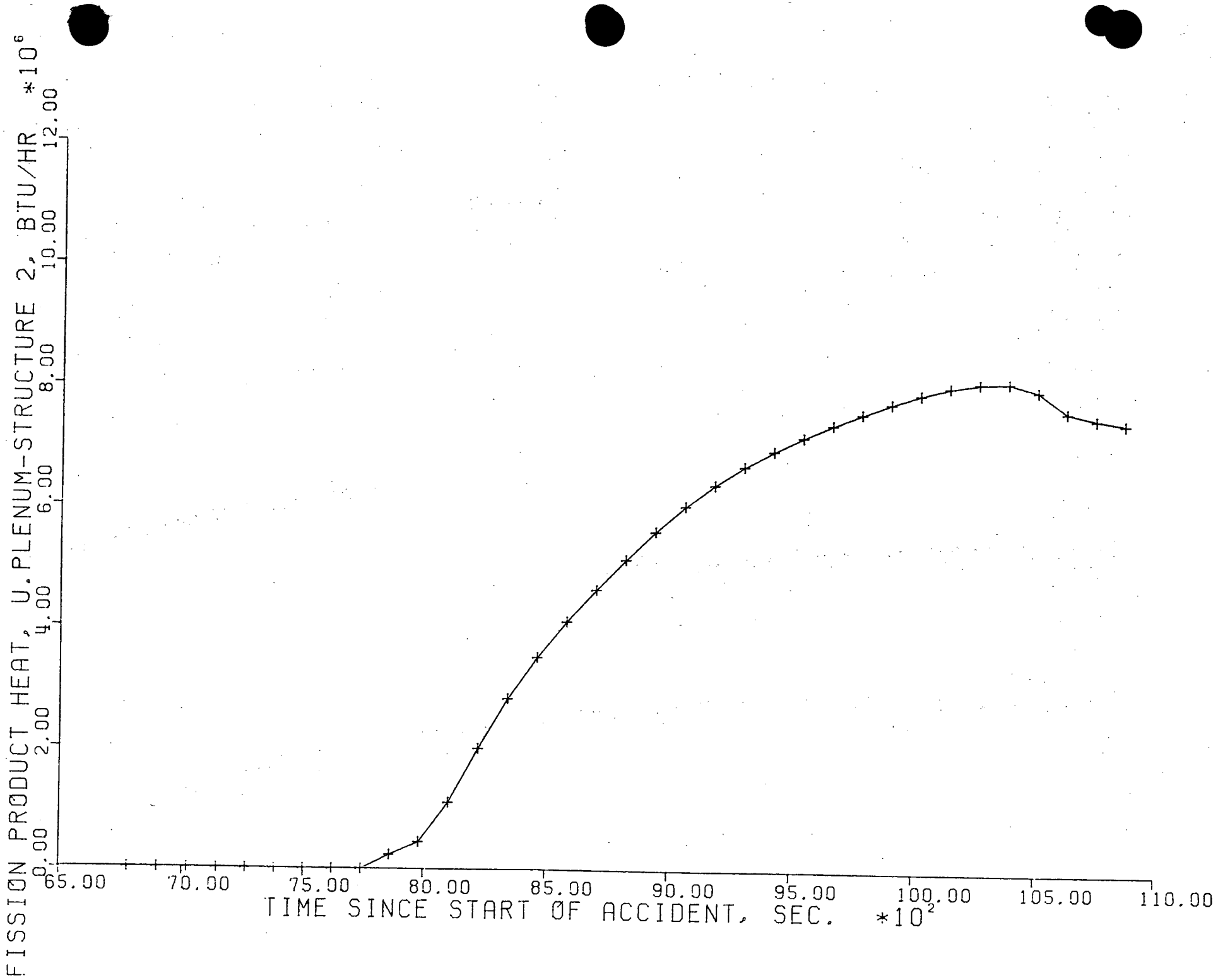
FISSION PRODUCT HEAT, U.PLENUM-STRUCTURE 2, BTU/HR *10^6
0.00
2.00
4.00
6.00
8.00
10.00
12.00
65.00
70.00
75.00
80.00
85.00
90.00
95.00
100.00
105.00
110.00
TIME SINCE START OF ACCIDENT, SEC. *10^2

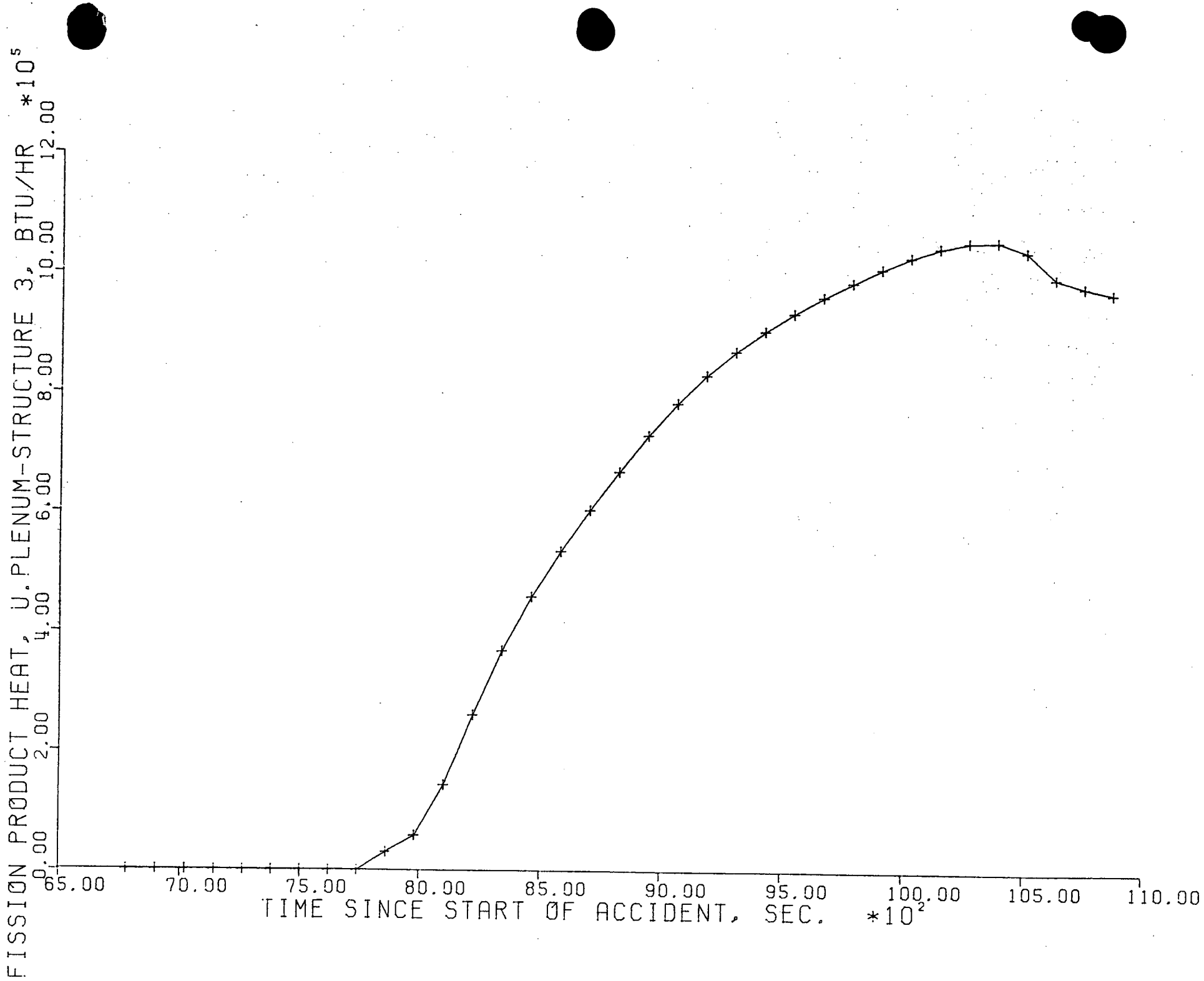
FISSION PRODUCT HEAT, U. PLENUM-STRUCTURE 3, BTU/HR *10^5
0.00
2.00
4.00
6.00
8.00
10.00
12.00
65.00
70.00
75.00
80.00
85.00
90.00
95.00
100.00
105.00
110.00
TIME SINCE START OF ACCIDENT, SEC. *10^2

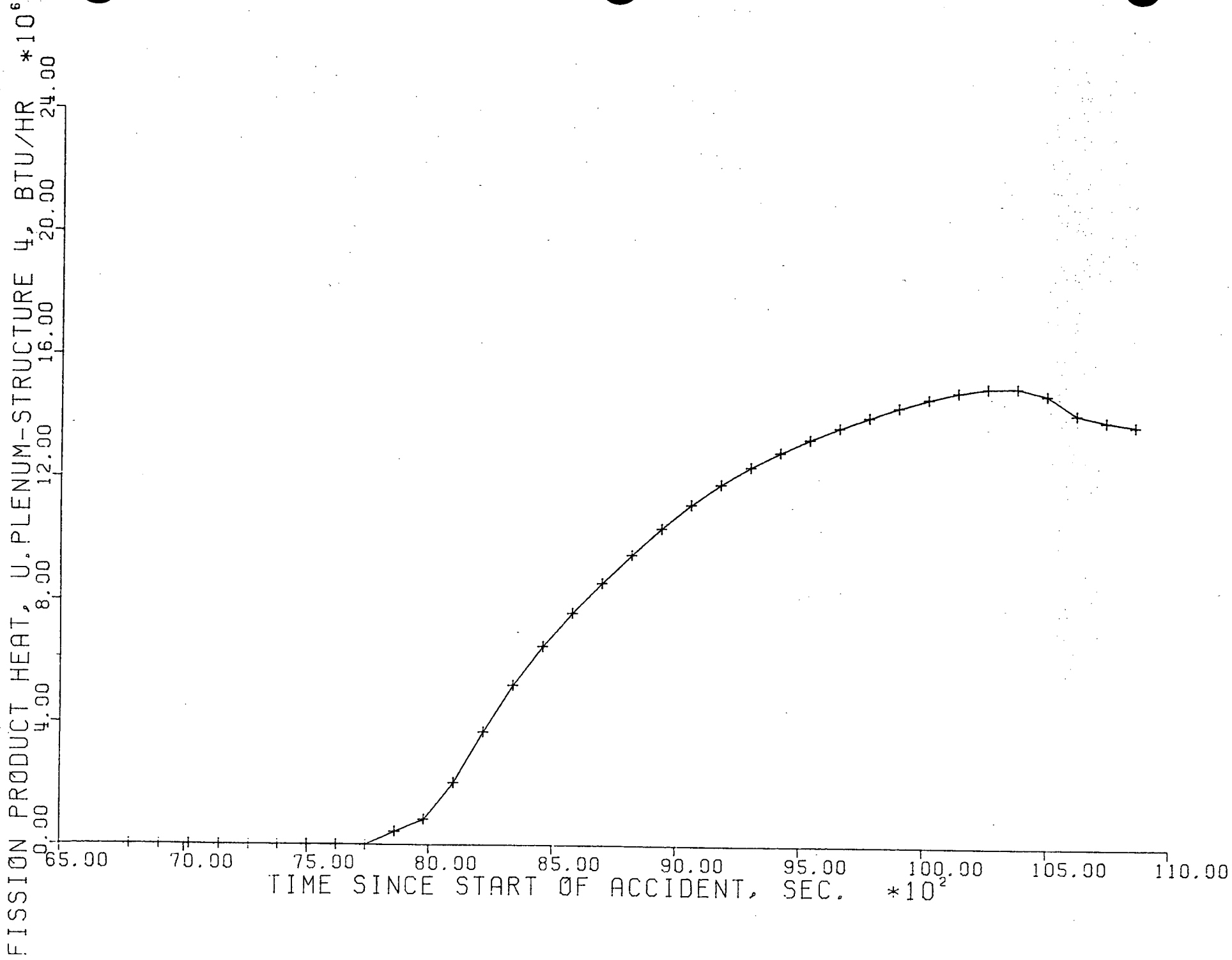
FISSION PRODUCT HEAT, U.PLENUM-STRUCTURE 4, BTU/HR *10^6
0.00
4.00
8.00
12.00
16.00
20.00
24.00
65.00
70.00
75.00
80.00
85.00
90.00
95.00
100.00
105.00
110.00
TIME SINCE START OF ACCIDENT, SEC. *10^2

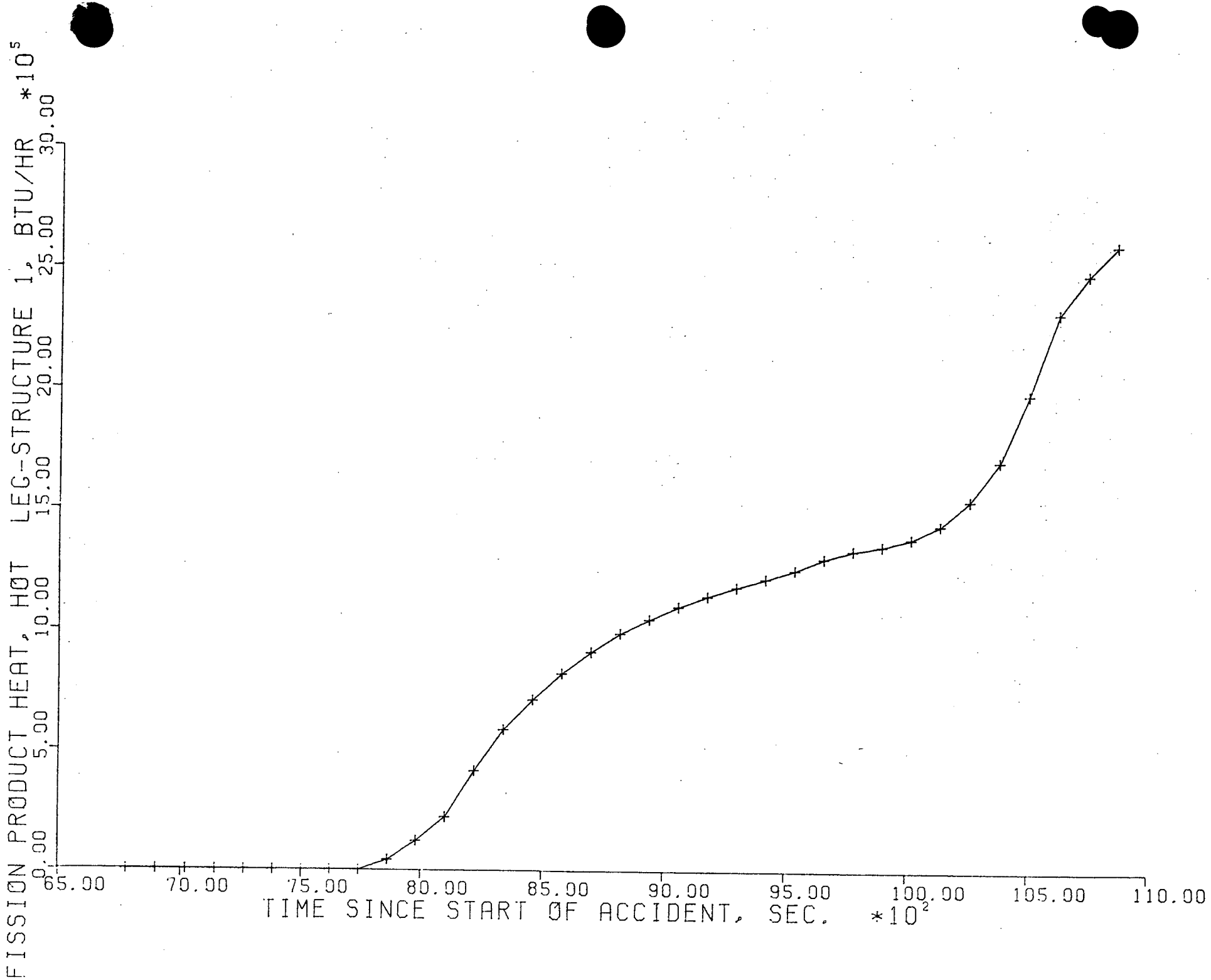
FISSION PRODUCT HEAT, HOT LEG-STRUCTURE 1, BTU/HR *10^5
0.00
5.00
10.00
15.00
20.00
25.00
30.00
65.00
70.00
75.00
80.00
85.00
90.00
95.00
100.00
105.00
110.00
TIME SINCE START OF ACCIDENT, SEC. *10^2

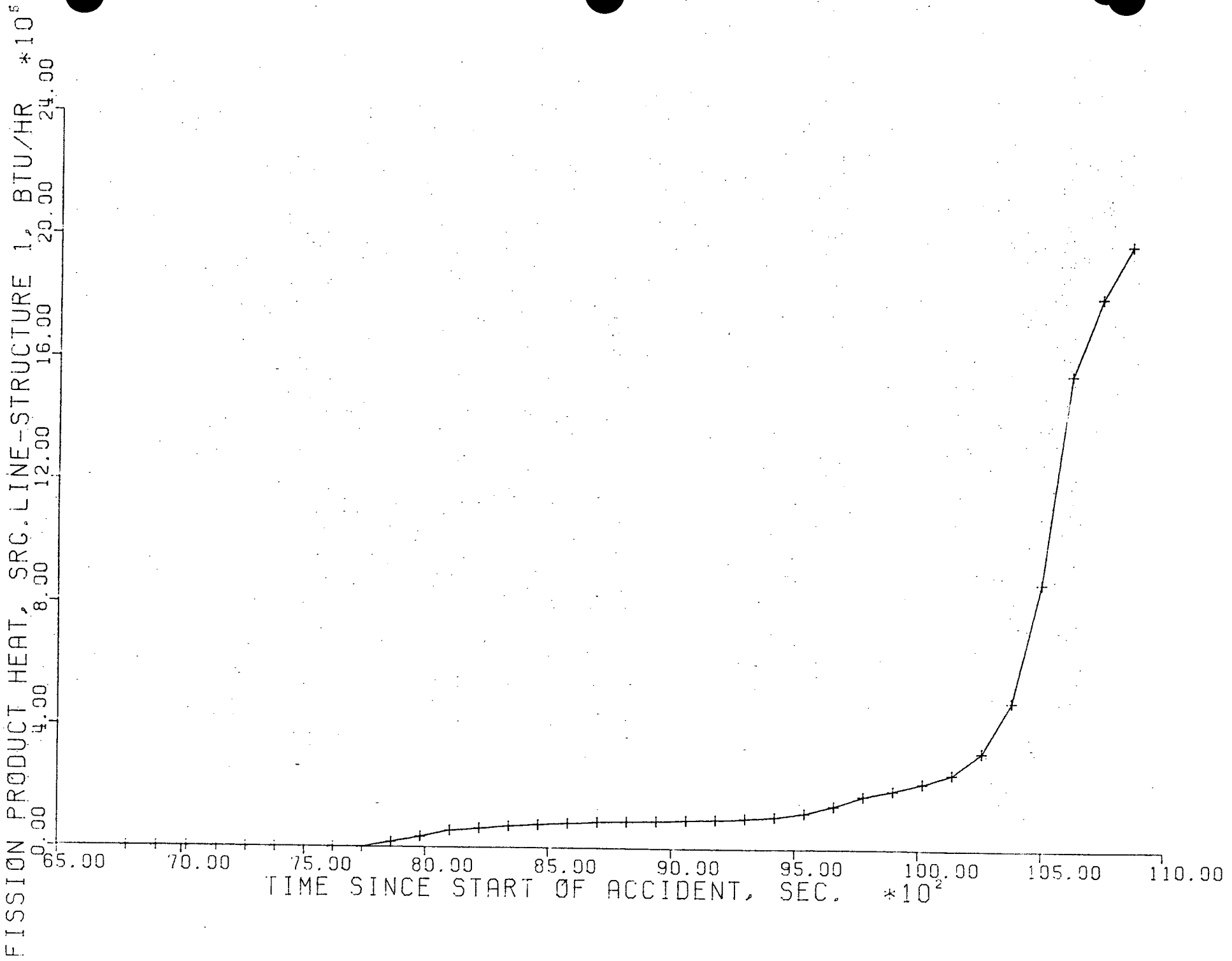
FISSION PRODUCT HEAT, SRC. LINE-STRUCTURE 1, BTU/HR *10^5
0.00
4.00
8.00
12.00
16.00
20.00
24.00
65.00
70.00
75.00
80.00
85.00
90.00
95.00
100.00
105.00
110.00
TIME SINCE START OF ACCIDENT, SEC. *10^2

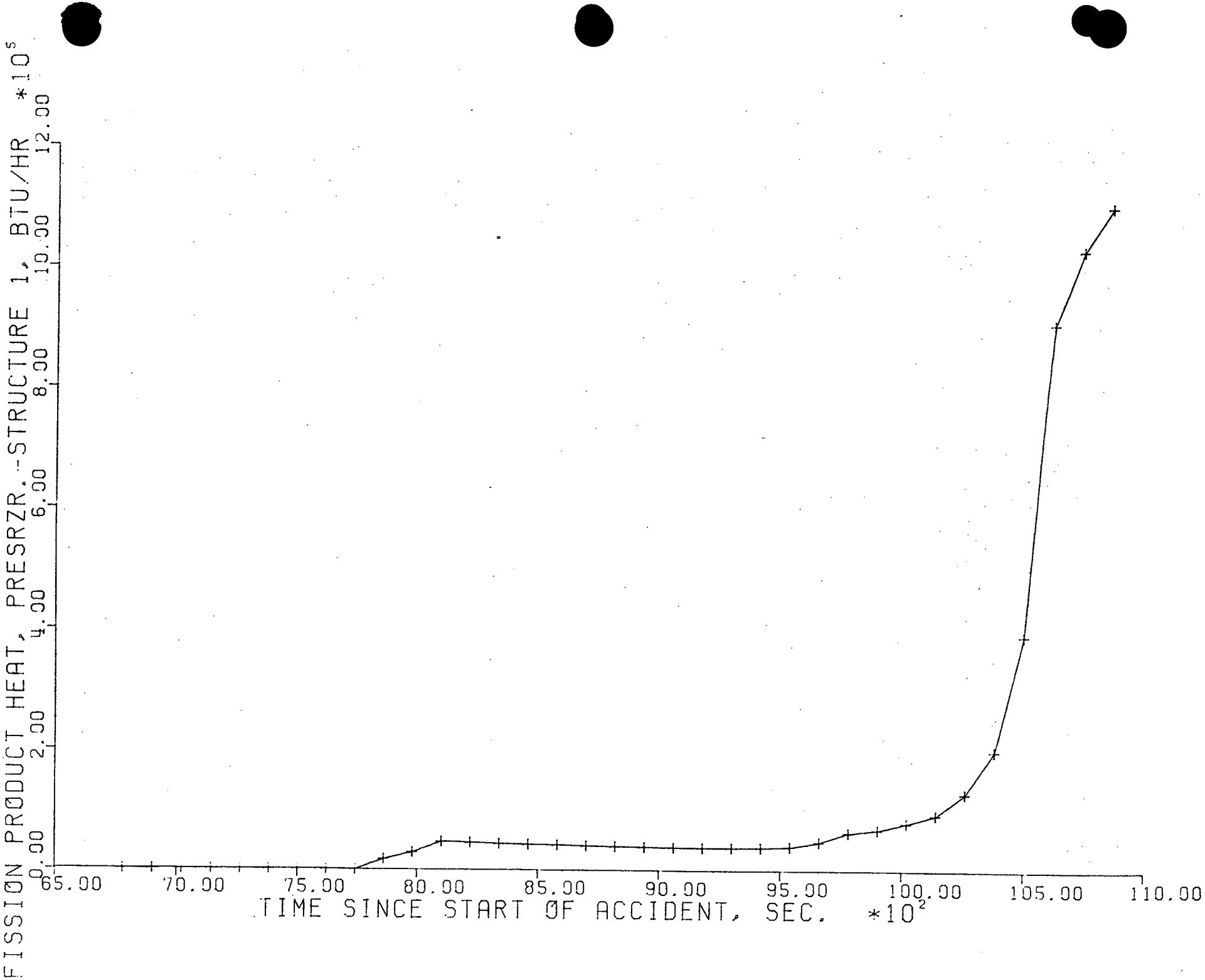
FISSION PRODUCT HEAT, PRESRZR.-STRUCTURE 1, BTU/HR *10^5
0.00
2.00
4.00
6.00
8.00
10.00
12.00
65.00
70.00
75.00
80.00
85.00
90.00
95.00
100.00
105.00
110.00
TIME SINCE START OF ACCIDENT, SEC. *10^2

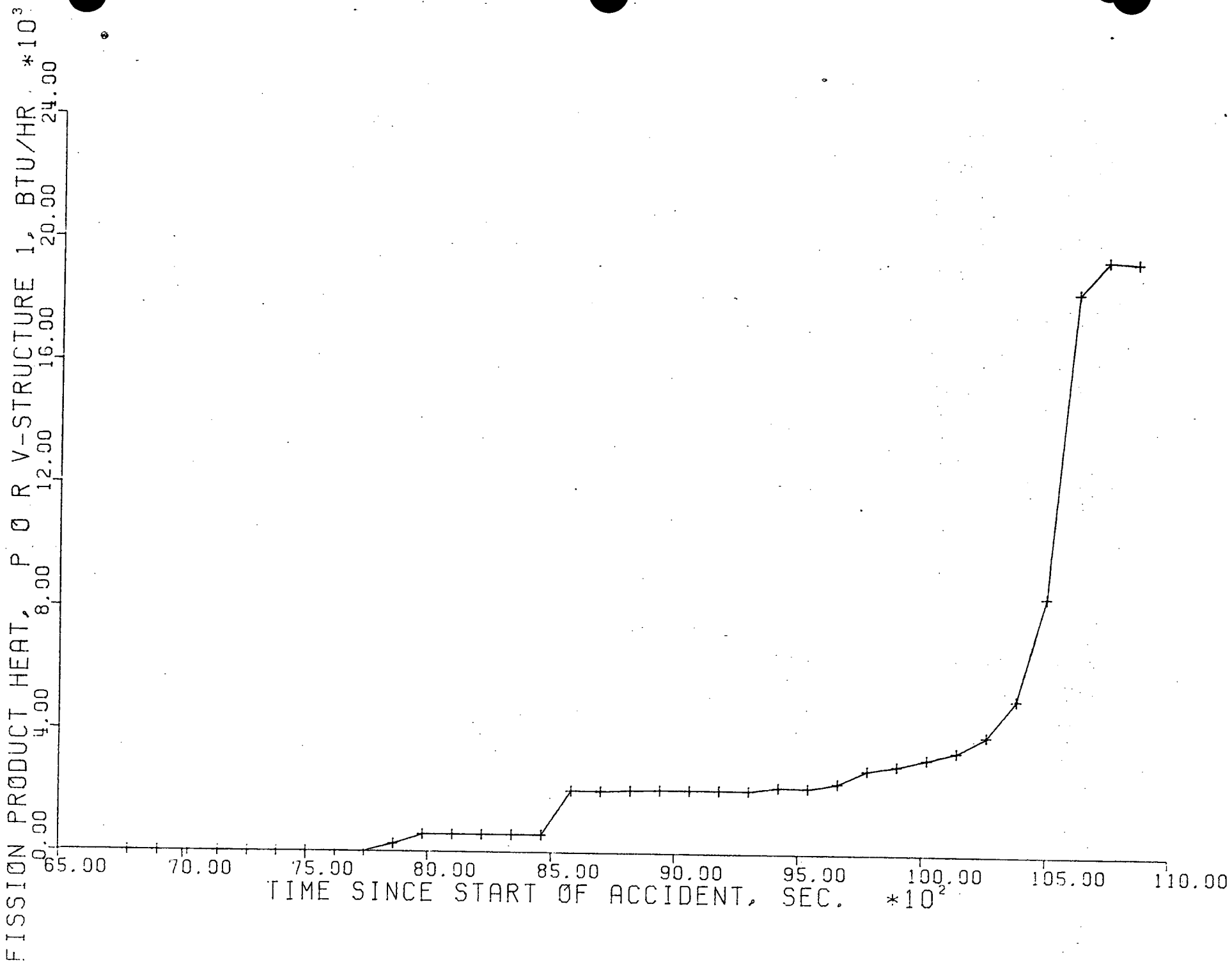
FISSION PRODUCT HEAT, P 0 R V-STRUCTURE 1, BTU/HR *10³
0.00
4.00
8.00
12.00
16.00
20.00
24.00
65.00
70.00
75.00
80.00
85.00
90.00
95.00
100.00
105.00
110.00
TIME SINCE START OF ACCIDENT, SEC. *10²

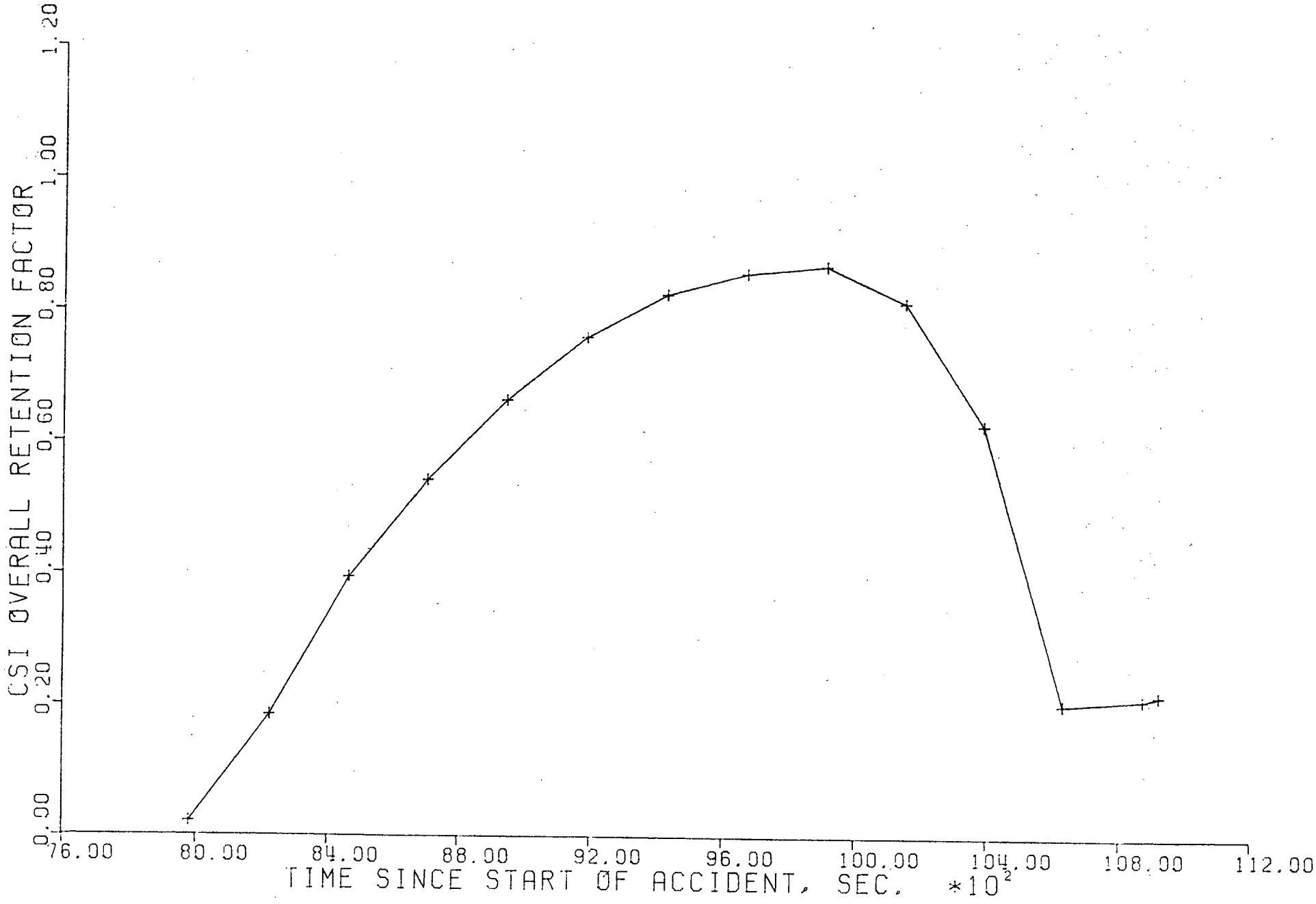
CSI OVERALL RETENTION FACTOR
0.00
0.20
0.40
0.60
0.80
1.00
1.20
76.00
80.00
84.00
88.00
92.00
96.00
100.00
104.00
108.00
112.00
TIME SINCE START OF ACCIDENT, SEC. *10²

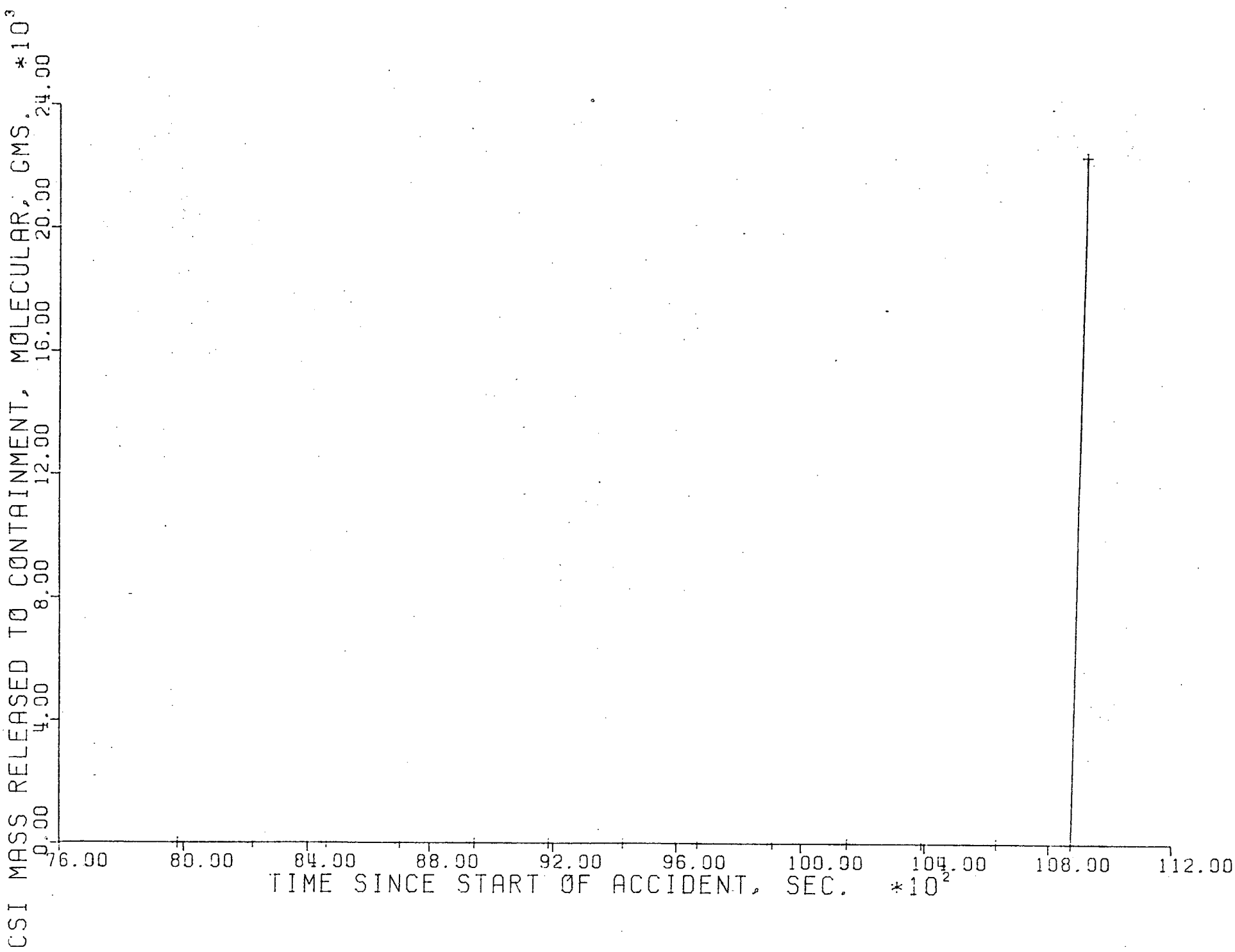
CSI MASS RELEASED TO CONTAINMENT, MOLECULAR, GMS. *10^3
0.00
4.00
8.00
12.00
16.00
20.00
24.00
76.00
80.00
84.00
88.00
92.00
96.00
100.00
104.00
108.00
112.00
TIME SINCE START OF ACCIDENT, SEC. *10^2

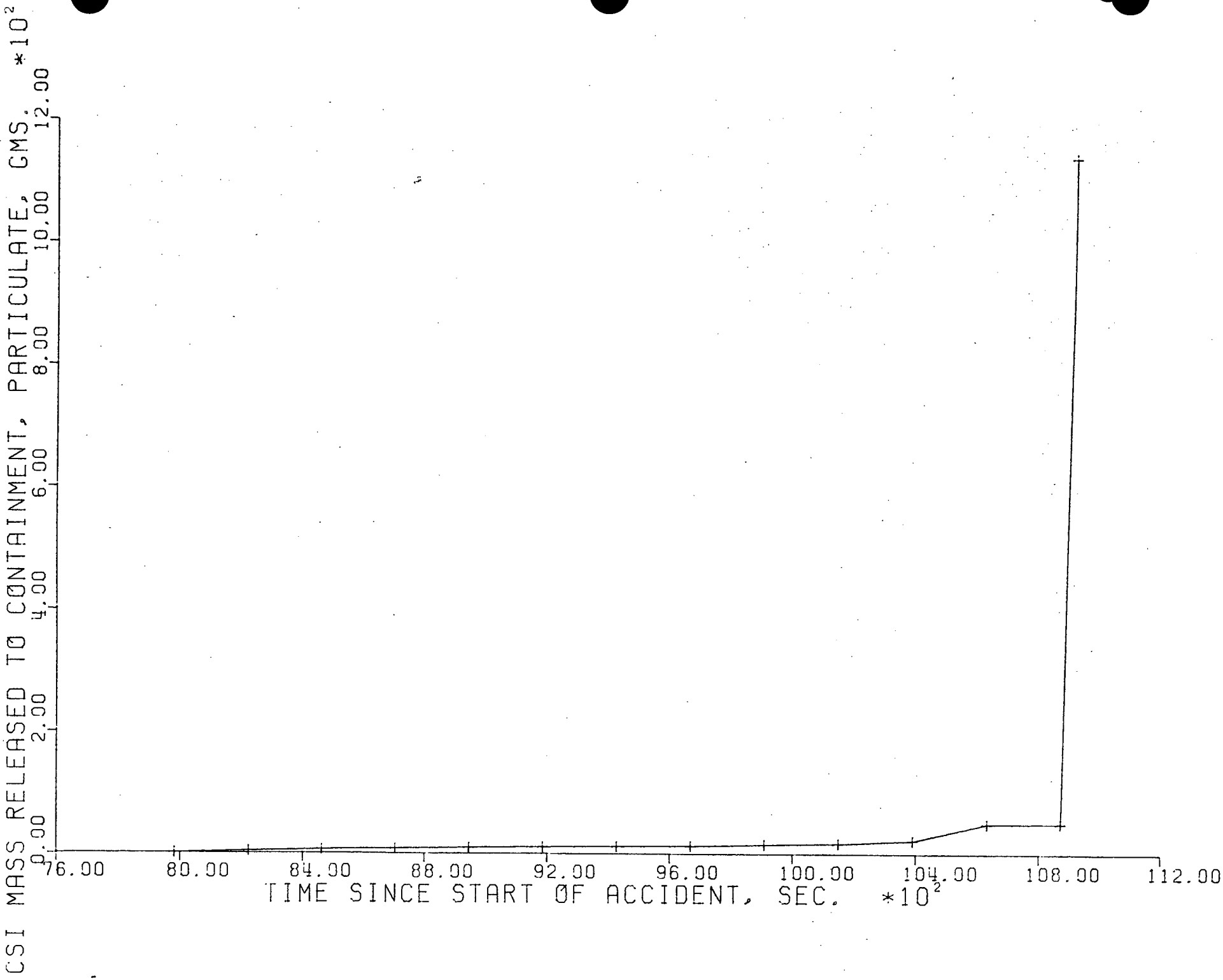
CSI MASS RELEASED TO CONTAINMENT, PARTICULATE, GMS. *10²
0.00
2.00
4.00
6.00
8.00
10.00
12.00
76.00
80.00
84.00
88.00
92.00
96.00
100.00
104.00
108.00
112.00
TIME SINCE START OF ACCIDENT, SEC. *10²

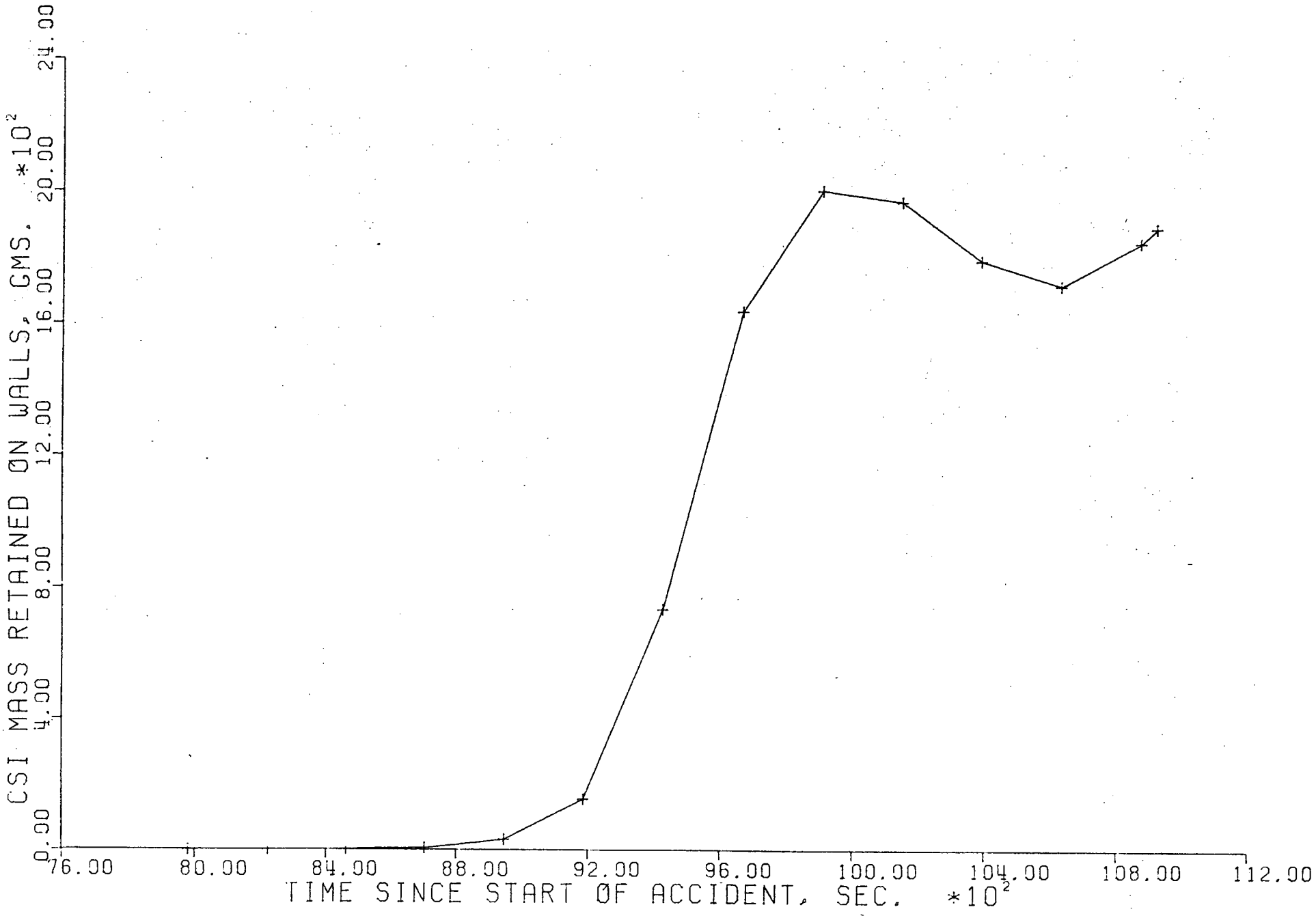
CSI MASS RETAINED ON WALLS, GMS. *10²
0.00
4.00
8.00
12.00
16.00
20.00
24.00
76.00
80.00
84.00
88.00
92.00
96.00
100.00
104.00
108.00
112.00
TIME SINCE START OF ACCIDENT, SEC. *10²

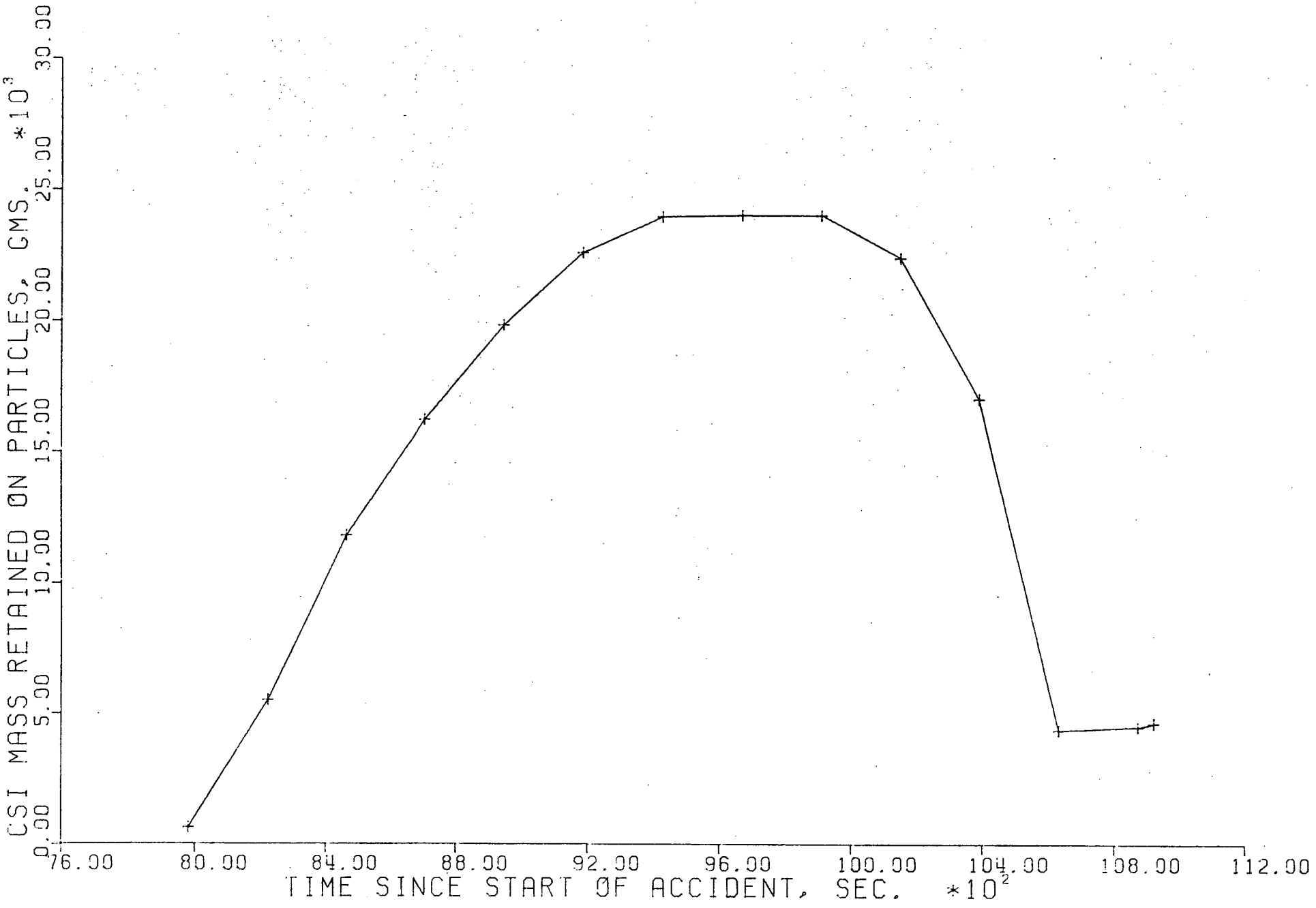
CSI MASS RETAINED ON PARTICLES, GMS. *10^3
0.00
5.00
10.00
15.00
20.00
25.00
30.00
76.00
80.00
84.00
88.00
92.00
96.00
100.00
104.00
108.00
112.00
TIME SINCE START OF ACCIDENT, SEC. *10^2

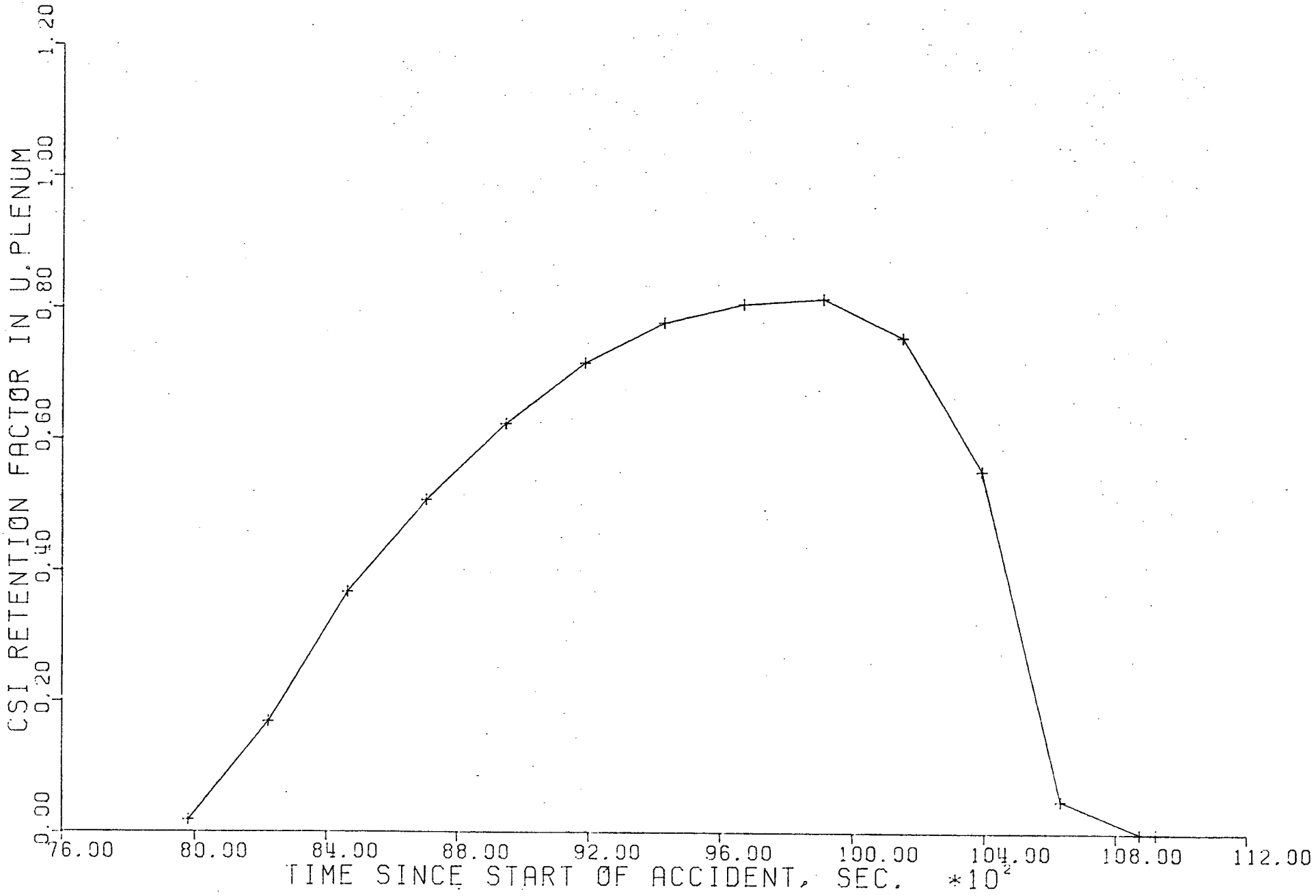
CSI RETENTION FACTOR IN U.PLENUM
0.00
0.20
0.40
0.60
0.80
1.00
1.20
76.00
80.00
84.00
88.00
92.00
96.00
100.00
104.00
108.00
112.00
TIME SINCE START OF ACCIDENT, SEC. *10²

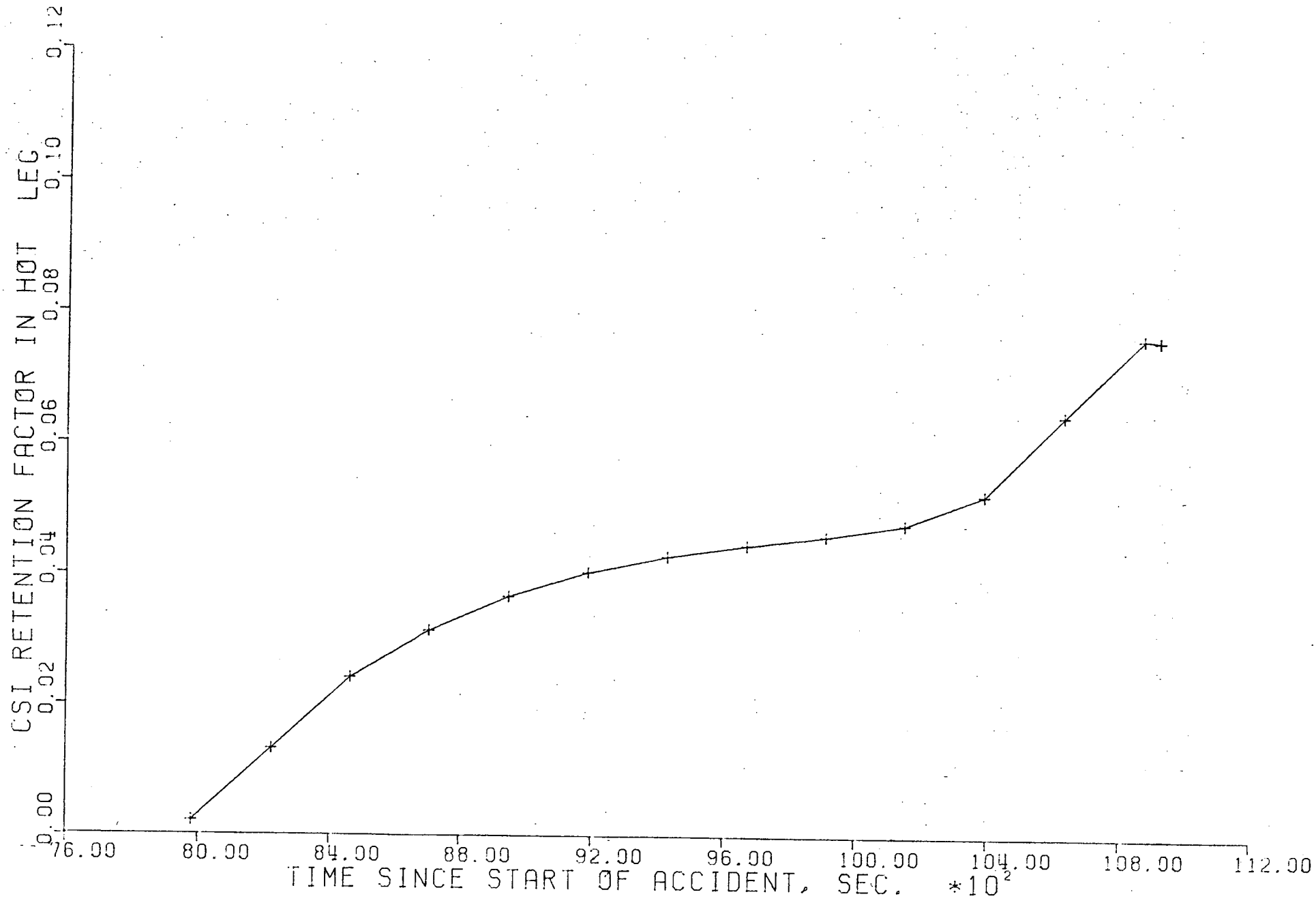
CSI RETENTION FACTOR IN HOT LEG
0.00
0.02
0.04
0.06
0.08
0.10
0.12
76.00
80.00
84.00
88.00
92.00
96.00
100.00
104.00
108.00
112.00
TIME SINCE START OF ACCIDENT, SEC. *10²

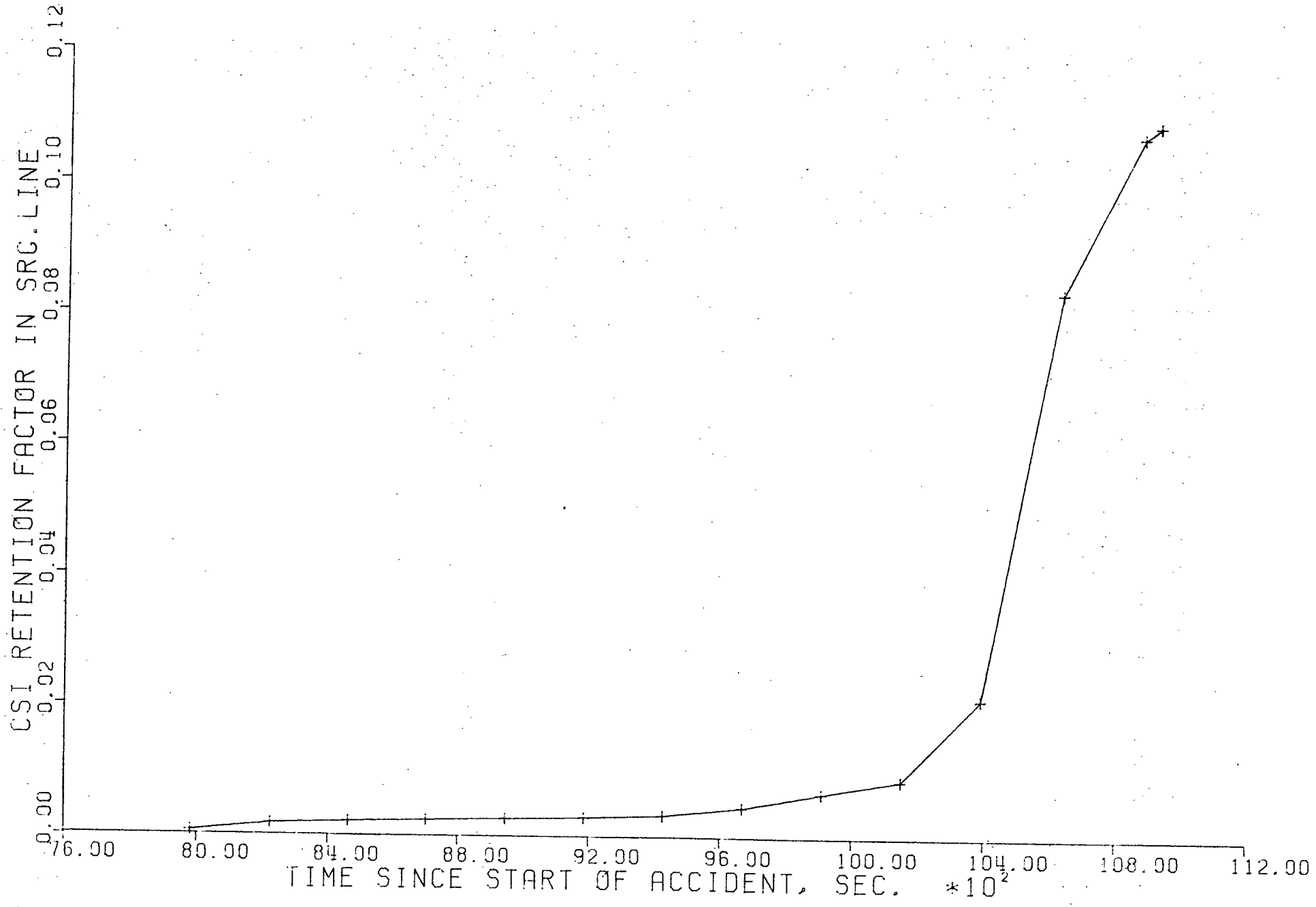
CSI RETENTION FACTOR IN SRC. LINE
0.00
0.02
0.04
0.06
0.08
0.10
0.12
76.00
80.00
84.00
88.00
92.00
96.00
100.00
104.00
108.00
112.00
TIME SINCE START OF ACCIDENT, SEC. *10²

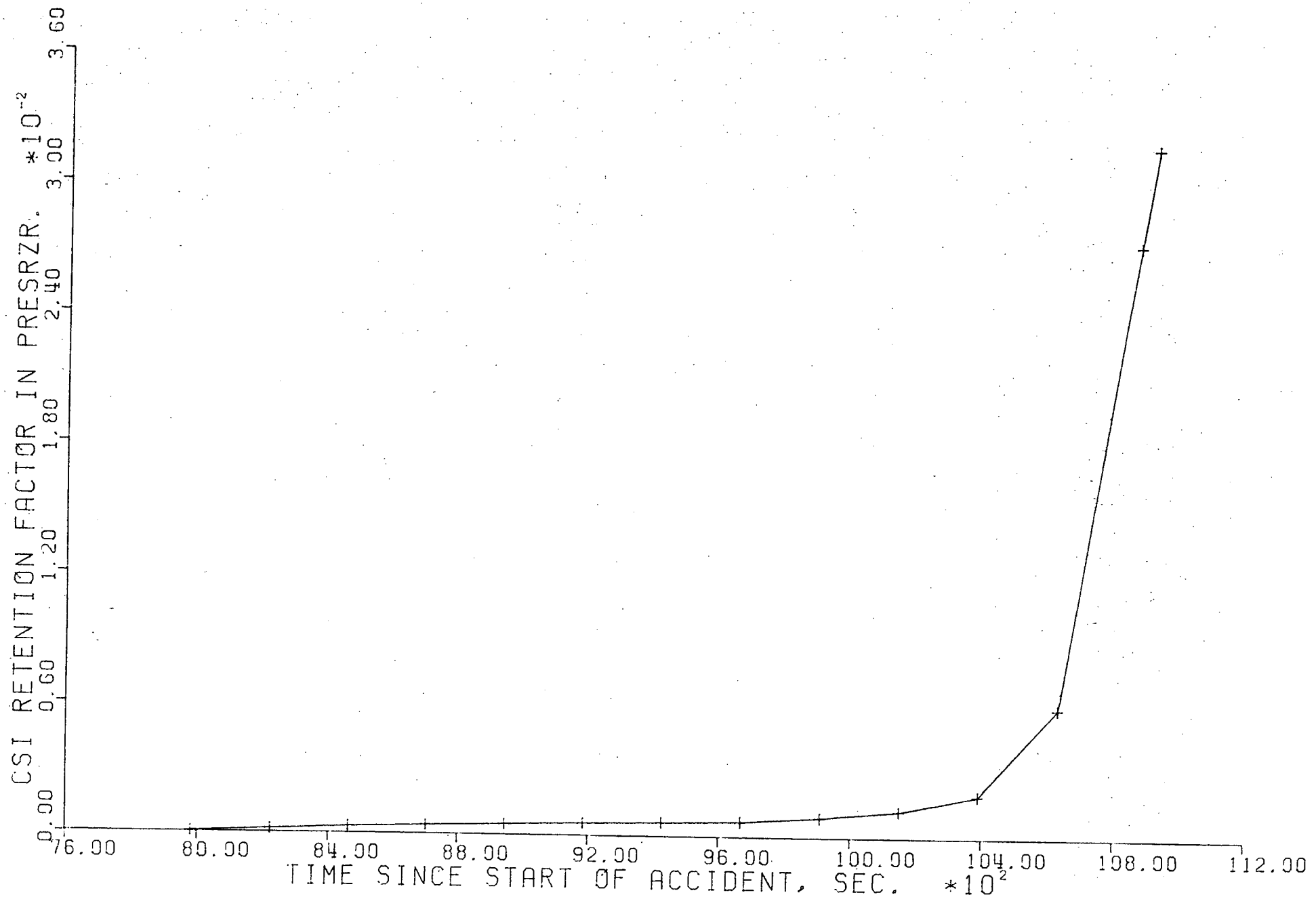
CSI RETENTION FACTOR IN PRESRZR. *10⁻²
0.00
0.60
1.20
1.80
2.40
3.00
3.60
76.00
80.00
84.00
88.00
92.00
96.00
100.00
104.00
108.00
112.00
TIME SINCE START OF ACCIDENT, SEC. *10²

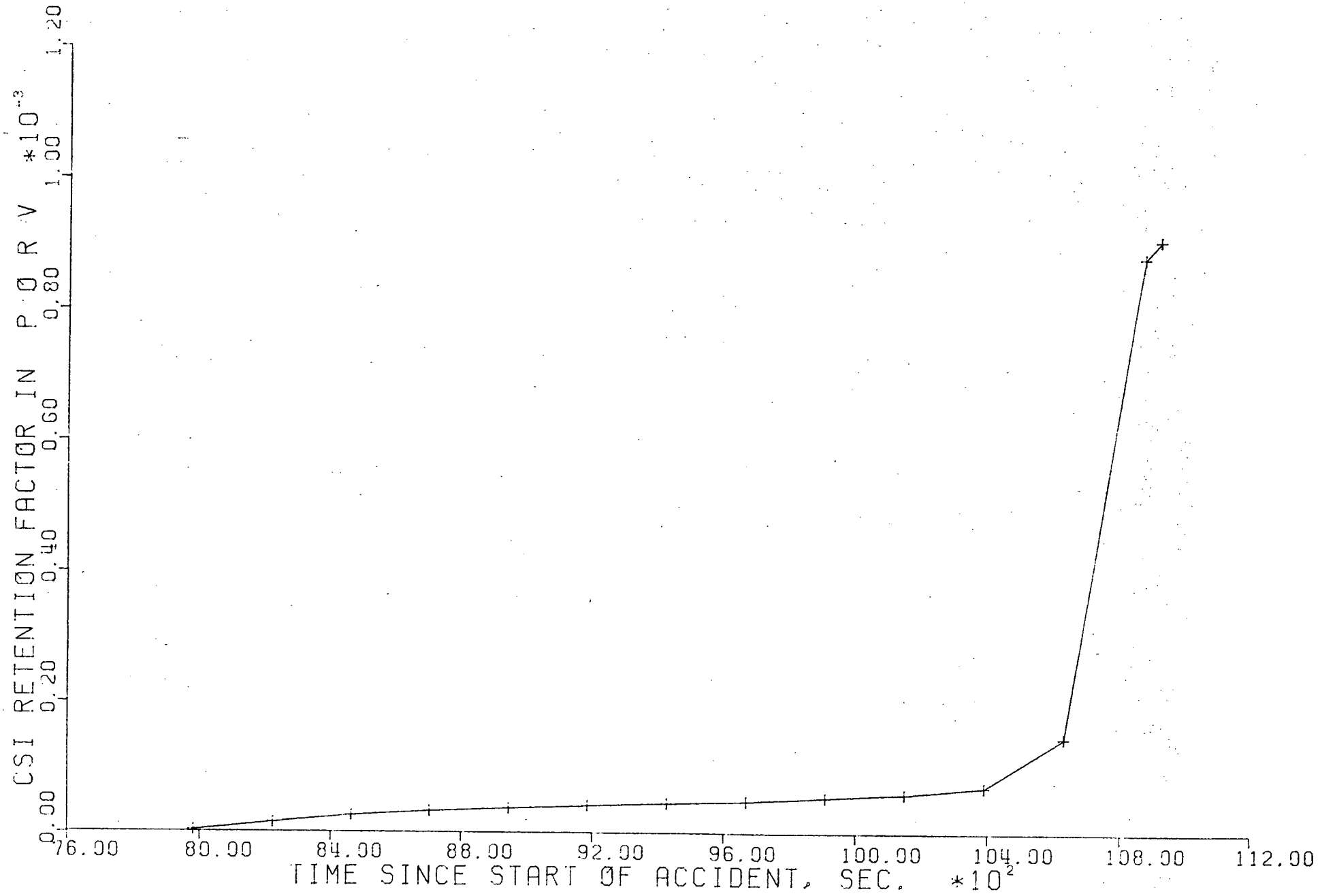
CSI RETENTION FACTOR IN P Ø R V *10⁻³
0.00
0.20
0.40
0.60
0.80
1.00
1.20
76.00
80.00
84.00
88.00
92.00
96.00
100.00
104.00
108.00
112.00
TIME SINCE START ØF ACCIDENT, SEC. *10²

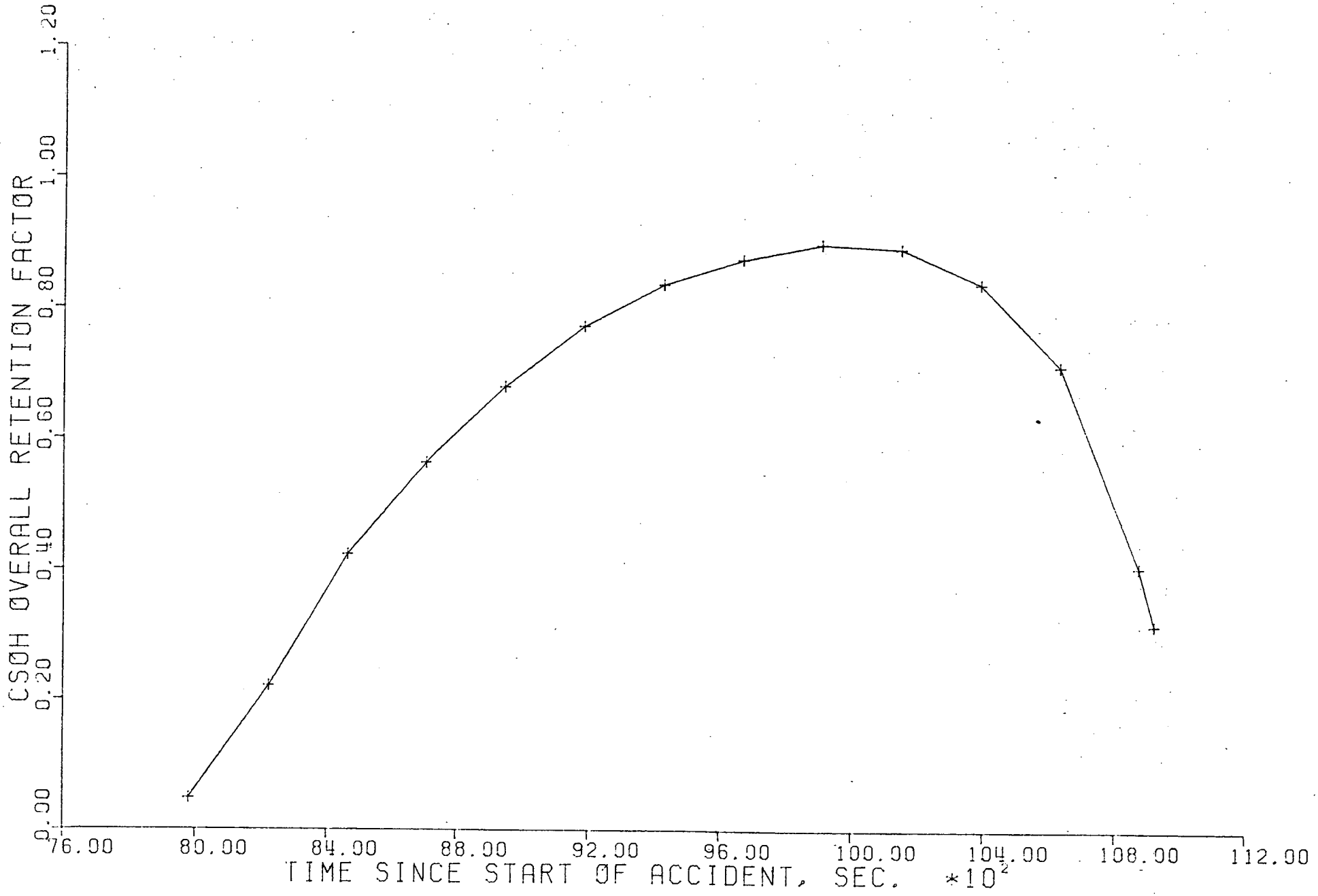
CSOH OVERALL RETENTION FACTOR
0.00
0.20
0.40
0.60
0.80
1.00
1.20
76.00
80.00
84.00
88.00
92.00
96.00
100.00
104.00
108.00
112.00
TIME SINCE START OF ACCIDENT, SEC. *10²

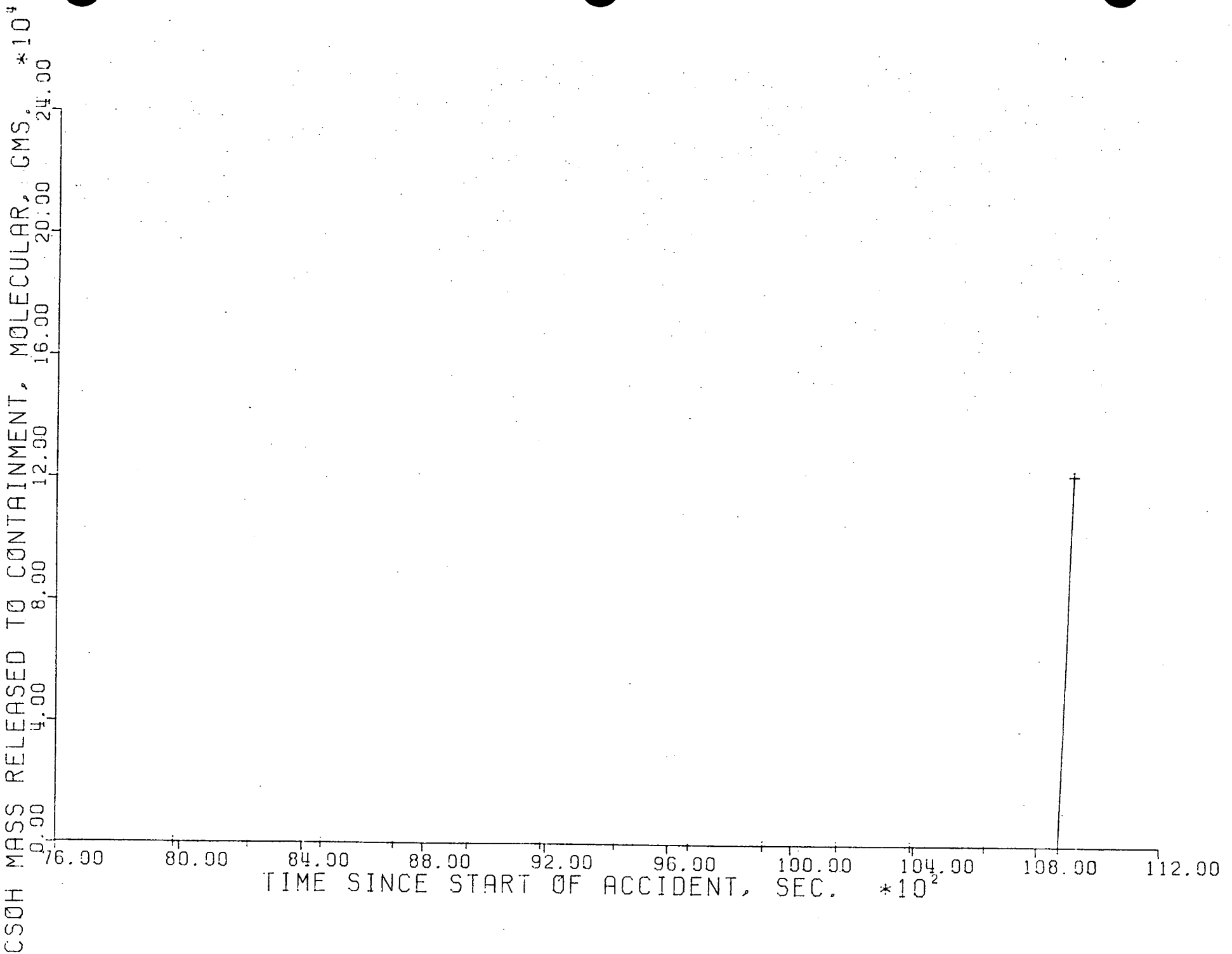
CSOH MASS RELEASED TO CONTAINMENT, MOLECULAR, GMS. *10⁴
0.00
4.00
8.00
12.00
16.00
20.00
24.00
76.00
80.00
84.00
88.00
92.00
96.00
100.00
104.00
108.00
112.00
TIME SINCE START OF ACCIDENT, SEC. *10²

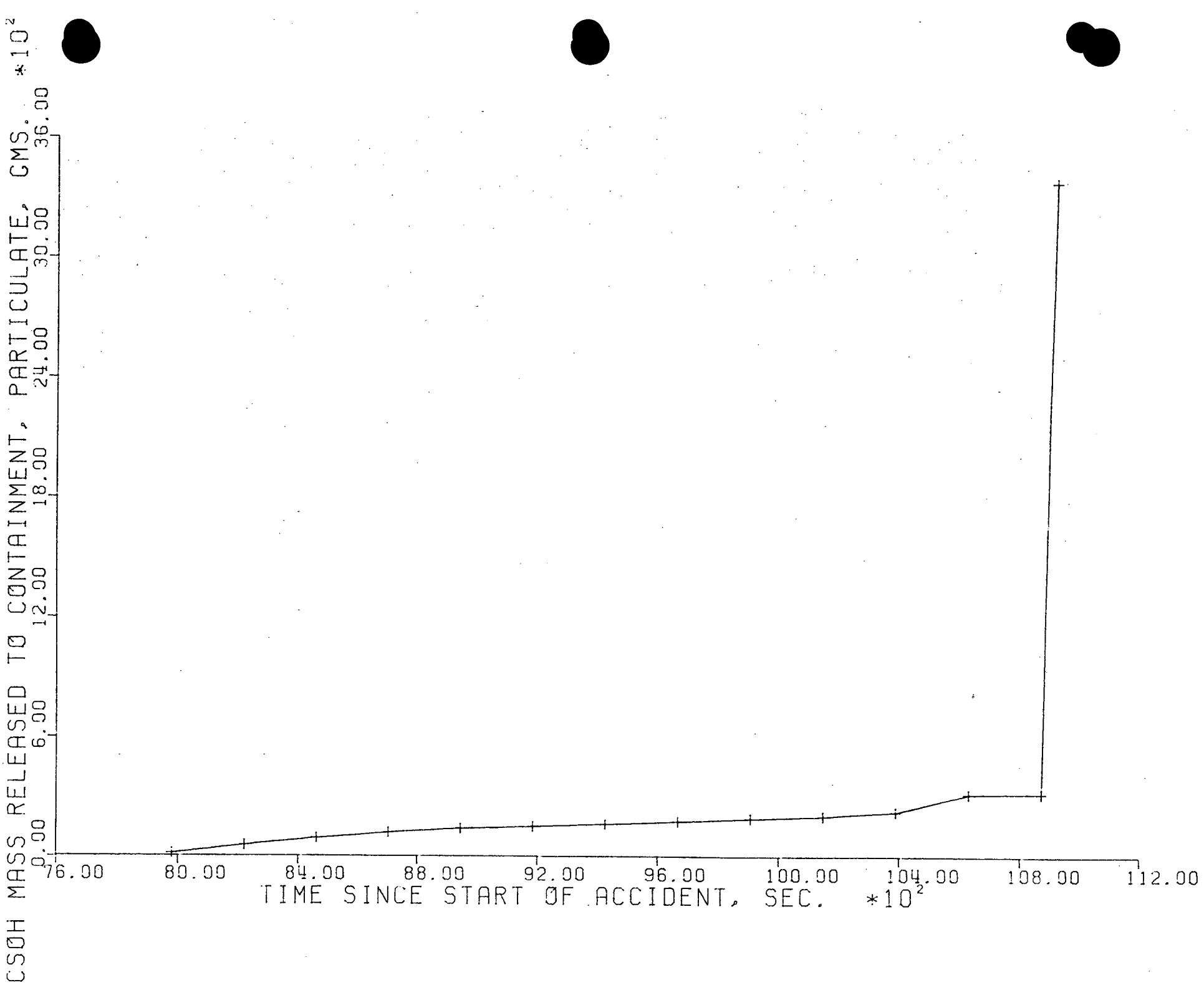
CSOH MASS RELEASED TO CONTAINMENT, PARTICULATE, CMS. *10²
0.00
6.00
12.00
18.00
24.00
30.00
36.00
76.00
80.00
84.00
88.00
92.00
96.00
100.00
104.00
108.00
112.00
TIME SINCE START OF ACCIDENT, SEC. *10²

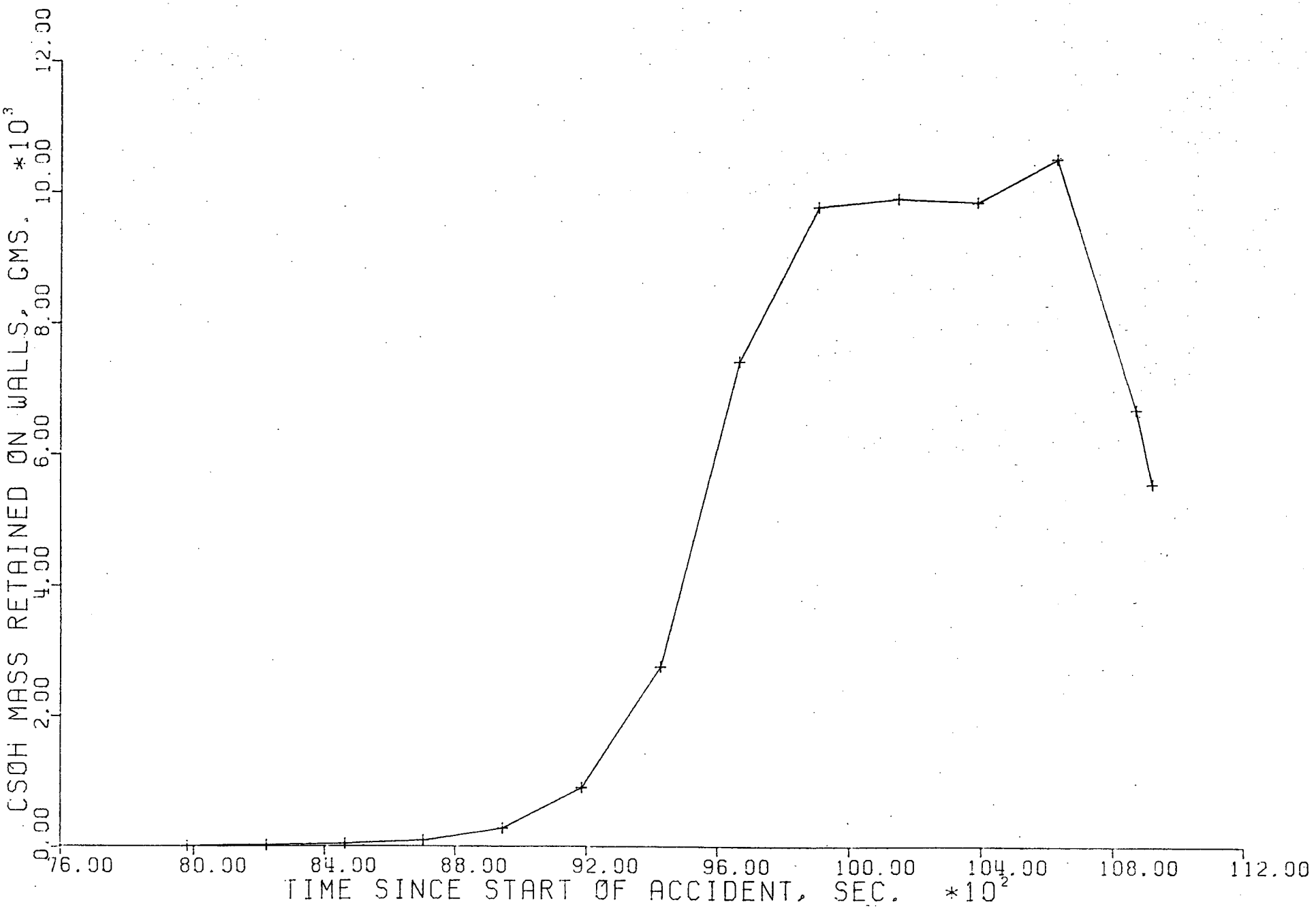
CSOH MASS RETAINED ON WALLS, GMS. *10^3
0.00
2.00
4.00
6.00
8.00
10.00
12.00
76.00
80.00
84.00
88.00
92.00
96.00
100.00
104.00
108.00
112.00
TIME SINCE START OF ACCIDENT, SEC. *10^2

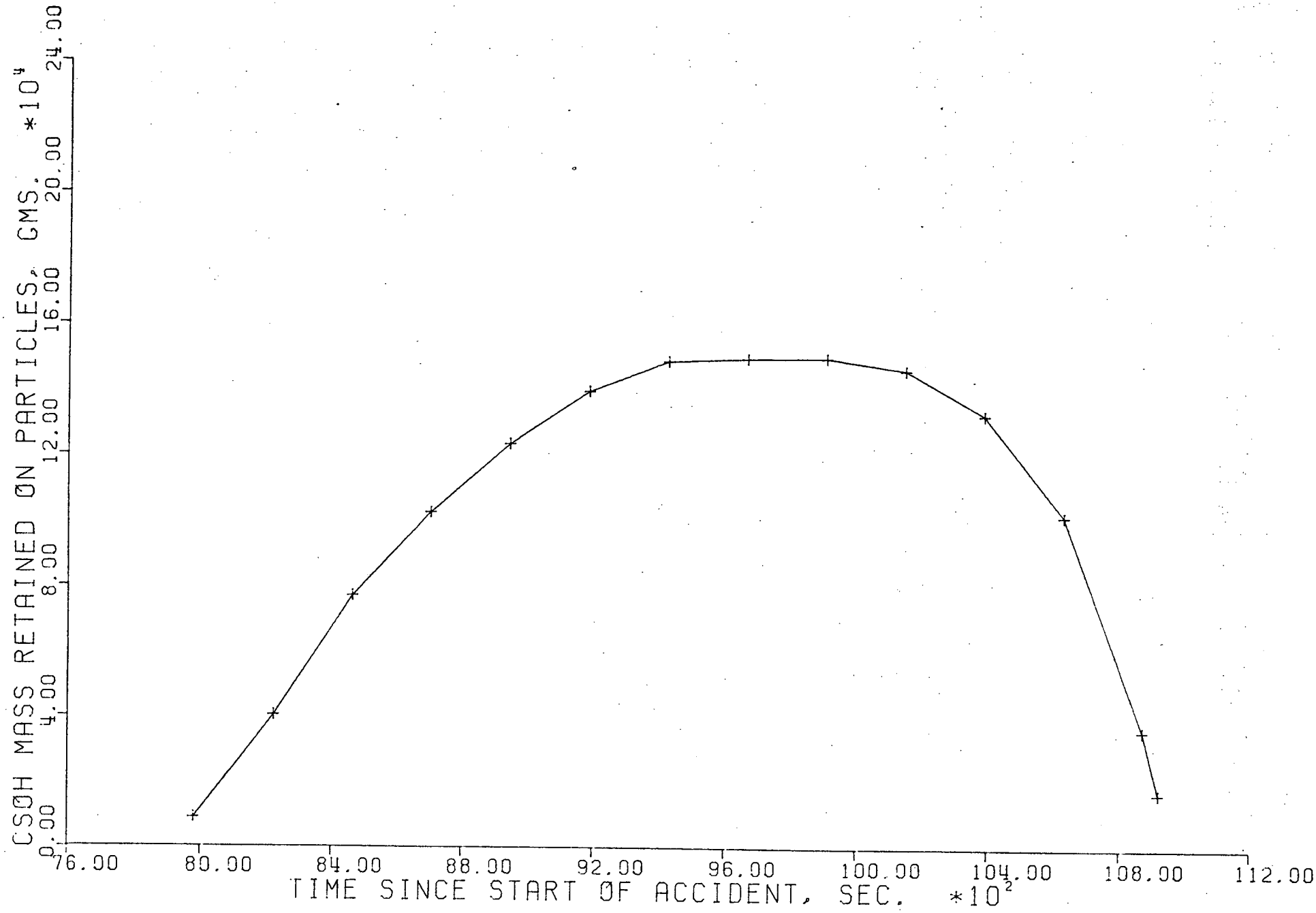
CSØH MASS RETAINED ØN PARTICLES, GMS. *10⁴
0.00
4.00
8.00
12.00
16.00
20.00
24.00
76.00
80.00
84.00
88.00
92.00
96.00
100.00
104.00
108.00
112.00
TIME SINCE START ØF ACCIDENT, SEC. *10²

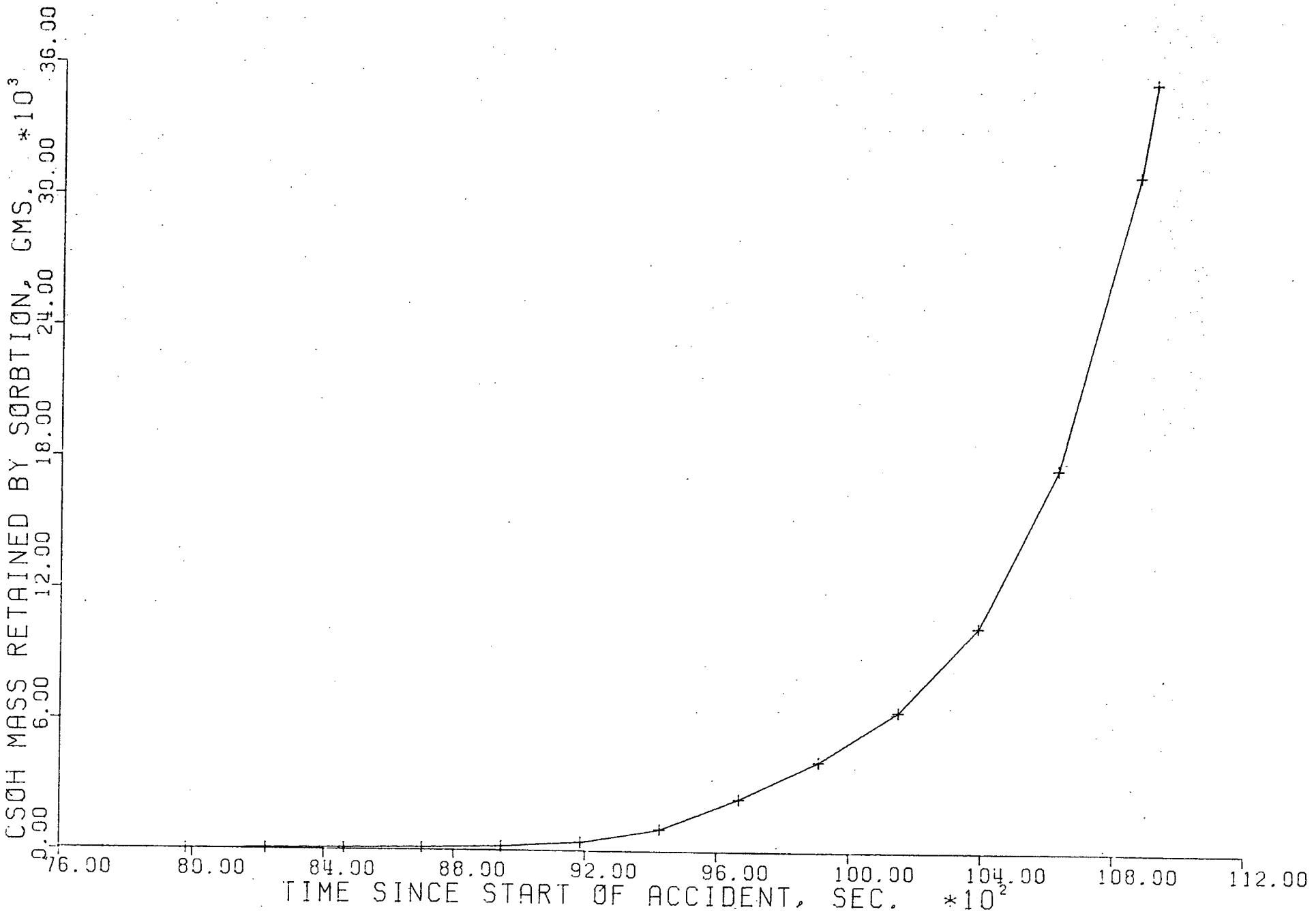
CSOH MASS RETAINED BY SORBTION, GMS. *10^3
0.00
6.00
12.00
18.00
24.00
30.00
36.00
76.00
80.00
84.00
88.00
92.00
96.00
100.00
104.00
108.00
112.00
TIME SINCE START OF ACCIDENT, SEC. *10^2

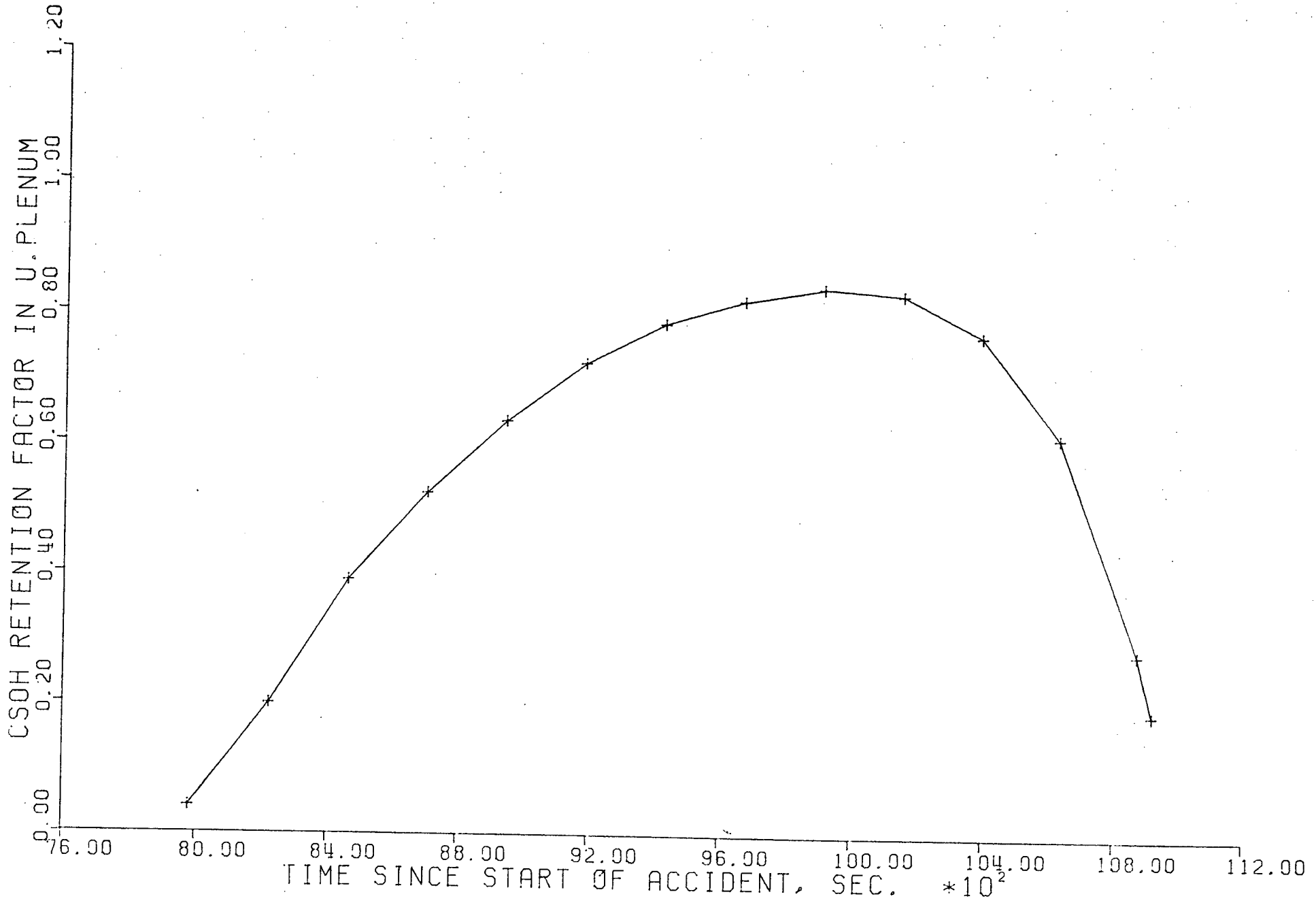
CSOH RETENTION FACTOR IN U.PLENUM
0.00
0.20
0.40
0.60
0.80
1.00
1.20
76.00
80.00
84.00
88.00
92.00
96.00
100.00
104.00
108.00
112.00
TIME SINCE START OF ACCIDENT, SEC. *10²

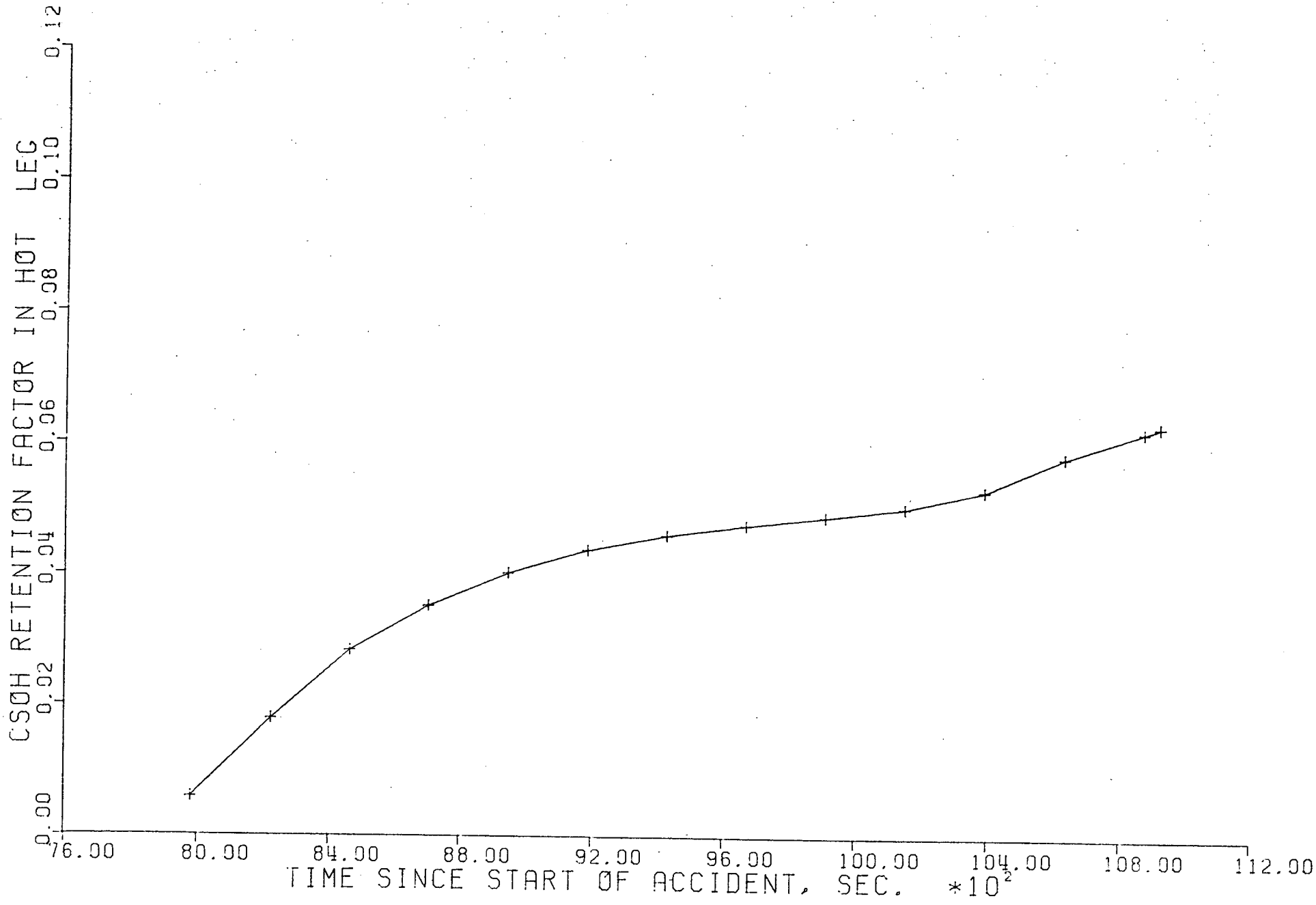
CSOH RETENTION FACTOR IN HOT LEG
0.00
0.02
0.04
0.06
0.08
0.10
0.12
76.00
80.00
84.00
88.00
92.00
96.00
100.00
104.00
108.00
112.00
TIME SINCE START OF ACCIDENT, SEC. *10²

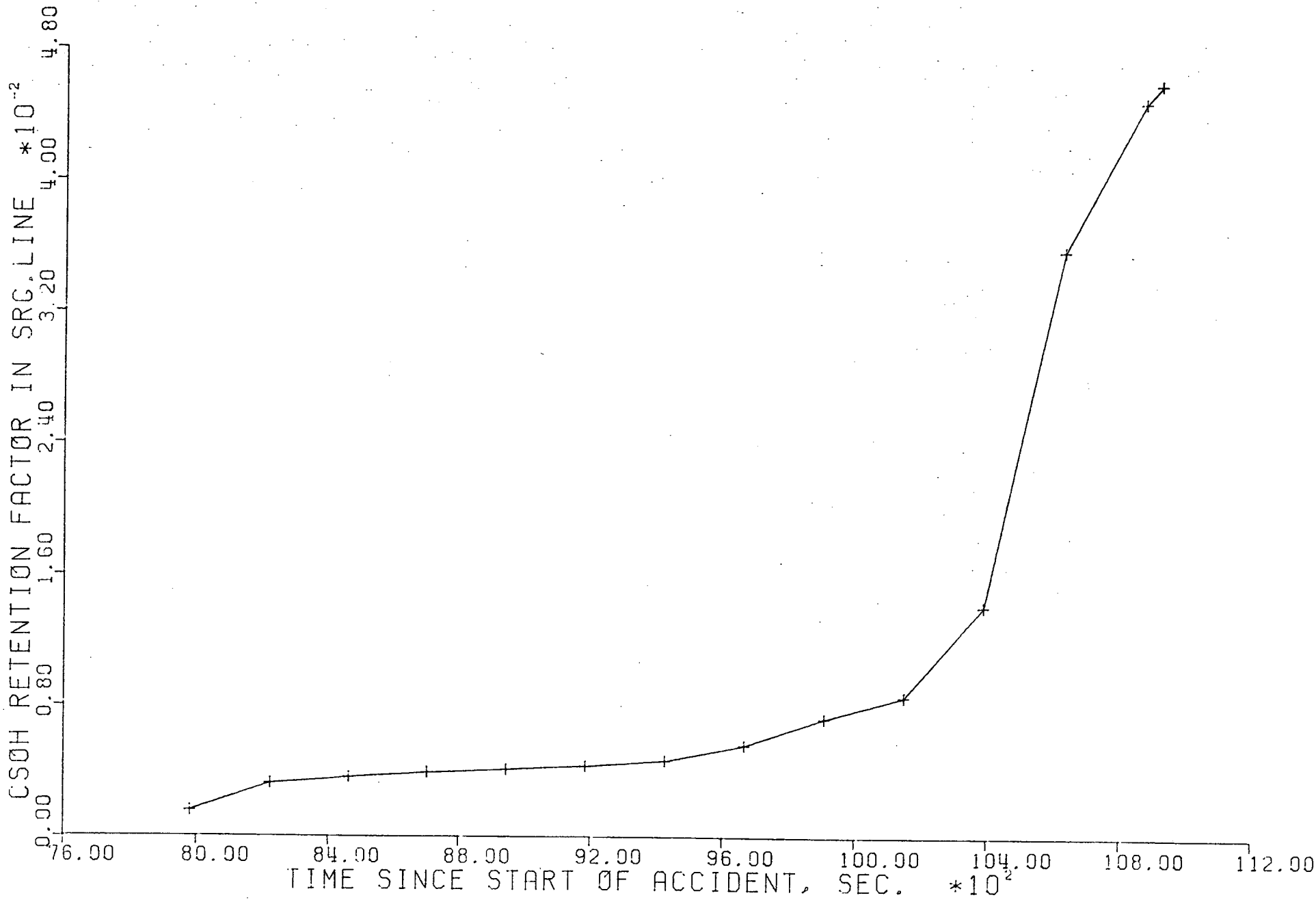
CSOH RETENTION FACTOR IN SRG. LINE *10⁻²
0.00
0.80
1.60
2.40
3.20
4.00
4.80
76.00
80.00
84.00
88.00
92.00
96.00
100.00
104.00
108.00
112.00
TIME SINCE START OF ACCIDENT, SEC. *10²

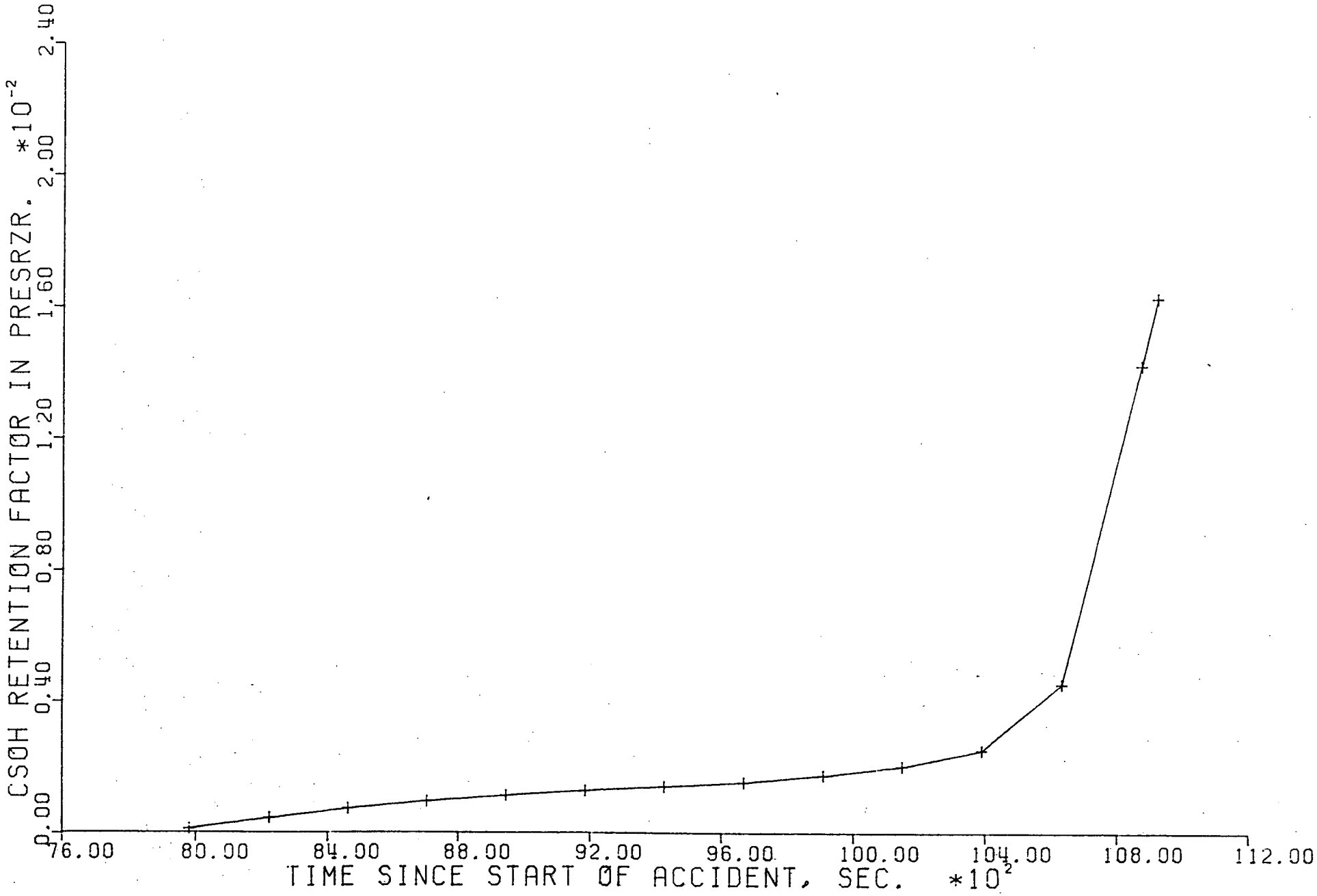
CSOH RETENTION FACTOR IN PRESRZR. *10⁻²
0.00
0.40
0.80
1.20
1.60
2.00
2.40
76.00
80.00
84.00
88.00
92.00
96.00
100.00
104.00
108.00
112.00
TIME SINCE START OF ACCIDENT, SEC. *10²

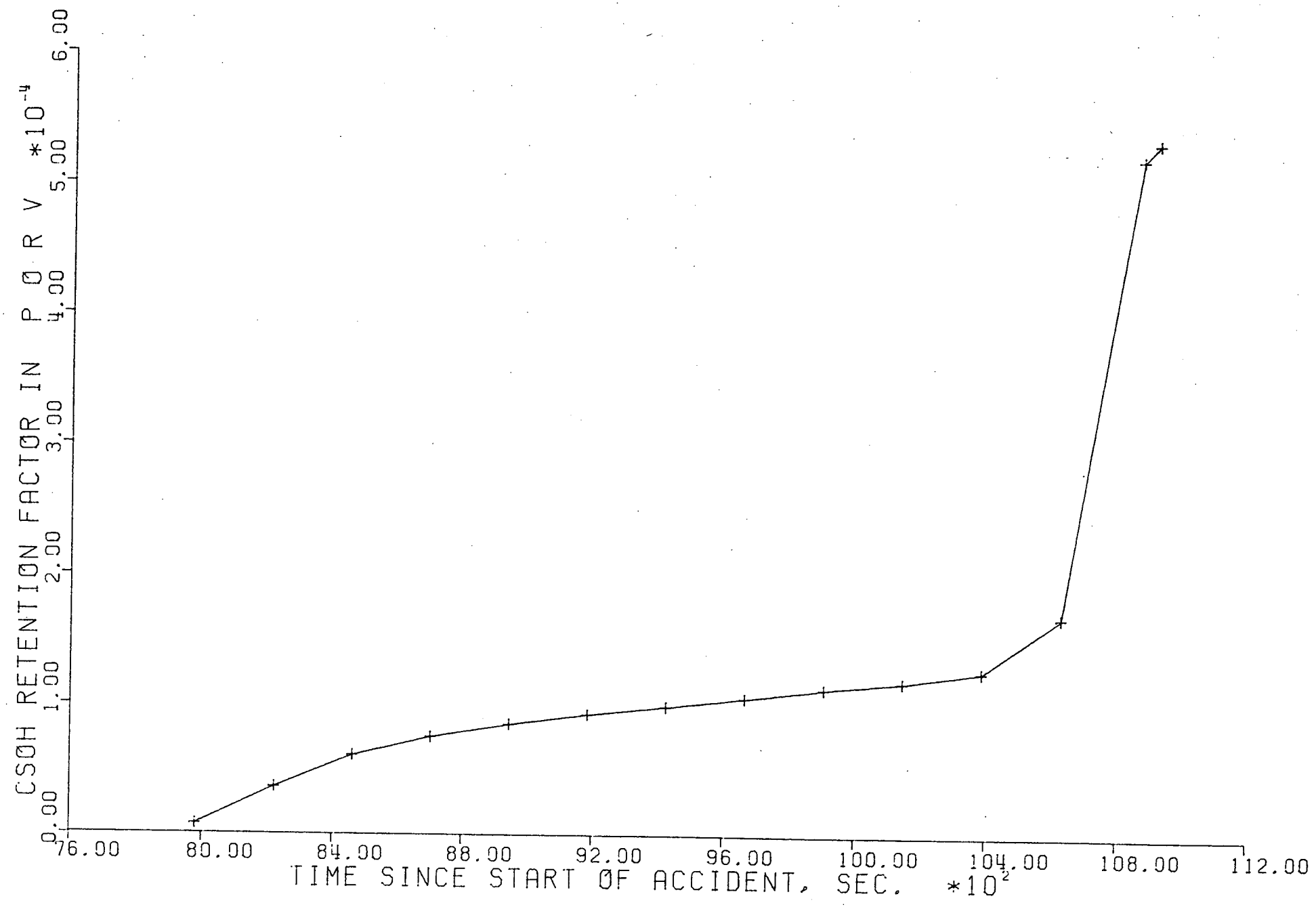
CSOH RETENTION FACTOR IN P O R V *10⁻⁴
0.00
1.00
2.00
3.00
4.00
5.00
6.00
76.00
80.00
84.00
88.00
92.00
96.00
100.00
104.00
108.00
112.00
TIME SINCE START OF ACCIDENT, SEC. *10²

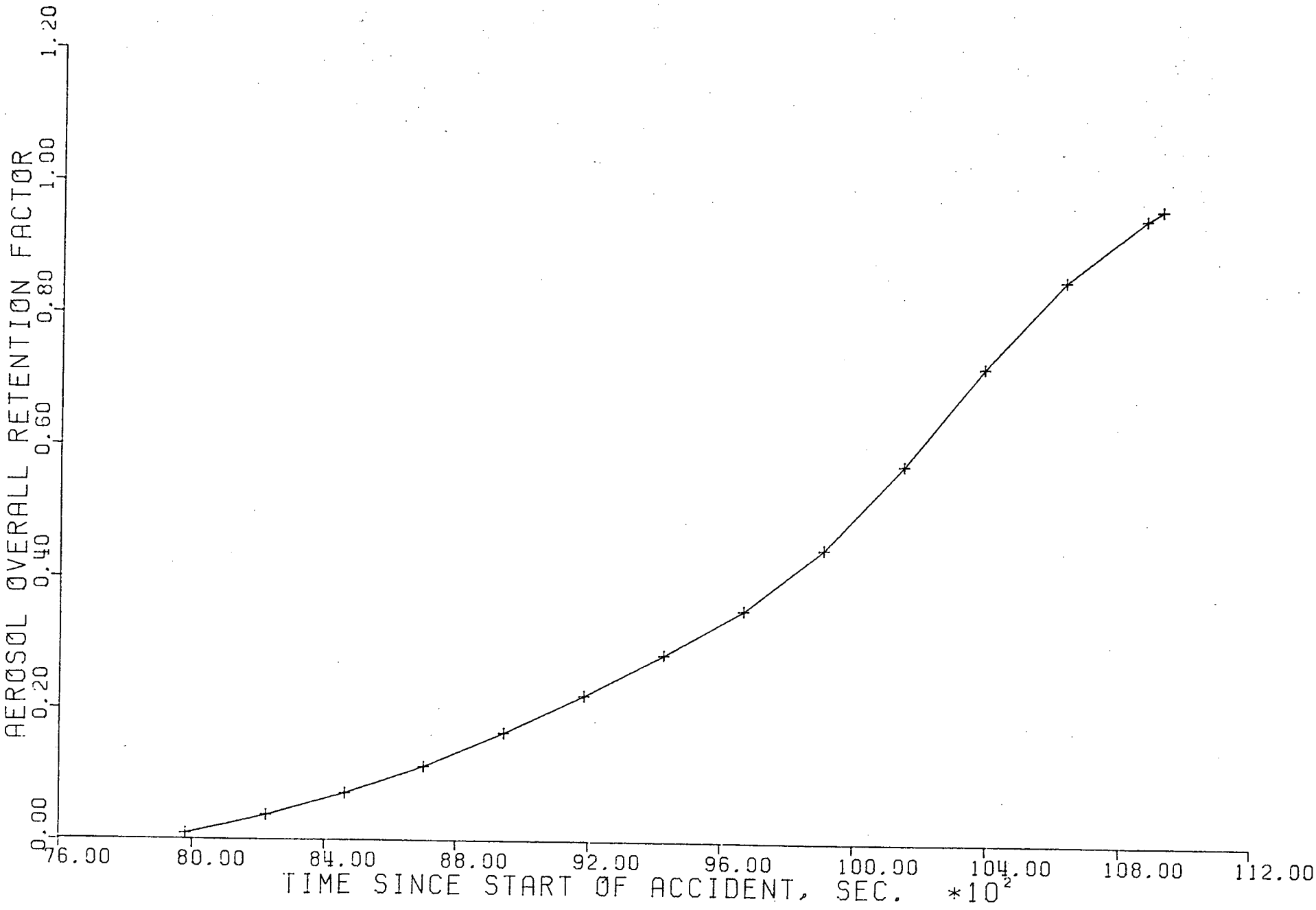
AEROSOL OVERALL RETENTION FACTOR
0.00
0.20
0.40
0.60
0.80
1.00
1.20
76.00
80.00
84.00
88.00
92.00
96.00
100.00
104.00
108.00
112.00
TIME SINCE START OF ACCIDENT, SEC. *10²

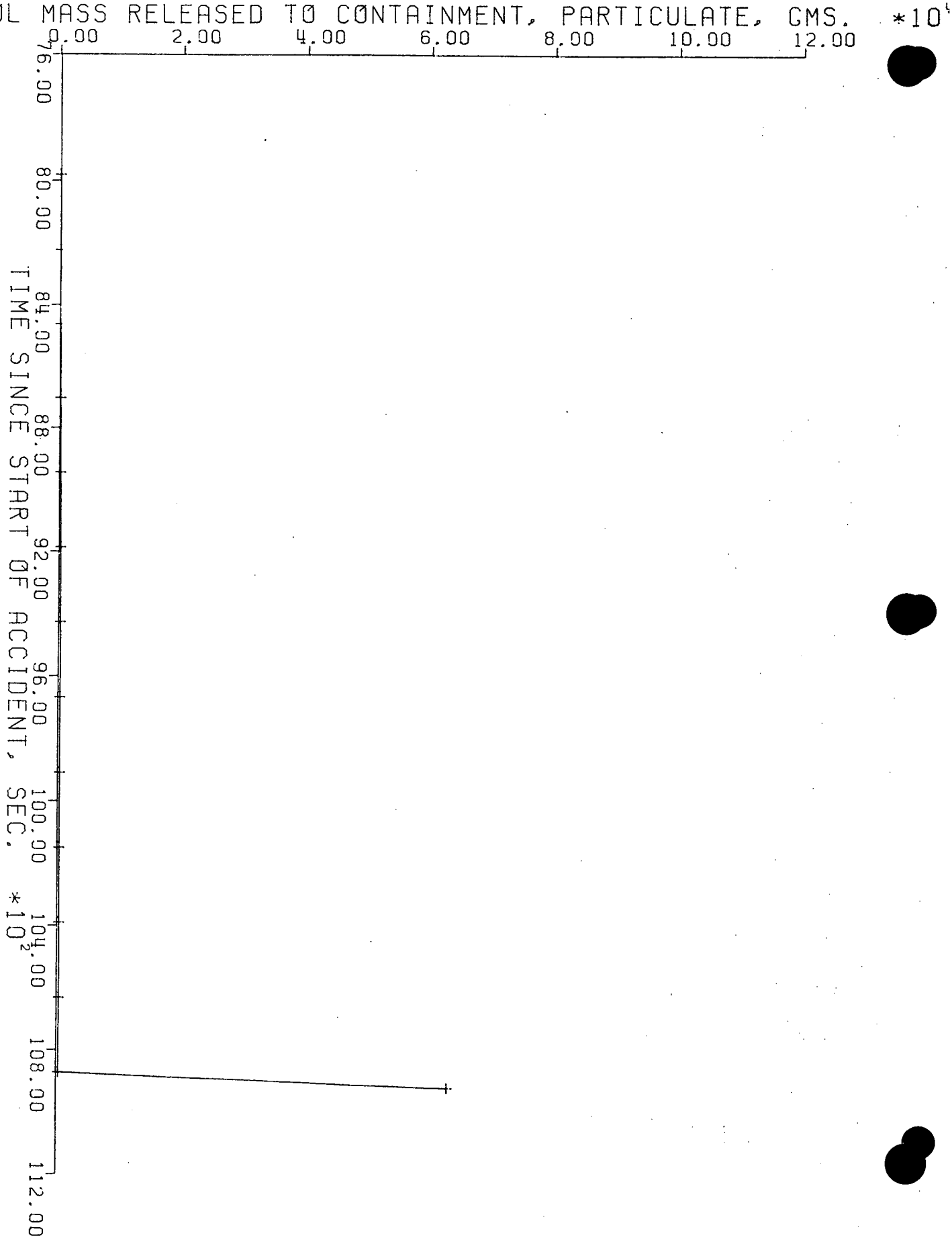
AERØSØL MASS RELEASED TØ CØNTAINMENT, PARTICULATE, GMS. *10⁴
0.00
2.00
4.00
6.00
8.00
10.00
12.00
TIME SINCE START ØF ACCIDENT, SEC. *10²
76.00
80.00
84.00
88.00
92.00
96.00
100.00
104.00
108.00
112.00

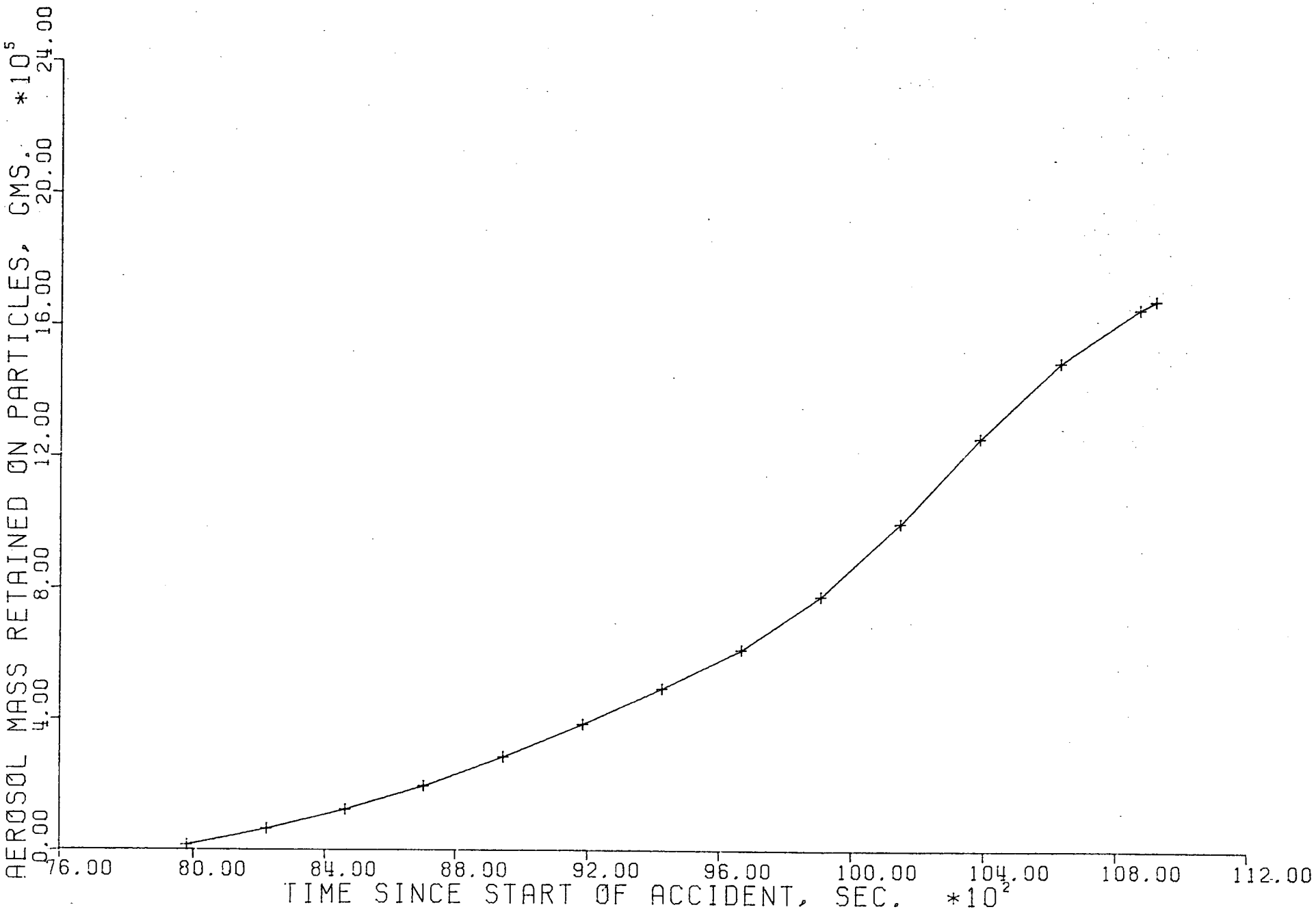
AERØSØL MASS RETAINED ØN PARTICLES, GMS. *10^5
0.00
4.00
8.00
12.00
16.00
20.00
24.00
76.00
80.00
84.00
88.00
92.00
96.00
100.00
104.00
108.00
112.00
TIME SINCE START ØF ACCIDENT, SEC. *10^2

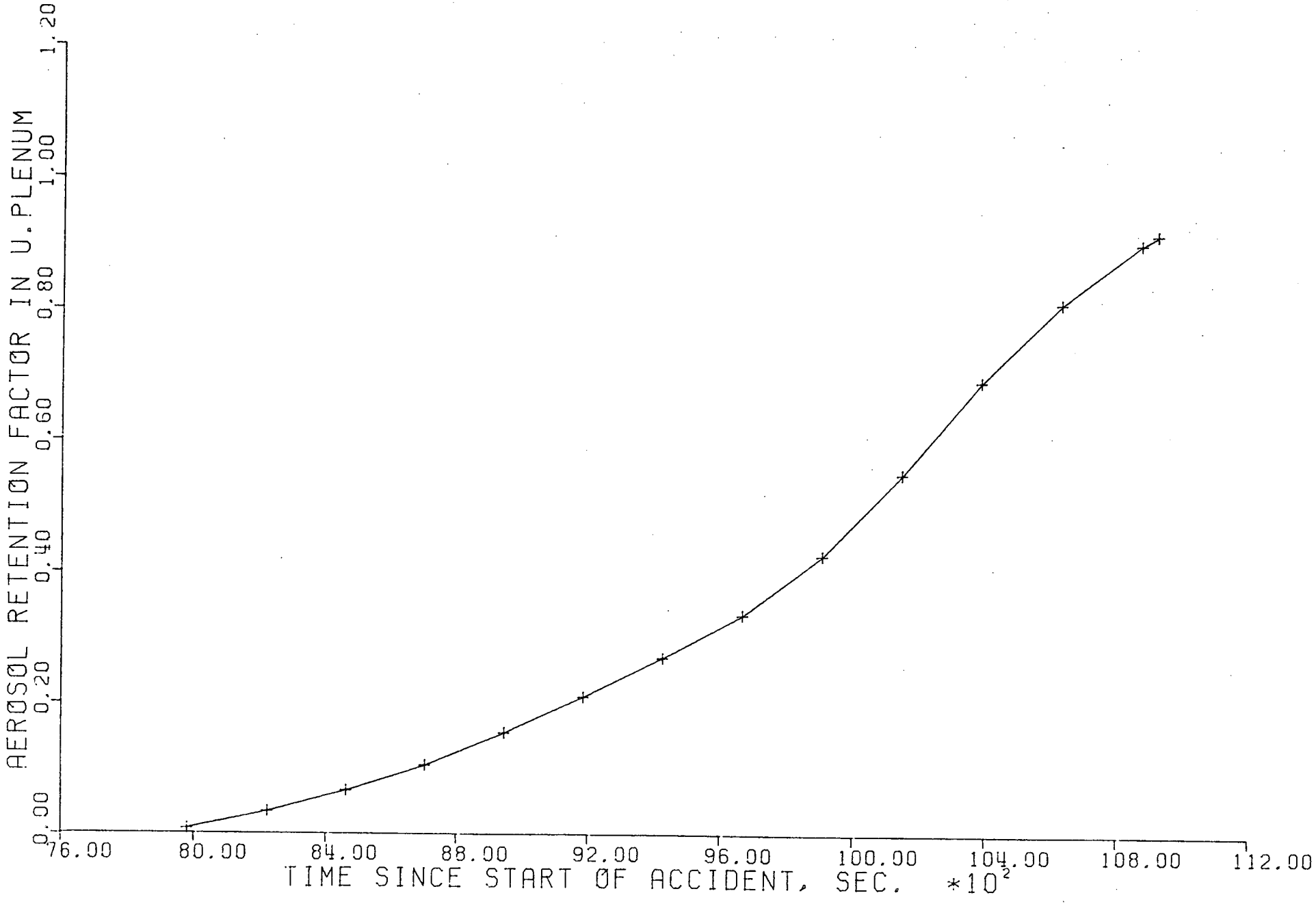
AERØSØL RETENTIØN FACTØR IN U.PLENUM
0.00
0.20
0.40
0.60
0.80
1.00
1.20
76.00
80.00
84.00
88.00
92.00
96.00
100.00
104.00
108.00
112.00
TIME SINCE START ØF ACCIDENT, SEC. *10²

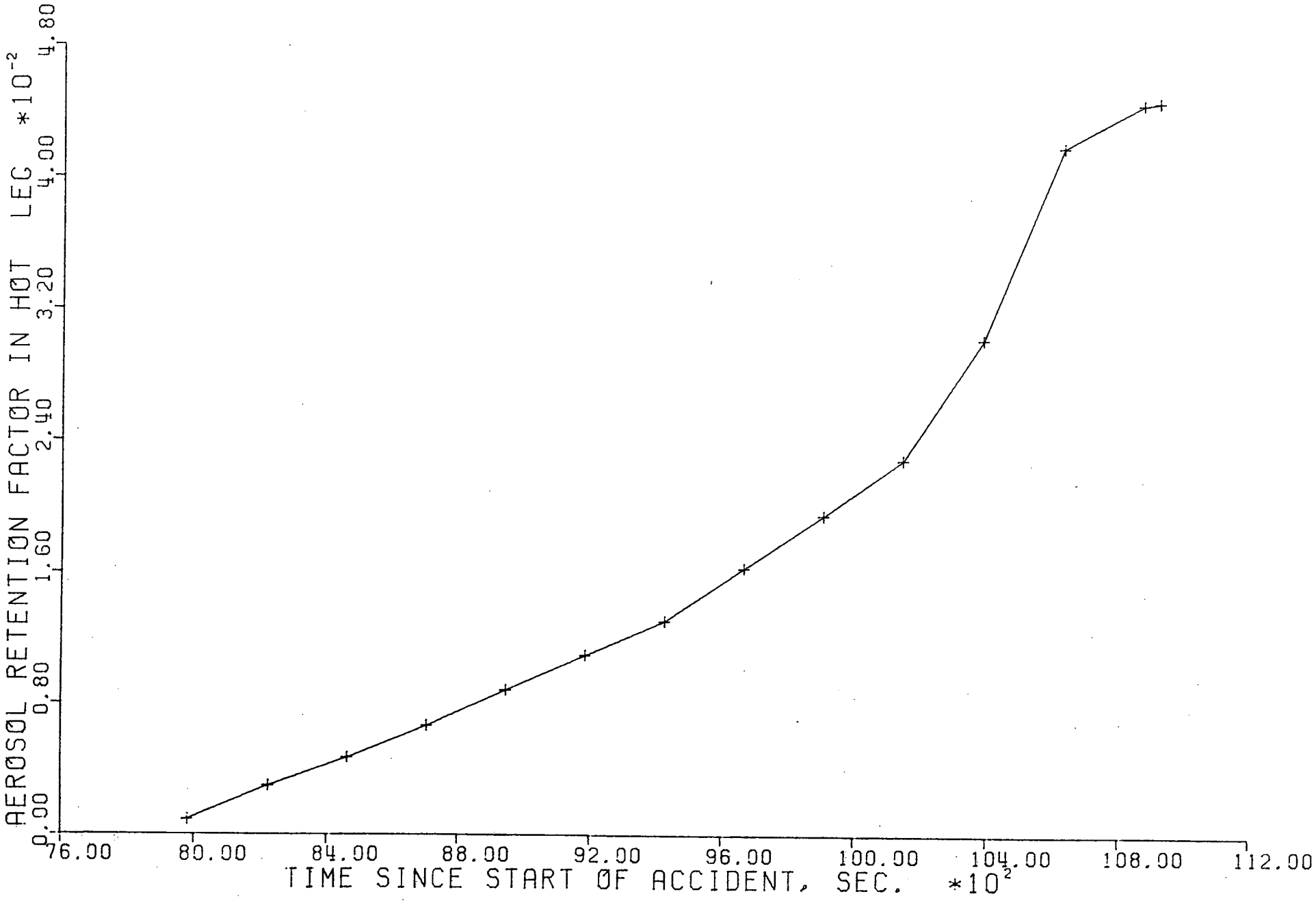
AEROSOL RETENTION FACTOR IN HOT LEG *10-2
0.00
0.80
1.60
2.40
3.20
4.00
4.80
76.00
80.00
84.00
88.00
92.00
96.00
100.00
104.00
108.00
112.00
TIME SINCE START OF ACCIDENT, SEC. *10²

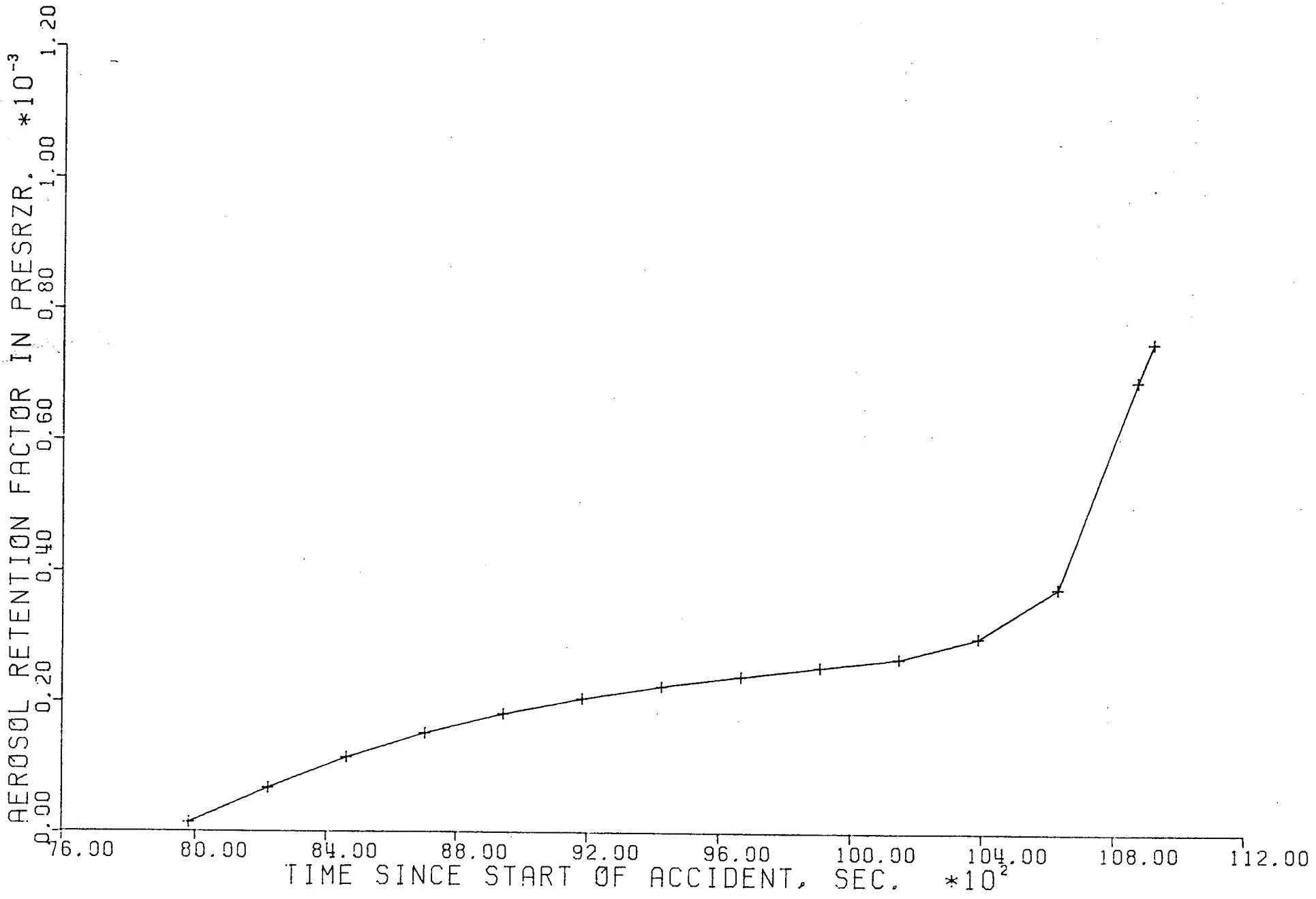
AEROSOL RETENTION FACTOR IN PRESRZR. *10-3
0.00
0.20
0.40
0.60
0.80
1.00
1.20
76.00
80.00
84.00
88.00
92.00
96.00
100.00
104.00
108.00
112.00
TIME SINCE START OF ACCIDENT, SEC. *10²

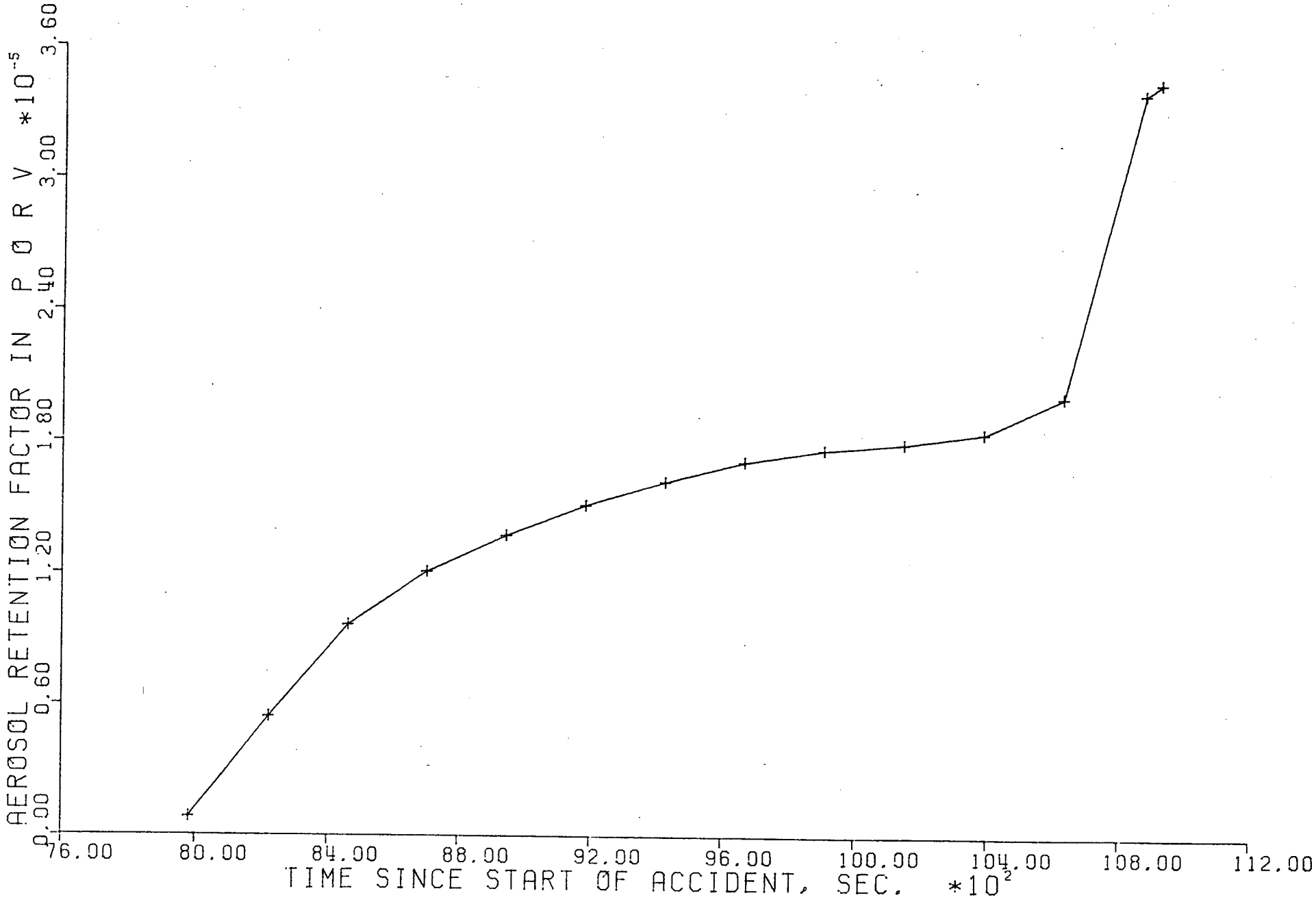
AEROSOL RETENTION FACTOR IN P Ø R V *10⁻⁵
0.00
0.60
1.20
1.80
2.40
3.00
3.60
76.00
80.00
84.00
88.00
92.00
96.00
100.00
104.00
108.00
112.00
TIME SINCE START OF ACCIDENT, SEC. *10²

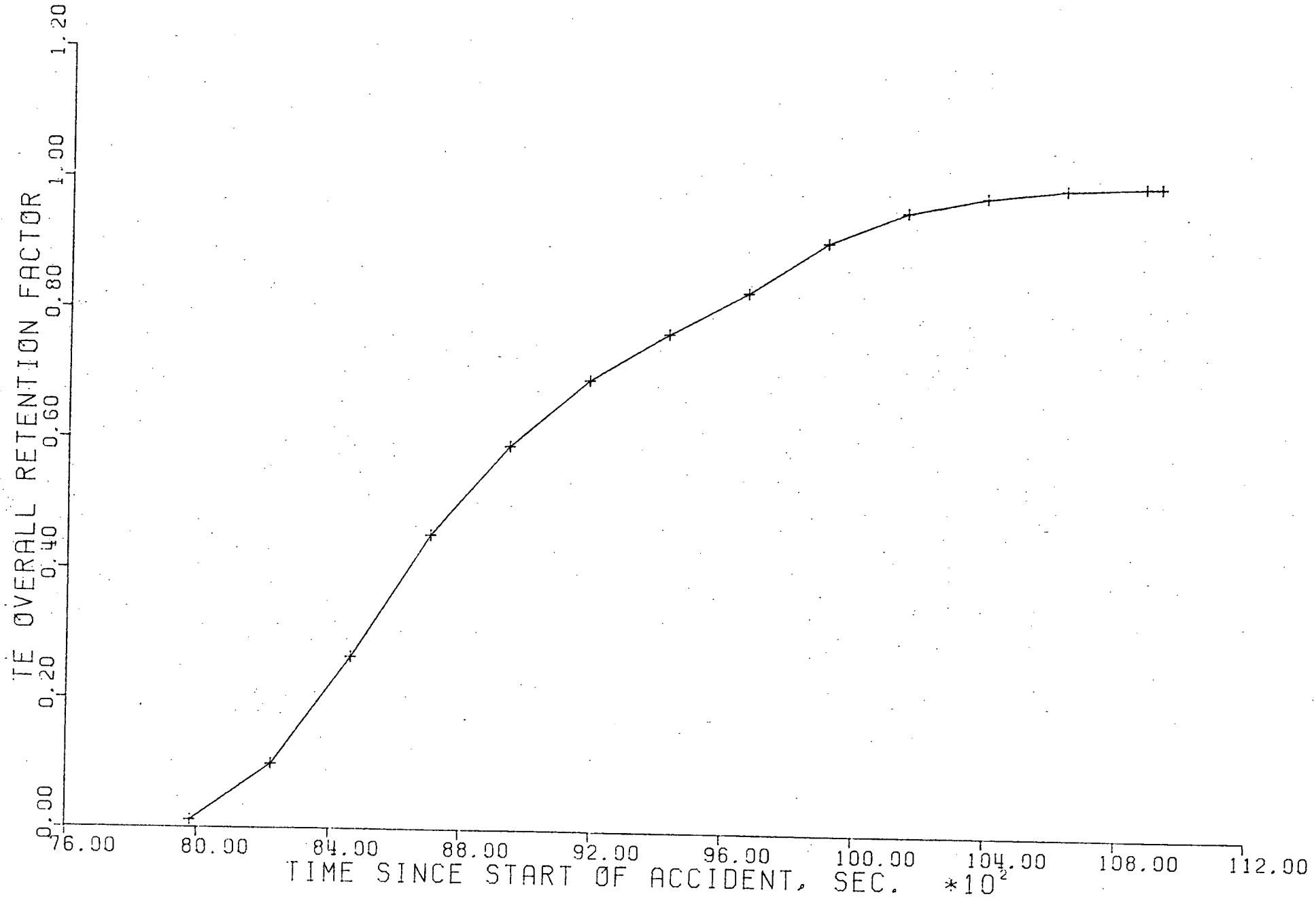
IE OVERALL RETENTION FACTOR
0.00
0.20
0.40
0.60
0.80
1.00
1.20
76.00
80.00
84.00
88.00
92.00
96.00
100.00
104.00
108.00
112.00
TIME SINCE START OF ACCIDENT, SEC. *10²

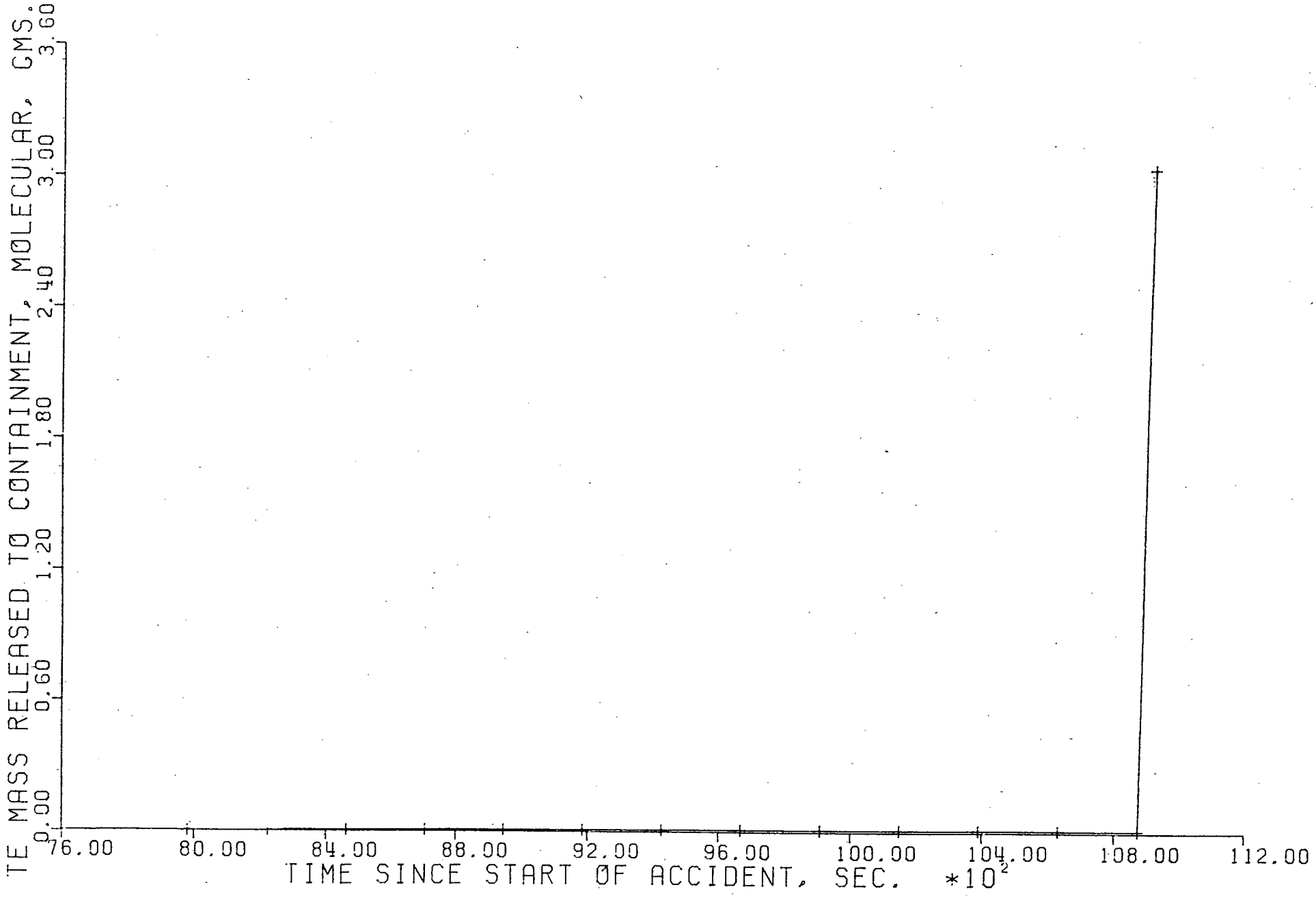
TE MASS RELEASED TO CONTAINMENT, MOLECULAR, GMS.
0.00
0.60
1.20
1.80
2.40
3.00
3.60
76.00
80.00
84.00
88.00
92.00
96.00
100.00
104.00
108.00
112.00
TIME SINCE START OF ACCIDENT, SEC. *10²

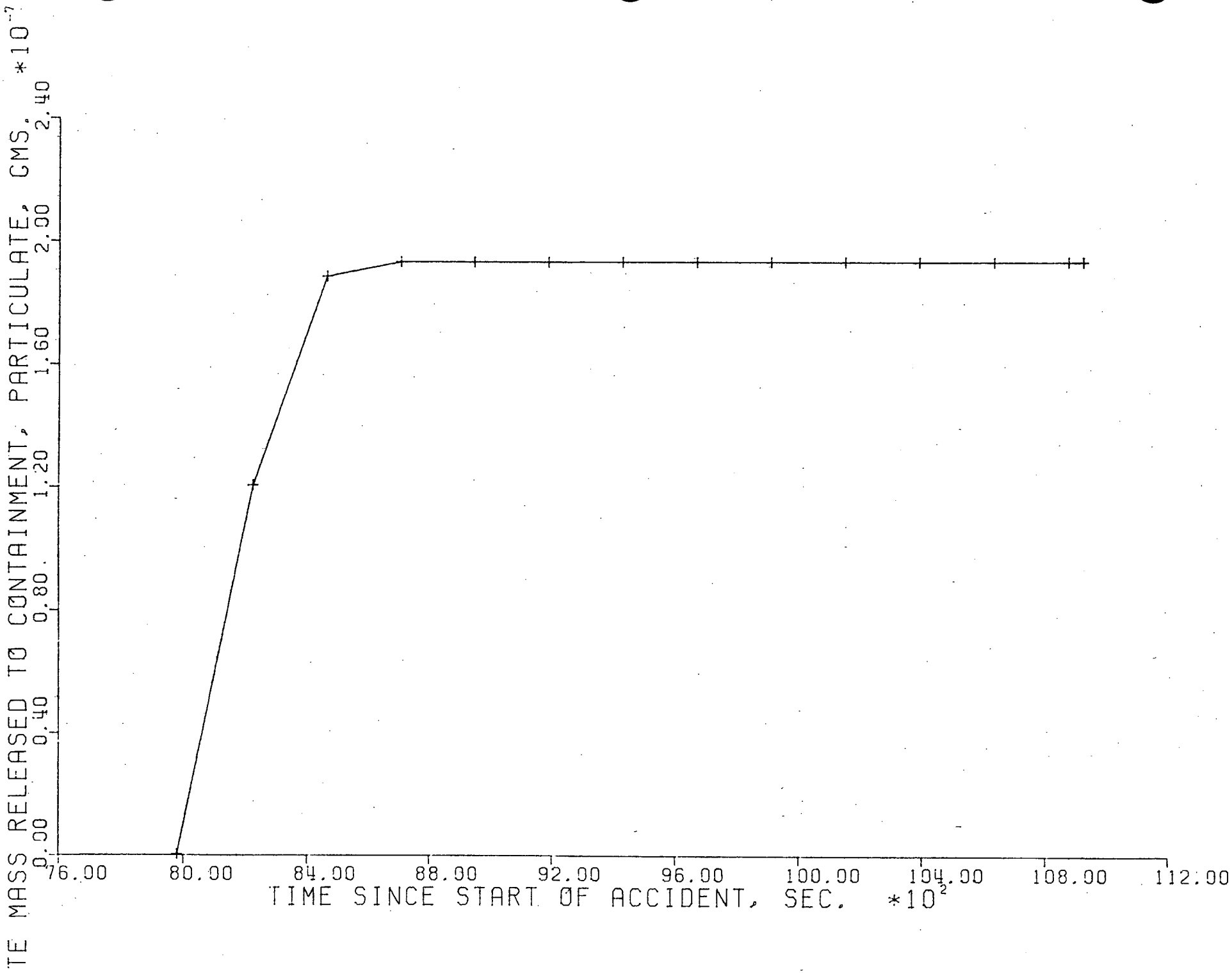
TE MASS RELEASED TO CONTAINMENT, PARTICULATE, CMS. *10⁻⁷
0.00
0.40
0.80
1.20
1.60
2.00
2.40
76.00
80.00
84.00
88.00
92.00
96.00
100.00
104.00
108.00
112.00
TIME SINCE START OF ACCIDENT, SEC. *10²

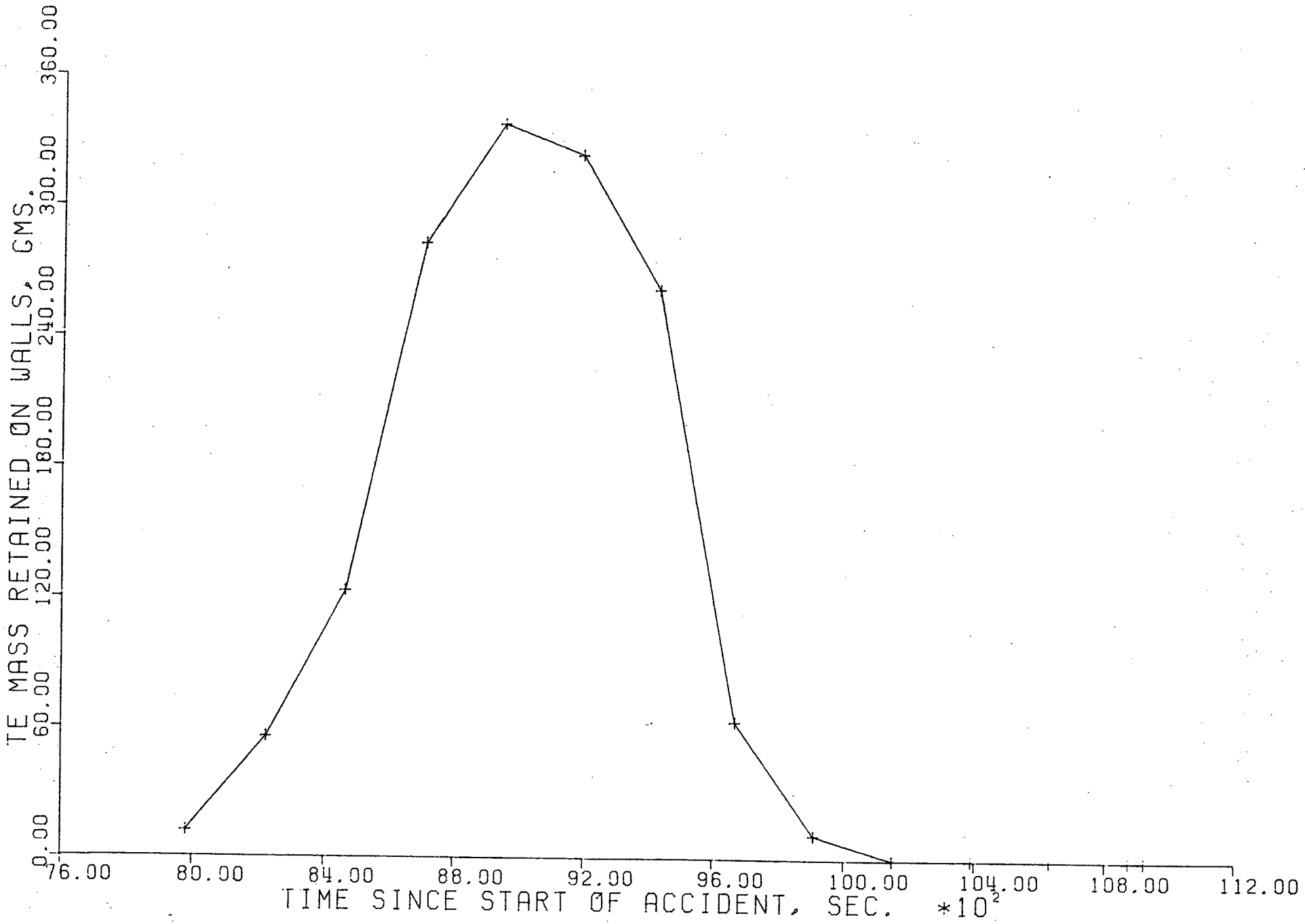
TE MASS RETAINED ON WALLS, GMS.
0.00
60.00
120.00
180.00
240.00
300.00
360.00
76.00
80.00
84.00
88.00
92.00
96.00
100.00
104.00
108.00
112.00
TIME SINCE START OF ACCIDENT, SEC. *10²

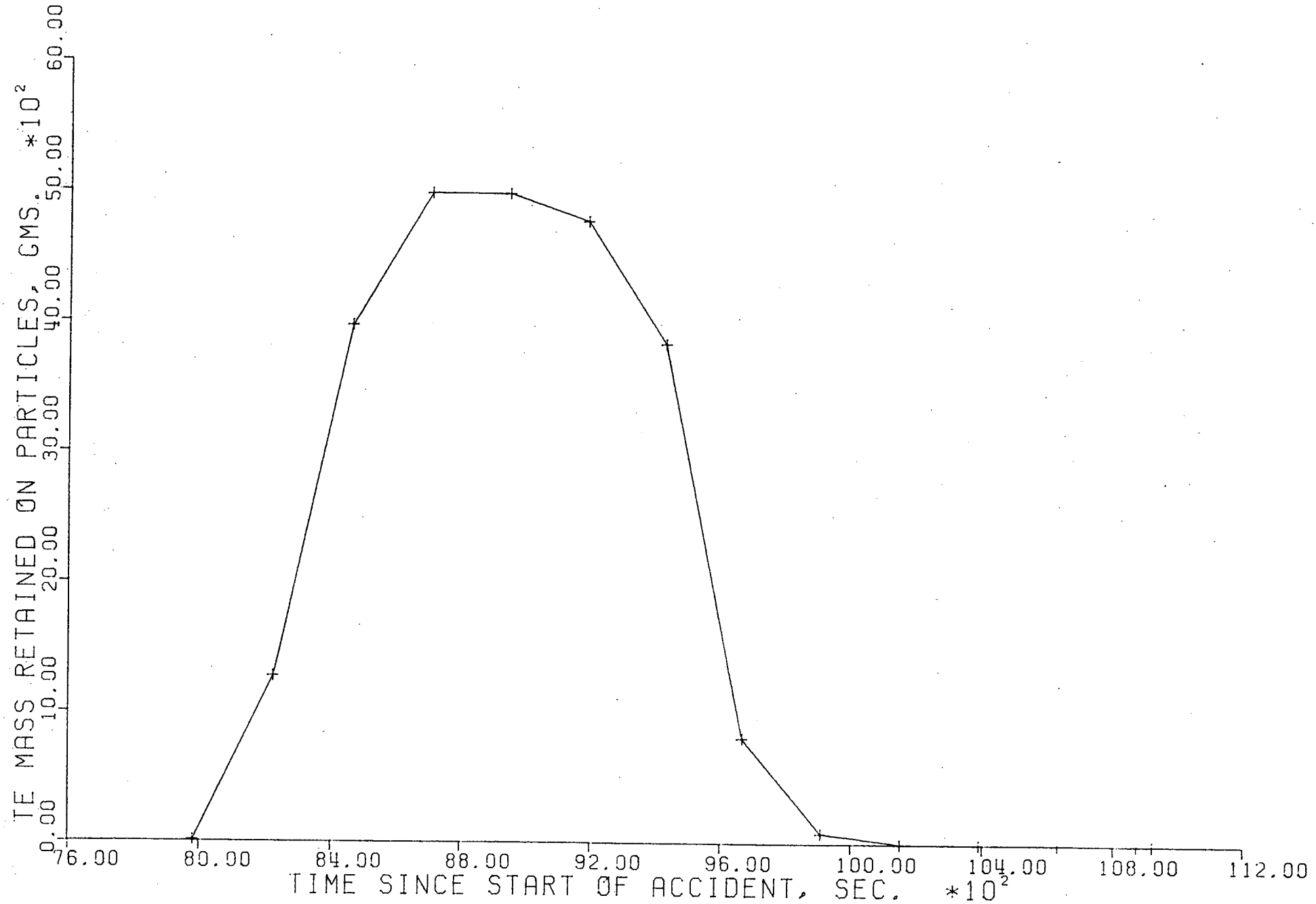
TE MASS RETAINED ON PARTICLES, GMS. *10²
0.00
10.00
20.00
30.00
40.00
50.00
60.00
76.00
80.00
84.00
88.00
92.00
96.00
100.00
104.00
108.00
112.00
TIME SINCE START OF ACCIDENT, SEC. *10²

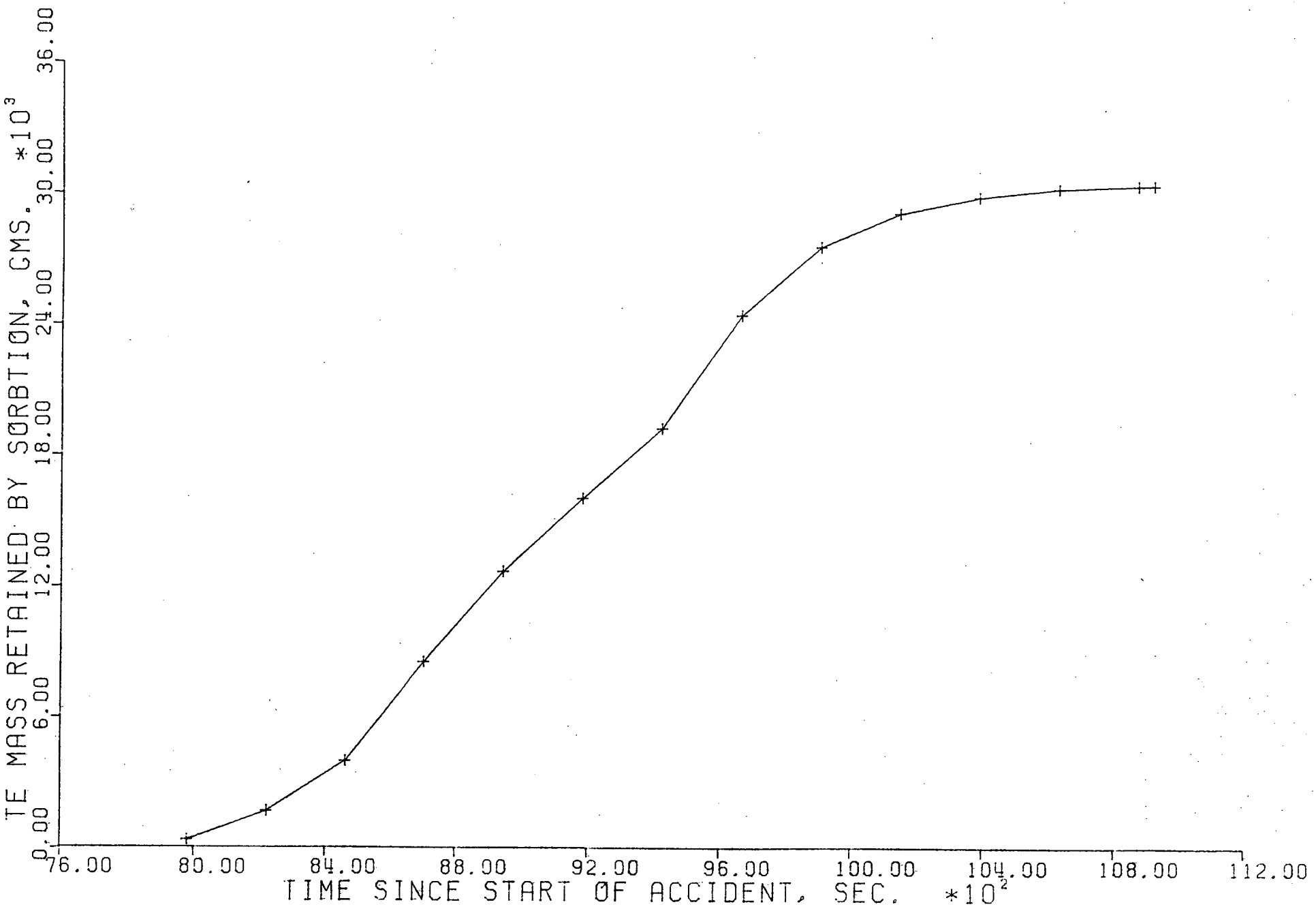
TE MASS RETAINED BY SORBTION, CMS. *10^3
0.00
6.00
12.00
18.00
24.00
30.00
36.00
76.00
80.00
84.00
88.00
92.00
96.00
100.00
104.00
108.00
112.00
TIME SINCE START OF ACCIDENT, SEC. *10^2

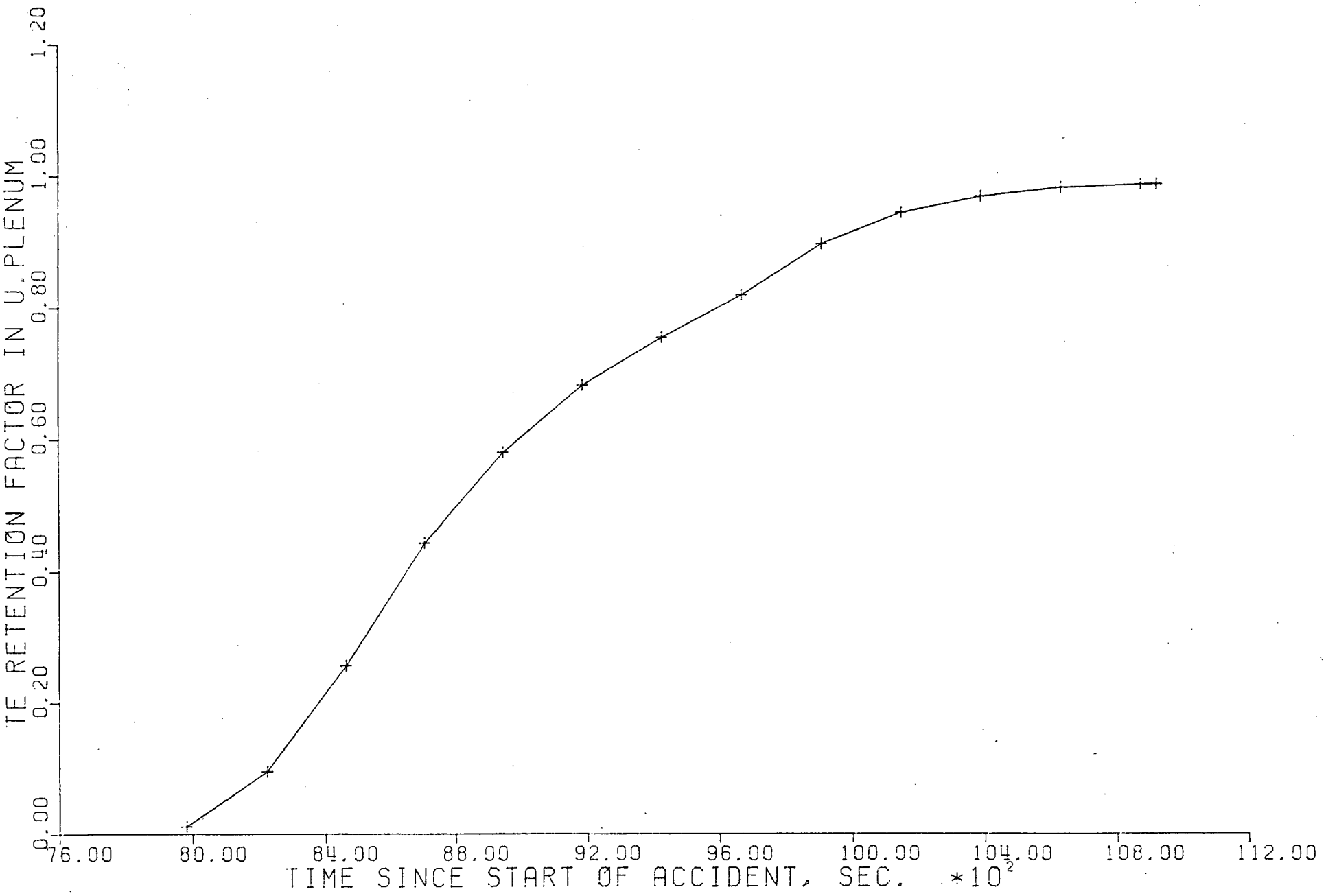
TE RETENTION FACTOR IN U.PLENUM
0.00
0.20
0.40
0.60
0.80
1.00
1.20
76.00
80.00
84.00
88.00
92.00
96.00
100.00
104.00
108.00
112.00
TIME SINCE START OF ACCIDENT, SEC. *10²

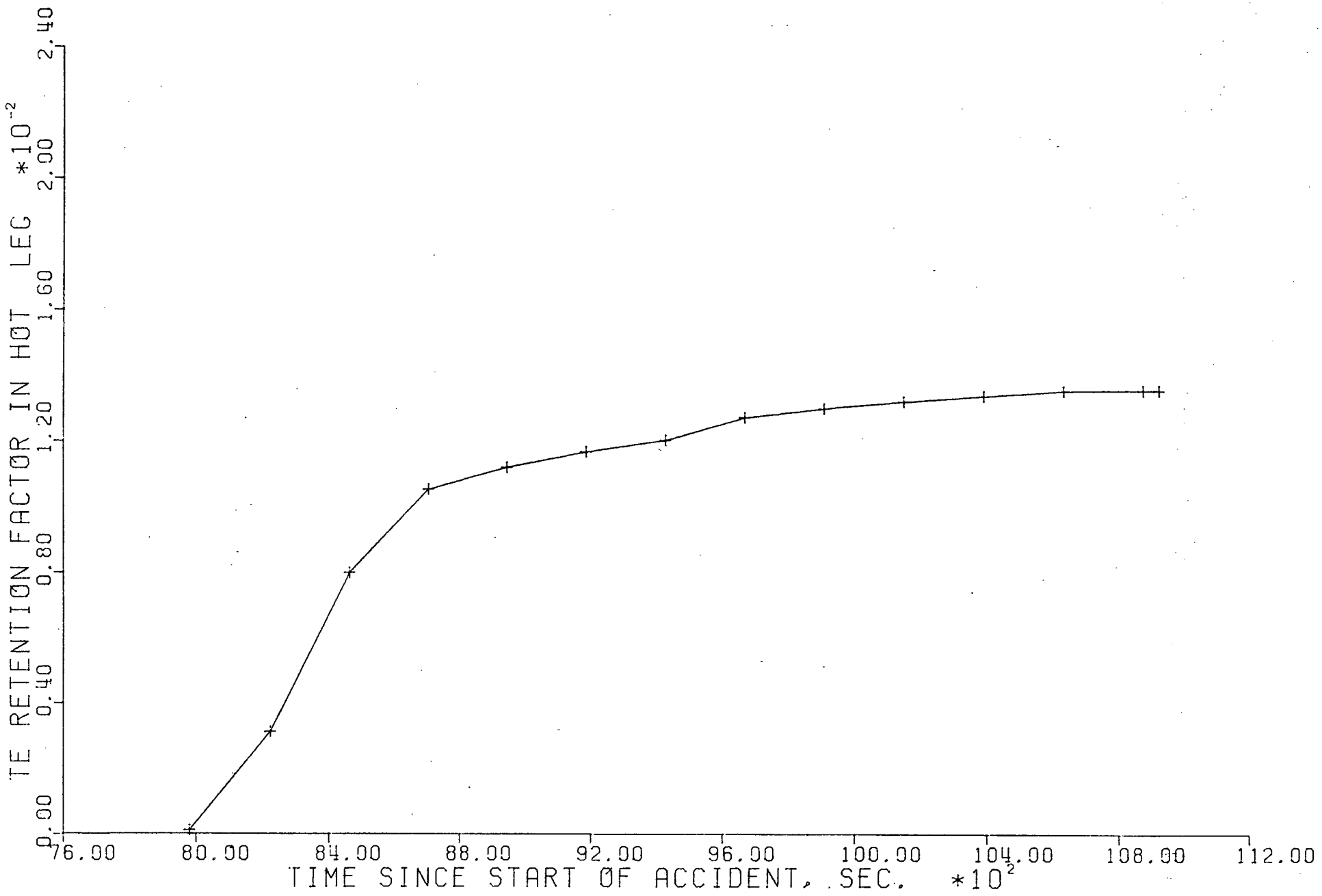
TE RETENTION FACTOR IN HOT LEG *10^-2
0.00
0.40
0.80
1.20
1.60
2.00
2.40
76.00
80.00
84.00
88.00
92.00
96.00
100.00
104.00
108.00
112.00
TIME SINCE START OF ACCIDENT, SEC. *10^2

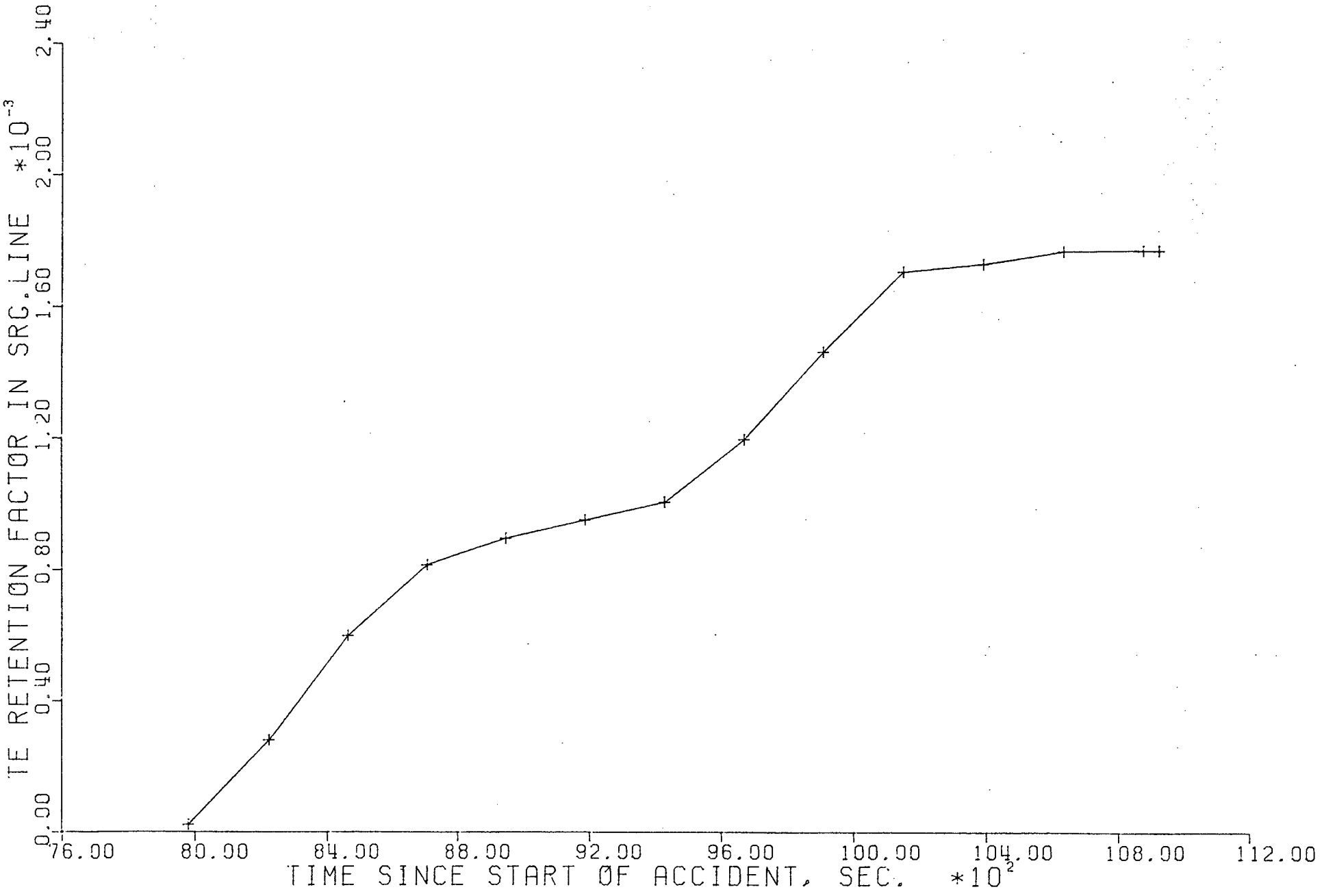
IE RETENTION FACTOR IN SRC.LINE *10^-3
0.00
0.40
0.80
1.20
1.60
2.00
2.40
76.00
80.00
84.00
88.00
92.00
96.00
100.00
104.00
108.00
112.00
TIME SINCE START OF ACCIDENT, SEC. *10^2

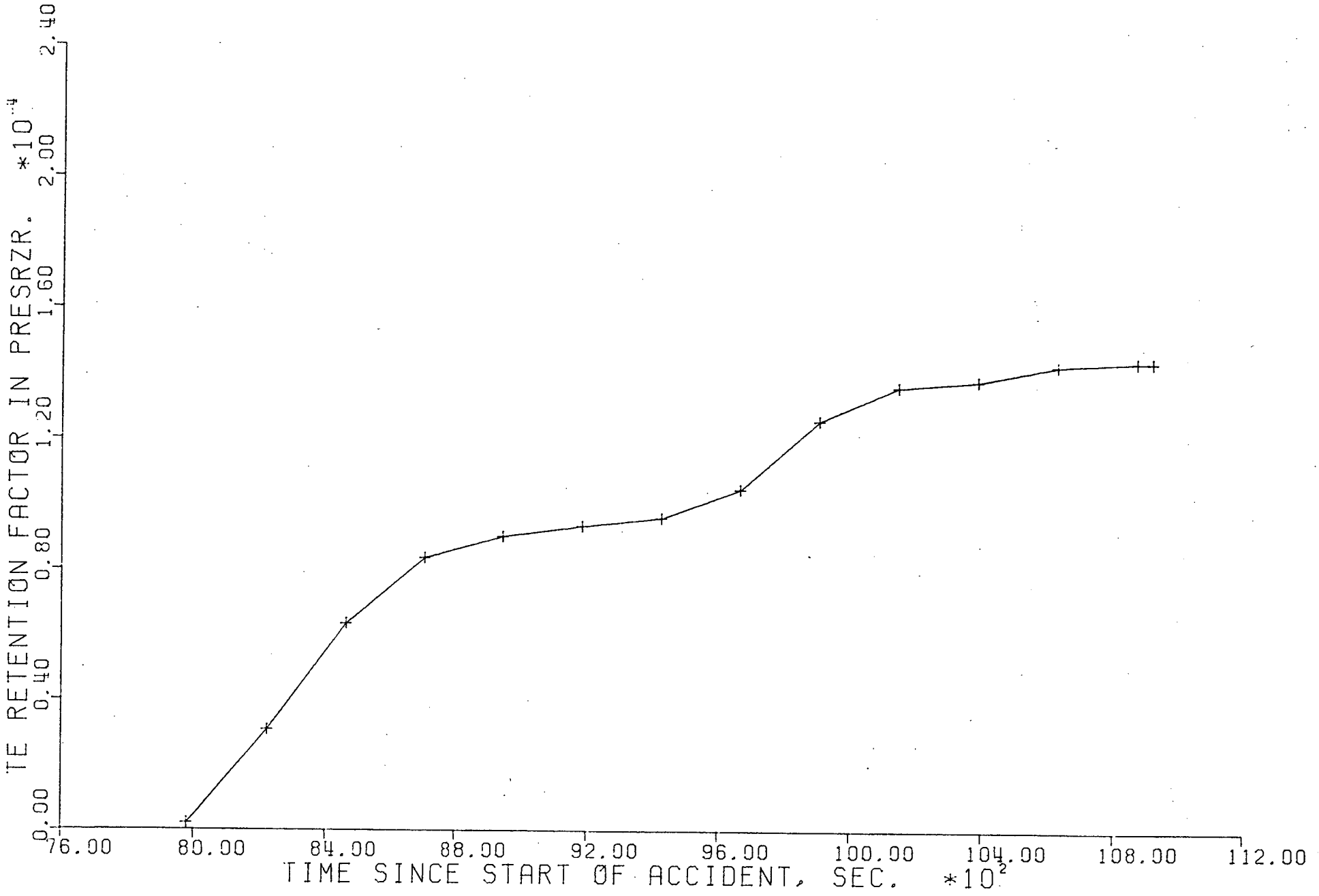
TE RETENTION FACTOR IN PRESRZR. *10⁻⁴
0.00
0.40
0.80
1.20
1.60
2.00
2.40
76.00
80.00
84.00
88.00
92.00
96.00
100.00
104.00
108.00
112.00
TIME SINCE START OF ACCIDENT, SEC. *10²

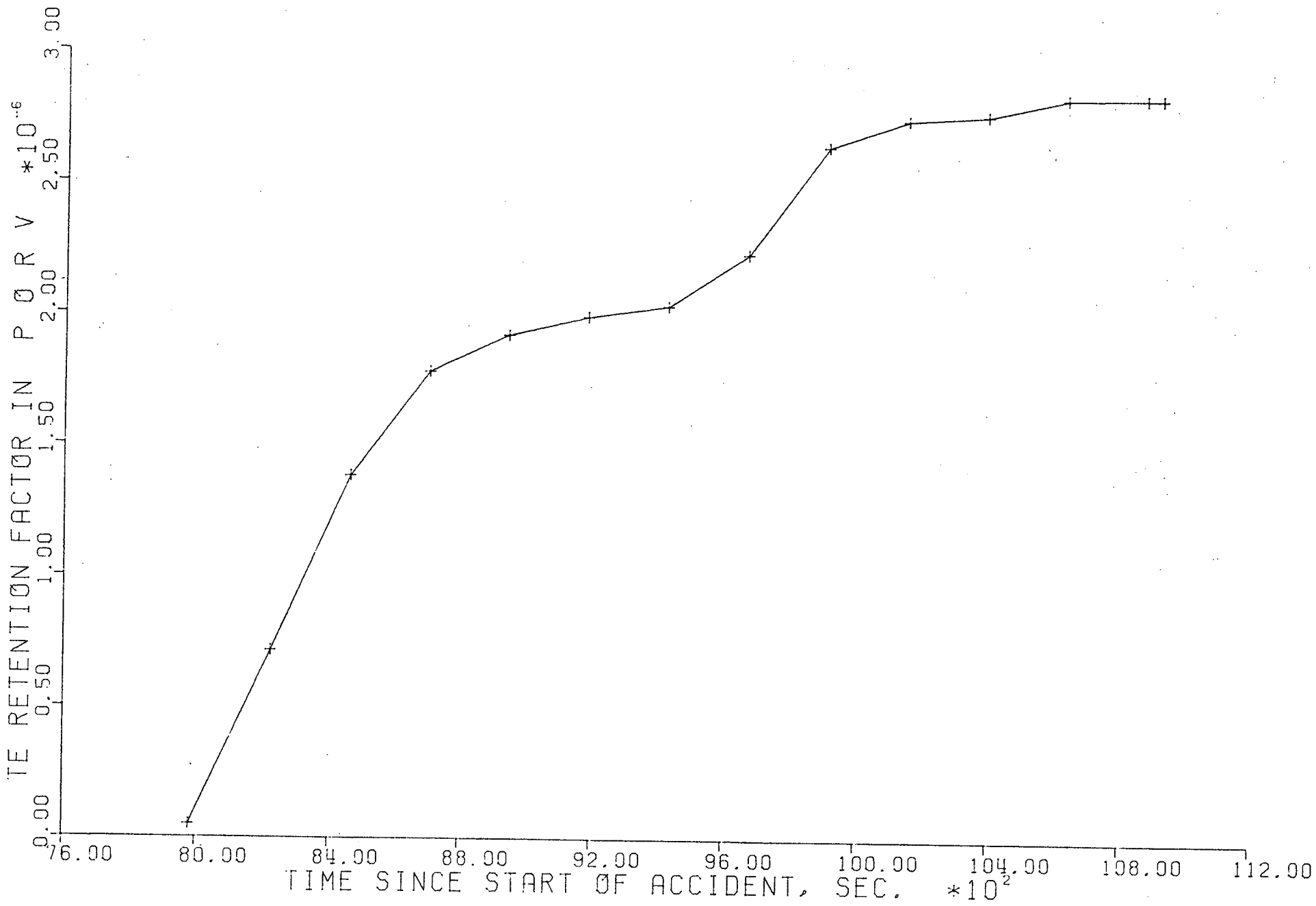
TE RETENTION FACTOR IN P Ø R V *10^-6
0.00
0.50
1.00
1.50
2.00
2.50
3.00
76.00
80.00
84.00
88.00
92.00
96.00
100.00
104.00
108.00
112.00
TIME SINCE START ØF ACCIDENT, SEC. *10^2

Section 5.2 Figures

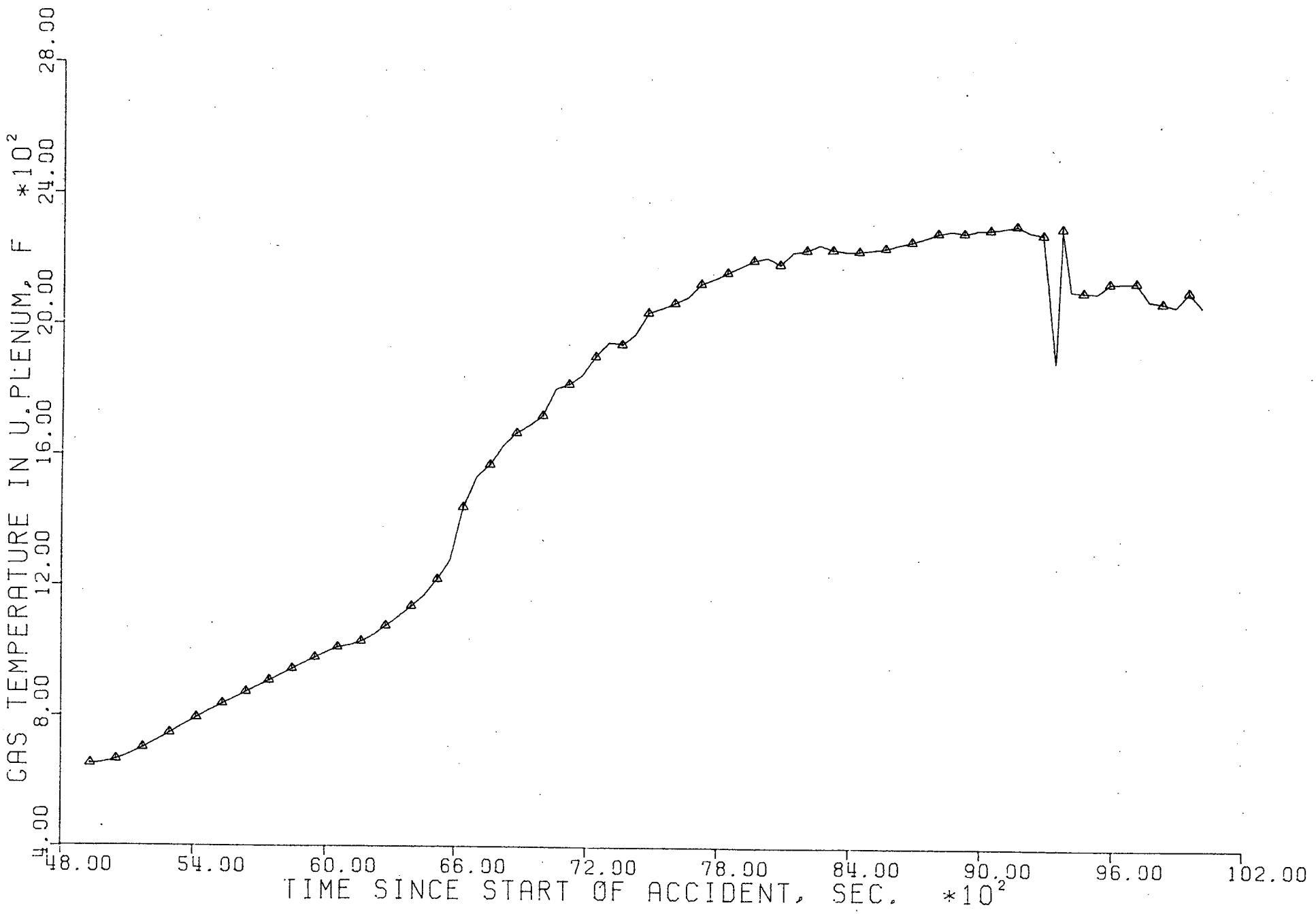
GAS TEMPERATURE IN U.PLENUM, F *10²
4.00
8.00
12.00
16.00
20.00
24.00
28.00
48.00
54.00
60.00
66.00
72.00
78.00
84.00
90.00
96.00
102.00
TIME SINCE START OF ACCIDENT, SEC. *10²

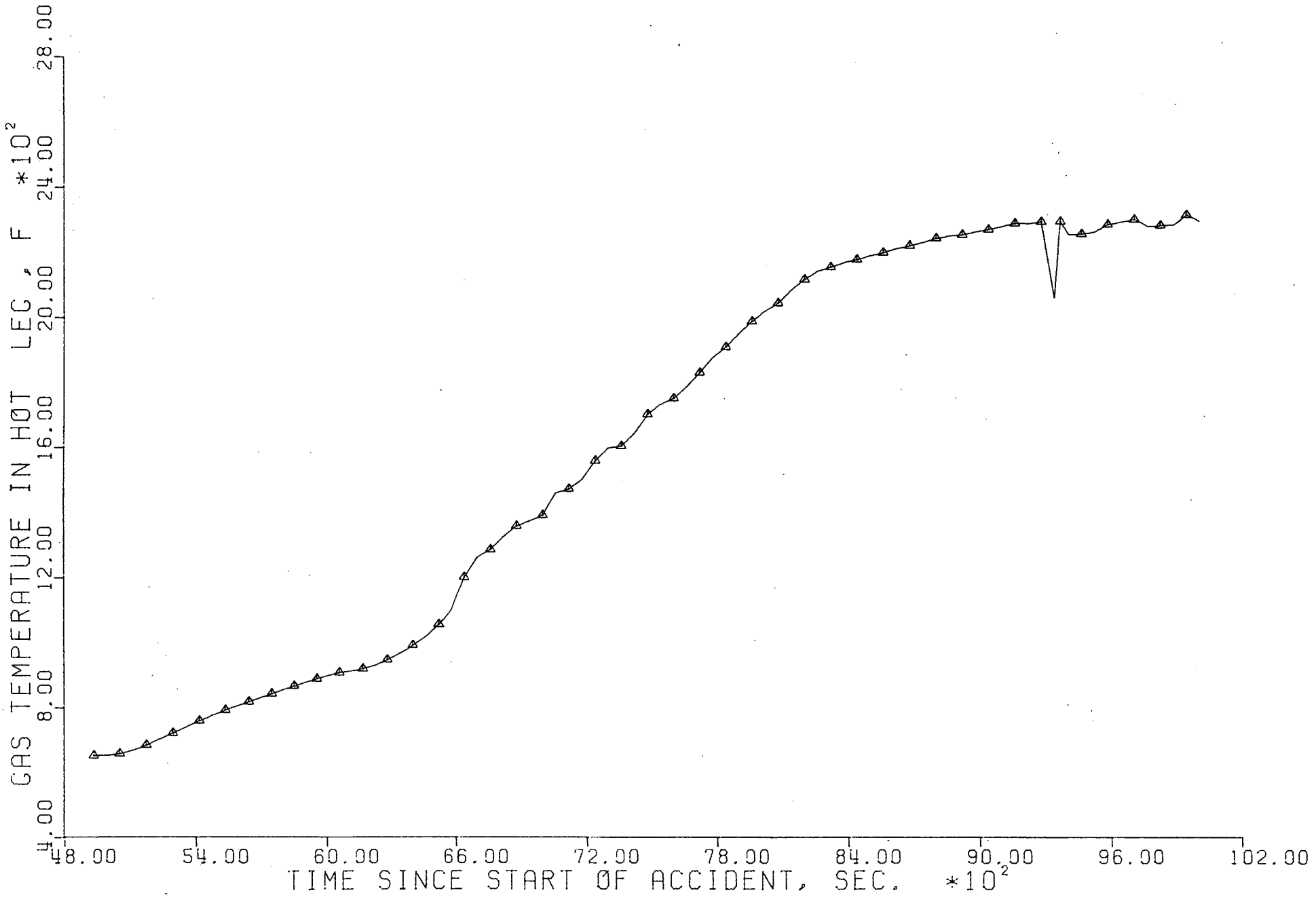
GAS TEMPERATURE IN HOT LEG, F *10²
4.00
8.00
12.00
16.00
20.00
24.00
28.00
48.00
54.00
60.00
66.00
72.00
78.00
84.00
90.00
96.00
102.00
TIME SINCE START OF ACCIDENT, SEC. *10²

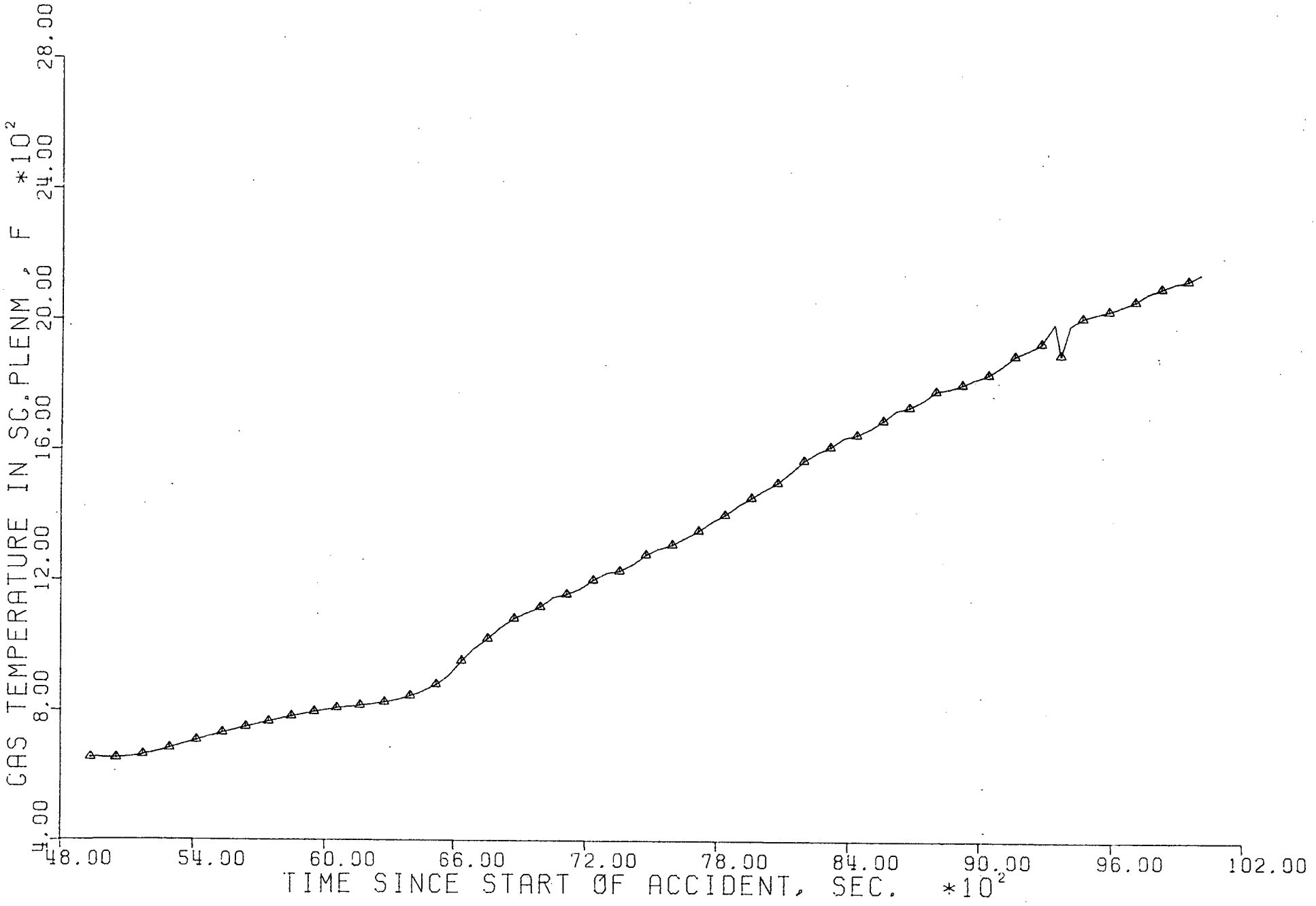
GAS TEMPERATURE IN SC. PLENM., F *10²
4.00
8.00
12.00
16.00
20.00
24.00
28.00
48.00
54.00
60.00
66.00
72.00
78.00
84.00
90.00
96.00
102.00
TIME SINCE START OF ACCIDENT, SEC. *10²

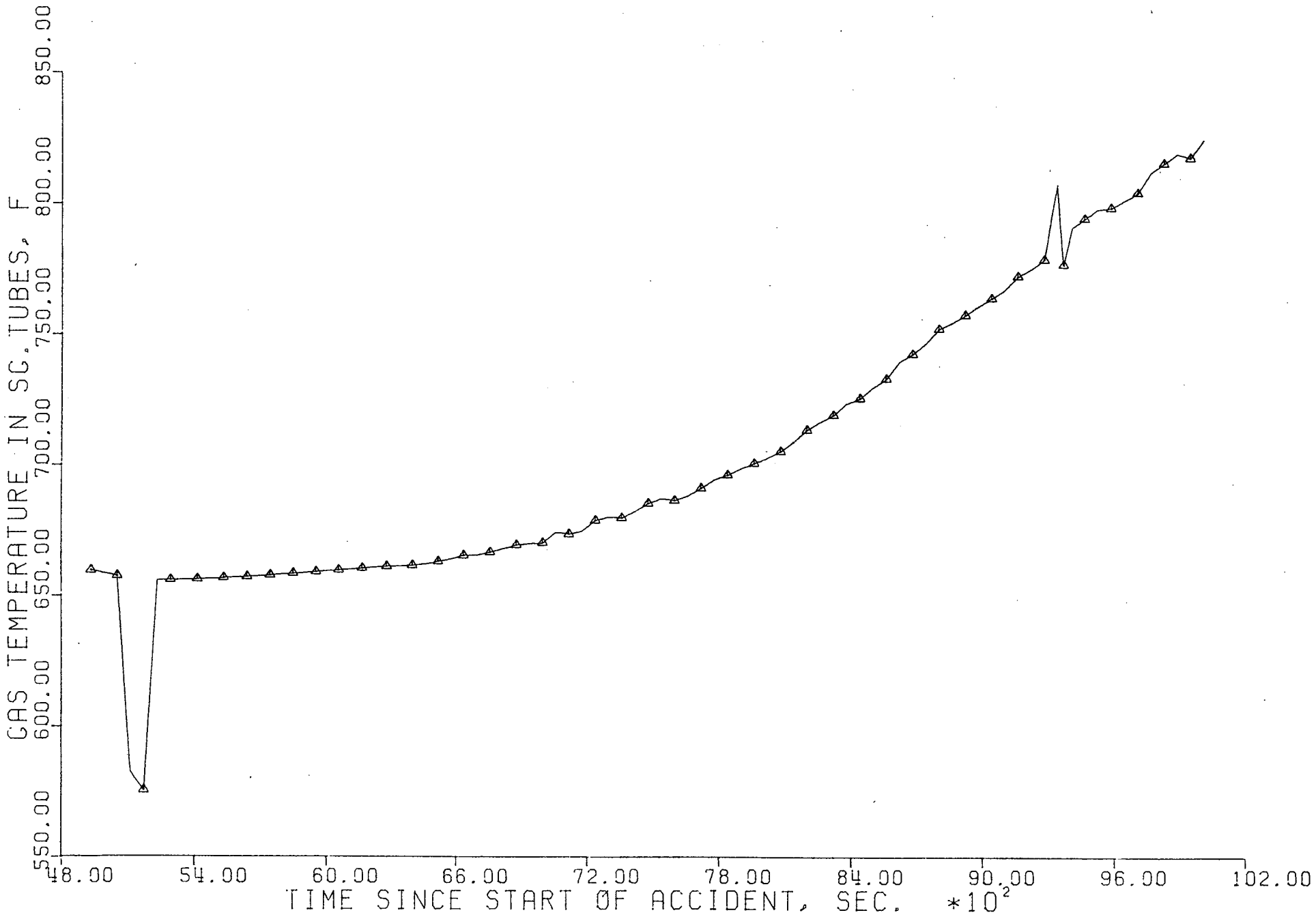
GAS TEMPERATURE IN SG. TUBES, F
850.00
800.00
750.00
700.00
650.00
600.00
550.00
48.00
54.00
60.00
66.00
72.00
78.00
84.00
90.00
96.00
102.00
TIME SINCE START OF ACCIDENT, SEC. *10²

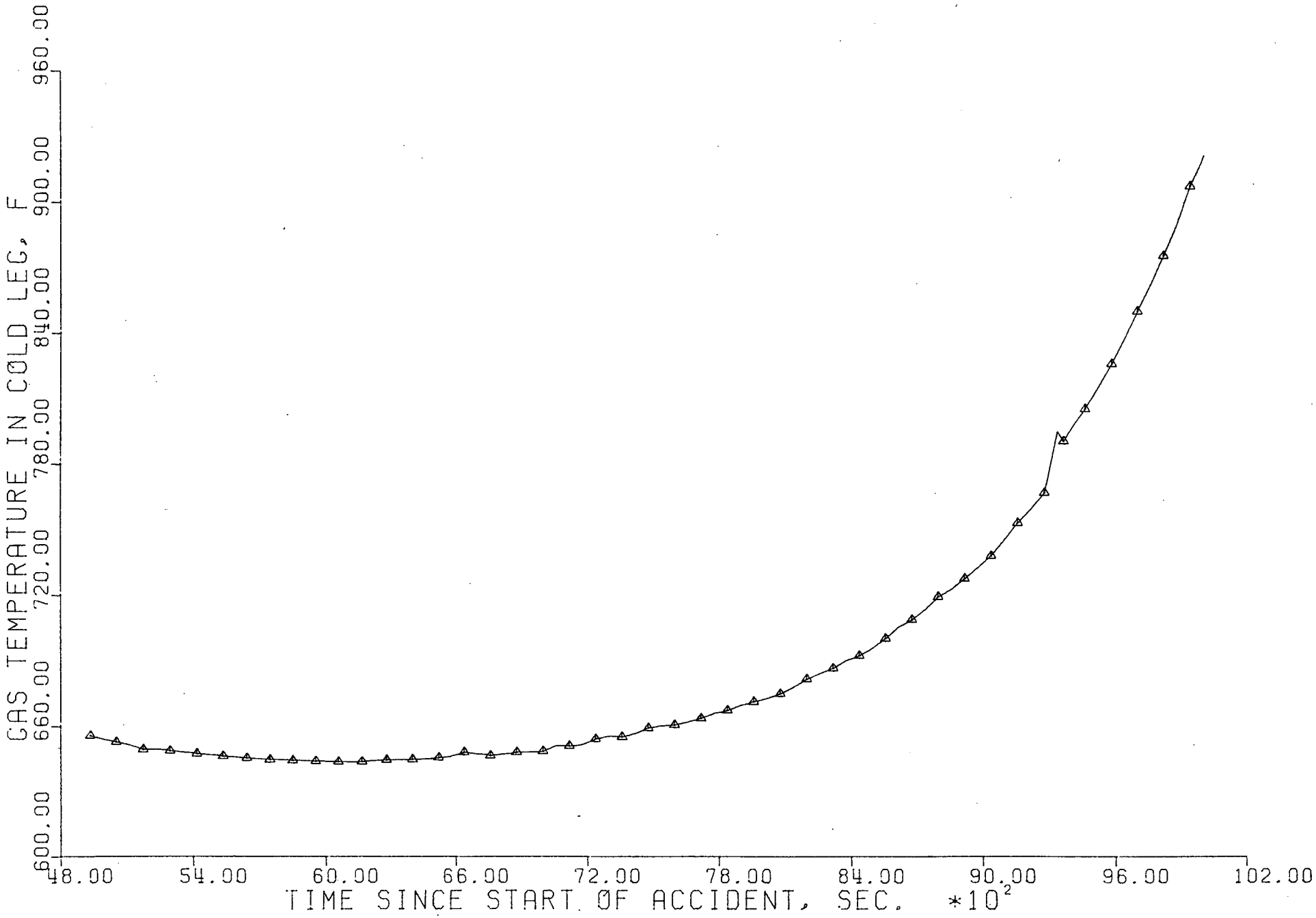
GAS TEMPERATURE IN COLD LEG, F
600.00
660.00
720.00
780.00
840.00
900.00
960.00
48.00
54.00
60.00
66.00
72.00
78.00
84.00
90.00
96.00
102.00
TIME SINCE START OF ACCIDENT, SEC. *10²

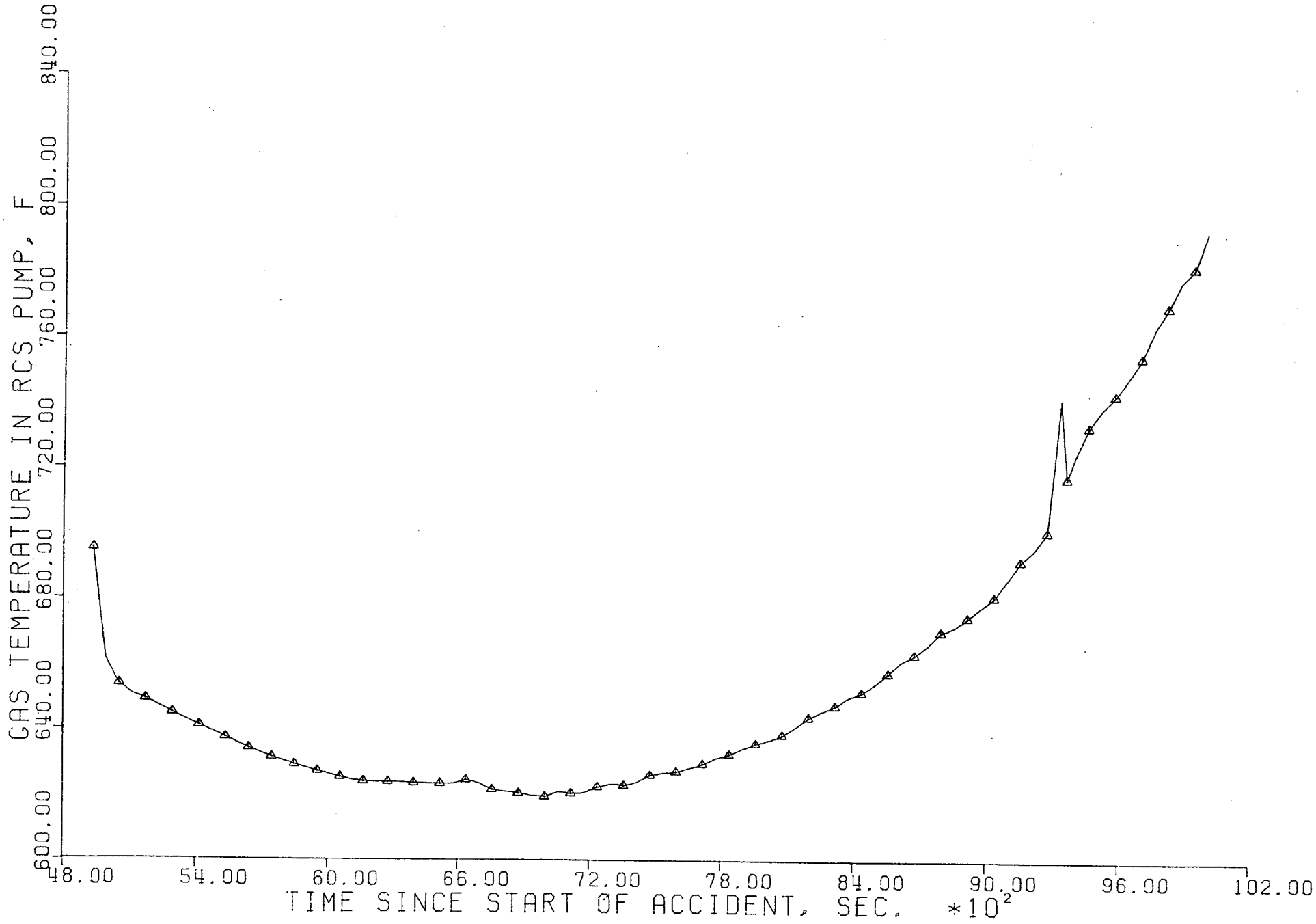
GAS TEMPERATURE IN RCS PUMP, F
600.00
640.00
680.00
720.00
760.00
800.00
840.00
48.00
54.00
60.00
66.00
72.00
78.00
84.00
90.00
96.00
102.00
TIME SINCE START OF ACCIDENT, SEC. *10²

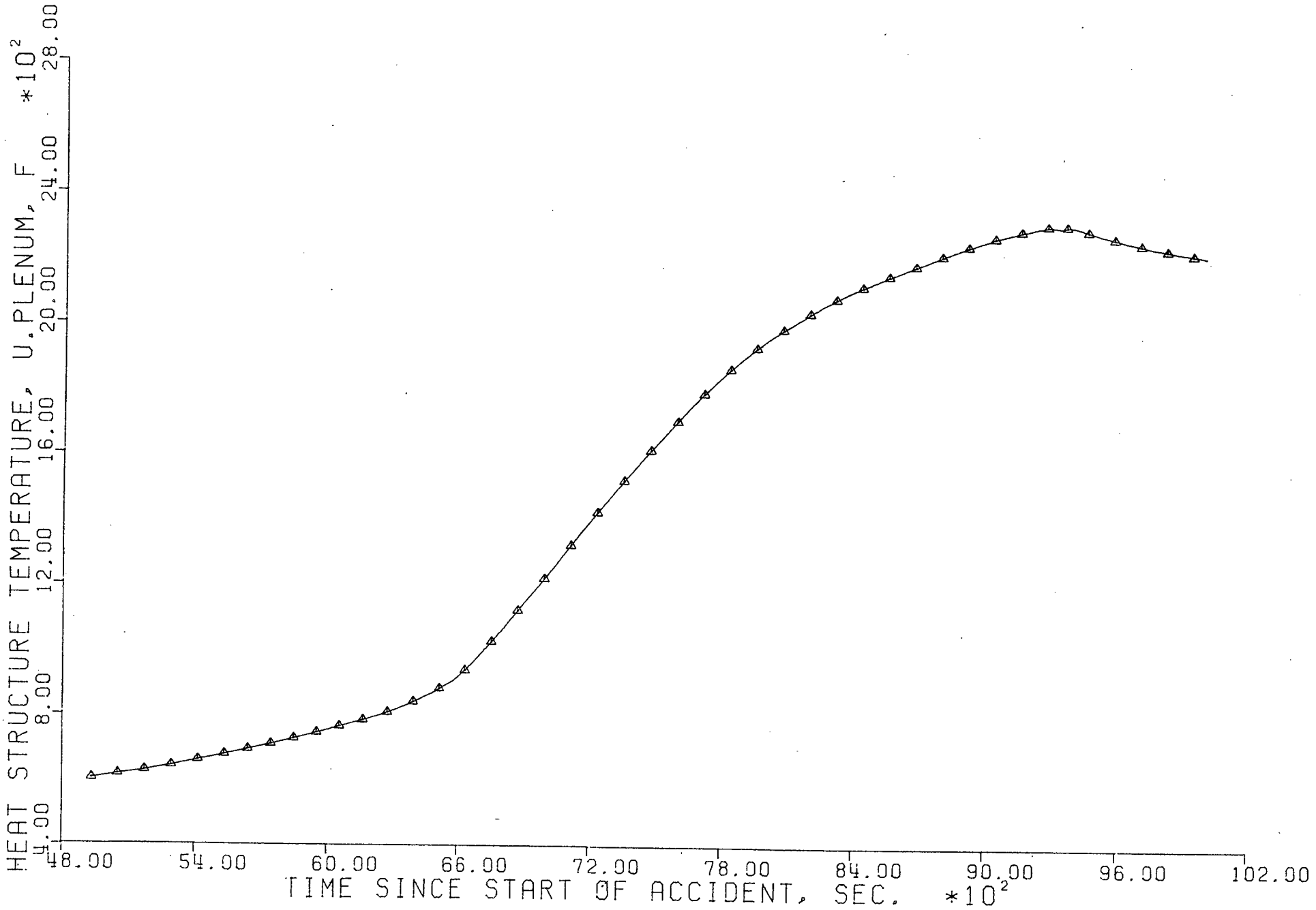
HEAT STRUCTURE TEMPERATURE, U.PLENUM, F *10²
4.00
8.00
12.00
16.00
20.00
24.00
28.00
48.00
54.00
60.00
66.00
72.00
78.00
84.00
90.00
96.00
102.00
TIME SINCE START OF ACCIDENT, SEC. *10²

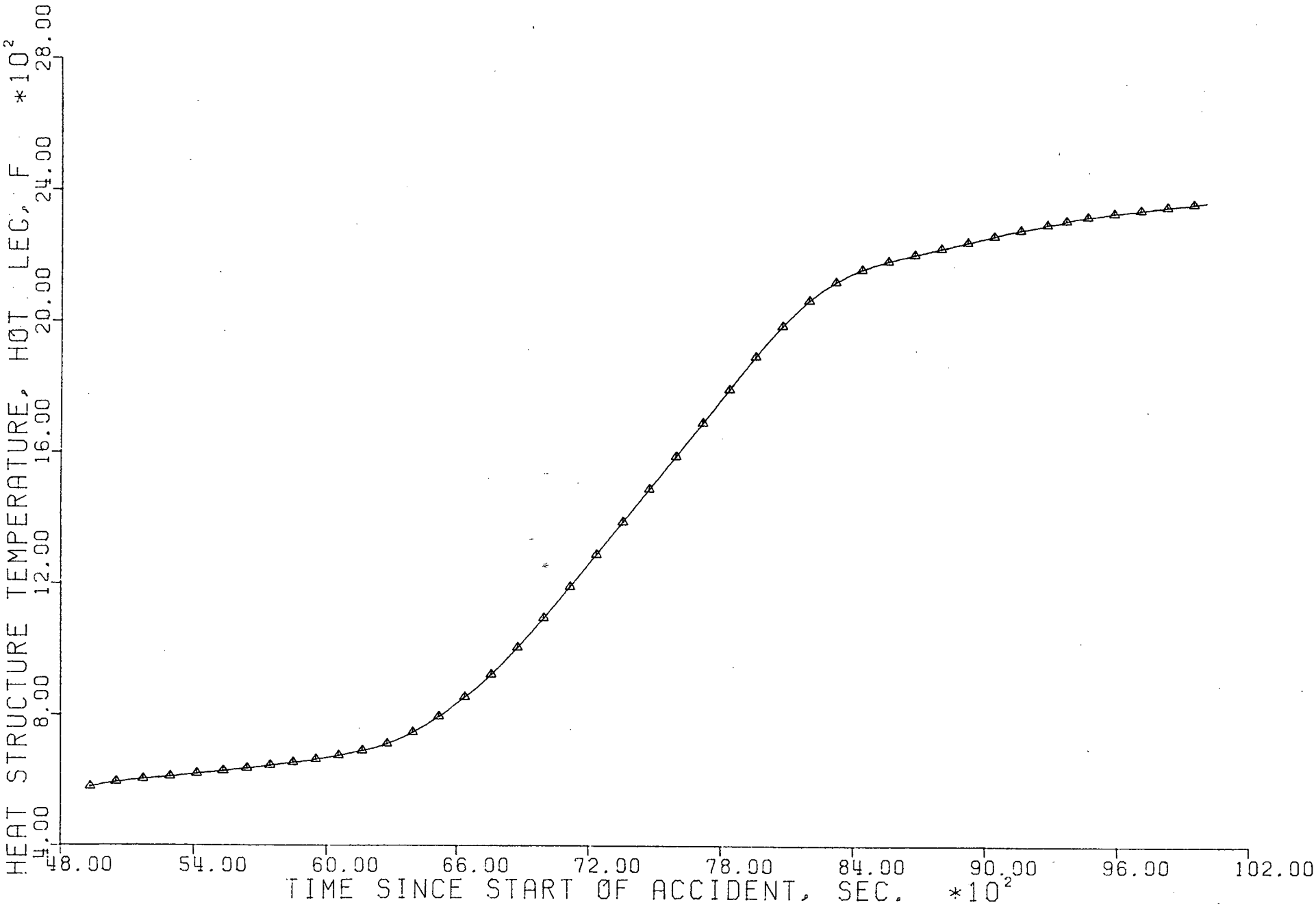
HEAT STRUCTURE TEMPERATURE, HOT LEG, F *10²
4.00
8.00
12.00
16.00
20.00
24.00
28.00
48.00
54.00
60.00
66.00
72.00
78.00
84.00
90.00
96.00
102.00
TIME SINCE START OF ACCIDENT, SEC. *10²

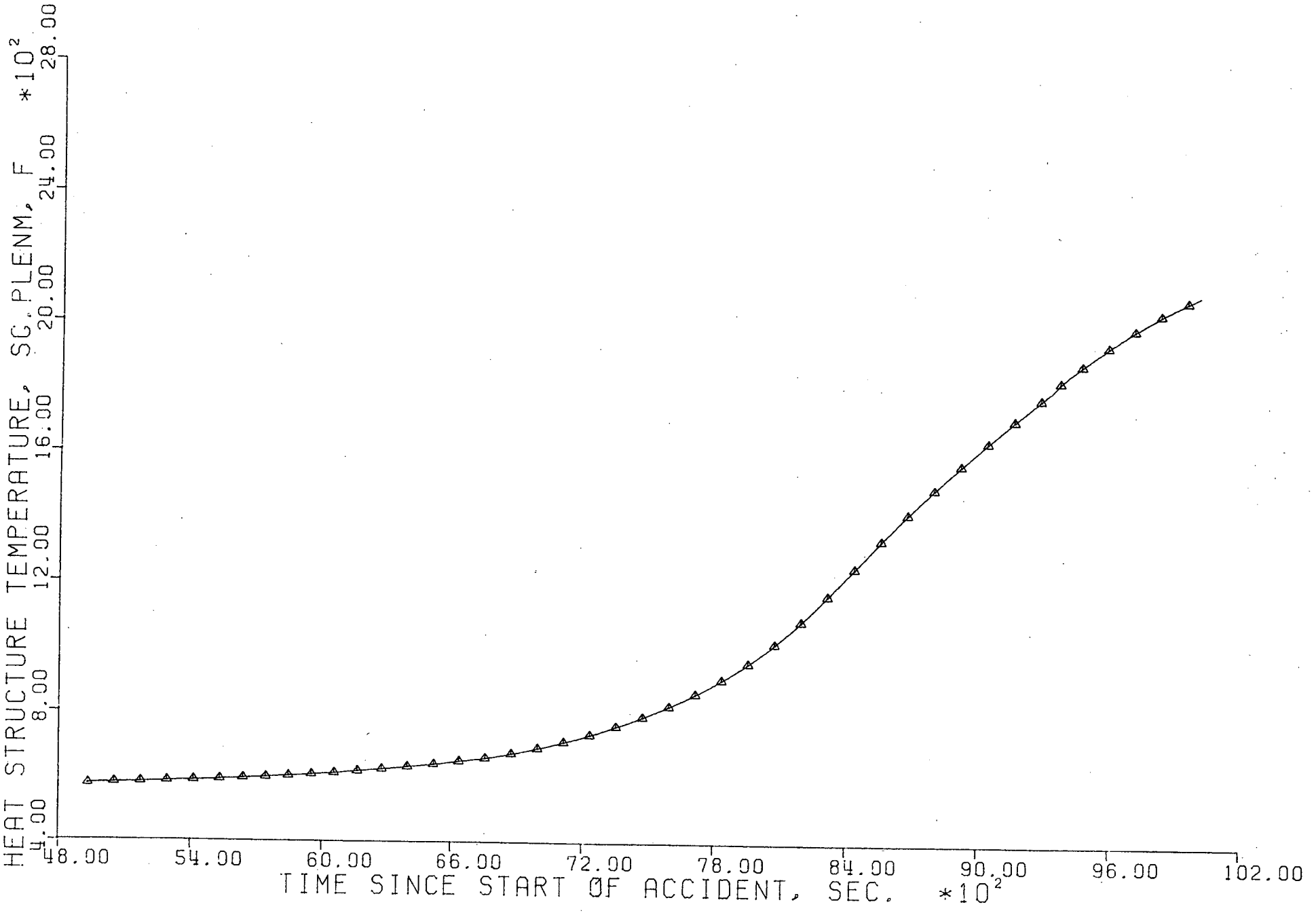
HEAT STRUCTURE TEMPERATURE, SC. PLENM, F *10²
4.00
8.00
12.00
16.00
20.00
24.00
28.00
48.00
54.00
60.00
66.00
72.00
78.00
84.00
90.00
96.00
102.00
TIME SINCE START OF ACCIDENT, SEC. *10²

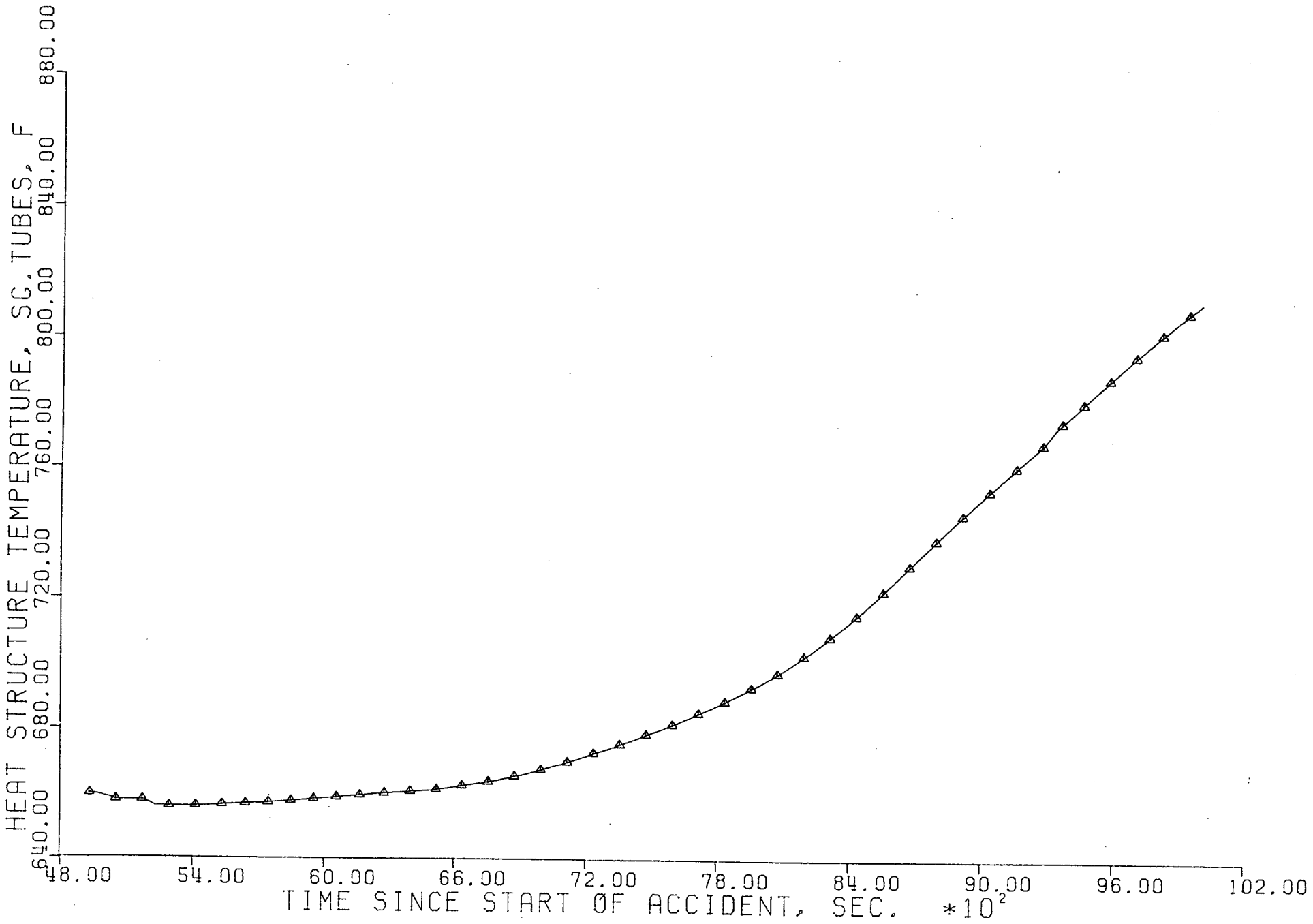
HEAT STRUCTURE TEMPERATURE, SC. TUBES, F
640.00
680.00
720.00
760.00
800.00
840.00
880.00
48.00
54.00
60.00
66.00
72.00
78.00
84.00
90.00
96.00
102.00
TIME SINCE START OF ACCIDENT, SEC. *10²

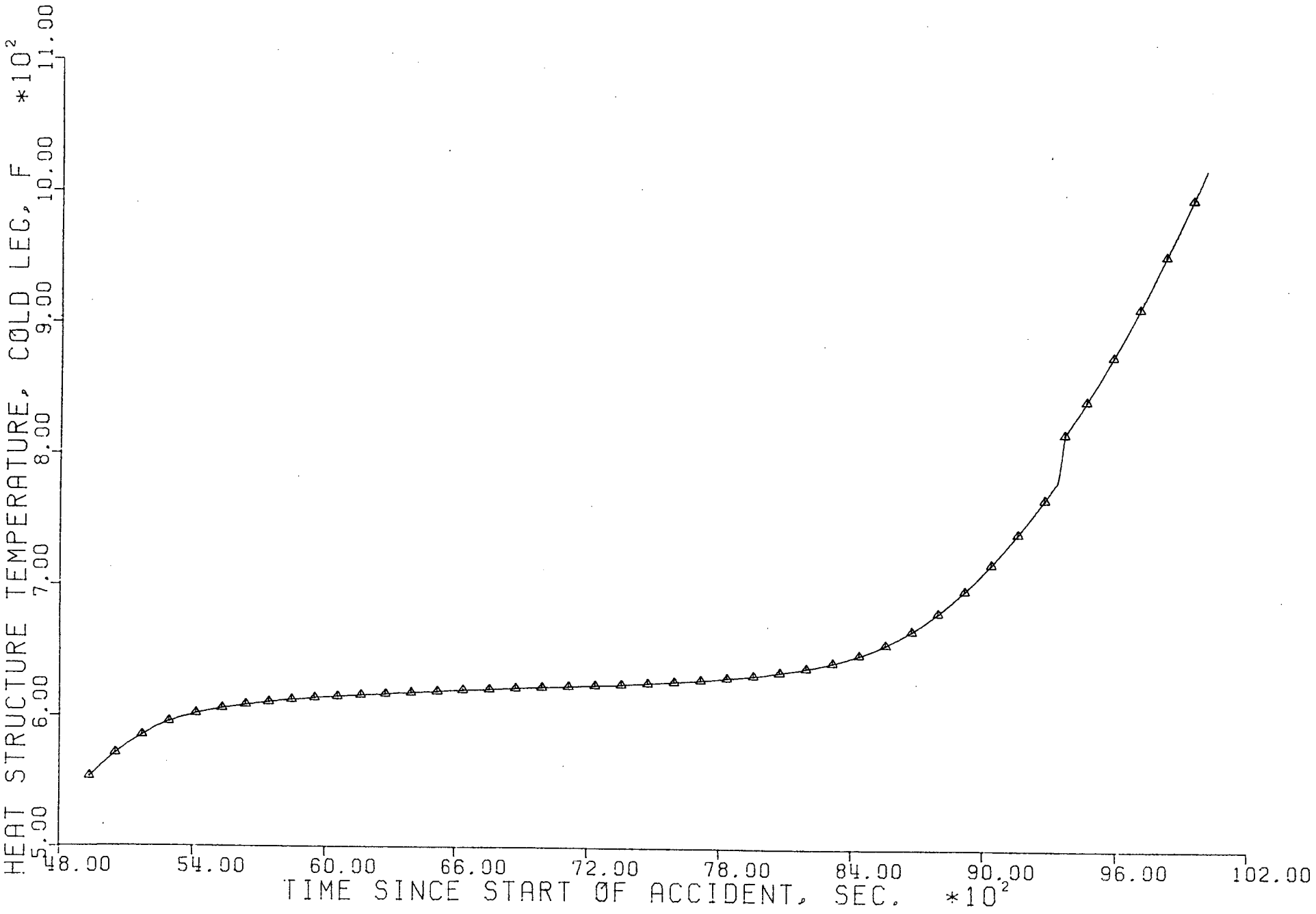
HEAT STRUCTURE TEMPERATURE, COLD LEG, F *10²
5.00
6.00
7.00
8.00
9.00
10.00
11.00
48.00
54.00
60.00
66.00
72.00
78.00
84.00
90.00
96.00
102.00
TIME SINCE START OF ACCIDENT, SEC. *10²

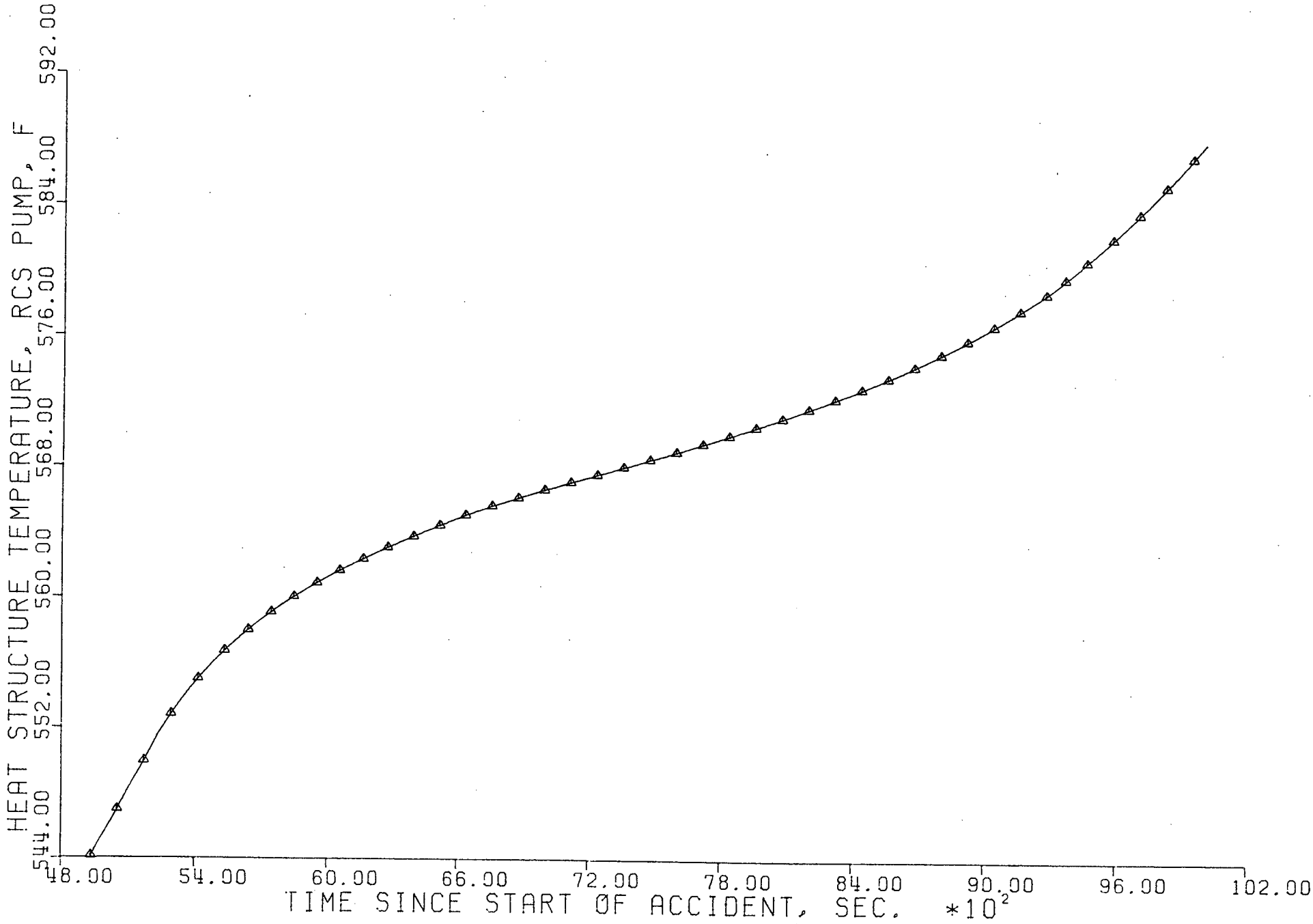
HEAT STRUCTURE TEMPERATURE, RCS PUMP, F
544.00
552.00
560.00
568.00
576.00
584.00
592.00
48.00
54.00
60.00
66.00
72.00
78.00
84.00
90.00
96.00
102.00
TIME SINCE START OF ACCIDENT, SEC. *10²

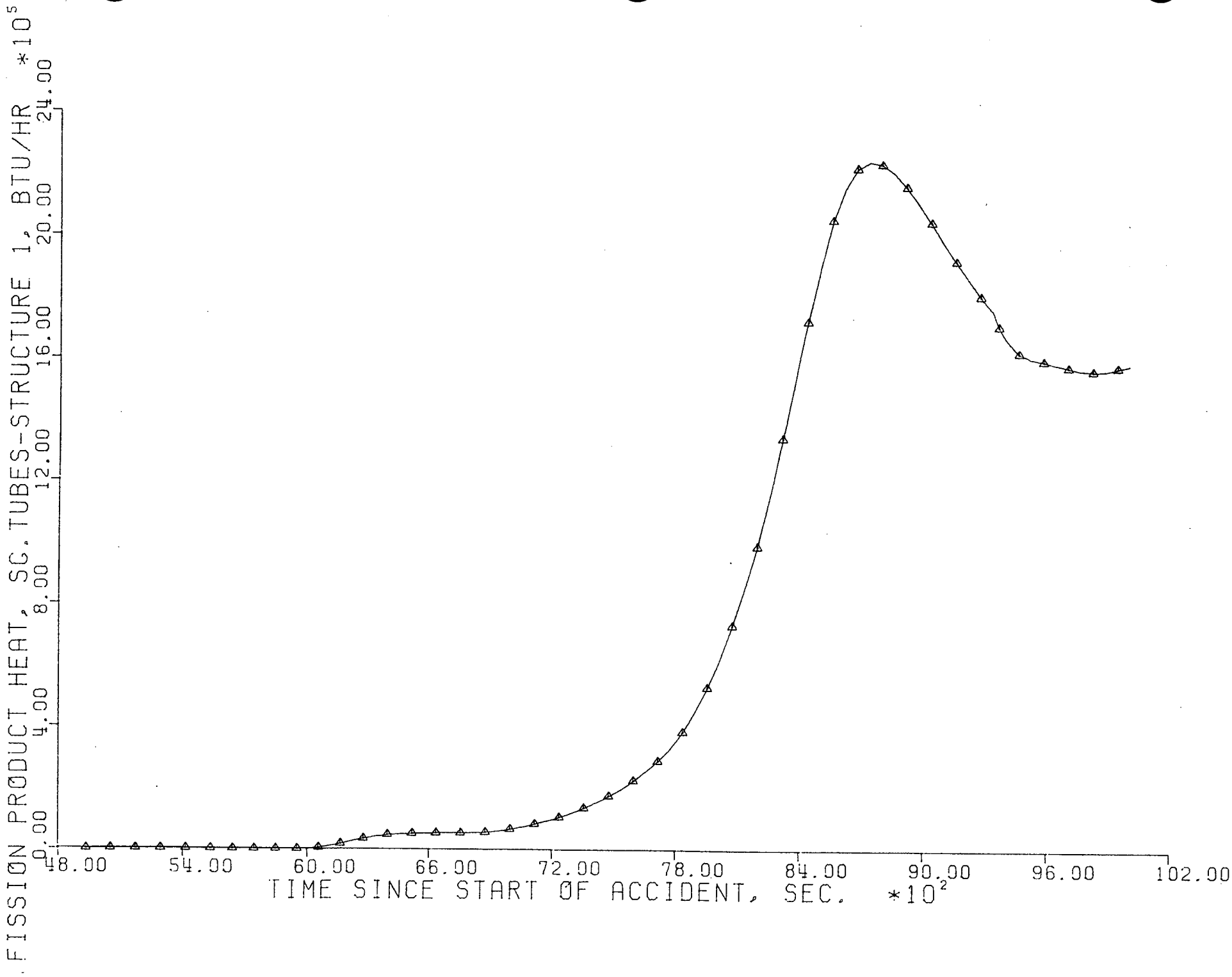
FISSION PRODUCT HEAT, SG. TUBES-STRUCTURE 1, BTU/HR *10^5
0.00
4.00
8.00
12.00
16.00
20.00
24.00
48.00
54.00
60.00
66.00
72.00
78.00
84.00
90.00
96.00
102.00
TIME SINCE START OF ACCIDENT, SEC. *10^2

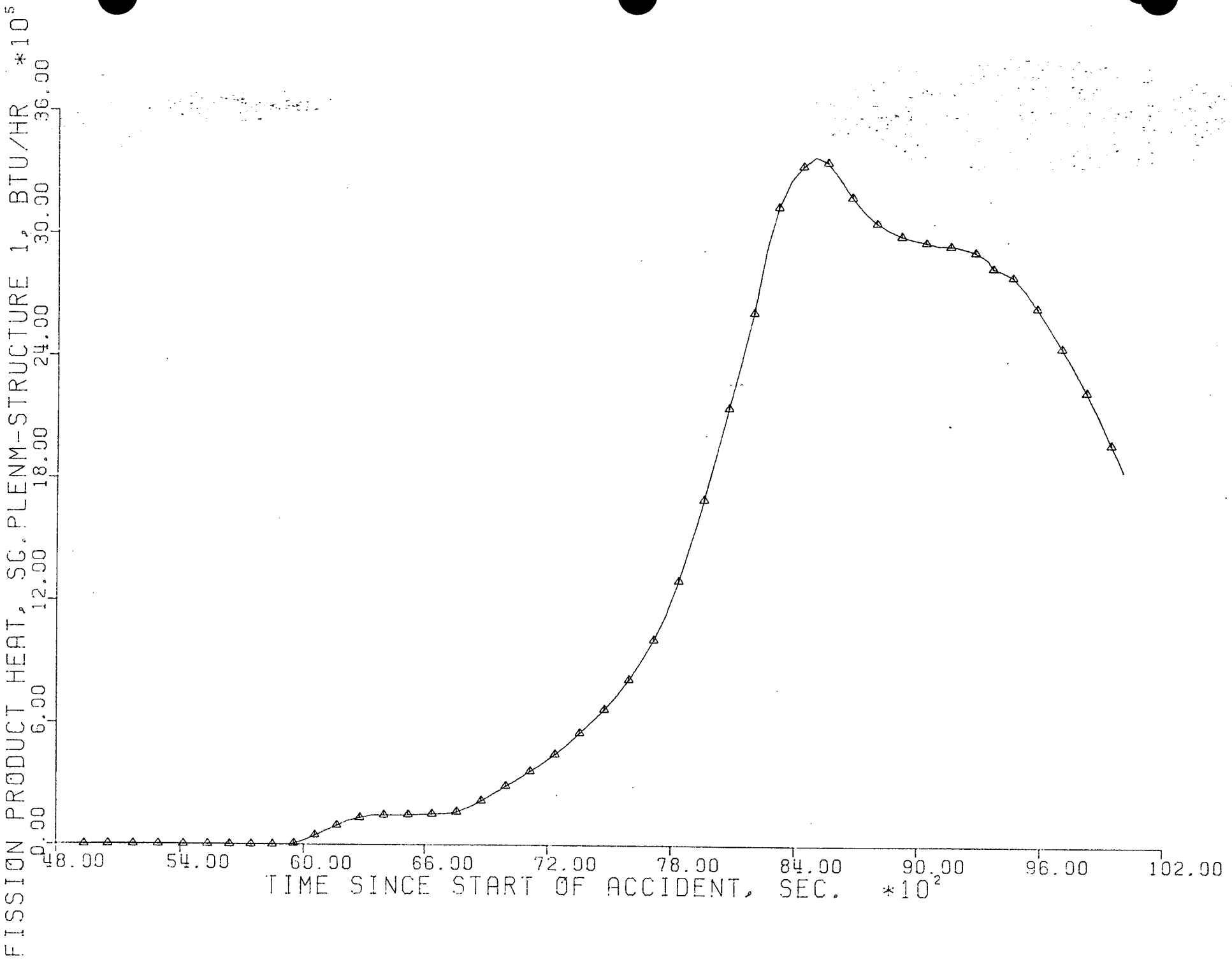
FISSION PRODUCT HEAT, SG. PLENM-STRUCTURE 1, BTU/HR *10^5
0.00
6.00
12.00
18.00
24.00
30.00
36.00
48.00
54.00
60.00
66.00
72.00
78.00
84.00
90.00
96.00
102.00
TIME SINCE START OF ACCIDENT, SEC. *10^2

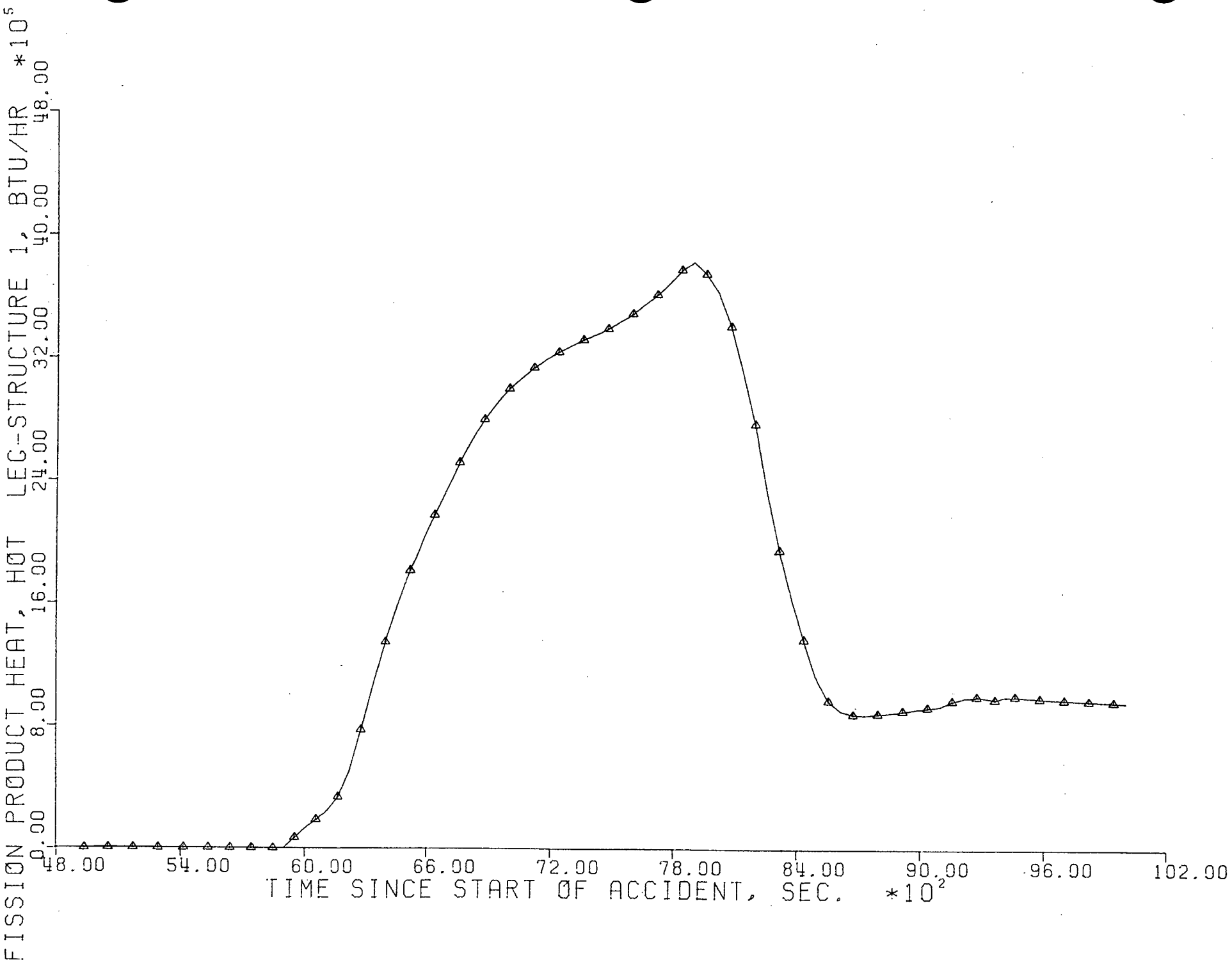
FISSION PRODUCT HEAT, HOT LEG-STRUCTURE 1, BTU/HR *10^5
0.00
8.00
16.00
24.00
32.00
40.00
48.00
48.00
54.00
60.00
66.00
72.00
78.00
84.00
90.00
96.00
102.00
TIME SINCE START OF ACCIDENT, SEC. *10^2

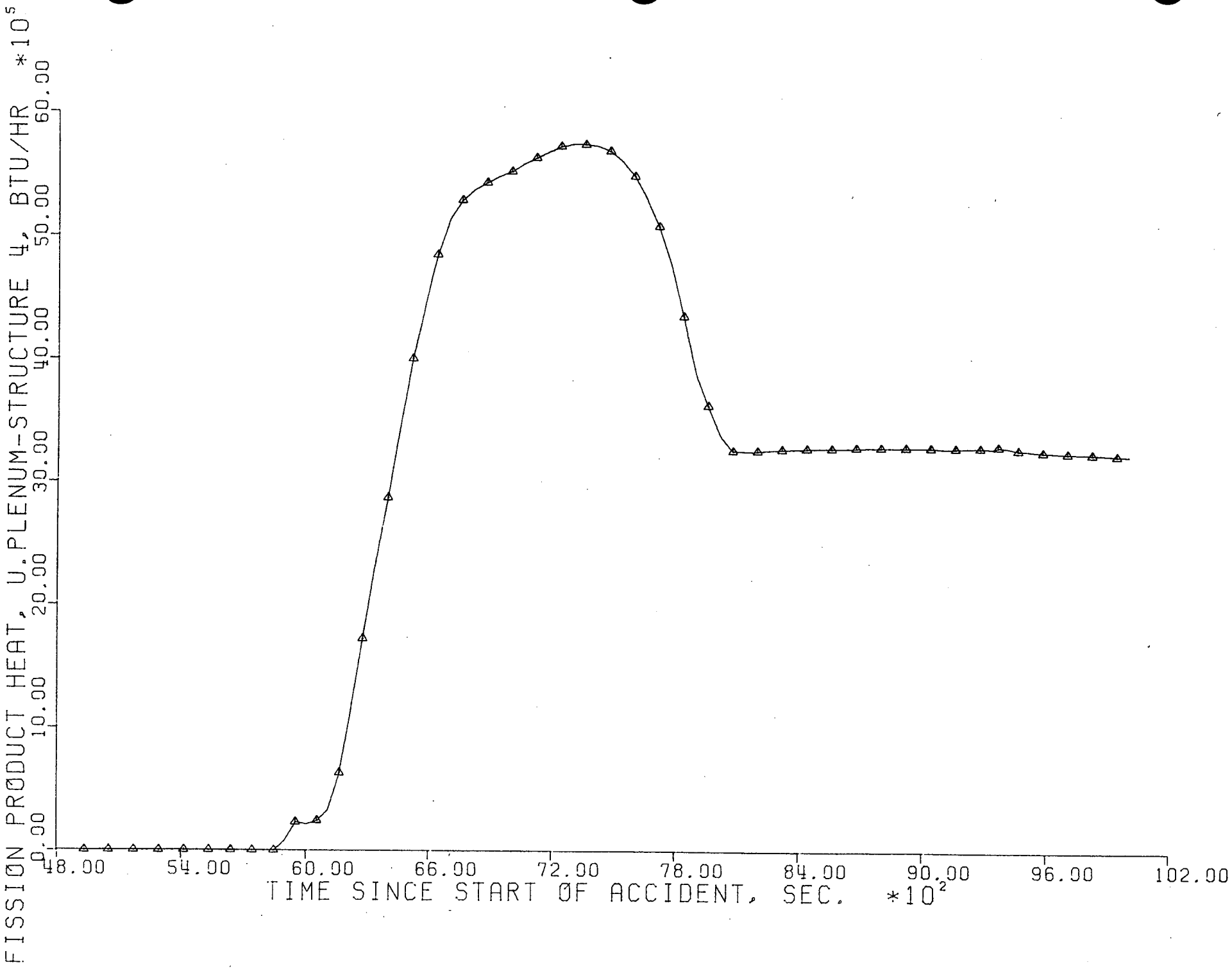
FISSION PRODUCT HEAT, U.PLENUM-STRUCTURE 4, BTU/HR *10^5
0.00
10.00
20.00
30.00
40.00
50.00
60.00
48.00
54.00
60.00
66.00
72.00
78.00
84.00
90.00
96.00
102.00
TIME SINCE START OF ACCIDENT, SEC. *10^2

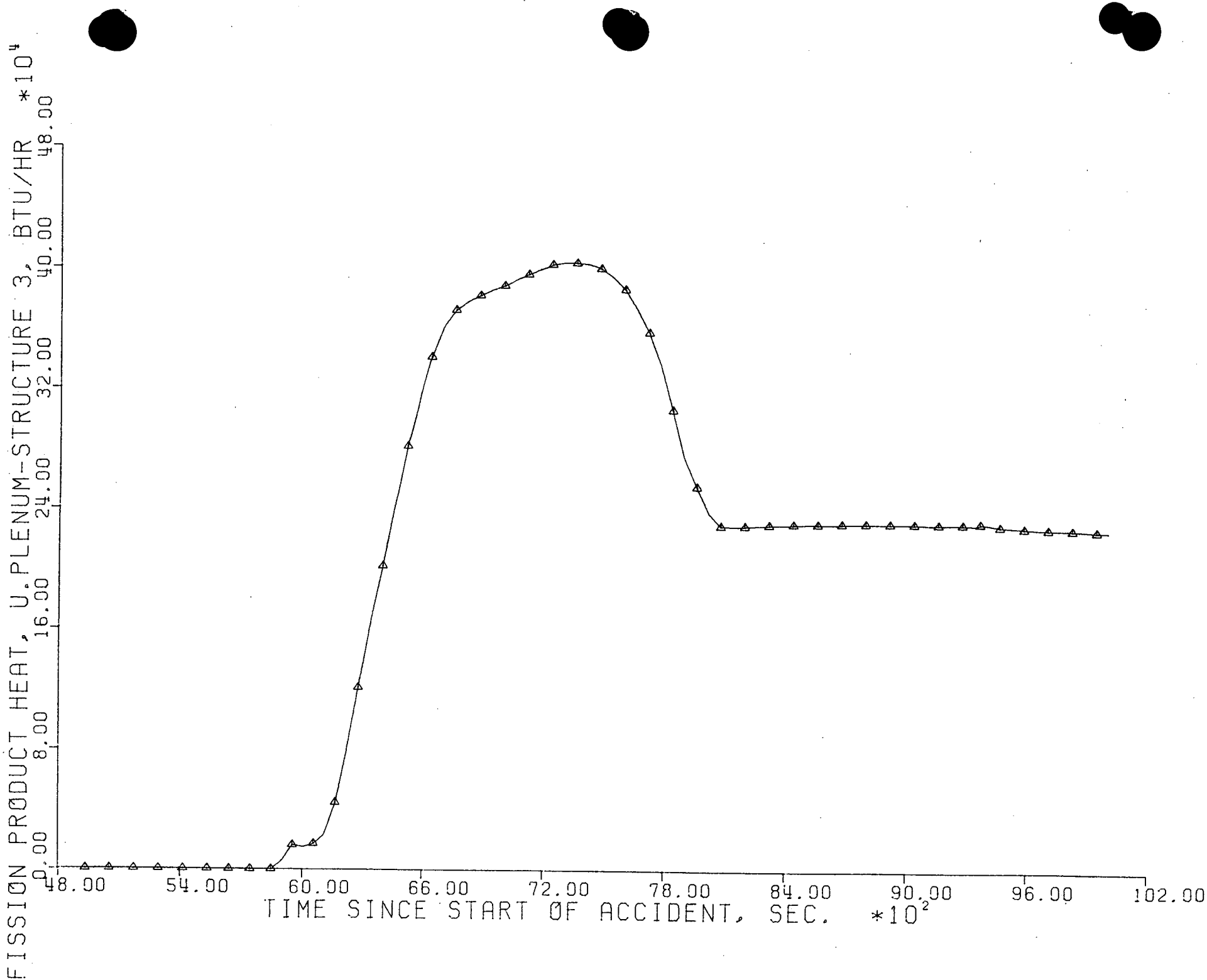
FISSION PRODUCT HEAT, U.PLENUM-STRUCTURE 3, BTU/HR *10^4
0.00
8.00
16.00
24.00
32.00
40.00
48.00
48.00
54.00
60.00
66.00
72.00
78.00
84.00
90.00
96.00
102.00
TIME SINCE START OF ACCIDENT, SEC. *10^2

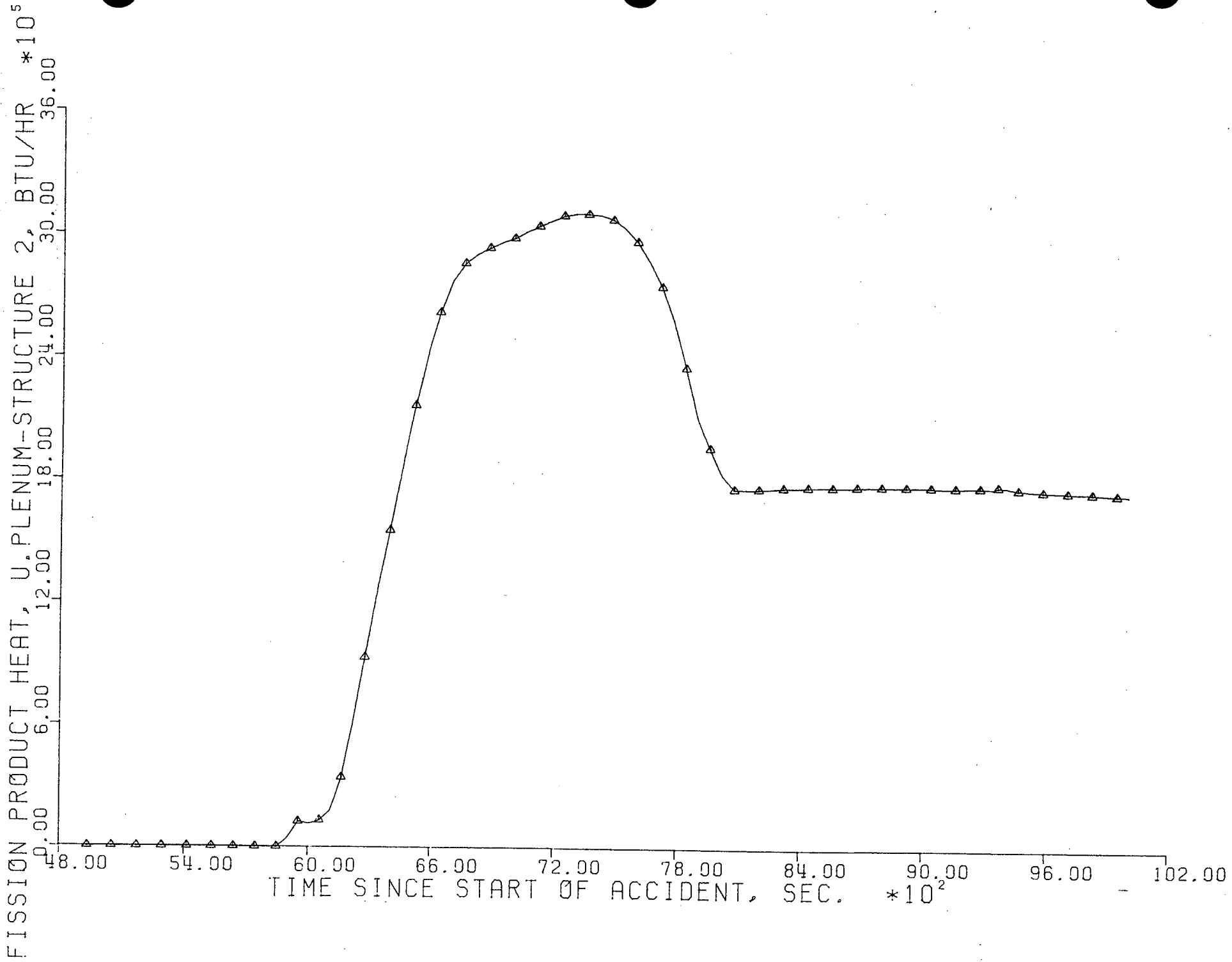
FISSION PRODUCT HEAT, U.PLENUM-STRUCTURE 2, BTU/HR *10^5
0.00
6.00
12.00
18.00
24.00
30.00
36.00
48.00
54.00
60.00
66.00
72.00
78.00
84.00
90.00
96.00
102.00
TIME SINCE START OF ACCIDENT, SEC. *10^2

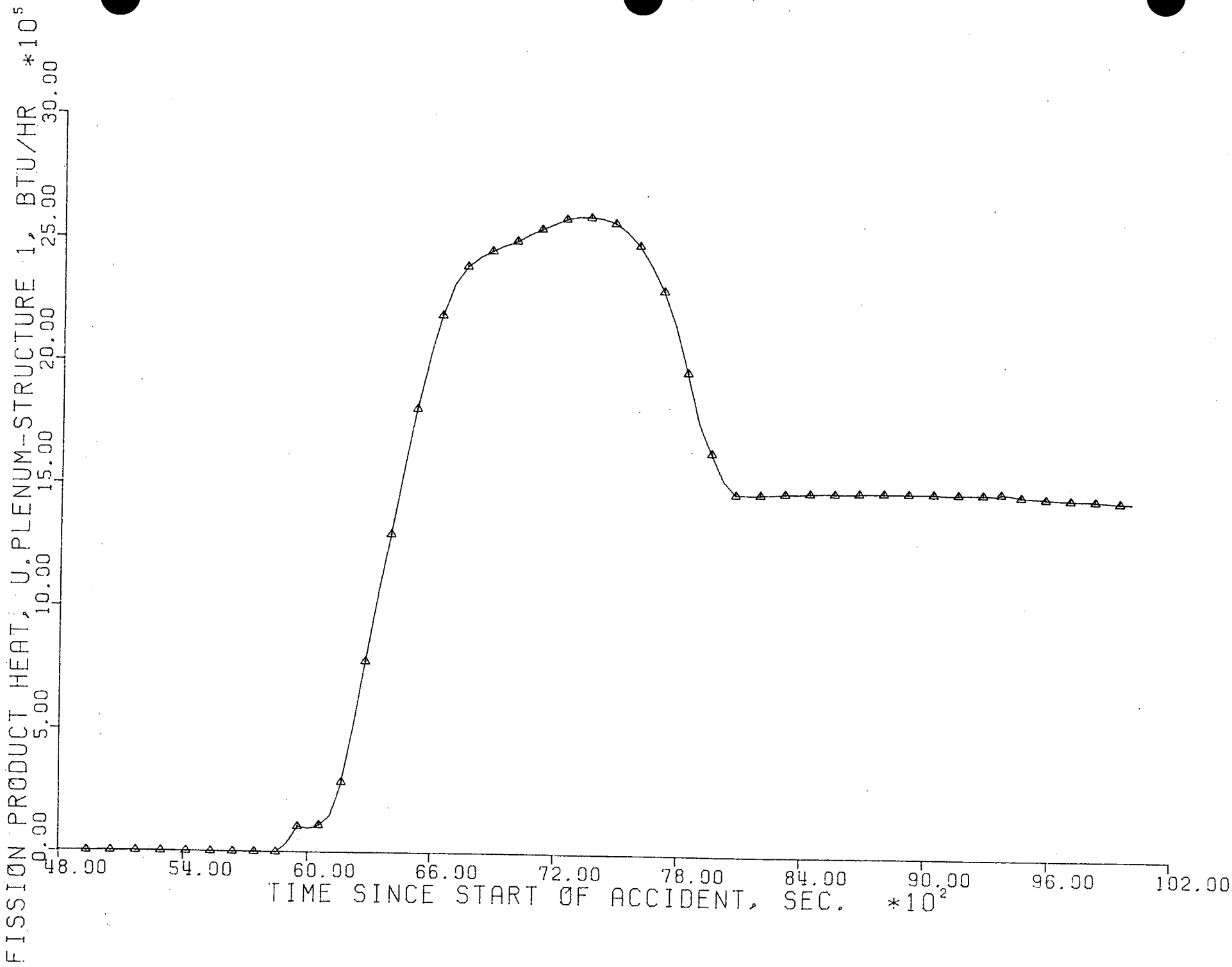
FISSION PRODUCT HEAT, U.PLENUM-STRUCTURE 1, BTU/HR *10^5
0.00
5.00
10.00
15.00
20.00
25.00
30.00
48.00
54.00
60.00
66.00
72.00
78.00
84.00
90.00
96.00
102.00
TIME SINCE START OF ACCIDENT, SEC. *10^2

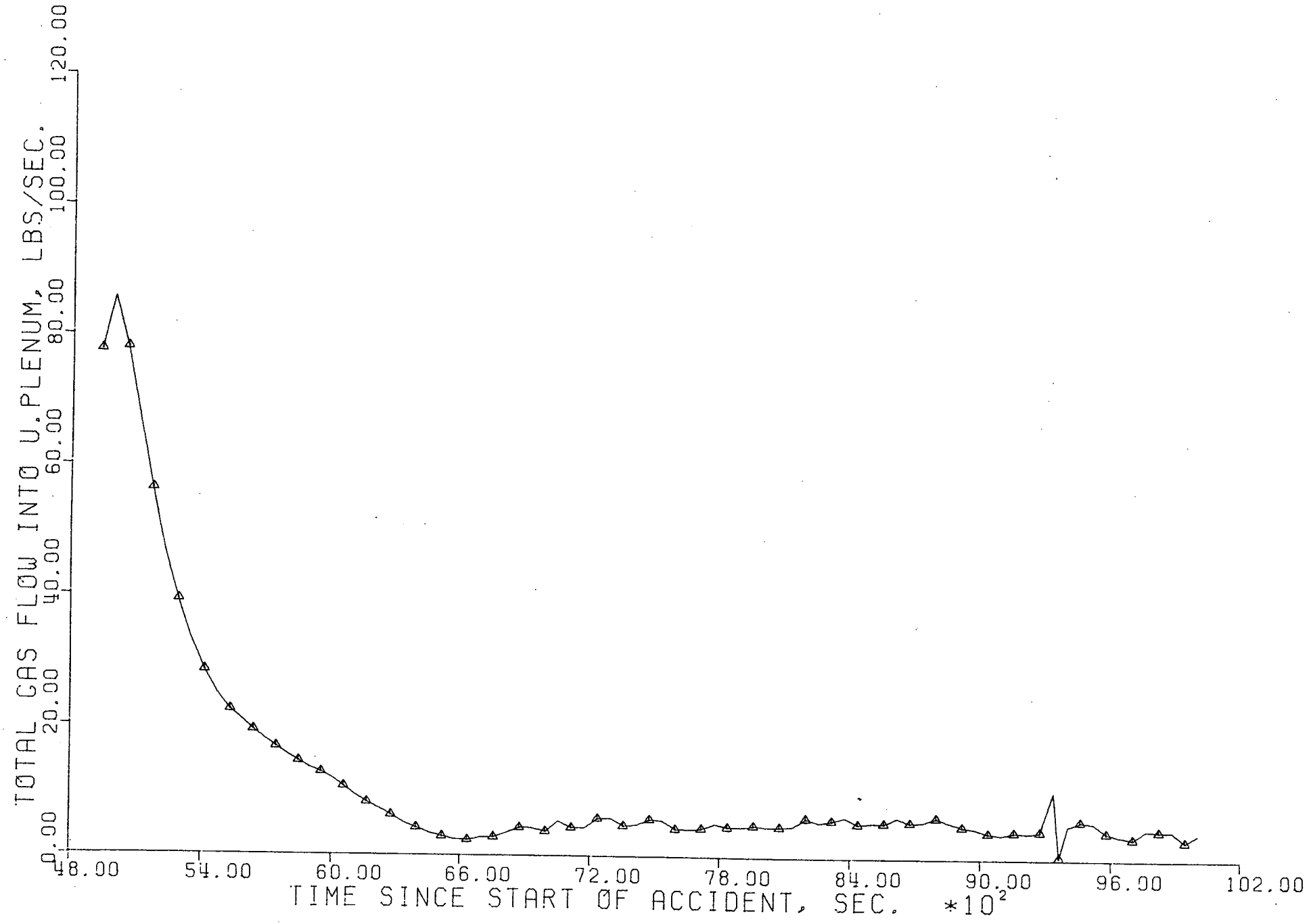
TOTAL GAS FLOW INTO U.PLENUM, LBS/SEC.
0.00
20.00
40.00
60.00
80.00
100.00
120.00
48.00
54.00
60.00
66.00
72.00
78.00
84.00
90.00
96.00
102.00
TIME SINCE START OF ACCIDENT, SEC. *10²

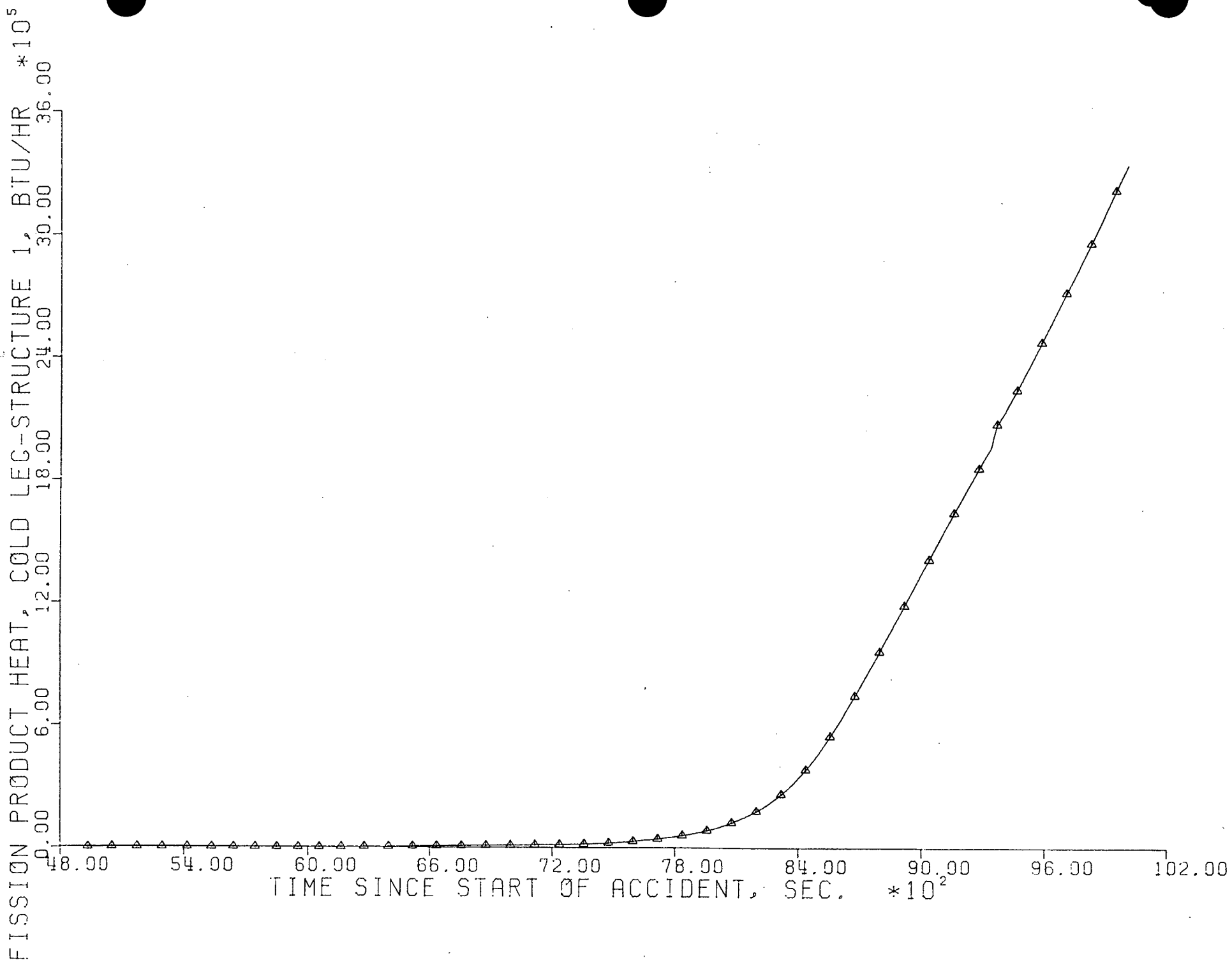
FISSION PRODUCT HEAT, COLD LEG-STRUCTURE 1, BTU/HR *10^5
0.00
6.00
12.00
18.00
24.00
30.00
36.00
48.00
54.00
60.00
66.00
72.00
78.00
84.00
90.00
96.00
102.00
TIME SINCE START OF ACCIDENT, SEC. *10^2

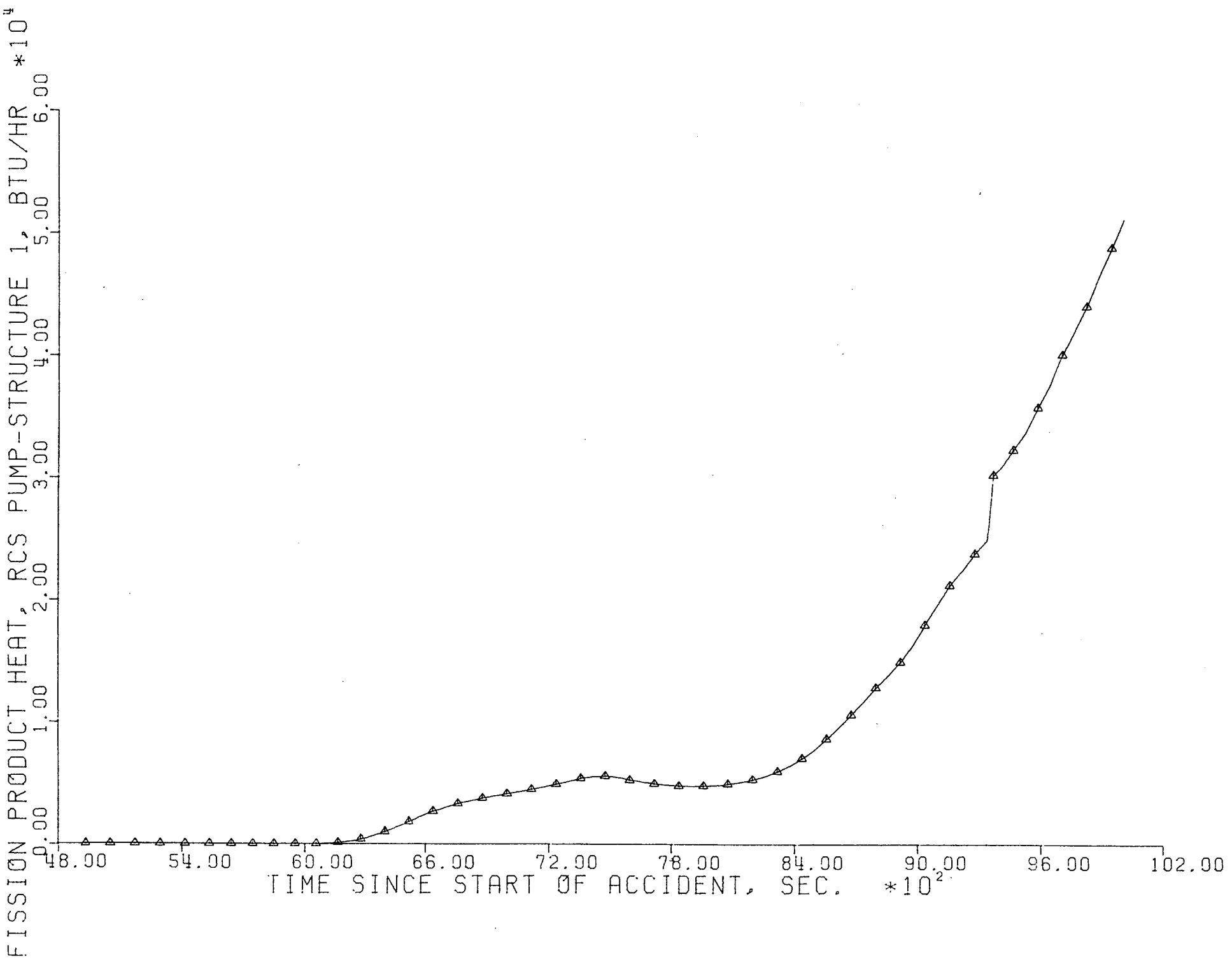
FISSION PRODUCT HEAT, RCS PUMP-STRUCTURE 1, BTU/HR *10^4
0.00
1.00
2.00
3.00
4.00
5.00
6.00
48.00
54.00
60.00
66.00
72.00
78.00
84.00
90.00
96.00
102.00
TIME SINCE START OF ACCIDENT, SEC. *10^2

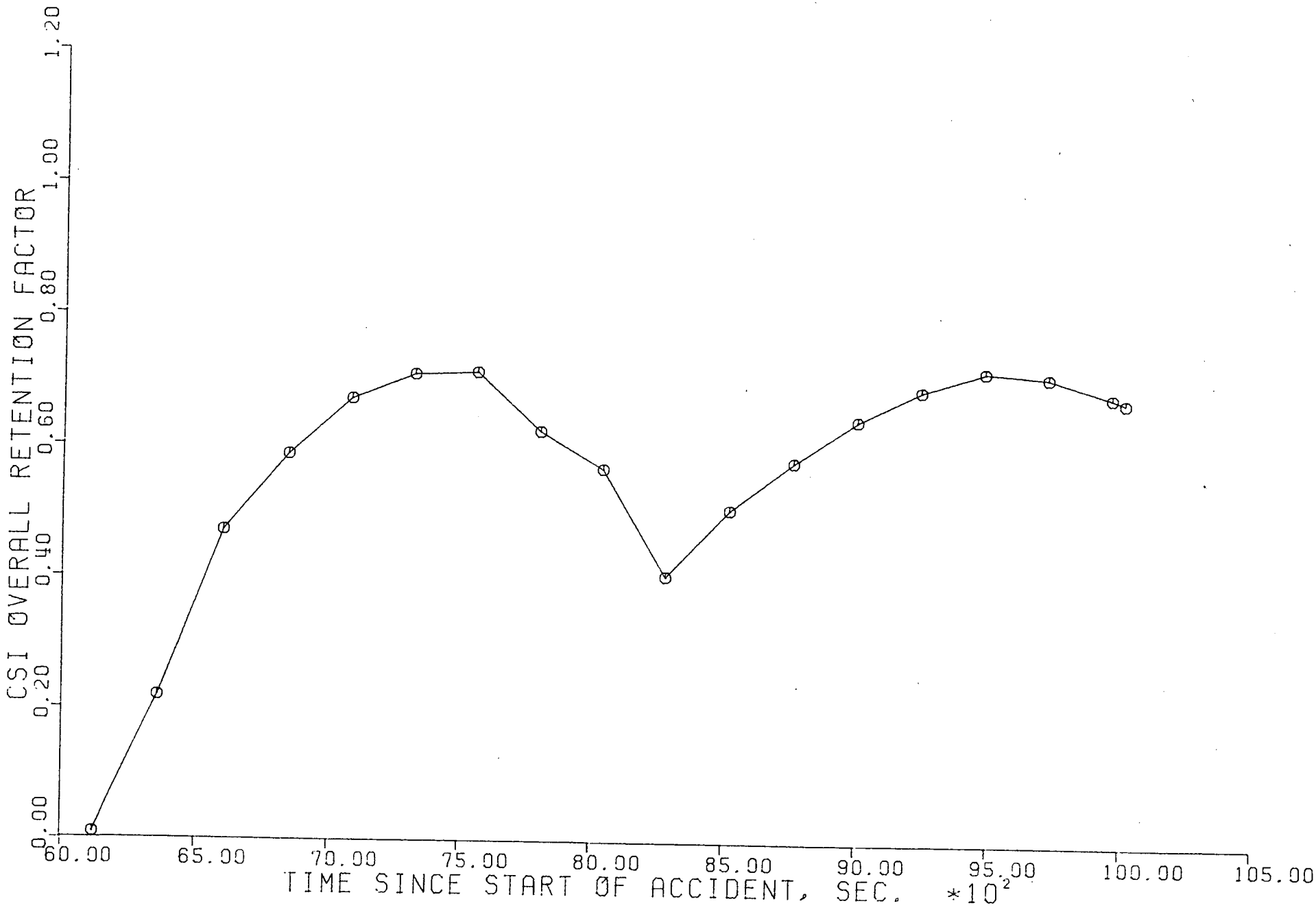
CSI OVERALL RETENTION FACTOR
0.00
0.20
0.40
0.60
0.80
1.00
1.20
60.00
65.00
70.00
75.00
80.00
85.00
90.00
95.00
100.00
105.00
TIME SINCE START OF ACCIDENT, SEC. *10²

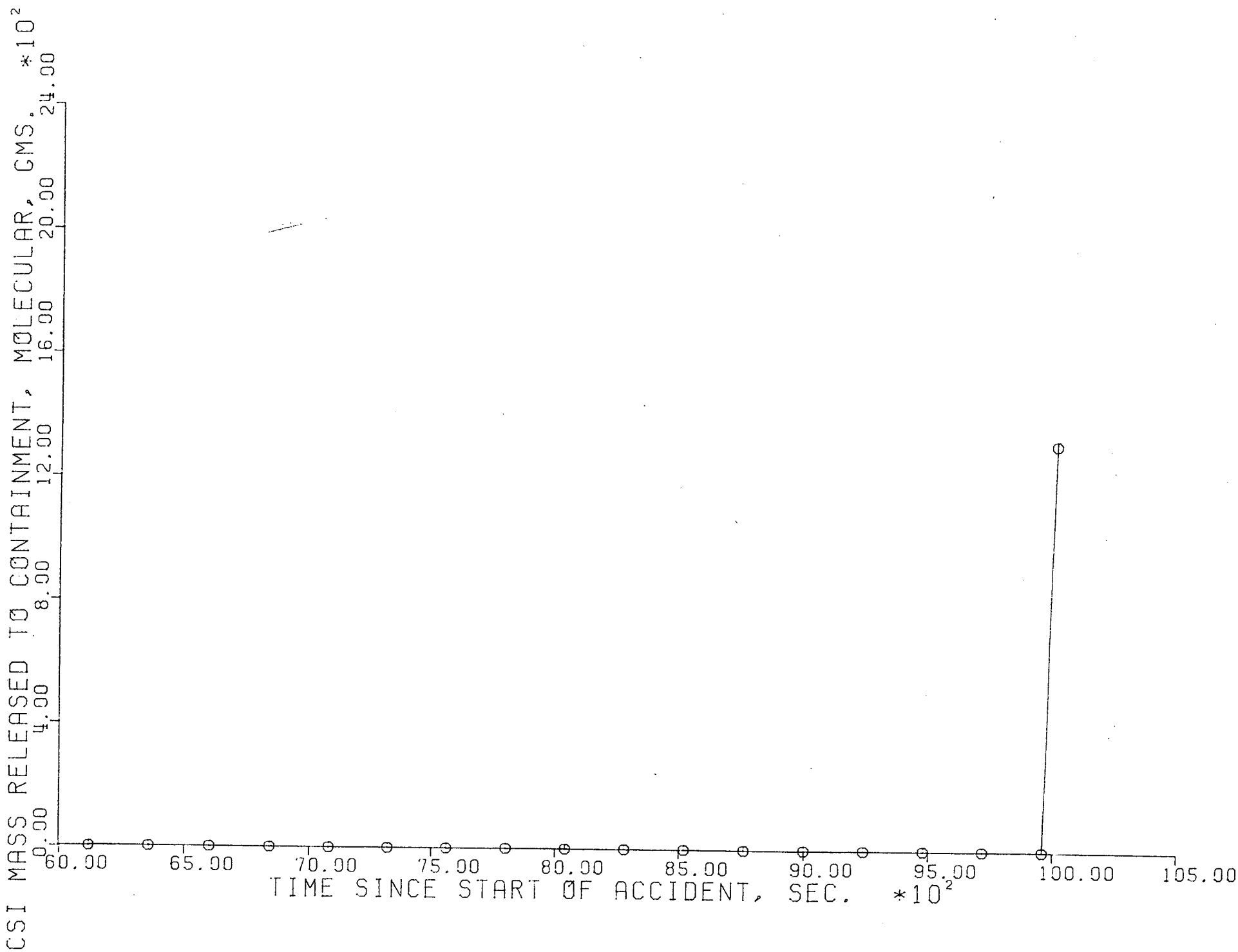
CSI MASS RELEASED TO CONTAINMENT, MOLECULAR, CMS. *10²
0.00
4.00
8.00
12.00
16.00
20.00
24.00
60.00
65.00
70.00
75.00
80.00
85.00
90.00
95.00
100.00
105.00
TIME SINCE START OF ACCIDENT, SEC. *10²

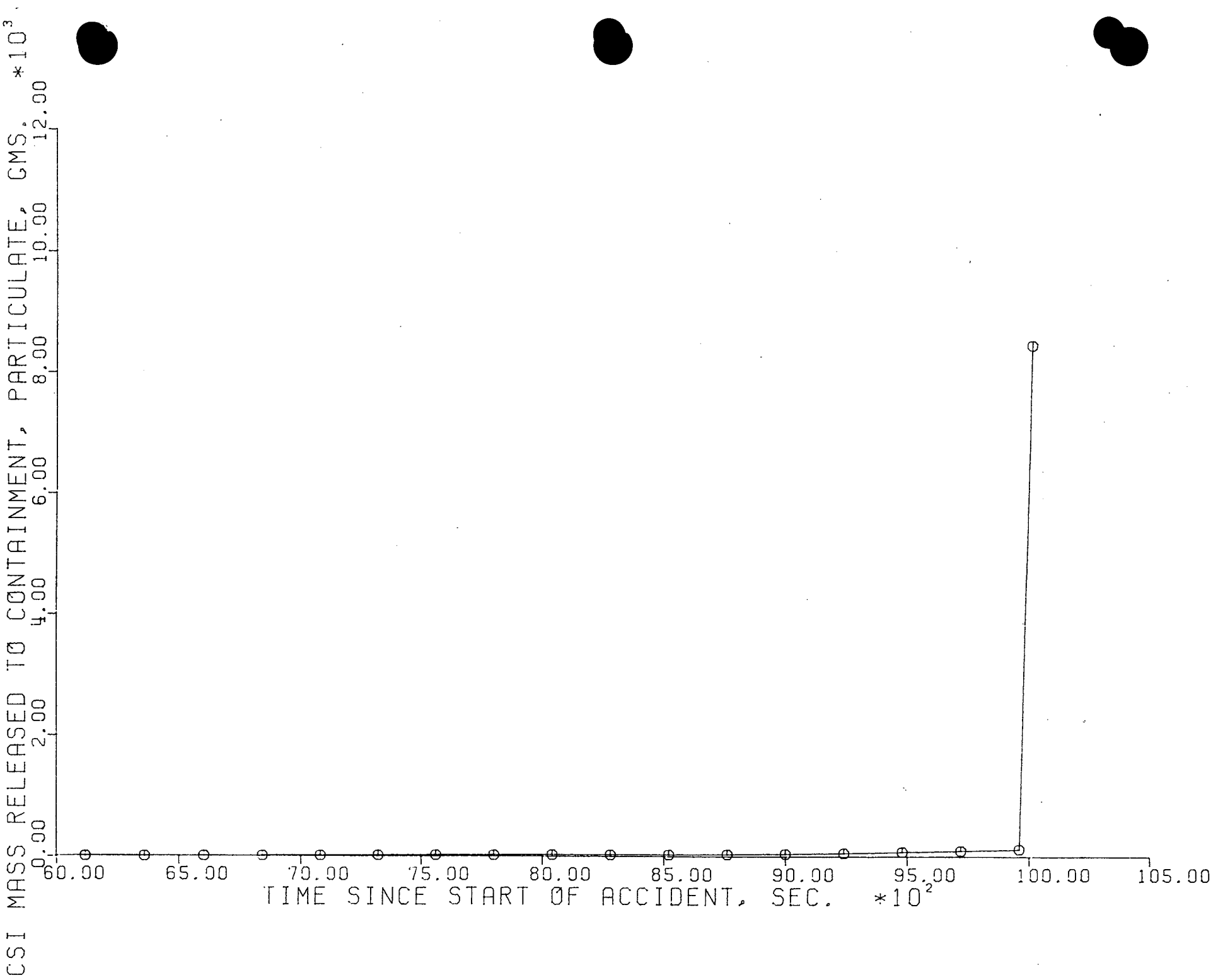
CSI MASS RELEASED TO CONTAINMENT, PARTICULATE, GMS. *10^3
0.00
2.00
4.00
6.00
8.00
10.00
12.00
60.00
65.00
70.00
75.00
80.00
85.00
90.00
95.00
100.00
105.00
TIME SINCE START OF ACCIDENT, SEC. *10^2

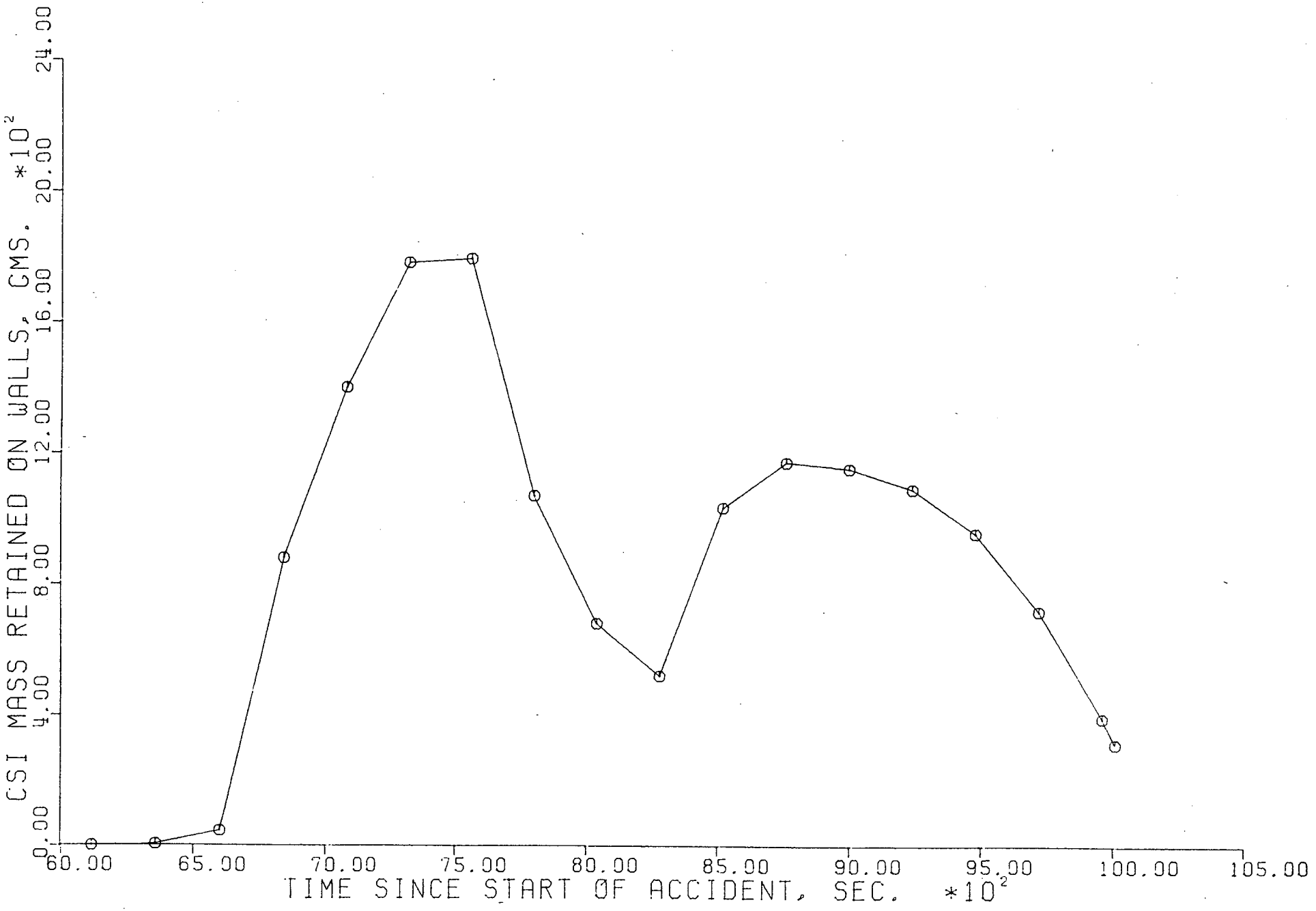
CSI MASS RETAINED ON WALLS, GMS. *10^2
0.00
4.00
8.00
12.00
16.00
20.00
24.00
60.00
65.00
70.00
75.00
80.00
85.00
90.00
95.00
100.00
105.00
TIME SINCE START OF ACCIDENT, SEC. *10^2

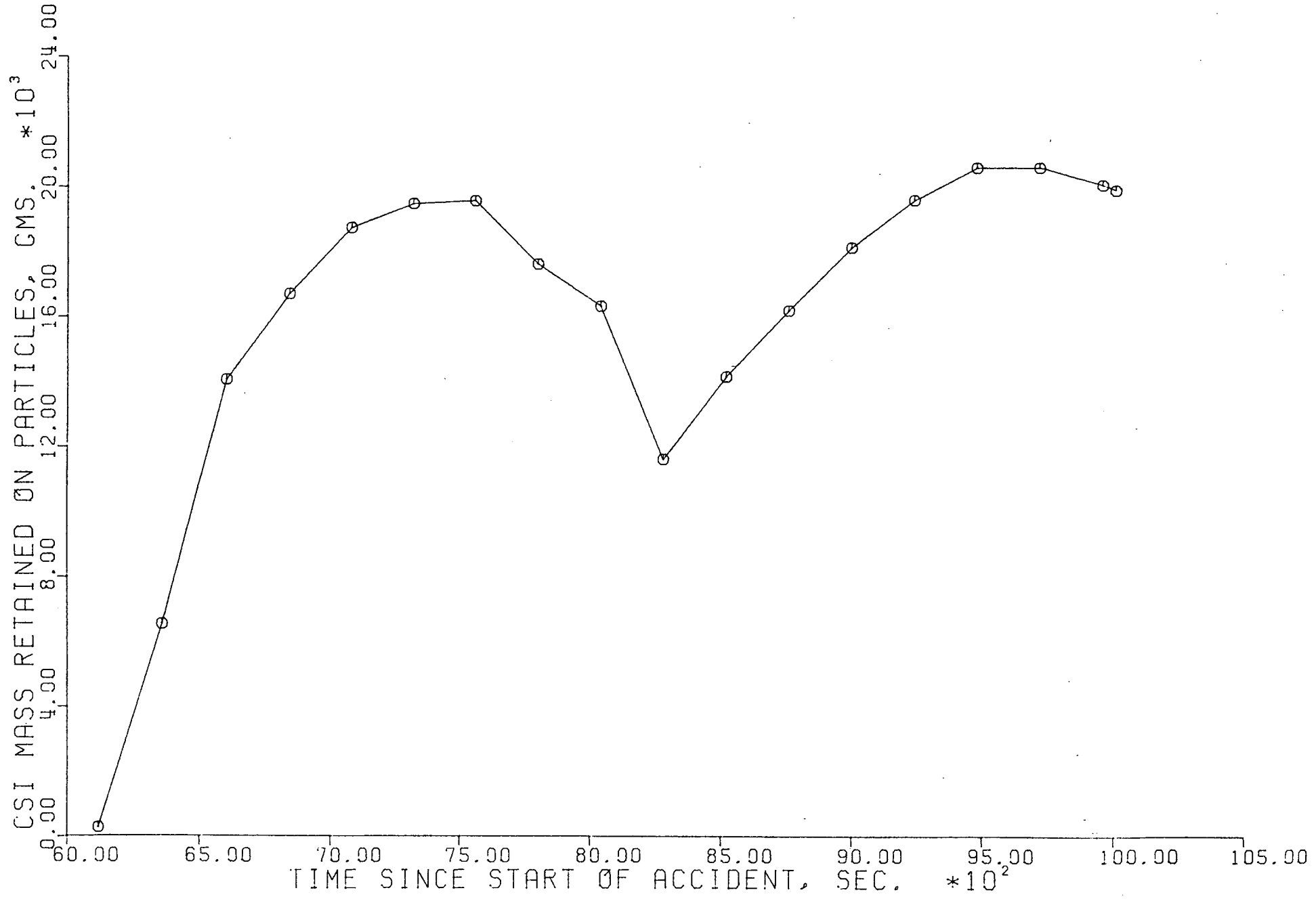
CSI MASS RETAINED ON PARTICLES, GMS. *10³
0.00
4.00
8.00
12.00
16.00
20.00
24.00
60.00
65.00
70.00
75.00
80.00
85.00
90.00
95.00
100.00
105.00
TIME SINCE START OF ACCIDENT, SEC. *10²

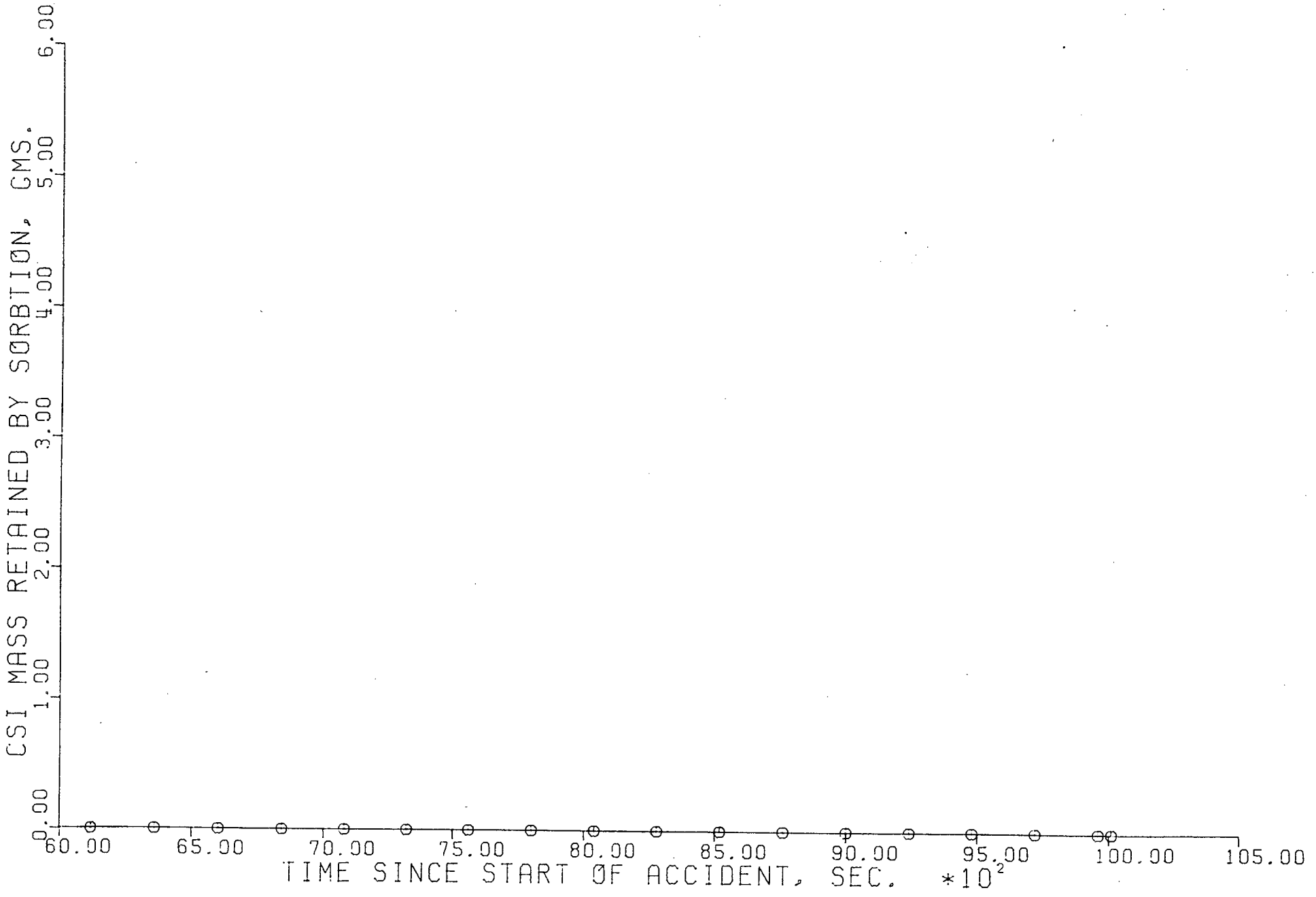
CSI MASS RETAINED BY SORBTION, GMS.
0.00
1.00
2.00
3.00
4.00
5.00
6.00
60.00
65.00
70.00
75.00
80.00
85.00
90.00
95.00
100.00
105.00
TIME SINCE START OF ACCIDENT, SEC. *10^2

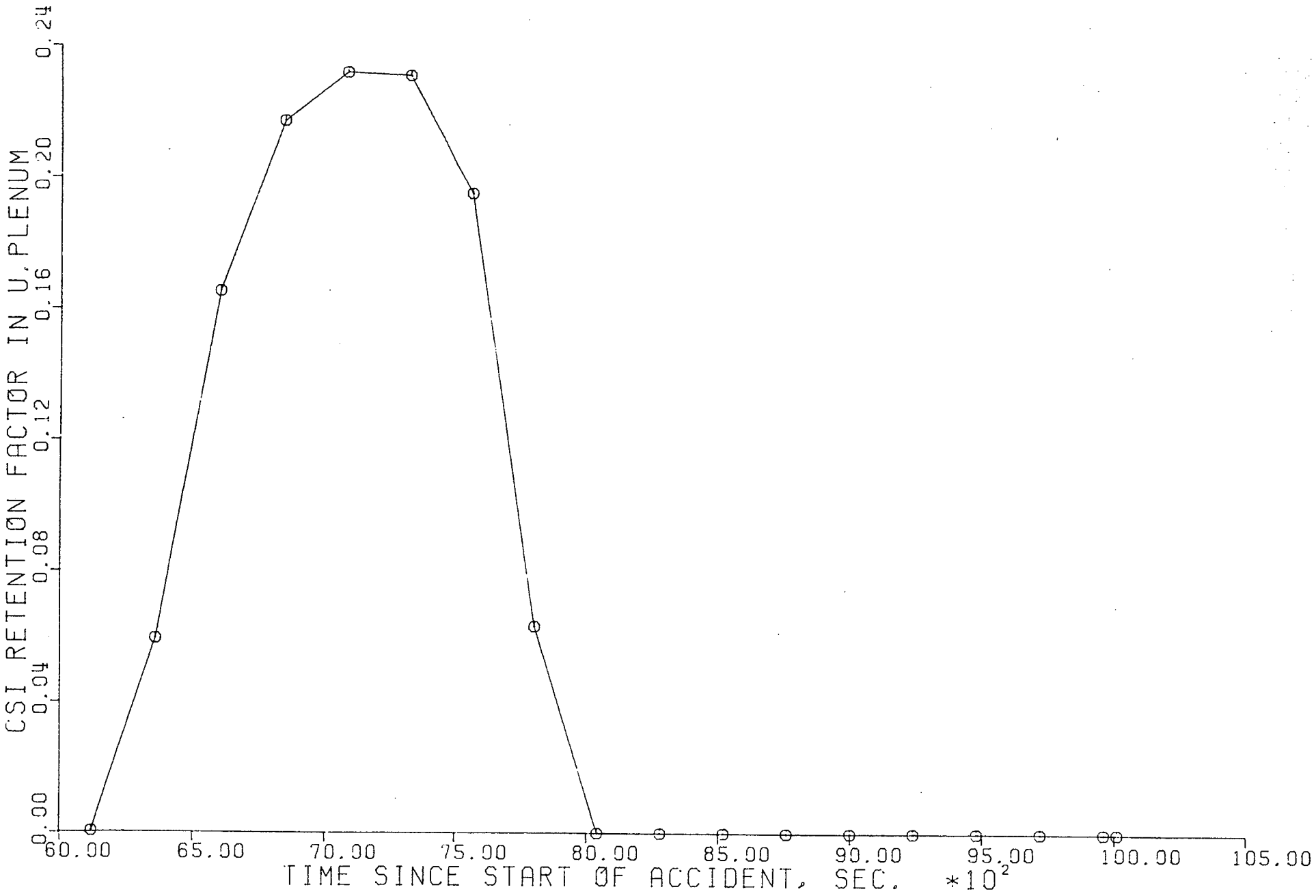
CSI RETENTION FACTOR IN U. PLENUM
0.00
0.04
0.08
0.12
0.16
0.20
0.24
60.00
65.00
70.00
75.00
80.00
85.00
90.00
95.00
100.00
105.00
TIME SINCE START OF ACCIDENT, SEC. *10²

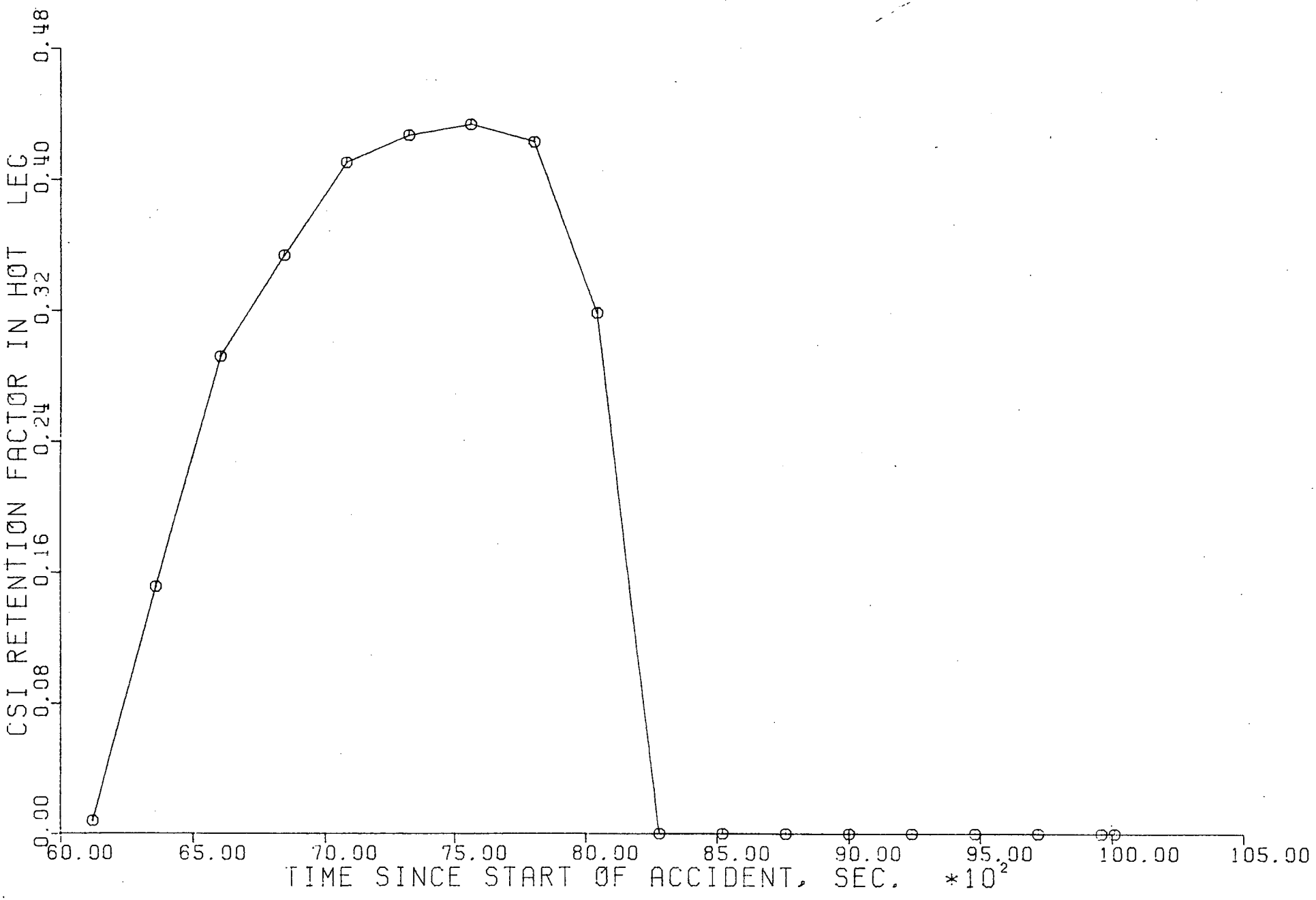
CSI RETENTION FACTOR IN HOT LEG
0.00
0.08
0.16
0.24
0.32
0.40
0.48
60.00
65.00
70.00
75.00
80.00
85.00
90.00
95.00
100.00
105.00
TIME SINCE START OF ACCIDENT, SEC. *10²

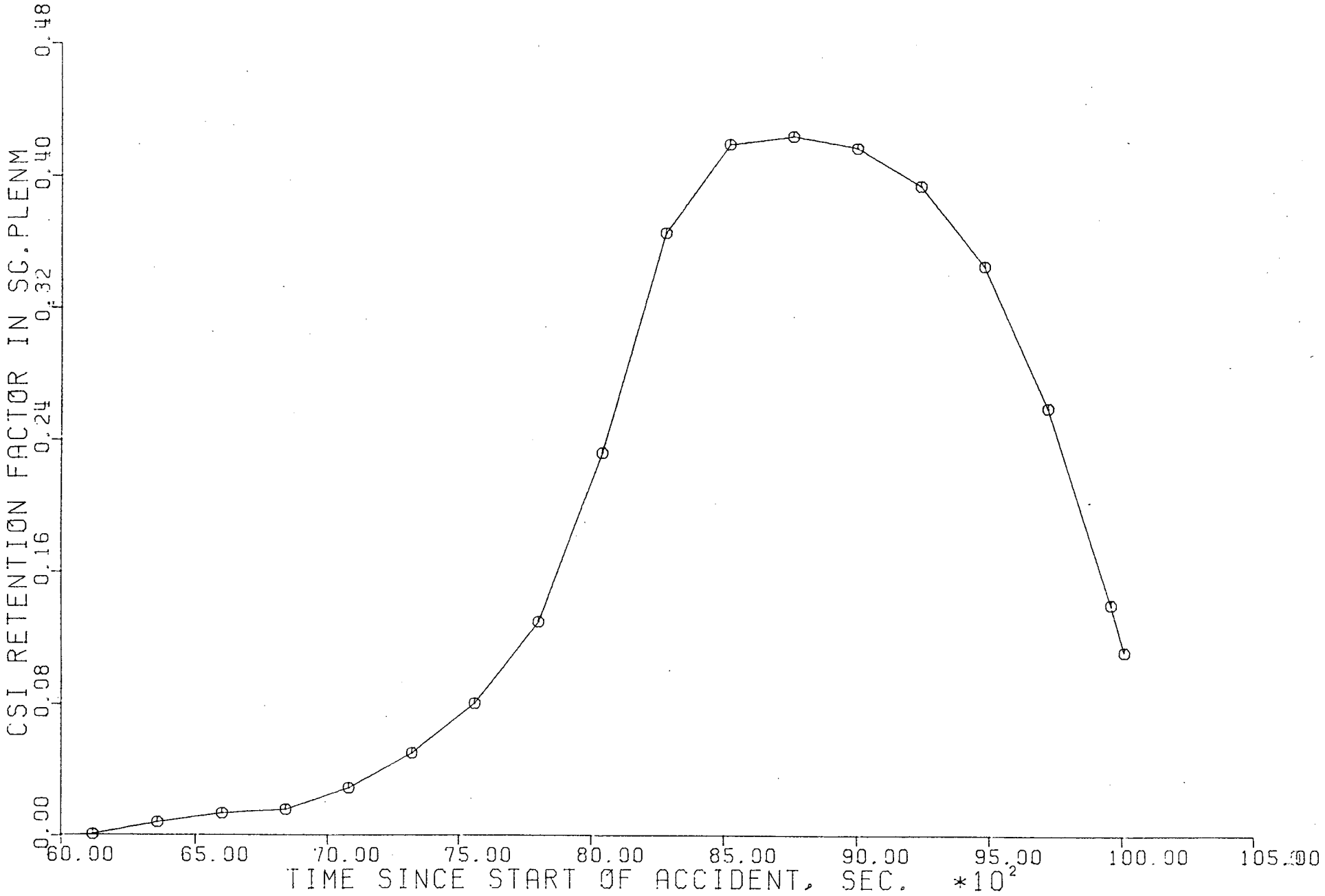
CSI RETENTION FACTOR IN SG. PLENM
0.00
0.08
0.16
0.24
0.32
0.40
0.48
60.00
65.00
70.00
75.00
80.00
85.00
90.00
95.00
100.00
105.00
TIME SINCE START OF ACCIDENT, SEC. *10²

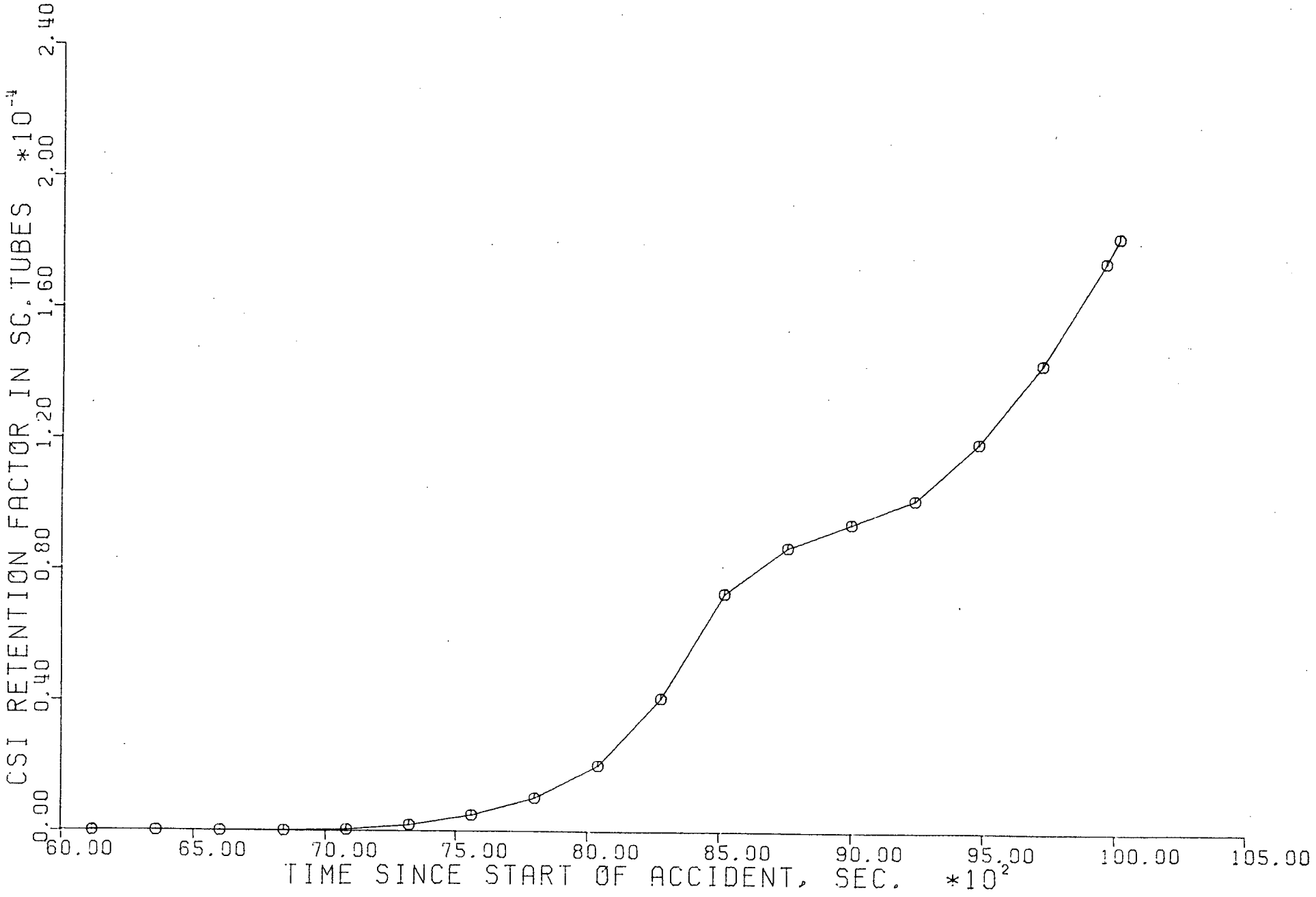
CSI RETENTION FACTOR IN SG. TUBES *10⁻⁴
0.00
0.40
0.80
1.20
1.60
2.00
2.40
60.00
65.00
70.00
75.00
80.00
85.00
90.00
95.00
100.00
105.00
TIME SINCE START OF ACCIDENT, SEC. *10²

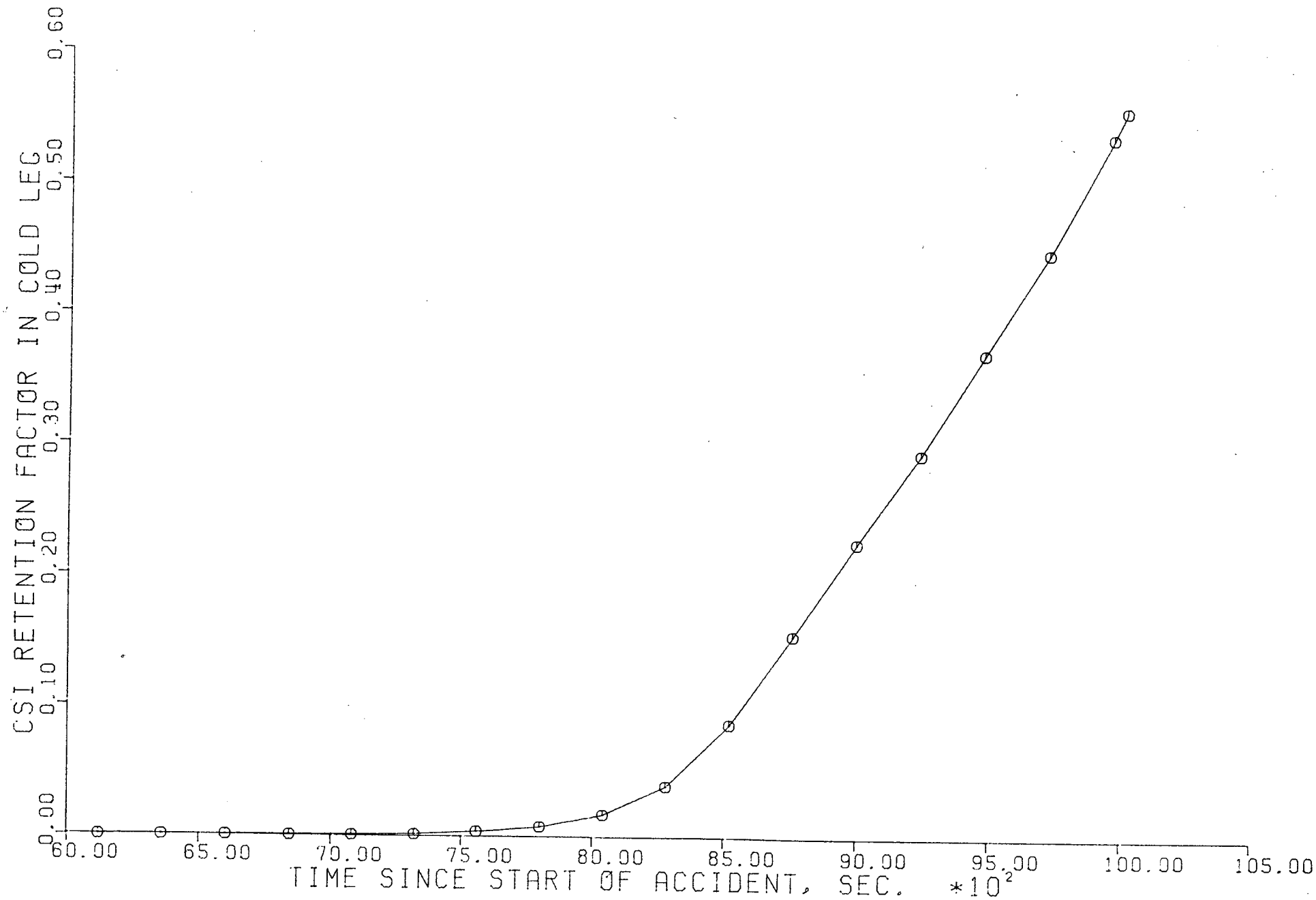
CSI RETENTION FACTOR IN COLD LEG
0.00
0.10
0.20
0.30
0.40
0.50
0.60
60.00
65.00
70.00
75.00
80.00
85.00
90.00
95.00
100.00
105.00
TIME SINCE START OF ACCIDENT, SEC. *10²

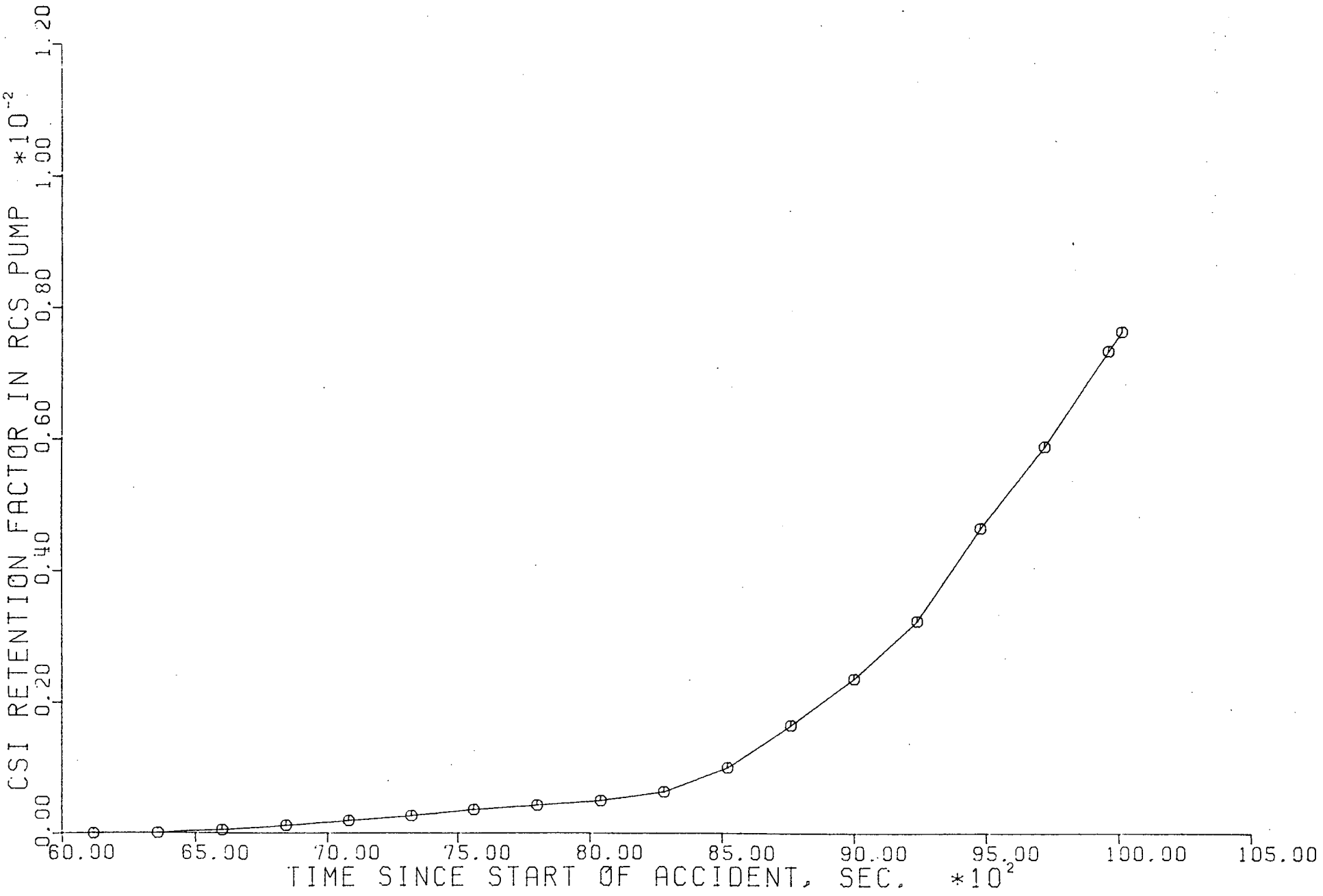
CSI RETENTION FACTOR IN RCS PUMP *10-2
0.00
0.20
0.40
0.60
0.80
1.00
1.20
60.00
65.00
70.00
75.00
80.00
85.00
90.00
95.00
100.00
105.00
TIME SINCE START OF ACCIDENT, SEC. *10²

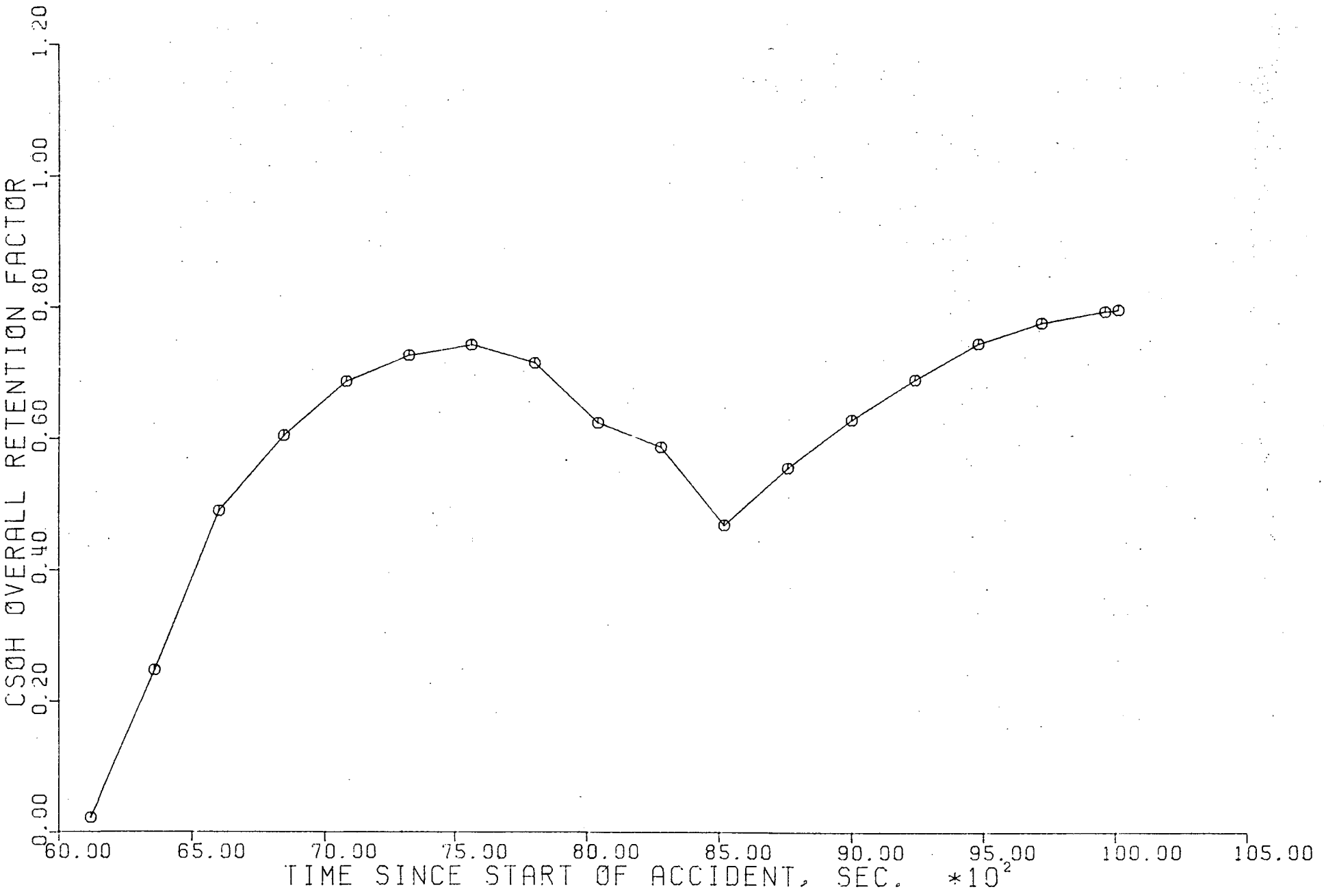
CSØH ØVERALL RETENTIØN FACTØR
0.00
0.20
0.40
0.60
0.80
1.00
1.20
60.00
65.00
70.00
75.00
80.00
85.00
90.00
95.00
100.00
105.00
TIME SINCE START ØF ACCIDENT, SEC. *10²

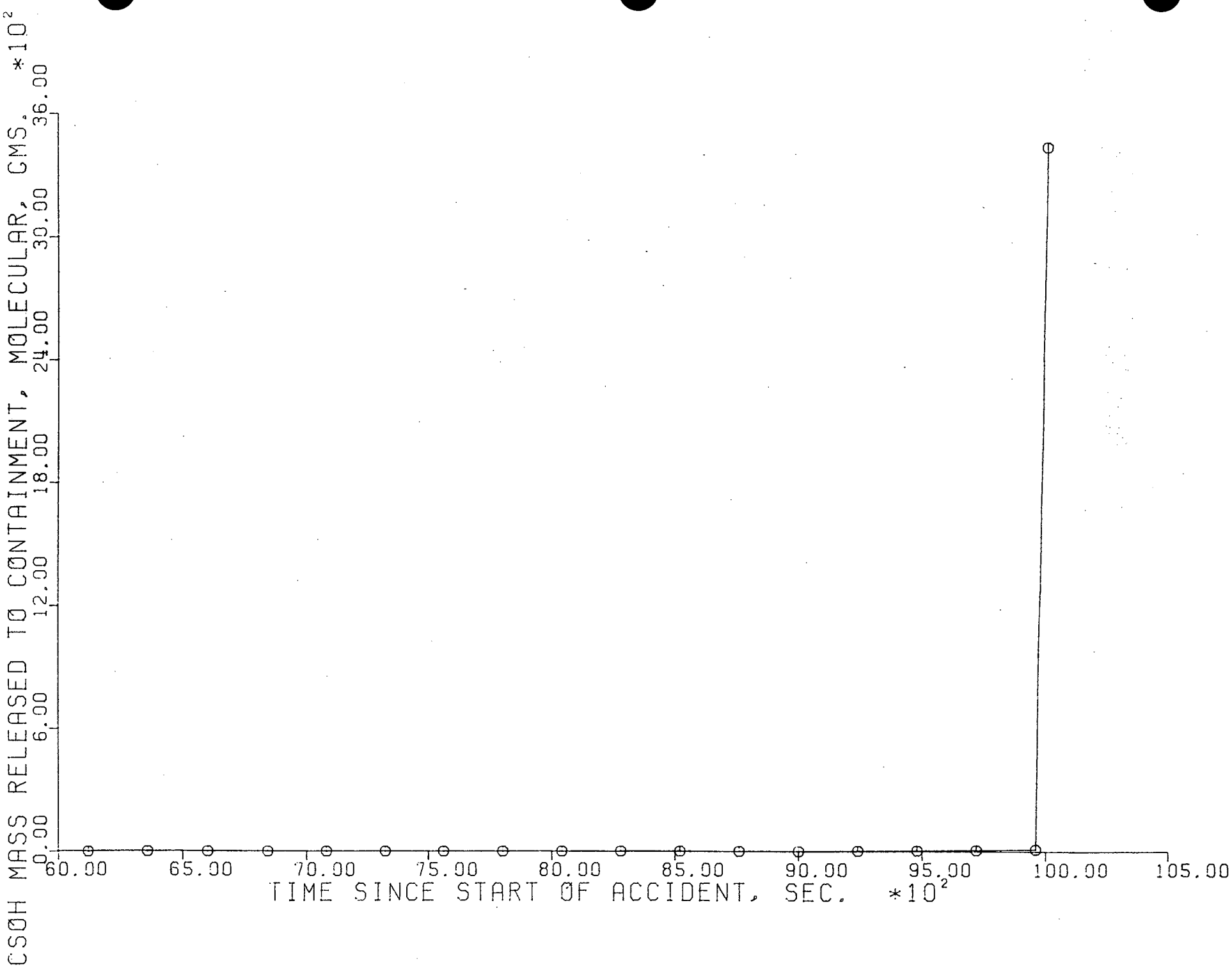
CSOH MASS RELEASED TO CONTAINMENT, MOLECULAR, GMS. *10²
0.00
6.00
12.00
18.00
24.00
30.00
36.00
60.00
65.00
70.00
75.00
80.00
85.00
90.00
95.00
100.00
105.00
TIME SINCE START OF ACCIDENT, SEC. *10²

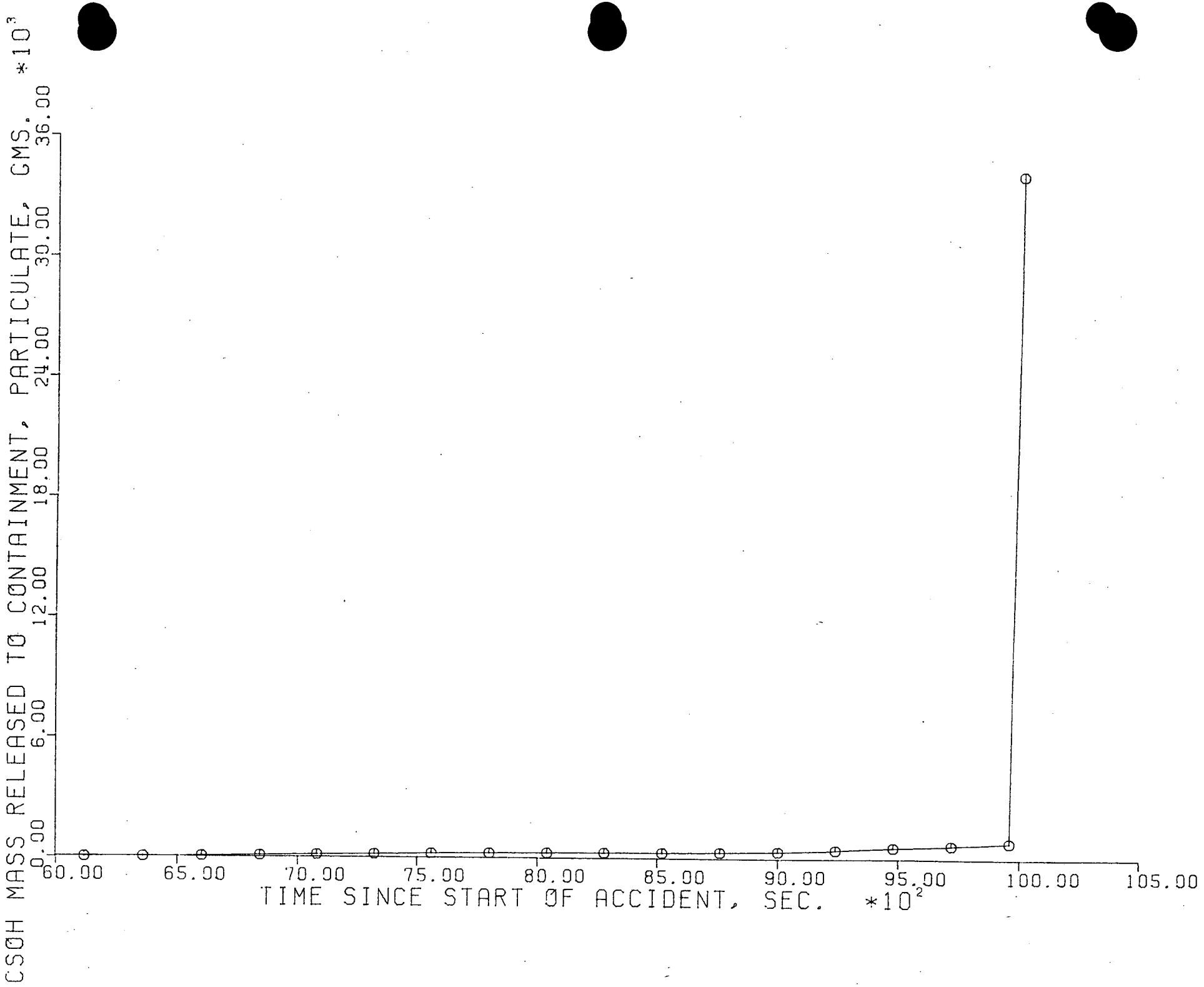
CSOH MASS RELEASED TO CONTAINMENT, PARTICULATE, CMS. *10³
0.00
6.00
12.00
18.00
24.00
30.00
36.00
60.00
65.00
70.00
75.00
80.00
85.00
90.00
95.00
100.00
105.00
TIME SINCE START OF ACCIDENT, SEC. *10²

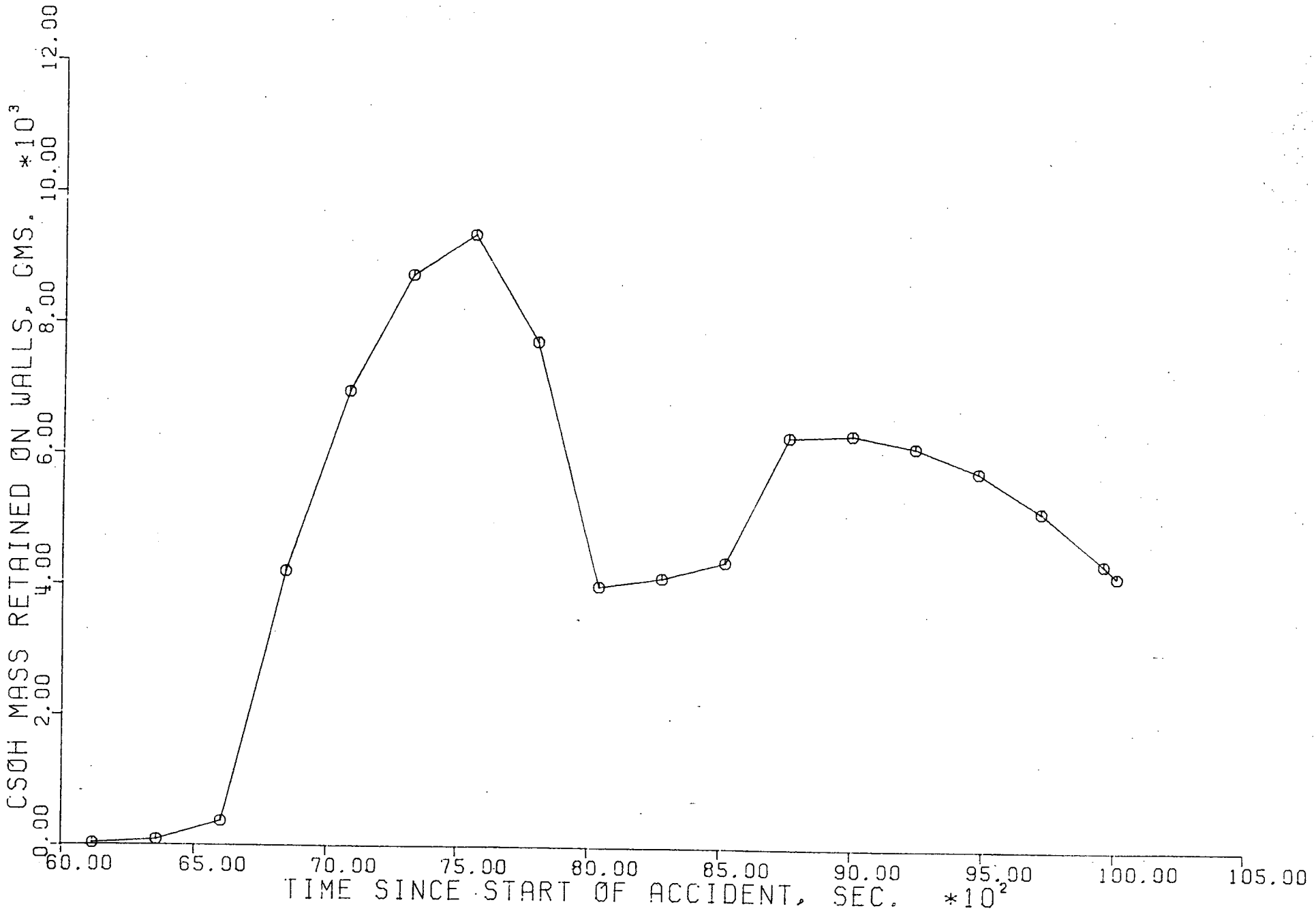
CSØH MASS RETAINED ØN WALLS, GMS. *10^3
0.00
2.00
4.00
6.00
8.00
10.00
12.00
60.00
65.00
70.00
75.00
80.00
85.00
90.00
95.00
100.00
105.00
TIME SINCE START ØF ACCIDENT, SEC. *10^2

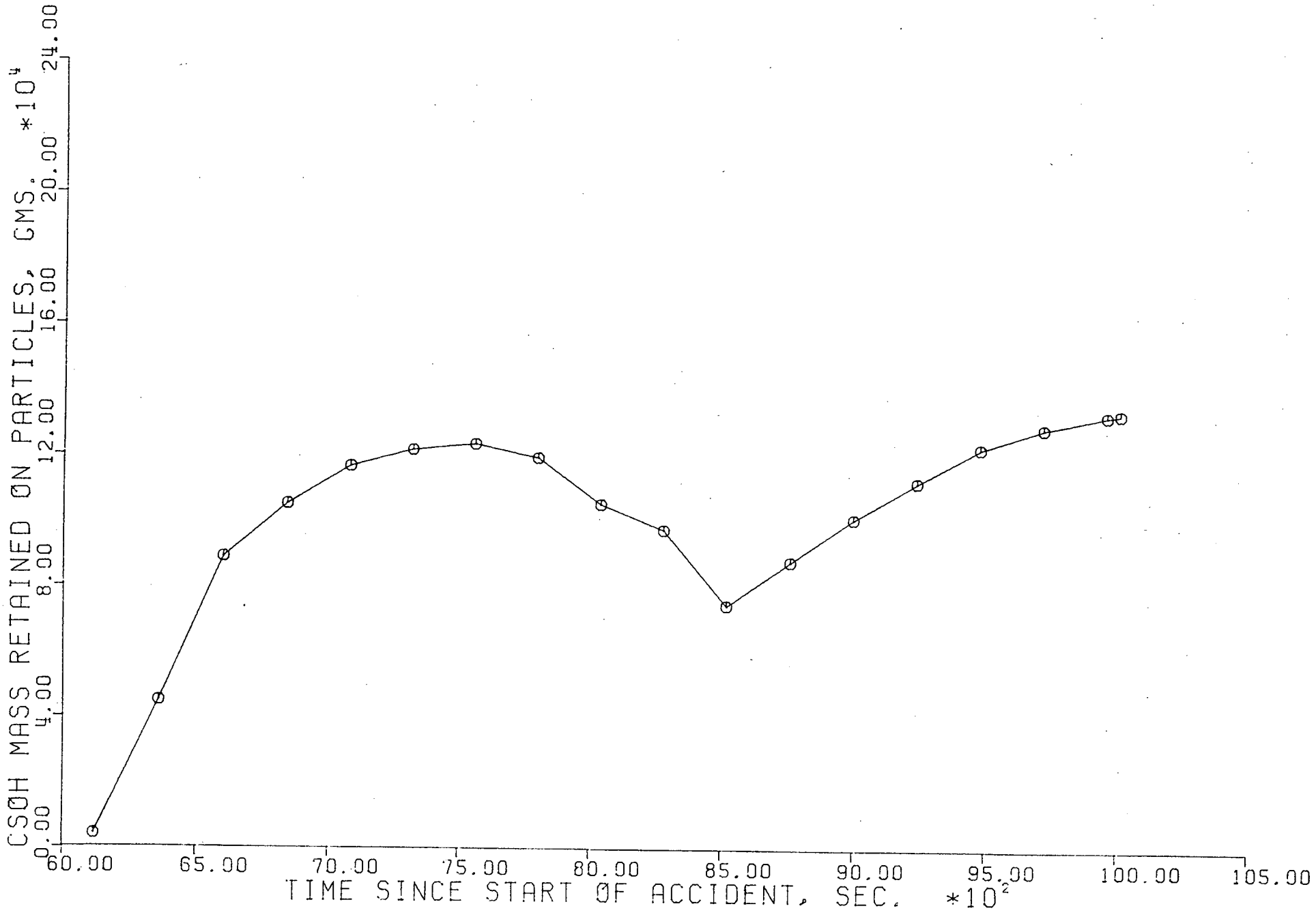
CSOH MASS RETAINED ON PARTICLES, GMS. *10^4
0.00
4.00
8.00
12.00
16.00
20.00
24.00
60.00
65.00
70.00
75.00
80.00
85.00
90.00
95.00
100.00
105.00
TIME SINCE START OF ACCIDENT, SEC. *10^2

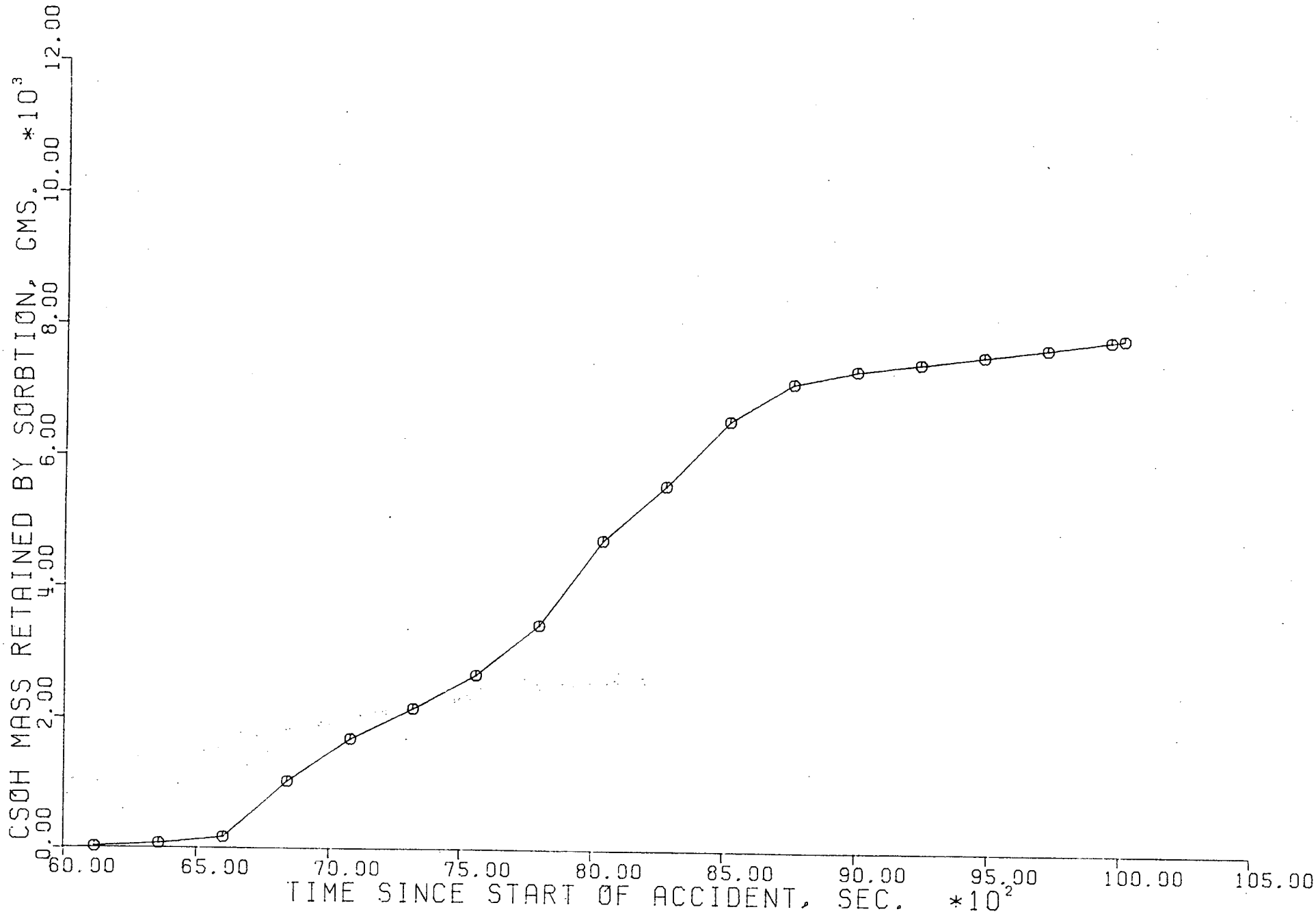
CSOH MASS RETAINED BY SORBTION, GMS. *10³
0.00
2.00
4.00
6.00
8.00
10.00
12.00
60.00
65.00
70.00
75.00
80.00
85.00
90.00
95.00
100.00
105.00
TIME SINCE START OF ACCIDENT, SEC. *10²

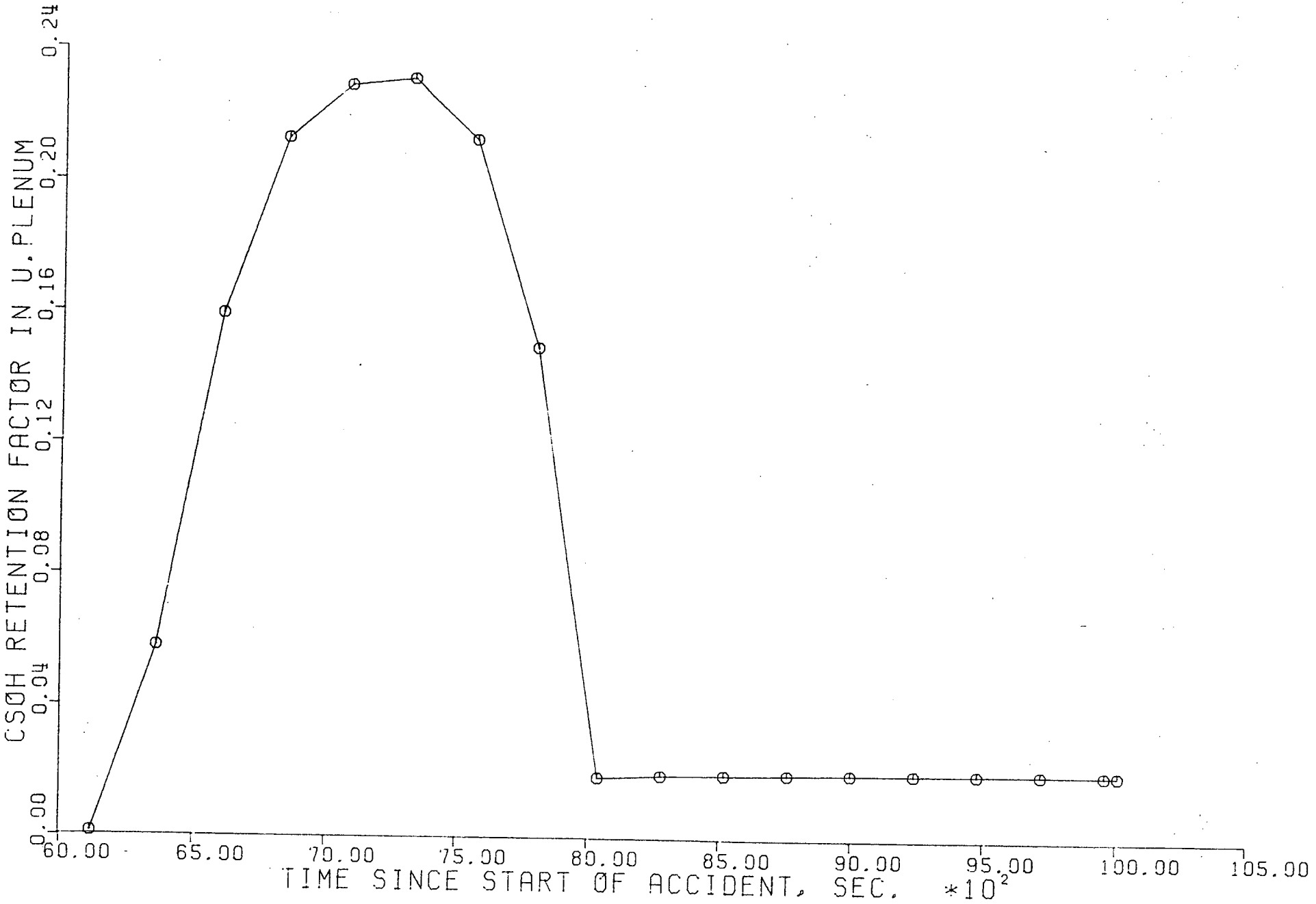
CSOH RETENTION FACTOR IN U.PLENUM
0.00
0.04
0.08
0.12
0.16
0.20
0.24
60.00
65.00
70.00
75.00
80.00
85.00
90.00
95.00
100.00
105.00
TIME SINCE START OF ACCIDENT, SEC. *10²

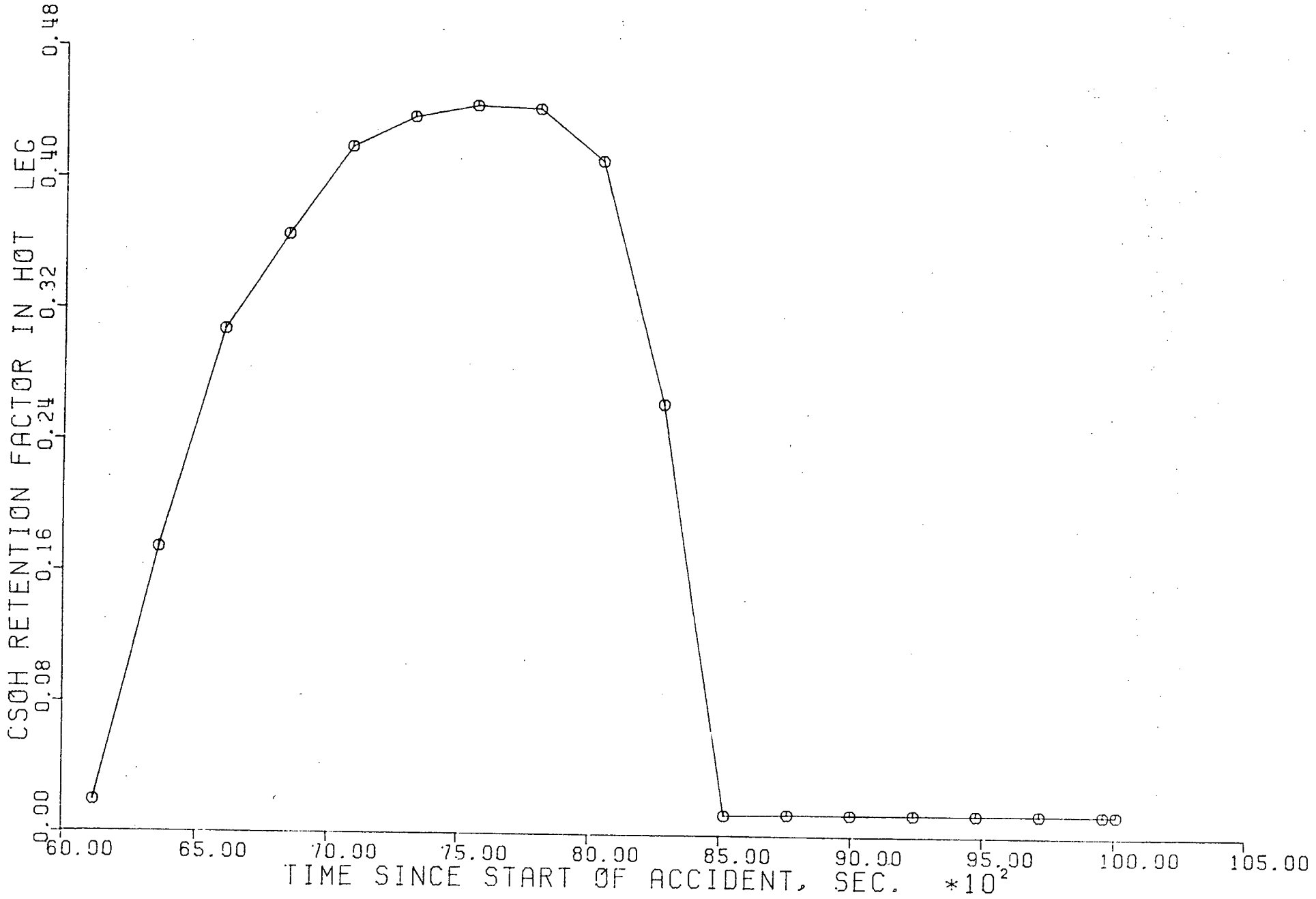
CSOH RETENTION FACTOR IN HOT LEG
0.00
0.08
0.16
0.24
0.32
0.40
0.48
60.00
65.00
70.00
75.00
80.00
85.00
90.00
95.00
100.00
105.00
TIME SINCE START OF ACCIDENT, SEC. *10²

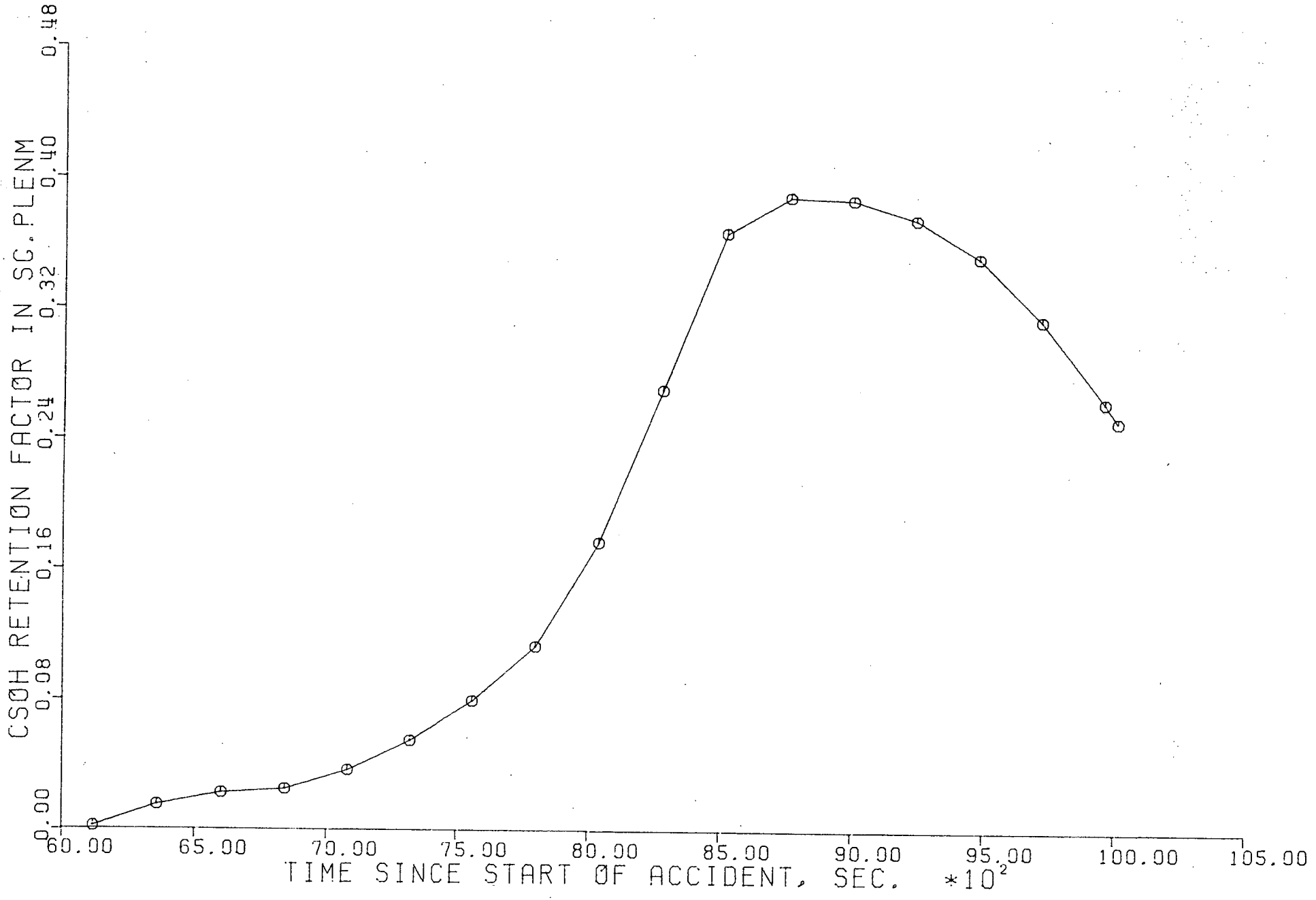
CSOH RETENTION FACTOR IN SG. PLENM
0.00
0.08
0.16
0.24
0.32
0.40
0.48
60.00
65.00
70.00
75.00
80.00
85.00
90.00
95.00
100.00
105.00
TIME SINCE START OF ACCIDENT, SEC. *10²

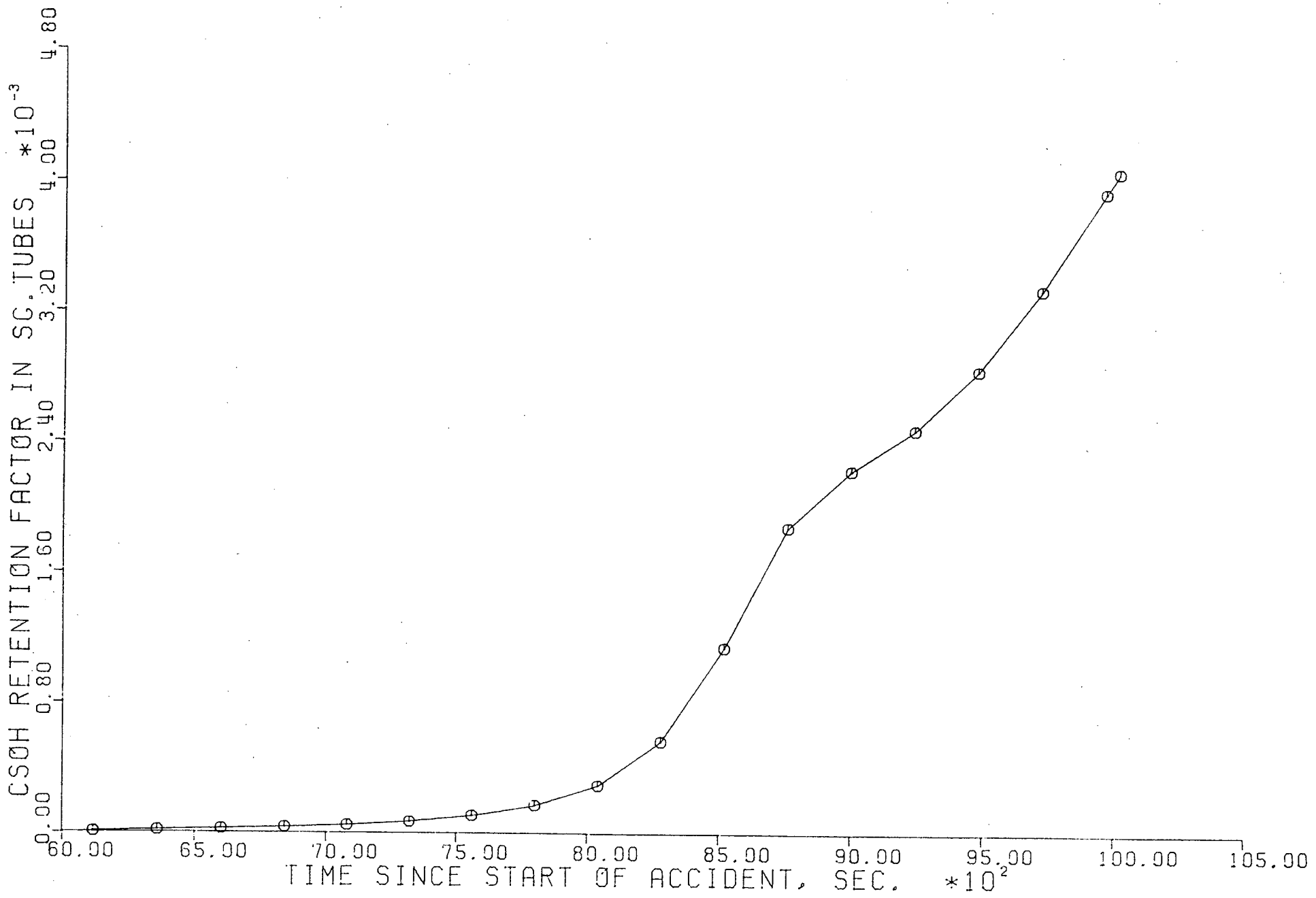
CSØH RETENTION FACTOR IN SG. TUBES *10⁻³
0.00
0.80
1.60
2.40
3.20
4.00
4.80
60.00
65.00
70.00
75.00
80.00
85.00
90.00
95.00
100.00
105.00
TIME SINCE START OF ACCIDENT, SEC. *10²

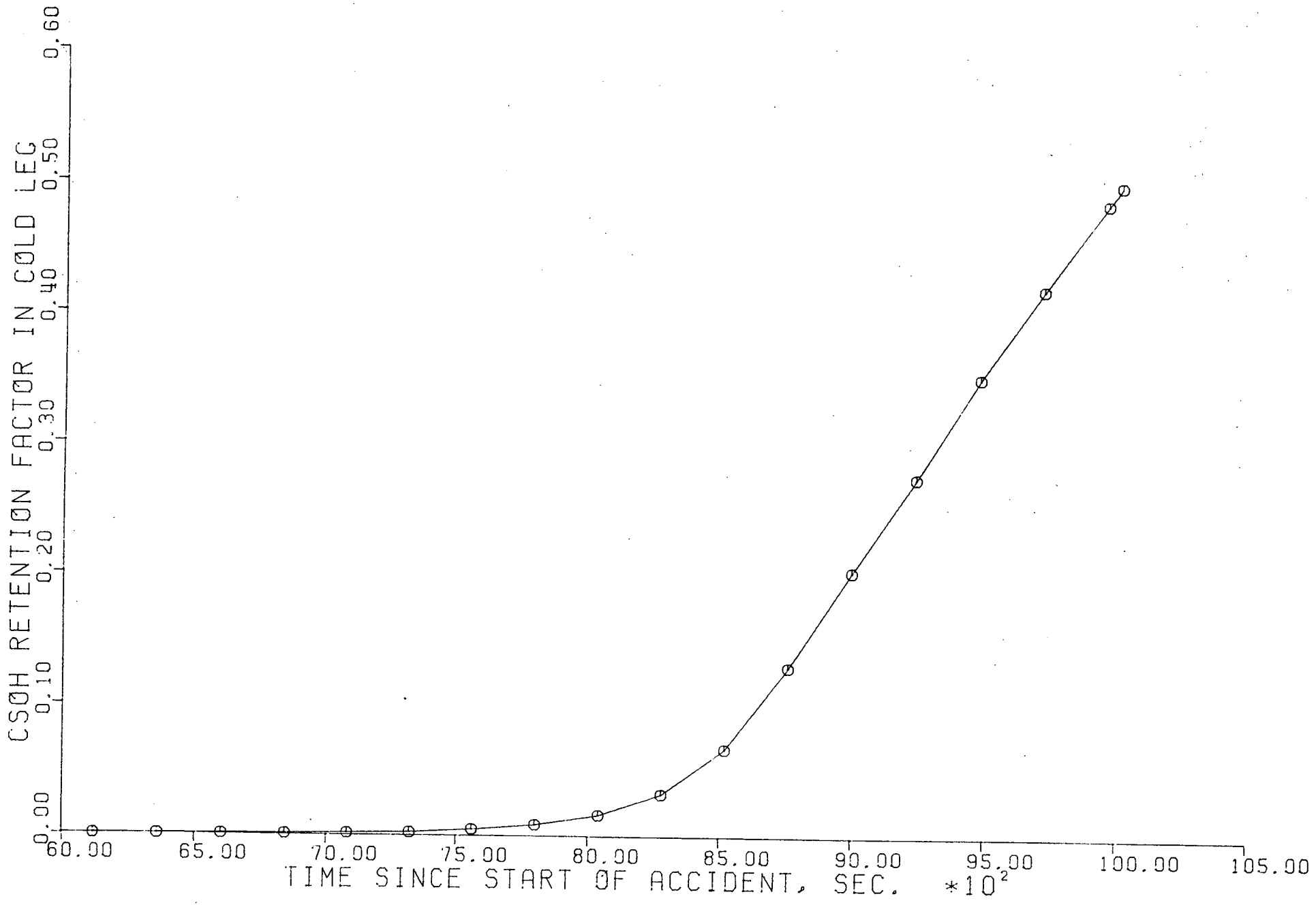
CSØH RETENTION FACTØR IN CØLD LEG
0.00
0.10
0.20
0.30
0.40
0.50
0.60
60.00
65.00
70.00
75.00
80.00
85.00
90.00
95.00
100.00
105.00
TIME SINCE START ØF ACCIDENT, SEC. *10²

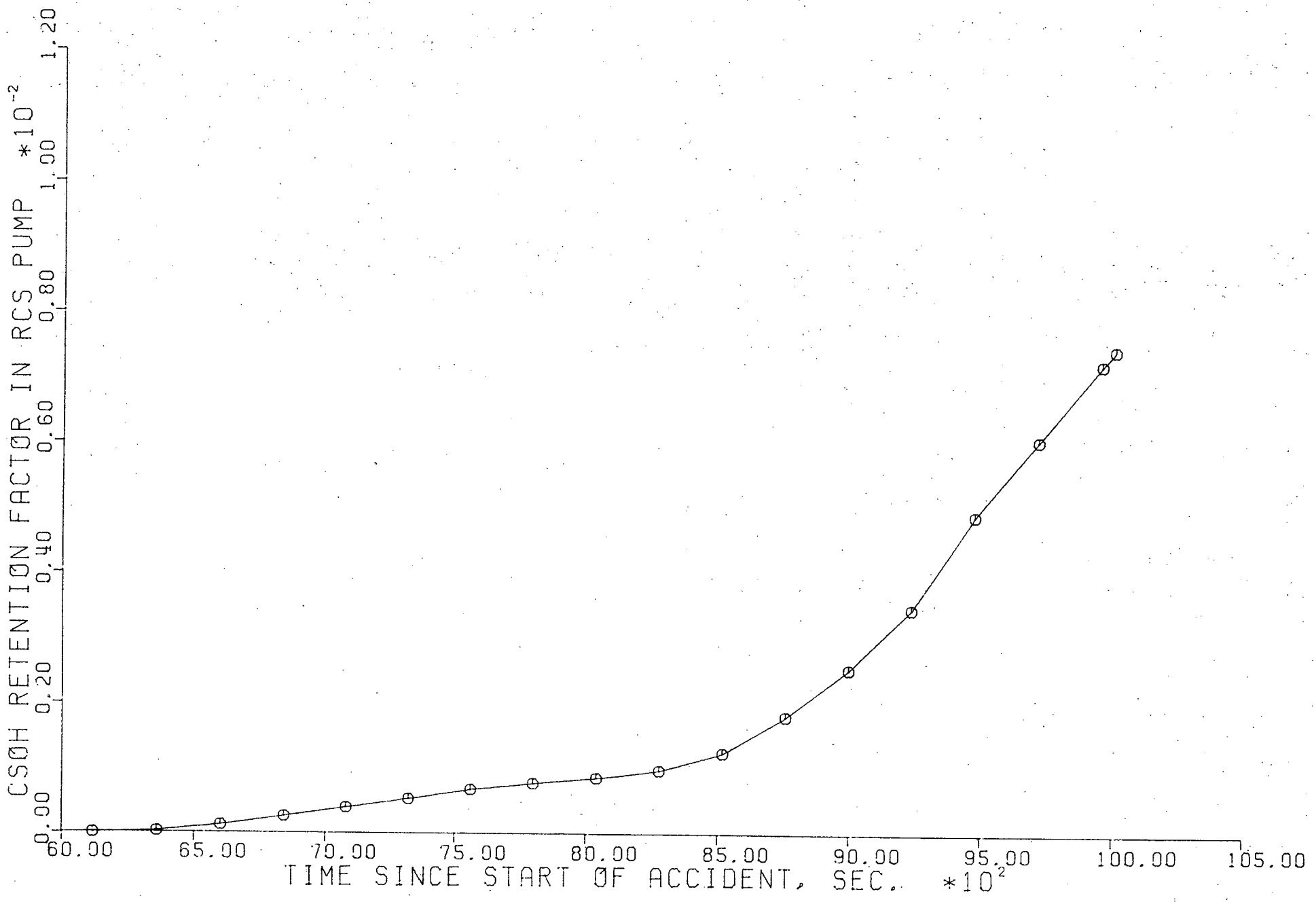
CSOH RETENTION FACTOR IN RCS PUMP *10-2
0.00
0.20
0.40
0.60
0.80
1.00
1.20
60.00
65.00
70.00
75.00
80.00
85.00
90.00
95.00
100.00
105.00
TIME SINCE START OF ACCIDENT, SEC. *10^2

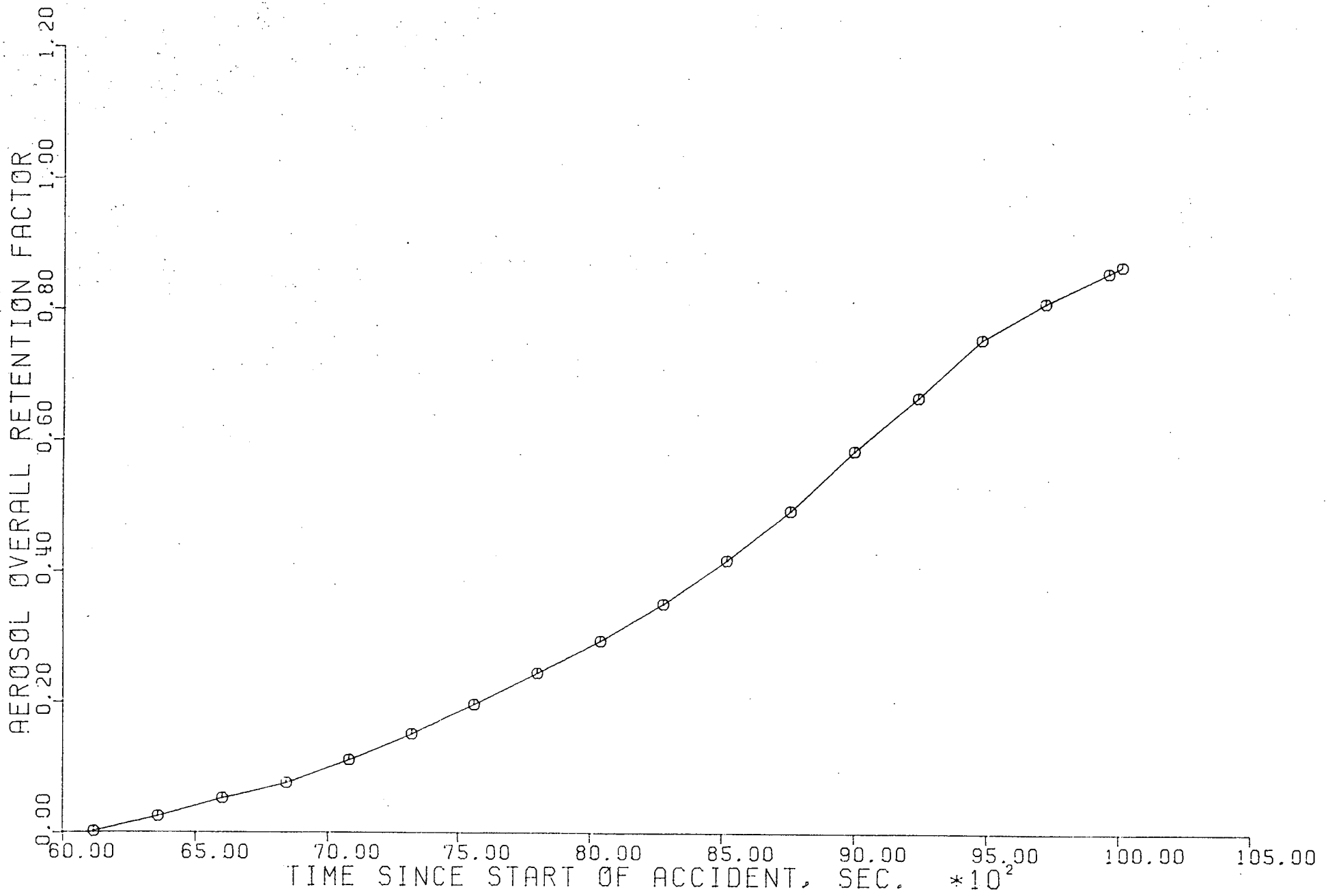
AEROSOL OVERALL RETENTION FACTOR
0.00
0.20
0.40
0.60
0.80
1.00
1.20
60.00
65.00
70.00
75.00
80.00
85.00
90.00
95.00
100.00
105.00
TIME SINCE START OF ACCIDENT, SEC. *10²

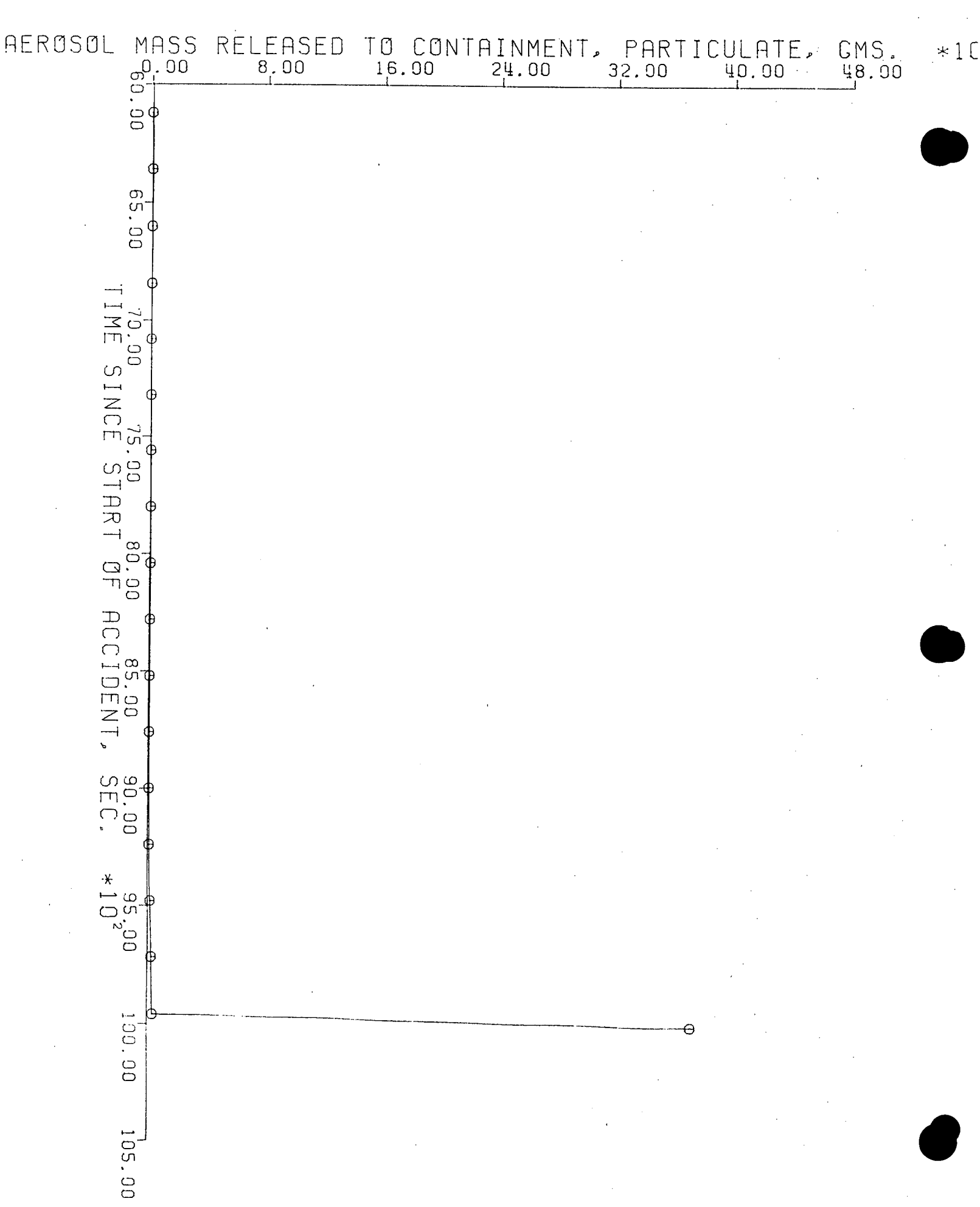
AEROSOL MASS RELEASED TO CONTAINMENT, PARTICULATE, GMS. *10
0.00
8.00
16.00
24.00
32.00
40.00
48.00
60.00
65.00
70.00
75.00
80.00
85.00
90.00
95.00
100.00
105.00
TIME SINCE START OF ACCIDENT, SEC. *10²

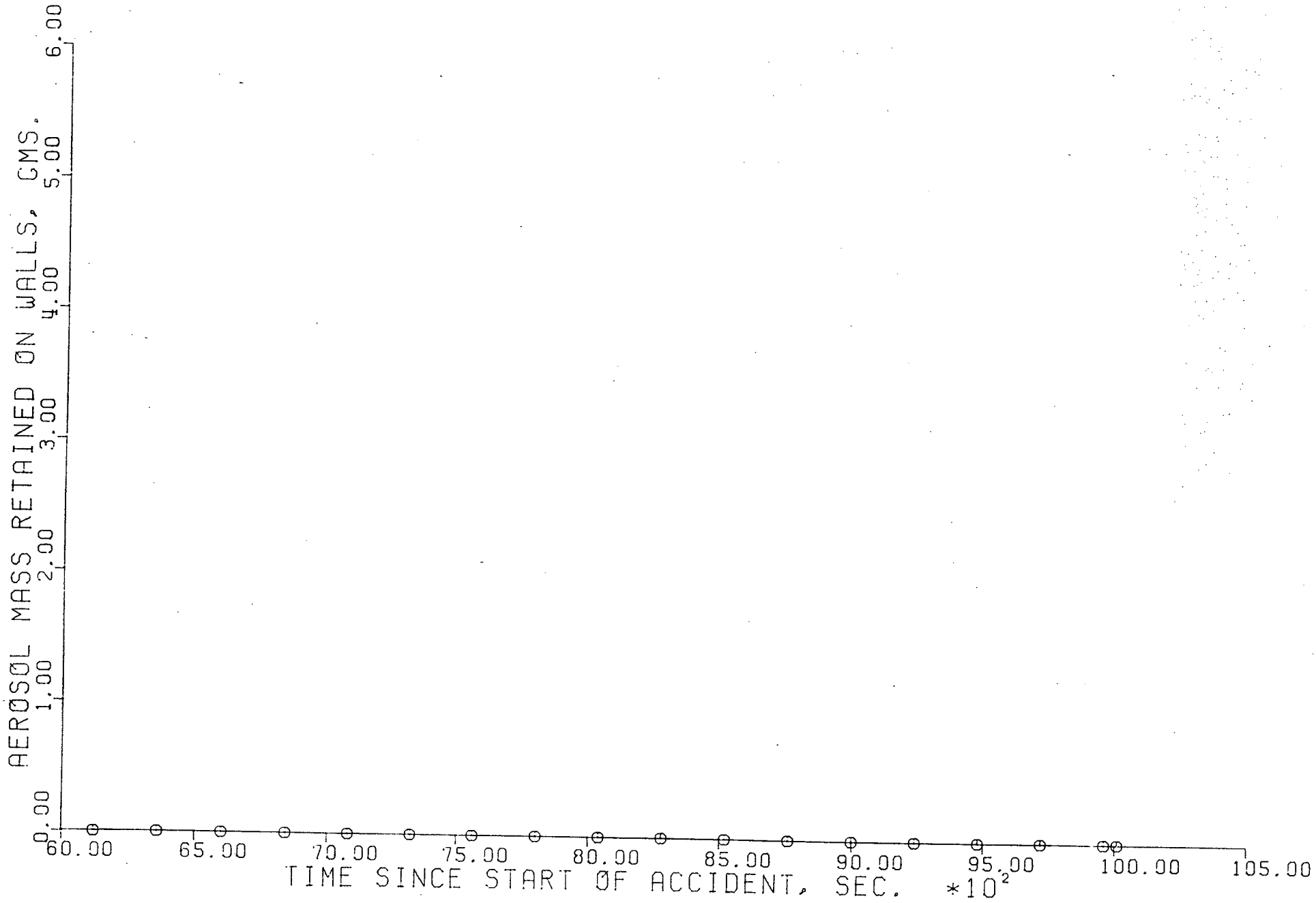
AEROSOL MASS RETAINED ON WALLS, CMS.
0.00
1.00
2.00
3.00
4.00
5.00
6.00
60.00
65.00
70.00
75.00
80.00
85.00
90.00
95.00
100.00
105.00
TIME SINCE START OF ACCIDENT, SEC. *10²

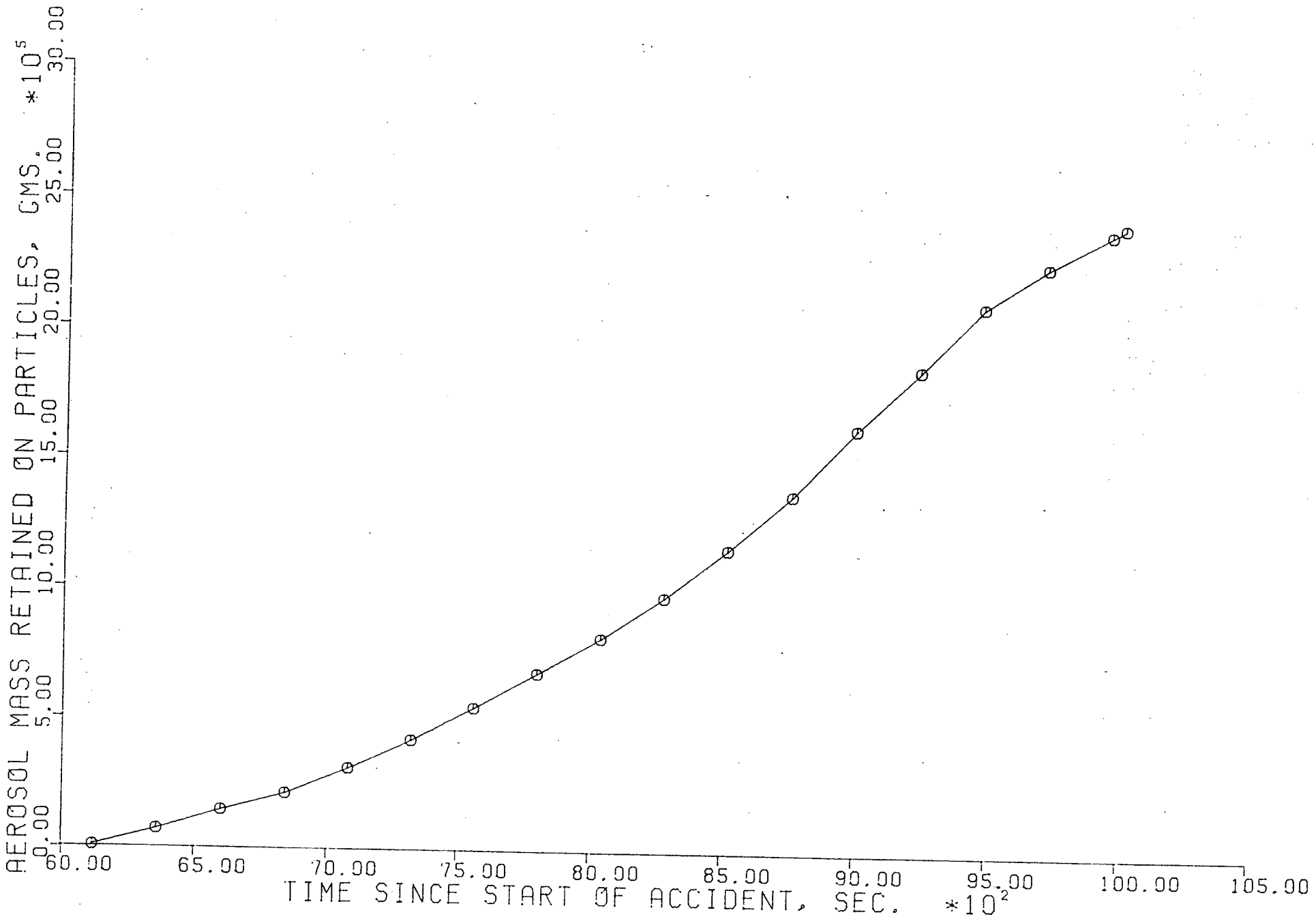
AEROSOL MASS RETAINED ON PARTICLES, GMS. *10^5
0.00
5.00
10.00
15.00
20.00
25.00
30.00
60.00
65.00
70.00
75.00
80.00
85.00
90.00
95.00
100.00
105.00
TIME SINCE START OF ACCIDENT, SEC. *10^2

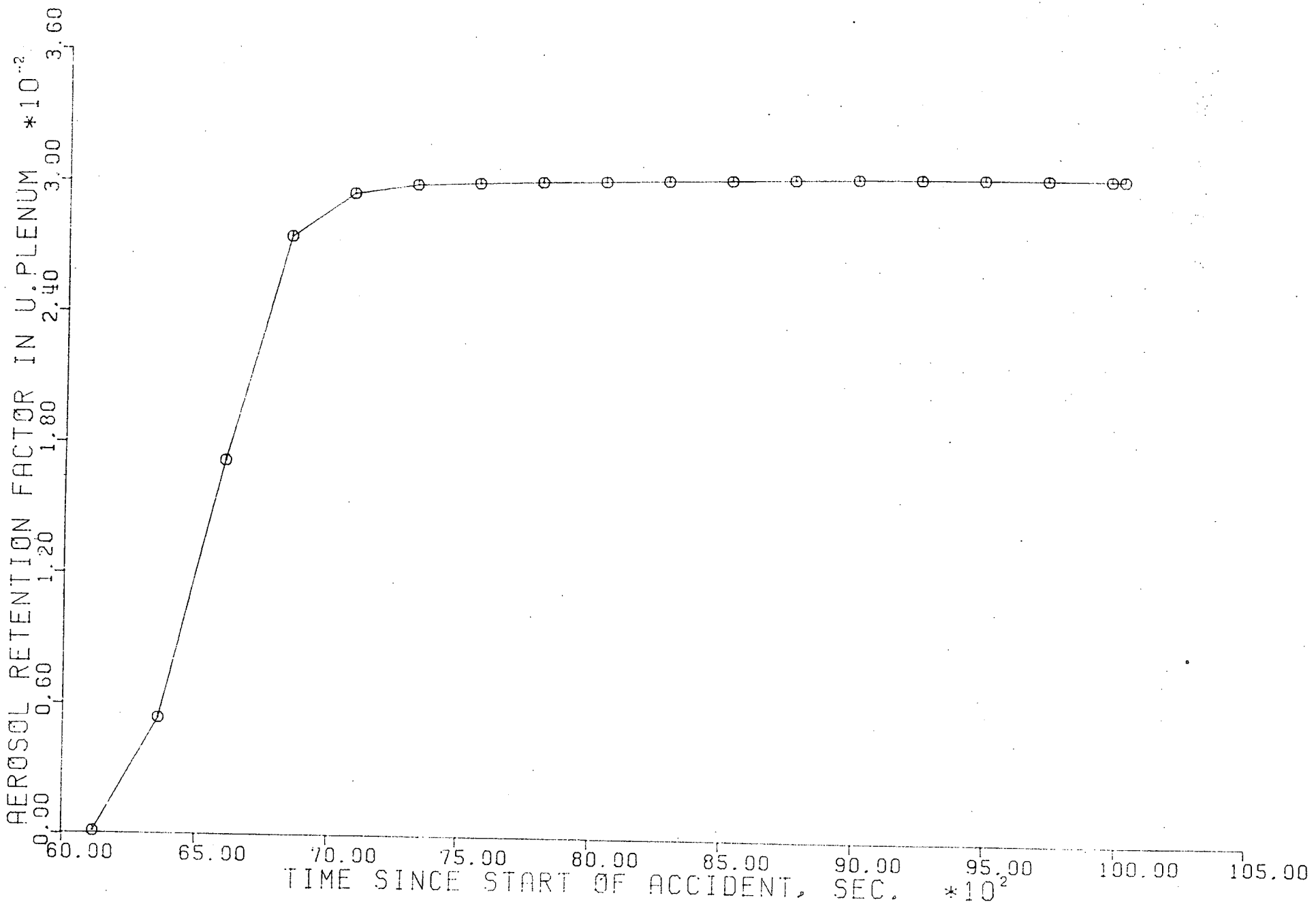
AEROSOL RETENTION FACTOR IN U.PLENUM *10⁻²
0.00
0.60
1.20
1.80
2.40
3.00
3.60
60.00
65.00
70.00
75.00
80.00
85.00
90.00
95.00
100.00
105.00
TIME SINCE START OF ACCIDENT, SEC. *10²

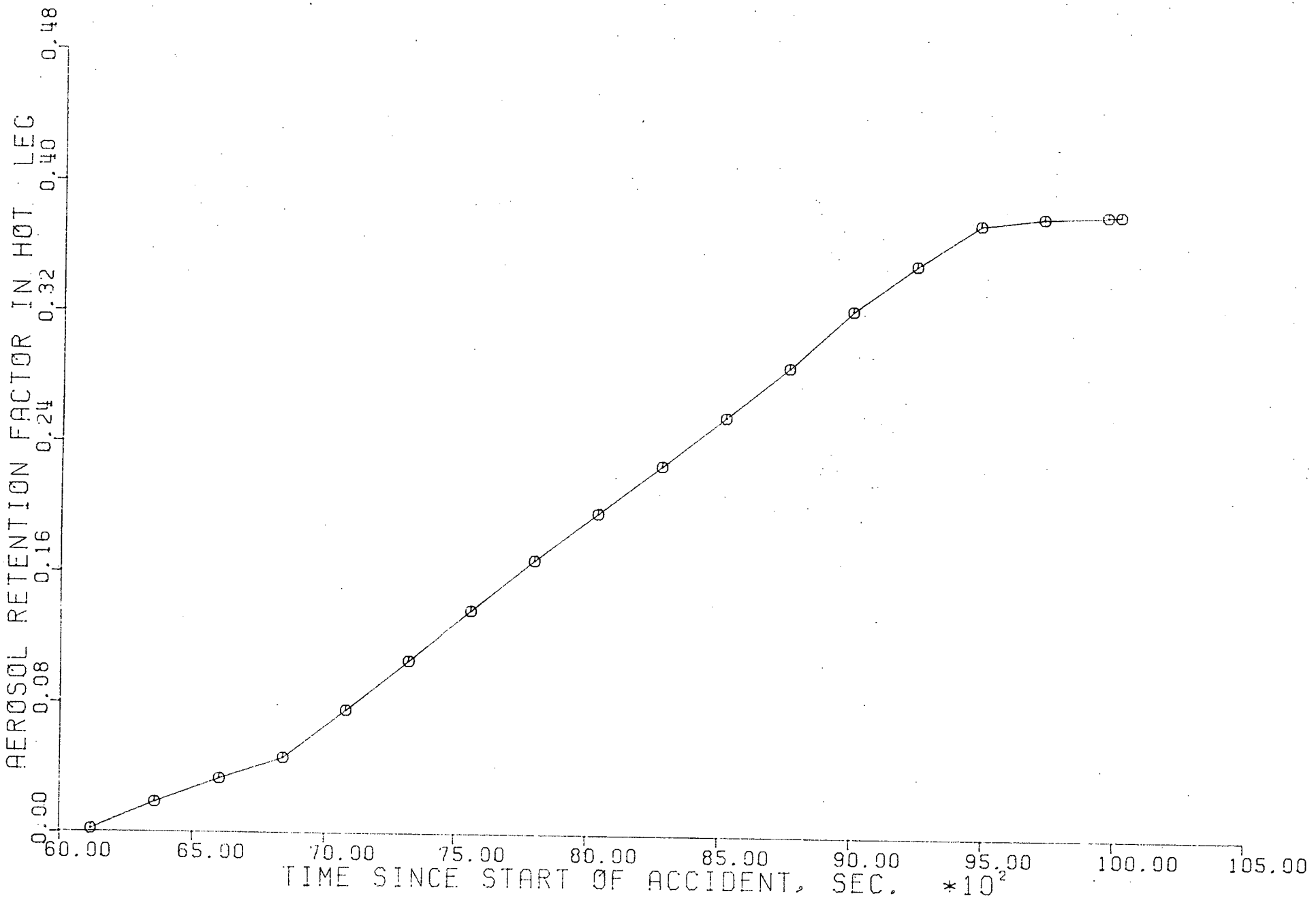
AEROSOL RETENTION FACTOR IN HOT LEG
0.00
0.08
0.16
0.24
0.32
0.40
0.48
60.00
65.00
70.00
75.00
80.00
85.00
90.00
95.00
100.00
105.00
TIME SINCE START OF ACCIDENT, SEC. *10²

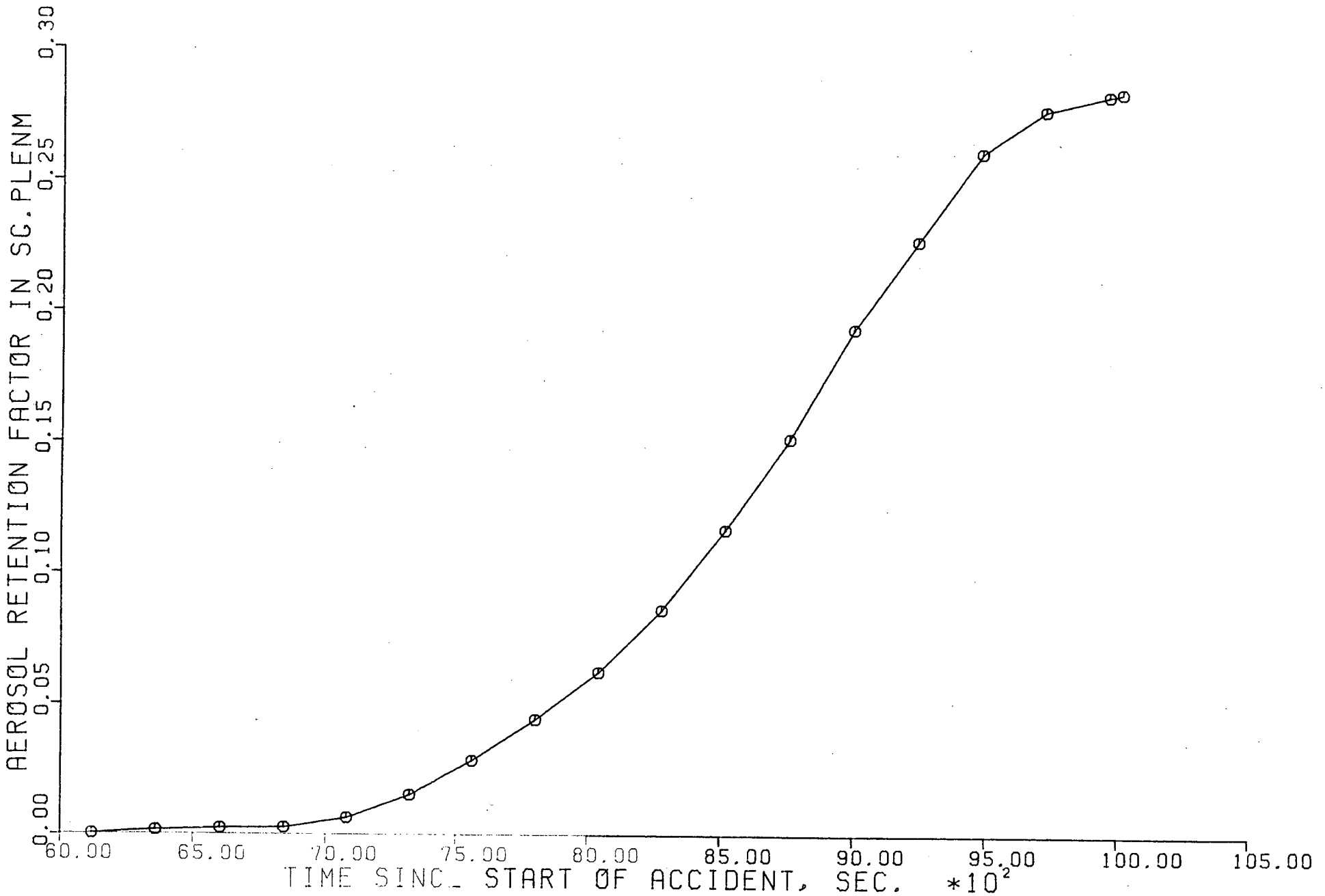
AERØSØL RETENTIØN FACTØR IN SG. PLENM
0.00
0.05
0.10
0.15
0.20
0.25
0.30
60.00
65.00
70.00
75.00
80.00
85.00
90.00
95.00
100.00
105.00
TIME SINCE START ØF ACCIDENT, SEC. *10²

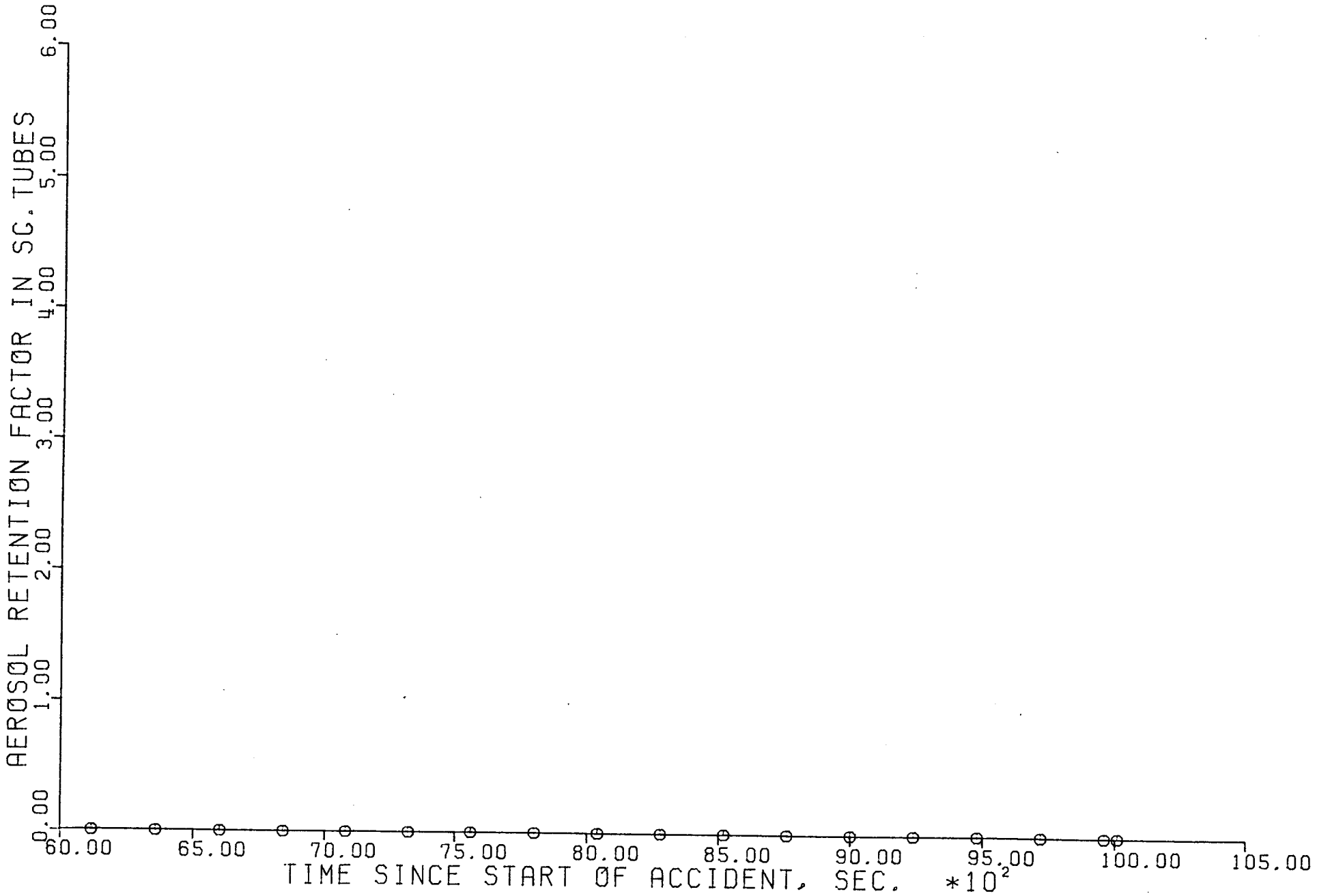
AEROSOL RETENTION FACTOR IN SG. TUBES
0.00
1.00
2.00
3.00
4.00
5.00
6.00
60.00
65.00
70.00
75.00
80.00
85.00
90.00
95.00
100.00
105.00
TIME SINCE START OF ACCIDENT, SEC. *10²

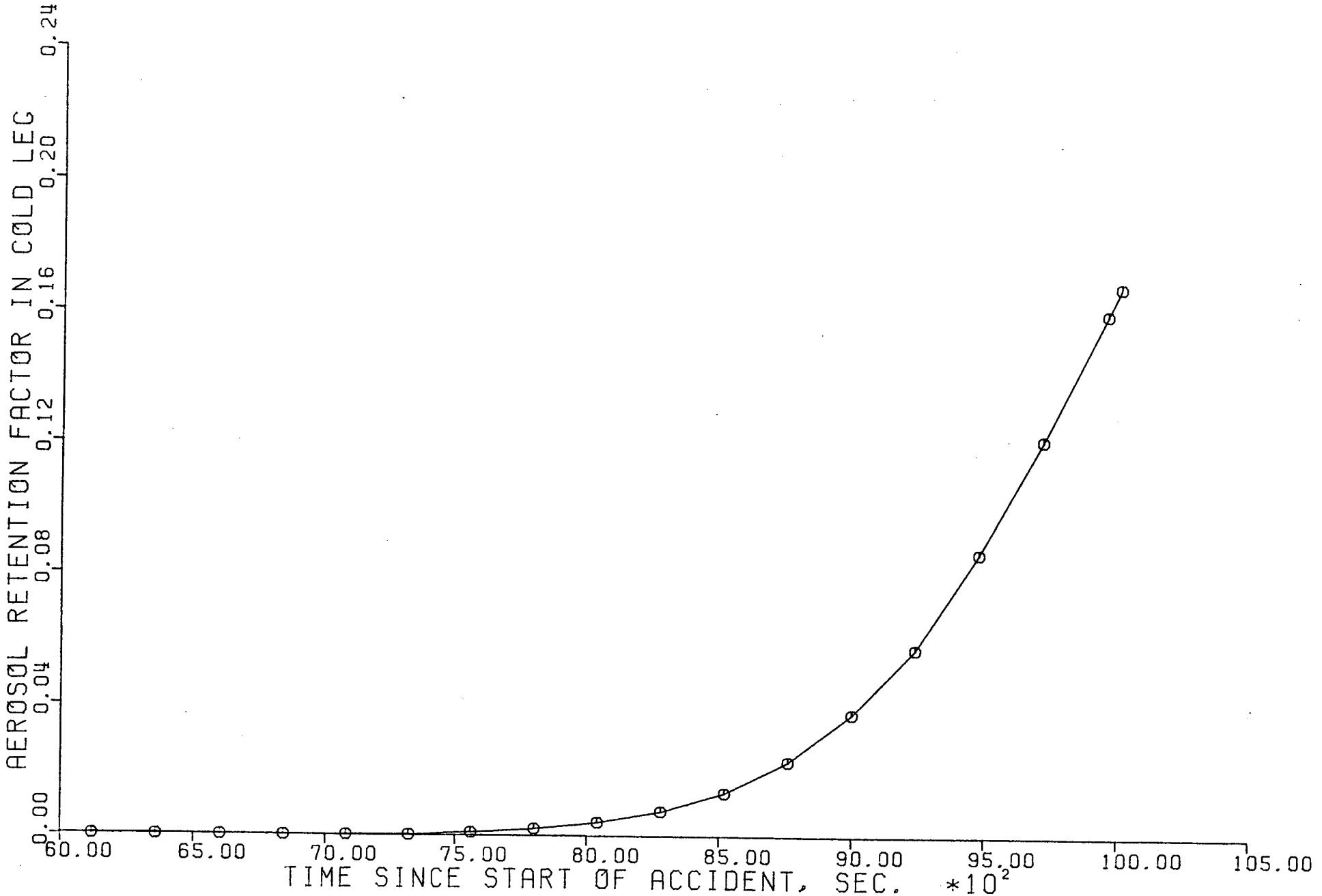
AEROSOL RETENTION FACTOR IN COLD LEG
0.00
0.04
0.08
0.12
0.16
0.20
0.24
60.00
65.00
70.00
75.00
80.00
85.00
90.00
95.00
100.00
105.00
TIME SINCE START OF ACCIDENT, SEC. *10²

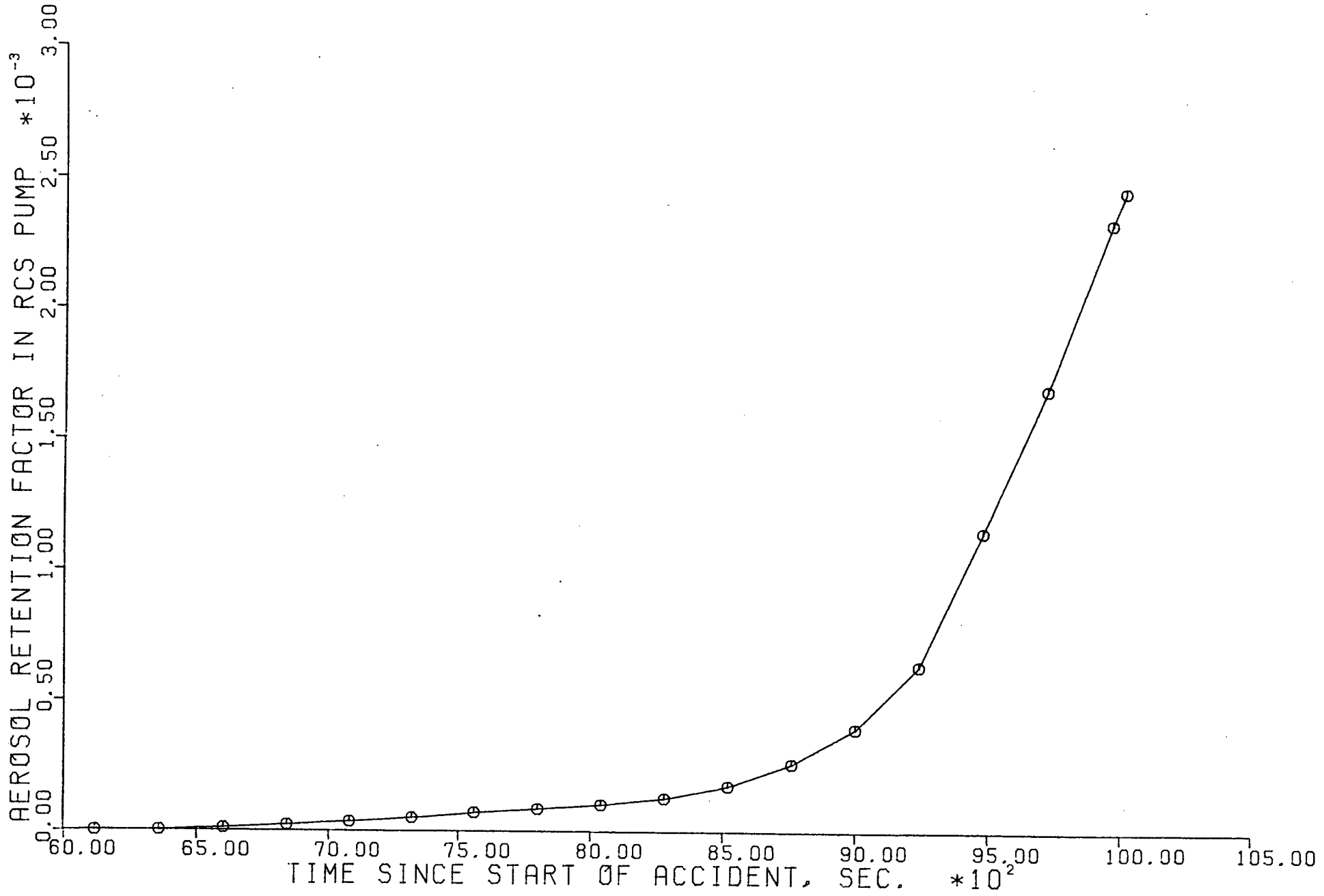
AERØSØL RETENTION FACTØR IN RCS PUMP *10^-3
3.00
2.50
2.00
1.50
1.00
0.50
0.00
60.00
65.00
70.00
75.00
80.00
85.00
90.00
95.00
100.00
105.00
TIME SINCE START ØF ACCIDENT, SEC. *10^2

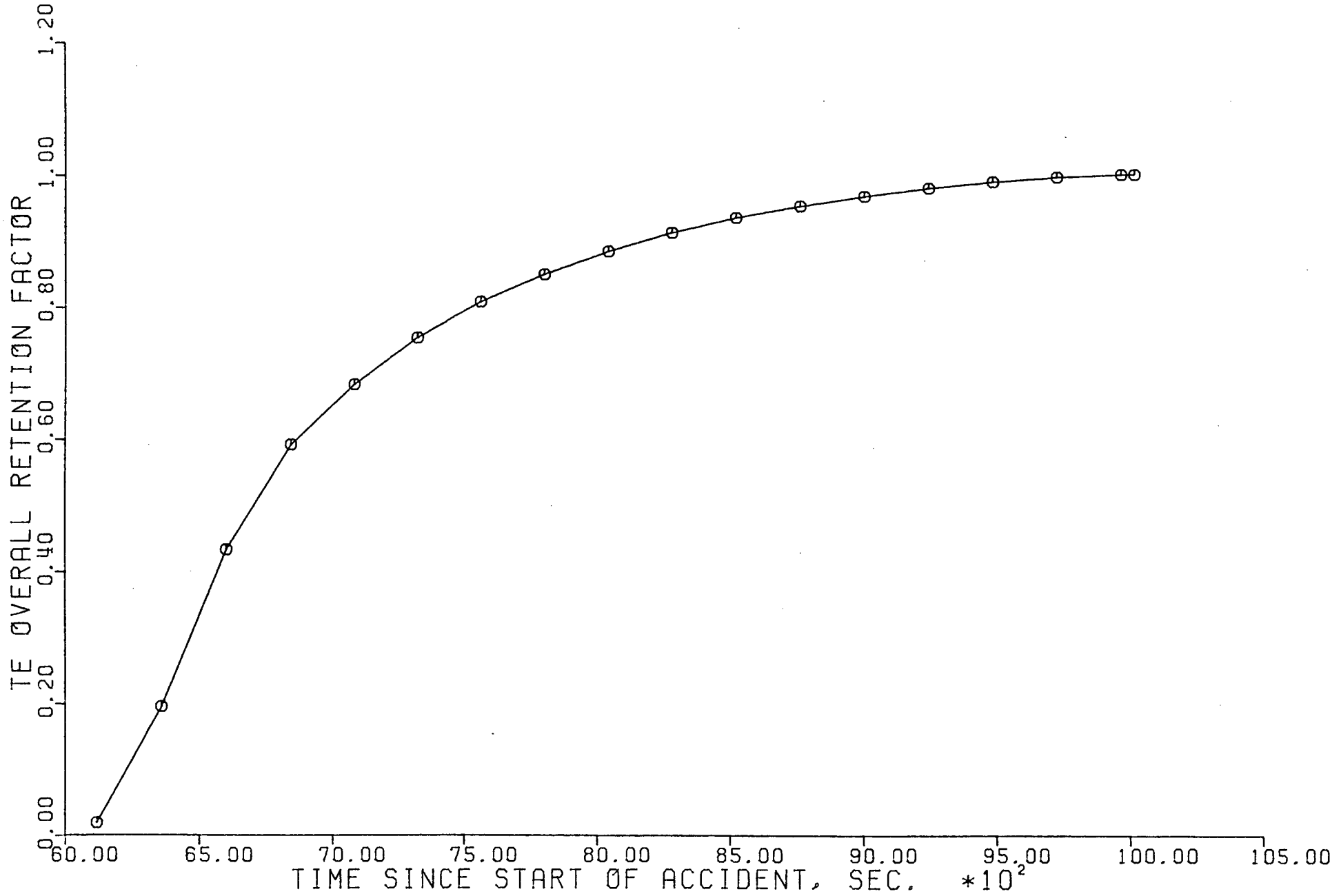
TE OVERALL RETENTION FACTOR
0.00
0.20
0.40
0.60
0.80
1.00
1.20
60.00
65.00
70.00
75.00
80.00
85.00
90.00
95.00
100.00
105.00
TIME SINCE START OF ACCIDENT, SEC. *10²

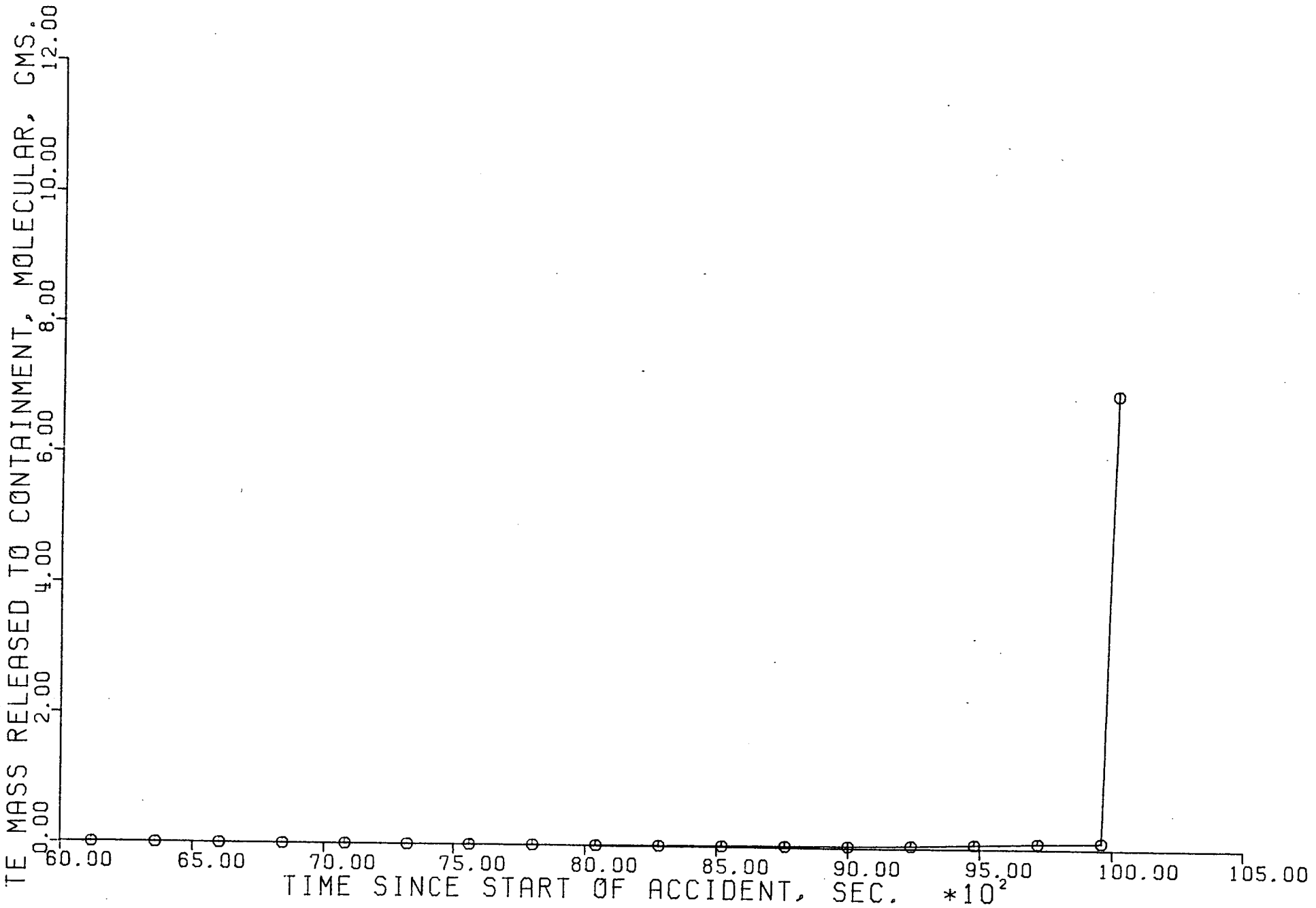
TE MASS RELEASED TO CONTAINMENT, MOLECULAR, GMS.
0.00
2.00
4.00
6.00
8.00
10.00
12.00
60.00
65.00
70.00
75.00
80.00
85.00
90.00
95.00
100.00
105.00
TIME SINCE START OF ACCIDENT, SEC. *10²

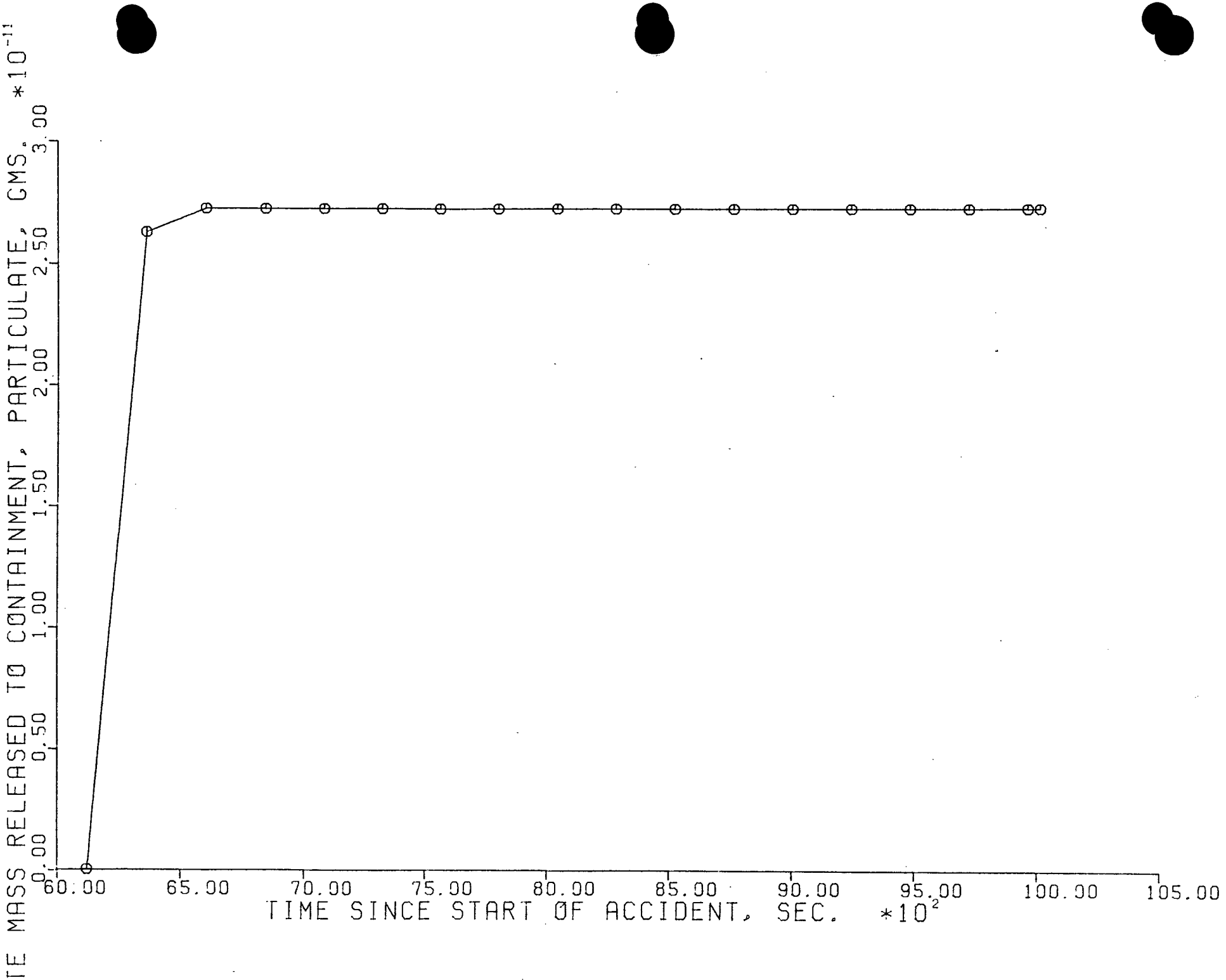
TE MASS RELEASED TO CONTAINMENT, PARTICULATE, CMS. *10^-11
0.00
0.50
1.00
1.50
2.00
2.50
3.00
60.00
65.00
70.00
75.00
80.00
85.00
90.00
95.00
100.00
105.00
TIME SINCE START OF ACCIDENT, SEC. *10^2

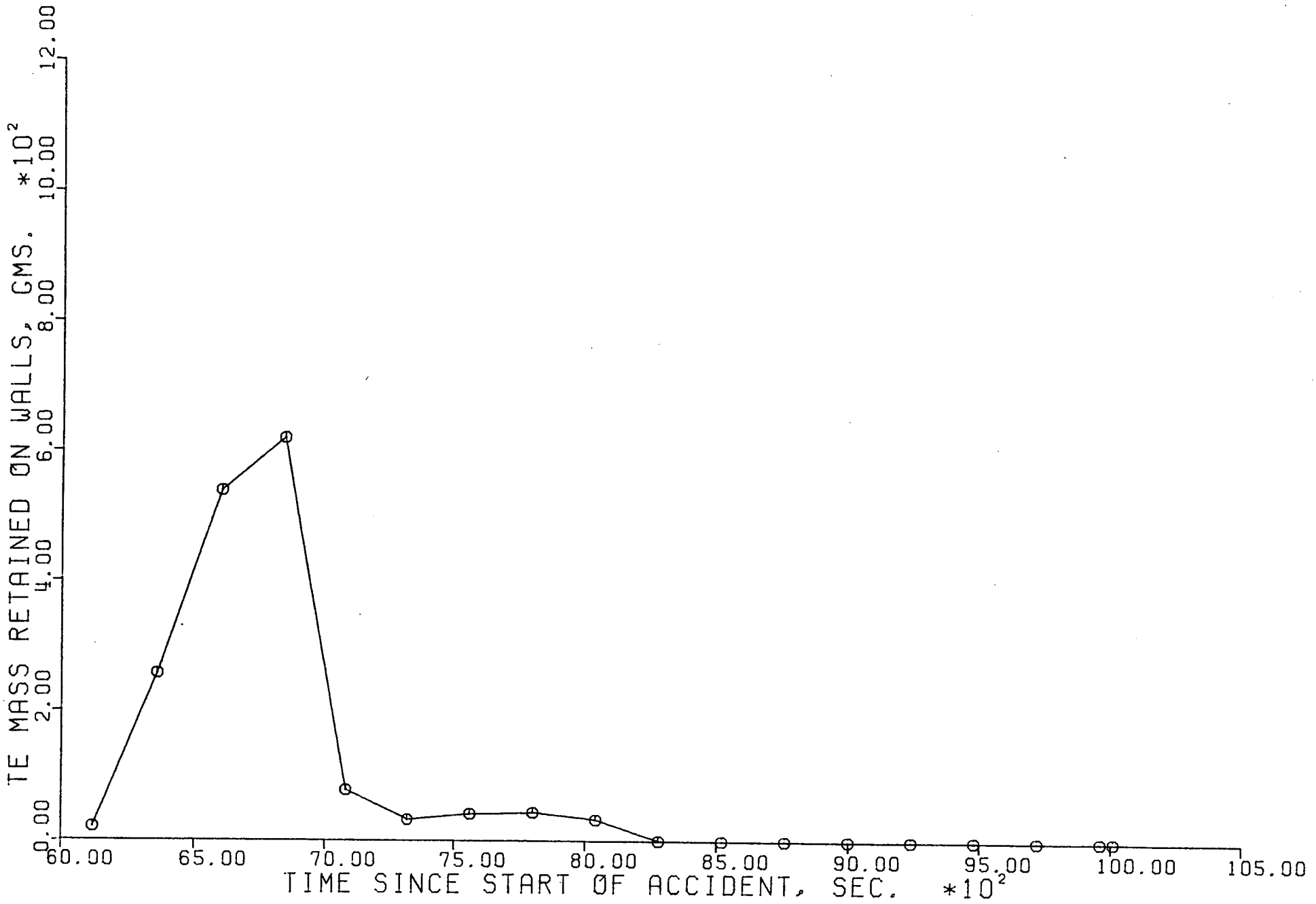
TE MASS RETAINED ON WALLS, GMS. *10²
0.00
2.00
4.00
6.00
8.00
10.00
12.00
60.00
65.00
70.00
75.00
80.00
85.00
90.00
95.00
100.00
105.00
TIME SINCE START OF ACCIDENT, SEC. *10²

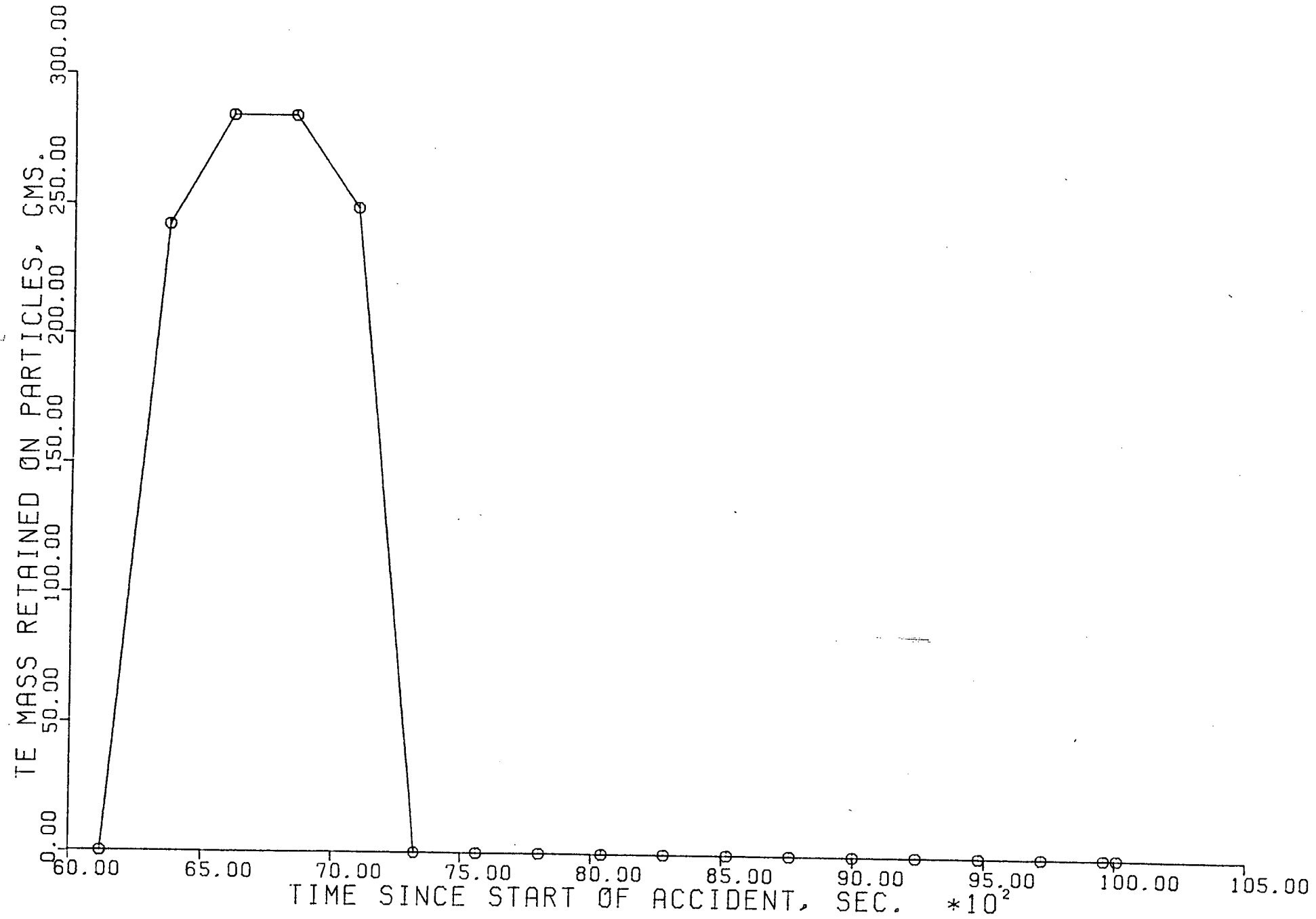
TE MASS RETAINED ON PARTICLES, GMS.
0.00
50.00
100.00
150.00
200.00
250.00
300.00
60.00
65.00
70.00
75.00
80.00
85.00
90.00
95.00
100.00
105.00
TIME SINCE START OF ACCIDENT, SEC. *10²

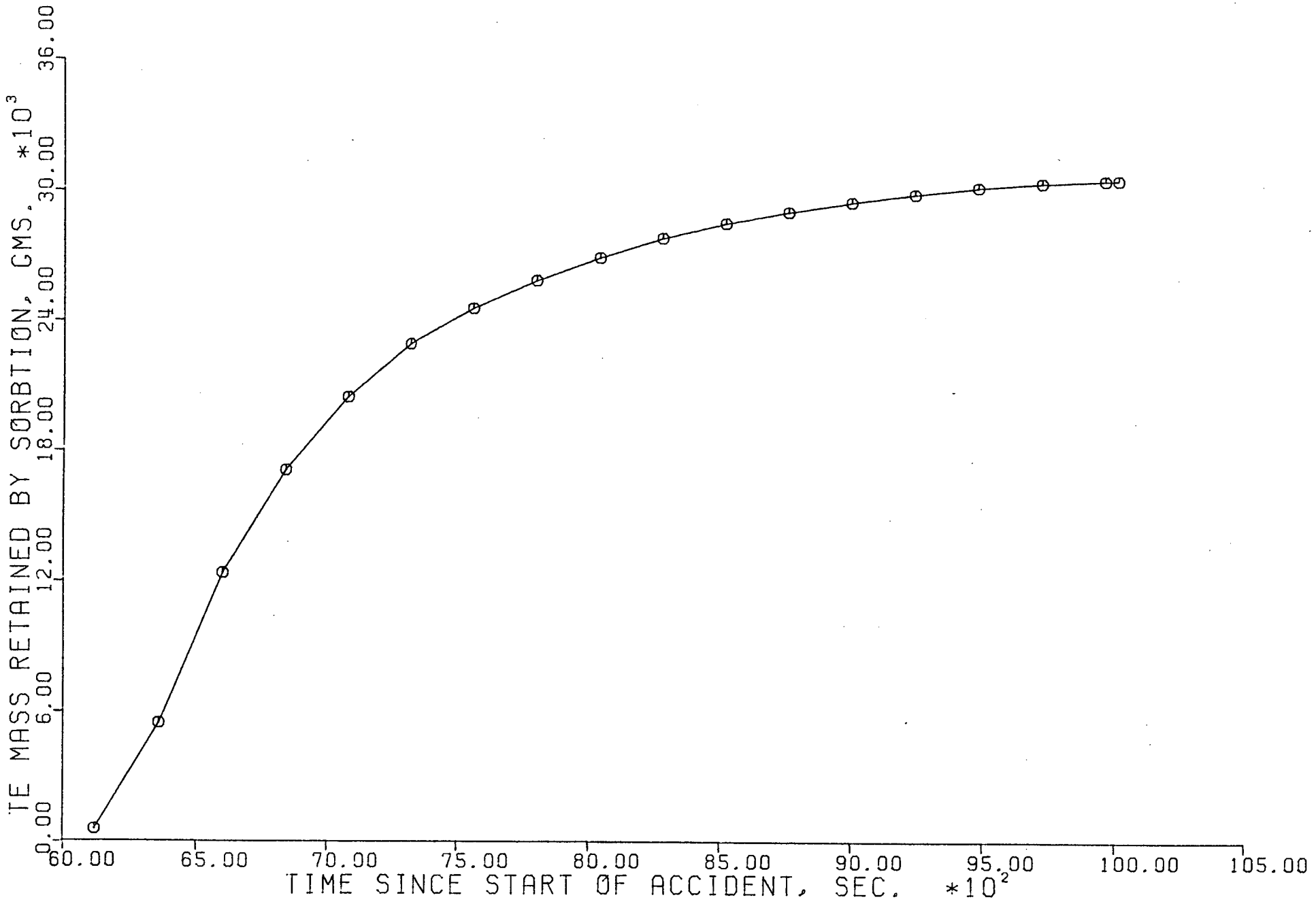
TE MASS RETAINED BY SORBTION, GMS. *10^3
0.00
6.00
12.00
18.00
24.00
30.00
36.00
60.00
65.00
70.00
75.00
80.00
85.00
90.00
95.00
100.00
105.00
TIME SINCE START OF ACCIDENT, SEC. *10^2

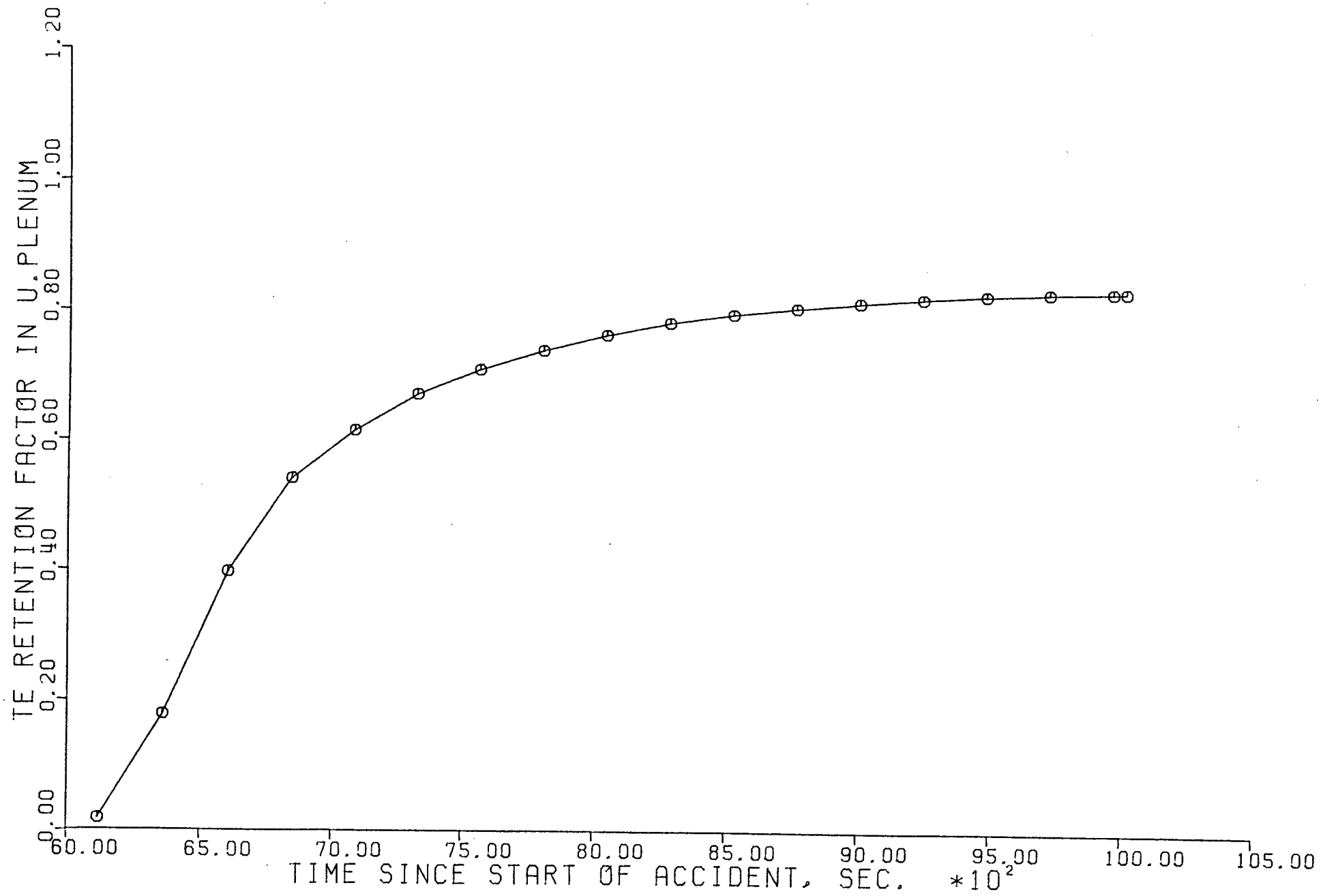
TE RETENTION FACTOR IN U.PLENUM
0.00
0.20
0.40
0.60
0.80
1.00
1.20
60.00
65.00
70.00
75.00
80.00
85.00
90.00
95.00
100.00
105.00
TIME SINCE START OF ACCIDENT, SEC. *10²

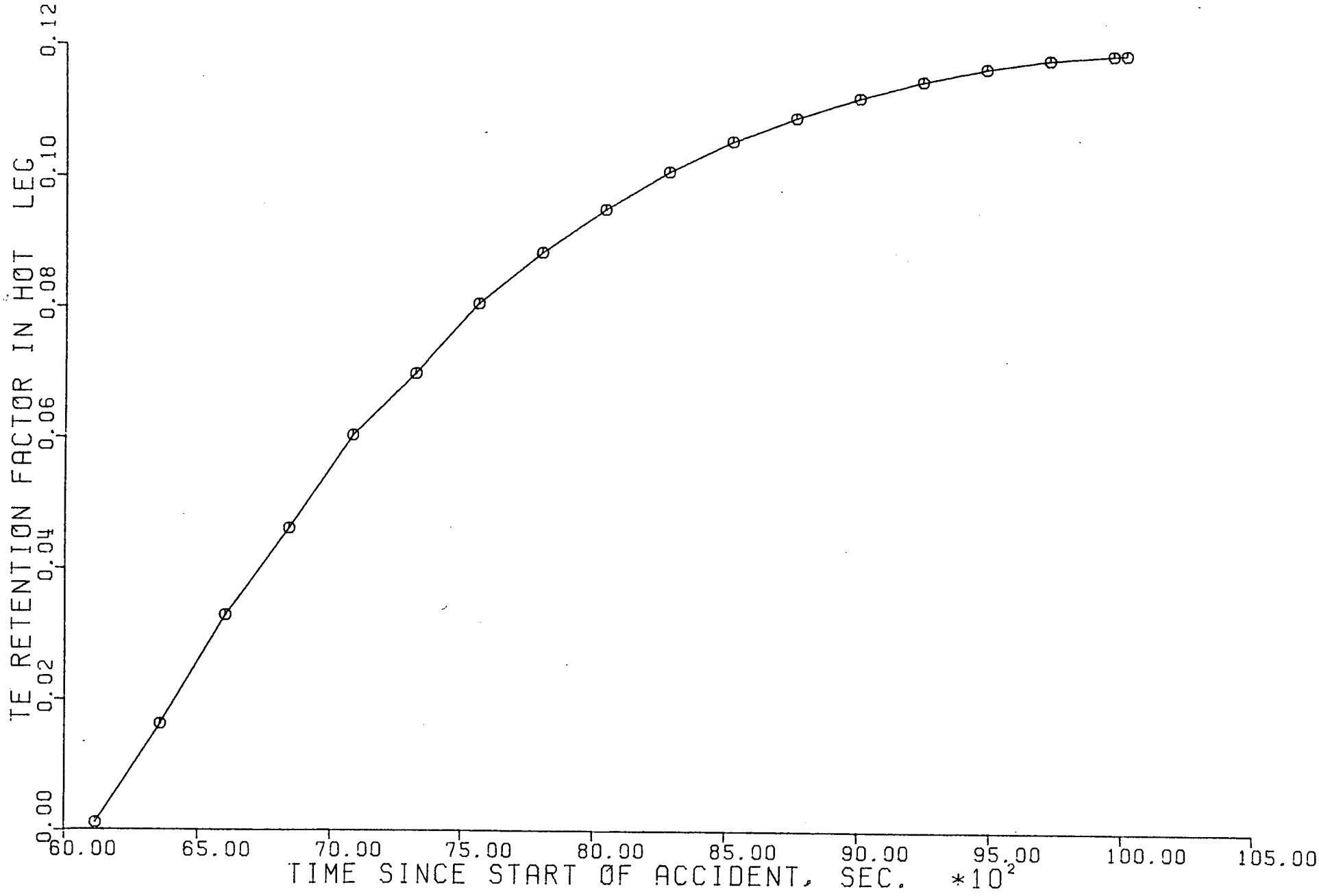
TE RETENTION FACTOR IN HOT LEG
0.00
0.02
0.04
0.06
0.08
0.10
0.12
60.00
65.00
70.00
75.00
80.00
85.00
90.00
95.00
100.00
105.00
TIME SINCE START OF ACCIDENT, SEC. *10²

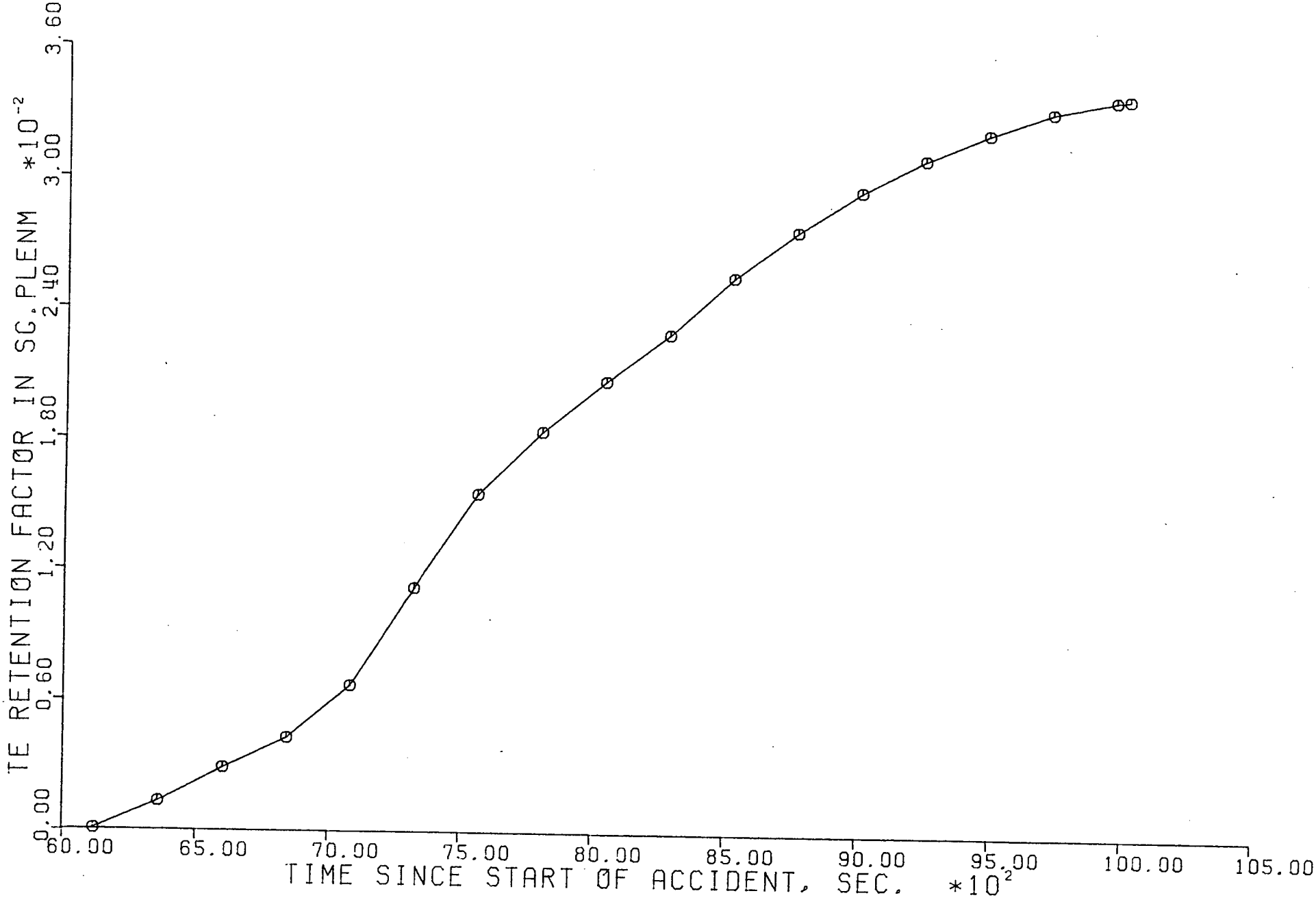
TE RETENTION FACTOR IN SG. PLENM *10⁻²
0.00
0.60
1.20
1.80
2.40
3.00
3.60
60.00
65.00
70.00
75.00
80.00
85.00
90.00
95.00
100.00
105.00
TIME SINCE START OF ACCIDENT, SEC. *10²

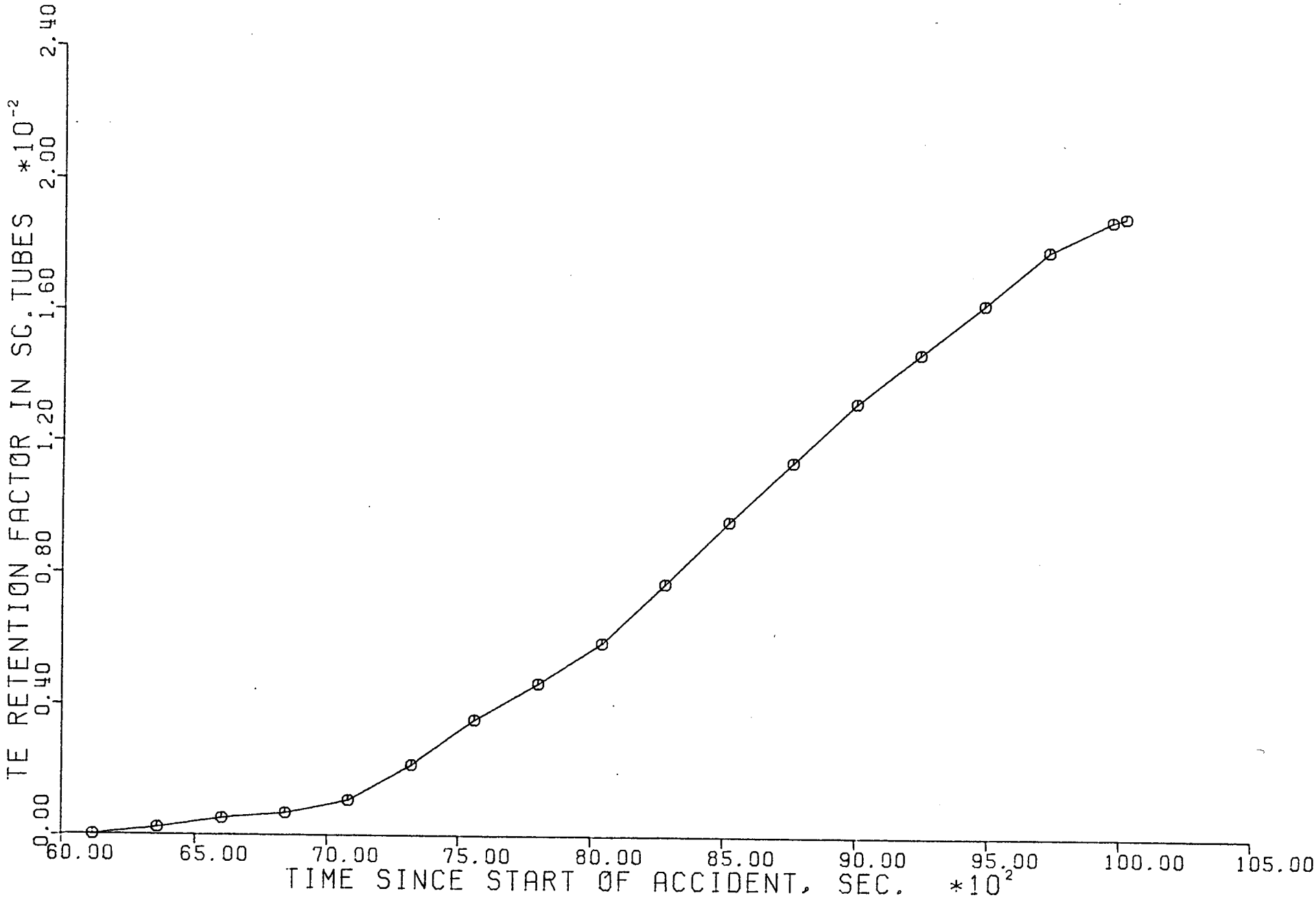
TE RETENTION FACTOR IN SG. TUBES *10⁻²
0.00
0.40
0.80
1.20
1.60
2.00
2.40
60.00
65.00
70.00
75.00
80.00
85.00
90.00
95.00
100.00
105.00
TIME SINCE START OF ACCIDENT, SEC. *10²

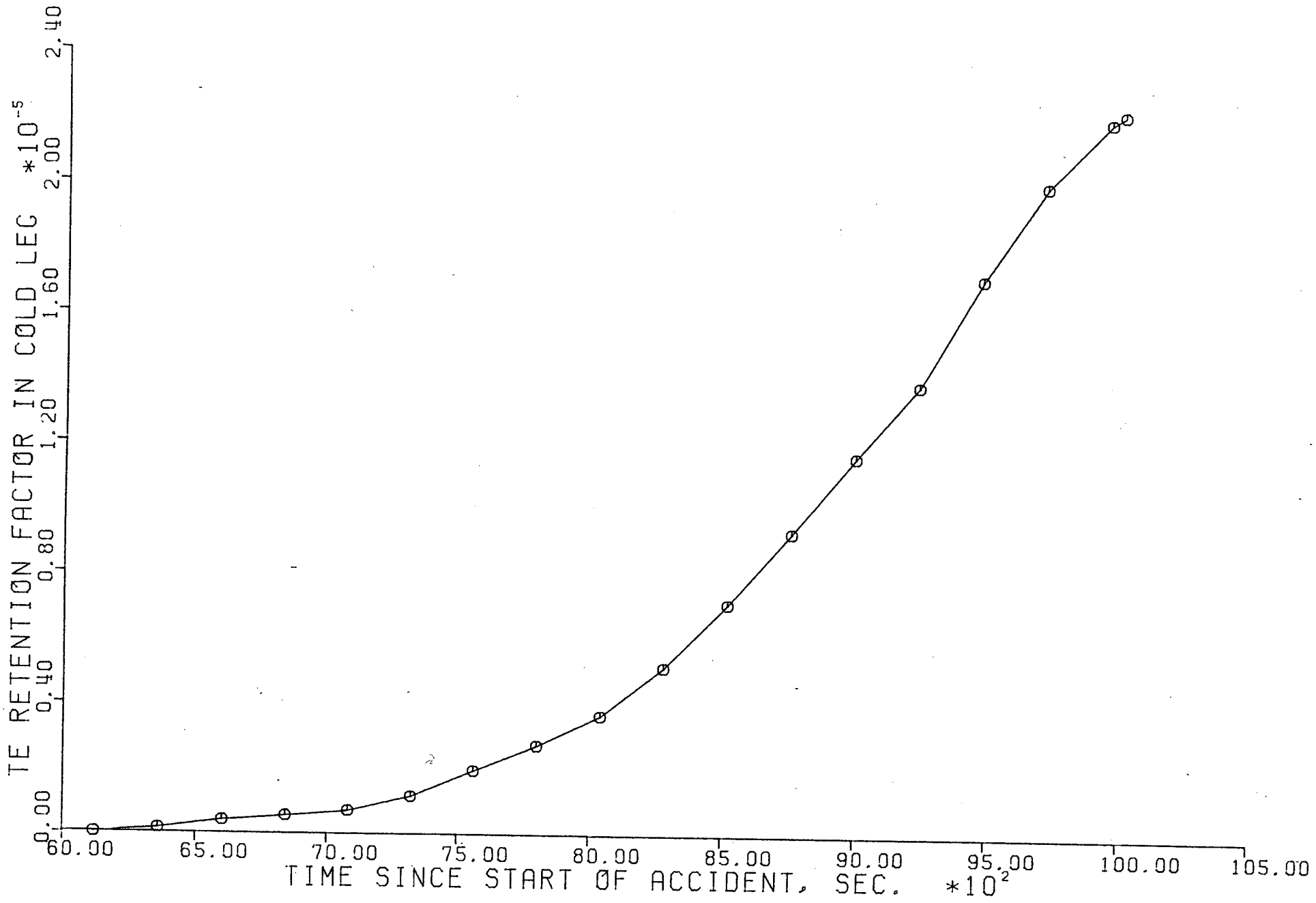
TE RETENTION FACTOR IN COLD LEG *10^-5
0.00
0.40
0.80
1.20
1.60
2.00
2.40
60.00
65.00
70.00
75.00
80.00
85.00
90.00
95.00
100.00
105.00
TIME SINCE START OF ACCIDENT, SEC. *10^2

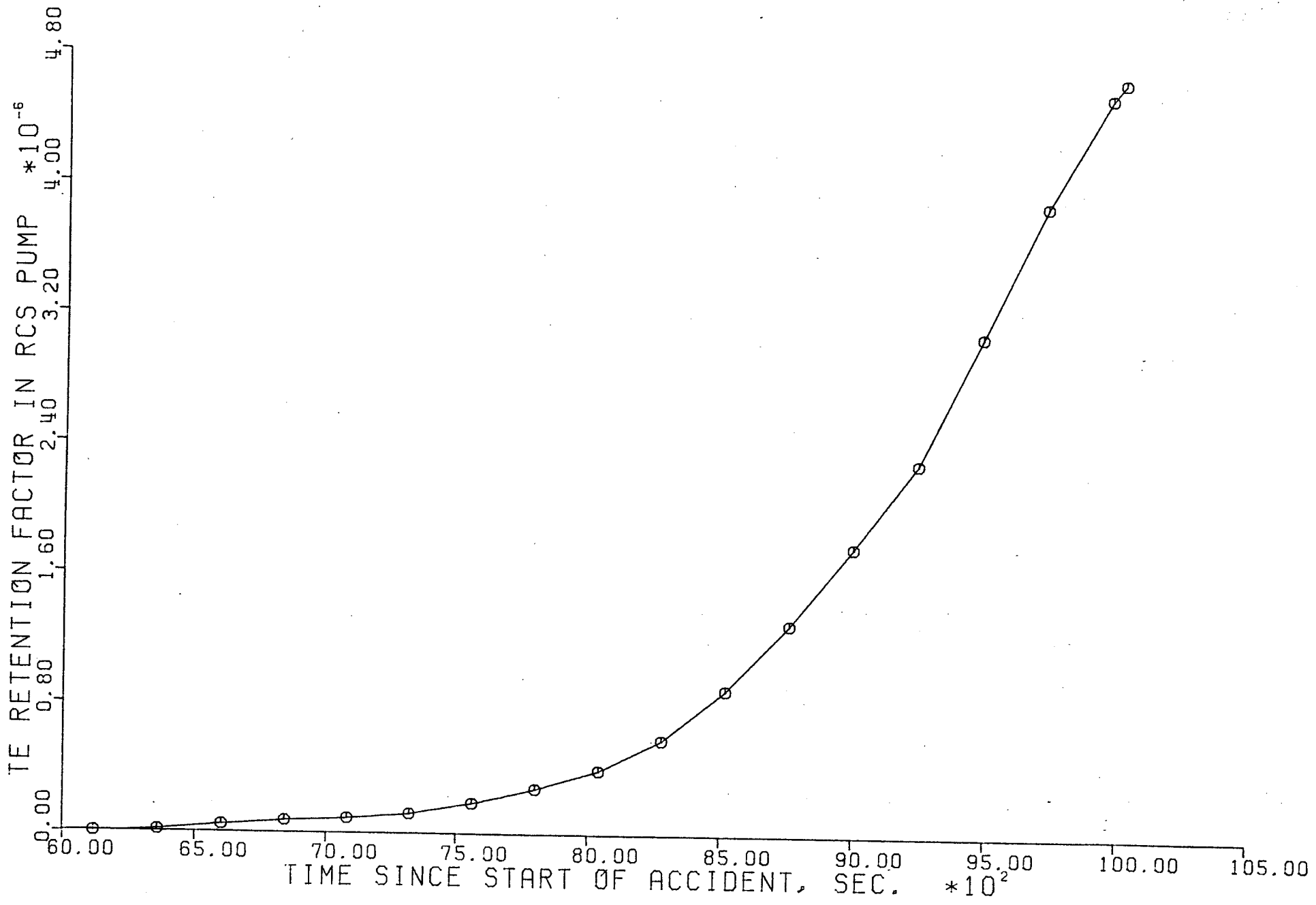
TE RETENTION FACTOR IN RCS PUMP *10⁻⁶
0.00
0.80
1.60
2.40
3.20
4.00
4.80
60.00
65.00
70.00
75.00
80.00
85.00
90.00
95.00
100.00
105.00
TIME SINCE START OF ACCIDENT, SEC. *10²